ENG 345-(EQC 2001/464)

Influence of precast prestressed flooring on the seismic performance of reinforced concrete perimeter frame buildings

DBN Lau, R C Fenwick, B J Davidson (University of Auckland)

The School of Engineering

THE UNIVERSITY OF AUCKLAND
NEW ZEALAND

Department of
Civil and
Environmental
Engineering

Influence of Precast Prestressed Flooring on the Seismic Performance of Reinforced Concrete Perimeter Frame Buildings

by

David Beng Non Lau

Richard C. Fenwick

Barry J. Davidson

April 2007

School of Engineering
Report No. 653

Whakapukahatanga Taiao
New Zealand Maori for
Strengthening the environment - built and natural

For further information contact:
Department of Civil and Environmental Engineering, School of Engineering
The University of Auckland, Private Bag 92019, Auckland, New Zealand
Telephone 64-9-3737599 ext.88166 or ext. 85715 Facsimile 64-9-3737462
Web www.cee.auckland.ac.nz Email cee-enquiries@auckland.ac.nz

INFLUENCE OF PRECAST PRESTRESSED FLOORING ON THE SEISMIC PERFORMANCE OF REINFORCED CONCRETE PERIMETER FRAME BUILDINGS

by:

David Beng Non Lau

Richard C. Fenwick

Barry J. Davidson

School of Engineering Report No. 653

Department of Civil and Environmental Engineering

The University of Auckland

New Zealand

April 2007

Abstract

Lateral load tests of reinforced concrete perimeter frames with diaphragms have shown that the addition of a floor slab (diaphragm) can have a major influence on structural performance. Three moment resisting frames were tested. Two of these frames were tested without a floor slab being attached to the beams, while the remaining frame was tested with the addition of a typical floor slab containing prestressed units. The tests showed that the addition of the floor slab increased the strength of the beams appreciably and as a result the lateral strength of the frame was increased by close to 80%. Clearly a strength increase of this order of magnitude is of major concern in seismic design in cases where it is essential to avoid the premature formation of a column sway mechanism. The test results presented together with an analytical study show the origins of this strength increase. Understanding these mechanisms is a first step in establishing a design method for assessing over-strength values in perimeter frames, which contain floors with prestressed units.

Acknowledgements

This report was prepared by the authors on the research completed by the first author for his PhD degree. The authors would like to acknowledge the financial support of the Earthquake Commission to the first author, enabling him to complete his research.

The authors would also like to acknowledge the generous support of Fletcher Reinforcing and Stahlton Prestressed Concrete Systems who contributed the materials for the tests described in this report. .

Table of Contents

Notation

Chapter 2

A_g = gross area of section.

b_w = width of beam web.

d = effective depth of beam, distance from extreme compression fibre of beam to centroid of tension reinforcement.

d' = distance from extreme compression fibre of beam to centroid of compression reinforcement.

δ_{eu} = elongation at mid-depth of beam containing uni-directional plastic hinges

e = elongation of the reinforcement in the compression zone of the plastic hinges in the beam.

f_c' = specified compressive strength of concrete.

F_c = axial force required to just close the cracks in the compression zone due to contact stress effects.

l = clear span length of beam, between column faces.

L = span of beam.

L_d = bar development length.

L_n = clear span of hollowcore unit.

M_{pos} = maximum positive flexural strength at end of beam.

M_{neg} = maximum negative flexural strength at end of beam.

θ = rotation sustained by the plastic hinges.

$\sum \theta$ = sum of rotations of the plastic hinges in a beam bay.

t_s = thickness of slab.

T_1 = tension force in hollowcore topping reinforcement.

T_2 = tension force in hollowcore topping reinforcement.

V_c = nominal shear force resistance provided by concrete mechanisms.

V_o = shear force due to truss-like action associated with shear resistance in reversing plastic hinges.

w_{max} = maximum uniformly distributed load on that a beam can sustain for reversing hinges to form.

Chapter 3

α = angle of the diagonal members to the horizontal of a segment of beam instrumentation.

b_N = displacement reading at the bottom of column '*N*' (=A,B or C).

d_B = distance from the centroid of segment to the bottom of column.

d_T	=	distance from the centroid of segment to the top of column.
δ_{fl}	=	lateral deflection at mid-span of the beam bay.
δ_x	=	change in length of member 'x'.
δ_s	=	lateral deflection due to shear.
Δ_x	=	as shown in Figures 3.23.
ΔX	=	change in the distance of segment X of a DEMEC arrangement.
E	=	elongation in a segment of beam instrumentation.
e_{AB}	=	average elongation of the beam between columns 'A' and 'B'.
e_{BC}	=	average elongation of the beam between columns 'B' and 'C'.
e_{max}	=	reinforcement strain at maximum stress.
f_{max}	=	maximum stress of reinforcement.
$f_c^{'}$	=	specified compressive strength of concrete.
f_y	=	yield stress of reinforcement.
G	=	change in depth of a segment of beam instrumentation.
h	=	distance between top and bottom members of a segment of beam instrumentation.
h_c	=	height of the column from the base to the beam centreline.
h_d	=	initial vertical distance of DEMEC arrangement as shown in Figure 3.27.
L	=	distance between the column centres.
l_{fl}	=	flexural component of lateral deflection of column
l_s	=	shear component of lateral deflection of column.
π	=	pi (= 3.141593)
θ	=	rotation sustained by a segment of beam instrumentation.
θ_N	=	rotation of the segment N.
θ_x	=	rotations of the columns as shown on Figures 3.23.
θ_X	=	angle in triangular DEMEC arrangement as shown in Figure 3.27 (also θ_Y and θ_{X2}).
S	=	shear deformation in a segment of beam instrumentation.
S_n	=	shear deformation of segment n.
S_N	=	shear deformation in segment N.
t	=	the target displacement.
t_{AB}	=	displacement reading of the displacement between the top of columns 'A' and 'B'.
t_{BC}	=	displacement reading of the displacement between the top of columns 'B' and 'C'.
t_N	=	displacement reading at the top of column 'N' (=A, B or C).

u_1 = horizontal displacement of DEMEC point.

u_2 = vertical displacement of DEMEC point.

X = measured distance of a DEMEC arrangement as shown in Figure 3.27 (similarly segments Y and Z).

X_0 = initial measurement of a DEMEC arrangement.

x_n = distance from column centre to the centroid of each segment n.

Chapter 5

C_c = crack width at central transverse beam.

E_s = elongation in floor slab.

γ = shear deformation of column.

Chapter 7

A_n = area of member 'n' of elongating hinge model.

A_v = area of transverse reinforcement in beam section.

α = angle of diagonal compression strut.

B = width of beam section.

C_d = diagonal compression force.

C_y^n = compression force at yield of member 'n'.

D = depth of beam section.

d_d = depth of the compression stress block of the flexible slab at the beam face.

Δ_d = vertical deflection of diagonal slab.

E_n = modulus of elasticity of member 'n' of elongating hinge model.

ε_y = yield strain of member.

f_v = yield stress of transverse reinforcement in beam section.

I_{cr} = moment of inertia of cracked section.

I_e = effective moment of inertia of concrete section.

I_g = moment of inertia of gross concrete section.

L_{db} = basic development length of a straight bar.

L_{dh} = development length of hooked bars.

L_n = length of member 'n' of elongating hinge model.

L_t = length of tension tie under yield extension.

M_a = moment applied to a section.

M_{cr} = cracking moment of a section.

M_d = moment that can be resisted by the slab.

M_y = flexural strength based on assumed rectangular compression stress block.

θ_d = rotation of diagonal slab.

s = spacing between transverse reinforcement.

T_t = tension force in ties.

T_y^n = tension force at yield of member '*n*'.

V_d = shear force along the interface between slab and beam.

V_s = shear resistance provided by the transverse reinforcement.

w_d = width of diagonal compression strut.

Chapter 8

C = compression force in beam.

ε_{face} = strain in reinforcement at column face.

ε_s = strain measured across gauge length.

ε_{yield} = strain in reinforcement at yield.

T_{beam} = tension force passive longitudinal reinforcement in beam.

T_{rein} = equivalent tension force from the slab reinforcement acting with the perimeter frame beams at the central column.

T_{slab} = tension force in slab, equivalent to an additional force applied to the beam at mid-height of the floor slab.

Chapter 1

Introduction

1.1 Background

It was in the 1950s that the use of prestressed precast flooring began to expand concurrently with the building industry boom in the United States. Due to the high quality and cost-effectiveness demonstrated by the products, investment was placed into the promotion and commissioning in this form of construction. As a result, many precast prestressed flooring products were introduced, which became industry standards such as the double tee, single tee, flat slab, rib (or joist) and infill system followed by the hollow core system in the early 1960s [P1].

Since the 1960s there has been increase in the use of precast prestressed flooring at the expense of cast-in-place floors in the New Zealand construction industry. This can be attributed to the high cost of labour and formwork required for cast-in-place construction. General design provisions for the design of reinforced and prestressed concrete floor slabs are contained in the standards for design loadings and concrete structures, *NZS 4203:1992* [S1] and *NZS 3101:1995* [S2]. However, not all aspects of the design and construction of precast concrete components are covered. With such an extensive use of this form of construction, there is a need for more understanding of how this type of flooring interacts with other structural elements, particularly under seismic conditions.

It has only been in the last two decades that attention has been drawn to the interaction of floor slabs with moment resisting frame systems. Previous research on individual reinforced concrete beam-column joint assemblies with floor slabs identified the influence of slabs on beam-column connections, and the contribution they made to strength [S3, D1, P2, A1, C1 and F1]. However, moment resisting frames have a high level of indeterminacy, which is not present in tests on individual beam column sub-

assemblies. Indeterminacy allows forces to be redistributed and added to this, the phenomenon such as elongation of beams can induce significant additional actions. Comparisons of experimental results have shown that the response of individual beam-column joints sub-assemblies to that of multiple beam-column joint sub-assemblies (both with and without floor slabs) are significantly different, primarily due to the indeterminacy of a frame subassembly. Subsequently, researchers have undertaken tests of reinforced concrete frame subassemblies representing typical levels of a multistorey moment resisting building with and without floor slabs [Q1, Z1, Z2, F2]. While methods for design based on the results of tests of cast-in-place diaphragms can be validly extrapolated, the same may not be true of diaphragm with precast flooring elements.

1.2 General Concept of Seismic Design

New Zealand is situated in a seismically active region. Therefore, structural engineers must consider, and take precautionary measures to mitigate the effects of earthquakes. On the one hand, structures require a level of protection against damage to non-structural elements in order to minimise the disruption to normal operations in smaller magnitude earthquakes [A2]. This requires a minimum level of stiffness to be provided throughout the building to limit the amount of lateral movement in the building. On the other hand, it is generally uneconomical to design structures to resist the largest likely earthquake and remain undamaged. Therefore for the design of structures in seismic zones, most design standards have adopted the following recommendations as design performance criteria:

(a) Resists minor earthquakes with no damage.

(b) Resists moderate earthquakes without structural damage but with some non-structural damage.

(c) Resist major earthquakes without collapse, but sustaining structural and non-structural damage, even unrepairable, but most importantly, without the loss of life.

The objectives above require structures to behave elastically in the event of moderate earthquakes that may be expected to occur in the life of the building. More importantly the building should be able to survive without collapse in a major earthquake. In order to avoid collapse, the structural members must behave in a ductile manner and be able to absorb and dissipate energy by inelastic deformation [P3]. The following specific structural properties have to be considered in order to satisfy the requirements for seismic design mentioned above:

(a) *Stiffness* - A realistic estimate of the stiffness needs to be made in order to reliably quantify, and thus control, the deformation of the structure. This property is estimated from section geometric properties and elastic moduli of construction materials. However it is not simple with reinforced concrete members, as cracking and the distribution of forces in the members influence the stiffness.

(b) *Strength* - For the past 70 years, since design for seismic resistance has been required by standards, strength and performance have often been considered to go hand in hand. However, there has been a realisation that increasing the strength alone does not necessarily enhance performance. The development of capacity design principles in the 1970s [P3], showed that the distribution of strength throughout a building was more important than the absolute design base shear value.

(c) *Ductility* - The ability of the structure and its members to deform in the inelastic domain is generally given the term *ductility*. In order to ensure survival in a major earthquake, the members have to be able to retain a high proportion of their initial strength while sustaining repeated inelastic deformations. This includes the ability of the members to absorb energy by hysteretic behaviour. The fundamental source of ductility is the material (or strain) ductility. This is exhibited by the stress-strain response of the material. Concrete is inherently a brittle material, and suited to carry compression stresses. On the other hand, steel is a ductile material, but when subjected to compression, is susceptible to buckling if not restrained. However in

structural engineering, the curvature ductility of a section and the displacement ductility of a member is of more relevance. The moment-curvature relationship describes the response of the section. From a moment-curvature analysis, it is possible to determine displacement from a curvature distribution of a member. The displacement ductility of a member indicates the ability of the member to displace beyond its yield displacement. In this report where the term 'ductility' is used (given the symbol μ), it is in reference to the displacement ductility of the member or structure.

Though not covered in detail in this thesis, another method of protecting structures from the damaging effects of earthquake ground motions is by base or seismic isolation, where the structure is uncoupled from the ground. To achieve this, additional flexibility is introduced at the base of the structure, which effectively increases the period of vibration of the structure. The combined structure-mounting system is designed such that the period of vibration is sufficiently long so that the structure is isolated from the greatest disturbing motions.

Energy dissipation devices are generally used in conjunction with base isolation to introduce extra damping into the system. This keeps the deflections of the structure relative to the foundation down to acceptable limits and absorbs the energy that would otherwise have to be adsorbed (with damage) by a structure without base isolation. Isolation may be provided for structures with longer fundamental periods, but the design is more complex as there may be more than one significant mode of vibration, and overturning effects may also be important [S5]. A common form of base isolation device is the lead-rubber bearing, which is similar to the laminated steel and rubber bearings used to allow movements due to thermal and other effects to occur on bridges, but with the addition of lead core as energy dissipator.

1.3 Background to Seismic Design of Moment-Resisting Reinforced Concrete Building

Moment resisting frames are one of the most widespread forms of structures used for modern multistorey commercial and residential buildings. Such frames can carry

gravity loads while providing the necessary resistance for lateral forces generated from wind and earthquake ground motion. There are essentially two types of moment resisting frame structures. The first of these, given the term 'uniform frame building' (see Figure 1.1(a)), is where the frames are spaced at regular intervals and are designed to perform the dual act of supporting the gravity loads as well as providing lateral resistance.

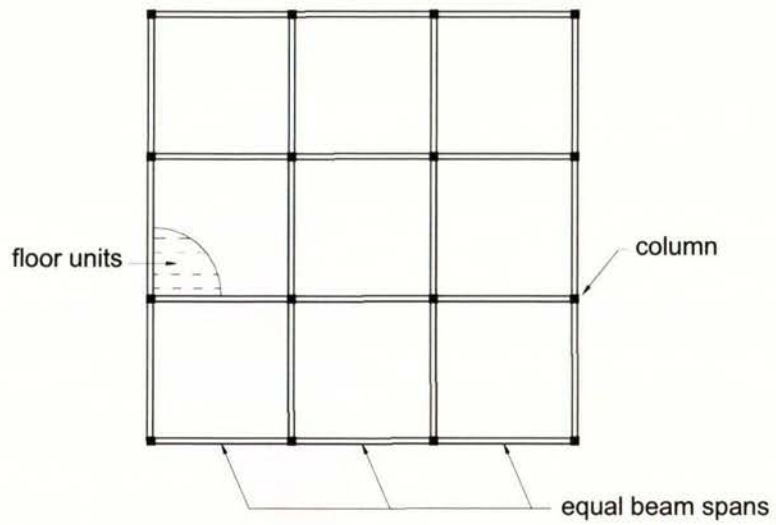

(a) Uniform frame building

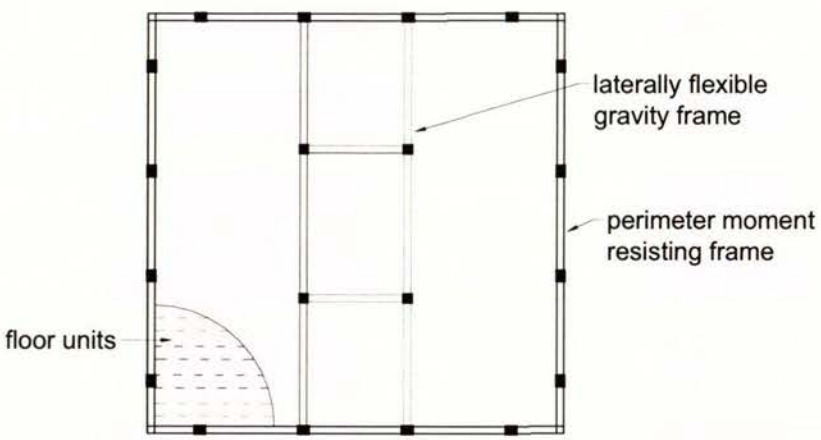

(b) Perimeter frame building

Figure 1.1: Typical plan configuration of moment resisting frame buildings.

The second type of frame, as shown in Figure 1.1(b), is the 'perimeter frame building', where relatively stiff perimeter frames resist the majority of the lateral wind and seismic forces and laterally flexible internal framing supports the majority of the gravity loads. These structures have the advantage that they contain relatively few internal columns compared with the uniform frame building. A common feature of the perimeter frame structure is that the span of the floor slab is greater than the span of the beams in the perimeter frames.

Figure 1.2 shows three possible mechanisms of plastic deformation for a frame building as a result of lateral loading. The column side-sway mechanism, shown in Figure 1.2(a), has plastic hinges that form only in the columns of one storey. This mode of deformation requires large curvature ductility demand in the plastic hinges, which cannot be sufficiently supplied from the columns when the frame is several stories high [P3].

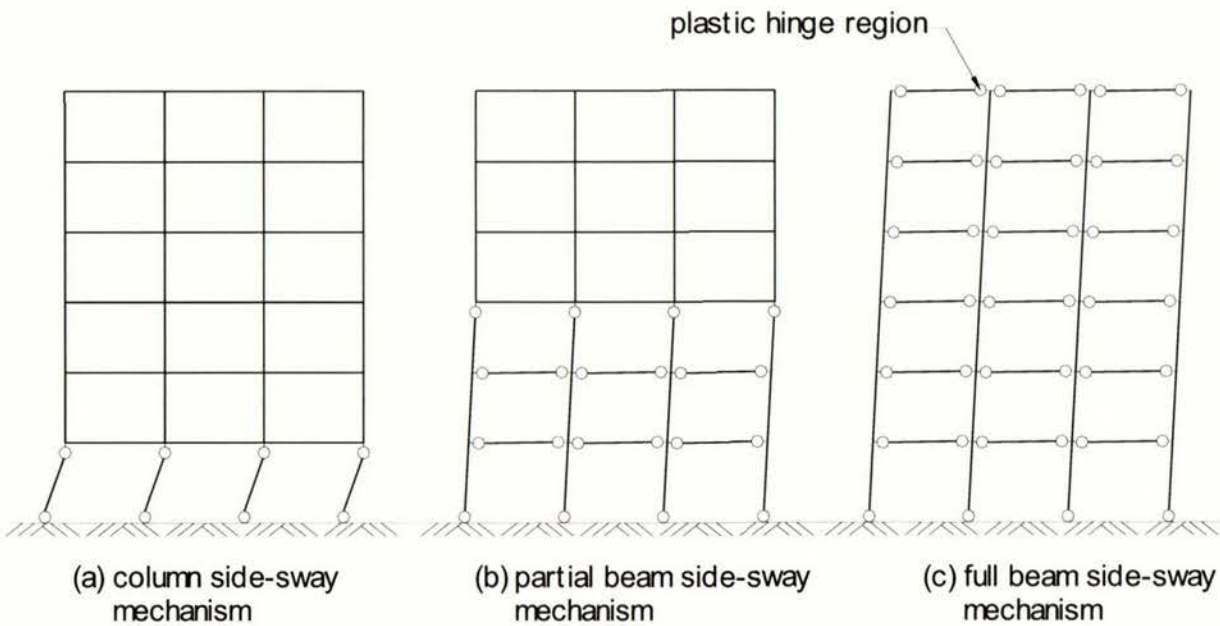

Figure 1.2: Possible modes of deformation in multi-storey building.

Alternatively more desirable mode of deformation for tall multistorey building can be obtained by designing for the partial and full beam side-sway mechanisms, as shown by Figures 1.2(b) and (c). In the full beam side-sway mechanism plastic hinges are confined to the beams and at the base of the columns. In the partial side-sway

mechanism most hinges are located in the beams, at the base of the columns and at selected locations in columns. For the same amount of displacement, the curvature demands in the members are much smaller for the beam side-sway mechanisms when compared to that of the column side-sway mechanism. P-delta actions should be considered as these can contribute to multiple column hinging.

In order to achieve the desired mode of failure, a design philosophy known as *capacity design* forms the core of seismic design of multistorey reinforced concrete buildings. This design procedure was initially proposed by Hollings [H1], and consequently has been developed and incorporated in New Zealand structural standards [P3, P4, P5, P6]. The approach involves the design of members in the frame in accordance with the 'weak beam and strong column' philosophy [P7].

This design process can be summarized in the following:

- The potential plastic hinge zones are selected by proportioning the members. To ensure that the chosen mechanism develops in preference to other failure modes, the potential plastic hinge zones are designed to be the weak links or fuses in the structure. In the case of the full beam side-sway mechanism the potential plastic hinge zones are located in the beams, with column hinging limited to just above the column bases (as shown by Figure 1.2(c)).

- The members within the potential plastic hinge zones are designed to have dependable flexural strengths and detailed to ensure they can sustain the required inelastic deformation.

- Shear and anchorage failures are inhibited within members that contain plastic hinges by ensuring that the strengths of these failure modes exceed that of the potential plastic hinges at flexural over-strength. The member over-strength is calculated based on the likely increased strength due to for example, higher than specified characteristic yield stress and strain hardening of reinforcement in reinforced concrete sections.

- In regions outside potential plastic hinge zones, protection against inelastic deformation is provided by ensuring that the strength exceeds the maximum demands that can be imposed from over-strength actions sustained in the potential plastic hinges.

With this approach it is essential that the member over-strengths are realistically determined. Underestimates may result in the formation of unintended column failure modes, while overestimates increase the structural costs.

With the formation of plastic hinge zones, the tensile strains in the reinforcement are appreciably larger than the compressive strains in the concrete and as a consequence the member increases in length. Beams in ductile frames tend to elongate with the formation of plastic hinges. The restraint provided by floor slabs to this elongation increases the flexural strength of the plastic hinge zones. This strength increase is primarily a function of the beam elongation, the in-plane strength of the slab, the structural arrangement of the slab in relation to the frames and the strength of the connections between the slab and the frame. If the strength enhancement due to these factors is under-assessed, it is possible that in the event of a major earthquake, the intended ductile beam-sway mechanism may be replaced by the non-ductile column-sway mechanism, leading to premature structural collapse.

A model of a unidirectional plastic hinge was incorporated into a time history analysis of a six-storey three bay frame building [F3, F7]. The results were compared against a non-elongating analysis of the same structure. It was found that elongation caused the maximum interstorey deflection and the plastic hinge rotations of the column base in the first storey to be doubled in critical regions. In addition it was pointed out that elongation could result in precast floor units being pulled off their supports. This has important implications for the detailing of supports for precast flooring components and external cladding. It was observed that precast flooring systems performed poorly during the 1994 Northridge Earthquake [N1], with collapse occurring due to loss of seating.

1.4 Research Objectives

The seismic performance of ductile moment resisting frames has been extensively researched in New Zealand and elsewhere, and design rules have been developed from this work. As part of this effort the interaction of in-situ floor slabs with the beams of ductile moment resisting frames has been studied. In particular the interactions between beams and in-situ slabs have been considered and rules have been developed and included in the New Zealand Concrete Standard for the amount of slab reinforcement which should be included with the beam reinforcement, in assessing both the design and over-strength values. However, while the research work on which these rules are founded relates well to reinforced concrete slabs supported by beams at regular centres, such as illustrated in Figure 1.1(a), it does not model the case where perimeter frames are used. Two particular aspects are of concern:

- The use of precast prestressed units in floor diaphragm which will tend to restrain beam elongation, inducing forces that may increase the flexural strength of the perimeter frame.

- The effect of using precast prestressed units which span greater than the beams in the perimeter frame, which is likely to concentrate cracking at specific locations and induces failure which may not have been expected previously.

The research described in this thesis aims to bring more understanding to the interaction of plastic hinge zones and diaphragms and the potential problems that might arise with large deformations imposed on the structure. This is a natural continuation to research work on the behaviour of ductile reinforced concrete members in moment resisting frames carried out previously in the University of Auckland. In particular, the elongation of plastic hinge members and the effect it has on the overall behaviour of reinforced concrete frame elements was studied [M1, F2, F11].

1.5 Outline of Thesis

The literature review on previous studies related to this work is presented in Chapter 2. Chapter 3 describes the experimental programme, including the details of the test units, the test arrangements, equipment and test procedures. Chapter 4 reports on the experimental results from the first test, Unit 1, while the experimental results of Unit 2 and 3 are contained in Chapters 5 and 6 respectively. Chapter 7 presents analytical models developed to model the effects of elongating hinge and interaction of floor slabs in frames. The experimental results and observations are discussed in Chapter 8. General conclusions are contained in Chapter 9.

Chapter 2

Literature Review

2.1 Introduction

In this chapter, the mechanisms of elongation in plastic hinges are described. The results of a number of tests in which elongation has been observed are reviewed. The influence of elongation of frames with insitu floor slabs and the stability of precast flooring elements are also examined. In-plane diaphragm actions in structures are also reviewed.

2.2 Plastic Hinges and Mechanisms of Elongation

When beams are subjected to inelastic cyclic displacements, two types of plastic hinge can form. The type that develops depends on the ratio of the gravity and seismic actions applied to the beam. The two forms of plastic hinges are:

1. Uni-directional or gravity dominated plastic hinges,
2. Reversing or seismic dominated plastic hinges.

With both plastic hinge types, the yielding in tension of the flexural reinforcement causes the beam to elongate. Structural actions associated with elongation have received little attention in the literature until recently, and its influence on the performance of seismically designed reinforced concrete structures has been largely neglected. Test results have indicated that member elongation is quite significant. Typically both uni-directional and reversing plastic hinges elongate by 2 to 5% of the beam depth before strength degradation occurs [F4, M1, R1, M2]. The inelastic load deformation characteristics of uni-directional and reversing plastic hinges are different, as discussed in the following subsections.

2.2.1 Uni-directional plastic hinge

In a frame, uni-directional plastic hinges may form in a beam in a severe earthquake if the level of gravity and vertical loading that is supported simultaneously with the earthquake induced lateral forces exceeds a critical value. Hence this form is known as a gravity dominated plastic hinge [F3]. The positive and negative moment plastic hinges develop at different locations along the beam. This is shown in Figure 2.1. This form of hinge may be expected in a severe earthquake in a proportion of the beams in uniform frame structures (see Figure 1.1(a) of *Chapter 1*), which have been designed for the dual purpose of providing both seismic and gravity load resistance.

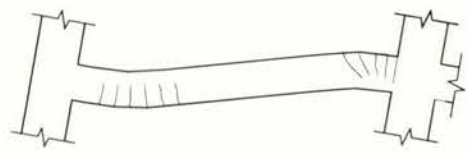

(a) Frame sways to right

(b) Frame sways to left

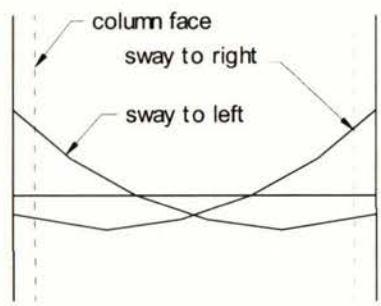

(c) Bending moment diagram

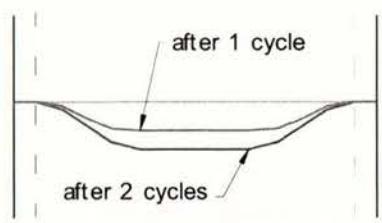

(d) Deflected shape of beam

Figure 2.1: Uni-directional plastic hinges in beam.

The formation of uni-directional plastic hinges in a beam of a seismic resistant frame is shown in Figure 2.1. As the frame sways to the right, as shown in Figure 2.1(a), a positive moment (sagging bending moment) plastic hinge forms to the left of the mid-span while a negative moment (hogging bending moment) plastic hinge forms next to the face of the right hand column. When the frame reverses in sway direction, as illustrated in Figure 2.1(b), the opposite situation develops as a positive moment plastic hinge forms in the span to the right of the mid-span as a negative moment plastic hinge forms adjacent to the face of the left hand column. The bending moment diagrams associated with these actions are shown in Figure 2.1(c).

Subsequent inelastic deformation of the structure in either direction causes the plastic hinge rotations to increase. The accumulation of rotation is accompanied by increasing deflection to produce the deflected shape illustrated in Figure 2.1(d). In order to survive an earthquake of high intensity, the plastic hinges must be able to sustain high rotations [M1], which are appreciably greater than the corresponding rotations sustained in reversing plastic hinges. Analyses indicate that with uni-directional plastic hinges imposed rotations are typically two to four times the corresponding values imposed on reversing plastic hinges [F5]. Additional reinforcement may be added to prevent formation of uni-directional plastic hinges. This consists of reinforcement lapped to the bottom longitudinal reinforcement along the beam length and stopped before the ends of the beam.

2.2.2 Reversing plastic hinge

Reversing plastic hinges are formed within the beams of a frame where seismically induced moments dictate the behaviour of the system. This type of plastic hinging occurs in a severe earthquake, provided that the maximum positive and negative bending moments occur at the ends of the beam. In beams with uniform longitudinal reinforcement, the maximum uniformly distributed load, w_{max}, that a beam can sustain for reversing hinges to form is given by:

$$w_{max} = \frac{2(M_{pos} + M_{neg})}{l^2} \qquad \textit{Equation 2.1}$$

where M_{pos} and M_{neg} are the maximum positive and negative flexural strengths at each end of the beam,

l is the clear span of the beam between the column faces.

If the distributed force, w_{max}, exceeds the value given by Equation 2.1, uni-directional plastic hinges form [F6].

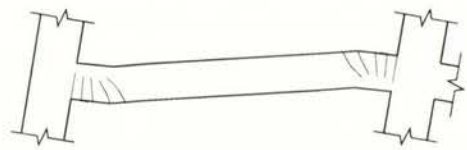

(a) Frame sways to right

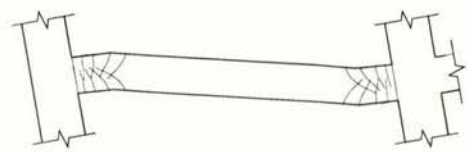

(b) Frame sways to left

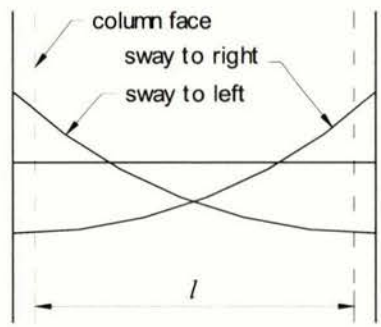

(c) Bending moment diagram

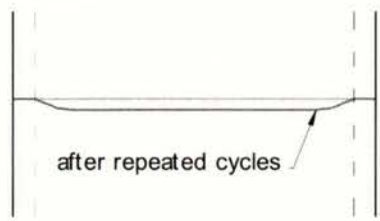

(d) Deflected shape of beam

Figure 2.2: Reversing plastic hinges in a beam.

As the structure sways to the right, as shown in Figure 2.2(a), positive and negative moment plastic hinges form in the beam adjacent to the left and the right of the column faces respectively. The inelastic rotation of the plastic hinges reverses, shown in Figure 2.2(b), as the frame sways in the other direction. The bending moment diagram associated with this behaviour is shown in Figure 2.2(c). In this case, as shown in Figure 2.2(d), the deflected shape of the beam does not change with subsequent load cycles and the plastic hinge rotation is closely related to the interstorey drift. A significant amount of elongation in the beam length can result from repeated inelastic rotations of this type of plastic hinge.

2.2.3 Elongation in plastic hinge zones

Plastic hinge elongation was first observed by Paulay in 1969, in a series of tests carried out on spandrel beams of shear walls [P8]. The rotations of the plastic hinges in the beams develop mainly from the yielding of the reinforcement by flexural tension. Elongation occurs, as the tensile strains in the reinforcement are appreciably greater than the compressive strains.

Elongation in uni-directional plastic hinge zone

Elongation in uni-directional plastic hinges occurs primarily as a result of inelastic rotations. An idealised form of elongation sustained by a beam containing uni-directional hinges after recurring cyclic loading is shown in Figure 2.3. The extensive yielding of the reinforcement of a test beam is shown in Figure 2.4. It can be seen that the reinforcement in the compression zone sustains little strain and the rotation arises primarily from the tensile strains in the reinforcement. This demonstrated that the strains in the compression zone reinforcement are small and could be ignored. Based on this, the resultant elongation at mid-height of the beam, δ_{eu}, may be found by multiplying the plastic hinge rotation by half the distance between the top and bottom reinforcement, as given by *Equation 2.2*.

$$\delta_{eu} = \frac{\Sigma\theta\left(d - d'\right)}{2} \qquad \textit{Equation 2.2}$$

where $\Sigma\theta$ is the sum of rotations of the plastic hinges in the beam bay,

$(d - d')$ is the distance between the centroids of the compressive and the tensile longitudinal reinforcement.

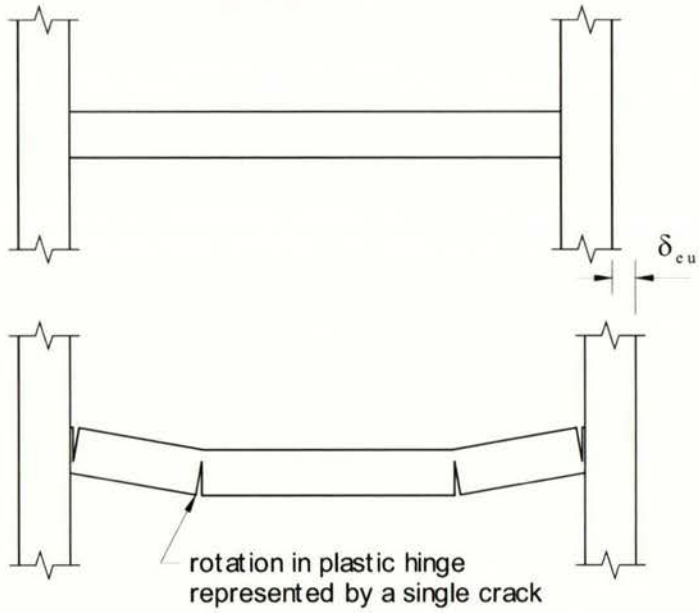

Figure 2.3: Elongation in beam due to formation of uni-directional hinges [M2].

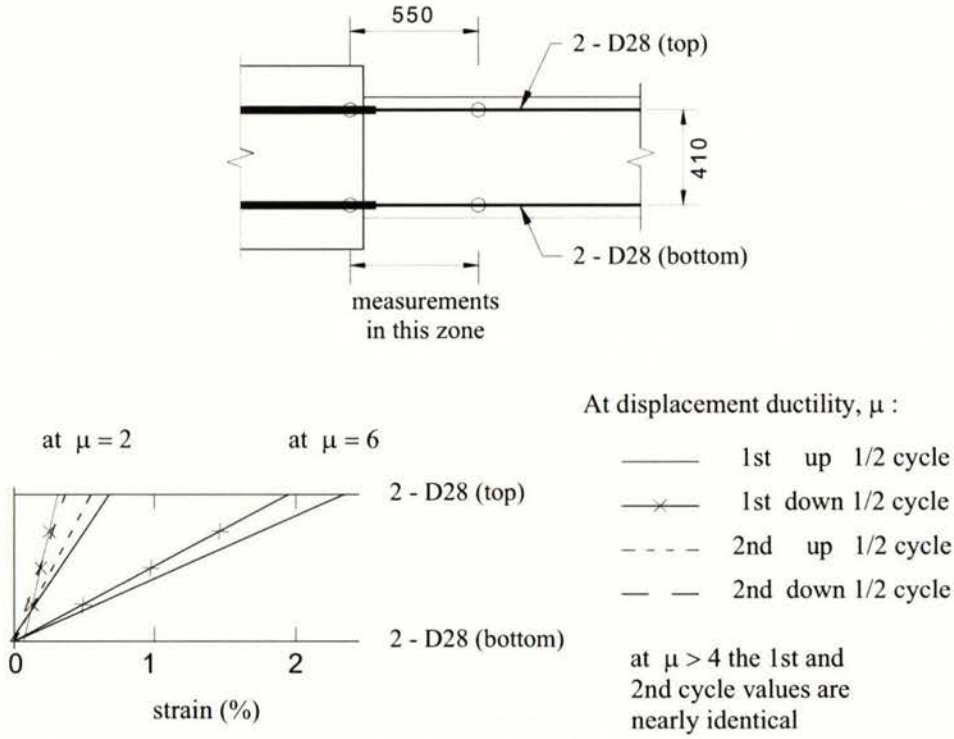

Figure 2.4: Elongation of reinforcement in a uni-directional plastic hinge at column face of a test beam [F6].

A uni-directional plastic hinge model has been developed in the University of Auckland, which has been implemented into the dynamic analysis program DRAIN-2DX and used to analyse a number of structures, which formed uni-directional plastic hinges [F7]. This model was later extended to include both the uni-directional and the reversing plastic hinges with the addition of shear deformation [D2].

Elongation in reversing plastic hinge zone

Figure 2.5 shows the strain patterns in of a reversing plastic hinge formed in a test beam [F6]. The strain patterns are markedly different from that of the uni-directional plastic hinge as shown in Figure 2.3.

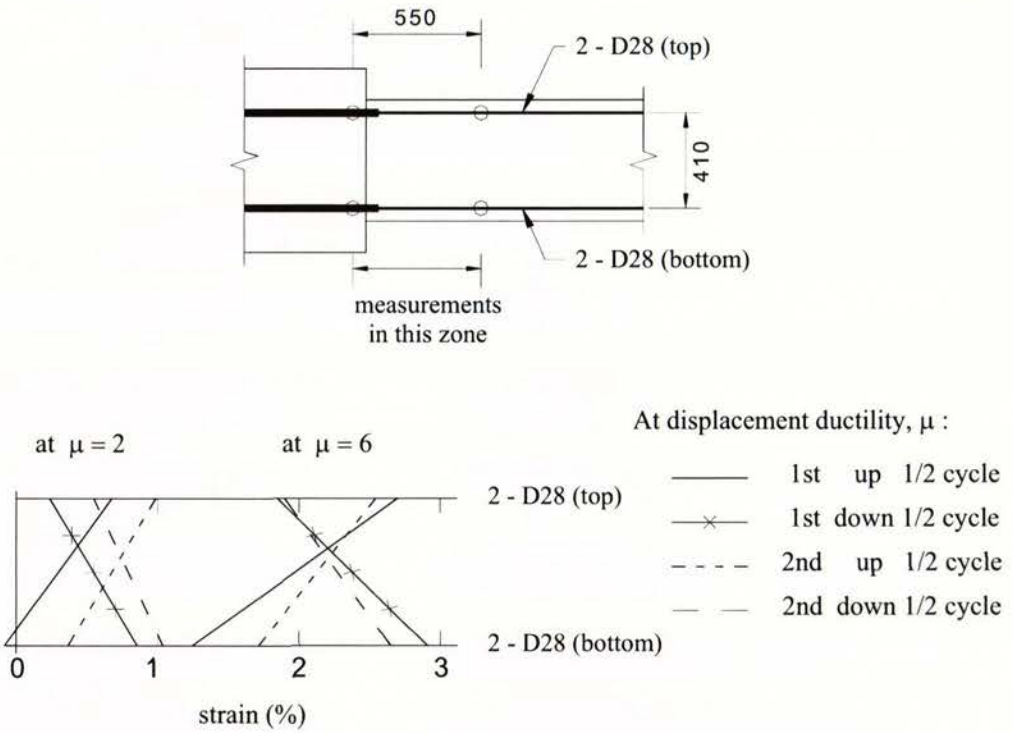

Figure 2.5: Elongation of reinforcement in a reversing plastic hinge of a test beam [F6].

A reversing plastic hinge acts as a uni-directional plastic hinge on the application of initial inelastic displacement, where the reinforcement yields in the tension zone and a small compression strain is sustained by the compression zone reinforcement. On reversal of loading direction, the reinforcement in the compression zone, which had yielded in tension in the previous half cycle, does not fully yield back in compression.

With additional inelastic loading cycles, the reinforcement continues to increase in length until buckling of the bars occurs. The extension of the reinforcement causes the cracks in the compression zones to remain open. *Equation 2.3* was proposed to calculate the elongation, δ_{cr}, in reversing plastic hinges [F6]:

$$\delta_{cr} = e + \frac{\Sigma\theta\left(d - d'\right)}{2} \qquad \textit{Equation 2.3}$$

where e is the elongation of the reinforcement of the plastic hinge in the beam which had yielded in tension in the previous half cycle and has not fully yielded back in compression.

Two principle reasons were given for the explanation of why the longitudinal reinforcement in the compression zone of a reversing hinge does not fully yield back, thus preventing the cracks from closing [F6]. These are:

1. *Contact stress effect* - arises when the concrete cracks in tension and the tensile longitudinal steel yields and dislodges aggregate particles into the cracks. When the loading direction reverses and the longitudinal steel goes into compression, these aggregate particles sustain local contact compression pressure, restricting the closure of the cracks [B1].

2. *Mechanism of shear resistance in plastic hinge zones* - with the formation of intersecting diagonal cracks in the hinge zone, the shear resistance is provided by a truss like action, as shown in Figure 2.6. In this mechanism, the diagonal compression struts are sustained by the concrete while the tension ties are sustained by the transverse reinforcement. From the equilibrium requirements shown in Figure 2.6(b), it can be seen that the flexural tension force, T, is always larger than the flexural compression force, C, at the same section. As a consequence, the inelastic rotations in the hinge zone tend to occur more by the yielding of the tension reinforcement than the reinforcement in the compression zone. Under repeated cyclic loading, this results in longitudinal extension (or elongation) of the plastic hinge.

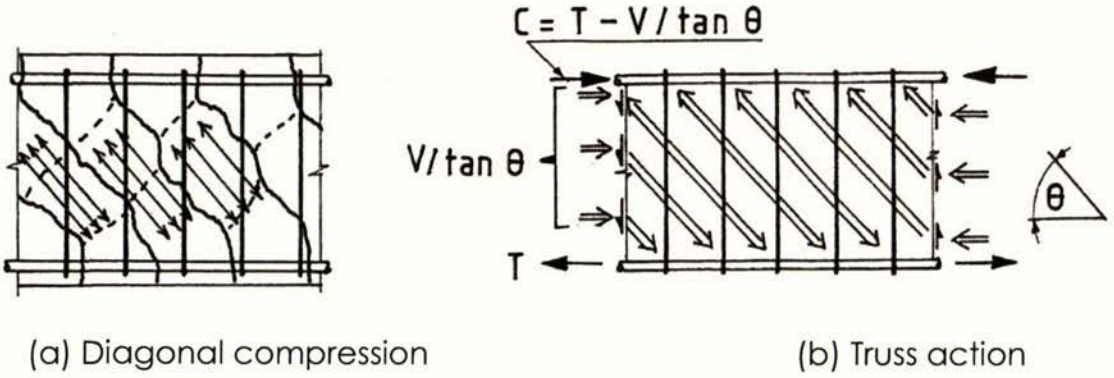

Figure 2.6: Mechanism of shear resistance in reversing plastic hinge [F6].

A model of plastic hinge zone substructure, as illustrated in Figure 2.7, was developed in the University of Auckland [D2, D3]. The steel and concrete truss elements, which are pinned at the end to the rigid arms, are placed at the centroids of the beam reinforcement. It can be seen from this model that once the steel truss element yields in tension, the plastic hinge increases in length. Under the tensile action, the concrete cracks and is assumed to have negligible stiffness, therefore the elongation has little impact on the cracked concrete element response while in tension. In the compression zone, the concrete truss element does not significantly reduce in length due to its large compression stiffness. The length of the plastic hinge is only updated once the loading direction reverses.

Significant shear deformations occur in plastic hinges of reinforced concrete beams subjected to inelastic cyclic loading. In the model shown by Figure 2.7, the shear resistance of the hinge is provided by the shear link. This element has no axial and flexural stiffness. The behaviour of this element incorporates a modified version of shear deformation theory developed by Fenwick and Thom [F8]. It applies to members containing equal areas of tension and compression reinforcement and assumes that axial loads are negligible. The following conclusions established from experimental observations formed the basis of the response of the shear link:

- Strain distribution is approximately linear along the length of the plastic hinge.
- The cracks in the compression zone remain open (zero axial load).

- Extensive transverse reinforcement yielding occurs at the high strain end of plastic hinges.
- The shear resistance provided by the concrete (ie. the V_c component) is negligible once intersecting diagonal cracks form in a reversing plastic hinge. The shear is resisted by tension forces in the stirrup and diagonal compression in the concrete.
- At load levels in excess of that causing yielding in the transverse reinforcement, repeated cycles of shear will cause the concrete in the web to spall in a manner which suggests a compression failure.

The hinge model was implemented into a two dimensional nonlinear computer package DRAIN-2D, which is capable of performing static and dynamic analyses. The cyclic response from analytical simulations of reinforced concrete members incorporating the hinge substructure were compared against experimental results from four cantilever beams, a portal frame and a two-storey three bay bent. The load versus displacement and moment versus rotation response closely followed those obtained experimentally.

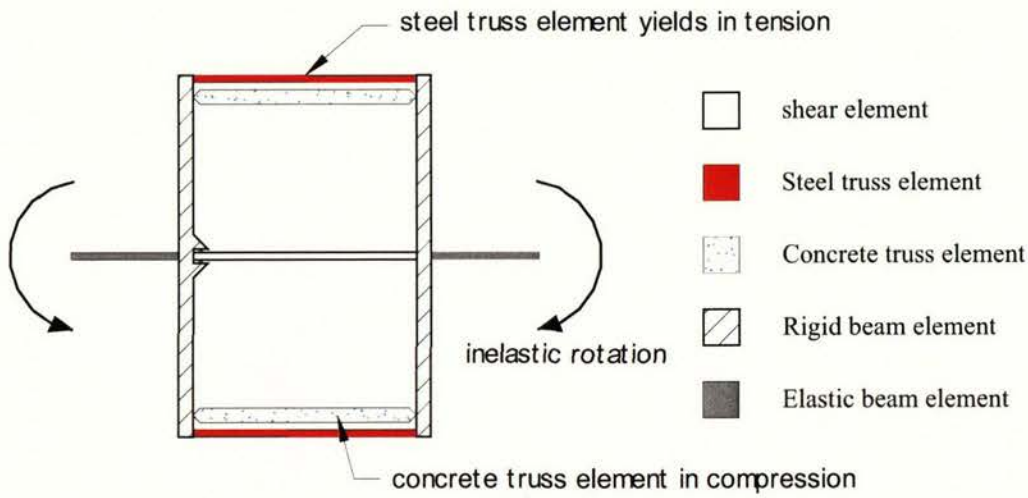

Figure 2.7: Model of elongating plastic hinge in beam [D2].

Analytical predictions of beam elongation, shear and flexural deformations were in reasonable agreement with values measured in experiments. However, the model was unable to represent accurately the effects of concrete contact stresses and reinforcement bar buckling and kinking. The effects of axial loading on the plastic hinge zone was not considered.

2.3 Previous Reporting on Elongation

The elongation that develops within the plastic hinges during testing of statically determinate units such as beams and beam-column subassemblies does not induce reactions within the members and is therefore easily overlooked. However, on formation of plastic hinge within statically indeterminate structures, a redistribution of internal forces occurs throughout the structure. The resulting internal actions are a function of the extent of plastic deformations, relative stiffness and overall configuration of the members within the structure. Hence elongation induced effects such as frame dilatency (or expansion), loss of floor support and induced axial forces in floor slab can be important in indeterminate structures.

Elongation in reinforced concrete members has been observed by researchers, who have highlighted different aspects of plastic hinge elongation and its effects. These are briefly reviewed in the following sections.

2.3.1 University of Auckland, New Zealand

In this section, research carried out within the University of Auckland relating to elongation in reinforced concrete members is reviewed. Experiments where elongation was observed, and also tests where elongation was studied in detail, are presented. Also included are test programs of moment-resisting reinforced concrete frames, where their behaviour under cyclic loading was studied. In particular, the effect that elongation has on the overall performance was evaluated.

Elongation in reinforced concrete members

Elongation has been measured in many tests conducted at the University of Auckland. This action was first observed and reported by Fenwick and Fong in 1979 [F9], where five reinforced concrete cantilever beams were subjected to cyclic loading. These beams were 500mm deep by 200mm wide and had different span lengths. The increase in the length of beams was between 13 to 19mm in magnitude, which corresponded to elongation of 2.6 to 3.8% of beam depth. Fenwick and Nguyen tested a beam-column connection, where elongation of 4.4% of beam depth was measured [F10]. Another

series of tests reported by Fenwick *et al* in 1981 [F4], involved testing of eight cantilever beams. Elongation measurements of 2.5 to 4.1% of beam depth were recorded.

Two identical beams were made and tested to enable the performance of uni-directional and reversing plastic hinges to be compared [F6]. The first beam was subjected to cyclic loading, but the force in the upward direction was limited to 3/4 of the theoretical strength. The beam was loaded in the downward direction such that a uni-directional plastic hinge was formed. For this beam, measurements indicated that the strain sustained in the compression zone reinforcement was negligible provided that it had not been yielded in tension in previous load cycles. As shown in Figure 2.8, the elongation measured from the beam and from a test of a portal frame (see later) correlated well with the calculated values obtained from *Equation 2.2* in which *e* was zero.

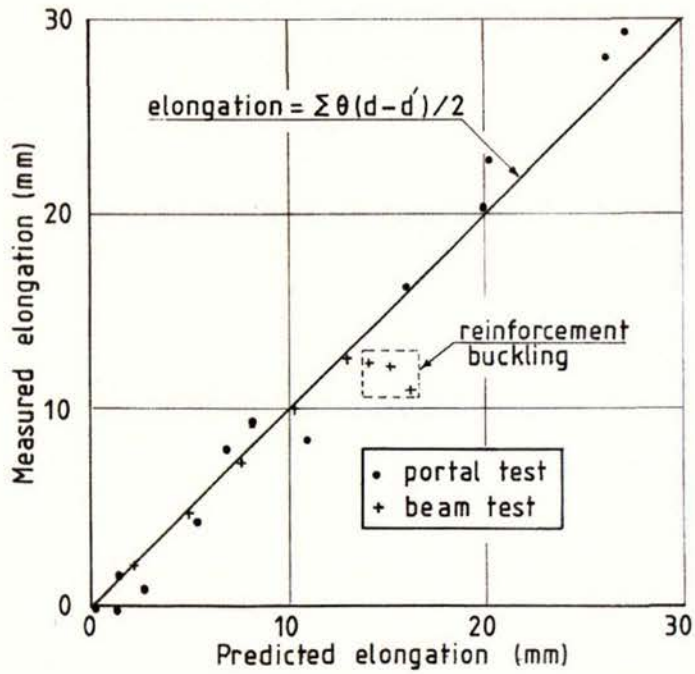

Figure 2.8: Predicted and measured elongation in members forming uni-directional hinges [F6].

For the second beam, cyclic loading was applied to impose equal displacement in both directions such that a reversing plastic hinge was formed. On the initial inelastic displacement, it acted as a uni-directional plastic hinge and a small compression strain was sustained by the compression zone reinforcement. On the reversal of the loading

direction, the reinforcement in the compression zone, which had yielded in tension during the previous half cycle, did not fully yield back in compression. With continued cyclic loading, the compression reinforcement continued to elongate.

Three more cantilever beams were tested under cyclic loading so that reversing plastic hinges were formed [F6]. Two of the beams were rectangular (500mm deep by 200mm wide), the first beam reinforced with five 20mm deformed longitudinal bars in both the top and bottom, and the second beam with five 20mm bars in the top and three 20mm bars as bottom reinforcement. A third beam had a tee-shaped cross-section with 500mm deep by 200mm wide wed and 80mm thick flanges, 700mm wide both sides of the web. It was reinforced with five 20mm longitudinal bars in both the top and bottom and ten 10mm bars in the flanges. The test results showed that the beams with unequal areas of top and bottom reinforcement sustained slightly larger elongation when the larger area of steel is in compression, in comparison to the beam with equal areas of top and bottom reinforcement. Slightly smaller elongation was measured in the reverse direction than the corresponding beam with equal top and bottom reinforcement areas. It was found that the slab in the tee-section beam was ineffective in restraining the elongation.

Four beams, which were identical in section (500mm by 200mm), were subjected to cyclic loading under differing axial load levels for each beam [F7, T2]. Three of the beams were subjected to axial load levels of $0.039\,A_g f_c^{'}$, $0.068\,A_g f_c^{'}$ and $0.145\,A_g f_c^{'}$ (where A_g is the gross sectional area and $f_c^{'}$ is the unconfined concrete compression strength). Three of the beams were tested dynamically at speeds comparable to that of a major earthquake. The fourth beam (subjected to axial force of $0.145\,A_g f_c^{'}$) was tested slowly over a period of two days. It was found that elongation decreased with increasing axial load. This is shown in Figure 2.9.

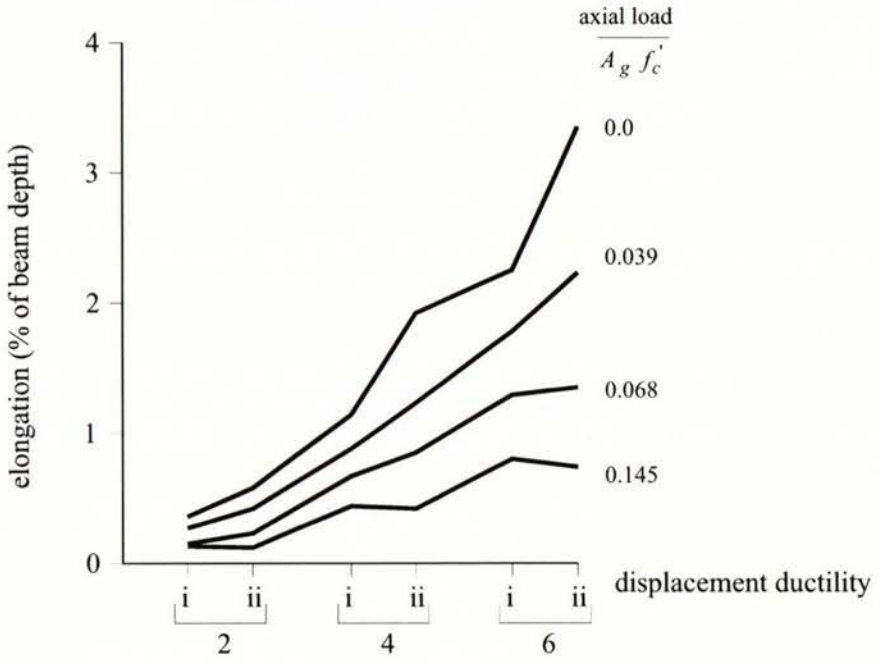

Figure 2.9: Elongation of beams subjected to axial loads [F7].

To close the cracks in a reversing plastic hinge in a beam with equal top and bottom reinforcement an axial force must act. The axial force that acts must increase the magnitude of the force in the compression zone so that the compression force is equal to the tension force. The difference in the tension and compression forces is due to the mechanism of shear resistance in a reversing plastic hinge, which can be represented by a truss like action (see *Section 2.2.3* and Figure 2.6).

It was proposed that and axial force of $0.05\, A_g f_c'$ was required to close the cracks due to contact stress effects (wedging action of the dislocated aggregate particles in the crack). On this basis it was proposed that the axial force level, F_c, required to just close the cracks in the compression zone is given by:

$$F_c = V_o + 0.05\, A_g f_c' \qquad \textit{Equation 2.4}$$

where V_o is the shear force due to truss like action associated with shear resistance in reversing plastic hinges.

Reinforced concrete portal frame

In an investigation into the performance of structures, which form uni-directional plastic hinges in a severe earthquake, a reinforced concrete portal frame was built and tested [M1]. Two constant point loads were applied to the beam to represent gravity loads, while a lateral force, which reversed in direction, acted just above the beam level to represent seismic actions, see Figure 2.10.

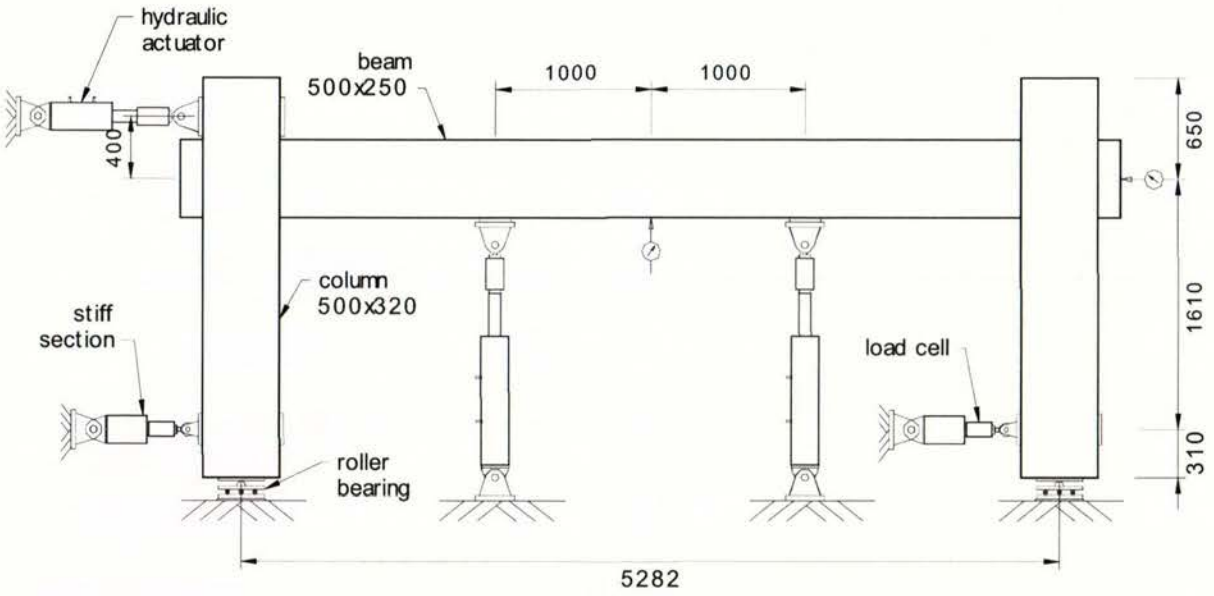

Figure 2.10: Test arrangement of portal frame [M1].

During the test predominantly uni-directional plastic hinges formed. Positive moment plastic hinge rotations accumulated near the vertical load points and negative moment hinges accumulated in the beam near the column faces. The progressive increase in plastic hinge rotations was reflected in the increasing mid-span deflection, which reached 1.1% of the span during the second cycle to displacement ductility 6. Beam elongation was between 30 to 40mm depending on the direction of loading while the corresponding average lateral displacement was less than ±60mm. In a load cycle in which the imposed drift was ±3.4%, buckling occurred in the compression reinforcement, which led to the lateral strength being reduced to less than 80% of the theoretical strength.

Stiffness degradation in plastic hinges is largely a function of the shear deformation that occurs when the shear reverses in direction [F6]. For the portal frame, shear reversal did not occur and hence pinching of the load deflection curves did not develop to any appreciable extent, as shown in Figure 2.11. Consequently, there was very little stiffness degradation until failure was imminent and the longitudinal reinforcement started to buckle.

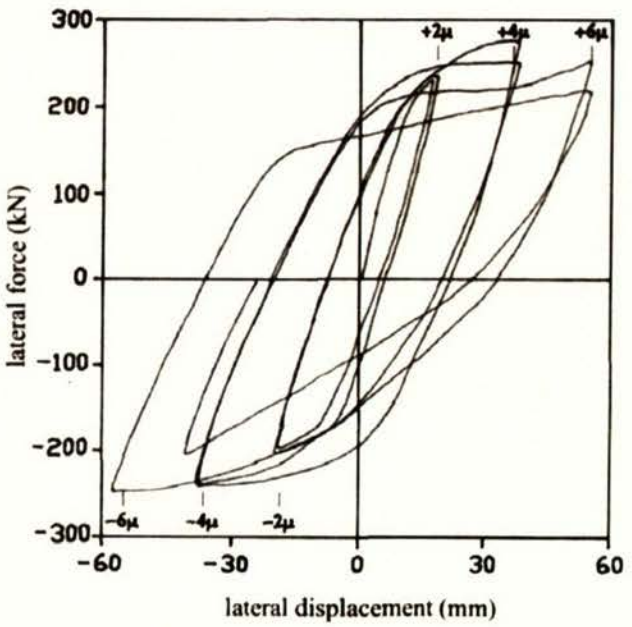

Figure 2.11: Load versus displacement response at mid-point of portal frame [M1].

Three-bay reinforced concrete bent with and without slab

Two 1/3 scaled test units were designed to model a level of an internal three-bay frame in a multistorey building [F2]. One of the units had a slab and the other was without. The unit with the composite slab had transverse beams, which cantilevered out from each column. The aim was to assess the influence of the slab on behaviour. The reinforcing details in the main beam and columns were identical for both units. The test arrangement for the composite frame slab unit is shown in Figure 2.12(a) and (b), and the beam and slab section is shown by Figure 2.12(c).

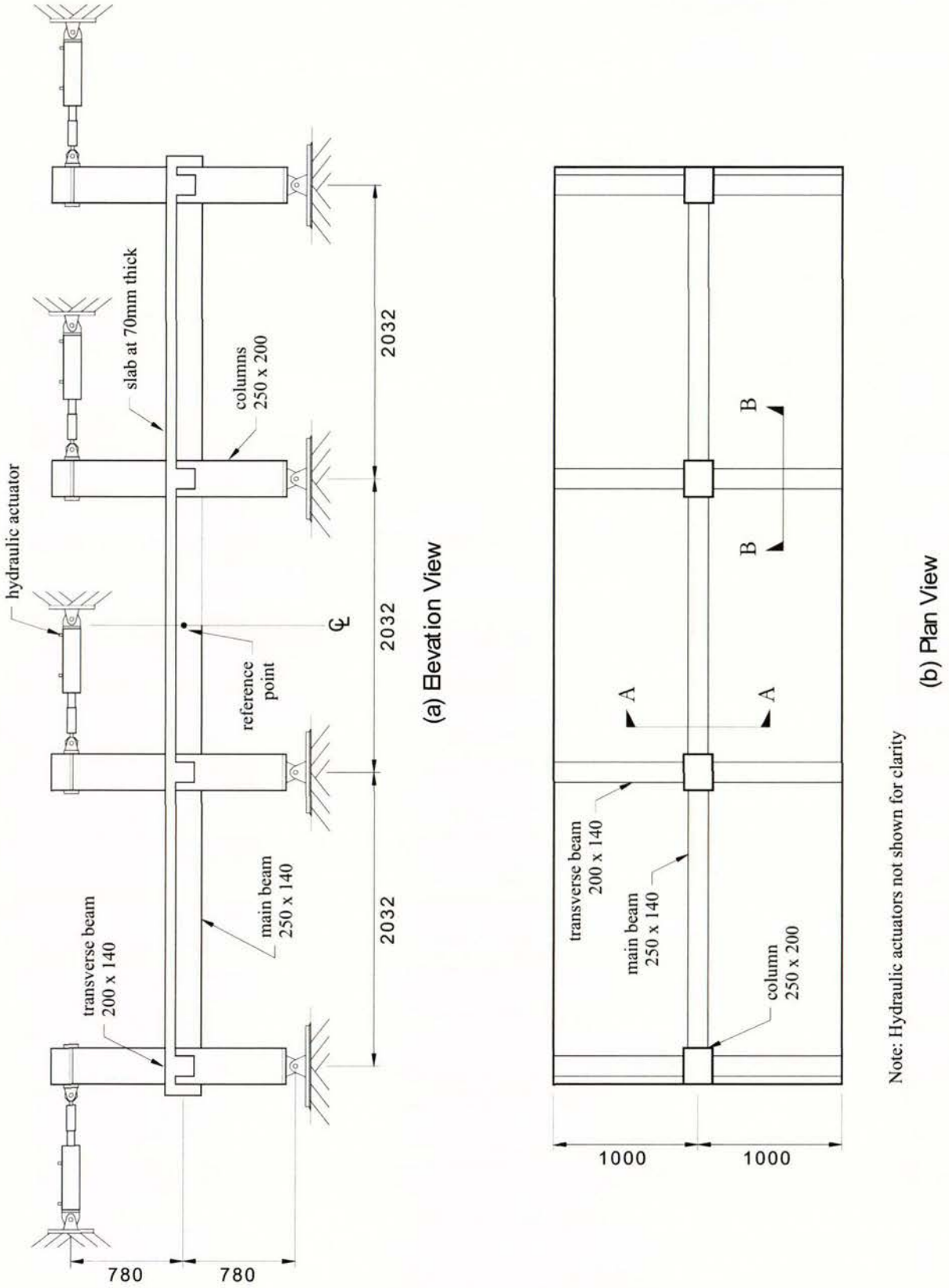

Figure 2.12: Two-bay reinforced concrete frame with floor slab [F2]. (continued)

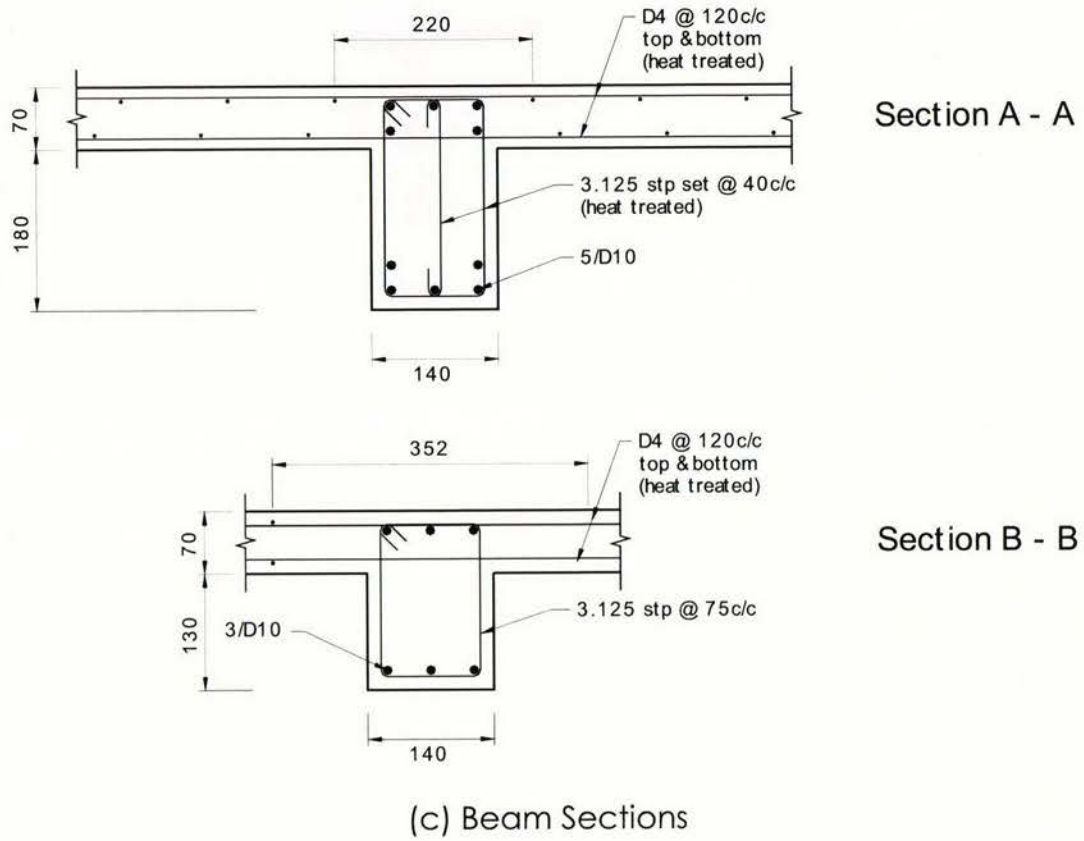

Figure 2.12: Two-bay reinforced concrete frame with floor slab [F2]. (concluded)

One way hinges were fixed to the column bases and lateral forces were applied by reversing pin ended hydraulic actuators fixed to the top of each column, as shown in the figure. During the tests, the lateral forces applied to each of the external columns were kept at half the value applied to each the internal columns. With this arrangement, the columns provided no restraint to the elongation of the beams.

In both units, diagonal shear cracks in the beam hinges were well defined at the end of the ductility 2 cycles. Spalling of cover concrete started during the cycles to ductility 4. Some crushing of web concrete was evident in the ductility 6 cycles.

The presence of the slab significantly increased the strength and stiffness of the unit. The load versus deflection diagram for both tests is presented in Figure 2.13. The ductility 1 displacement for the unit without the slab was 7.4mm while the corresponding value for the unit with the slab was 5.2mm. These lateral displacements corresponded to interstorey drifts of 0.95% and 0.67% respectively. For the unit

without the slab the maximum lateral strength was 124kN, which was recorded during the ductility 4 cycle (equivalent interstorey drift of 3.7%). For the unit with the slab, at 2% interstorey drift, the reinforcement within the full width of the slab had yielded.

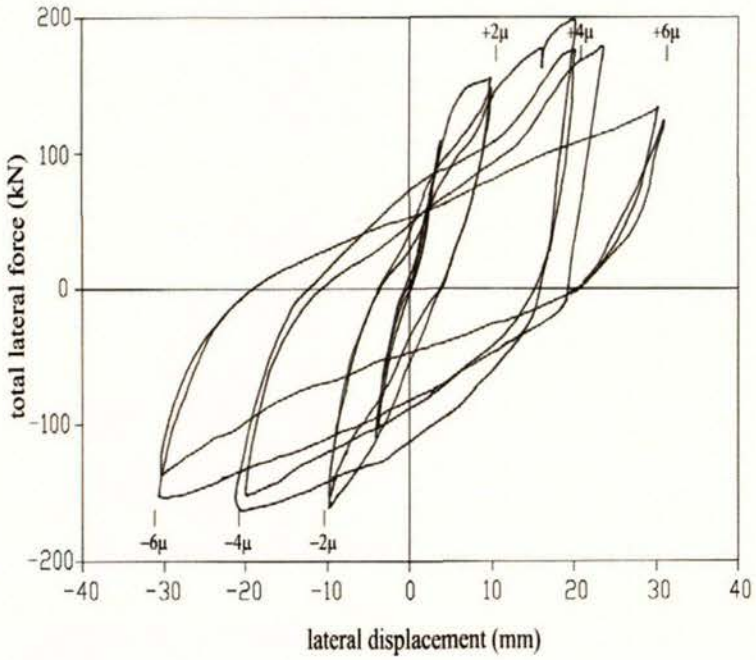

(a) With slab

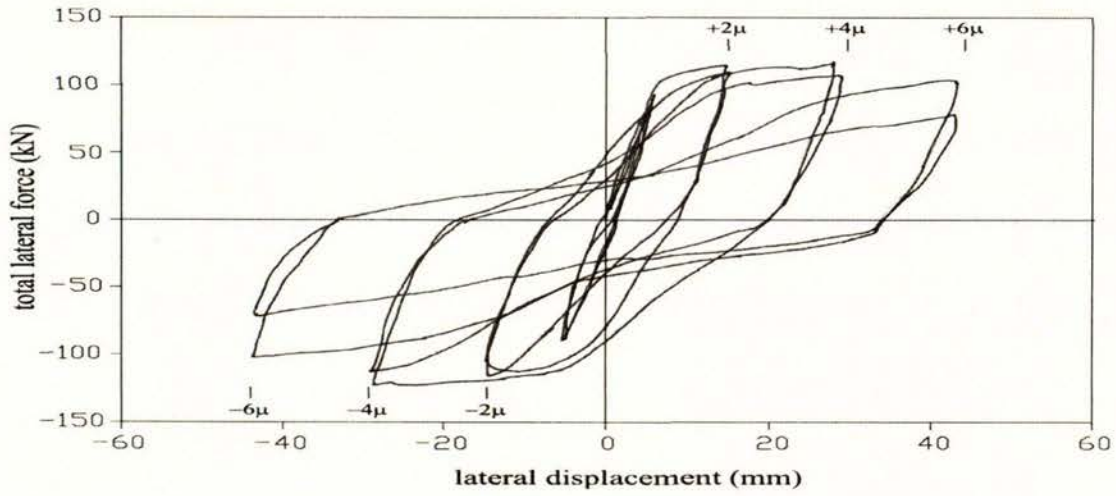

(b) Without slab

Figure 2.13: Load versus displacement response of reference point of three-bay bent [F2]. (figures size adjusted from original to match scales)

The maximum lateral strength of 196kN was reached during the ductility 4 cycles at an interstorey drift of 2.7%. The slab cantilevered out from the beam web by a clear 3.7 beam depths on each side. For comparison, the current New Zealand concrete design standard [S2] requires an equivalent width of 1.75 beam depths on each side of the web to be considered to contribute to the beam flexural strength in negative bending.

During the tests, it was evident that the plastic hinges adjacent to the exterior columns sustained more damage than the other plastic hinges. This was due to greater rotations that were forced onto these hinges as the elongation in the beams forced larger lateral displacement on the external columns relative to the internal columns. This is illustrated in Figure 2.14 and it was observed in both test units. However, this situation would not occur to the same extent in a multistorey building as the external columns are constrained by the beams in the higher levels.

For the unit without the slab, it was found that elongation amounted to a maximum of 35mm, which corresponded to an average elongation of 2.3% of beam depth per plastic hinge. At interstorey drift of 4%, the compression reinforcement in the plastic hinges started to buckle. This led to some reduction in the elongation of the beams. For the composite slab unit, elongation peaked at 28mm, or an average of 1.9% of beam depth per plastic hinge. The elongation versus interstorey drift is shown for both units in Figure 2.15. It can be seen that there is little difference between the units, indicating that the longitudinal slab had only a small influence on the magnitude of the elongation that developed.

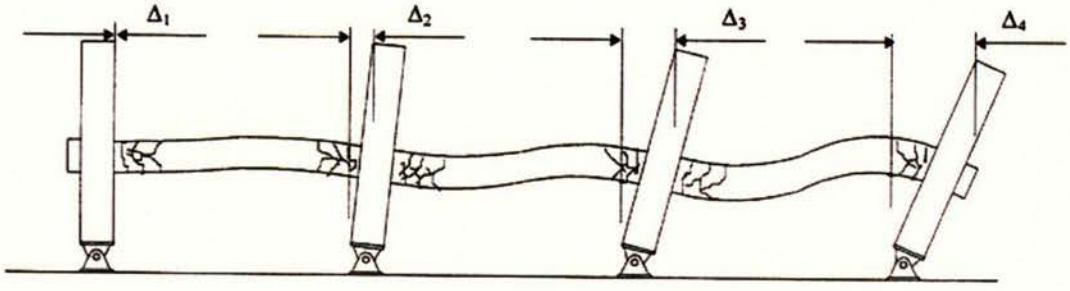

Figure 2.14: Differences in column lateral displacement [F2].

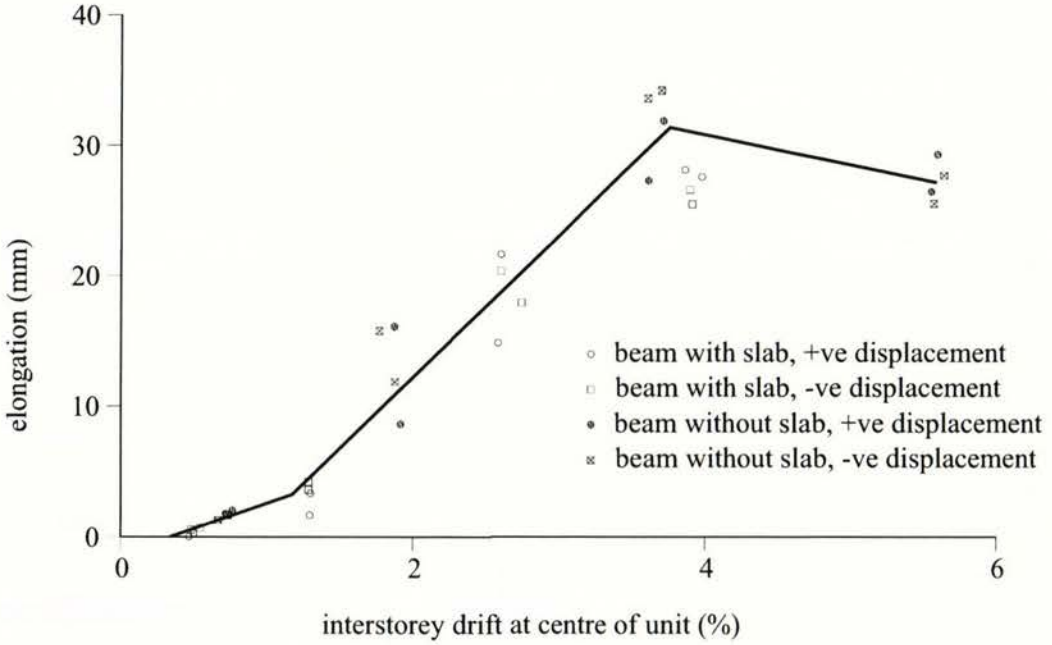

Figure 2.15: Comparison of elongation measurements from three-bay bents [F2].

2 ½-storey reinforced concrete frame

An approximately 1/3 scaled, 2 ½-storey three-bay reinforced concrete frame was built and tested by Fenwick *et al* [F11]. The unit was designed to a strength level that would correspond to a structure of about eight storeys. The reinforcement details were designed such that under cyclic loading, plastic hinges would be confined to the beams close to the column faces and to the columns close to the face of the foundation beam.

Lateral forces representing the storey seismic shear were introduced into the frame by pin-ended hydraulic actuators acting on each of the four columns, at a level equivalent to the mid-height of the third storey (as shown in Figure 2.16). The lateral forces were maintained throughout the test in a ratio of one to two for the external and internal columns respectively. With this arrangement, no artificial restraint to beam elongation was provided by the loading system.

The theoretical ultimate lateral strength of the frame was 192kN. The average displacement measured at 120kN was linearly extrapolated to obtain a ductility 1 displacement of 16.5mm, which corresponded to an interstorey drift of 0.63%.

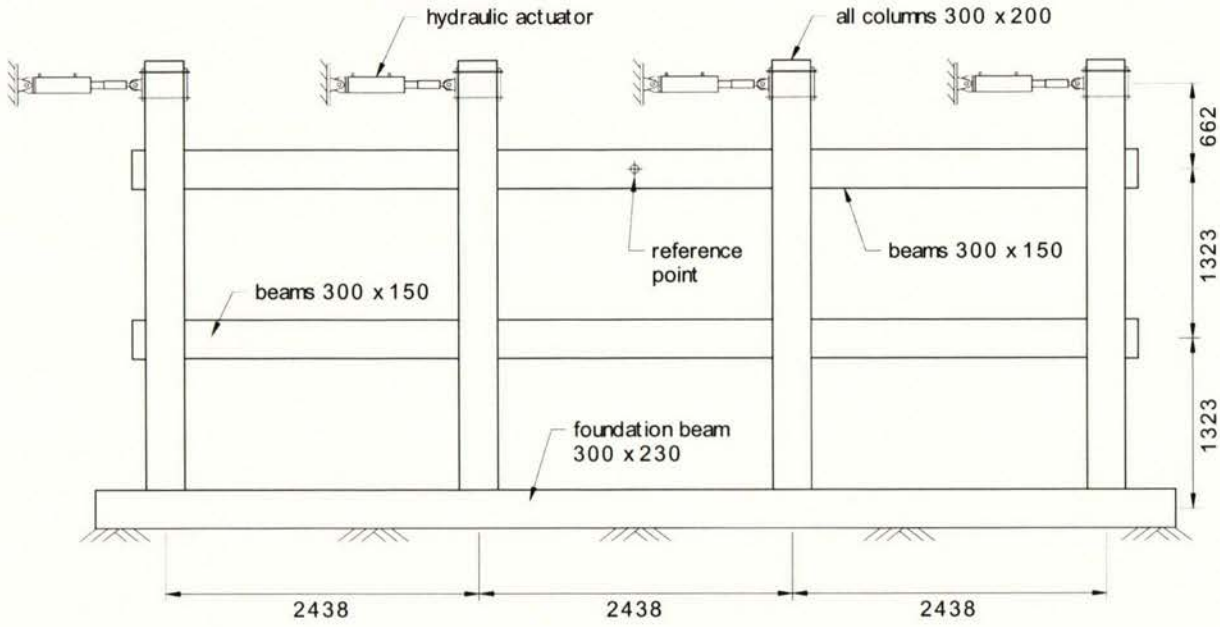

Figure 2.16: 2 ½ storey test frame by Fenwick *et al* [F11].

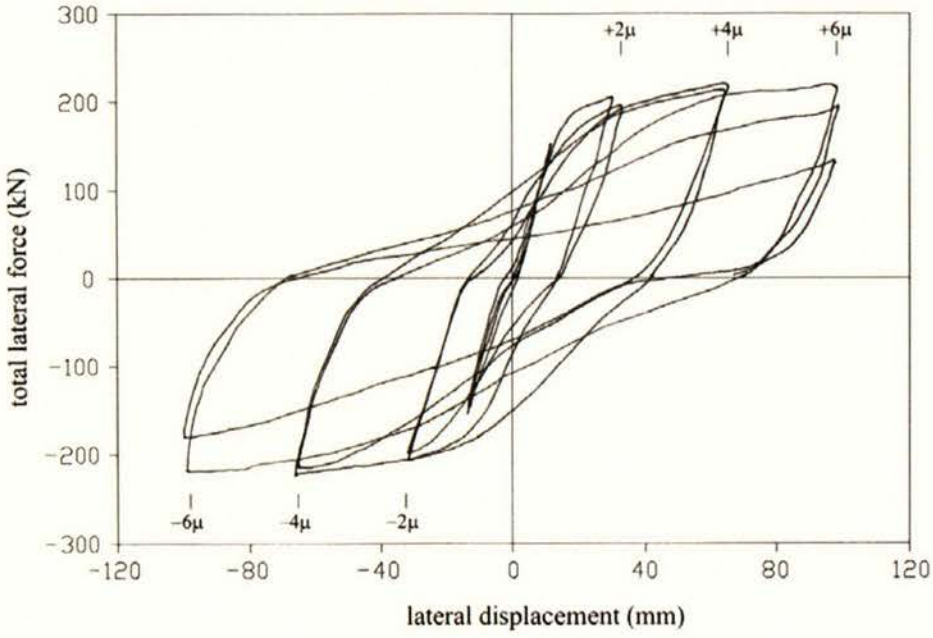

Figure 2.17: Load versus displacement response at reference point of 2 ½ storey frame [F11].

The lateral deflection of the reference point (as shown in Figure 2.16) is plotted against the total applied lateral force in Figure 2.17. It can be seen that stiffness degradation occurred in the ductility 2 cycles. This was due to shear deformation in the plastic hinge zones. With subsequent ductility 4 and 6 cycles, stiffness degradation continued

to increase with increasing shear deformation. Two complete cycles at ductility 6 were sustained with storey shears exceeding or reaching the calculated ultimate value. However, in the first half of the third ductility 6 cycle, the strength decreased to 71% of the theoretical ultimate value.

Plastic hinging in the beams was accompanied by significant elongation. This reached 53mm in the top line of beams and 45mm in the bottom beams (see Figure 2.19). These values correspond to an average elongation, which is in the range of 2.5 to 3.0% of beam depth for each plastic hinge. This elongation had a significant influence on the overall behaviour of the frame. As illustrated in Figure 2.18, the elongation of the lower beam forced the left hand side column outwards, increasing the shear sustained by it. In addition to this, axial tension was induced in the upper beams and axial compression in the lower beams. Axial tension in the upper beams led to an increase of shear deformation and concrete spalling in the associated plastic hinges, when compared to those in the lower level.

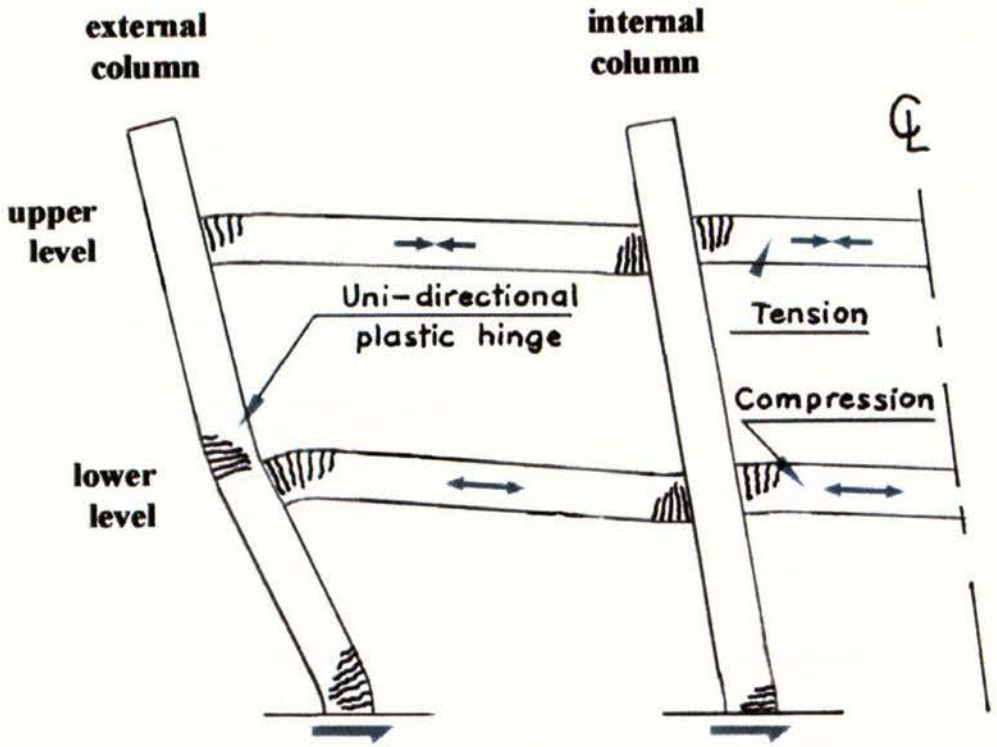

Figure 2.18: Deformed shape of 2 ½ storey test frame [F11].

The elongation in each level in the beams is shown in Figure 2.19. Beam elongation increased the rotation in the plastic hinges at the base of the external columns. This behaviour should to be considered when designing the shear and confinement reinforcement in the columns.

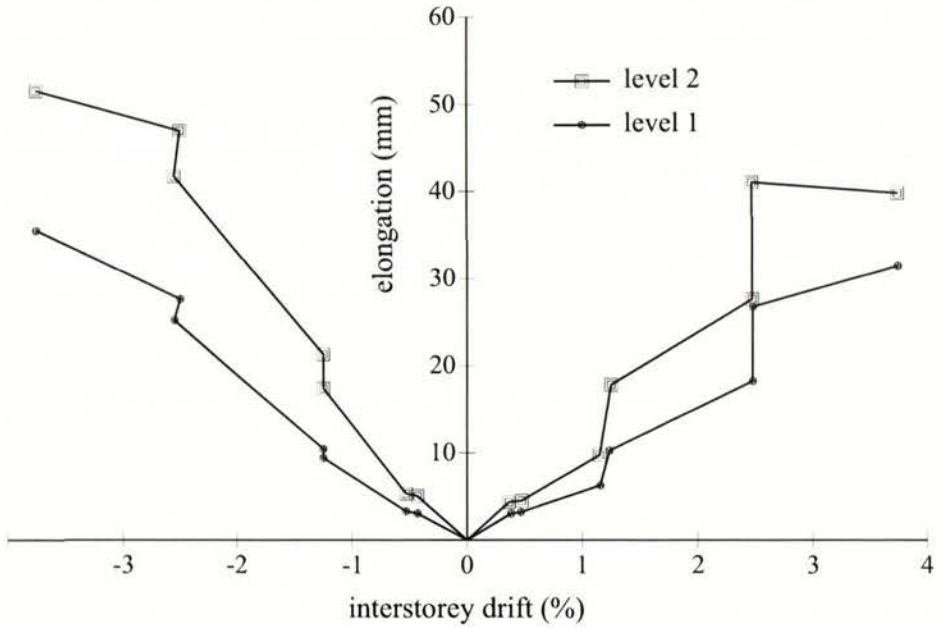

Figure 2.19: Elongation of beams in 2 ½ storey frame [F11].

2.3.2 University of Canterbury, New Zealand

Cheung recorded elongations between 2.5 to 4% of beam depth per plastic hinge in tests performed on beam-column with insitu slab units [C1]. Cheung *et al* [C2], postulated that beam elongation in the presence of a composite slab would cause the beam to go into compression, and act as a strut to resist the tension force sustained by the longitudinal (mesh) reinforcement in the slab. This strut and tie mechanism is shown in Figure 2.20. As indicated in the diagrams, the mechanism around the interior columns is dependant on the magnitude of the tension force sustained by the longitudinal reinforcement in the slab. The mechanism around the exterior columns relies on the anchorage of the slab reinforcement in the exterior transverse beams. In both cases, the strength of the beams was enhanced due to the introduction of the compression forces into the beams.

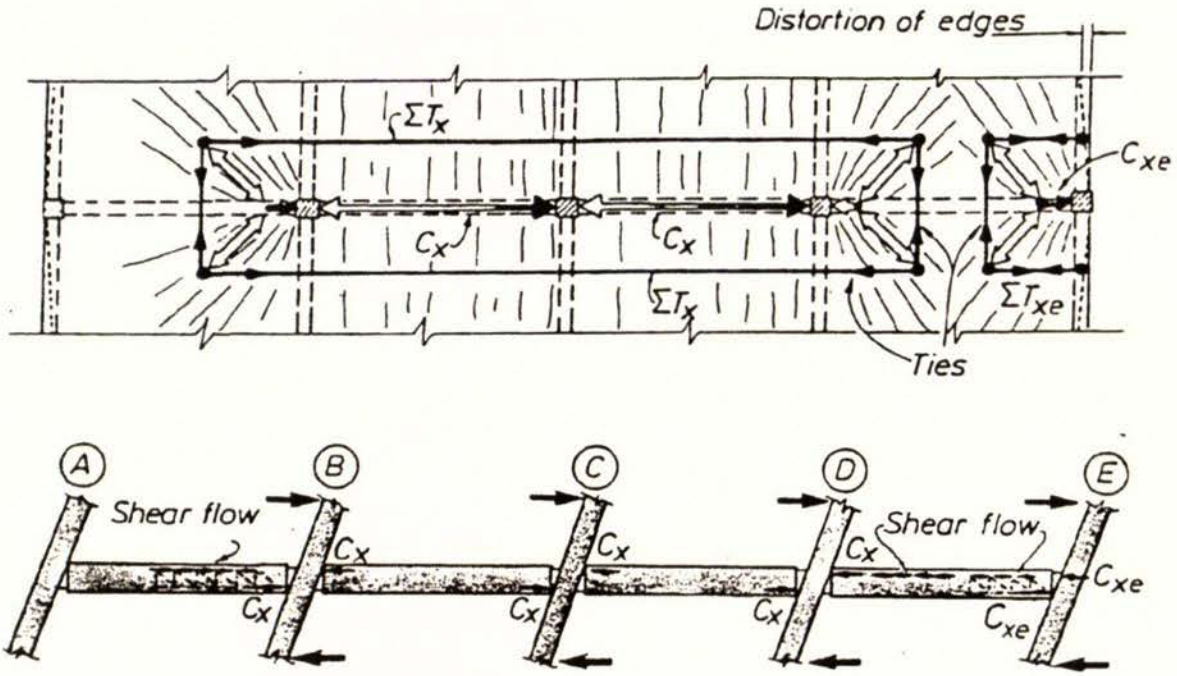

Figure 2.20: Strut and tie mechanism in floor slab [C2].

Restrepo tested a number of beam-column subassemblies and noted that elongation occurred when inelastic displacements were applied [R1]. He measured elongations between 2.1 to 2.8% of beam depth on various types of precast concrete beam-column units. From his and other tests, he concluded that the elongation in the test units containing two plastic hinges lay between θ (*d-d'*) and twice this value, where θ is the rotation sustained by the plastic hinges. The expression θ (*d-d'*) was proposed by Megget and Fenwick for the prediction of elongation in uni-directional plastic hinges [M1].

2.3.3 United States of America

Beam elongation was reported by Zerbe and Durrani, who carried out tests on beam-column connections and two-bay beam-column subassemblies with and without slabs [Z1, Z2]. The lateral loads were applied to a stiff loading beam, which was connected to the tops of the columns. The columns were pinned at their bases to a rigid support, as illustrated in Figure 2.21. The authors compared the elongation in the two-bay frame with tests performed on one internal and two external statically determinate beam-column units. The elongation measured on the beam-column units were summed for comparison with the total elongation in the frame unit. It was found that the total

elongation at 4.0% interstorey drift was 9.5mm for the frame unit, and 15.0mm for the beam-column units. These values correspond to 0.8 and 1.2% of beam depth per plastic hinge for the frame unit and the beam-column units respectively.

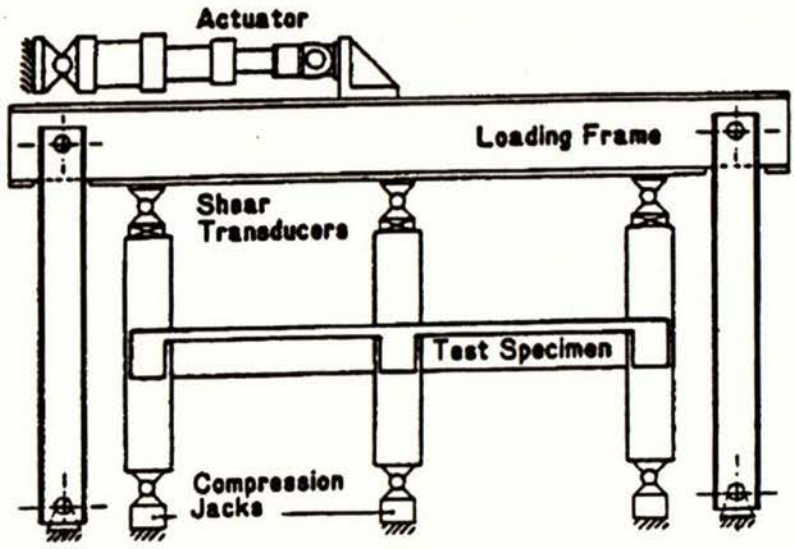

Figure 2.21: Test arrangement of two-bay frame with floor slab [Z2].

The authors suggested that the difference in the elongation measured was due to the flexural stiffness of the columns, which resulted in axial compression in the beams, therefore restraining the elongation in the beams of the frame unit. Significant cracking of the outer faces of the external columns supported this suggestion. However, it appeared that it was the loading system that restrained the elongation since the tops of the columns were fixed in position relative to each other. The authors later commented that at large drift levels, the main beams could be restrained against axial elongation and that the testing arrangement more accurately represents the first storey in a multi-storey building. However, as shown by Figure 2.18, this may not be totally correct, where the test showed that the columns above the first level were forced outwards as the beams in the lower level elongated.

Qi and Pantazopoulou tested a 1/4 scaled two-bay beam-column subassembly with an insitu slab, as shown in Figure 2.22 [Q1]. The frame was built to represent the first one and a half storey of an internal frame. The researchers attempted to avoid introducing unrealistic restraint to elongation in the beams by controlling MTS actuators such that

the relative displacement at the ends of each actuator was set equal to the measured elongation within the respective span.

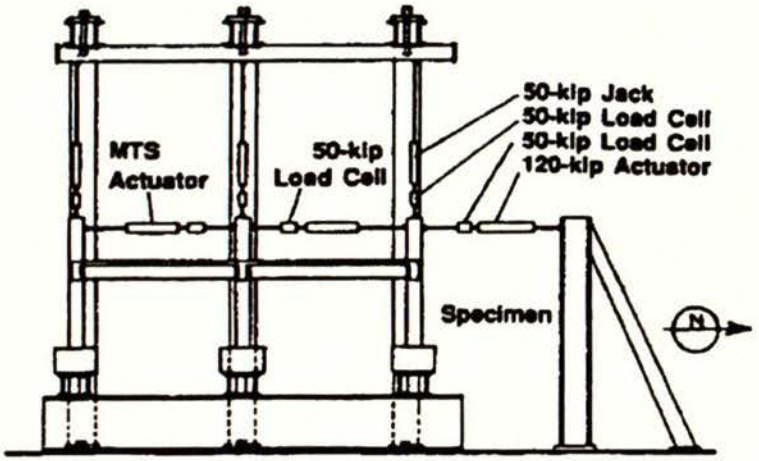

Figure 2.22: Test arrangement of two-bay frame with floor slab [Q1].

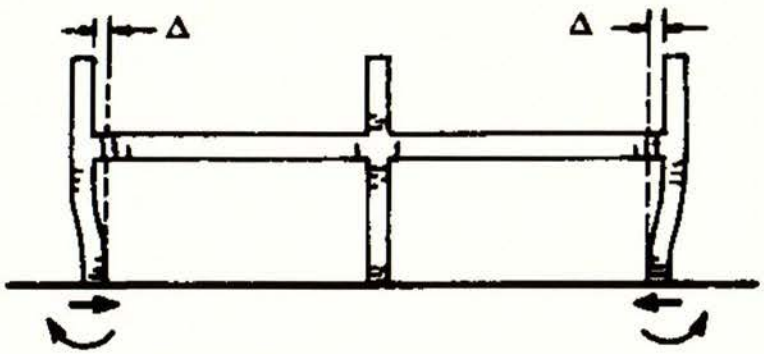

Figure 2.23: Effect of elongation in the beams in the level [Q1].

Throughout the test, they noted that the distribution of the base shear at the foundation was affected by the direction of loading. They attributed this alternating pattern of base shear distribution to a combination of overturning moments created by the application of lateral loads and residual beam deformations. The residual beam deformations, which resulted from inelastic strains in the reinforcement, cracking of the concrete and bond deterioration, accumulated to produce an overall expansion in the beams as shown in Figure 2.23. The elongation of the beams averaged 1.6% of the beam depth for each plastic hinge in the later loading cycles. This action introduced additional flexural moments and shear forces in the columns. The additional shear in the columns induced axial compression forces in the beams.

2.3.4 Japan

Hinge elongation was observed during the testing of a full scale seven-storey wall-frame building built on a large strong floor. This work was carried out as part of the U.S.-Japan Cooperative Earthquake Engineering Program [W1]. Substantial elongation was found in the wall due to the formation of a plastic hinge at its base. This resulted in axial tension forces being induced in the surrounding columns and axial compression being induced in the wall. This greatly increased the lateral strength above that predicted by standard methods of analysis. In practice it is unlikely that this level of strength enhancement would be obtained, as the additional axial compression force in the wall would, in all probability, have caused the foundations to fail.

Sakata and Wada tested 1/20 scaled concrete frame models to study the effects of deformation in multiple bay, medium height frame structures [S6]. Because of the small size of the models, they were able to devise a system of applying independent lateral loads to the columns of the test models without introducing additional restraint to the elongation of the beams. They showed that elongation could be expected to be larger in the higher levels when compared to the lower levels of the structure.

2.4 Stability of Precast Flooring Elements

Elongation of the beam plastic hinges may cause loss of seating for precast floor units. The situation is particularly severe for perimeter frame structures where the elongation from the plastic hinges in several beams can be applied to one span of precast units. The effect that this has on the connections of precast elements with cast in place topping and supporting beam has been investigated by Mejia-McMaster and Park, who tested three different connections between the ends of precast, pretensioned concrete hollowcore units [M3]. The first part of the test involved the downward loading on the floor unit, which had been constructed without bearing on the supporting beam. This was carried out to investigate the shear friction capacity provided by the topping slab. The second part involved application of horizontal load until seating was lost, followed by vertical loading to investigate the vertical reaction provided by the kinking action of tie bars.

From this study, the authors recommended that special reinforcement should be used at the end supports of hollowcore floor units to prevent collapse in the event of inadequate seating lengths for imposed movements in an earthquake. Proper design of tie bars, by shear friction could be implemented in the event of loss of support without horizontal movement, or by kinking effect of bar if horizontal movement occurred. It was also concluded that straight lengths of tie bars with hooks should be placed within the units, as shown in Figure 2.24(a). The bars should be plain, rather than deformed, in order to allow yielding to propagate along the bar, therefore allowing for large plastic elongation. Figure 2.24(b) shows an alternative detail, which has a diagonal tie bar compared to the straight tie bar shown in Figure 2.24(a). However, this is a less desirable detail, as kinking of the tie bar may be accompanied by cracking of the floor unit along the diagonal tie bar.

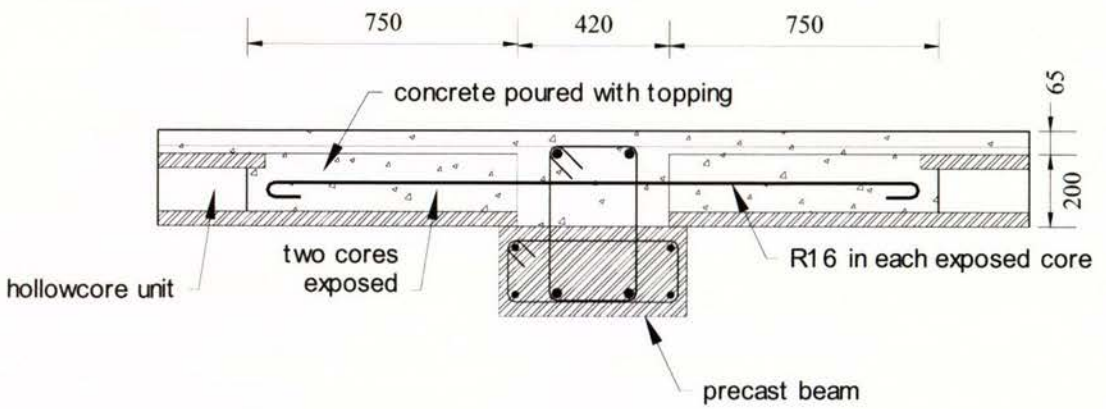

(a) Connection 'Type 1'

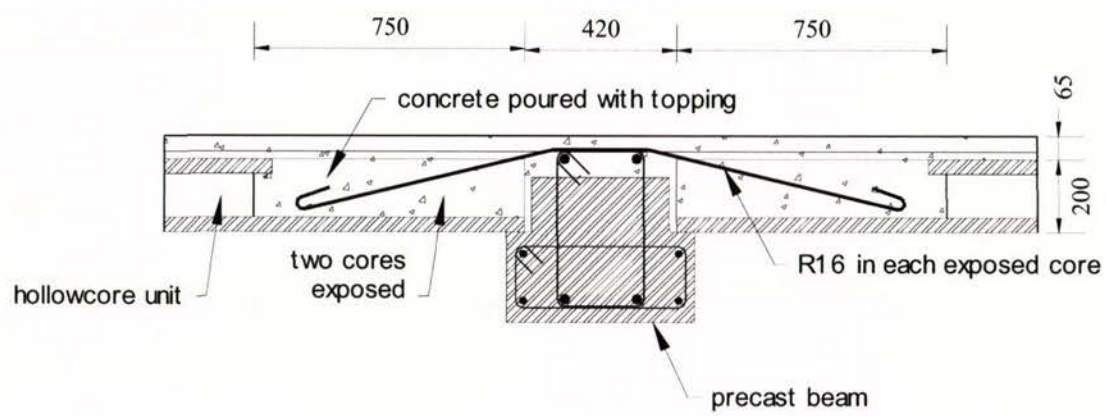

(b) Connection 'Type 3'

Figure 2.24: Recommended connections tested by Mejia-McMaster & Park [M3].

Three further tests on different connections at the ends of hollowcore units were carried out by Oliver *et al* [O1]. The first of these was the traditional detail of deformed starter bars going into cast-in place topping slab with additional steel fibres. This unit behaved unsatisfactorily and it fell when the seating was lost. The second and third units were detailed with additional plain bar 'paperclip' ties (see Figure 2.25(a)), with the difference being steel fibres added to cast-in-place topping in unit three. Units 2 and 3 failed with fracture of the 'paperclip' legs at corresponding interstorey drift of 1.4% and 2.1% respectively.

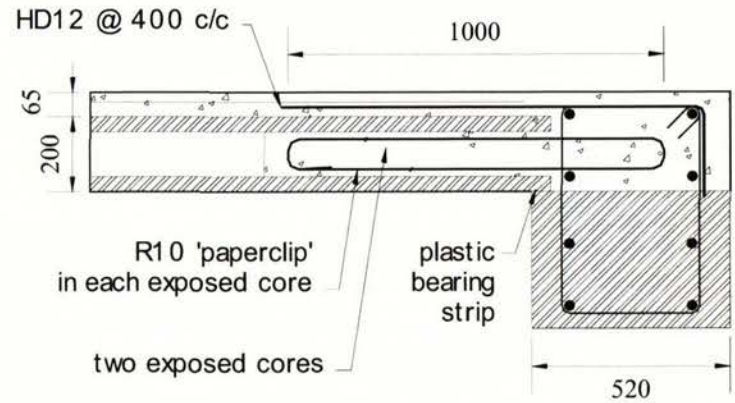

(a) 'Paperclip' connection

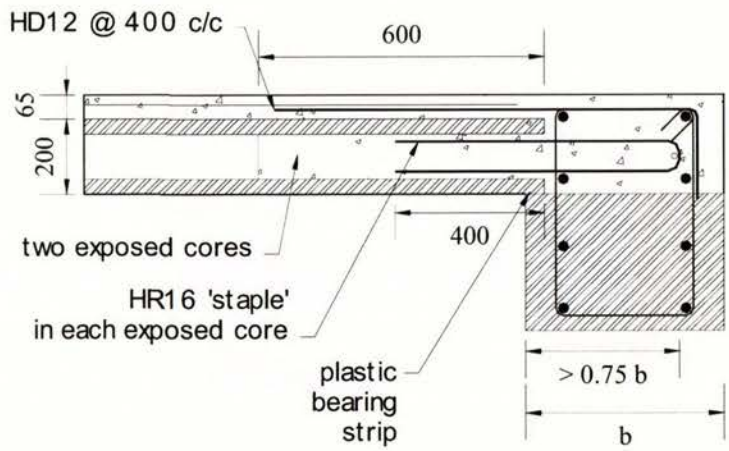

(b) 'Staple' connection

Figure 2.25: Hollowcore floor connection details tested by Oliver *et al* [O1].

It was concluded that this detail might be suited for buildings with structural walls or where precast floors span individual bays in the frame, but not in situations where large deformation demands are expected, when precast floors span multiple bays in the

perimeter frame. It was also found that deformed bars traditionally placed in topping slabs to transfer seismic forces in the diaphragm may not have sufficient deformation capacity to resist the effects of beam elongation.

The authors recommended a 'staple' connection detail shown in Figure 2.25(b). This detail utilises flexural strength of plain 16mm bars to resist gravity loads when unseating occurs. The de-bonding of the plain bars within the cores should prevent significant axial strains from occurring, therefore allowing large horizontal displacements without the loss of support. A number of acceptable support arrangements of precast flooring are also shown by a publication titled '*Guidelines for use of Structural Precast Concrete in Buildings*' [N2].

2.5 Effective Slab Width for Calculation of Beam Flexural Strength

The contribution of the strength of a slab in tension to the performance of reinforced concrete beams in frames has been examined in several projects. A number of researchers have proposed that the contribution of a slab can be assessed from the longitudinal reinforcement confined in a specified effective width for the calculation of beam flexural strength. It should be noted that the discussion below apply to cast insitu slabs, and not to necessarily to composite insitu slabs with precast elements (see later).

For beams at internal columns, Zerbe and Durrani [Z2] recommended including the width of the slab equal to two beam depths on each side of the beam for the calculation of the negative flexural capacity of the beams. For external columns they recommended that the width should be reduced to one beam depth on each side of beam if the torsional moment induced in the transverse beams by tension forces in the slab reinforcement (based on two beam depths on each side) exceeds the torsional strength of the transverse beam.

Pantazopoulou *et al* [P9], developed an analytical model to estimate the effective slab width and proposed an effective width of 1.5 beam depths from the beam face on each side of the beam should be considered for assessing the strength at first yield, and

increasing this to three beam depths on each side for large drift levels. The same values applied for both internal and external joints.

Qi and Pantazopoulou [Q1] found that for exterior connections, the computed flexural strength with an effective slab width of one beam depth on each side of the beam compared well with the estimated strength from experimental data. This was calculated by taking into account the torsional strength of the transverse beam at the exterior supports. For interior connections, the estimated effective beam depth at 2.0% interstorey drift was one beam depth on each side, and at 5.8% it was estimated to be 2.5 beam depths on each side.

The practical implications of amendments in the ACI 318-99 [A3] that include the estimation of nominal beam flexural capacity in seismic design of frame connections were reviewed by Pantazopoulou and French [P10]. ACI 318-99 calls for an effective width of slab reinforcement to be included for calculation of nominal flexural strength of beams under negative (hogging) bending for seismic response. The recommendation is that the effective width of slab on each side of the beam should be the lesser of:

$L/4$ or $b_w + 16\, t_s$ or centre to centre spacing of beams.

where L is the span of the beam
b_w is the width of beam web
t_s is the thickness of slab.

These values of effective slab participation were obtained from experimental results for tests and correspond to a lateral drift of 2% [P10]. As the effect of slab participation is greatly influenced by the structural drift, greater widths of slab might be effective at larger drifts.

In this paper the authors reviewed 15 years of previous related research from the United States, Canada, New Zealand and Japan. Pantazopoulou and French recommended that designers should consider the effects of slab participation on structural strength and stiffness, overall structure shear demand and capacity, beam shear demand, bar cut-offs and joint confinement.

On the basis of test results, Cheung *et al* [C2] recommended that the effective slab width for the estimating of the negative flexural strength of beams should be taken as the lesser of:

- 1/4 of the span of the beam, extending each side from the centre of the beam section;
- 1/2 of the span of the slab, transverse to the beam under consideration, extending each side from the centre of the beam section;
- Where the beam frames into an exterior column, 1/4 of the span of the transverse edge beam, extending each side from the centre of the beam section;
- Where the beam frames into an exterior column but no transverse beam is present, 1/2 the column width extending each side from the centre of the beam section.

These recommendations were adopted in the 1995 New Zealand concrete structures standard [S2].

McBride *et al* [M2], tested a three-bay beam-column-floor unit (see Figure 2.12), and found that before yielding, the effective slab width was 1.4 beam depths on each side of the beam. At an interstorey drift beyond 2.0%, it was found that nearly the full slab width, which corresponded to 3.7 beam depths on each side of the beam, was effective for beam strength calculations. The authors suggested that the provisions in the 1995 New Zealand concrete code [S2], which gives a value of one quarter of the beam span between internal columns, should be revised to prevent significant underestimates of beam over-strengths.

2.6 Strength Enhancement from Precast-Prestressed Flooring

It is important to assess the likely strength enhancement of the beams due to the restraining forces from floor diaphragms. An underestimate of this strength

enhancement can lead to non-ductile failure modes, such as shear failure in beams or forcing plastic hinges into columns, leading to a possible column-sway failure mode.

Fenwick *et al* in an analytical study consider a case where the elongation in the beams may be restrained by precast pretensioned units built into the floor [F12]. This is shown in Figure 2.26(a), where the precast units span more than one bay of the moment resisting frame. This situation is common in perimeter frame buildings. A number of outcomes are possible due to the interaction of the pretensioned units and the perimeter beams. Firstly, the restraint provided may induce high shear forces at the interface with the beam as illustrated in Figure 2.26(b). This might lead to a complete shear failure at this interface, or alternatively it could lead to a significant increase of the negative moment flexural strength in the beam.

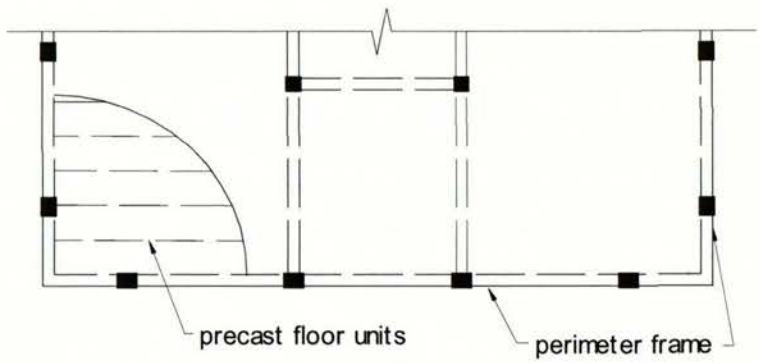

(a) Plan of perimeter frame and diaphragm

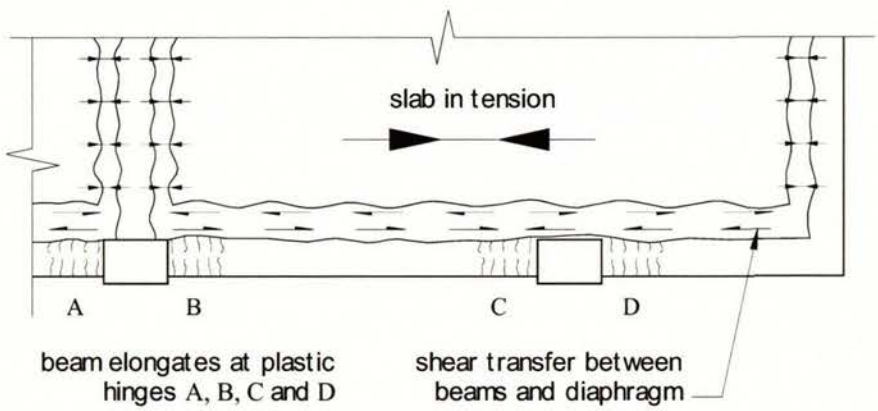

(b) Shear forces at interface between beams and diaphragm

Figure 2.26: Interaction of beams and diaphragm due to elongation in beams [F12]. (continued)

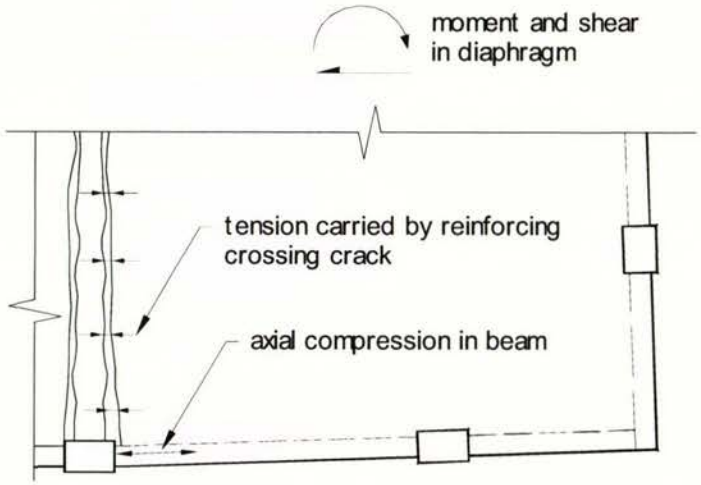

(c) Portion of floor acting as deep beam

Figure 2.26: Interaction of beams and diaphragm due to elongation in beams [F12]. (concluded)

The authors estimated that the potential flexural over-strength of plastic hinge C for the specific detail examined was 2.3 times the value that would normally be calculated if these actions were ignored [F12].

A further source of strength enhancement of beams due to diaphragm restraint to elongation of beams needs to be considered. Elongation of perimeter frame beams could generate wide cracks in the topping concrete on either side of the transverse beam. This situation is shown in Figure 2.26(c). Forces are transferred across these cracks by reinforcement in the insitu concrete. It can be seen that the floor is acting as a deep beam, with bending moment and shear forces being sustained. These actions together with the force transmitted across the cracks apply an axial force to the beams in the frame, which could increase in flexural strength in negative bending substantially. For the case examined, the estimated strength increase was 1.8 times the value that would be obtained ignoring the interaction with the floor slab [F12].

2.7 Preliminary Results from Testing of a Precast Hollowcore Floor Slab Subassembly

The structural interactions between reinforced concrete perimeter frames and commonly used precast, prestressed floor systems in modern buildings were investigated in a

collaborative effort between Universities of Auckland and Canterbury. At both universities, the main aims were to examine the effects that the elongation of beams had on structural integrity (e.g. seating lengths of floor units) and on strength enhancement of beams in negative bending.

A full scale subassembly was constructed and tested at the University of Canterbury [M4]. It consisted of a two-bay reinforced concrete frame with a single span on each end in the transverse direction. The floor system consisted of 300mm deep hollowcore units with 75mm cast insitu topping. The test setup is shown in Figure 2.27. A complex test rig was set up such that shear forces were applied at the top and bottom of the columns, while the drift angle between each column was kept the same. The displacements applied by the test rig were controlled such that elongation of the beams were neither promoted nor restrained.

Signs of distress to the seating detail were noticed at a relatively early stage of interstorey drift at 0.35%. At 1.9% drift, a significant tear developed in the floor along the joint between the first and second floor unit (see Figure 2.27). This was due to the elongation of the beams, which caused the central column to move outwards (orthogonal to direction of loading), taking the first hollowcore floor unit with it.

By the end of 2.0% drift in the reverse direction, the entire seating had been damaged with some of the units dropping by 10mm. Splitting of the web in the first hollowcore unit was also observed. At this stage the central column had moved outwards by 25mm. The structure was displaced up to 2.5% interstorey drift. The authors reasoned that in an actual building, the separation of the column and the floor unit closest to the perimeter frame from the rest of the floor could occur on several floors, and it is possible that columns would fail by buckling as the lack in effective restraint would increase their effective lengths, hence reducing axial load capacities.

The loading rigs were then moved to the outer frames and the structure was displaced in the transverse direction. The structure was subsequently displaced in steps, and eventually up to 3.5% interstorey drift in this direction. Splitting of the webs in the first hollowcore unit was extensive, and the floor had dropped by 60mm at this stage. The

loading rigs were then transferred again to the main frame and the unit was displaced up to 2.0% interstorey drift. At this stage, the entire bottom section of the first hollowcore unit dropped. At reversal of displacements to 2.5% interstorey drift, the entire floor failed when design live loads were applied. Even though the floor failed, the perimeter frame beams, columns and beam-column joints were relatively undamaged.

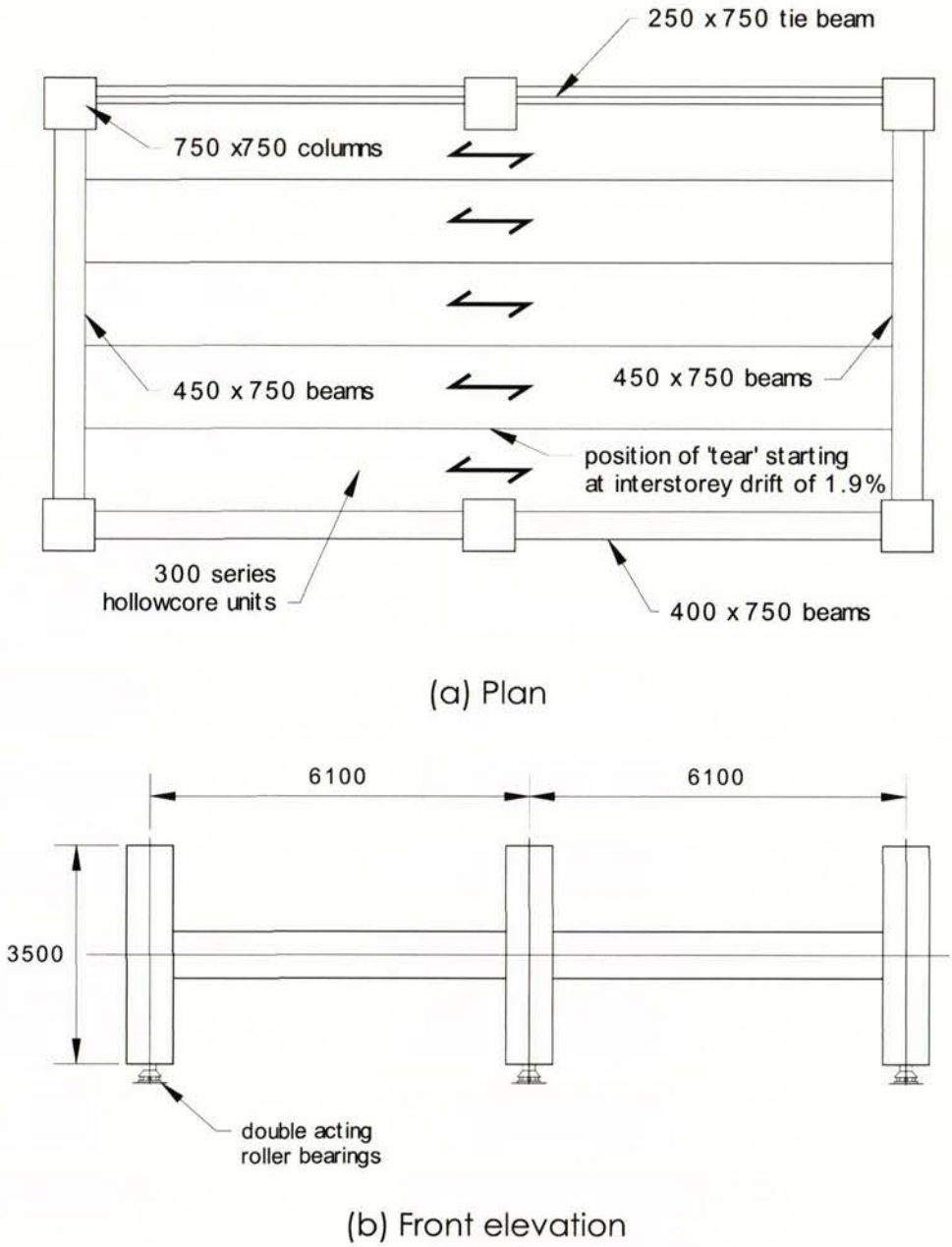

Figure 2.27: Basic test setup of frame-floor slab subassembly [M4]. (continued)

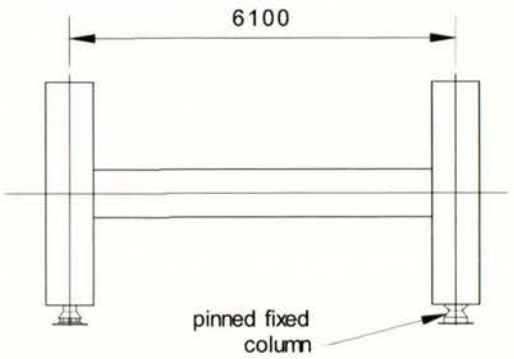

(c) Side elevation

Figure 2.27: Basic test setup of frame-floor slab subassembly [M4]. (concluded)

One of the major observations from this work was the way in which the seating of the hollowcore units failed [M6]. Instead of sliding relative to the beam, there was enough bond or friction to cause the unit to fracture at the ends of the units (see Figure 2.28).

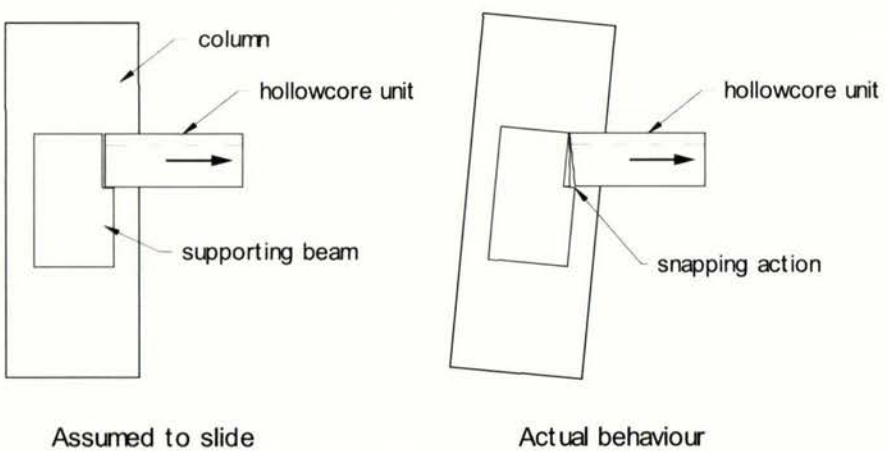

Figure 2.28: Behaviour of hollowcore to supporting beam [M6].

A technical advisory group [T1] was formed to discuss these results and recommended details were made and tested. These recommendations have been incorporated in a recent amendment to the New Zealand Concrete Structures Standard [S7]. The first recommended detail (see Figure 2.29(a)) requires a compressible backing material between the end of the floor unit and the beam, with a low friction bearing strip. This detail allows the end of the floor unit to slide and the beam to rotate relative to the floor unit without causing a fracture to the end of the floor unit. The second detail (see Figure 2.29(b)) require plain round bars placed at the bottoms of the filled cells of the

hollowcore units. However for both details, care is needed in placing reinforcing steel in the topping crossing the hollowcore unit and the supporting beam as very high strains could be induced at this section due to elongation and rotation. The tie forces resulting from this could induce flexural and axial tension failure or shear failure of the hollowcore unit (see later).

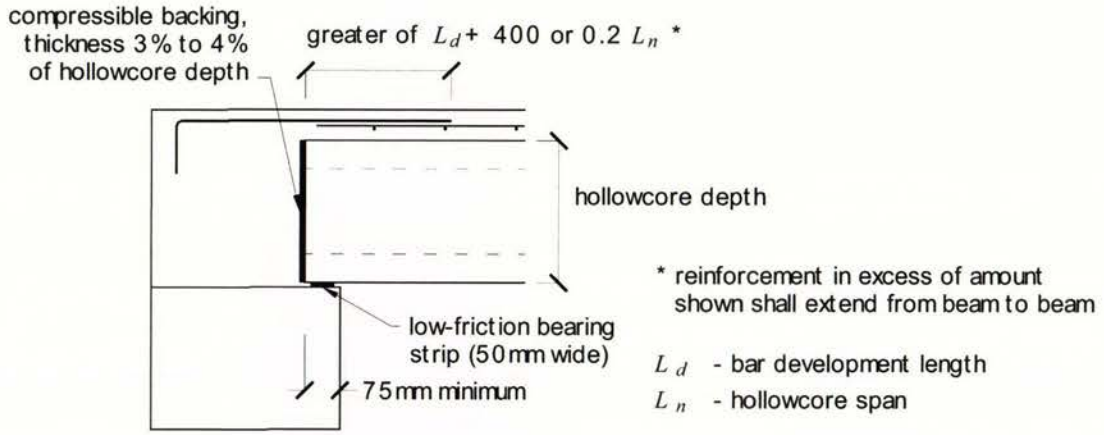

(a) Hollowcore with compressible backing on low-friction bearing strip

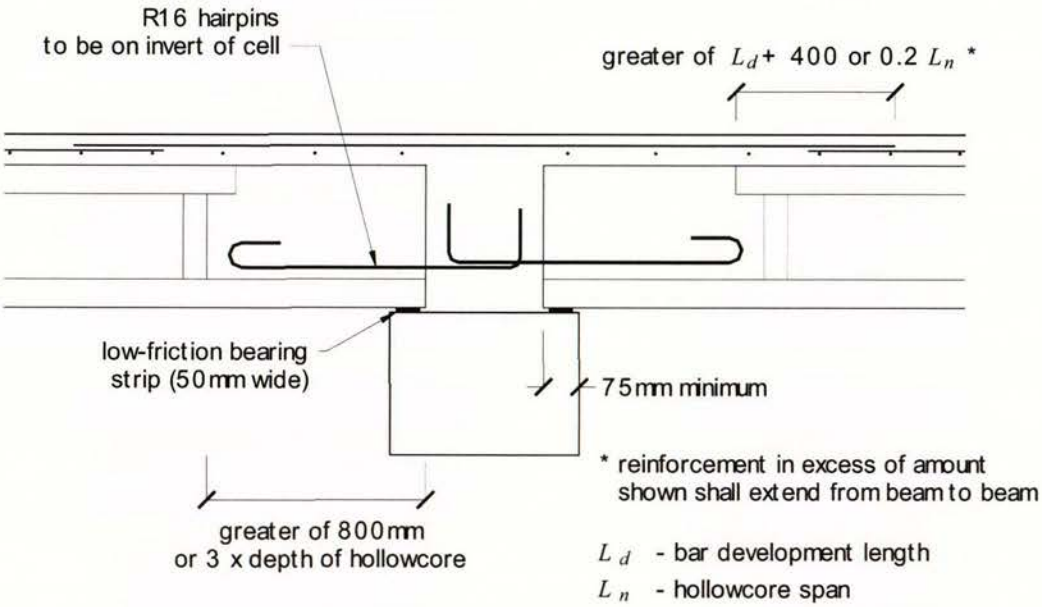

(b) Hollowcore with 2 – 2 leg R6 hairpins on low-friction bearing strip

Figure 2.29: Hollowcore seating detail in amendment to New Zealand Concrete Structures Standard [S7].

The performance of the first hollowcore unit adjacent to the frame was also emphasised. In particular the relative vertical displacement between the frame beam and the floor slab caused the hollowcore unit to fail by the splitting of the webs in the hollowcore unit. It was proposed that the first hollowcore unit should be placed at some distance away from the perimeter beam with a cast insitu slab (or linking slab) in between, as shown by Figure 2.30, allowing a more flexible interface between the two elements. A detail similar to this was also incorporated in the recent amendment to the New Zealand Standard [S7].

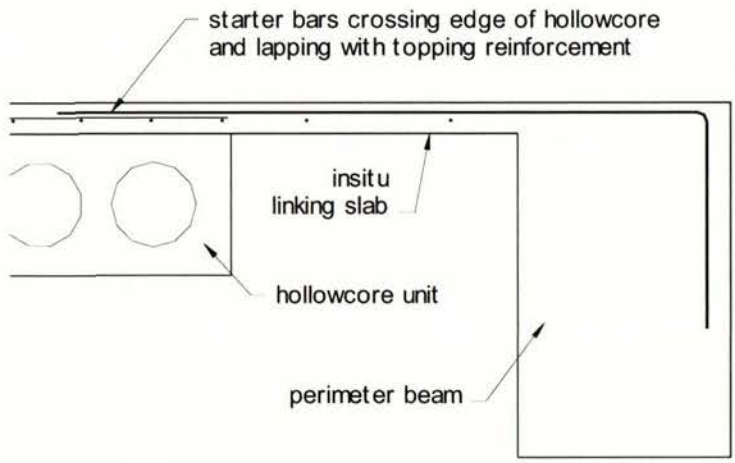

Figure 2.30: Hollowcore unit parallel to perimeter beam [S7].

The problem of the relative vertical displacement was also pointed out by Fenwick *et al* [F12]. In their experiment, the floor unit performed more favourably (no brittle failure of floor unit) due to a flexible insitu slab between the perimeter frame and the first precast floor unit.

Due to the tear formed between the floor and the column, Matthews *et al* also proposed that tie reinforcement between the floor diaphragm and the column should be placed transverse to the perimeter frame (see Figure 2.31(b)). The New Zealand Concrete Structures Standard specified that the bars should be placed at 45° to the beams (see Figure 2.31(a)), but Matthews commented that this could contribute to the perimeter beam over-strength actions. The recommended detail by the standard showed a transverse beam which can help in tying back the column. However, no clear provision was given for an intermediate column placed between floor spans.

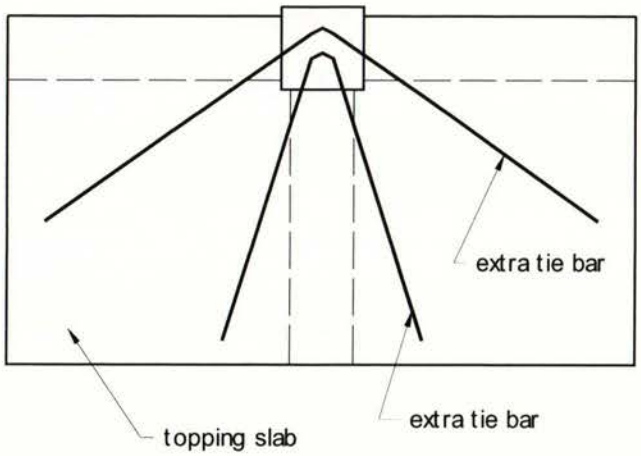

(a) Detail recommended by New Zealand Standard [S4].

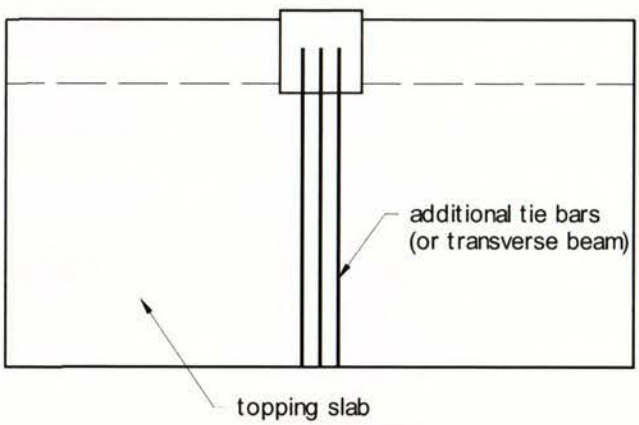

(b) Detail recommended by Matthews [M6].

Figure 2.31: Details for tie-back of perimeter column.

Fenwick *et al* conducted an analytical study into the different actions that may arise in hollowcore floor diaphragms [F14]. The authors looked at the problems associated with the seating of hollowcore units, such as that listed below:

- unreinforced concrete core in hollowcore units due to placement of dam 75mm from the end of the unit (had been until recently standard practice),
- reinforced cores and insitu topping, similar to that shown in Figure 2.24 & Figure 2.25,
- details recently incorporated in the amendments to the New Zealand Structures Standard, shown by Figures 2.29.

From their analysis, elongation and rotation of supporting beams relative to the floor unit can induce significant tension force in the topping reinforcement connecting the floor unit and the supporting beam. It was shown the force resulting from this, in combination with gravity loading and vertical seismic forces (high seismic zone for example Wellington), the floor units could fail in negative bending unless the topping is reinforced with passive reinforcement or prestressing strands near the top of the unit. An analysis of the shear stresses that could develop in the webs of the hollowcore units also indicated there is significant danger of diagonal tension failure in the units.

In addition to the above, the authors looked at the vertical differential displacement between the hollowcore units and the perimeter frame parallel to the units. They commented that three possible failure modes could result even with the recommended detail shown by Figure 2.30:

- Failure of the linking slab due to combined longitudinal shear, vertical shear and flexure.

- The longitudinal shear in the linking slab induces axial tension and negative moments to the hollowcore unit adjacent to it, and if the magnitude of the forces are large enough, the hollowcore unit could fail by breaking at the top.

- The vertical shear and bending moments transmitted by the linking slab induce torsion in the hollowcore unit and tension in the nearest web, which could result in splitting along the web.

The interaction of hollowcore units and beams transverse to the units (supporting beam) were also considered by Fenwick *et al* [F14]. Due to rotation of the plastic hinges in the beams (750mm deep beam), it was suggested that the vertical deflection over the width of a typical 300mm deep hollowcore unit (1200mm wide) could be 30mm. This would cause extensive damage to any hollowcore within this zone. Therefore, avoiding supporting hollowcore units on potential plastic hinge zones in beams can help to avoid the damage that would be induced.

When the transverse beam is subjected to bending, tensile strains are applied to the floor slab. As a result, any transverse reinforcement in the topping could sustain tension forces. Standard design practice requires designers to take the transverse reinforcement into account for calculating beam flexural over-strength. Any change in the tension force in the topping reinforcement (T_1 - T_2, see Figure 2.32) must be resisted by a shear force, such as friction at the seated edge of the floor unit if it is supported on a mortar bed. Therefore the hollowcore unit is subjected to Vierendeel truss type actions, which could result in a flexural shear failure of unreinforced webs. However, if the units are supported on low friction bearing strips, the tension force in the transverse reinforcement cannot change, and significant lateral displacements must develop between the beam and the hollowcore units. The effectiveness of transverse reinforcement in the topping concrete is also reduced as the tension force remains constant over the bay and makes no overall contribution to the lateral strength. Any force in this reinforcement results from the elongation of the beam only.

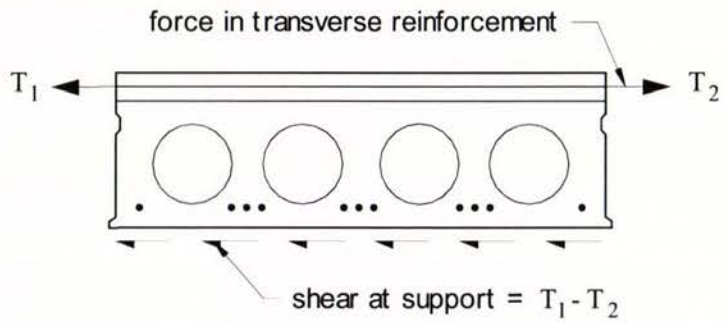

Figure 2.32: Vierendeel truss action in hollowcore [F14].

From their study, Fenwick *et al* gave an alternative proposal for the seating of hollowcore units on supporting beams [F14]. This is illustrated in Figure 2.33. The following comments expand on the corresponding numbered captions in the diagram:

1. Tie reinforcement used to transfer tension forces to enable the floor to maintain its function as a diaphragm. This is located at the ends of the units in filled concrete cells and is placed close to the pretensioned strands in the bottom such that the negative moments and associated shear stresses are reduced.

2. A hard board sheet placed against the end of the unit to create a break in the concrete. This is used to limit the magnitude of the forces transmitted into the hollowcore units.

3. Longitudinal reinforcement is added to the topping to ensure that the hollowcore unit has a greater flexural and axial strength than the critical section (end of unit at the support).

4. Additional pretensioned strands added to the top of the units to increase negative moment capacity. Also this increases the height of the zero stress fibre in the zone close to the supports which increases the shear strength of the section when subjected to negative bending.

5. Soft packing around the tie bars enable vertical movement to occur between the hollowcore unit and the beam without causing splitting cracks. This movement arises from the rotation of the beam and hollowcore unit about the low-friction strip.

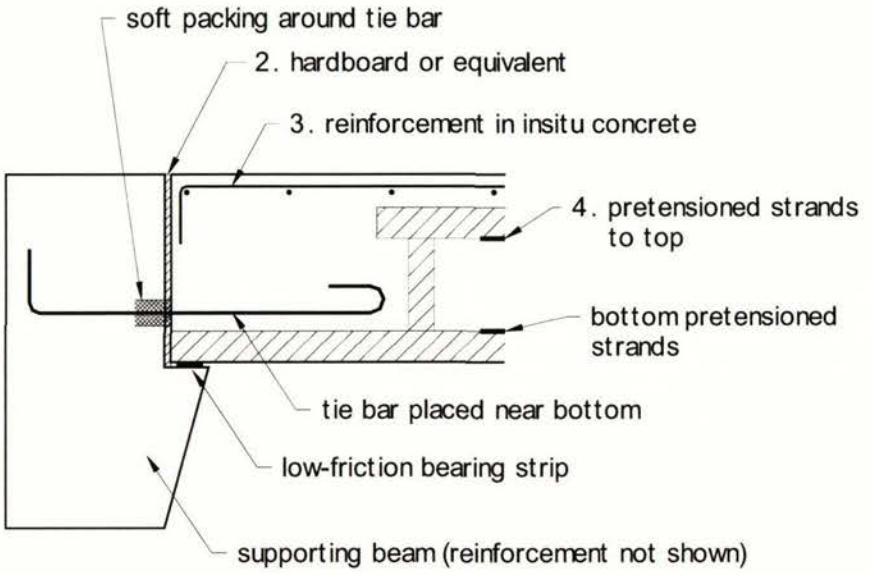

Figure 2.33: Proposed detail to improve seismic performance of hollowcore units [F14].

Chapter 3

Experimental Programme

3.1 Introduction

In this chapter the experimental programme is described, starting from the design considerations, a description of the construction, instrumentation and the testing procedures adopted for the test units. Also included are the test results on the component materials.

3.2 Design Considerations

Three frame subassemblies were constructed for the experimental phase of the project. One of these frames was constructed integrally with a floor slab, which contained precast prestressed units. These were designed to represent one storey of a ductile, moment resisting perimeter frame of a multistorey building (see Figure 3.1), and as such it would be expected to form reversing plastic hinges in the beams in the event of a design level earthquake. Cyclic lateral forces were applied to the top and bottom of the columns to simulate seismic forces (more details in *Section 3.6*). These positions represent the mid-height of a storey in a frame building, where the points of inflexion in the columns are expected to form.

The experimental units were detailed in accordance with the New Zealand Concrete Structures Standard, NZS 3101:1995 [S2]. The choice of structural system for this project was based on the perimeter frame building design example contained in the 'Examples of Concrete Structural Design to New Zealand Standard 3101', or commonly known in New Zealand as the 'Red Book' [C3]. However, instead of incorporating the 'hollowcore' flooring system, the 'interspan' or 'rib and infill' flooring system was used for one of the units. The experimental units were scaled to approximately 1/3 of typical member sizes so that it could be accommodated in the space and equipment available to

the facilities in the University of Auckland Test Hall. A summary of the design calculations of the experimental units have been included in *Appendix 1* of this report.

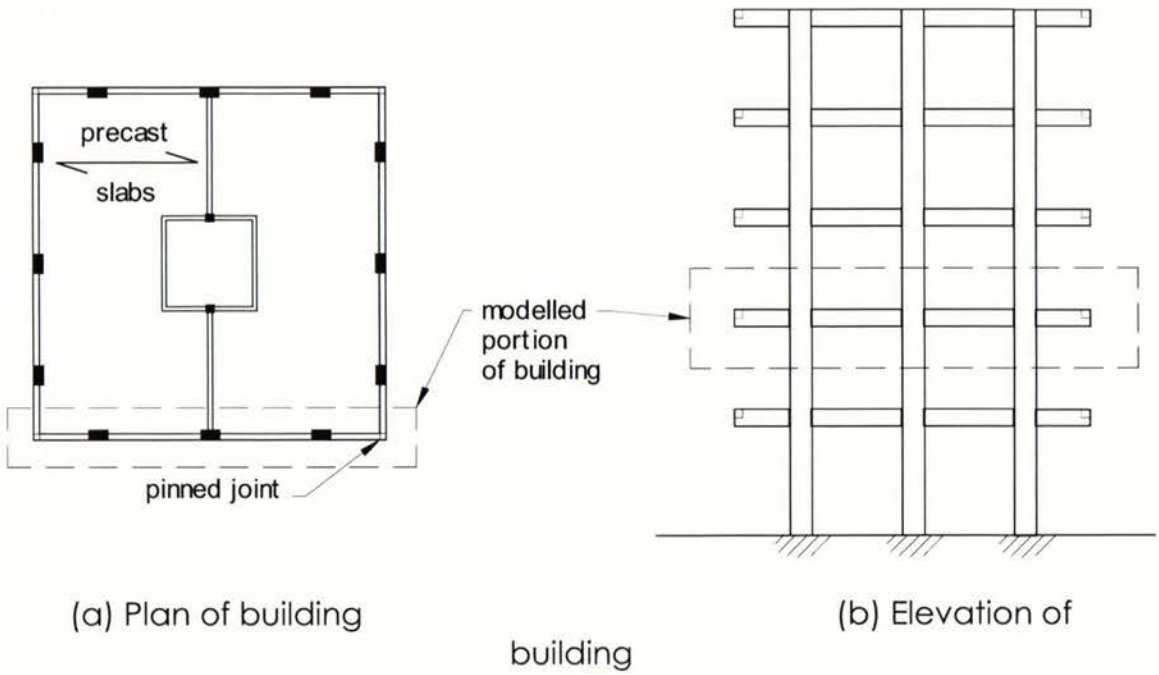

Figure 3.1: Typical level of frame in a building modeled by test units.

3.3 Description of Experimental Units

The primary objective of this project was to investigate the influence of a precast-prestressed flooring system on the structural performance of a perimeter frame. To achieve this, at least two beam-column frame sub-assemblies were required. The first of these, Unit 1, involved a level of a two-bay bent with cantilever beam extensions on each end. The second test, Unit 2, contained the same frame as in Unit 1, but with the addition of precast floor ribs and floor concrete topping. The precast floor ribs were positioned parallel with the perimeter frame and were supported on three beams perpendicular to the perimeter frame. The depth of floor slab was approximately half the length of the frame in plan.

The first test was intended to serve as a benchmark for comparison against the second test, as well as reaffirming findings from previous research. It also allowed the method of loading to be trialled and refined before the more complicated second unit was tested. Subsequent to testing Unit 1, changes to the experimental arrangement and procedures

were made for Unit 2 and a third unit (Unit 3) to be built and tested. This unit had a similar frame to Units 1 and 2, but was tested using the same procedure employed for Unit 2.

3.3.1 Test Frame Units: Units 1, 2 and 3

The dimensions and cross sections of the beams and columns of the experimental frames subassemblies are shown in Figure 3.2. The distance between the loading points at the top and bottom of the columns was 1230mm. The distance between the centres of each column was 2032mm. And the dimension from the centre of the outside columns to the end of the cantilevers was 1284mm.

The beams were 300mm deep and 130mm wide. They were reinforced with equal top and bottom longitudinal reinforcement, which consisted of three 12mm deformed bars along the entire length of the frame unit. Grade 300 bars, which had a design yield stress of 300MPa, were used. This grade was chosen as the use of high strength reinforcement reduces the stiffness of the beams and gives problems in the anchorage of the bars. Grade 300, 6mm diameter transverse reinforcement was placed in the beams at 65mm centres in the potential plastic hinge zones, in accordance with the anti-buckling and confinement requirements of the code [S2]. The stirrup spacing was increased to 100mm outside of the plastic hinge zones.

The columns were 300 deep and 200mm wide. These were reinforced longitudinally by twelve, Grade 430 (design yield stress of 430MPa), 12mm deformed bars running along the entire height of each column. The columns were deliberately over-designed for two reasons:

1. Obtain a 'weak beam and strong column' design, to ensure that the columns remained elastic throughout the test,
2. To allow for the anticipated strength enhancement effects of the beams in the second test, Unit 2, due to the addition of the slab.

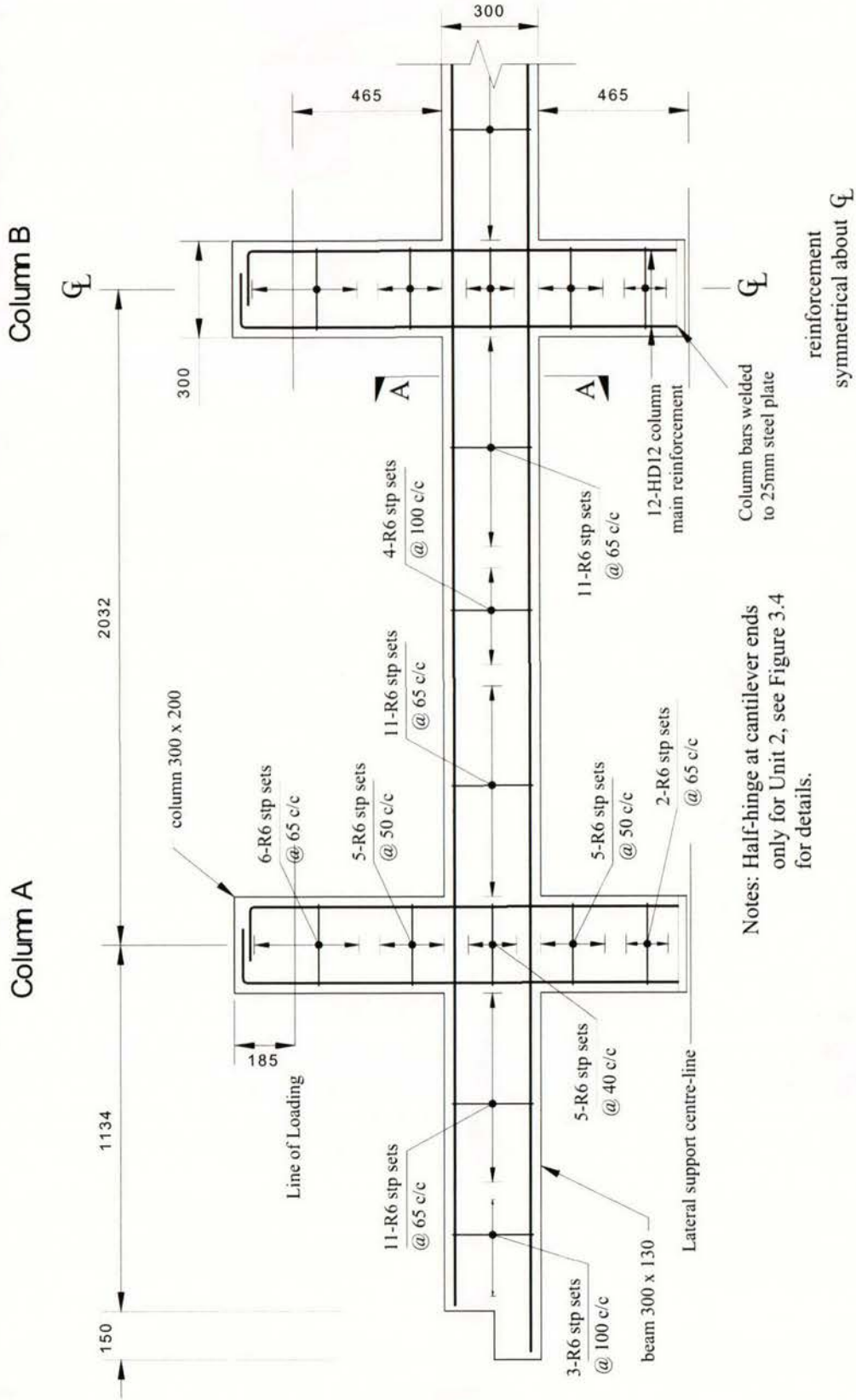

(a) Elevation of frame unit

Figure 3.2: Reinforcement details of the test frames. (continued)

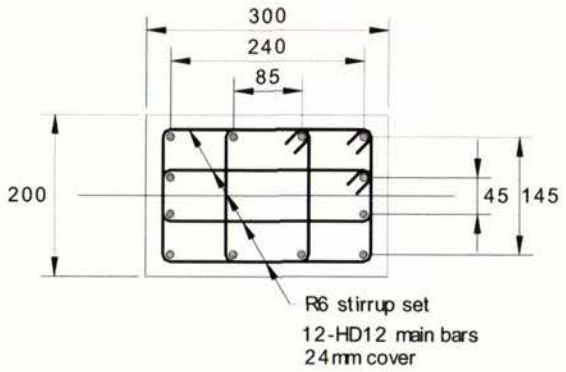

(b) Section A-A: Column cross section

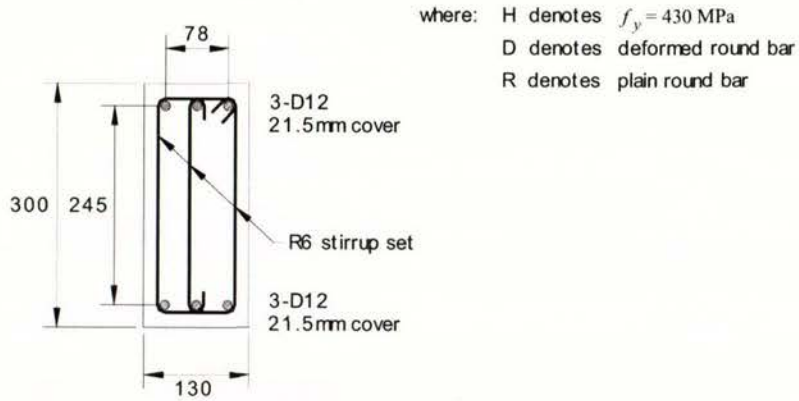

(c) Section B-B: Beam cross-section
(flange not shown for Unit 2)

Figure 3.2: Reinforcement details of test frames. (concluded)

Grade 300, 6mm diameter bars were used for transverse reinforcement in the columns. The centre-to-centre spacing of stirrup sets was 50mm in the potential plastic hinge zones immediately above and below the beam face. This was increased to 65mm outside of these zones. Stirrup sets in the beam-column joints were spaced at 40mm centre-to-centre in order to provide sufficient strength to these critical regions.

The sectional flexural strengths of the members (without adjacent flanges) are listed in Table 3.1 (see worked example calculation for Unit 1 in Section A1.5, *Appendix I*). These values were calculated using the average yield stress of the reinforcement determined from tension tests and the average compression strength found from concrete cylinder tests. The rectangular compression stress block defined in the New Zealand Concrete Structures Standard [S1] was used in these calculations. Generally for calculation of beam flexural over-strength in New Zealand, the design yield stress is

increased by an over-strength factor of 1.25. This factor is made up of two parts, the first of these being an allowance of 10% to account for the likely underestimate of the actual yield stress, and secondly 15% to allow for strain hardening characteristics of steel reinforcement. However, as the actual yield stress is known for these test specimens the flexural over-strength was taken as the product of the yield tension force in the reinforcement multiplied by 1.15, and the distance between the centroids of the top and bottom reinforcement.

It can be seen that the central column has a theoretical ultimate moment capacity equal to approximately 2.5 times the flexural over-strength of the beam. It was anticipated that this should give an adequate margin to protect the columns from failure for the strength increase in the beams in Unit 2 due to addition of floor slab.

Table 3.1: Calculated theoretical flexural strength of sections

Section	design flexural strength (kNm)			theoretical over-strength (kNm)
	average f_y (MPa)	average f_c' (MPa)	design strength	
Beams:				
Unit 1	309	30.8	27.0	29.6
Unit 2*	309	32.5	27.0	29.6
Unit 3	315	26.1	27.1	30.1
Columns:				
Unit 1	460	30.8	75.4	
Unit 2	460	32.5	76.8	
Unit 3	466	26.1	74.2	

* flange not included for Unit 2, calculation including flanges see *Chapter 5* pgs. 130-132.

3.3.2 Test Frame-Slab Unit: Unit 2

The structural details of Unit 2 are shown in Figure 3.3. Where possible, the details were designed according to common best practice. The floor consisted of two spans of precast 'rib and infill' units with 40mm of insitu concrete topping. These units were Stahlton's 900 Ti 200 rib and infill units (see Figure 3.3 b)). The insitu slab was cast on

timber, supported by the ribs. This timber was removed before the unit was tested. As shown in Figure 3.3(a), each precast unit spanned 3125mm from the outer transverse beam adjoined to the end of the cantilever in the main beam, to the central transverse beam extending from the central column.

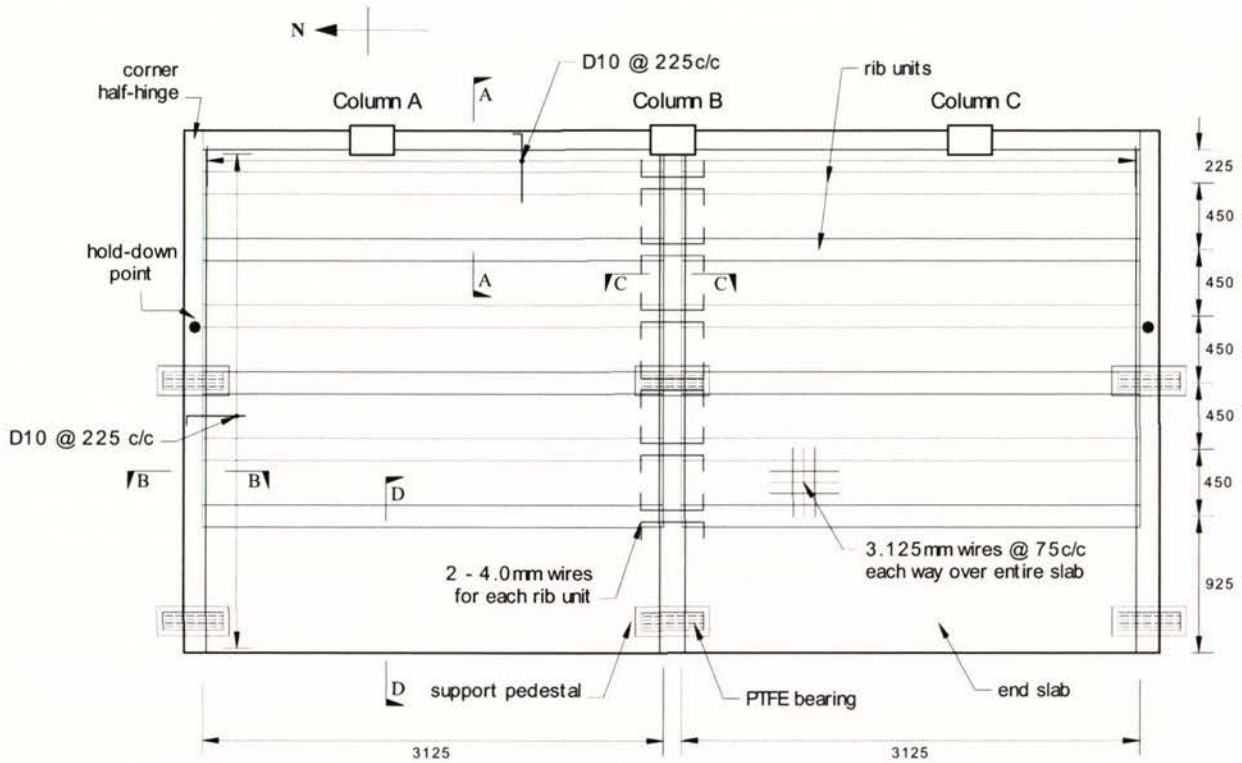

(a) Plan view of Unit 2

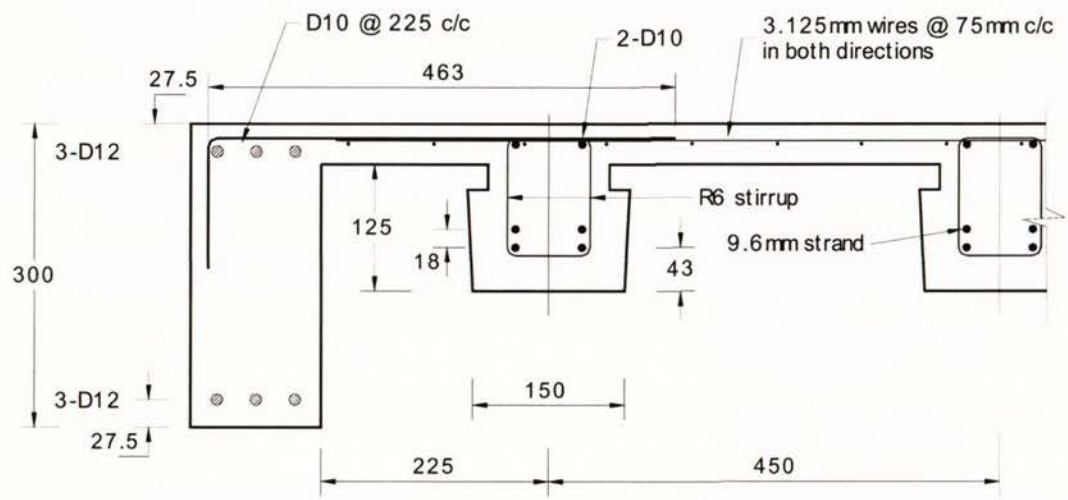

(b) Section A-A: Frame beam and rib units

Figure 3.3: Diagrams of test Unit 2. (continued)

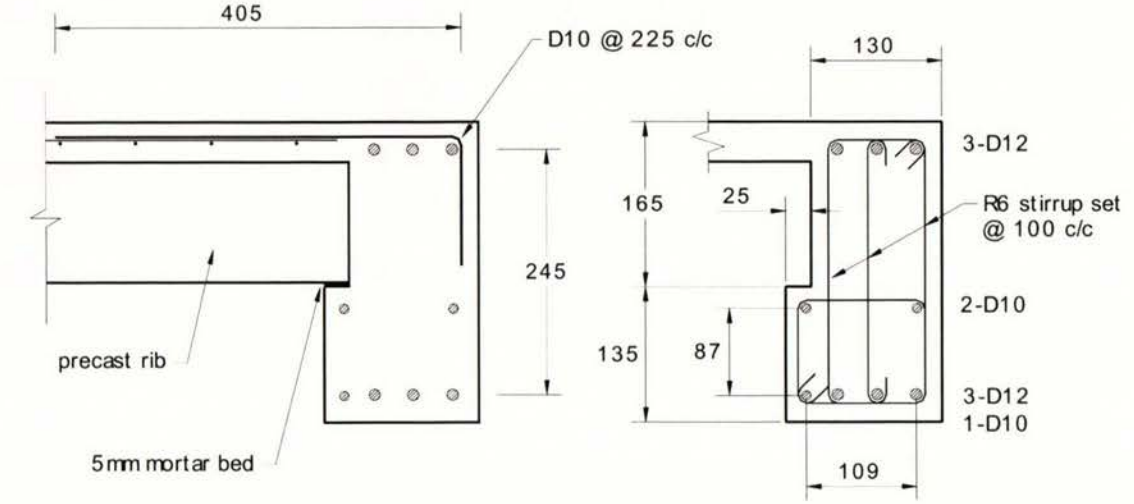

(c) Section B-B: Outer transverse beam

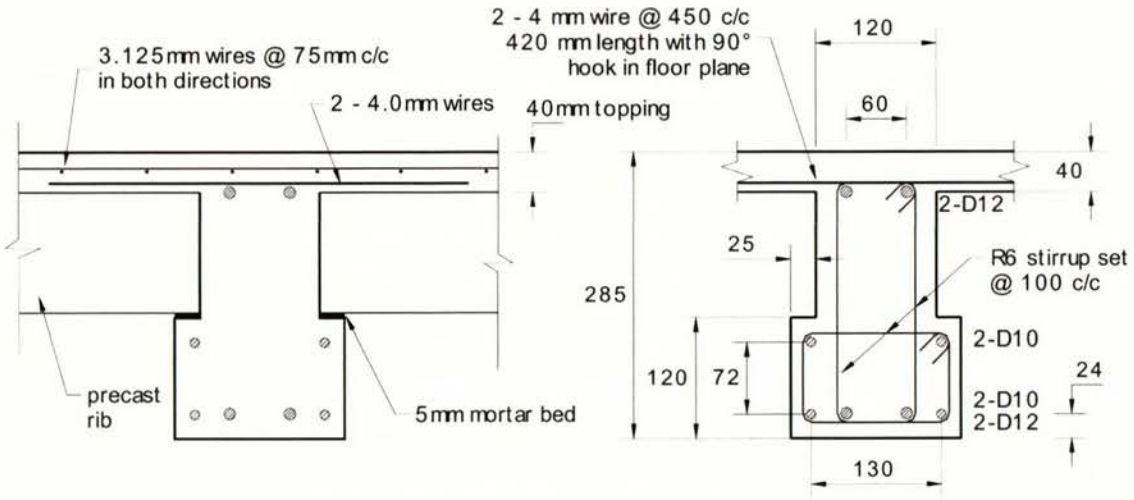

(d) Section C-C: Centre transverse beam

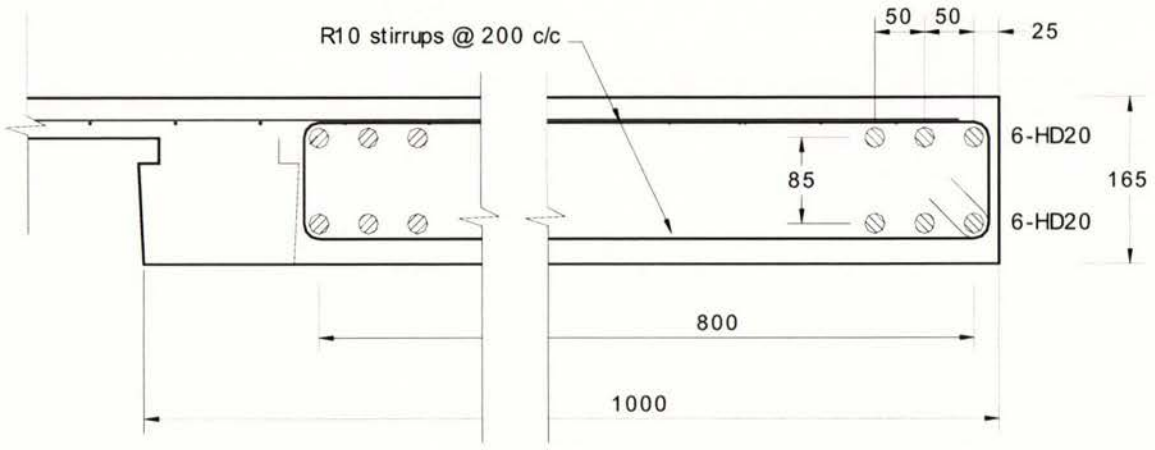

(e) Section D-D: End slab

Figure 3.3: Diagrams of test Unit 2. (concluded)

The first precast unit was spaced at 225mm from the face of the frame beam, and five subsequent units were spaced at 450mm centre-to-centre. The sixth unit was joined to a solid end slab, which was 165mm deep and reinforced with six, high tensile 20mm reinforcing bars on each side (see Figure 3.3(e)). The end slab acted as a stiff boundary condition, to model the continuation of a floor diaphragm in a building. The floor was supported at two locations for each transverse beam by pedestals bolted down to the strong floor. PTFE bearings were used to allow the floor to slide over the pedestals during the test.

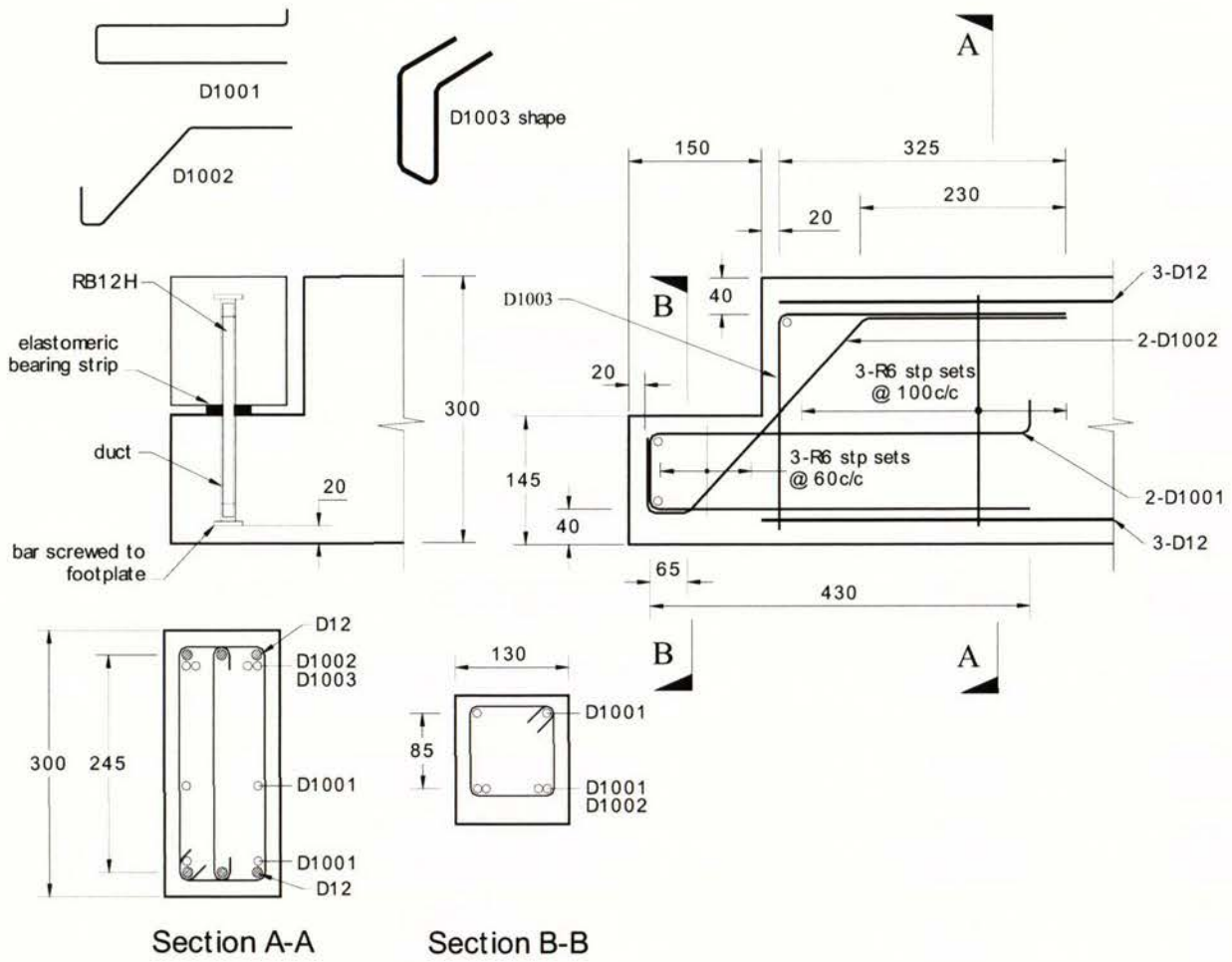

Figure 3.4: Corner half-hinge connection details.

The insitu concrete above the ribs was reinforced with mesh, which consisted of 3.125mm wires spaced at 75mm centre-to-centre in both directions. Joining the frame beam to the floor were 10mm deformed starter bars spaced at 225mm (see Figure 3.3(c)). The continuity reinforcing between each of the ribs and the central transverse

beam was provided by two 4.0mm wires (see Figure 3.3(d)). A seating width of 25mm was provided for the ribs along the transverse beams. The cantilever and transverse beams were connected with half-hinge joints as shown in Figure 3.4. A 12mm Reid bar (indicated by RB12H, f_y = 500MPa) with footplates screwed to the bar was used to provide the tension connection in the joint.

3.4 Testing of Materials

The materials used for the test units, namely steel reinforcement and concrete, were tested prior to the test of the units. The following subsections describe this process.

3.4.1 Steel reinforcement tension testing

The reinforcement was attained in two batches, the first was used for Units 1 and 2 and the second for Unit 3. Axial tension tests on samples of the reinforcement were carried out to determine the stress-strain relationships. The samples were obtained from each batch of reinforcement and were tested in direct tension without turning the bars to remove deformed patterns. The results of the tests on the reinforcement used in the beams and columns of the frames are summarised in Table 3.2, and details are given in *Appendix 2*. Additional steel reinforcement was required for the floor slab and transverse beams of Unit 2. The properties obtained from tests on these are shown in Table 3.3.

The 12mm bars were tested on the Avery Universal Testing Machine situated in the Structures Test Hall. The Grade 300, 12mm bar used in the beams of the frame for Units 1 and 2 had an average yield stress of 309MPa, while for Unit 3 it was 315MPa. These bars were ductile, as indicated by the high strain levels of 23 to 25% at maximum stress. The Grade 430, 12mm bars used in the columns yielded at an average of 461MPa for Units 1 and 2 and 466MPa for Unit 3. The strain at failure was between 25 to 26%. The stress-strain plot for tests on three samples of Grade 300 D12 bars are shown in Figure 3.5.

The plain round 6mm bars were tested on the Instron Testing Machine located in the Civil Materials Laboratory. These bars yielded at an average of 358MPa for Units 1

and 2 and 361MPa for Unit 3. An average ultimate stress of 468MPa for Units 1 and 2 was reached at strain levels ranging from 11 to 12%, and for Unit 3 it was 463MPa at strains between 9.5 to 10.5%.

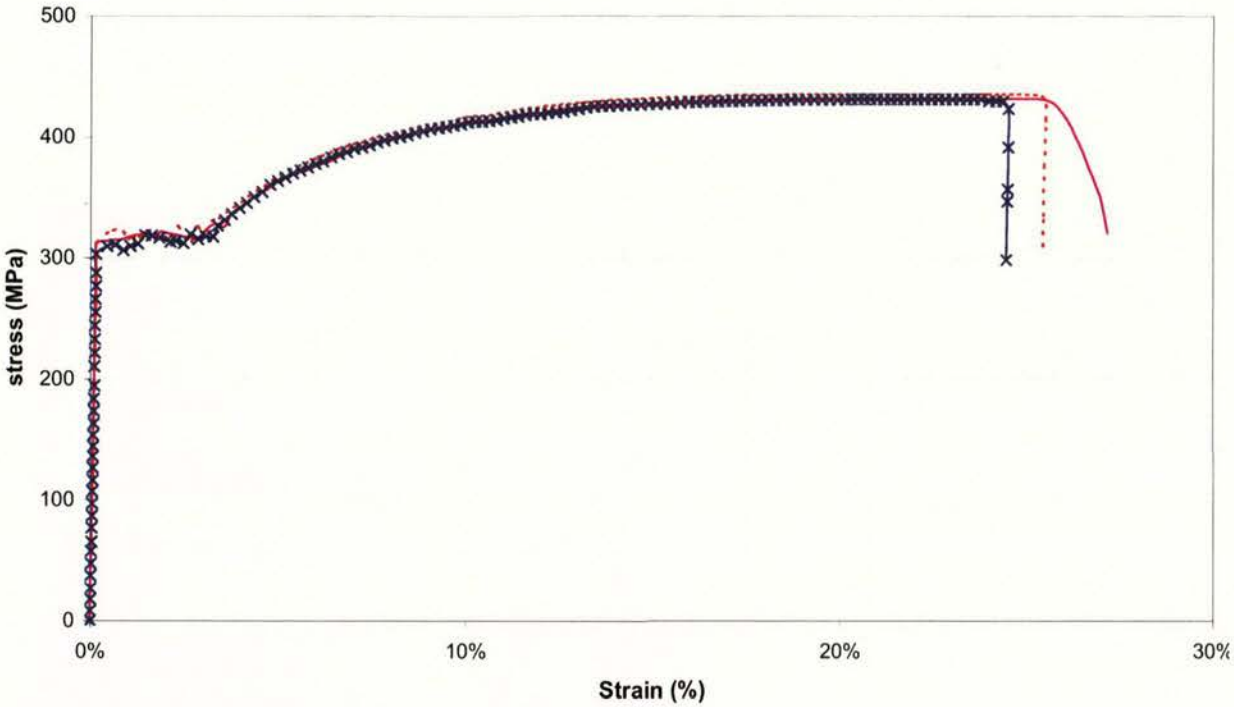

Figure 3.5: Stress-strain plot of 12mm diameter beam longitudinal reinforcement.

The steel reinforcement properties used in the floor slab of Unit 2 are summarized in Table 3.3. The 3.125mm and the 4.0mm diameter wires were tested on the Instron Testing Machine in the Mechanics of Materials laboratory as shown in Figure 3.6. The 3.125mm and 4.0mm wires had an average yield stress of 408MPa and 431MPa respectively.

Deformed 10mm bars were used in the corner half-hinge joints, nominal reinforcing in the transverse beams and starter bars connecting the frame beam to the floor. These were found to have an average yield stress of 313MPa and an average ultimate stress of 437MPa. The strains at which ultimate stresses were sustained ranged from 18.7 to 19.6%.

Table 3.2: Steel reinforcement stress-strain properties.

Description	yield stress f_y (MPa)	maximum stress f_{max} (MPa)	strain at maximum stress ε_{max} (%)
D12			
Beam longitudinal bars	303	431	23.6
Unit 1 and 2	313	431	25.5
	312	435	24.6
	314	442	24.9
Unit 3	315	441	26.4
	316	441	24.3
HD12			
Column longitudinal bars	457	606	14.9
Unit 1 and 2	469	609	15.6
	456	609	17.8
	462	614	15.8
Unit 3	462	609	16.3
	475	612	14.6
R6			
Transverse reinforcement	369	470	11.2
Unit 1 and 2	350	470	11.2
	355	463	12.3
	354	464	9.7
Unit 3	363	462	10.5
	365	464	9.9

Figure 3.6: Testing of wire reinforcement on Instron Test Machine.

Table 3.3: Steel reinforcement stress-strain properties - floor slab of Unit 2.

Description	yield stress f_y (MPa)	maximum stress f_{max} (MPa)	strain at maximum stress ε_{max} (%)
3.125mm wire Floor mesh	398 423 403	479 483 480	- 11.40 15.76
4.0mm wire Rib end and central transverse beam continuity bars	439 420 433	502 483 497	11.32 11.59 12.39
D10 Starter bars, half-hinge joint and transverse beam bars	312 316 312	439 439 434	18.95 18.69 19.63
D12B Transverse beam longitudinal bars	312 315 316	423 455 452	22.50 22.40 22.52
HD20 End slab longitudinal bars	312 315 316	423 455 452	22.50 22.40 22.52

3.4.2 Concrete Compression Testing

Concrete cylinders were prepared with all concrete pours. These were tested using the Contest Concrete Testing Machine in the Civil Materials Laboratory. The results of the tests are summarized in Table 3.4.

Units 1 and 3 were constructed in a single pour (see *Section 3.5*). Concrete test cylinders were damp cured with the test unit for seven days. Three of these were tested twenty eight days after the pour and a further three immediately before the Unit 1 was tested. It was found that the average strength was 29.8MPa in both instances. Similarly, the concrete cylinder strength of Unit 3 was found to be 24.8MPa after twenty eight days, and was 26.1MPa just before testing commenced.

The frame-floor slab unit, Unit 2, was poured in four stages. This is described in more detail in *Section 3.5*. The concrete for the first three stages were obtained from ready

mixed concrete suppliers. The concrete for the final stage was prepared in the laboratory. The average strength of concrete from the ready mixed concrete suppliers was 31MPa, whereas the concrete mixed in the laboratory had an average strength of 39MPa.

Table 3.4: Concrete compression test results.

Description	number of tests	age at test (days)	individual specimen strengths f_c' (MPa)	average strength f_c' (MPa)
Unit 1: Frame Unit	3	28	29.6, 30.9, 29.2	29.9
Whole unit	3	130	30.4, 29.8, 32.2	30.8
Unit 2: Stage 1	3	28	25.6, 26.4, 24.0	25.4
Half of transverse beams	3	246	29.1, 29.2, 28.8	29.0
Unit 2: Stage 2	3	28	29.6, 29.9, 29.1	29.5
Bottom half of columns and frame beams	3	216	33.1, 31.7, 32.6	32.5
Unit 2: Stage 3	3	28	26.9, 32.7, 28.9	29.3
Floor and beams	3	167	28.4, 32.8, 32.2	31.9
Unit 2: Stage 4	2	28	37.4, 35.6	36.5
Top half of columns	4	155	43.1, 41.3, 36.3, 35.6	39.1
Unit 3: Frame Unit	3	28	24.2, 25.4, 24.8	24.8
Whole unit	3	130	26.0, 25.4, 26.9	26.1

3.5 Construction of Test Units

The test units were constructed in the Structures Test Hall. The majority of the steel reinforcement was obtained in straight lengths and cut to required lengths on site. The stirrups for the columns and the end slab (for Unit 2 only) were obtained pre-bent. However, the stirrups for the beams were bent on site from straight lengths of plain, round 6mm bars.

A base plate was used to attach the base of the columns to one-way pins, which were connected to the strong floor, and to the actuators that were used to adjust the position of the columns (see Figure 3.10). Details of the base plate are shown in Figure 3.7. The column longitudinal reinforcement were welded to slotted holes drilled into the 25mm thick base plate. Four threaded, 28mm diameter studs were welded to the plate to enable the pins to be bolted in place.

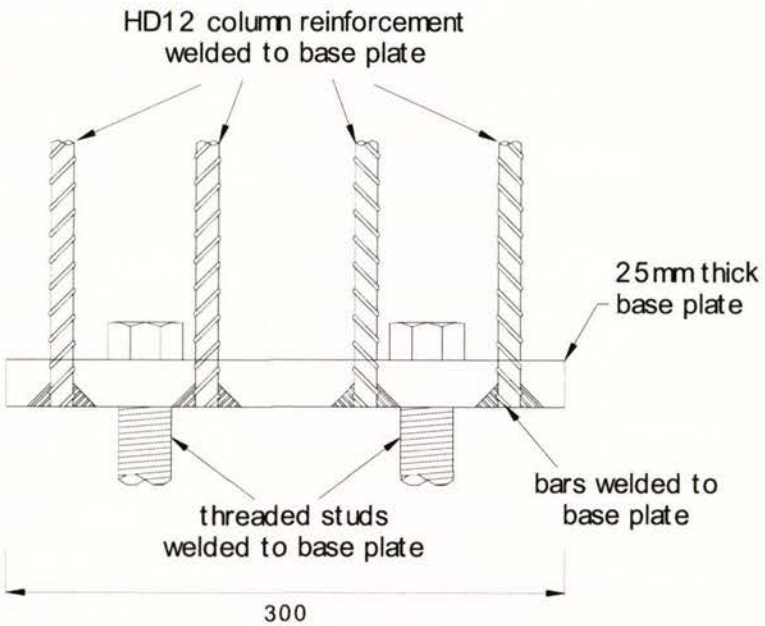

Figure 3.7: Detail of connection at column base.

The formwork for the unit was constructed out of 20mm thick particle-board supported on timber lengths. The formwork for Units 1 and 3 was made so that the units could be cast on their side in one pour. The concrete was obtained from a ready-mixed concrete supplier. The specified maximum aggregate size was 10mm. After initial set, the

exposed surface was covered with wet sacks and polythene sheeting for a period of seven days for curing.

The reinforcing cage for the frame portion of Unit 2 was constructed in the same way as for the other units apart from the additional work needed to reinforce the corner half-hinge joints at the end of the cantilevers. The stages of construction of the unit are described in Table 3.5.

Table 3.5: Stages in construction of Unit 2.

Stage	Description
I	The reinforcing cages for the transverse beams were built and formwork made. Concrete was poured up to the seating level. These beams were placed into position on the pedestals.
II	The formwork for the main frame was assembled around the reinforcement, which had been placed and tied to the final position. Concrete was poured approximately to the mid-height of the frame beams.
III	The ribs were placed into position on the transverse beams and timber infills placed. This was done while the formwork was put in place. The reinforcing for the end slab was put into place. The floor mesh reinforcing was placed and concrete was poured up to the top surface of the beams and floor. Timber infills between each rib unit were removed on the following day.
IV	The top half of the columns were cast.

Concrete for stages I, II and III was obtained from a ready mixed concrete supplier. Concrete for stage IV was mixed in the laboratory as only a small amount was needed. In all cases, where a construction joint was required, a retarding agent was used to enable the treated surface to be brushed so that the aggregate was exposed at the

junction to the new concrete. At each stage, concrete was cured under damp conditions for seven days. Figure 3.8 shows the unit in stage III, immediately before concrete pour.

Figure 3.8: Stage III of construction of Unit 2, immediately before concreting.

3.6 Loading Equipment and Arrangement

The test equipment and loading arrangement were different for Units 1 and 2. The arrangement for Unit 2 was revised after the testing of Unit 1. Unit 3 was similar in arrangement to Unit 2. The subsections below describe these arrangements.

3.6.1 Test arrangement of Unit 1

A photograph of the test arrangement of Unit 1 is shown in Figure 3.9 and the overall schematic in Figure 3.10. Reversing hydraulic actuators with a 200kN push and 150kN pull capacity were placed in the bays between columns 'A' and 'B' and 'B' and 'C'. These were operated by reversing hydraulic hand pumps. The pins to which the hydraulic actuators were attached to, at the each of the top of the columns, were held by bolts and packed to the side of the columns using sand and cement mortar. The main loading hydraulic jack with a capacity of 380kN push, 280kN pull was attached to the top of column 'A'. It was held by a buttress bolted on top of two thick walled steel universal sections (see Figure 3.10). These in turn were held together by bolts and

stressed down to the strong floor by high tensile McAlloy bars. Plates of steel were welded between the buttress and the steel section to provide adequate shear transfer.

The bottom of each column was pinned and supported vertically by 40mm thick steel 'sway' plates attached to pins, which were bolted to the strong floor as shown in Figure 3.10. This arrangement enabled the bottom the columns to displace laterally, along the direction of the frame. The bottom displacements of columns 'A' and 'C' were controlled by hydraulic actuators (with capacity of 150kN push, 100kN pull) pinned to the sides of the base plate of the respective columns. The hydraulic actuators were held on the other side by buttresses bolted to the strong floor. The bottom of column 'B' was restrained from moving to any large degree. By this arrangement, the loading components did not provide additional restraint to the elongation of the members, by allowing the outside columns to extend outwards from the middle column. Struts, which were pin ended, were attached to the strong wall and the top and bottom of the columns (see Figure 3.10). These struts allowed displacements to occur in the plane of the frame but restrained out of plane movement.

Figure 3.9: Test Arrangement of Unit 1 - motorised hydraulics control (foreground), datalogger (right), loading hydraulic actuators (top of columns), hand-pumps (on floor).

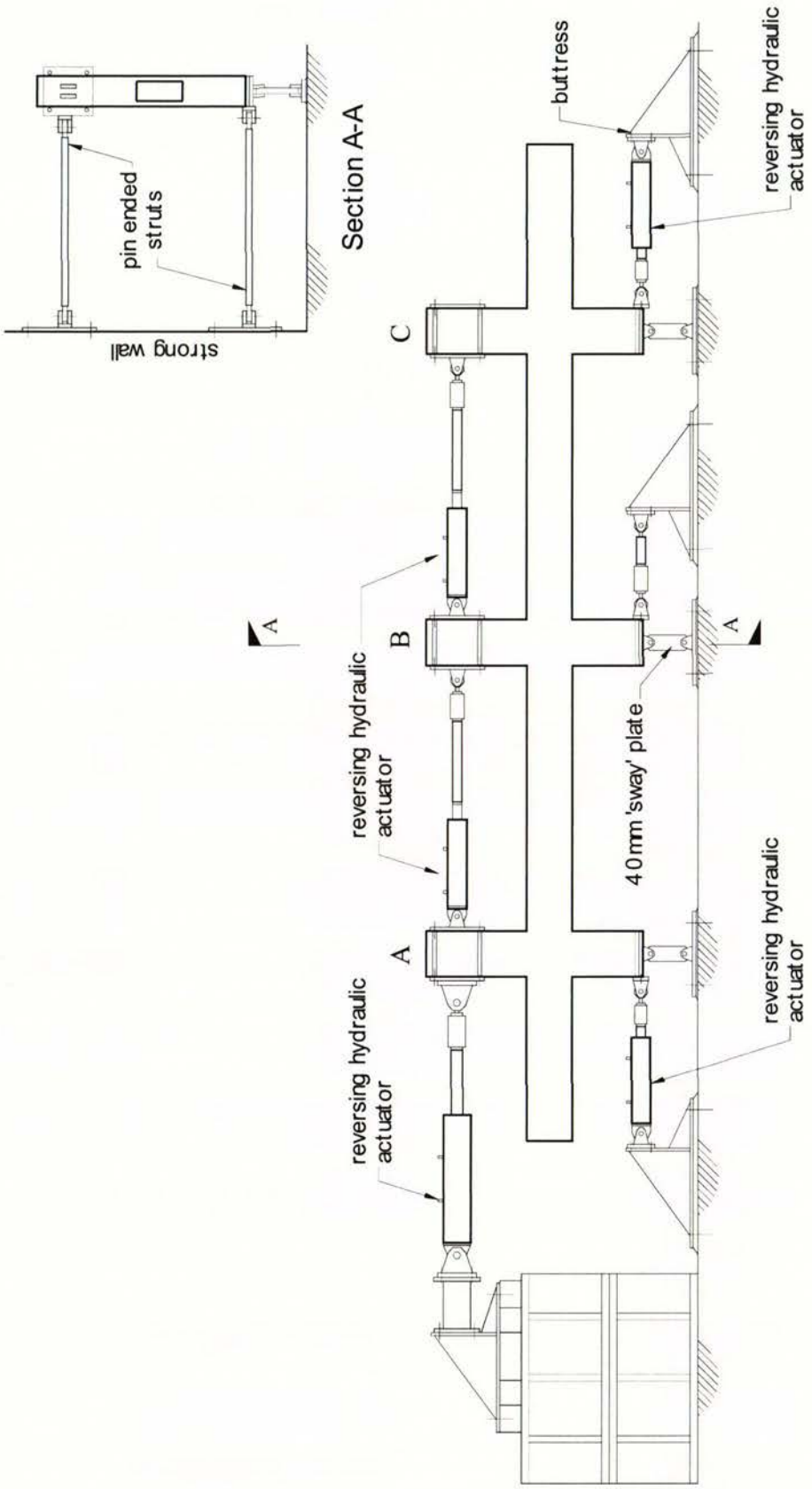

Figure 3.10: Schematic of test arrangement of Unit 1.

3.6.2 Test arrangement of Unit 2

The loading arrangement with Unit 1 was difficult to operate and control, and consequently a different arrangement was used for Unit 2. The main difference was in the way the top columns were loaded. This can be seen by comparing Figure 3.10 of Unit 1 and Figure 3.12 of Unit 2. The revised arrangement allowed the actuators at the top of the columns to be operated independently each other.

The central hydraulic actuator had a push capacity of 500kN and 280kN in the other direction. This had a shorter cylinder in comparison to the actuators used for the outside columns, which were had capacities of 380kN and 280kN in the push and pull directions respectively. This shorter length made it possible to fit this arrangement in the space available without obstructing the movement of the columns. The reaction force for the actuator to column 'B' was provided by a cantilever 250×250×9mm RHS, which was welded at the base to a 40mm thick square plate. This was stressed to strong wall with stressing bolts. Two additional braces were welded to the RHS and the plate. A vertical steel frame provided the reaction frame to the actuator at column 'C'. This was stressed to the strong wall and also braced diagonally against the floor. Apart from these changes, the other arrangements were similar to that employed for Unit 1.

Figure 3.11: Loading arrangement on Unit 2.

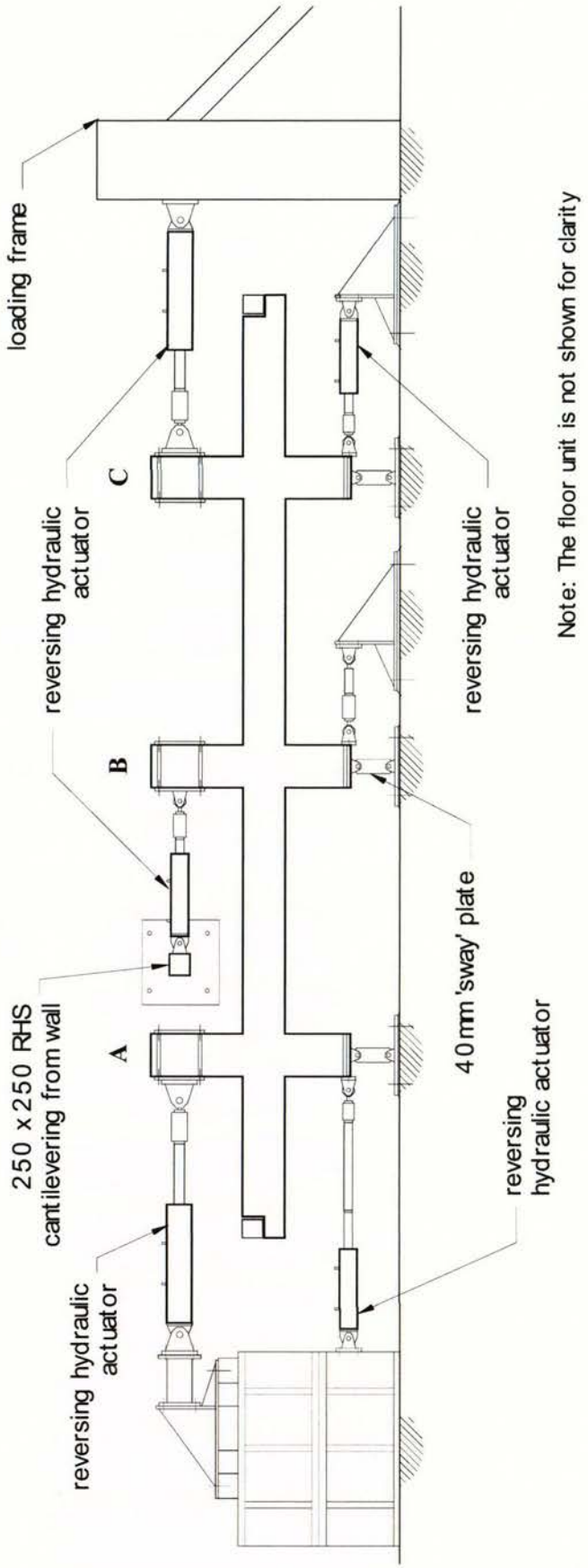

Figure 3.12: Schematic of test arrangement of Unit 2.

3.6.3 Additions to Unit 2

Concern was expressed over the possibility of splitting of the concrete above the starter bars that connect the main beam to the floor slab. These bars were placed on top of the mesh, and the cover concrete over these bars was approximately 15mm. It was decided that some form of retrofit work was needed to prevent possible premature failure by this mode. Strips of steel measuring 20mm wide, 100mm long and 2mm thick were epoxied onto the surface of the insitu concrete directly above the positions of the starter bars (see Figure 3.13(a)). Figure 3.13(b) shows a photograph taken of two of these during the test. The line on the floor, to the left in this photograph is a crack in the floor, which shows that the concrete was splitting above the bar.

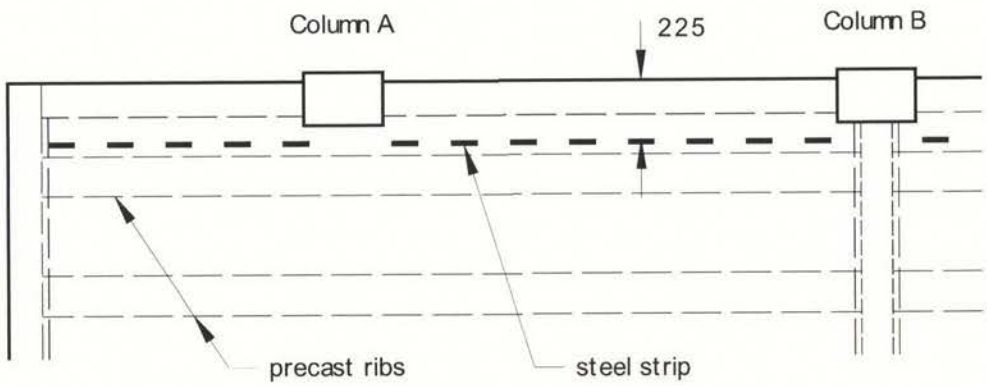

(a) Typical placement on floor

(b) Two steel strips on floor during test

Figure 3.13: Steel strips epoxied to concrete floor.

Additional weight was placed on the floor before testing commenced. The prestressing force in the bottom half of the ribs results in the negative bending of the composite section (floor rib and topping concrete). Stress redistribution due to creep and

shrinkage reduces the average flexural cracking moment of the section. Combined with tension in the floor slab (due to diaphragm forces in the plane of the floor generated from the interaction of the frame with the floor) this could result in failure in negative bending unless the floor is sufficiently reinforced with passive reinforcement. The addition of extra weight can contribute to balance out some of this action by increasing the negative moment capacity. An equivalent surface load of approximately 3.0kPa was applied to the first 1000 mm of the floor width.

Lead bars were used as additional weight nearer to the frame to allow strain measurements to be made with DEMEC gauges. When necessary the lead bars were moved temporarily when DEMEC gauge readings were taken. Sand bags, each weighing approximately 250N, were placed further away from the frame. A total of approximately 18kN of extra weight was placed onto the floor. Figure 3.14 shows the placement of the lead bars and the sand bags. During the test, a few sand bags were moved at a time to enable DEMEC gauge readings to be made.

Figure 3.14: Placement of extra mass on the floor.

3.6.4 Test arrangement of Unit 3

The loading arrangement for this test frame is shown by Figure 3.15. This arrangement was similar to Unit 2, which was described in Section 3.6.2. However the three 40mm thick sway plates at the bottom of the columns were replaced with load cells. These were used to monitor the axial forces acting in the columns, which enabled the shears in the beams to be determined.

Figure 3.15: Test arrangement of experimental Unit 3.

3.7 Measurement and Instrumentation

A substantial amount of instrumentation to record forces, displacements, and deformations was placed on the experimental units. Displacement measurements were made using portal displacement transducers and force readings were obtained from load cells. Other manual checks were made using tapes and rulers, DEMEC readings, theodolite and level sightings. The number of individual portal gauge and load cell readings that could be used for the Unit 1 test was restricted to 110 due to the channel capacity of the data acquisition system. A total of 104 displacement transducers were used for this test. For Unit 2, a second data acquisition system was acquired and used in conjunction with the first to allow for up to 206 channels to be monitored. A total of 170 displacement transducers and 153 DEMEC gauge reading points were to be

recorded. For Unit 3, a total of 131 channels were monitored during the experiment. The measurements and instrumentation for the experiments are further described in the following subsections.

3.7.1 Measurement of forces

In all the tests, lateral loads applied to the top of all the columns and the bottoms of the outside columns were measured by load cells coupled with the reversing hydraulic actuators. A load cell was used to monitor the lateral reaction force at the bottom of column 'B'. In Unit 3, additional load cells were placed at the bottom of the columns to measure the axial forces acting on the columns. Prior to the test, the load cells were calibrated on an Avery Universal Machine.

3.7.2 Measurement of displacements

The displacements of the top and bottom of the columns were measured using portal displacement transducers. Calibration of the transducers was conducted on the MTS load frame before the test. At the top of each column on Unit 1, a portal transducer was attached to the hydraulic jack and screwed on to the pinned joint at the side of the column (see Figure 3.16). With this arrangement, the absolute displacement at the top of column 'A' was monitored together with the displacement of column 'B' relative to column 'A', and column 'C' relative to column 'B'. This arrangement was modified for Units 2 and 3. Instead of using the standard sized portal transducers, larger portal transducers with an effective measurement range of ±60mm were manufactured. These transducers were attached to the column pin on one end and to an independent stand on the other end to enable the absolute displacement of each column to be measured.

During the testing of Unit 1, steel rulers and tapes were used to check the displacements against the electronic measurements obtained at displacement peaks. For Unit 2, additional portal transducers were mounted to measure the changes in the distance between the columns as a check against the absolute displacements of the columns. For Units 2 and 3 checks were made using theodolite sightings to steel rulers fixed to the columns.

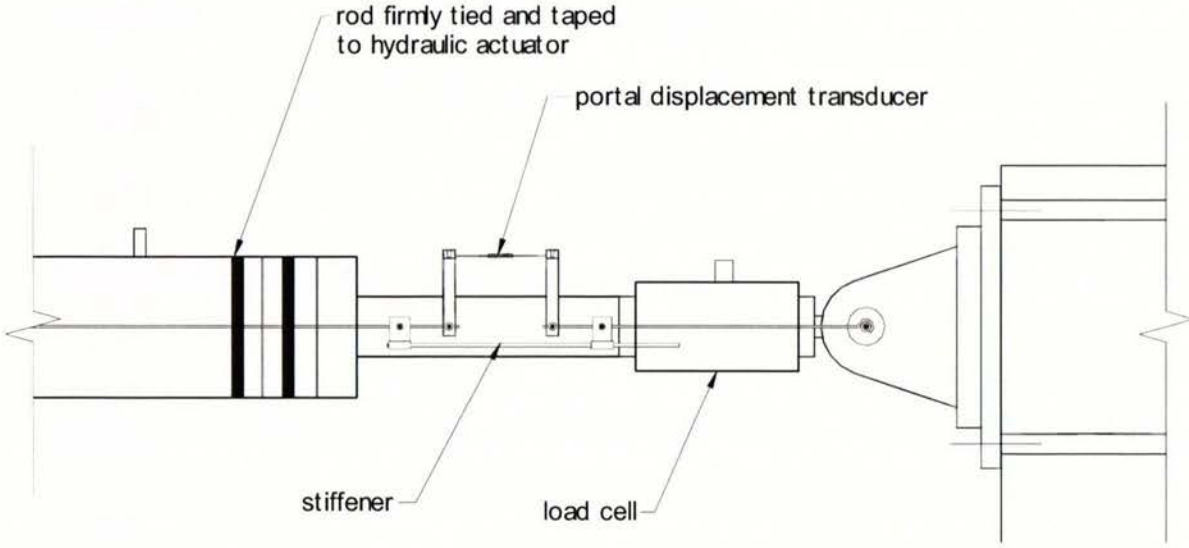

Figure 3.16: Typical placement of portal transducer at top of columns.

Portal transducers were used to measure the displacements of the bottom of the columns (see Figure 3.17). Steel rulers and tapes were used to check against the electronic readings at zero load positions and cycle peaks during testing. In Unit 2, additional portal transducers were mounted to measure the distance between the bottoms of the columns.

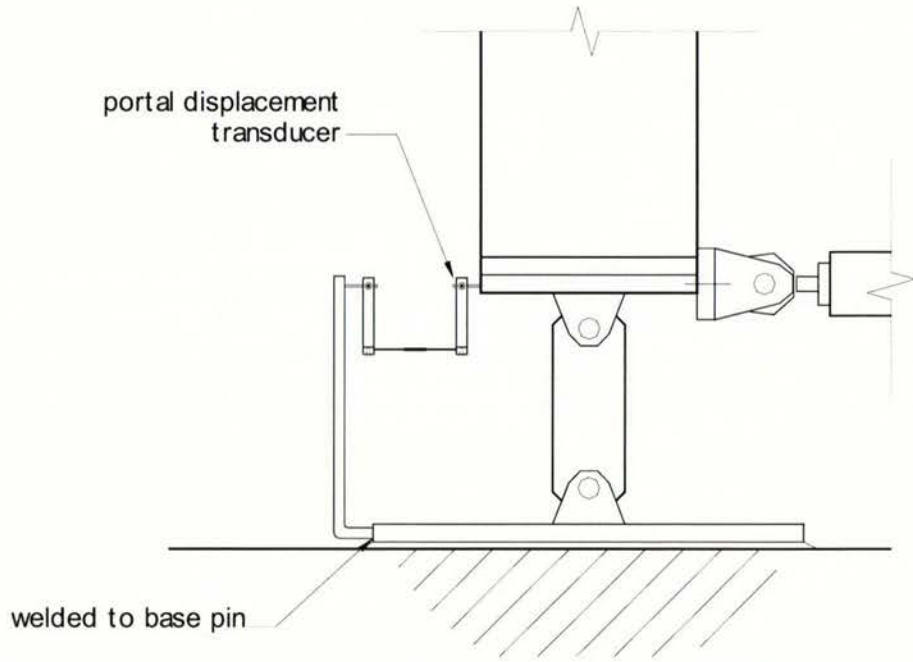

Figure 3.17: Typical placement of portal transducer at bottom of columns.

3.7.3 Measurement of beam elongation

The elongation between the column centrelines for the two internal beams was measured directly using portal transducers as shown in Figure 3.18. Two portal transducers were used to check one against the other during the tests, as well as obtaining an average value for controlling the test (see test procedure in section 3.8). The centres of the beam-column joints contained 12mm reinforcement bars, which had previously been positioned and cast in with the concrete. The 12mm bars were tapped so that aluminium discs could be attached to the bars by screws. Steel rods connected these to the portal transducers. Hooks glued along the beam were used to prevent sagging of the rods (also see Figure 3.19).

In Unit 2, due to the extension of the central transverse beam from column 'B', the aluminium disc could not be placed as in Units 1 and 3. Instead, a steel bar was cast into the transverse beam parallel to the longitudinal beam at mid depth so that the steel rods could be screwed into the bar. This was placed at the level of the mid-depth of the beams underneath the floor, as shown in Figure 3.19. The same arrangement was used to measure the elongation from the centre of each outside column to the respective end of the cantilever beam.

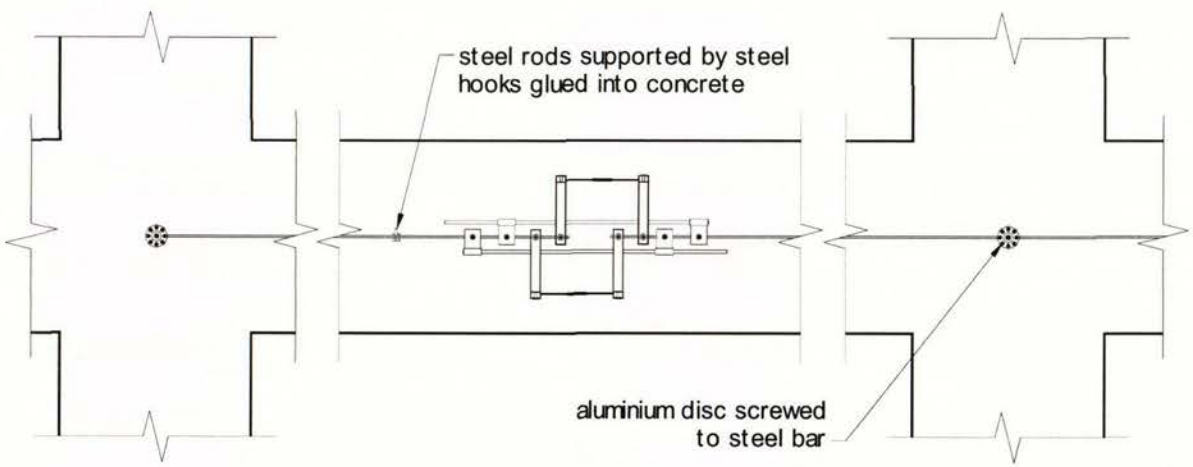

Figure 3.18: Instrumentation to measure direct elongation of beam between beam-column joints.

Figure 3.19: Measurement of elongation in beam, Unit 2.

3.7.4 Measurement of beam deformation

Steel studs were welded to the top and bottom line of the beam longitudinal reinforcement at specified positions after the fabrication of the reinforcement cages. These studs were used for mounting portal transducers. The studs were welded to the reinforcement such that the average strains could be measured as well as preventing studs from being dislodged as the concrete cracks. As illustrated in Figure 3.20, an aluminium disc was screwed to each steel stud and shown in Figure 3.21(b), 4mm rods were attached to the disc and the portal transducers. Prior to casting a grease impregnated tape was wrapped around the studs. These were removed after the concrete was cast to give a clear gap between the stud and the concrete (see Figure 3.20).

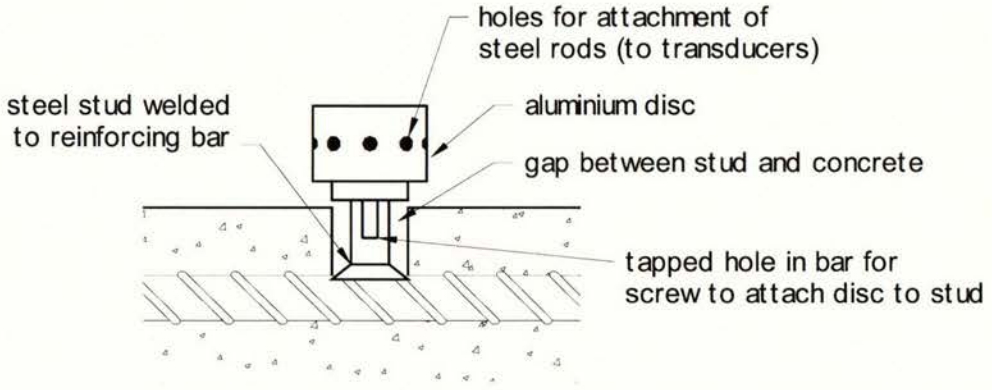

Figure 3.20: Measurement points on beams and columns.

The overall instrumentation scheme on the frame of the test units is shown in Figure 3.21(a). There was change of level at the beam-column face from the difference in the width of the columns to the beams. As shown in Figure 3.21(b), the steel rod was bent in order to allow a transducer to be placed. However, any slippage of beam reinforcement in the beam-column joints could not be effectively quantified and can only be visually observed.

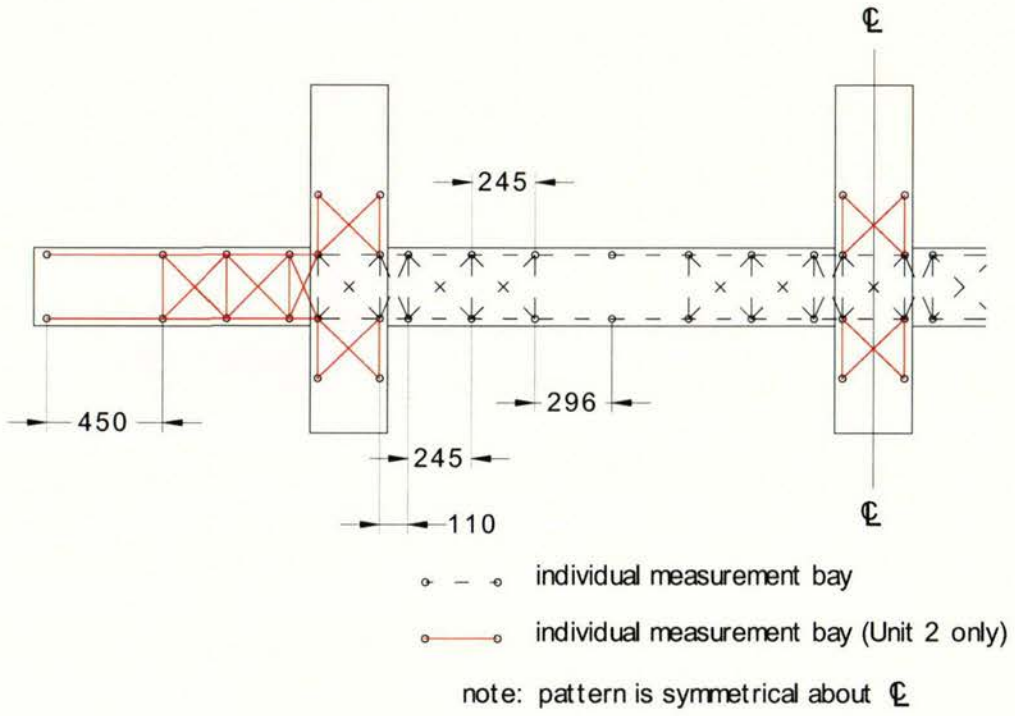

(a) Position of portal transducers on test frame

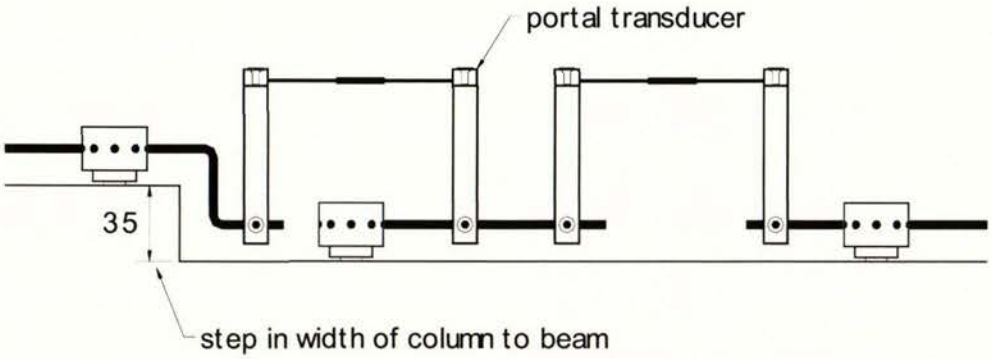

(b) Position of transducers at beam to column interface

Figure 3.21: Positions of portal transducers on test unit frames.

The portal transducers were arranged in a pattern so that the portal readings could be reduced to find the following components of beam deformation:

1. Flexural deformation (or rotation of each segment).
2. Shear deformation (in segments with diagonal gauges).
3. Elongation of the beam.
4. Expansion in depth of beam (in segments with gauges normal to the span of the member).

These deformation components were found from the readings as shown graphically in Figure 3.22. The summation of the components from each segment allows the resultant deformation of the beam to be found. As shown in Figure 3.22(a), pure rotation in this segment affects the length of top and bottom members (ie. members 'a' and 'b'). The effects of shear and depth expansion components on members 'a' and 'b' are typically so small as to be considered negligible, whereas elongation causes equal extension in both gauges. Therefore the rotation, θ, in a segment is given by:

$$\theta = \frac{\delta a - \delta b}{h} \qquad \textit{Equation 3.1}$$

where δa, δb are the changes in length of members 'a' and 'b', and

h is the distance between the top and bottom members.

From Figure 3.22(b), it can be seen that the shear component causes a change in length of the diagonal members. The elongation and depth expansion components cause the members to extend the same amount. Assuming that there is uniform curvature over the length of the gauges, an approximation of shear deformation, S, in one segment can be calculated from:

$$S = \frac{\delta e - \delta f}{2 \cos \alpha} \qquad \textit{Equation 3.2}$$

where δe, δf are the changes in length of members 'e' and 'f', and

α is the angle of member 'f' to the horizontal (equal angle to 'e').

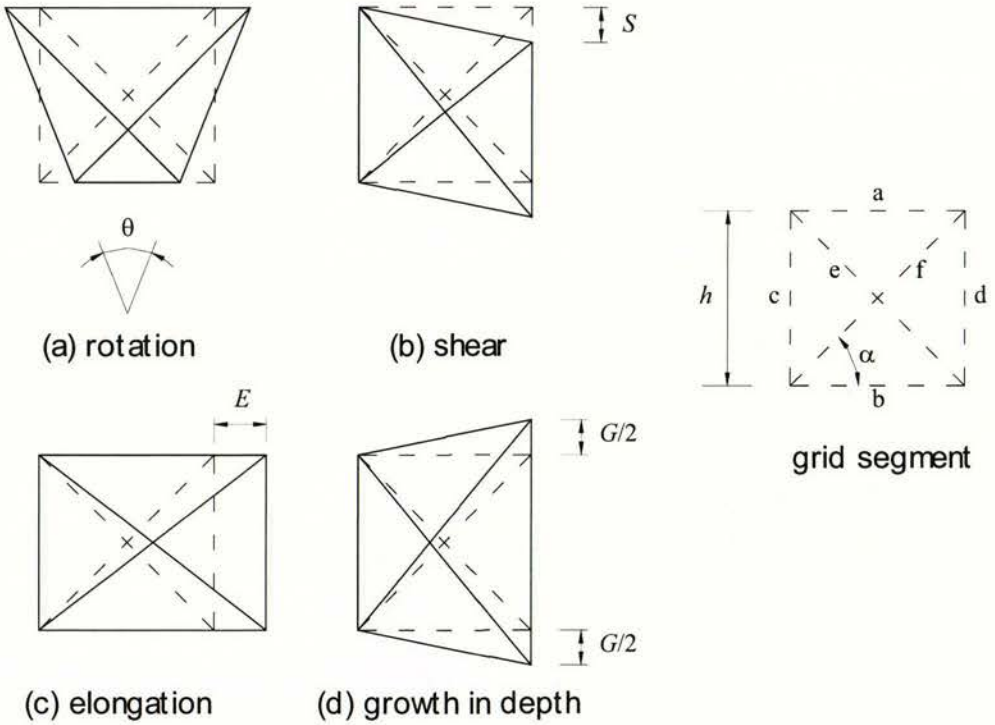

Figure 3.22: Deformation components in a single grid segment.

Elongation causes the top and bottom members to extend the same amount (Figure 3.22(c)) while rotation causes one of the members to extend while the other contracts. Shear and depth expansion have negligible effect to these members. Therefore the elongation in the segment, *E*, is given by the average change in length of the top and bottom members, as given by *Equation 3.3*:

$$E = \frac{\delta a + \delta b}{2} \qquad \textit{Equation 3.3}$$

As shown in Figure 3.22(d), the depth expansion, *G*, is given by the change in length of the vertical member:

$$G = \delta d \qquad \textit{Equation 3.4}$$

where δd is the change in length in the member 'd'.

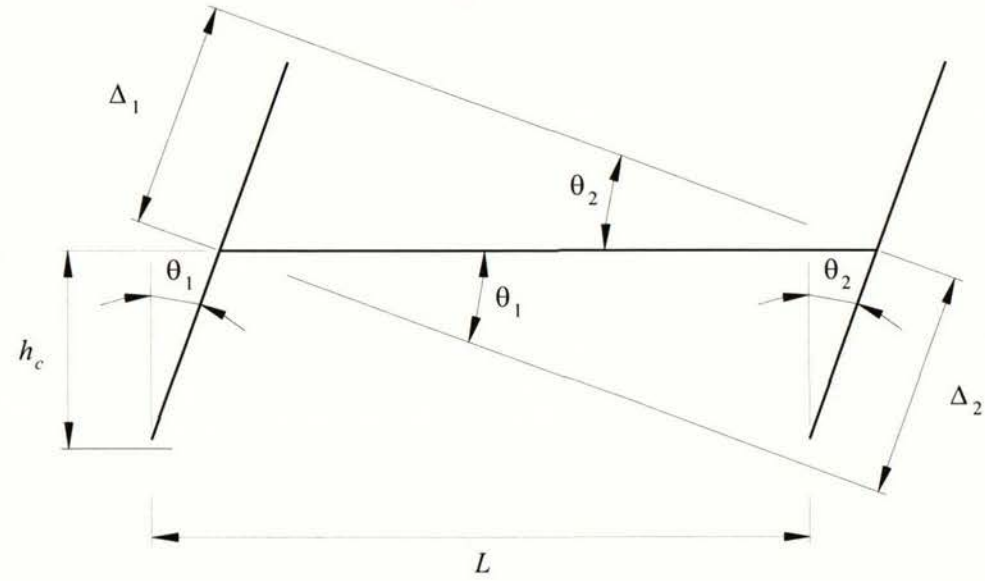

(a)

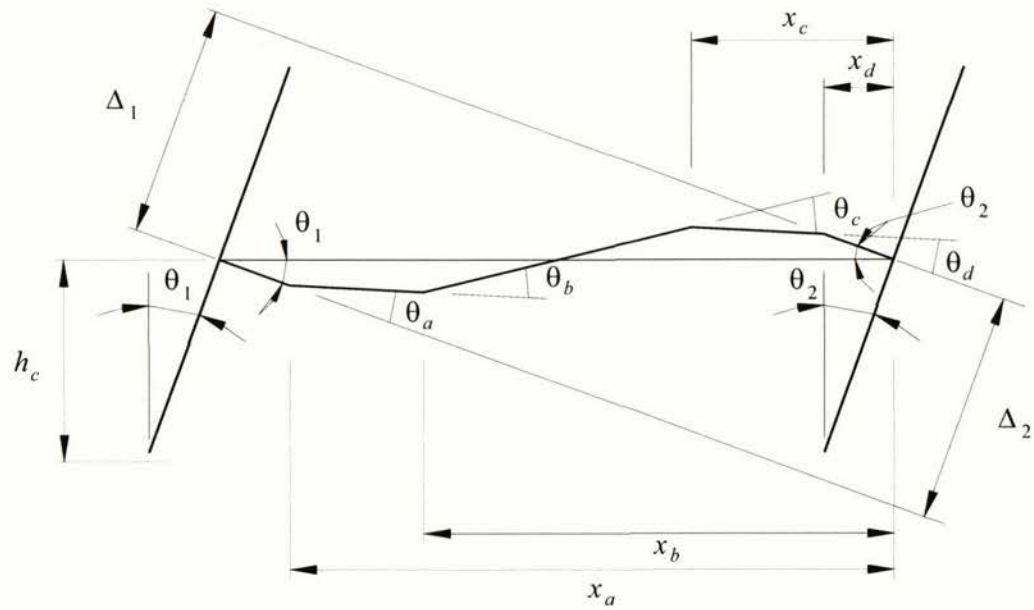

(b)

Figure 3.23: Elongation and flexural deformation component of mid-span deflection in each bay.

The lateral deflection of each bay due to flexural deformation and elongation can be calculated. Assuming that the columns are rigid, the lateral deflection of the mid-span of the bay is given by *Equation 3.5* and illustrated by Figures 3.23.

$$\delta_{fl} = \frac{(\theta_1 + \theta_2)h_c}{2} \qquad \textit{Equation 3.5}$$

where δ_{fl} is the lateral deflection at mid-span of the bay,

θ_1 and θ_2 are the rotations of the columns, and

h_c is the height of the column from the base to the beam centreline.

Referring to the geometry in Figure 3.23(a), the column rotations are given by:

$$\text{(a)}\ \ \theta_1 = \frac{\Delta_2}{L} \qquad \text{and} \qquad \text{(b)}\ \ \theta_2 = \frac{\Delta_1}{L} \qquad \textit{Equations 3.6}$$

where Δ_1 and Δ_2 are as shown in Figure 3.23(a), and

L is the distance between the column centres.

The rotation of the discrete segments (see *Equation 3.1*) can be used to calculate Δ_1 and Δ_2, as shown in Figure 3.23(b), and are given by *Equation 3.7*.

$$\text{(a)}\qquad \Delta_2 = \theta_a x_a + \theta_b x_b + \theta_c x_c + \theta_d x_d \qquad \textit{Equations 3.7}$$

$$\text{(b)}\qquad \Delta_1 = \theta_a (L - x_a) + \theta_b (L - x_b) + \theta_c (L - x_c) + \theta_d (L - x_d)$$

where θ_n is the rotation of segment n, and

x_n is the distance from column centre to the centroid of each segment 'n'.

The lateral deflection of the mid-span of each bay due to shear deformation of the beam can be calculated from summing the beam shear deformations of each segment. From consideration of Figure 3.24, the lateral deflection due to shear, δ_s, is given by *Equation 3.8*.

$$\delta_s = \frac{(S_a + S_b + S_c + S_d)h_c}{L} \qquad \textit{Equation 3.8}$$

where S_n is the shear deformation of segment n given by *Equation 3.2*.

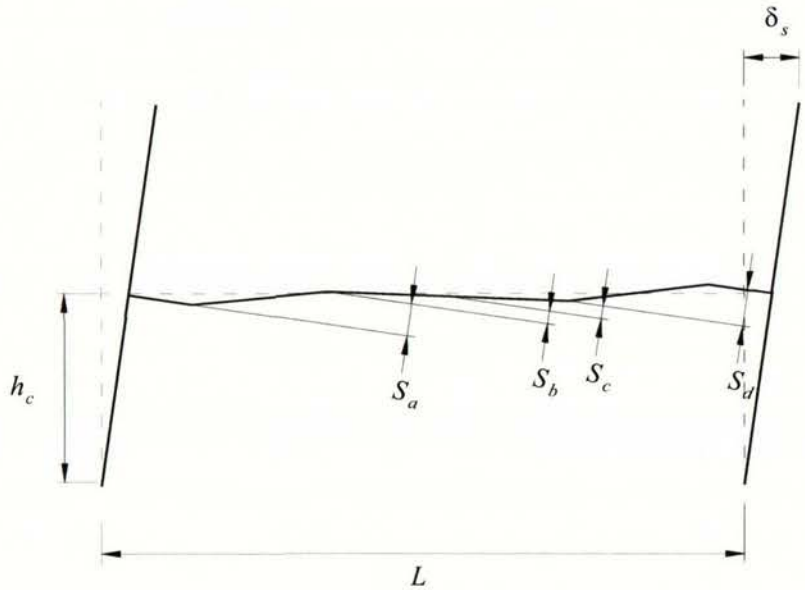

Figure 3.24: Shear component of mid-span lateral deflection of each bay.

Portal transducers were added to the columns immediately above and below the beam-column joint zone for Units 2 and 3. These gave additional information on the flexural and shear deformations at these regions. The equations below give the lateral displacement of a column between the top and the bottom of the column. The displacements at the top of the columns measured from the test can be compared against the interpolated flexural and shear components of lateral deflection in the bays (given by *Equations 3.5 - 3.8*) together with the average lateral displacement of the columns.

Figure 3.25 shows the flexural component of the lateral deflection of a column. The flexural component of lateral displacement at the top relative to the bottom of the column, l_{fl}, is given by:

$$l_{fl} = \theta_T d_T + 2(\theta_C h_c) + \theta_B d_B \qquad \textit{Equation 3.9}$$

where θ_N is the rotation of the segment N as shown in Figure 3.25,

d_T is from the centroid of segment to the top of column,

d_B is from the centroid of segment to the bottom of column, and

h_c is the height to the top/bottom of column from the centre of column.

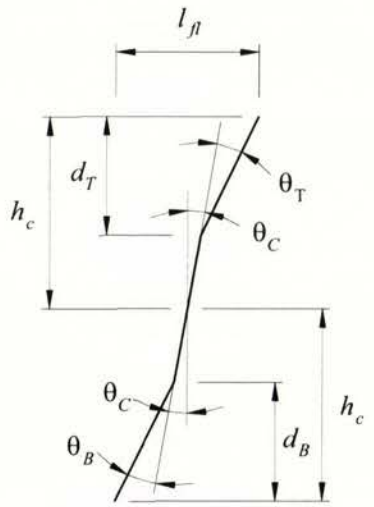

Figure 3.25: Flexural component of lateral deflection of column.

The shear component of lateral displacement, ℓ_s, is given by the sum of the shear deformation measured directly in each segment.

$$\ell_s = S_T + S_C + S_B \qquad \textit{Equation 3.10}$$

where S_N is the shear deformation in segment N given by *Equation 3.2*

3.7.5 Measurement of floor deformation in Unit 2

Portal transducers were attached to rods, which were epoxied into the slab at the ends of the first two rows of precast ribs. This was done to obtain a history of the cracking that was likely to occur at these locations. DEMEC points were placed along the entire length of the floor in a triangular pattern. This enabled local shear movement between the floor and the frame to be measured. Figure 3.26 shows the scheme of measurement points placed on the floor.

The DEMEC gauges were spaced at 200mm apart. The wider spaced gauges further from the frame were measured using a Vernier scale. Three separate DEMEC reference gauges were measured each time measurements were taken in order to allow corrections to be made for thermal strains. The localised shear movement in each triangular DEMEC arrangement (Figure 3.27) was determined in the following way:

(a) $X = X_0 + \Delta X$

where X is the measured distance as shown in Figure 3.27,

X_0 is the initial measurement, and

ΔX is the change in the distance.

(b) $Y = Y_0 + \Delta Y$

(c) $Z = Z_0 + \Delta Z$ *Equations 3.11*

And:

$$\theta_X = \cos^{-1}\left(\frac{Z^2 + Y^2 - X^2}{2ZY}\right) \quad \textit{Equation 3.12}$$

$$\theta_{X2} = \pi - \theta_X \quad \textit{Equation 3.13}$$

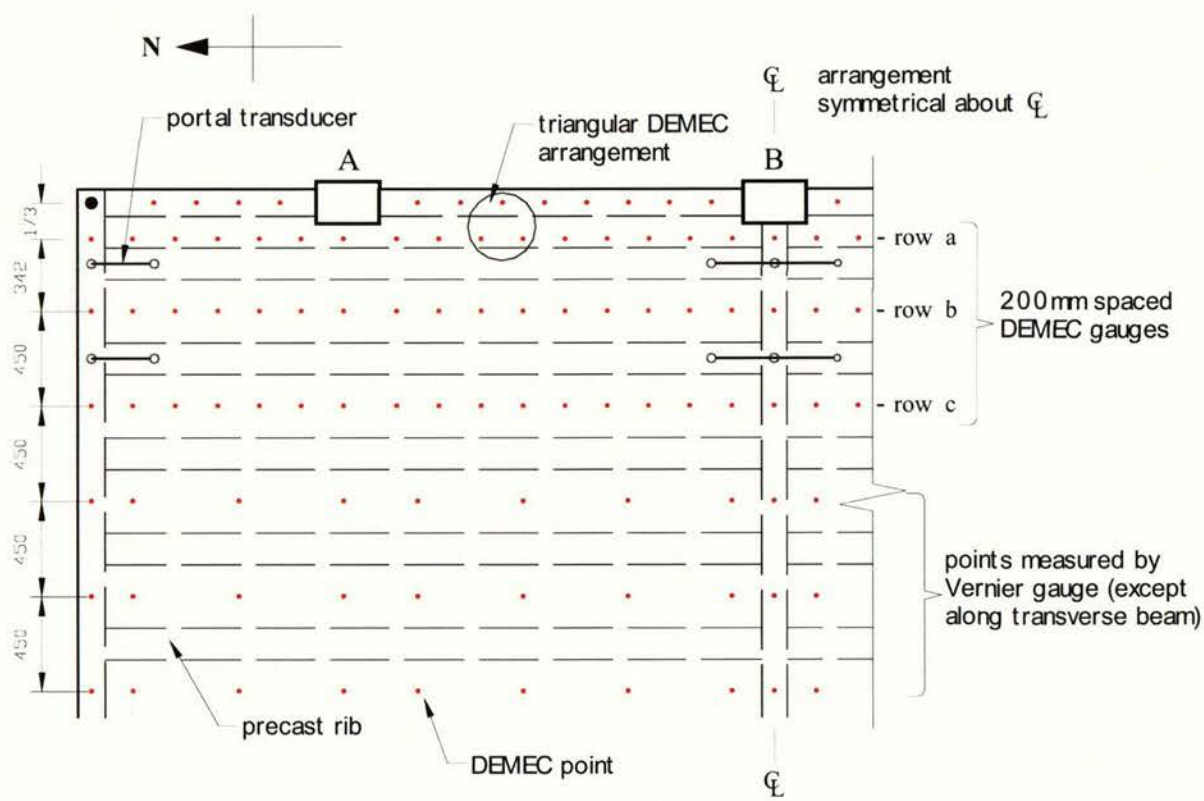

Figure 3.26: Scheme of measurement and instrumentation of floor of Unit 2.

Once the geometry of the deformed shape has been determined from the data and *Equations 3.10-13* the unknown displacements, u_1 and u_2 can be found using *Equations 3.14 and 3.15.*

$$u_1 = Y\cos\theta_{X2} \qquad \textit{Equation 3.14}$$

$$u_2 = Y\sin\theta_{X2} - h_d \qquad \textit{Equation 3.15}$$

where h_d is the distance shown in Figure 3.27.

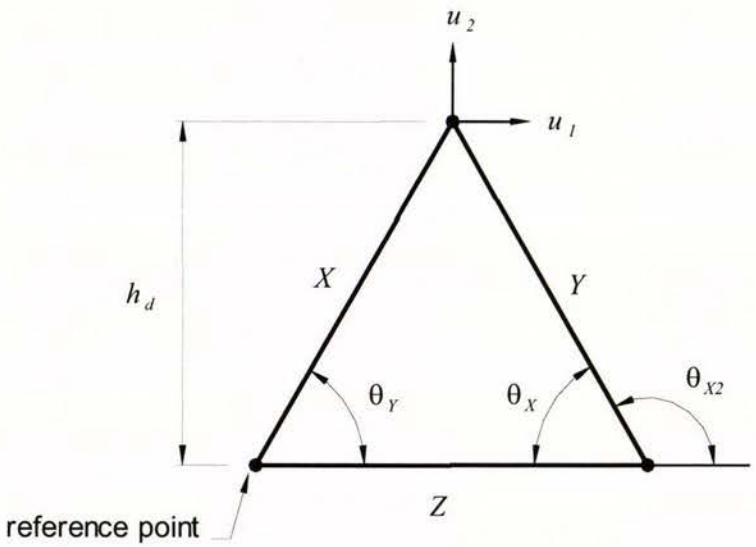

Figure 3.27: Geometry of triangular DEMEC arrangement.

3.8 Testing Procedure

Loads were applied at the top and bottom of columns to induce moments into the beams. It was important that the displacement of the three columns would remain parallel to one another during the test, as the columns in levels above the first storey of a building would remain relatively parallel as the building displaces during an earthquake. The procedure was also designed to minimise any restraining forces into the beams as these could influence the strength and elongation.

After completing the test for Unit 1, as mentioned in *Section 3.6*, the loading arrangement was re-designed. Therefore the procedure for testing was modified to suit. The following subsections describe the plan for the testing of both units.

3.8.1 Procedure for testing Unit 1

The unit was loaded up to approximately 3/4 of the design strength of the frame (based on design strength of beam section shown in Table 3.1) for two cycles. By linear extrapolation of the column displacement at this point, the ductility 1 displacement was determined. Two complete load cycles were then applied to give displacement ductilities of two, four and six. The planned lateral displacement sequence for the test is shown in Figure 3.28. As shown on the figure, for example the expression '+2Di' represents the peak displacement to first cycle in the positive direction to ductility 2, and '-4Dii' represents second cycle in the negative direction to ductility 4 (ie. +/- sign indicates direction, the number and 'D' indicates ductility displacement and the letter indicates the i^{th} cycle). Columns 'A', 'B' and 'C' were loaded and readjusted at a 1:2:1 ratio respectively, while adjustments were made to keep the columns parallel to one another. As the actuators were connected in a single line at the top of the columns, the load reading at column 'A' represented the total load on the unit. The difference of the load readings at column 'B' and 'C' represented the actual load on column 'B'.

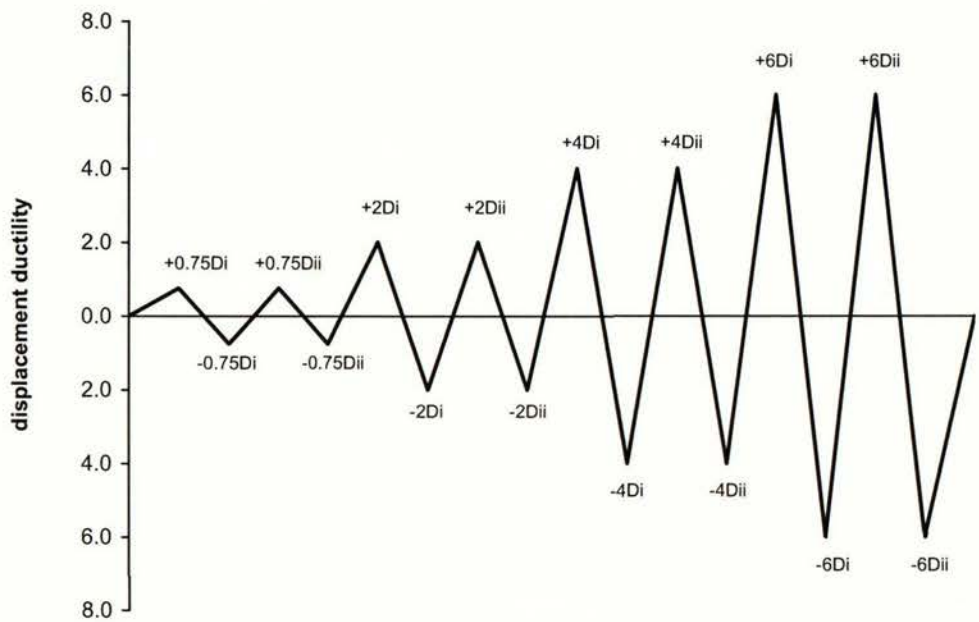

Figure 3.28: Planned displacement history for Unit 1

At least 20 load increments were taken to reach each peak displacement. For each load increment, the top of the columns were loaded to the target ratios. Then a scan of the readings was taken. Following this, the bottom actuators (external columns) were adjusted from the displacement at the top, such that the columns were parallel. The following equations were used:

$$b_A = t_{AB} + b_B \qquad \textit{Equation 3.16}$$

where b_A is the displacement reading at the bottom of column 'A',

b_B is the displacement reading at the bottom of column 'B', and

t_{AB} is the displacement reading of the displacement between the top of columns 'A' and 'B'.

Similarly:

$$b_C = t_{BC} + b_B \qquad \textit{Equation 3.17}$$

where b_C is the displacement reading at the bottom of column 'C',

b_B is the displacement reading at the bottom of column 'B', and

t_{BC} is the displacement reading of the displacement between the top of columns 'B' and 'C'.

After making adjustments to the bottom actuators, the load ratio at the top changed. This process was repeated until a satisfactorily small difference was achieved. At this stage the readings from the portal gauges and load cells were scanned and saved.

3.8.2 Procedure for testing Units 2 and 3

Unit 2 could not be loaded in the same way as Unit 1. This was due to a number of factors. Firstly, the loading arrangement and the instrumentation of the critical displacements had been modified. Secondly there was no way of determining the actions in the unit, therefore the columns could not be loaded at a pre-determined ratio. Thirdly, the point of first ductility could not be accurately calculated, since the yield strength of the unit could not be found due to uncertainty about the interaction of the

frame and diaphragm. Therefore, it was decided that this unit was to be displaced to predetermined interstorey drift levels. Unit 3 was also tested in a similar way as Unit 2.

For the initial elastic cycles, the unit was displaced to 0.1% interstorey drift for at least two cycles, and then up to 0.2% for another two cycles. Then the unit was displaced up to 0.5% interstorey drift. Two displacement cycles for each target drift level were taken and in increments of 0.5% drift until there was substantial falling off in performance.

The columns were loaded to a target displacement at each loading step. For each step within a cycle, not more than one-twentieth of the target displacement was imposed. Each column was displaced to:

(a) $t = t_A + b_A$

(b) $t = t_B + b_B$

(c) $t = t_C + b_C$ *Equations 3.18*

where t is the target displacement,

t_N is the displacement reading at the top of column N (=A, B or C), and

b_N is the displacement reading at the bottom of column N.

Then the bottom actuators were adjusted, such that the distance between the bottoms of the columns were equal to the average of the elongation of the beam in the respective bays. The following equations were used:

$$b_A = e_{AB} + b_B \qquad \textit{Equation 3.19}$$

where b_A is the displacement reading at the bottom of column 'A',

e_{AB} is the average elongation of the beam between columns 'A' and 'B',

b_B is the displacement reading at the bottom of column 'B'.

And:

$$b_C = e_{BC} + b_B \qquad \textit{Equation 3.20}$$

where b_C is the displacement reading at the bottom of column 'C',

e_{BC} is the average elongation of the beam between columns 'B' and 'C',

b_B is the displacement reading at the bottom of column 'B'.

This process was repeated until the errors were marginal. At each step the data was saved on file. This procedure was much easier in comparison to the procedure used for Unit 1, as the actuators were decoupled and as a result, changes made in any one of the actuators did not affect the others to a large extent. The new data acquisition programme also enabled the values given by *Equations 3.18-20* to be calculated simultaneously.

Chapter 4

Test Results of Unit 1

4.1 Introduction

This chapter presents the results from the testing of the plane frame unit, Unit 1. It contains general description of the crack patterns, load versus deflection characteristics, flexural and shear deformation and the elongation which developed in the beam members.

4.2 Displacement History

It had been intended to follow the loading sequence set out in *Section 3.8.1*. However, the displacements were recorded from the top of column 'A' instead of column 'B', which was the originally planned location. As a result of beam elongation, the exterior columns (columns 'A' and 'C') moved outwards, and this led to greater displacements being imposed on these columns than had been intended. The actual displacement history measured for column 'B' is shown in Figure 4.1 (the figure shows the intended displacement steps eg. +2Di, +4Di etc. and the actual drift displacement). As indicated in the figure, it was displaced up to a maximum of 5.9% interstorey drift in the positive direction, compared against 2.9% drift the other direction.

The controlling displacement should have been the difference in the lateral displacements of the top and the bottom of column 'B'. However, this would have been difficult to achieve with the test arrangement that was used, as the hydraulic actuator at column 'B' was coupled to column 'A'. In light of the difficulties encountered in this test, modifications were made to the test arrangement and procedure used for Units 2 and 3. As indicated by Figure 4.2, the columns were adequately parallel to one another throughout the test. The lateral displacement at any load stage was taken as the difference in displacement of each column measured between the lateral support and load points for the individual column (ie. between the top and bottom of column where

the actuator loads were applied as shown on Figure 3.10 of *Chapter 3*). The largest out of parallel between the columns throughout the test was 1.6mm during the cycle to +5.9% interstorey drift.

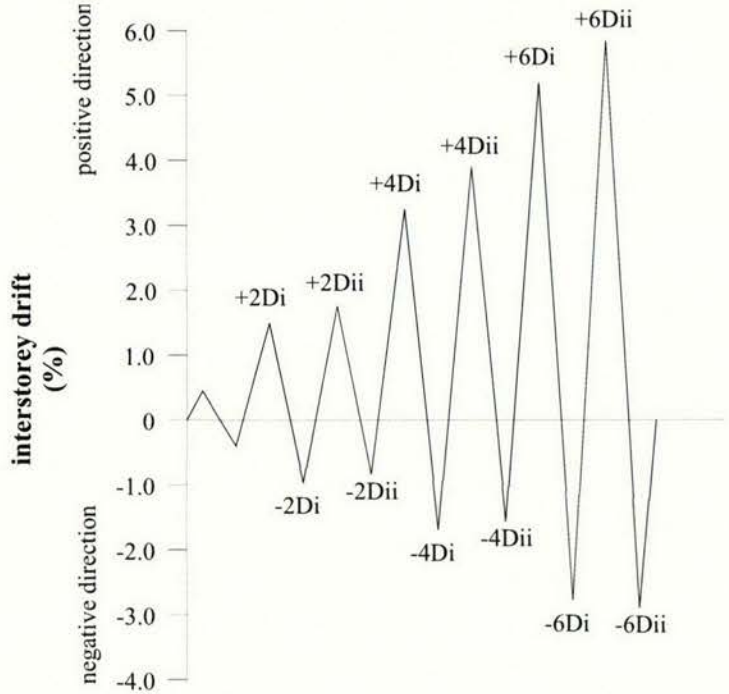

Figure 4.1: Actual displacement sequence applied to Unit 1.

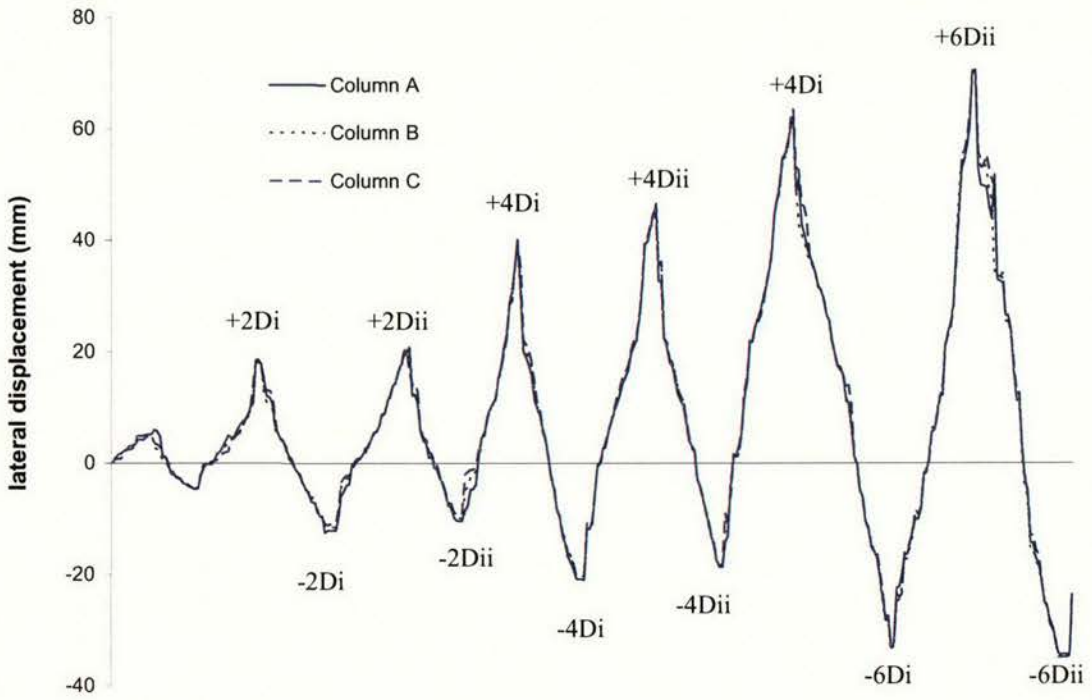

Figure 4.2: Lateral displacement history of columns.

4.3 General Behaviour and Observations During Test

The duration of the test was seven days. Early in the test a fault was found with the hydraulic hose fitting connected to the hydraulic actuator attached to column 'A'. The movement in the hydraulic cylinder was very small with large build up in pressure at the pumps. There was a sudden release of this pressure to the actuator, and as a result the frame was laterally displaced up to 9.5mm. This movement exceeded the yield displacement of the unit, described in *Section 4.4*. As a result, the test unit would have sustained a limited amount of damage in that it is expected that the initial stiffness was reduced. The unit was brought back to its zero position, actuator pressures released and the test was restarted.

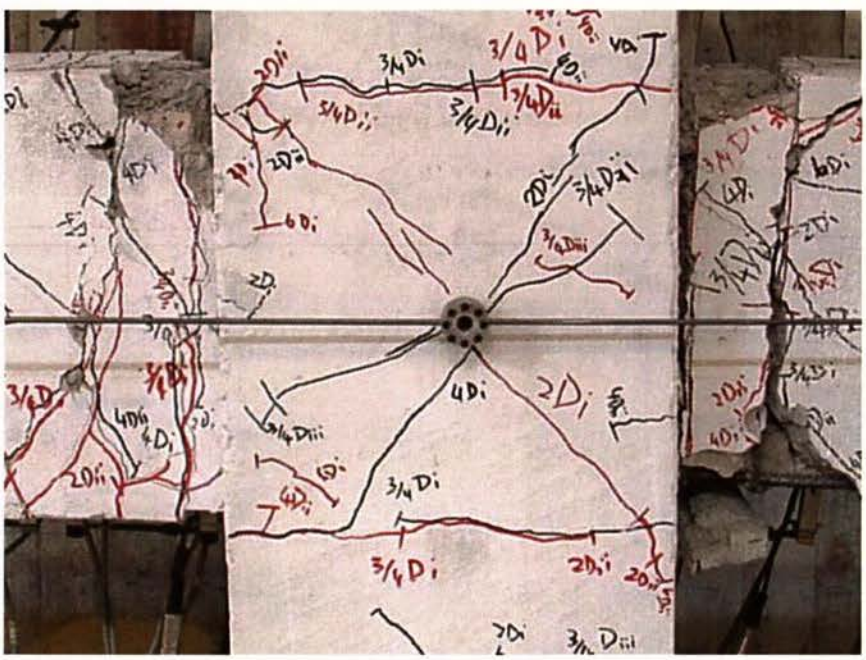

Figure 4.3: Central beam-column joint at the end of test.

At the end of the elastic cycles (up to 0.45% drift), fine flexural cracks were identified at the column faces and potential plastic hinge zones. There were six fine cracks less than 0.1mm wide on the tension side of the central column and two flexural cracks on each of the outside columns. As shown by Figure 4.3, a diagonal shear crack at about 45°, which was less than 0.1mm wide formed within the beam-column region of the central column during the second elastic positive half cycle. As shown in Figure 4.3, further diagonal cracking developed during the displacement to +1.8% and -0.8% drift

(+2Dii and -2Dii on Figure 4.3, where 'i' represents the first cycle at the target displacement, and 'ii' represents the second cycle). At no time did these diagonal cracks exceed 0.4mm in width. The three columns appeared to remain elastic throughout the test with only fine cracks measuring at a maximum of 0.5mm wide. At the peak displacement to +5.9% drift half cycle (intended +6Dii), six flexural cracks had formed on the tension sides of the central column.

Cracking in the beams was mainly confined in the plastic hinge zones, with only minor cracking occurring in the mid-span regions. Inclined diagonal shear cracking occurred near the column faces, which appear to initiate at the first and second stirrups in the beam. In the plastic hinge zone just to the right of the central column, these cracks were almost vertical and diverted to about 45° at the top and bottom of the beam. For the other plastic hinges, these cracks were approximately 70° to the horizontal through the middle third of the depth the beam but were inclined at about 45° above and below this zone. The development of these cracks is shown in Figure 4.4(a) to (b) for the plastic hinge zone located to the left of the central column. The black lines indicate cracks that opened or grew in length as the unit was loaded in the positive direction (southwards). The red lines indicate cracks formed in the negative direction. Also shown in these figures are the greater progressions of the black crack lines compared against the red crack lines as larger rotations were sustained by the plastic hinges in the positive direction of loading.

As Figure 4.5(a) shows, a 2mm wide crack formed near the column face at +1.5% drift (intended +2Di). This figure also shows cracking of the beam at the column face. By the end of the displacement to +3.9% drift cycles (intended +4Dii), this crack developed further to show signs of a possible pull out of top reinforcement bars from the joint. The strength of test unit decreased to 80% of its maximum value during displacement to +5.9% drift (intended +6Dii) when the beam longitudinal reinforcement slipped through the central beam-column joint, as shown in Figure 4.5(b).

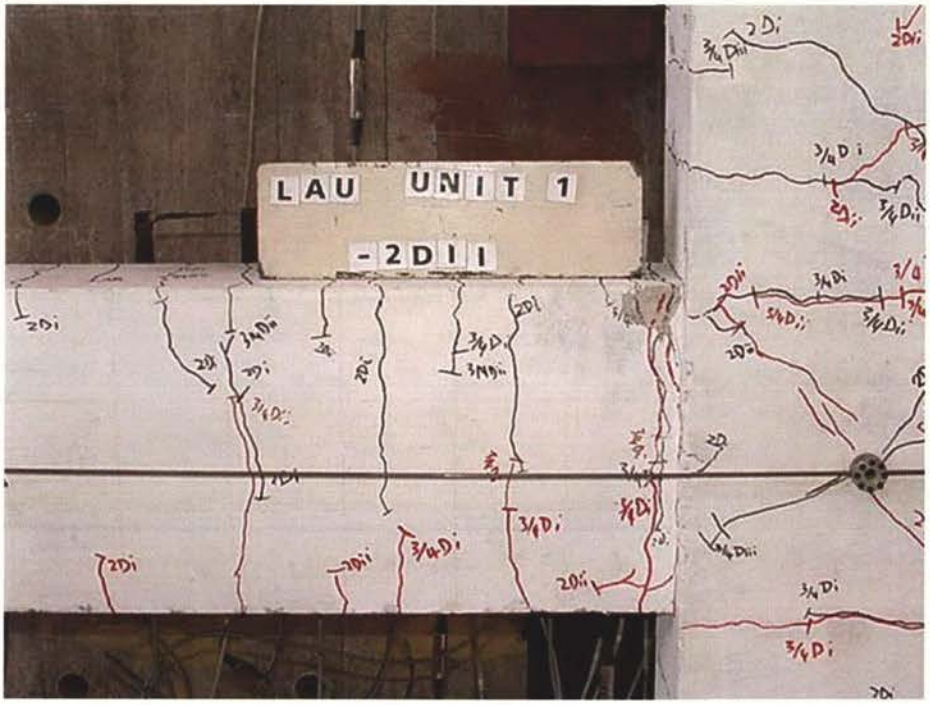

(a) At -0.8% drift

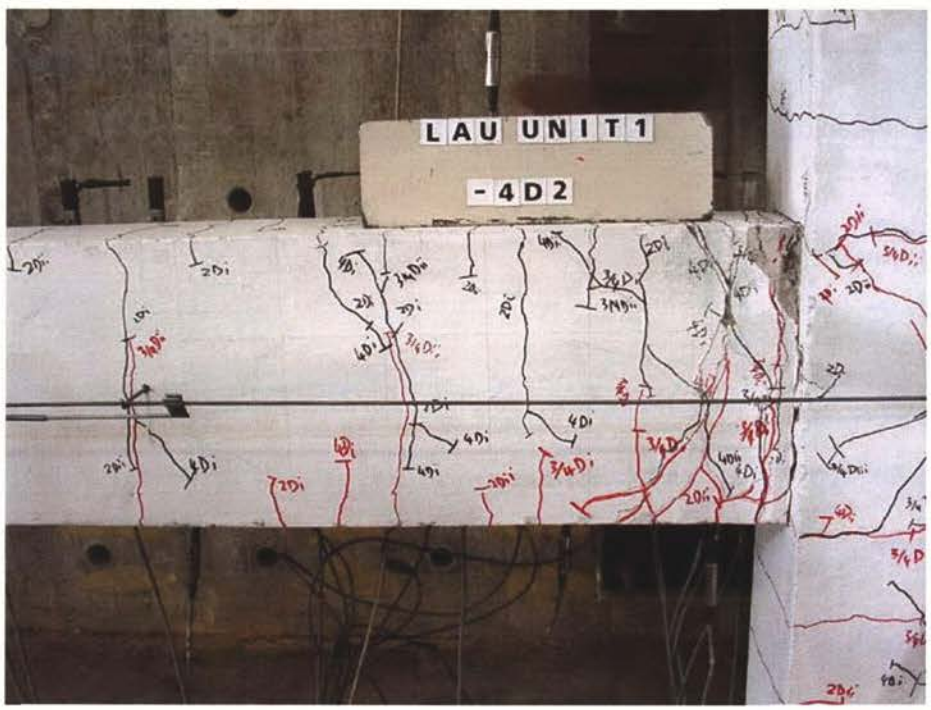

(b) At –1.6% drift

Figure 4.4: Progression of cracking in plastic hinge zone to the left of the central column (column 'B').

(a) At +1.5% drift

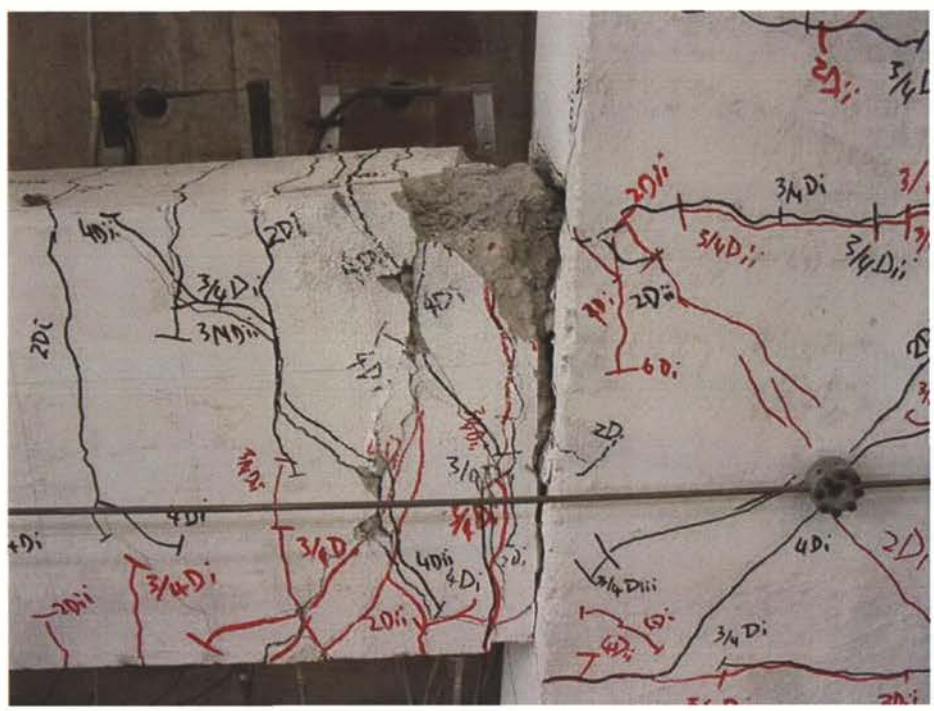

(b) At +5.9% drift

Figure 4.5: Cracking near column face of the central column.

4.4 Force versus Displacement Response

This section describes the force versus displacement response of the unit, as well as the response of each of the columns.

4.4.1 Overall unit response

Lateral forces of up to a maximum of 67.4kN were applied to the unit in the elastic cycles, which corresponded to 64% of the calculated theoretical lateral strength of 105.4kN (see section A1.5, *Appendix 1*). This was calculated based on the beam flexural strengths shown in Table 3.1 in *Chapter 3*. Figure 4.6 shows the force versus displacement response for the third elastic cycle in terms of the sum of the lateral load applied (load on main loading actuator at column 'A') against the lateral displacement at the top of column 'A'.

The extrapolated ductility 1 displacement was extrapolated as 8.1mm in the positive direction and 7.7mm in the negative direction, which corresponds to interstorey drifts of 0.68% and 0.64% respectively. The actual yield displacement would have been less, as the stiffness of the unit was reduced after the unplanned displacement that was applied at the beginning of the test (see *Section 4.2*). There seemed to be approximately 1mm of movement at low lateral force level or on changeover of loading direction. This movement could be attributed to the slack in the pins at the base of the columns.

The lateral force versus displacement response for the test unit is shown in Figure 4.7 (data included in *Appendix 3*). Part (a) of this figure shows the total lateral force plotted against the absolute displacement at the top of column 'A' (ie. measured displacement between the top of column 'A' and a stationary reference point), while Figure 4.7(b) is the total lateral force versus the average of the relative lateral displacement between the top and bottom of the three columns. The maximum lateral force in both directions of loading for the ductility 2 cycles was 115kN, which corresponds to 1.09 times the theoretical strength.

The maximum lateral force was 133kN (1.26 times theoretical strength) at +5.2% drift in the positive direction and 132kN (1.24 times theoretical strength) at -1.7% drift in the

negative direction of loading. Some pinching of the force versus displacement curve at the –1.6% drift half cycle (-4Dii) was noted. At this stage it was noticed that diagonal cracks had increased in width coupled with the spalling of cover concrete, particularly in the plastic hinge just to the right of the central column.

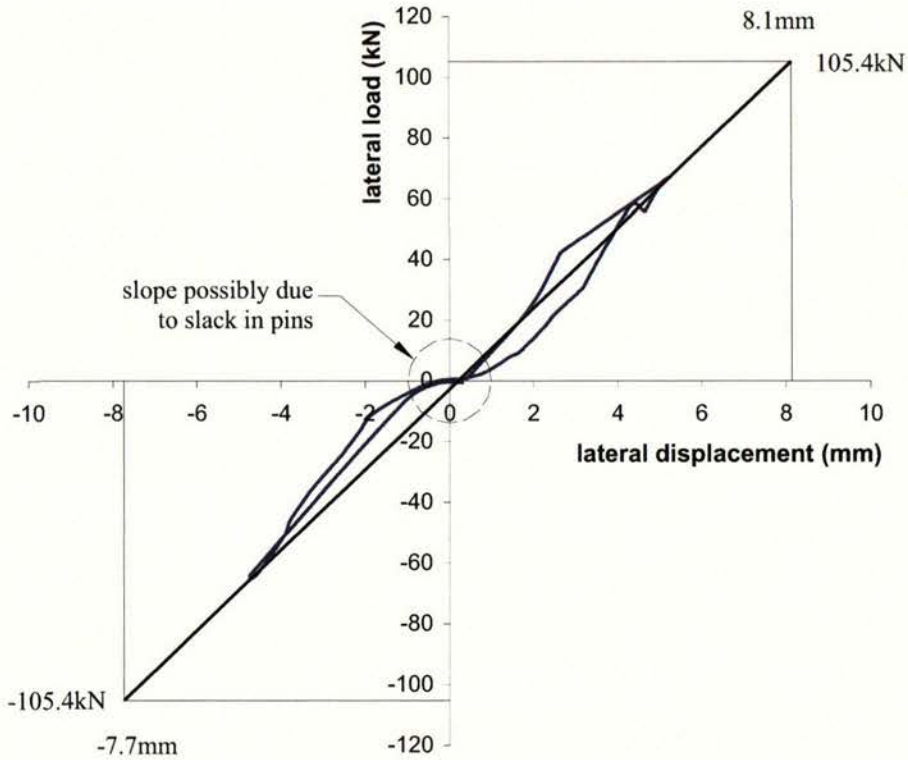

Figure 4.6: Elastic range total lateral force on frame against displacement at top of column 'A'.

The unit failed to reach 80% of the maximum strength in the final displacement cycle (+5.9% drift). The unit failed by loss of bond of the longitudinal beam bars in the central beam-column joint. At this stage, most of the cover concrete in the plastic hinges had spalled, revealing the main reinforcement. The reinforcement did not buckle greatly even though large rotations had been induced.

The differences in the sum of the lateral force applied at the top of the columns and the sum of the lateral forces resisted at the column bases at different stages of the experiment were small. This is shown by Table 4.1. The difference between the sum of the top and bottom lateral forces were typically 1 to 5 percent. At lower loads (between 10 to 30kN), the difference between the forces were typically 5 to 15 percent.

Table 4.1: Difference in sum of force applied to top and bottom of columns at peaks of displacement cycles.

displacement ductility, D	load at top (kN)	load at bottom (kN)	difference (kN)	difference (%)
at 0.64 of theoretical strength	67.1	65.0	2.1	3
	-65.1	-60.6	-4.5	7
2D	95.2	94.5	0.7	1
	-108.3	-102.6	-5.7	5
4D	128.9	129.9	1.0	1
	-124.4	-121.6	-2.8	2
6D	127.4	132.7	5.3	4
	-120.5	-121.6	-1.1	1
Note: Values are for 1st cycle of displacement step.				

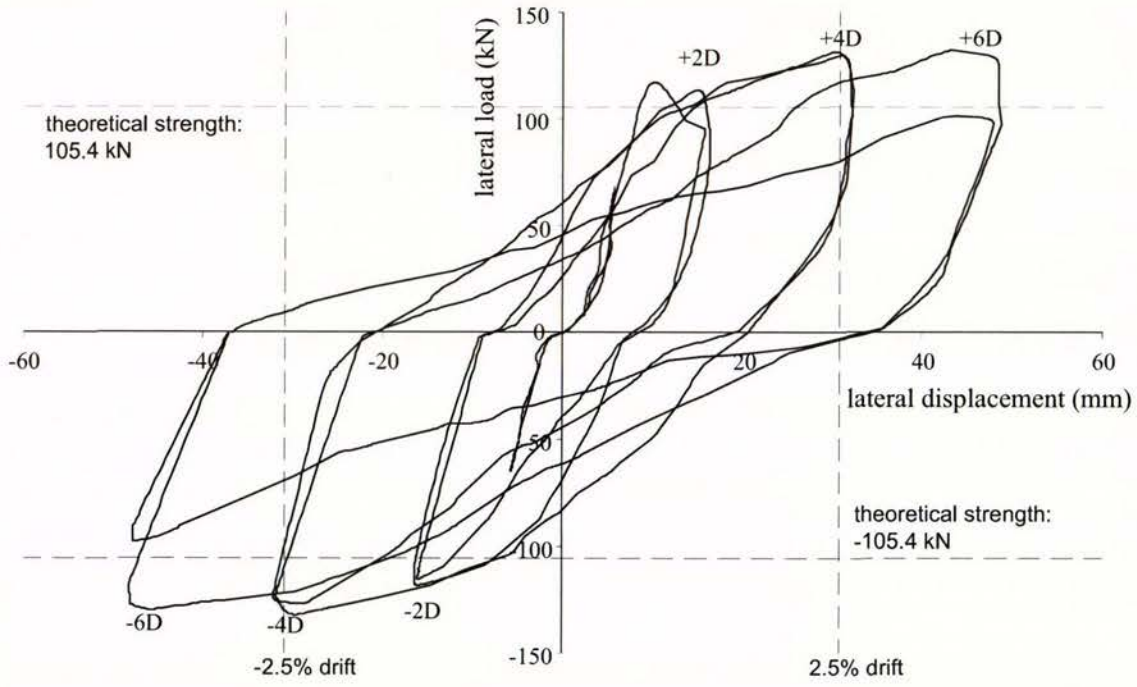

(a) Total lateral force versus load point absolute displacement of column 'A'

Figures 4.7: Total lateral force versus displacement at top of Column 'A'. (continued)

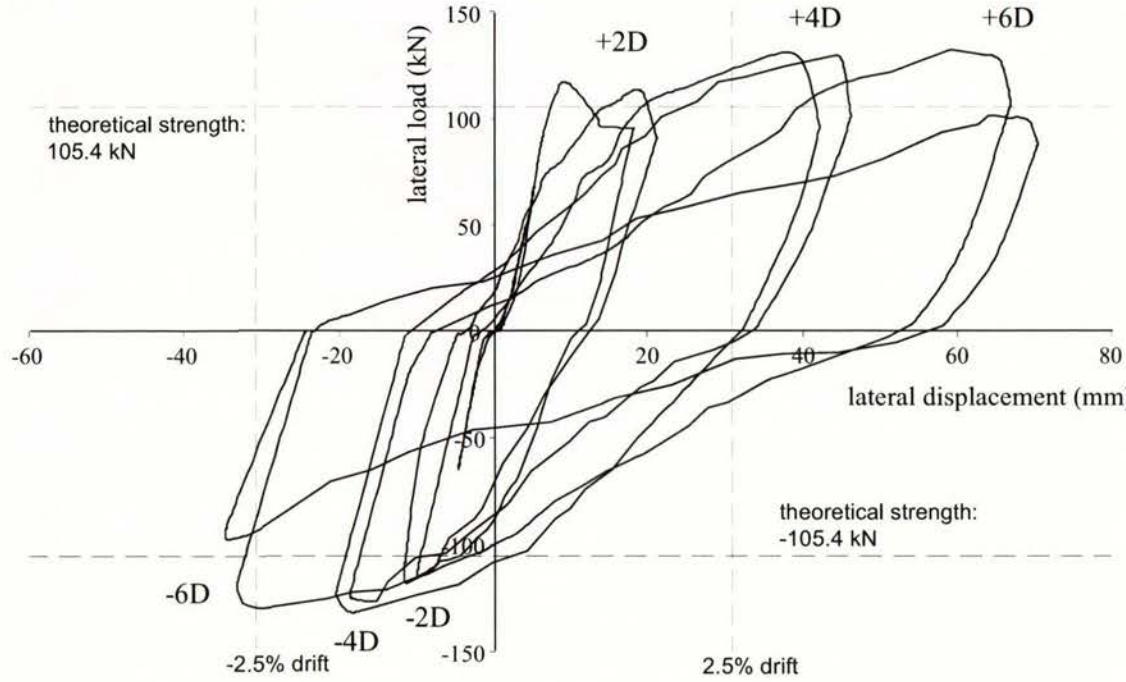

(b) Total lateral force versus average relative displacement

Figures 4.7: Total lateral force versus displacement at top of Column 'A'. (concluded)

4.4.2 Individual column response

The force versus displacement response for each column is presented in Figures 4.8. The forces plotted are those applied at the top of each corresponding column and the displacements are the relative lateral displacements measured between the top and bottom of each column. The irregularity of the plots is due to the nature of the test procedure, which involved very frequent adjustments to the loading equipment and also due to the relaxation of forces in the hydraulic actuators during the period when the displacement measurements were recorded.

It can be seen from Figure 4.8(a), (b) and (c) that in the cycle to +1.5% drift (+2Di), the beams, particularly around joints 'A' and 'C', responded elastically to reach the maximum load, followed by degradation in strength prior to reaching the peak displacement of that cycle.

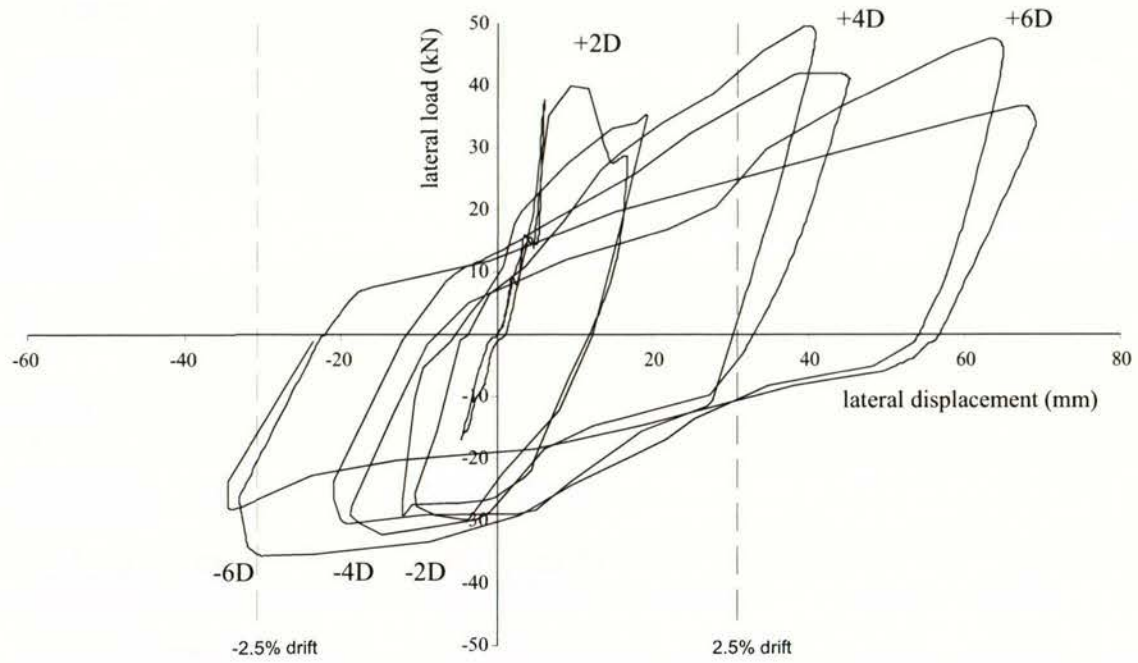

(a) Column 'A'

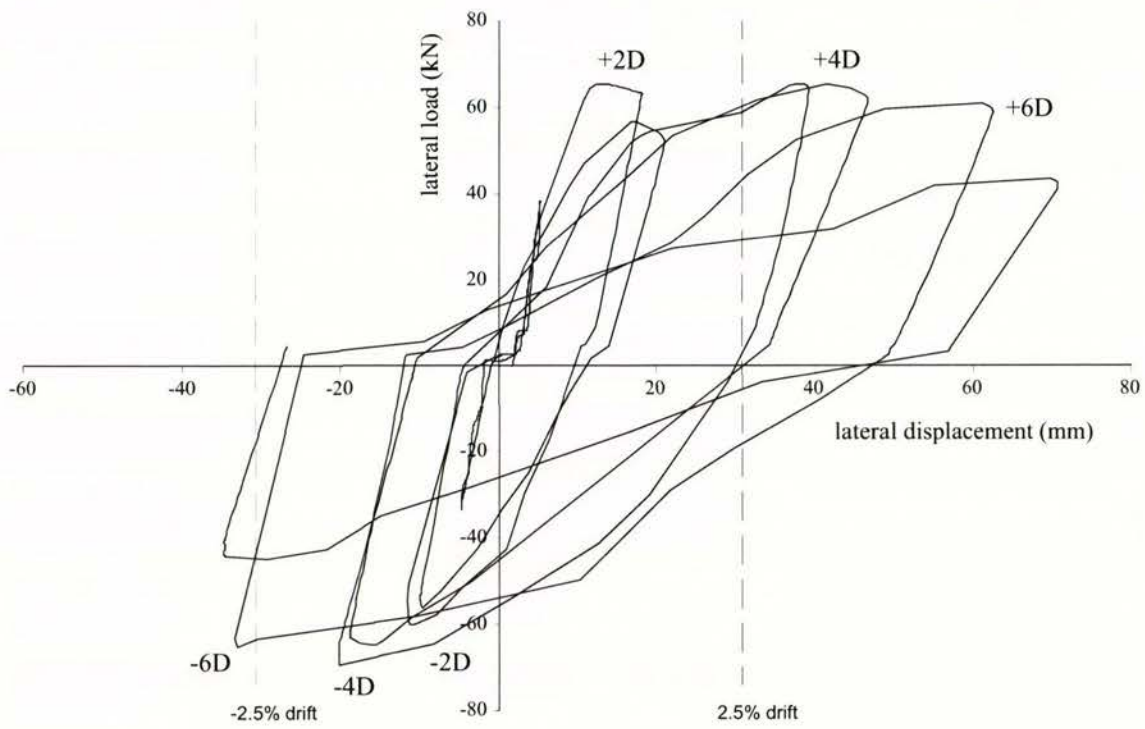

(b) Column 'B'

Figure 4.8: Force versus displacement response of individual columns. (continued)

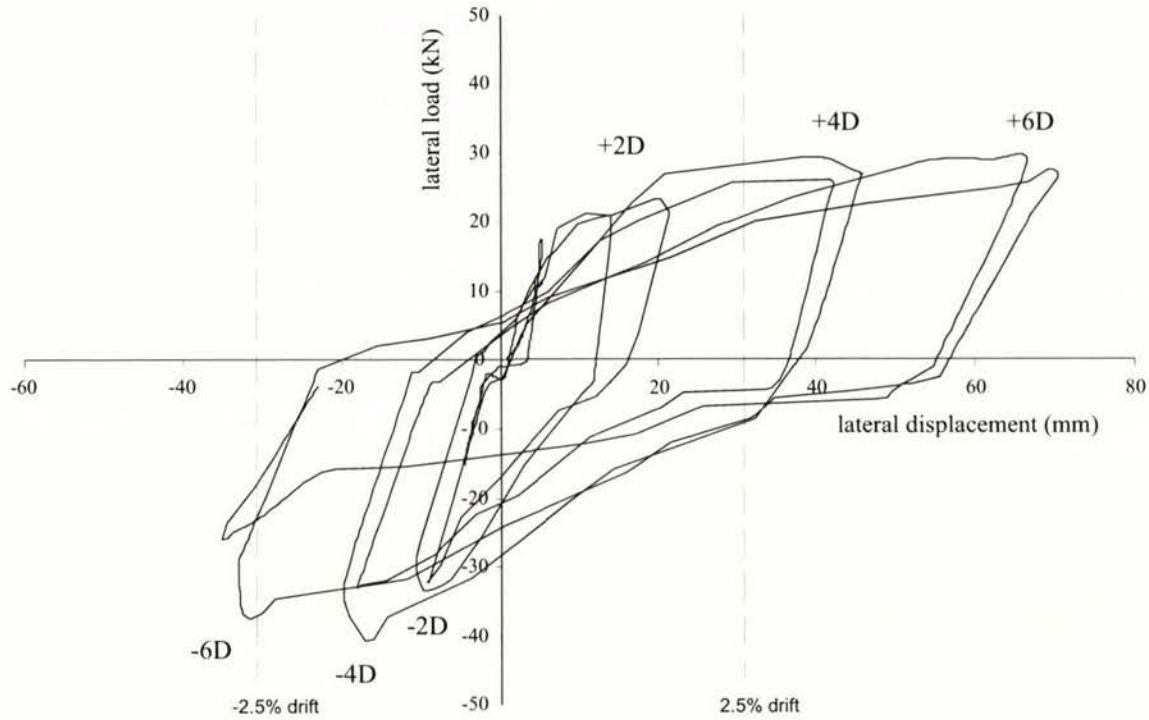

(c) Column 'C'

Figure 4.8: Force versus displacement response of individual columns. (concluded)

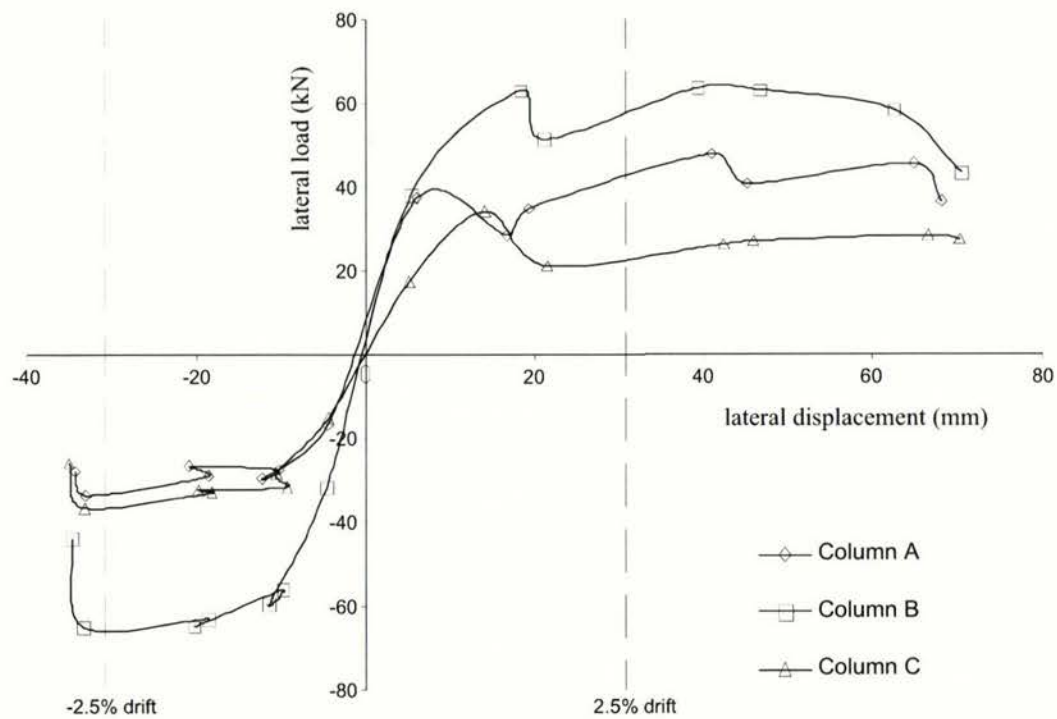

Figure 4.9: Peak lateral force versus displacement comparison of the columns.

The displacements for each column were similar to each other as adjustments were made at each step to keep them parallel. This is illustrated in Figure 4.9 (data included

in *Appendix 3*). Also noticeable in this chart is the smaller load in the forward direction sustained by column 'C' in comparison with column 'A'. The reverse is true for the reverse direction of loading, but to a lesser extent. The arrangement of the actuators (joined at the top of the three columns, see Section 3.6, *Chapter 3*) may have contributed to axial forces inadvertently applied through the beams as adjustments were made to the hydraulic actuators during the experiment.

4.5 Components of Deformation

The method and equations set out in *Section 3.7.4* were used to calculate the average lateral displacement at the top of the columns from the flexural and shear deformations measured on the beams and columns. Figure 4.10 compares the average lateral displacement measured directly at the top and bottom of the columns with the calculated displacements derived from the displacement measurements made on the test unit.

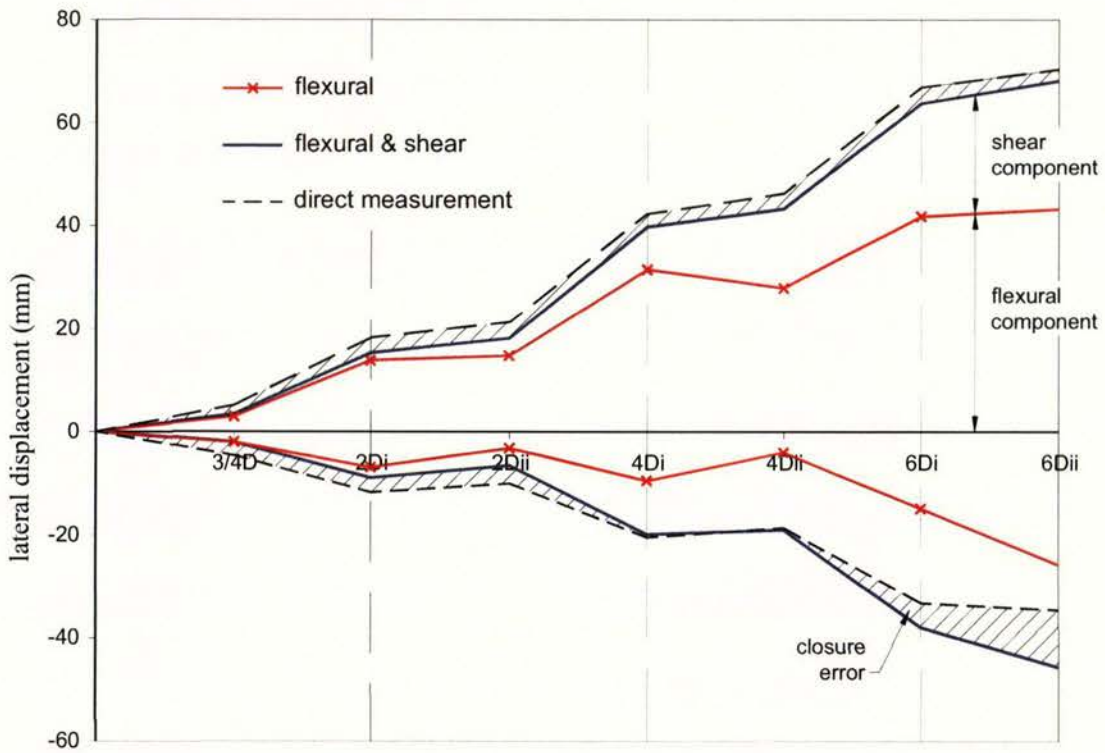

Figure 4.10: Flexural and shear components of deformation in Unit 1.

The results shown Figure 4.10 are the average values from the two beam bays and the three columns. The closure error shown could be attribute to a number of factors such

as slipping of bars in joints (especially at greater drifts), bending and twisting of rods between transducers (also see Figure 4.16), twisting of transducers and in accurate readings in transducers. Despite the closure error, it can be seen from Figure 4.10 that the calculated displacement closely matched the displacement from direct measurements of the displacements in the positive direction. In the negative direction, the match was good until the ductility 6 cycles. As expected, the contribution from shear deformation increased, as the magnitude of the peak displacements increased.

The plot of lateral displacement due to shear deformation is shown in Figure 4.11. This shows that the displacements due to shear in the positive direction was similar to that in the negative direction. Shear deformations became more prominent from the ductility 4 cycles and beyond, as shown in Figure 4.11.

The lateral displacement due to flexural deformation is shown in Figure 4.12. It can be seen from this figure that significant reduction in flexural stiffness of the frame occurs during the ductility 6 cycles.

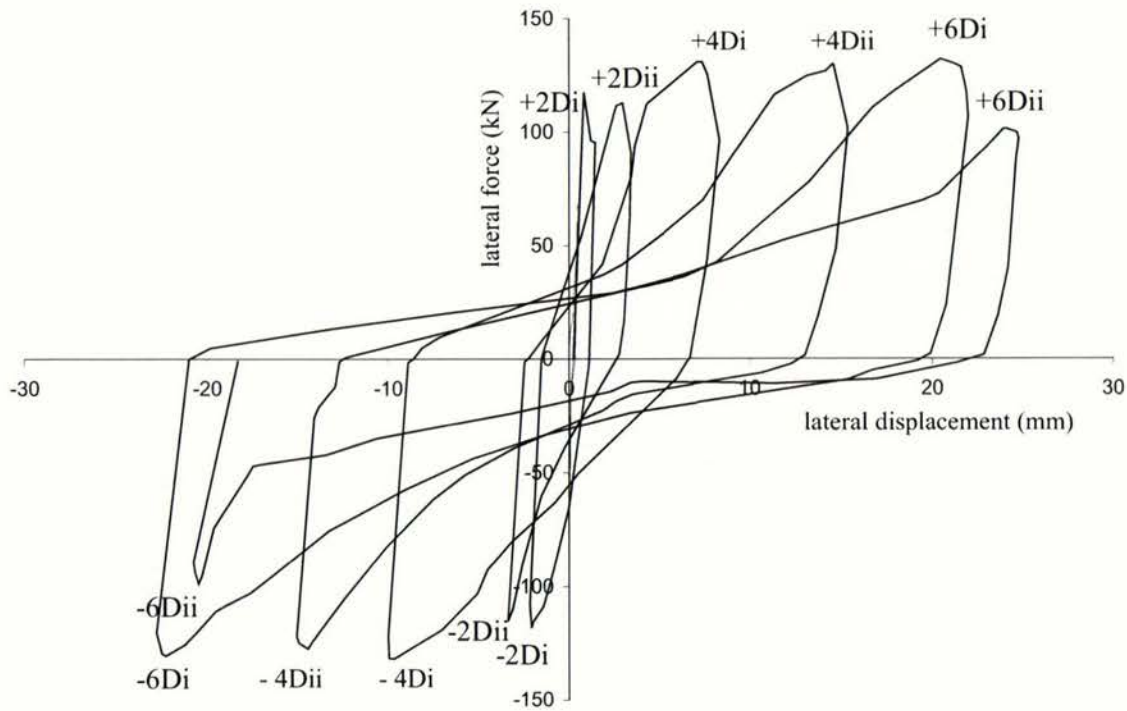

Figure 4.11: Lateral displacements from shear component of beams deformation against sum of lateral load.

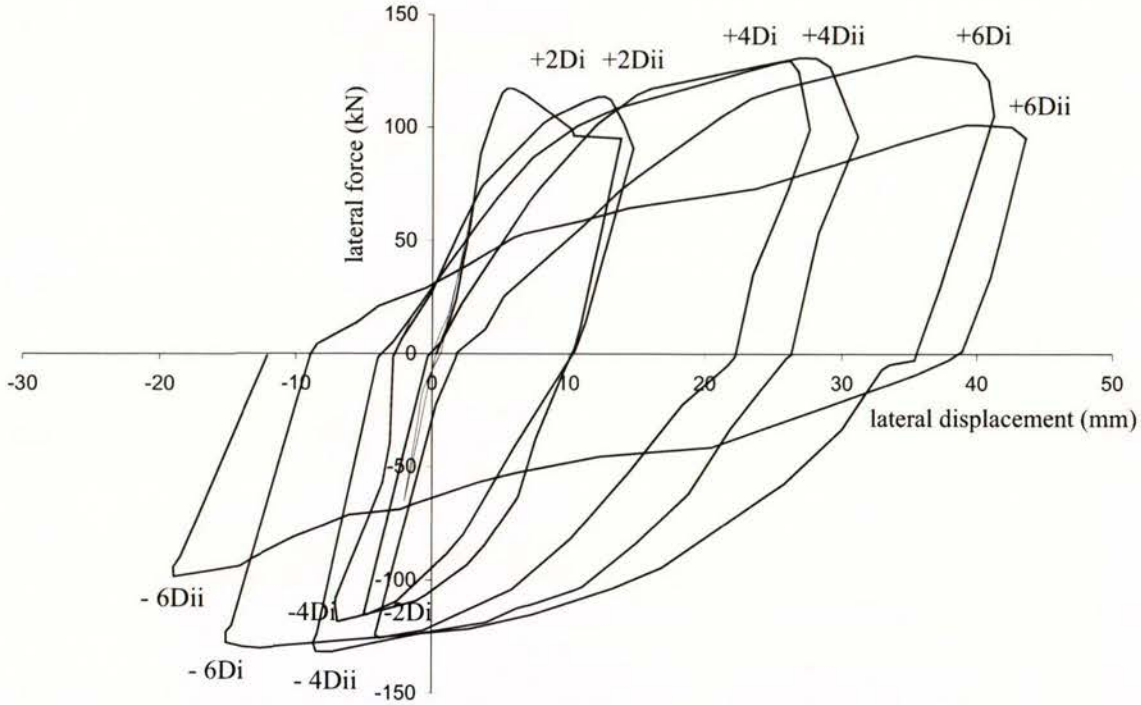

Figure 4.12: Lateral displacements from flexural component of beams deformation against sum of lateral load.

4.6 Elongation of Beams

Elongation along the centreline of the beams was measured by two means, firstly in a direct way by a displacement transducer spanning between the centres of the beam-column joints, and secondly by using the top and bottom line of instruments set up to measure beam deformations.

The total elongation being the sum of elongation for the two beams measured at peak positions is plotted against the displacement ductility in Figure 4.13 (data included in *Appendix 3*). As shown in the plot, the measurements by both methods were in close agreement until the second positive cycle of ductility 4 (+4Dii). The error between the two measurements could be due to the local buckling of the beam bars combined with the bending of the steel rod between the measurement points at the step between the beam and the column face. This is illustrated by Figure 4.14.

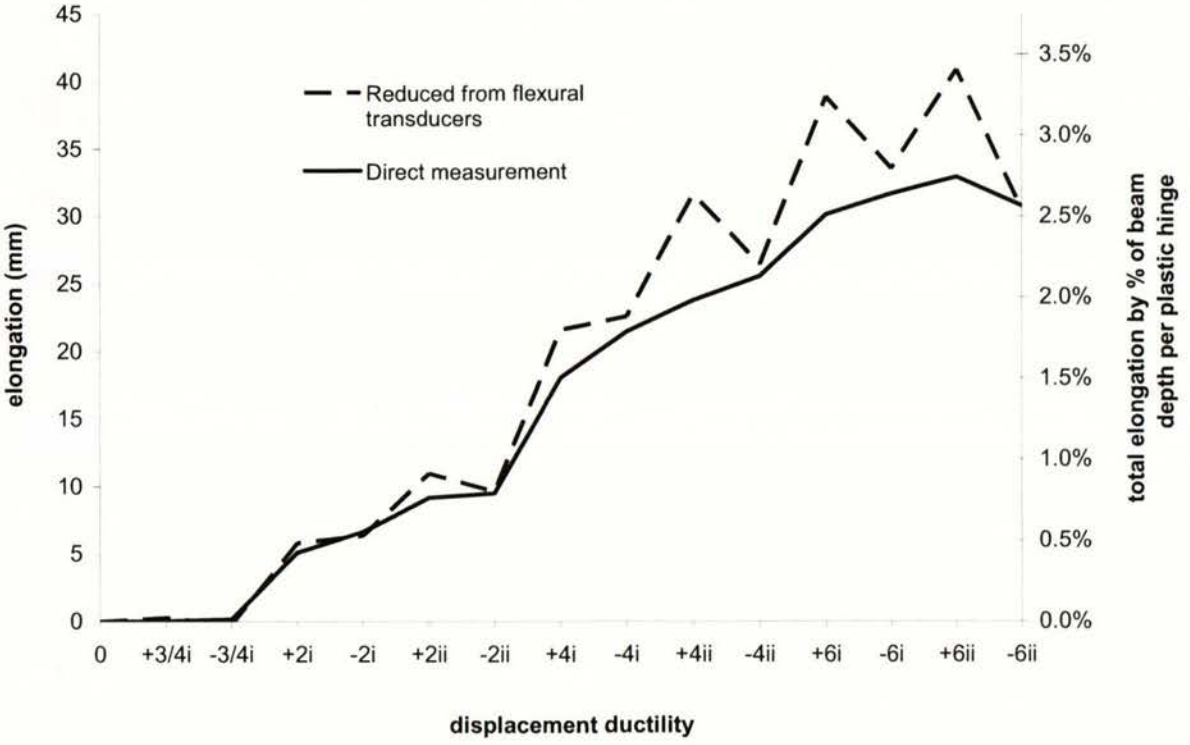

Figure 4.13: Total elongation of beams at peaks of ductility displacement.

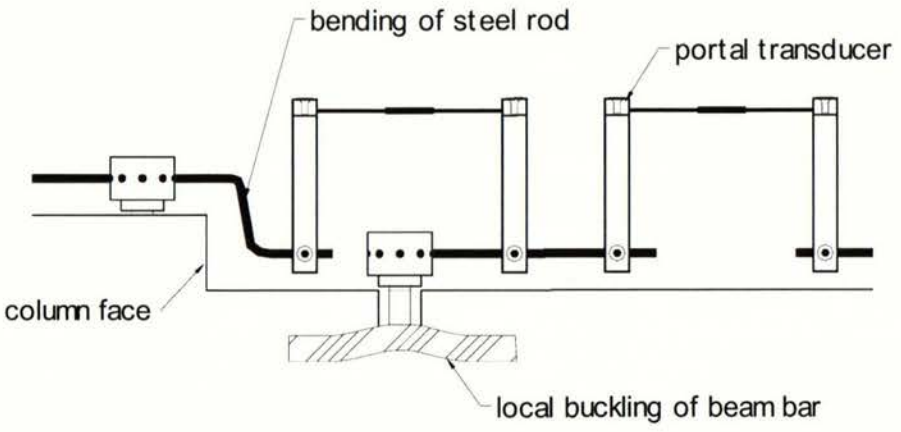

Figure 4.14: Error in instrumentation due to local buckling of beam bar and bending of steel rod.

The maximum recorded elongation of the frame in the elastic cycle was 0.3mm, but this likely to be on the low side, as the test was restarted after two earlier cycles had already been conducted (see *Section 4.3*). There is reason to believe from previous research that greater elongation of the beam occurs in the elastic cycles [M2]. Significant elongation of the beams started in the first ductility 2 cycle, with a total elongation of 5mm. This

corresponded to an average elongation of 0.4% of the beam depth for each of the four plastic hinges. The largest increase in elongation was during the first ductility 4 half cycle (+4Di), where the total elongation increased to a value of 18mm. The maximum elongation measured was 32.9mm, recorded at the peak of the second positive ductility 6 half cycle (+6Dii), which corresponds to an average elongation of 2.7% of beam depth for each plastic hinge. The reduction of elongation in the final half cycle was due to the loss of bond of the top row of beam reinforcement in the central beam-column joint, which resulted in the loss of stiffness in that region.

Figure 4.15 traces the history of total elongation with the application of lateral loads to the unit. It can be seen that the majority of the total elongation in the beams was during the positive direction of loading. This was due to the greater displacements imposed on the unit in the forward direction.

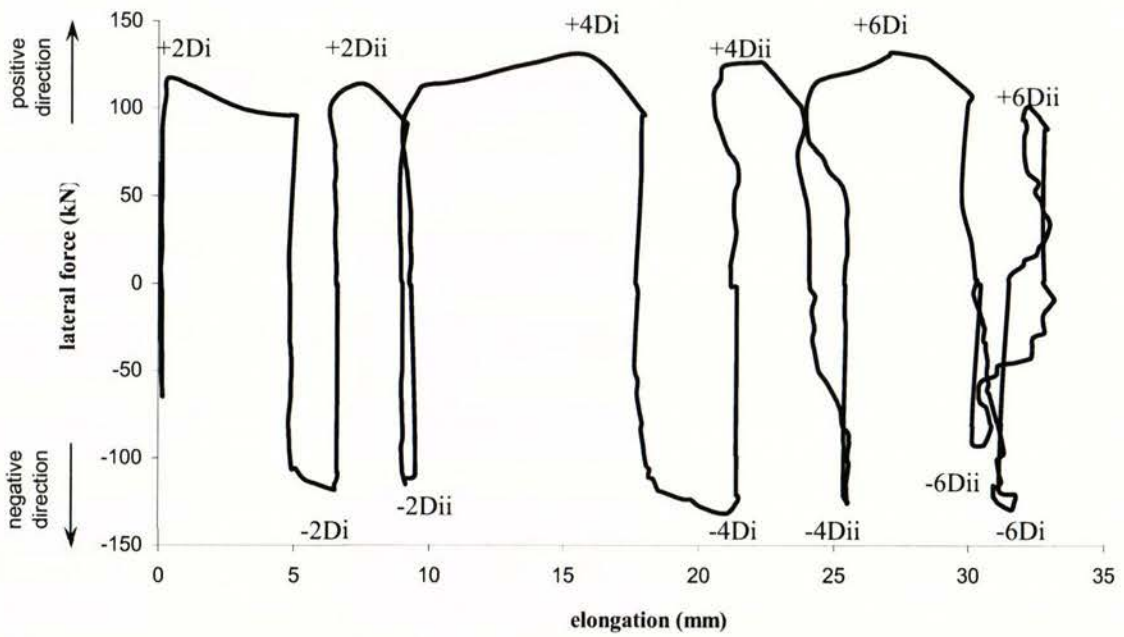

Figure 4.15: History of total elongation in terms of total applied lateral load.

Figure 4.16 shows the total elongation of the unit plotted against the ductility displacement cycles and subdivided into the two components, namely the rotational component and the component due to the extension of the compression reinforcement, *e* (see *Section 2.2.3* and *Equation 2.3*). The rotations in the elastic cycle resulted in the

small increase in length of the tension reinforcement. This increase was then negated by the reduction in length of the compression reinforcement at load reversal. In the first inelastic cycle, the tension reinforcement yielded, such that a permanent extension, *e*, was induced. In the first half cycle of ductility 4, it seemed that the extension had been compressed back to its original state. However, on load reversal, a large permanent extension had been induced, which accounted for 70% of the total elongation at that stage. This increased to 80% for the ductility 4 cycle, but was then reduced in the following ductility 6 cycle. The reduction in the extension of the bars was caused by the buckling of the compression reinforcement (top and bottom reinforcement, depending on direction of loading) during the ductility 6 cycles. By the end of the test, the permanent extension in the compression reinforcement accounted for more than 50% of the total elongation measured.

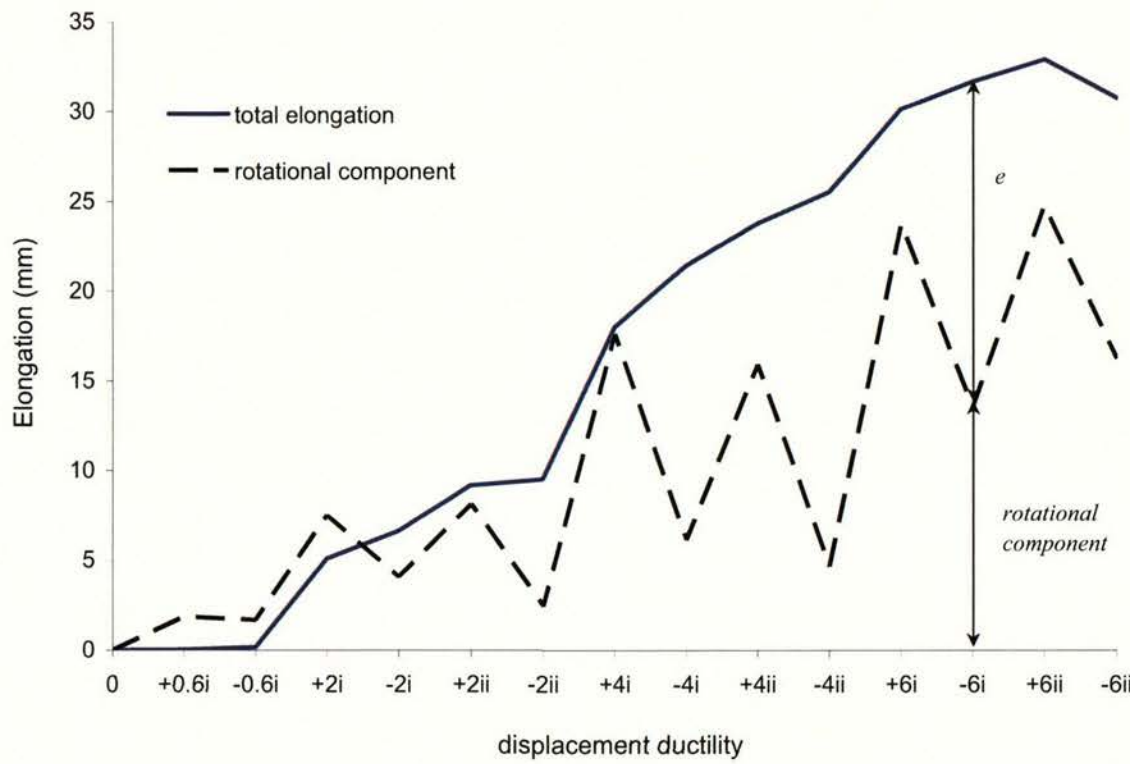

Figure 4.16: Compression reinforcement extension and rotational components of elongation.

Chapter 5

Test Results of Unit 2

5.1 Introduction

This chapter presents the results from the experiment on the frame with floor slab unit, Unit 2. The results include general observations made during testing and information collected and processed to determine the deformations that were sustained.

5.2 Displacement History

As previously described in *Section 3.8.2* of this report, the theoretical yield strength of Unit 2 could not be determined. Therefore, the unit could not be loaded to a predetermined load to determine the ductility 1 displacement. Instead, it was subjected to the displacement history shown in Figure 5.1 (drift displacement measured between pins at top and bottom of columns).

Initially, the unit underwent displacements up to $\pm 0.1\%$ interstorey drift for three complete cycles, followed by two cycles of displacements up to $\pm 0.2\%$ interstorey drift. At these stages, the equipment and testing procedure were fine tuned. After some reduction of data from the initial elastic phases, the unit was subjected to displacement cycles of $\pm 0.5\%$ interstorey drift for two complete cycles. As shown in Figure 5.1, further displacement cycles were set at steps of 0.5% interstorey drift, for two complete cycles at each step. One exception was for the displacement to $\pm 3.5\%$ interstorey drift, where the unit underwent three cycles at this level. This was done to provide more assurance that the unit was not going to fail before another displacement step was taken. The unit was then loaded for two further cycles up to $\pm 4.0\%$ then up to $\pm 4.5\%$ interstorey drift each, before testing ended.

Figure 5.2(a) shows the displacement history for each of the columns from 0.2 to 2.0% interstorey drift. As indicated by the figures, the columns were kept parallel to one

another. Throughout these displacement cycles, the largest out of parallel difference between the columns was 0.6mm at the peak of displacement cycle to ± 1.5% interstorey drift.

The displacement history for displacement cycles from ± 2.5% to ± 4.5% interstorey drift is shown in Figure 5.2(b). From 2.5 to 3.5% interstorey drift levels, at no time in the loading phases did the out of parallel difference between the columns exceed 0.2mm. In the worst case at ± 4.0% interstorey drift cycles was 0.4mm. The test unit was more difficult to control for the ± 4.5% interstorey drift cycles. At some stages the out of parallel difference was up to 0.7mm.

There were some differences during the unloading phase of each cycle (from peak to zero displacement) as the pressure release in the pumps was very difficult to control. The pattern was much the same for the other displacement cycles.

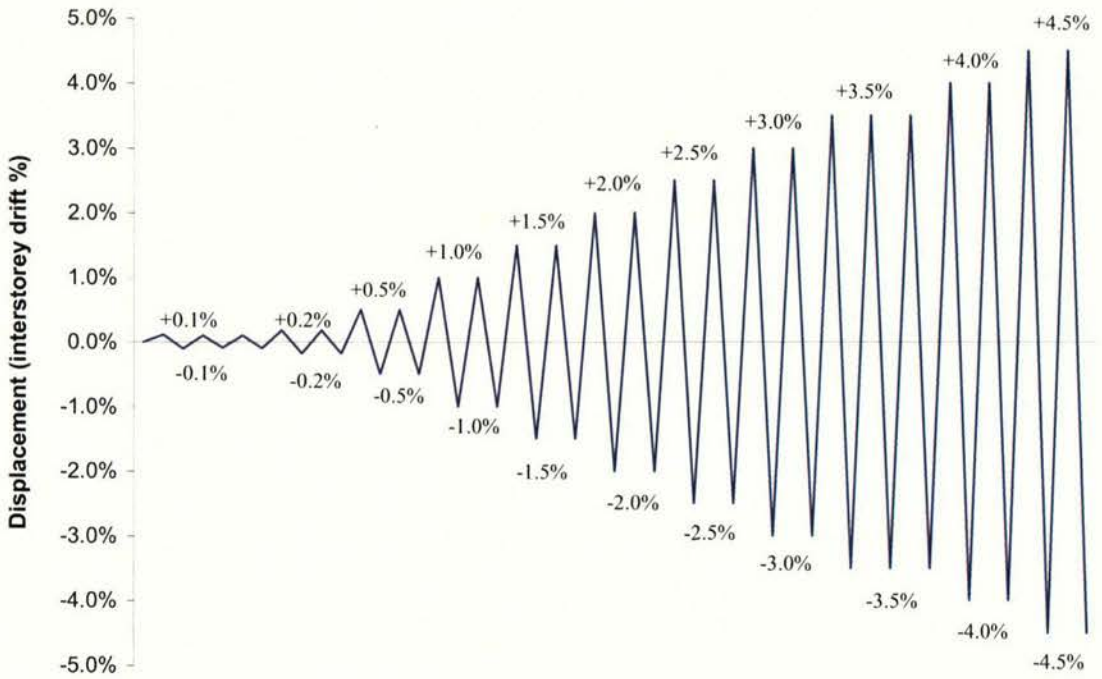

Figure 5.1: History of displacement levels applied to Unit 2.

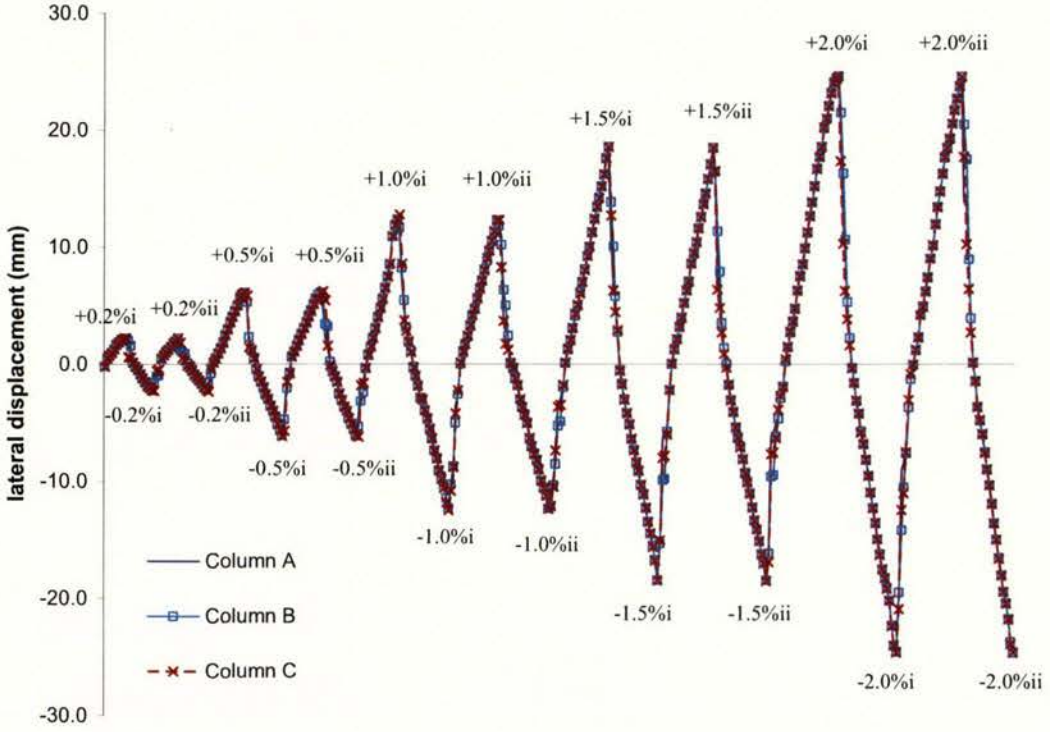

(a) From 0.2 to 2.0% interstorey drift

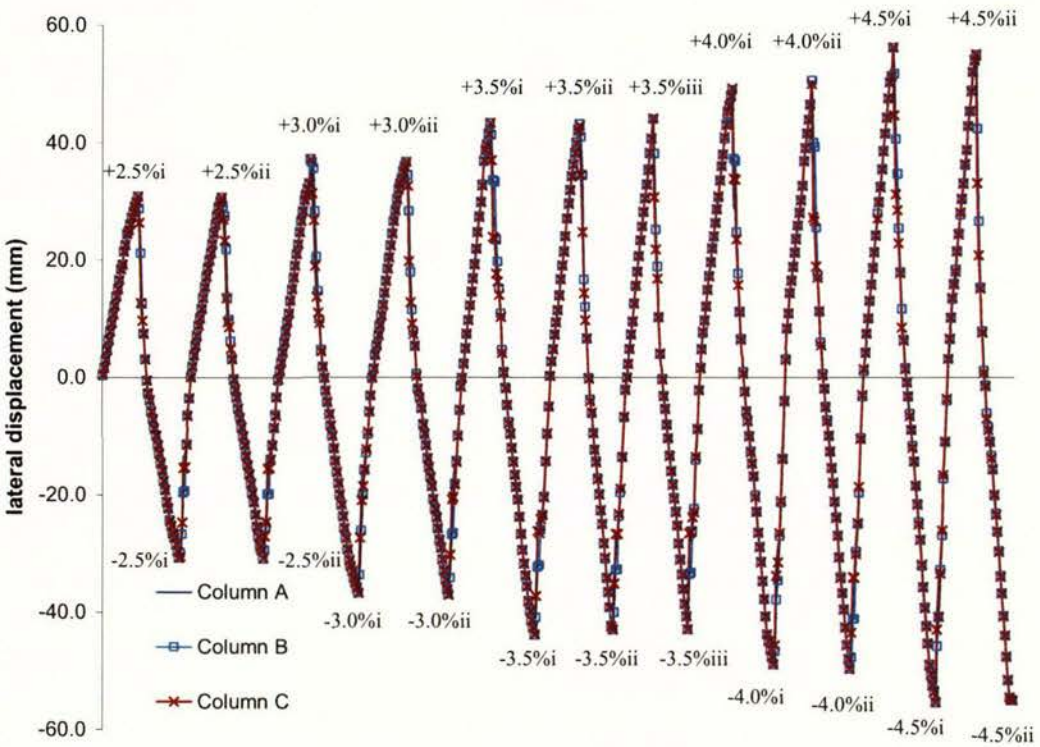

(b) From 2.5 to 4.5% interstorey drift

Figure 5.2: Lateral displacement history of columns.

5.3 General Behaviour and Observations During Test

Shrinkage cracks in the beams and floor were located and marked before the test. In the beams, cracks ran from the beam soffit to just above mid-depth. The shrinkage cracks formed in the floor topping around the mid-span region of both floor spans and were typically about 400mm in length. These ran across the slab, in directions perpendicular to the perimeter frame. A long crack formed along the support between the central transverse beam and the floor slab on the south side (which spans from column 'B' to the end support near column 'C'). This crack ran along the length of the transverse beam to the end-slab. The shrinkage cracks were difficult to see with the naked eye, and were less than 0.1mm in width.

Displacement cycles to 0.2% interstorey drift

The test lasted for a period of thirty two days. The initial elastic cycles were performed over four days. The unit was displaced up to ± 1.3mm at the top relative to the bottom of the column for three cycles. This corresponded to an interstorey drift of 0.1%. At these stages, the sum of lateral force peaked at ± 53kN. The unit was then loaded up to a maximum of 83kN in either direction for two cycles. The displacement reached at this level was consistently around the ± 2.2mm mark (± 0.2% interstorey drift). Over the duration of elastic loading, some problems were encountered with the instrumentation and the loading equipment. This involved replacing of four portal transducers, three data cables and a load cell. The load arrangement was also altered at the bottom of column 'C', where the extension bar connected to the actuator was buckling. A steel bracket was added to shorten the length and eliminate the need for an extension bar. The final arrangement is shown in Figure 3.11 of *Chapter 3*. At this stage as only small displacements imposed on the unit and consequently it was not damaged. Any deformation was limited to minor cracking which closed on unloading. The data collected from the test was checked to ensure that it was consistent. In particular, physical measurements were made to check against the column displacements and the elongation readings.

Displacement cycles to 0.5% interstorey drift

The next step in testing was to displace the unit up to ± 0.5% interstorey drift. Two displacement cycles to this level were applied. Minor flexural cracking was apparent in the potential plastic hinge zones and there was some diagonal cracking in the beam-column joint zones. In addition a limited amount of cracking occurred at the interface of the beam and floor around the columns and the beam potential plastic hinge zones. At this stage, cracks formed in the floor slab between the central transverse beam and the end supports of both floor spans (along the central transverse beam). At the peak displacement, this crack extended from the frame to the second rib unit of the south slab, while the crack formed up to the first unit in the north slab. In both cases the cracks were less than 0.2mm in width.

Displacement cycles to 1.0% interstorey drift

Crack patterns developed on the floor, which clearly showed that reinforcement in the floor slab was acting with the beam reinforcement. Diagonal cracks formed along the interface of the beam and floor were clear, showing shear transfer in this zone. This is shown in Figure 5.3 and in Figure 5.26(a), which shows a sketch of the cracks in the floor up to 1.0% interstorey drift. The red lines represent cracks formed at displacement in the positive direction (southward), while the black lines indicate cracks formed at negative displacement direction. It can be seen here that next to column 'A', diagonal cracks formed on the cantilever extension at the beam-floor interface to the left of the column. On reversal of loading direction, cracks were formed in the beam and diagonal cracking occurred at the beam-floor slab interface. Diagonal cracks were also found on the floor, starting from the end of the north slab (or left in figure) and cracking diagonally towards column 'A'. These appear to indicate compression struts, or compression forces from the precast rib flowing into the beam-column region. The crack pattern at the other south end of the unit (column 'C') was similar to that described above.

Cracks also formed parallel to the precast ribs, as shown in Figure 5.26(a), particularly around the beam-column joint zones next to the first row of precast ribs. This indicates bending of the insitu slab connecting the perimeter frame to the first precast rib. This is illustrated by Figures 5.8 and described in greater detail by the associated text.

There was further extension in the length of the cracks formed along the central transverse beam (see Figure 5.26(a)). Cracks were less than 0.3mm in width at this stage. Diagonal cracking was found on the beams in positive bending (sagging moment) in the plastic hinge zones. In negative bending (hogging moment), cracks formed at a smaller angle to the vertical than those formed in the previous half cycle.

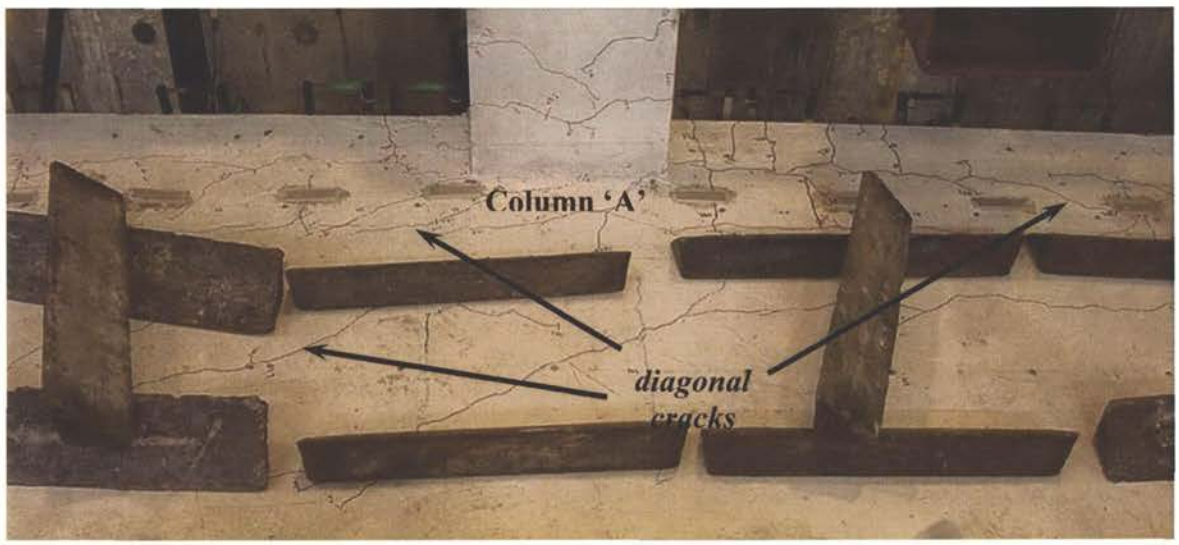

Figure 5.3: Diagonal cracking on floor in vicinity of column 'A', at 1.0% drift.

Displacement cycles to 1.5% interstorey drift

At displacements up to ± 1.5% interstorey drift, more floor cracks formed parallel to the perimeter frame (see Figure 5.26(b)). These were found in both spans, between the first and second row of rib units. Figure 5.4 shows a typical crack in the north span. This crack formed from the central transverse beam and propagated along next to the second rib unit (between the first and second rib units). The following are possible reasons for the formation of cracks parallel to the perimeter frame:

- The cracks formed parallel to the perimeter frame at the interface between the perimeter frame and the floor, and at the first precast rib are most likely due to vertical differential movement between the frame and the floor. This movement caused bending in the insitu slab linking the frame to the first rib (also see Figure 5.8).

- Elongation of the beams could cause the outer columns to move outwards, away from the floor slab (or perpendicular to the plane of the frame). This

movement is restrained by tension in the slab reinforcement, therefore causing cracks to form parallel to the frame (see Figure 5.5(a)). The test unit was restrained (perpendicular to the frame) at the top and bottom of the columns, and the movement at the centre of the column was not measured. However, in an actual building, this movement could be expected as the columns can only move outwards away from the floor to accommodate beam elongation and cracks in the floor.

- Beam elongation could cause the floor to act as a deep beam, as shown in Figure 5.5(b). Compression force due to this bending action is resisted partly by the floor slab and the outer transverse beam. The corresponding tension force is resisted partly by the floor slab and the central transverse beam. Due to this, shear is also resisted along the interface between the central transverse beam and the floor slab. These forces resulted in formation of cracks that branched from the central transverse beam and continued parallel to the perimeter frame (see Figure 5.4, denoted 'crack parallel to frame').

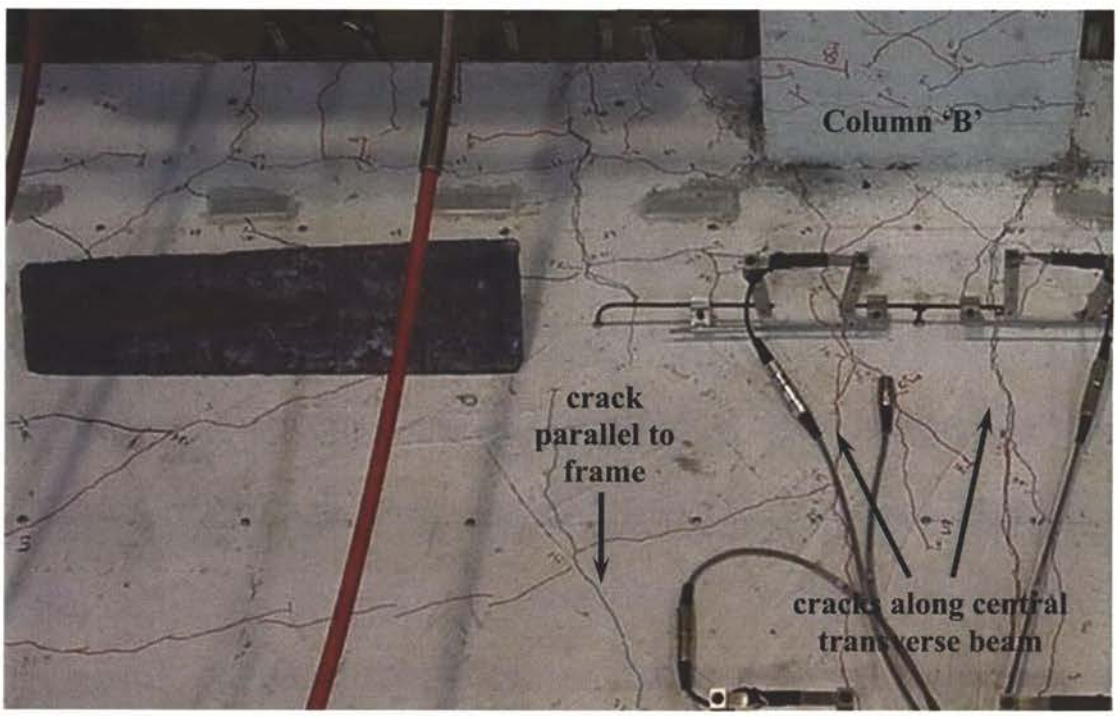

Figure 5.4: Longitudinal crack on floor alongside precast rib unit, 1.5% drift.

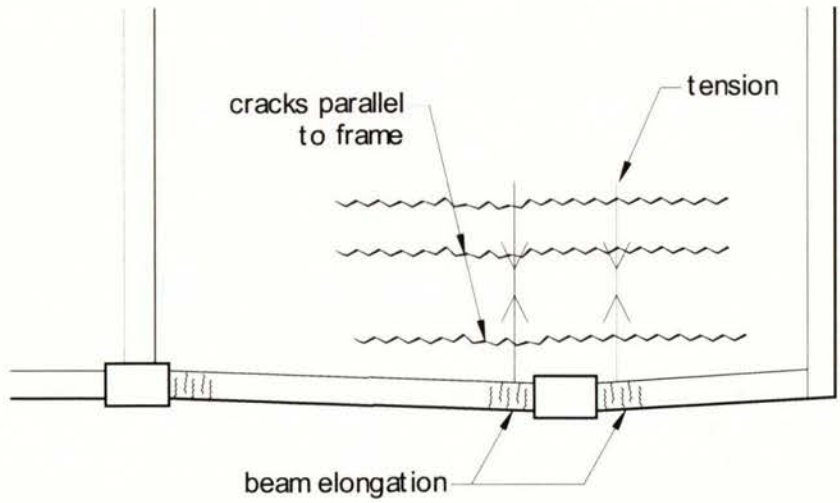

(a) Column moving outwards due to elongation

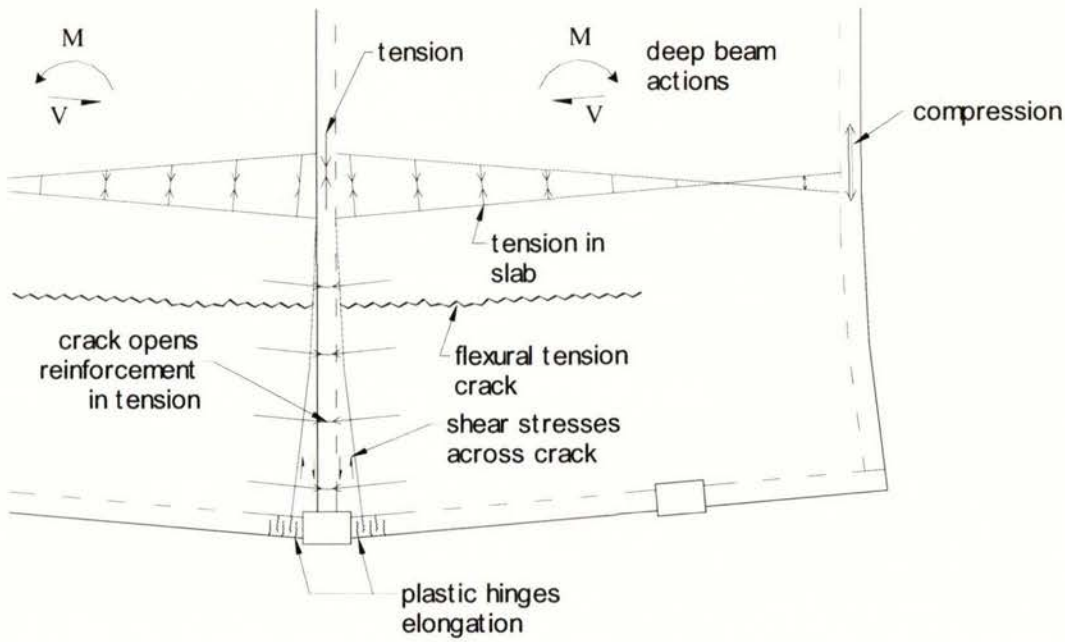

(b) Deep beam action in floor slab

Figure 5.5: Formation of cracks parallel to perimeter frame.

The crack along the central transverse beam and the floor opened to 2.1mm wide for the south span (see Figure 5.4), and 1.8mm for the north span at the end of the second cycle to 1.5% drift. There were also separation cracks at both ends of the floor (cantilevered ends). This is shown in Figures 5.6 and 5.26(b). These extended to mid-way between the first and second row of rib units. There was some limited spalling of cover concrete on the columns in compression at the beam face, above the floor. Cracks in the beam at column faces were about 3mm wide.

Displacement cycles to 2.0% interstorey drift

On the first cycle to 2.0% interstorey drift, damage was inflicted to the corner half-hinge joint at the north end. By the end of the second cycle, the Reid bar footplate in the half-hinge connection (see Figure 3.4 of *Chapter 3*) was exposed, as shown by Figure 5.6. This was due to the lifting up of the end of the transverse beam from the vertical movement at the end of the cantilever. Also visible in this figure is the separation crack between the floor slab and an external transverse beam.

There were further extensions in the lengths of the cracks parallel to the ribs. New cracks were found between the second and third ribs on both floor spans. The crack along the central transverse beam had extended to the end slab. There was some spalling of concrete at the beam and slab interface adjacent to column 'C' (see Figure 5.26(c)).

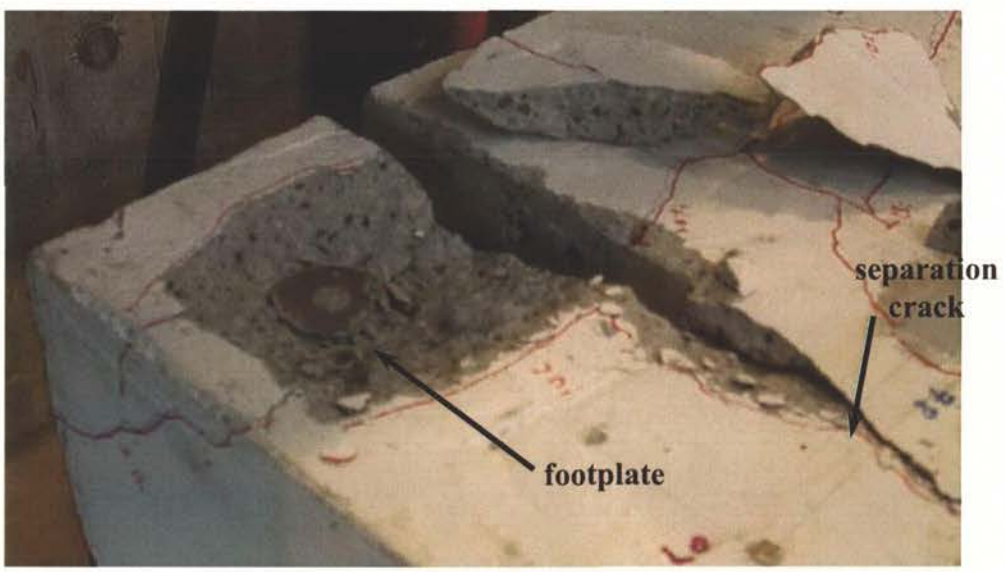

Figure 5.6: Damage to corner half-hinge joint at north end, at 2.0% drift.

Displacement cycles to 2.5% interstorey drift

On the first negative half cycle to 2.5% interstorey drift, spalling of concrete occurred at the beam and slab interface adjacent to column 'A'. This was similar to the event adjacent to column 'C' in previous cycle to 2.0% drift, and the positive half cycle to 2.5%. A diagonal crack in the floor from the south end towards column 'C' widened to 3.5mm. On reversal of loading direction, a diagonal crack in the north end slab, which extended towards column 'A' widened to a similar extent (see Figure 5.26(d)).

Longitudinal cracks (parallel to frame) were formed between the third and fourth ribs on both spans.

At this stage the vertical differential movement between the frame and the floor slab was obvious when a large crack formed at the beam to slab interface adjacent to column 'C'. This is shown in Figure 5.7(a). On the second negative half cycle to 2.5% drift, the same situation arose in the region close to column 'A', as shown in Figure 5.7(b). Figure 5.8(a) illustrates the vertical differential movement of the floor and the beam. As the frame is displaced laterally, the beams rotate. However, the slabs remained near straight because of the relatively stiff prestressed ribs. This relative displacement causes the floor to separate from the beam under positive rotation (sagging), giving rise to the crack at the floor and slab interface (see Figure 5.8(b)). In practise this movement could still be expected in an actual building as the crack patterns and widths indicate that the stiff end slab had little influence over this mode of local deformation, as the bending of the slab was limited to the slab between the frame and the first precast rib. However, the movement of the building in the direction perpendicular to the direction modelled in the test could influence the magnitude of this movement. Further studies would be required to investigate this effect.

(a) Next to column 'C'

Figures 5.7: Vertical movement of floor from beam at 2.5% interstorey drift. (continued)

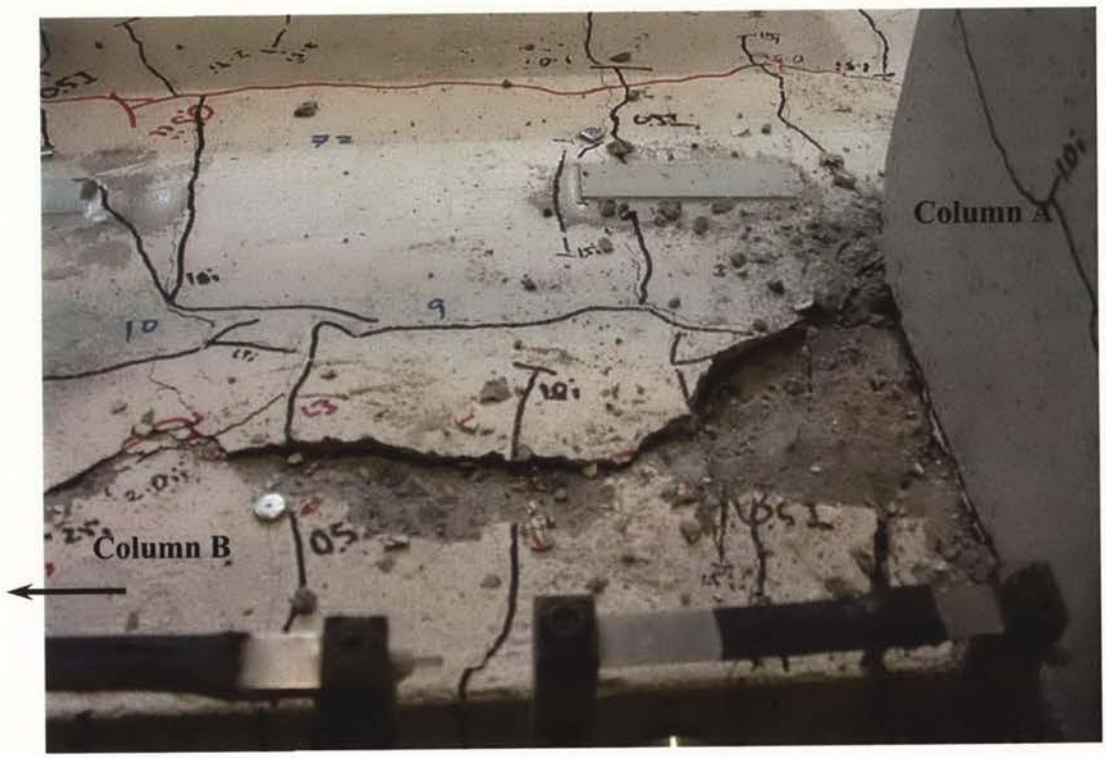

(b) Next to column 'A'

Figures 5.7: Vertical movement of floor from beam at 2.5% interstorey drift.
(concluded)

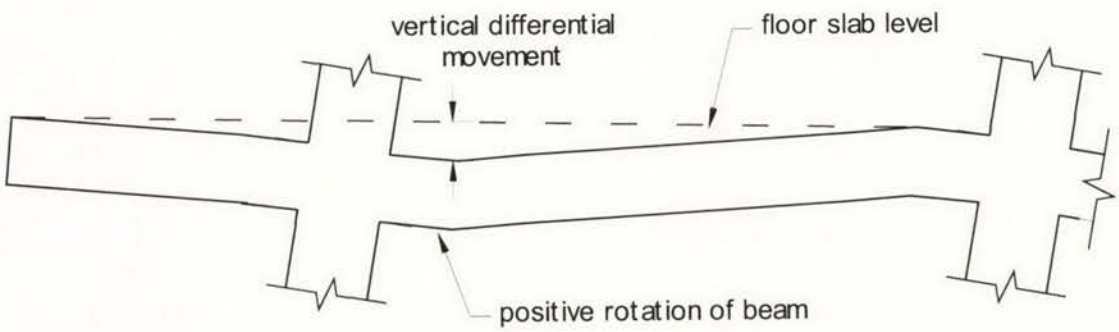

(a) Elevation view of vertical differential movement

Figures 5.8: Illustration of relative vertical movement between floor and beam.
(continued)

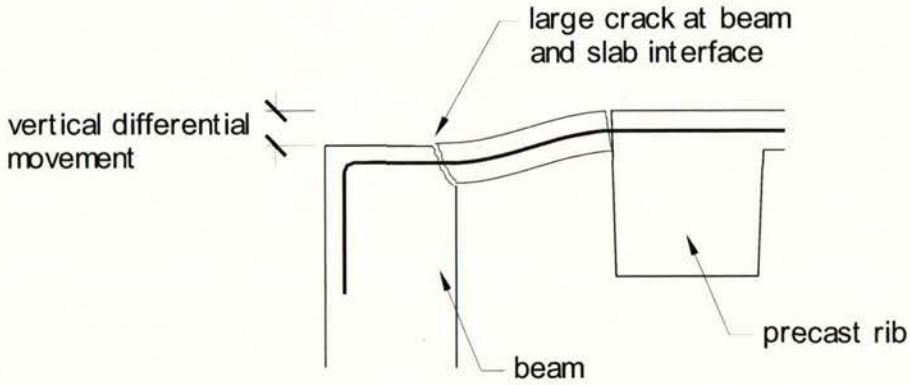

(b) Section view of floor slab and beam

Figures 5.8: Illustration of relative vertical movement between floor and beam. (concluded)

Displacement cycles to 3.0% interstorey drift

In the cycles up to ± 3.0% interstorey drift, more damage occurred at the large crack due to vertical differential movement of the floor and the beam adjacent to columns 'A' and 'C'. The first and second starter bars were exposed at these locations. In beam bay 'B'-'C', the crack had extended past the mid-span, as shown in Figure 5.9. There was some diagonal cracking in the first row of precast ribs at the ends of both spans. However, these cracks were small due to the restraint provided by the prestressed ribs. A sketch of the cracks in the floor at this stage is shown in Figure 5.26(d).

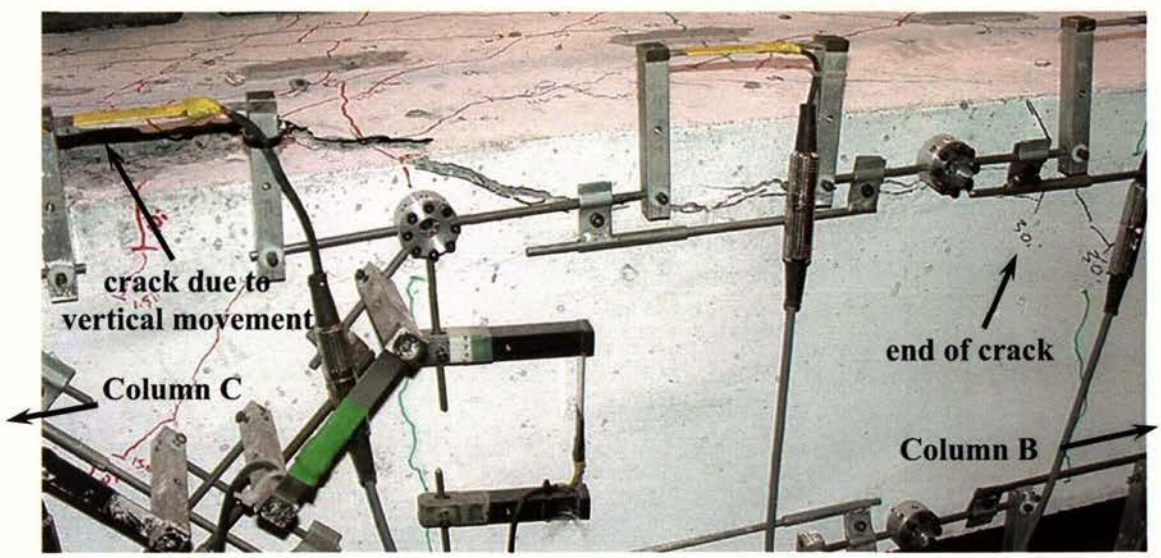

Figure 5.9: Elevation view of perimeter frame of extension of crack past mid-span of bay 'B' - 'C', at 3.0% interstorey drift.

Displacement cycles to 3.5% interstorey drift

In the first positive cycle to 3.5%, the crack associated with the vertical differential movement of the slab and beam extended past the mid-span of beam bay 'A'-'B'. The vertical movements between the slab and beam were more evident on the south cantilever extension. On reversal of loading, damage inflicted on the north cantilever extension was similar to the south extension in the previous half cycle. This is shown in Figure 5.10.

As a result of the concrete spalling at the beam and floor slab interfaces, the longitudinal beam reinforcement closest to the floor slab was exposed, particularly in plastic hinges next to columns 'A' and 'C'. Chunks of concrete from the floor around columns 'A' and 'C' had fallen off after the second cycle. The unit was subjected to a third cycle to 3.5% interstorey drift. However, no significant change was observed in this cycle.

Figure 5.10: Shearing and uplift of floor at north cantilever, at 3.5% drift.

Displacement cycles to 4.5% interstorey drift

More damage at the interface of the beams and floor was sustained around columns 'A' and 'C' after displacements to 4.0% interstorey drift. Damage to the plastic hinges next

to columns 'A' and 'C' was more severe, with buckling of longitudinal reinforcement and wide flexural cracks forming near to the column faces. Figures 5.11(a) and (b) show where concrete had fallen off around column 'C' and the starter bars exposed. The test was ended after two further cycles to 4.5% drift.

(a) Cantilever extension adjacent to column 'C'

(b) Region around column 'C'

Figure 5.11: Damage around column 'C' at the end of test.

5.4 Force versus Displacement Response

The force versus displacement response in the initial stages is shown in Figure 5.12. The displacement in this figure is the average relative displacement between the top and bottom for the three columns. This is referred to as 'lateral displacement' in the remainder of this document. It can be seen that at this stage, there was very little degradation in stiffness. The two cycles to ±0.2% drift were virtually identical. The maximum lateral force applied at this stage was 83kN at a lateral displacement of 2.2mm, and -81.5kN in the reverse direction at a lateral displacement of -2.2mm.

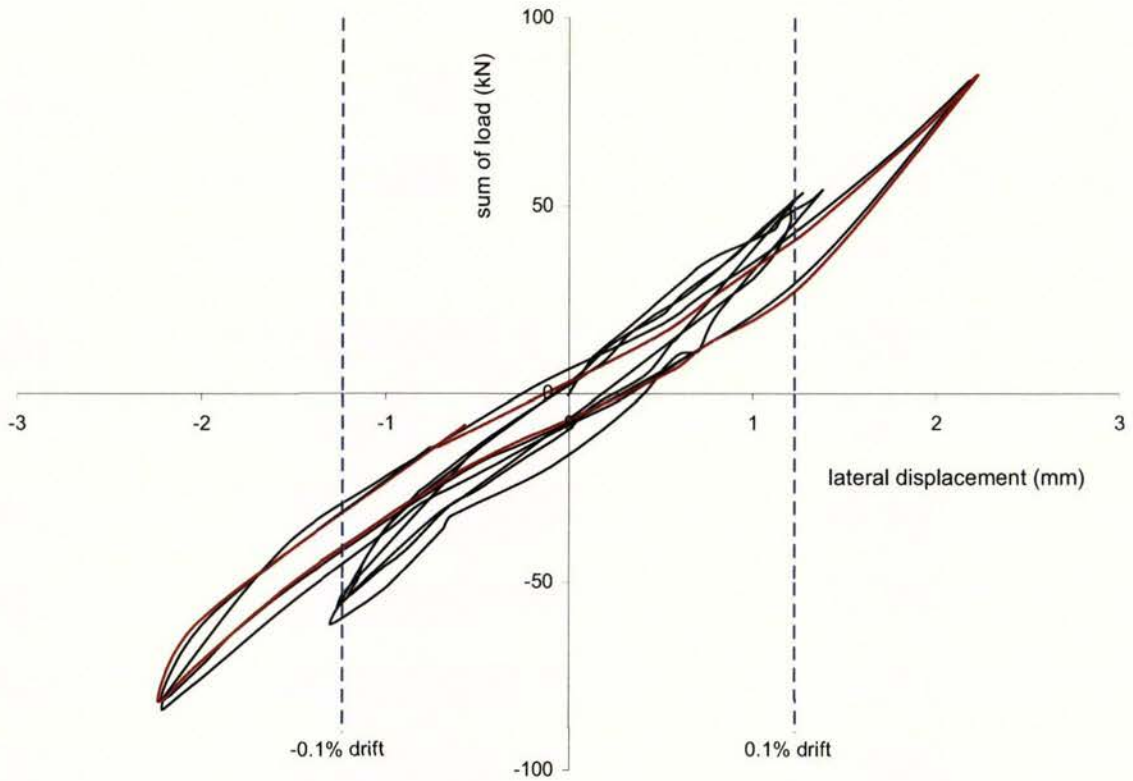

Figure 5.12: Force versus displacement response in initial loading stages, up to 0.2% interstorey drift.

The lateral force versus displacement response for the whole test is shown in Figure 5.13. Solid lines indicate the first cycle for each interstorey drift level and subsequent cycles are marked with dashed lines. Generally the unit was softer in the second cycle than in the first, which can be attributed to the flexural and shear cracking that occurred in the first cycle. There was more pinching in the load displacement relationship in the second cycle for each displacement step. The maximum lateral forces were reached at

the peak of displacement to 2.5% interstorey drift. The value in the positive direction was 313kN at 30.8mm and was -284kN at -30.8mm in the negative direction. The strength of the unit started to decline gradually in the subsequent cycles until it failed to reach 80% of the maximum value at the second cycle to 3.5% drift in the negative direction. It failed to reach 80% of the maximum value at the third cycle to 3.5% interstorey drift in the positive direction. However, the unit was taken to further displacement levels, as the lateral strength was still high compared to the test of the frame without the floor slab (*Chapter 4*). Testing was stopped after the second cycle to 4.5% interstorey drift, where the lateral strength reached at these levels was 166kN and -150kN in the positive and negative directions respectively.

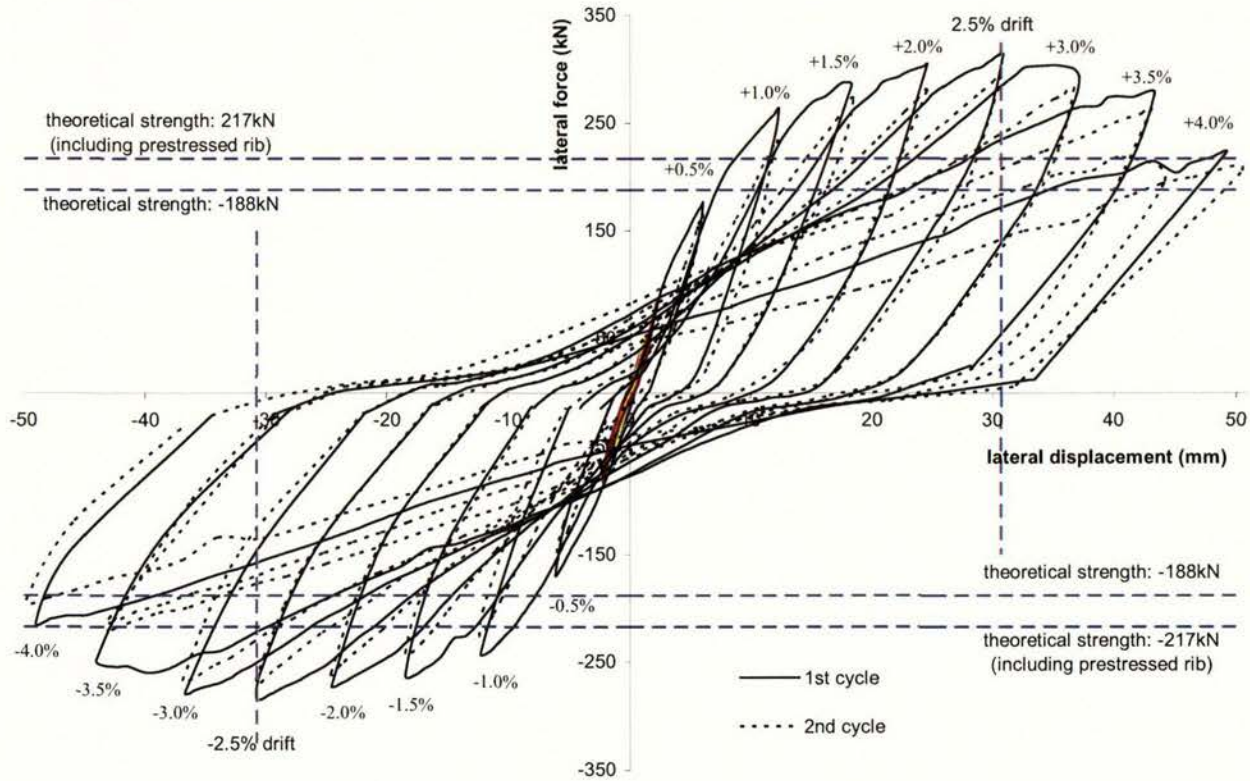

Figure 5.13: Lateral force versus average displacement response of Unit 2 (see values in Appendix 3).

The theoretical strength (lateral force) shown in Figure 5.13 was calculated based on the recommendations in the New Zealand Concrete Structures Standard [S2]. The strength was calculated by including effectively anchored longitudinal reinforcement within an effective slab width for the beams in negative bending. For this unit, the effective width

of floor slab included in beam flexural strength calculation was 443mm (equivalent to one quarter of the span of the beam, from the beam centreline). A precast prestressed floor rib was within this width (see Figure 5.14). Two theoretical strengths (lateral force) were considered; the first by ignoring the contribution of the prestressed strands in the floor rib, and the second by including the strands.

The values from material tests (see section 3.4 of *Chapter 3*) were used in calculation the theoretical strength (see worked example section A1.6, *Appendix 1*). Within the effective width, there were six 3.125mm wires, and two 10mm bars. However, adjacent to the central column, column 'B', the two lengths of 10mm reinforcement above the prestressed rib cannot be considered to contribute to beam strength as these were not effectively anchored. These bars were terminated at the ends of the prestressed ribs (ie. not connected at the transverse beam). The tension force at yield from the reinforcement within the effective slab width was 68kN. At joint 'B' the value was 18.8kN. The resultant flexural strength of the beam sections are shown in Table 5.1. By interpolating the bending moments to the column centrelines, the theoretical lateral strength of the unit was 188kN, neglecting the contribution of the prestressed rib within the effective slab width.

The tension force acting at mid-height of the slab is eccentric to the prestressed section. In calculating the strength of the prestressed rib, allowance must also be made for the bending moments due to gravity loads. Assuming that the compression strength of the rib concrete is 50MPa, and the prestressing strands (56mm^2 each) were initially stressed to 980MPa, an ultimate strength analysis indicates that each rib can resist an eccentric force of 69kN at the beam section adjacent to joint 'A' and an eccentric force 72kN adjacent to joint 'C'. The eccentric force acting in the rib adjacent to joint 'C' is greater due to slightly larger gravity load bending moment than the corresponding moment acting at the rib adjacent to joint 'A'. Adding to this the 68kN sustained by the passive reinforcement within the effective slab width gives a tension force capacity of 137kN at joint 'A' and 140kN at joint 'C'. The flexural strength of the beam sections are shown in Table 5.1. From these, the theoretical lateral strength of 217kN was calculated for the unit.

Table 5.1: Theoretical flexural strength of beams excluding prestressed strands.

	beam flexural strength at column faces (kNm)					
	Joint 'A'		Joint 'B'		Joint 'C'	
	-ve bending	+ve bending	-ve bending	+ve bending	-ve bending	+ve bending
excluding prestressed strands	-43.5	27.0	-31.7	27.0	-43.5	27.0
including prestressed strands	-59.4	27.0	-31.7	27.0	-58.8	27.0

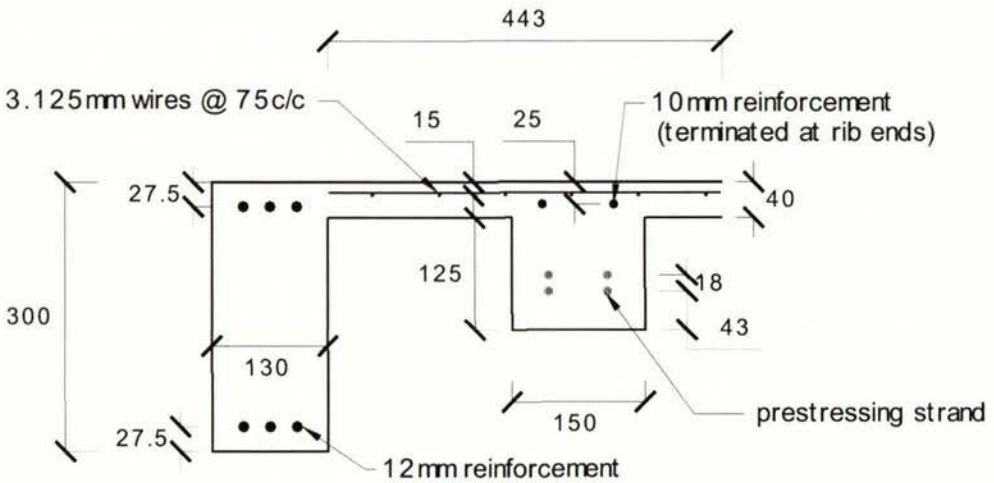

Figure 5.14: Effective width of slab contributing to beam flexural strength in negative bending.

The theoretical strengths calculated significantly underestimate the strength of the unit. In the negative direction of lateral displacement, the theoretical strength (including prestressed rib) was 76.4% of the measured peak force of -284kN. In the positive direction of displacement, the theoretical strength was 69.3% of the measured peak force of 313kN. These values clearly indicate that the theoretical strength calculation based on recommendations by the New Zealand Concrete Structures Standard may not be appropriate for this type of structure.

Allowing for two times the code recommended effective slab width and including two ribs for strength calculations, the lateral strength of the structure was 273kN. This value is closer in comparison with the measured peak forces. However extensive cracking should have occurred in the floor slab, across the top surface two prestressed ribs for the

tension force to develop. Such cracking was not observed (see Figures 5.26 (c) and (d)). Clearly the increase in strength of the unit had to come from other sources. Another source of strength enhancement is the deep beam action of the floor, resulting from the opening of crack along the central transverse beam due to beam elongation, as shown in Figure 5.5 (b). This is discussed in greater detail in *Chapter 8*.

Table 5.2: Difference in sum of force applied to top and bottom of columns at peaks of displacement cycles.

Interstorey Drift	Load at Top (kN)	Load at Bottom (kN)	Difference (kN)	Difference (%)
0.1%	49.5	41.0	8.5	17
	-52.8	-45.4	-7.5	14
0.2%	82.2	70.4	11.8	14
	-81.2	-73.9	-7.3	9
0.5%	176.3	160.5	15.8	9
	-169.1	-161.8	-7.3	4
1.0%	262.9	247.3	15.5	6
	-242.3	-232.8	-9.5	4
1.5%	285.1	277.2	7.9	3
	-261.4	-248.1	-13.3	5
2.0%	304.4	297.2	7.2	2
	-272.4	-259.9	-12.5	5
2.5%	313.2	307.4	5.8	2
	-284.0	-268.4	-15.6	5
3.0%	303.0	298.7	4.2	1
	-277.8	-262.5	-15.3	6
3.5%	276.4	273.5	2.9	1
	-246.5	-230.1	-16.4	7
4.0%	222.3	243.8	-21.5	-10
	-213.3	-179.6	-33.8	16
4.5%	211.5	240.5	-29.0	-14
	-182.6	-150.5	-32.1	18

Note:
Intersotrey drift %: displacement imposed on test.
Values are for 1st cycle of displacement step.

The sum of the lateral forces measured at the top of the columns did not equal the sum of forces measured at the bottom of the columns. Table 5.2 gives a summary of the forces at the peaks of the first lateral displacement cycle for each interstorey drift level. Up to 3.5% interstorey drift, the out of balance was between 2.9kN to 15.8kN for displacements in the positive direction, and was 7.3kN to 16.4kN for displacements in the negative direction. These differences were between 1 to 17% of the sum of the forces at the top of the columns in the positive direction up to 3.5% drift. In the negative direction, the corresponding values were 1 to 14%. This difference may be attributed to the friction force, which arose from the sliding of the floor unit on the supporting pedestals (as shown in Figure 3.3(a) in *Chapter 3*). The difference was high for the displacement cycles to 4.0 and 4.5% interstorey drift levels.

5.5 Moment Input to Beam-Column Joints

The moment applied to each beam-column joint was calculated from the sum of the lateral forces applied at the top and bottom of each column multiplied by the corresponding distance to the centre of the joint. Figure 5.15 shows a plot of the moment input for each of the beam-column joints at peaks of each cycle. Clearly for all stages, the moment applied to the central joint, joint 'B', was higher than the moment applied at both joints 'A' and 'C'. In the positive displacement cycles (top axis), the moment applied in joint 'C' was larger than that applied to joint 'A'. The reverse is true in the negative direction, though the margin was less. There were differences in the mechanism of slab contribution to the performance of the frame depending on the direction of loading. This was because two hinges in negative bending would form to one side of the frame centreline compared to one hinge in negative bending to the other side. This reverses on the change in loading direction. The strength increased when the slab was subjected to tension. Also noticeable for the plot was the drop off in moment input for the second cycle of each displacement step.

The theoretical bending strengths of joints at the column centrelines are shown on Figure 5.15. These were interpolated from the values shown in Table 5.1 (including prestressed rib). At the central joint, joint 'B', the value was 70kNm, while for the outside joints the greater value was 99kNm (98kNm for the lesser). The maximum

recorded moment input to joint 'B' was 150kNm, more than twice the theoretical value. For the outer joints, the maximum value was 136kNm, which is 1.37 times the theoretical value. It is clear from the comparisons that the code recommended method used for the calculation of beam strength is inappropriate. While the theoretical strength for the outer joints is comparable, the difference between the theoretical strength and the actual strength is significantly large. Clearly there is another source of strength enhancement to joint 'B'.

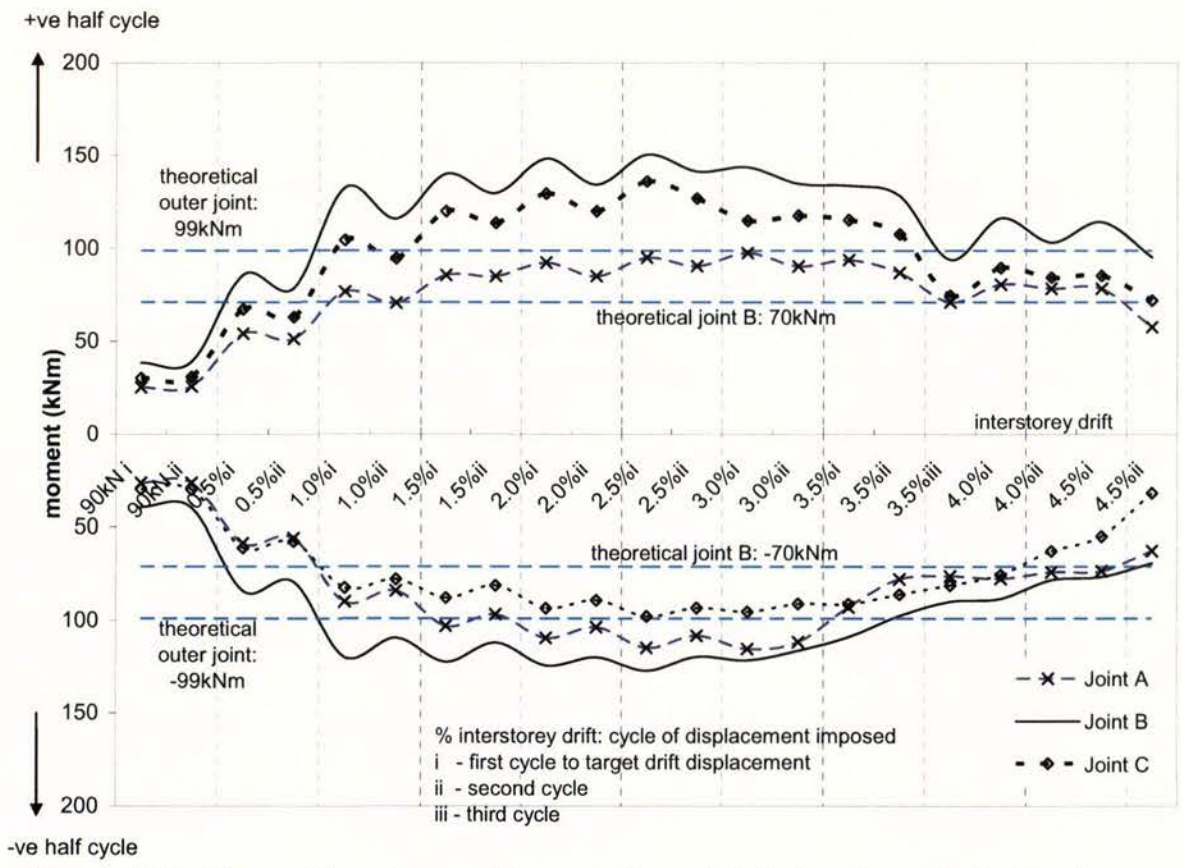

Figure 5.15: Moment input to each beam-column joint at cycle peaks (values in Appendix 3).

5.6 Components of Deformation

The method and equations set out in *Section 3.7.4* were used to calculate the average lateral displacement at the top of the columns from the flexural and shear deformations measured on the beams, columns and beam-column joint zone. Figure 5.16 compares the average lateral displacement measured directly at the top and bottom of the columns with the calculated displacements derived from the measurements. The results shown in the figure are the average values from the three columns.

It can be seen from Figure 5.16 that the calculated displacement closely matched the displacement from direct measurements until the displacements exceeded 3.0% interstorey drift. As expected, the contribution from shear deformation increased as the displacements got larger. The components of deformation were not calculated for the displacements to 4.5% interstorey drift, as some of the portal transducers were no longer operating due to excessive out of plane deformation.

The load versus displacement plot of the lateral displacement due to flexural deformation, against the sum of lateral load is shown in Figure 5.17. The plot of lateral displacement due to shear deformation is included as Figure 5.18. From Figure 5.17, it can be seen that the lateral displacement from flexural deformation was greater in the positive direction than the negative from displacements to 2.5% drift and onwards. This was compensated by greater lateral displacement due to shear deformation in the negative direction than the positive, shown by Figure 5.18. The decrease in the strength of the unit at displacements of 3.0% drifts and greater was accompanied by greater reduction in flexural and shear stiffness with increasing cycles and lateral drift. Comparison of the two plots shows that the reduction in shear stiffness was greater than the reduction in flexural stiffness.

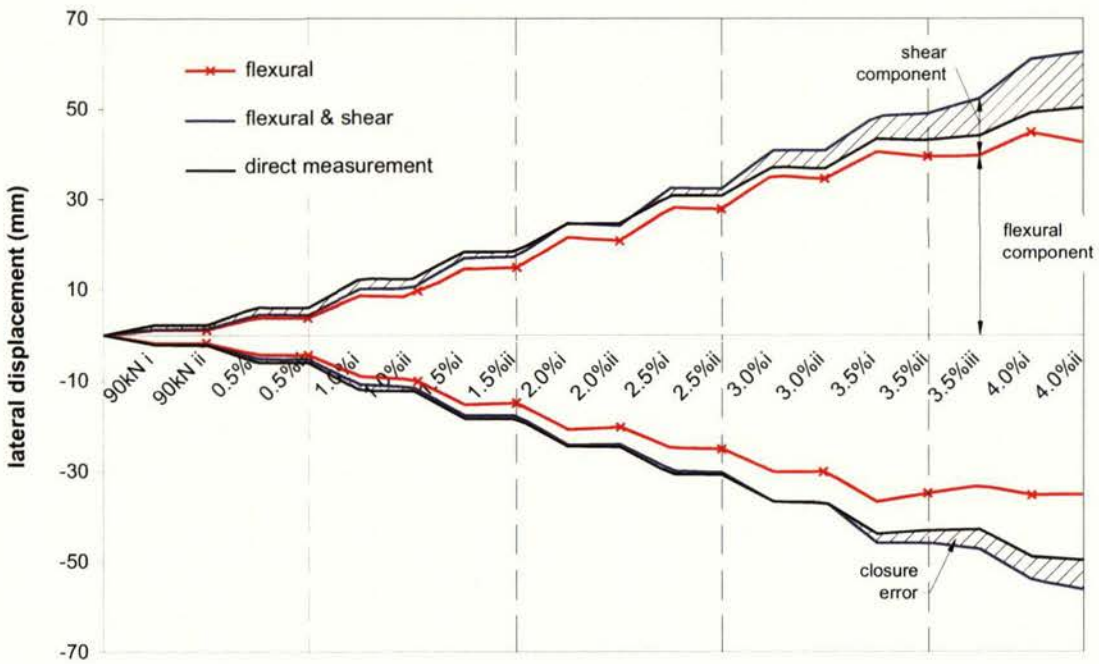

Figure 5.16: Flexural and shear components of deformation in Unit 2.

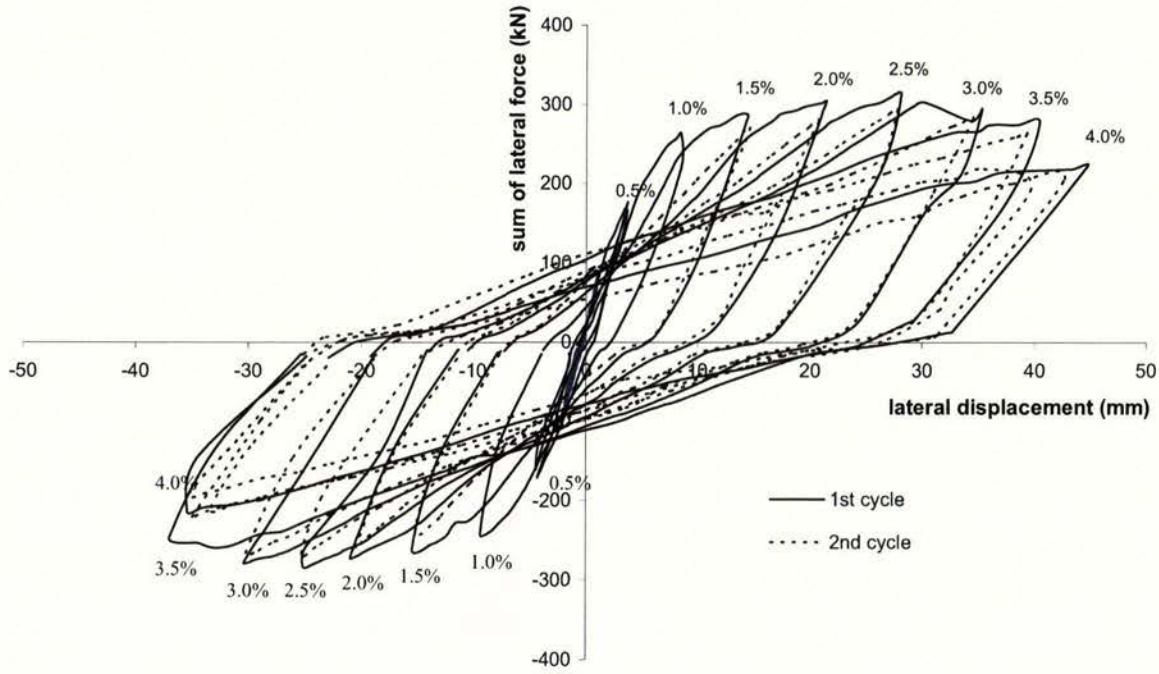

Figure 5.17: Lateral displacements from flexural deformations against the sum of lateral load.

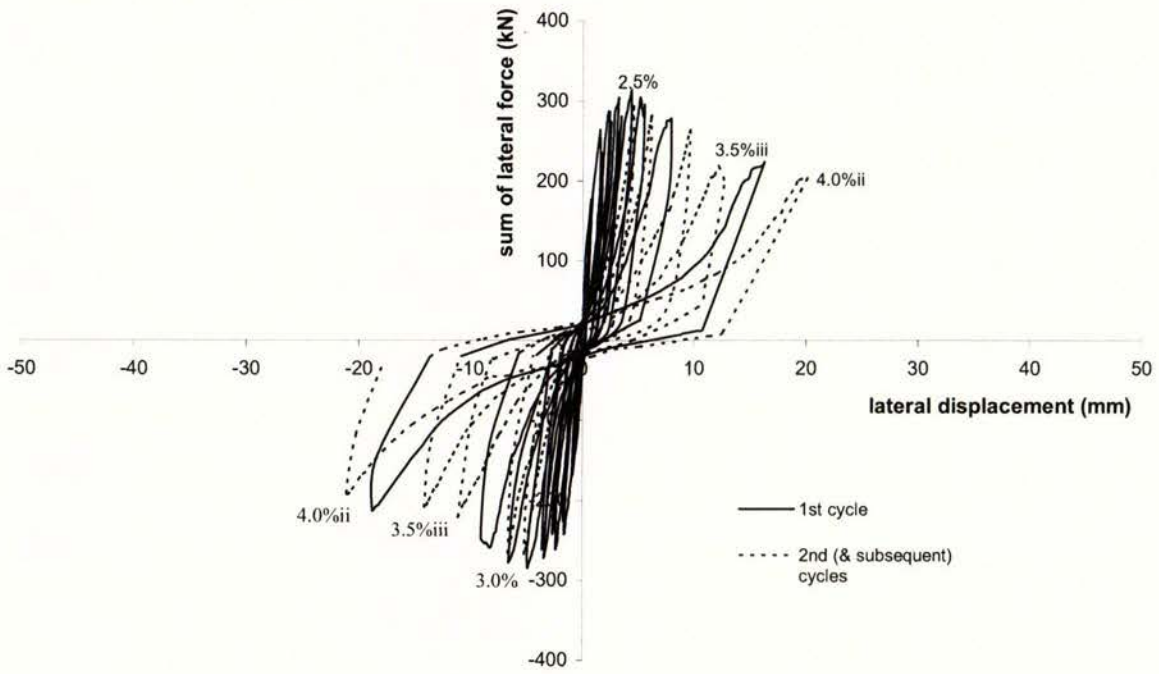

Figure 5.18: Lateral displacements from shear deformations against the sum of lateral load.

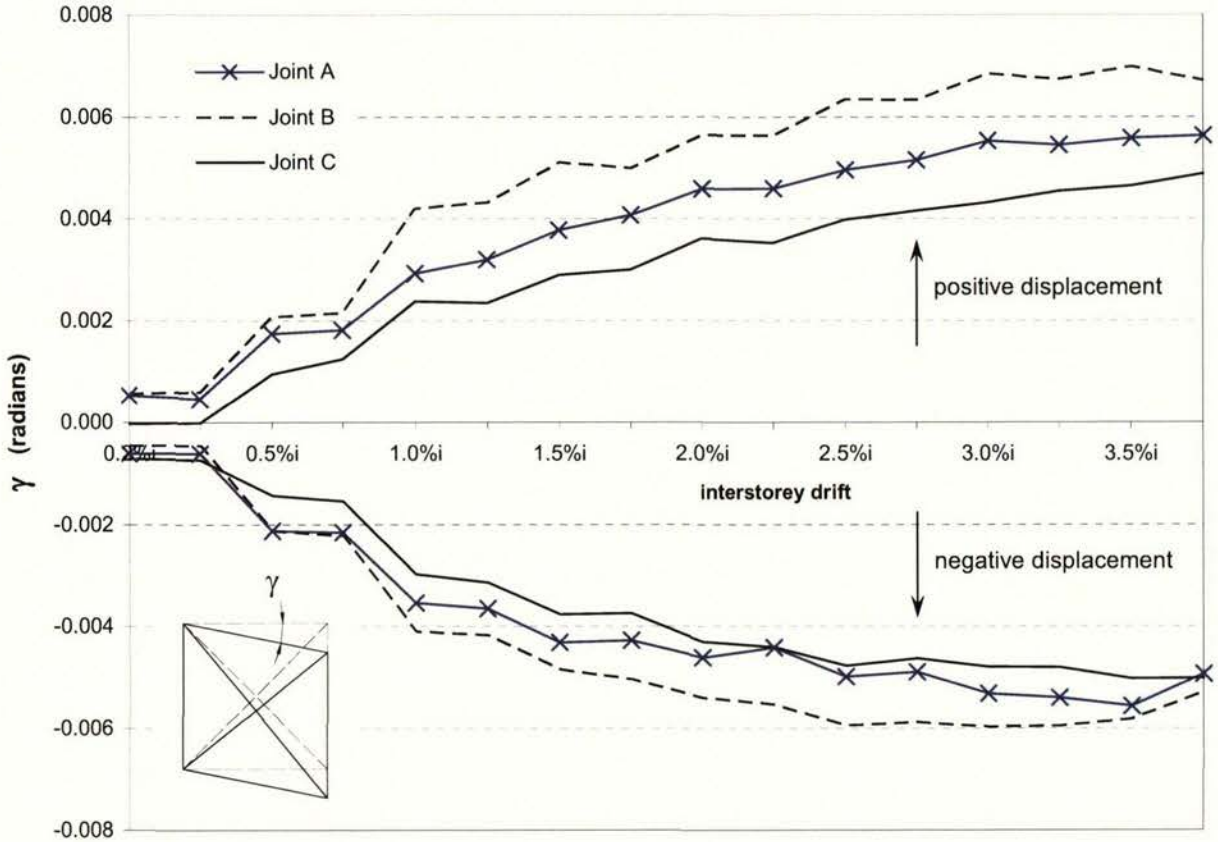

Figure 5.19: Shear deformation in beam-column joints.

Figure 5.19 shows the shear deformation within the beam-column joints at peak drift displacements. As expected, the shear deformation in joint 'B' was greater than the outer joints. Shear deformation in joint 'A' was about 20 to 30% greater than joint 'C' at displacements of 1.0% drift and greater in the positive direction. In the negative direction deformation in joint 'A' was a maximum of 15% greater than joint 'C'. This graph also shows that shear deformation in the beam-column joints increased at a greater rate up to 1.0% drift than at greater than 1.0% drift. This coincides with the pattern of strength increase shown in the lateral force against average lateral displacement plot shown by Figure 5.14.

5.7 Elongation of Beams

The recorded elongation over the whole length of the unit is shown in Figure 5.20 (see data included in Appendix 3). The values plotted were elongation readings taken at the peak of each lateral drift cycle. The solid line in Figure 5.20 is the elongation

measurement taken directly between the column centres, as described in *Section 3.7.3* (in *Chapter 3*) together with the measurements taken from each of the outside columns to the end of the cantilever extensions. The dashed line represents the calculated elongation from the measurements taken from the portal transducers mounted on the beams, which were used to calculate the flexural deformation. In this case the elongation was calculated from the sum of the elongation measured in each segment, as indicated in *Equation 3.3* (in *Chapter 3*). The closeness of the two lines in both plots is important, as it shows that the method used to measure the elongation directly was appropriate. This was important as the elongation from the direct measurement was used for controlling the test, where the columns were displaced parallel to one another in accordance with the elongation measured.

The maximum elongation measured at displacements up to 0.5% interstorey drift was 0.42mm. The initial elongation up to this stage was small and was mainly due to flexural cracking of the beams in the regions adjacent to the column faces. In both plots, it can be seen that the increase in the elongation of the beams was reasonably linear in two stages. Total elongation steadily increased from 0.5mm at displacement of 0.5% of interstorey drift up to a total of 16.5mm for the last cycle of 3.0% interstorey drift at an approximate rate of 1.4mm per cycle. Elongation increased at a much greater rate of approximately 6.2mm per cycle for the remaining displacement steps. This is coincidental with the decrease in the strength of the unit, and greater damage incurred at the beam-floor slab interface around columns 'A' and 'C' during the test. At these stages, the initial restraint to elongation of the beams from the prestressed flooring system was reduced, as the concrete around these areas fell off and the starter bars started to bend.

Figure 5.20 also plots the elongation in the beams in terms of the average elongation by percentage of the beam depth per plastic hinge. The average elongation per hinge for the entire frame was 0.92% of beam depth at 3.0% interstorey drift, and the maximum was 2.64% at the end of test (4.0% drift). However, these values do not represent actual level of elongation in the hinges. Figure 5.21 shows the average elongation for each plastic hinge within the two beam bays (four plastic hinges) and the average elongation per plastic hinge within the cantilever extensions (two plastic hinges).

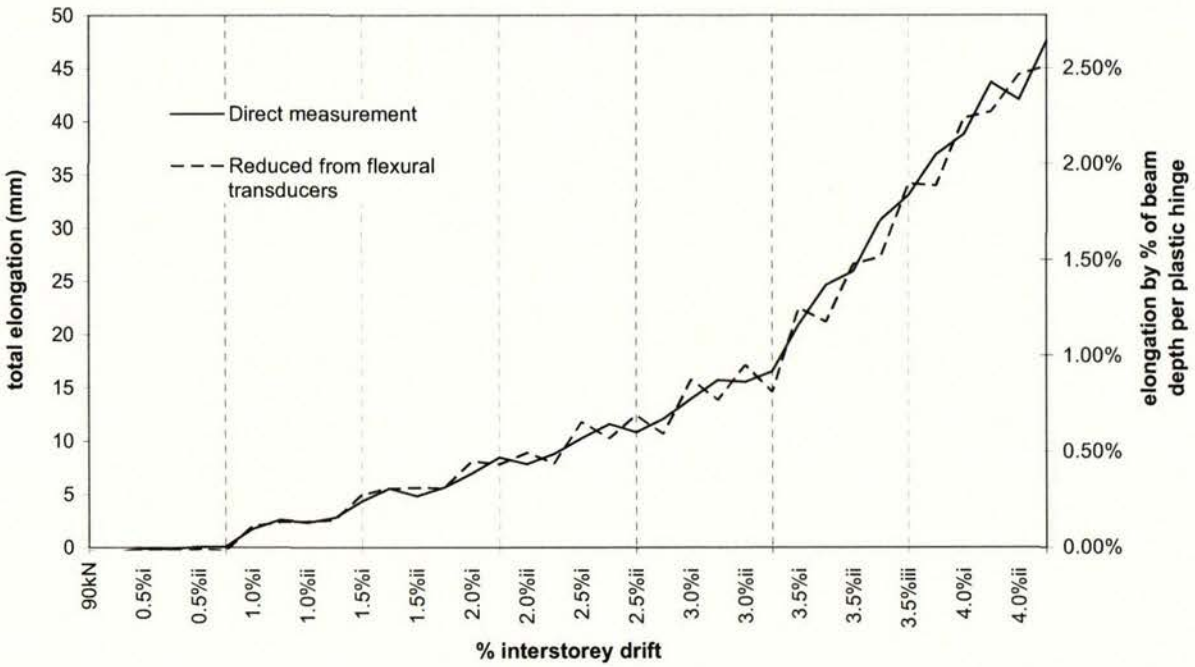

Figure 5.20: Total elongation of beams at peaks of lateral displacement steps (see values in Appendix 3).

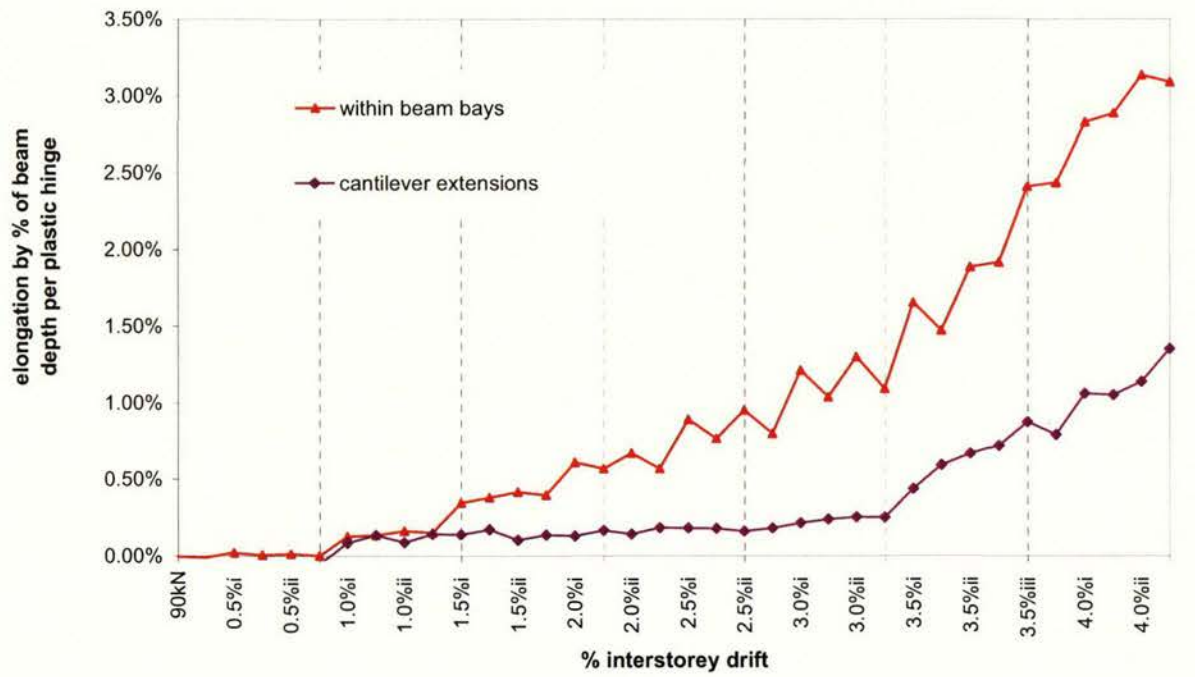

Figure 5.21: Elongation in hinges within beam bays compared to elongation in hinges in cantilever extensions (see values in Appendix 3).

Figure 5.21 shows that there is a large difference in the elongation recorded between the hinges within the beam bays and those in the cantilever extensions. At the peak of 3.0% interstorey drift, the average elongation per plastic hinge was 1.25% per plastic hinge,

while in the cantilevers the corresponding value was 0.25%. At the end of the test, elongation was 3.28% of beam depth per plastic hinge within the beam bays, while in the cantilevers it was 1.35%. The difference in elongation of the inner hinges and those in the cantilever extensions were due to the rotation sustained by the hinges. Figure 5.22 shows the average change in rotation of the plastic hinges, between the positive and negative peaks of the drift cycles. The rotations were measured over a distance of approximately one beam depth. As shown by the figure, the changes in rotation sustained by the inner hinges were greater than the hinges in the cantilever extensions.

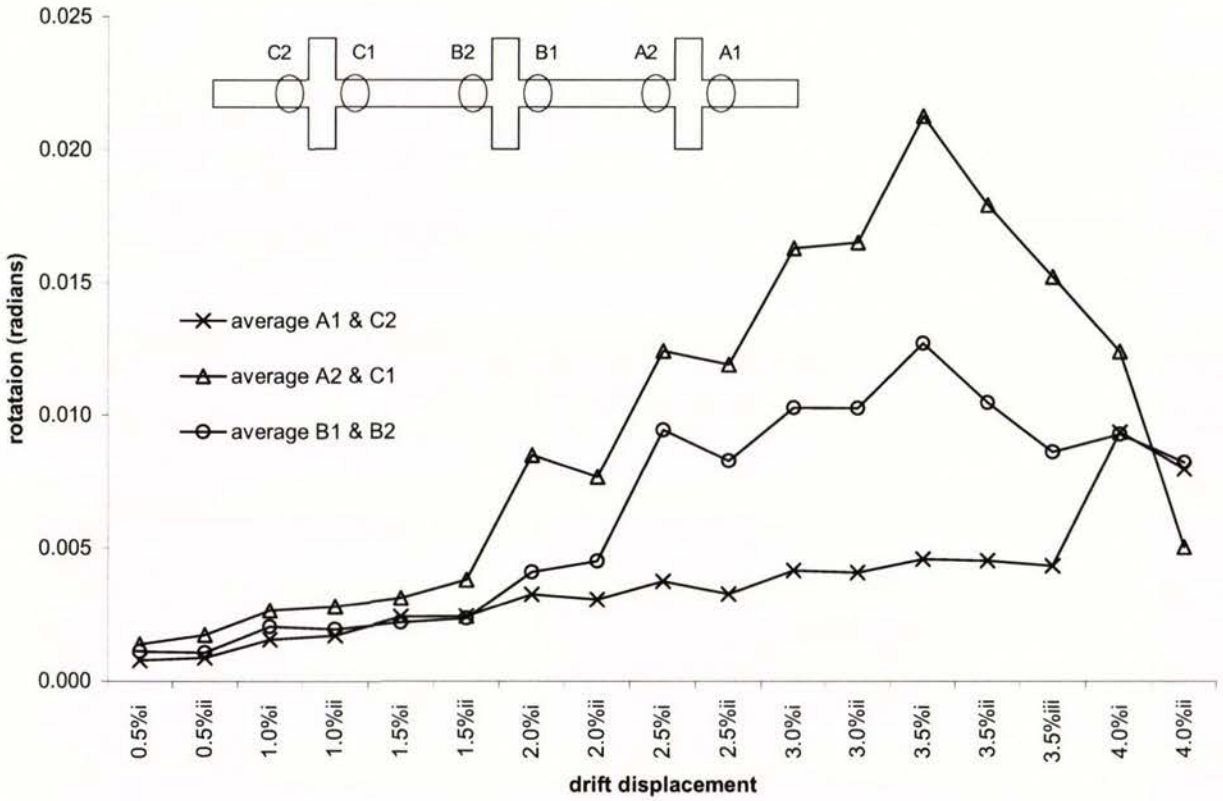

Figure 5.22: Change in rotation of plastic hinges between cycle peaks.

5.8 Slab Measurements

DEMEC points were placed on the slab as described in *Section 3.7.5* (*Chapter 3*). Figures 5.23 shows the elongation calculated from the DEMEC measurements obtained from the first three rows of measurement points compared against the direct elongation measurement of the beams. Measurements were only taken up to 3.0% drift as a number of the DEMEC points near the beam and floor interface had fallen off. The first

row of points (row a) were 110mm away from the inside beam face where the direct elongation was measured. The second row of points (row b) was 450mm, while the third (row c) was 900mm away from the beam face. The locations of the rows are shown in Figure 3.26 of *Chapter 3*.

There is good agreement between the direct elongation measurements and those taken from DEMEC points. In both floor spans (though more prevalent in the north span), as shown in Figure 5.23(a), elongation decreases as the frame reversed in drift direction. As the frame was displaced in the positive direction, in the north span, two plastic hinges were subjected to negative (hogging) bending and one plastic hinge was in positive bending. Therefore the reinforcement at the top of the two hinges elongated in tension and shortened in compression at the other hinge. On reversal of direction, at the top of the beams, two hinges shortened and one elongated. The elongation measured on the floor slab shown in Figure 5.23(a) exhibited this behaviour as the floor was located in the same plane as the top of the beams. As expected, as shown in Figures 5.23, the measured elongation in the floor was less than the elongation in the beams as the distance away from the beams increased.

The distribution of elongation on the floor slabs is shown in Figures 5.24. By comparing Figure 5.24(a) and (b), it can be seen that as the frame was displaced in the positive direction, the elongation in the north span increased while elongation in the south span decreased. The reverse is true as the frame was displaced in the negative direction. The crack width at peak displacements between the floor spans and the central transverse beam is shown in Figures 5.25. From comparison of Figures 5.24 and 5.25, it can be seen that a large proportion of the total elongation in the floor was due to the crack at the central transverse beam. The crack widths at the central transverse beam and the elongation of the floor slabs (measured at 100mm from the face of the beam) are compared in Table 5.3. It can be seen in both slabs that the crack width at the central transverse beam make up 55 to 79% of the total slab elongation in the north slab when the unit was displaced in the positive direction. In the south slab, it was 64 to 72% when displaced in the negative direction. On reversal of direction, the cracks at the central transverse beam close up, making up 8 to 20% of the total elongation in the north slab, and 0 to 16% in the south slab.

Table 5.3: Crack width between central transverse beam and north slab compared to elongation in floor slab at 110mm away from beam face.

drift displacement	North Slab		
	elongation in floor slab, E_s (mm)	crack width at central transverse beam, C_c (mm)	C_c / E_s (%)
+1.0%	1.1	0.6	55%
-1.0%	1.2	0.1	8%
+2.0%	4.4	3.2	73%
-2.0%	3.1	0.6	19%
+3.0%	8.1	6.4	79%
-3.0%	5.6	1.1	20%
	South Slab		
+1.0%	0.8	0.1	13%
-1.0%	1.4	0.9	64%
+2.0%	3.3	0	0%
-2.0%	4.7	3.4	72%
+3.0%	5.6	0.9	16%
-3.0%	8.8	6.1	69%

By comparing Figures 5.24(a) and 5.25(a) for displacements in the positive direction, it can be seen for the south slab that the majority of the total elongation near the face of the beam (first row of DEMEC points) was in the floor, as the crack width at the transverse beam was small. This pattern is similar for the negative direction in the north floor slab. This is explained by the opening of the diagonal cracks near the outer columns (see Figures 5.26) as the cracks at the central transverse beam reduced in width.

Figures 5.25 also show that the crack width between the floor slab and the transverse beam was larger in the south slab than in the north slab, particularly from the third rib and beyond. The plots show that the crack in the north slab closed more in comparison to the south slab as direction of displacement was reversed. The crack in the south slab also propagated further into the slab than the crack in the north slab throughout the entire test. This is shown by the crack patterns on the floor slab in Figures 5.26.

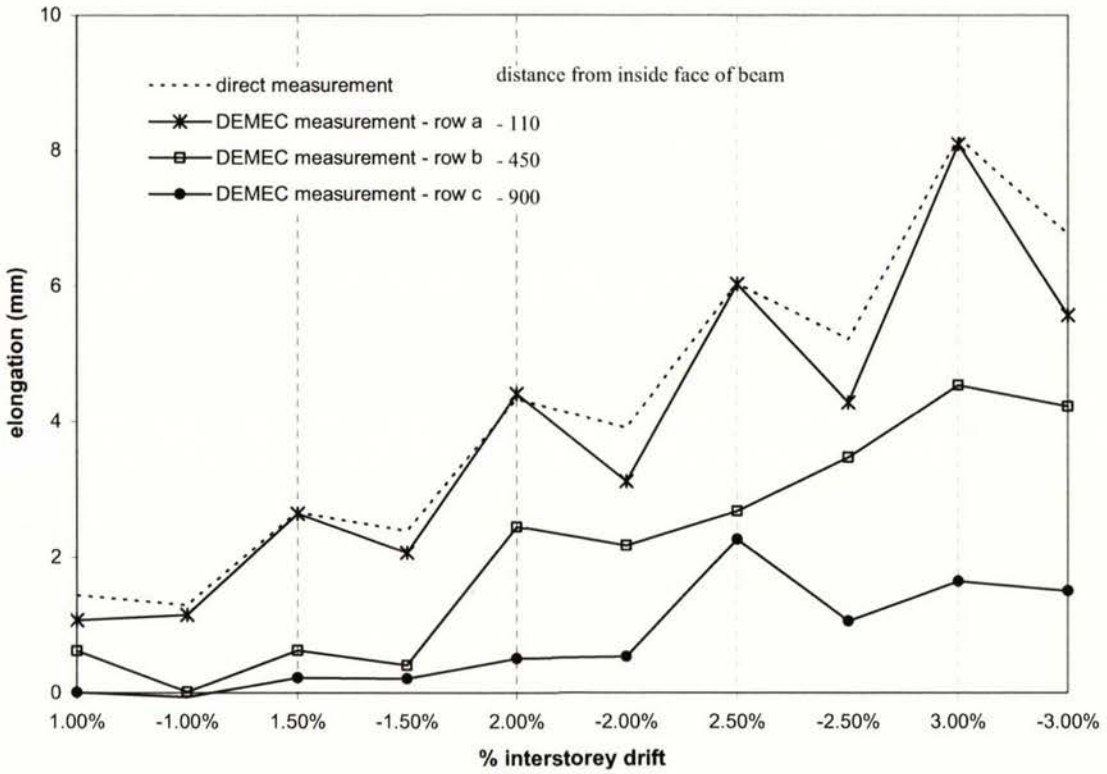

(a) North span

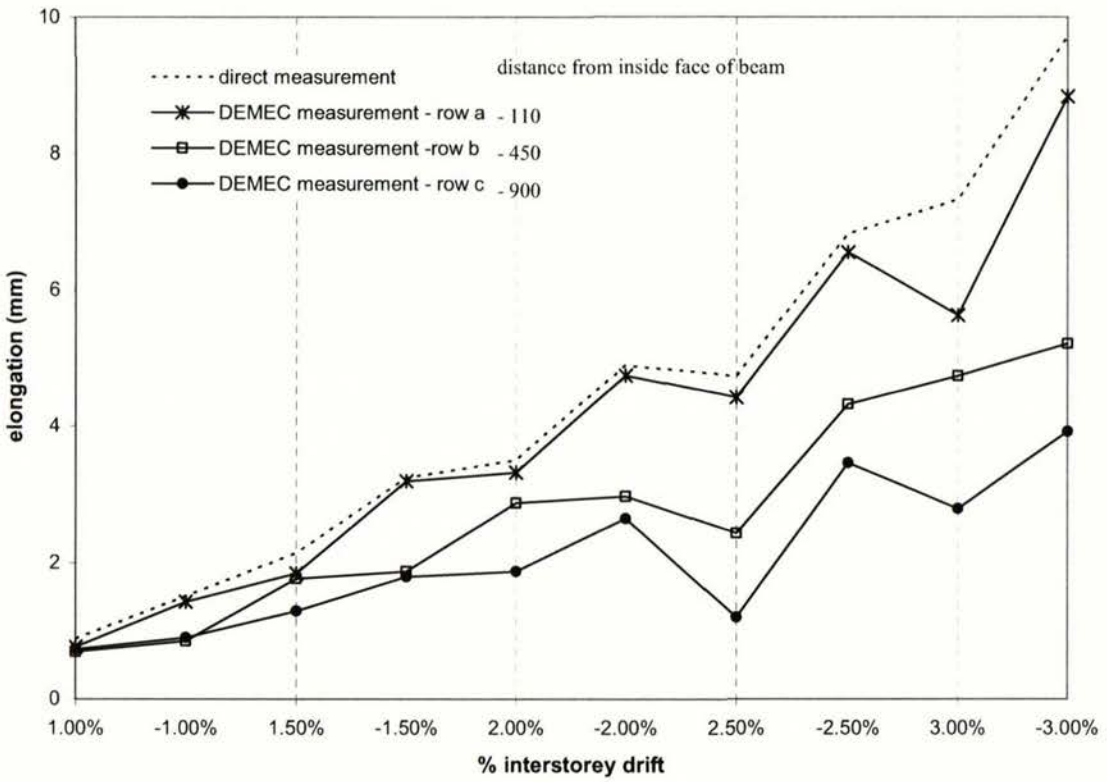

(b) South span

Figure 5.23: Total elongation measured on floor spans compared against elongation from direct measurements at peak displacements.

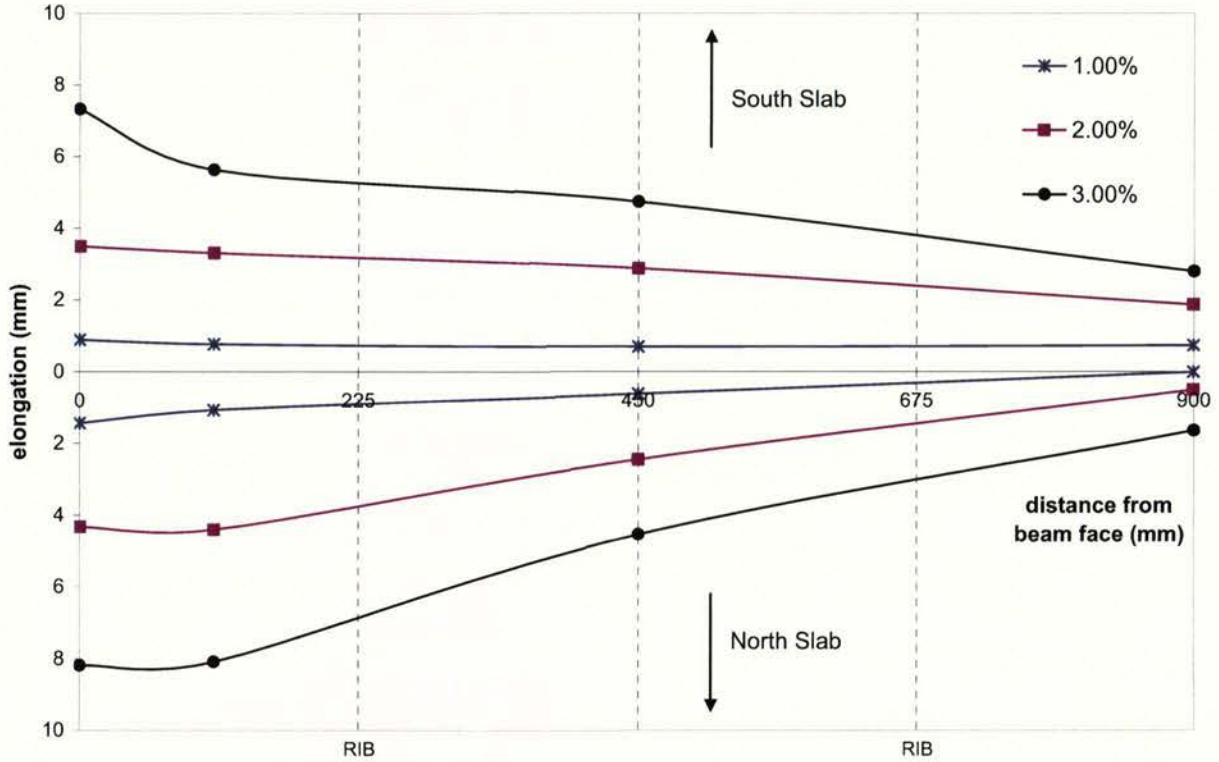

(a) Displacement in positive direction

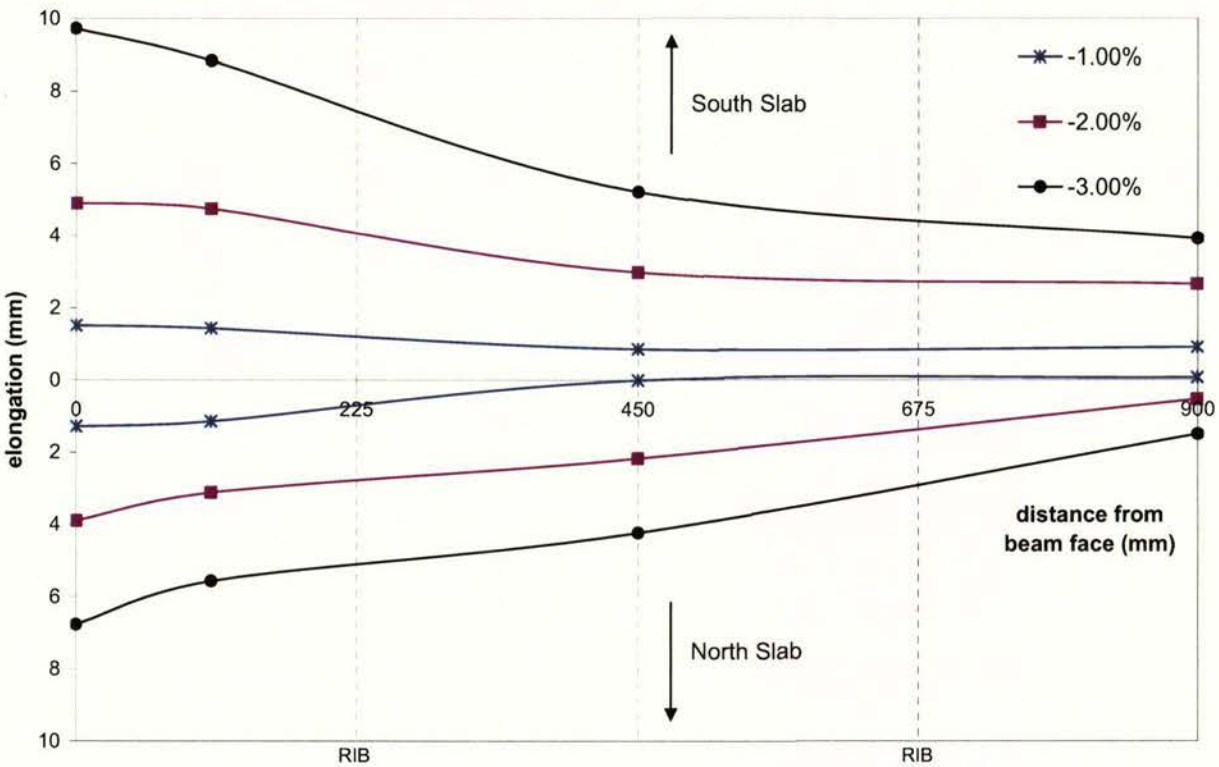

(b) Displacement in negative direction

Figure 5.24: Distribution of floor slab elongation at peak displacements.

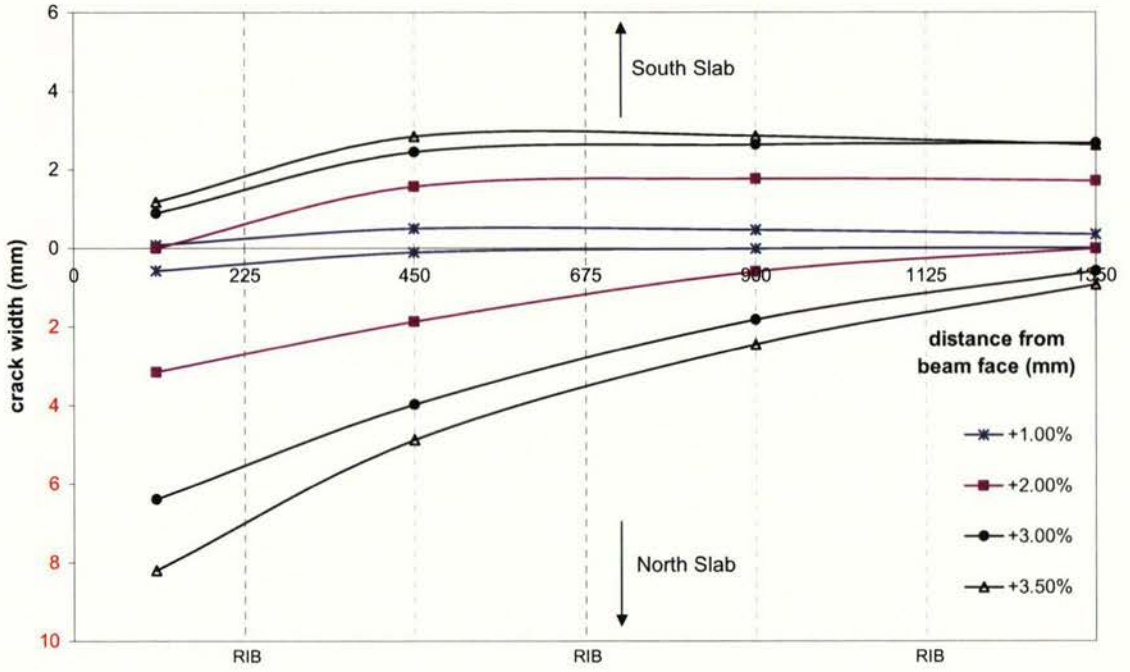

(a) Displacement in positive direction

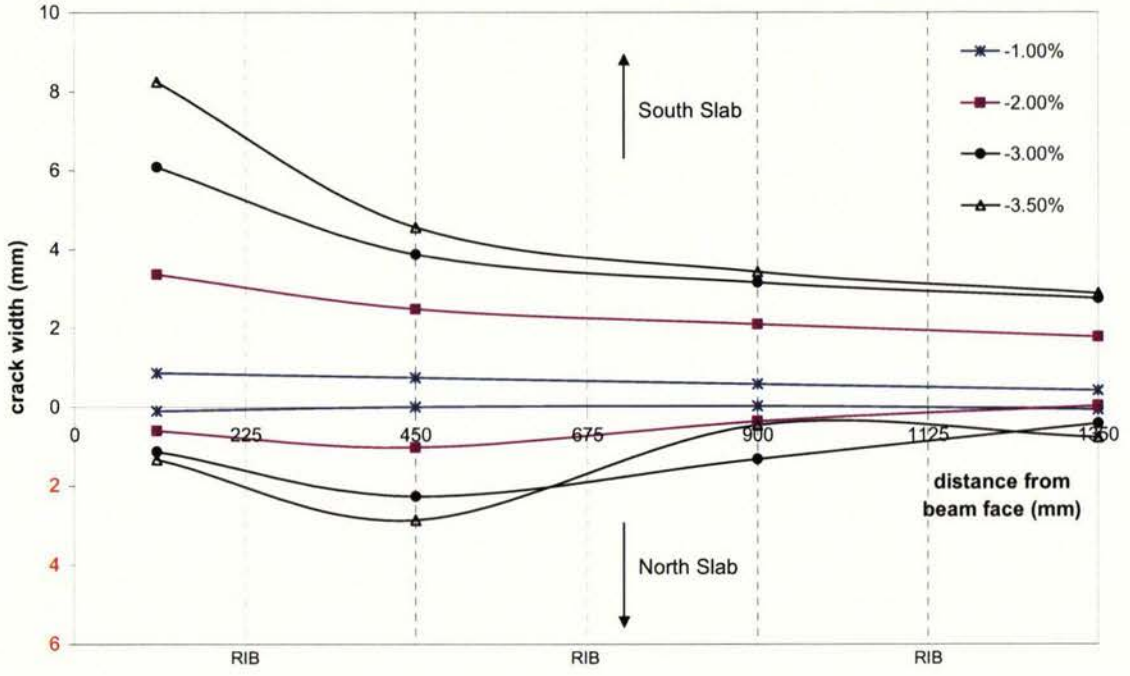

(b) Displacement in negative direction

Figure 5.25: Crack width between floor and central transverse beam measured at peak displacements.

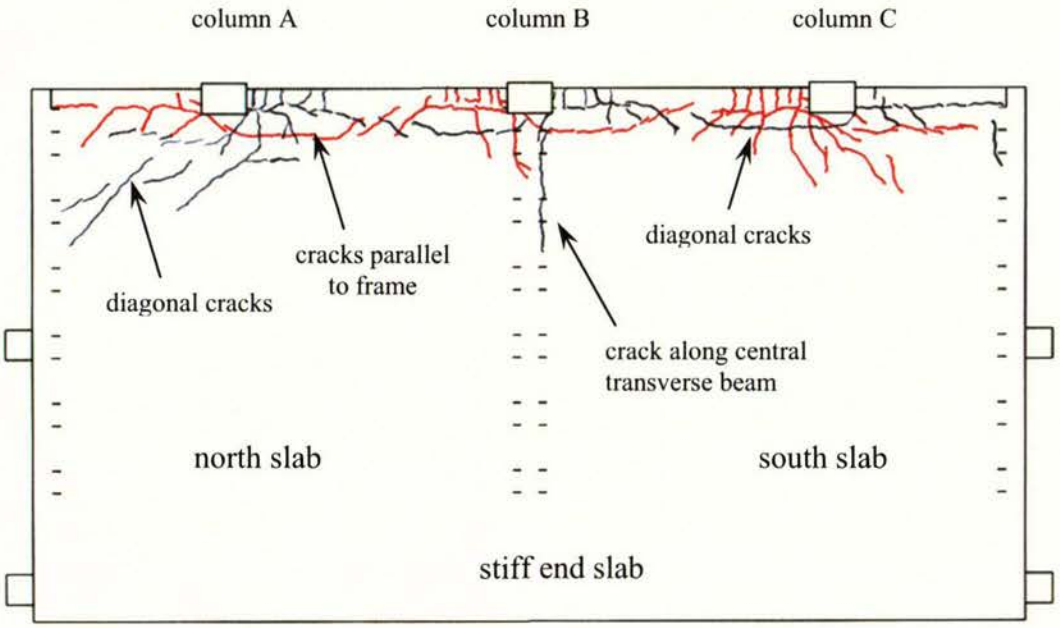

(a) Displacements up to 1.0% interstorey drift

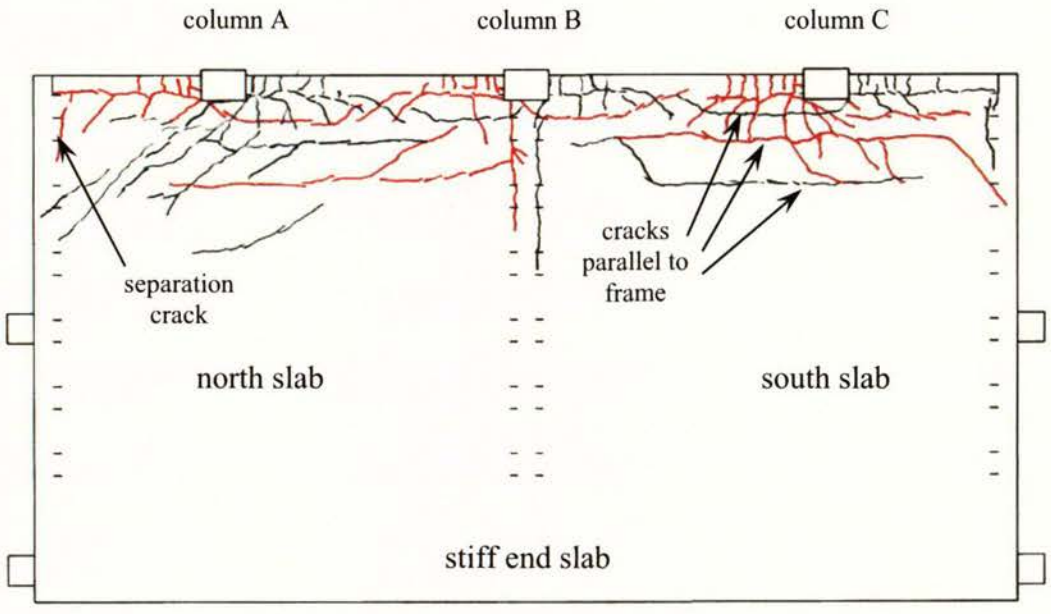

(b) Displacements up to 1.5% interstorey drift

Figure 5.26: Crack pattern on floor at different displacement levels. (continued)

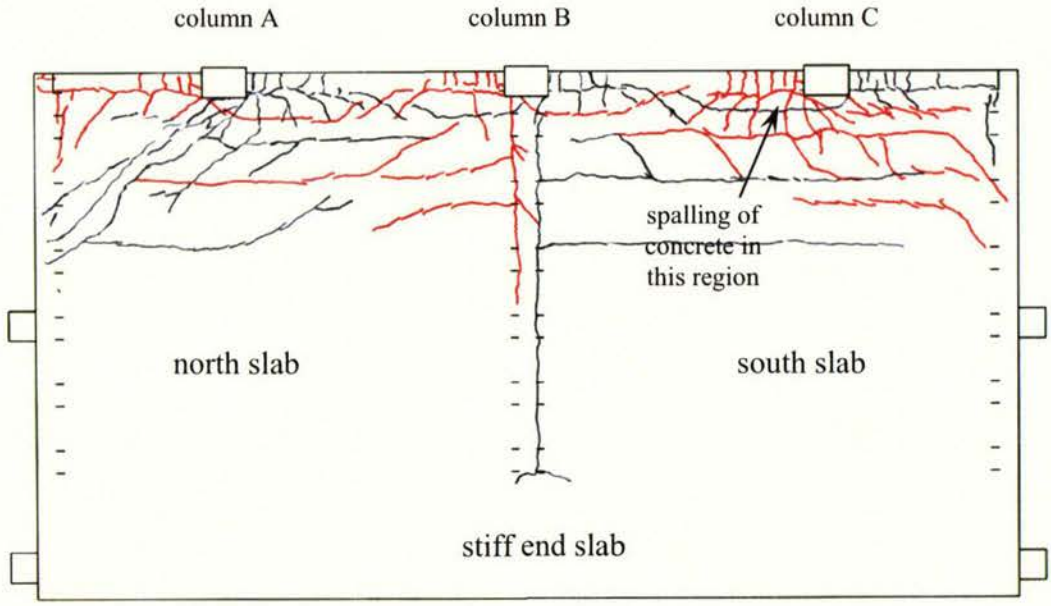

(c) Displacements up to 2.0% interstorey drift

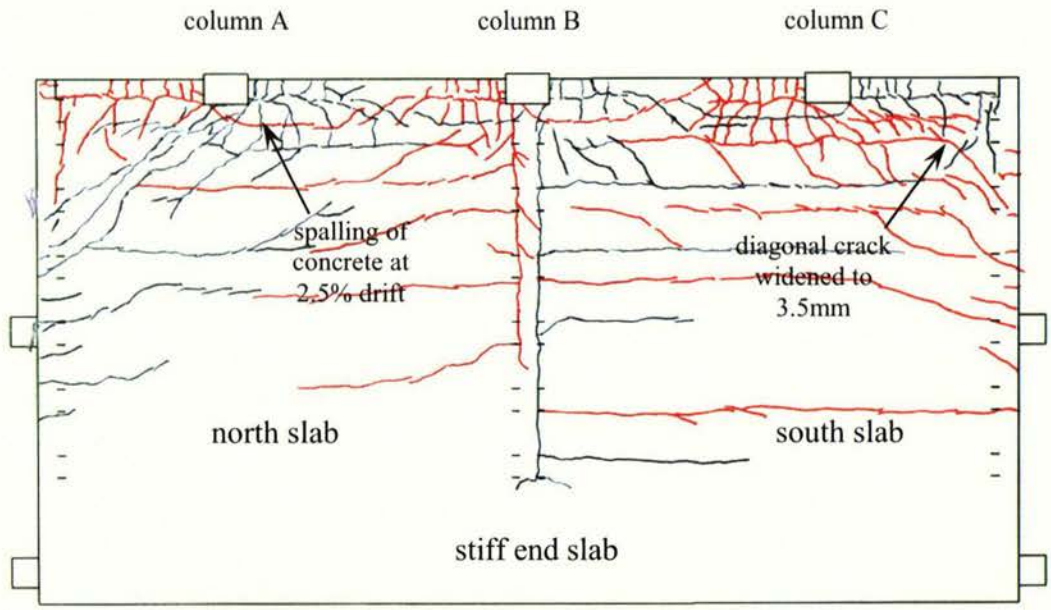

(d) Displacements up to 3.0% interstorey drift

Figure 5.26: Crack pattern on floor at different displacement levels. (concluded)

Chapter 6

Test Results of Unit 3

6.1 Introduction

This chapter presents the results from the experiment on the second of the plane frame units, Unit 3, together with general observations made during the experiment.

6.2 Displacement History

This unit was subjected to a similar displacement history that was applied to the frame-floor slab unit, Unit 2. This displacement history is shown by Figure 6.1. The percentage interstorey drift is the displacement applied, measured between the pin at the top and the bottom of the columns. Three displacement cycles up to ± 0.1% interstorey drift were applied to the frame, followed by two cycles of displacements up to ± 0.2% interstorey drift. The data collected from these test cycles were checked to ensure correct operation of the instrumentation. Then it underwent two cycles to 65% of the theoretical lateral strength calculated (flexural strength of beams calculated assuming rectangular stress block in beam compression) for the test unit based on material tests. As shown in Figure 6.1, further displacement cycles were set at steps of 0.5% interstorey drift, with two complete cycles at each step. The unit was displaced for two cycles at ± 3.5% interstorey drift before testing was concluded.

Figure 6.2 shows the displacement history for each of the columns from displacement at 65% of the theoretical lateral strength to 3.5% interstorey drift. As can be seen in the plot, the columns were kept parallel to one another up to 2.5% interstorey drift. Over these displacement cycles, the largest out of parallel difference between the columns was 0.7mm during a displacement cycle to ± 2.5% interstorey drift. On the following cycles, it became increasingly difficult to keep the columns parallel. This was due to some twisting at the base of column 'A' (discussed later). During the cycles to ± 3.0%

interstorey drift the largest out of parallel displacement was 2.4mm while during the cycles to ± 3.5% interstorey drift, the largest difference was 7.1mm.

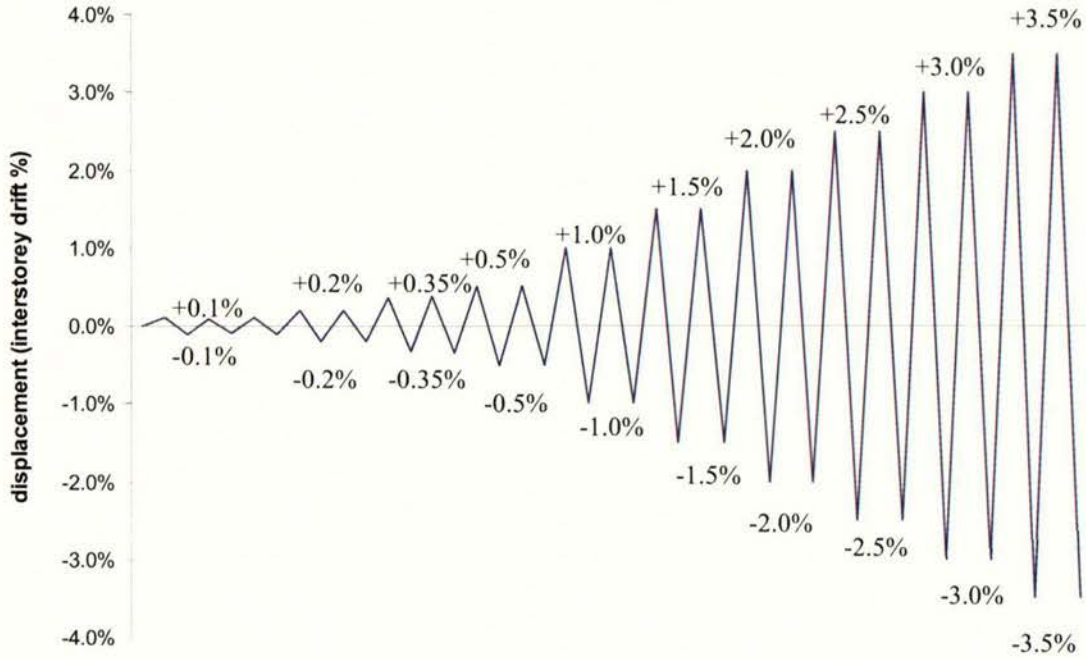

Figure 6.1: History of displacement levels applied to Unit 3.

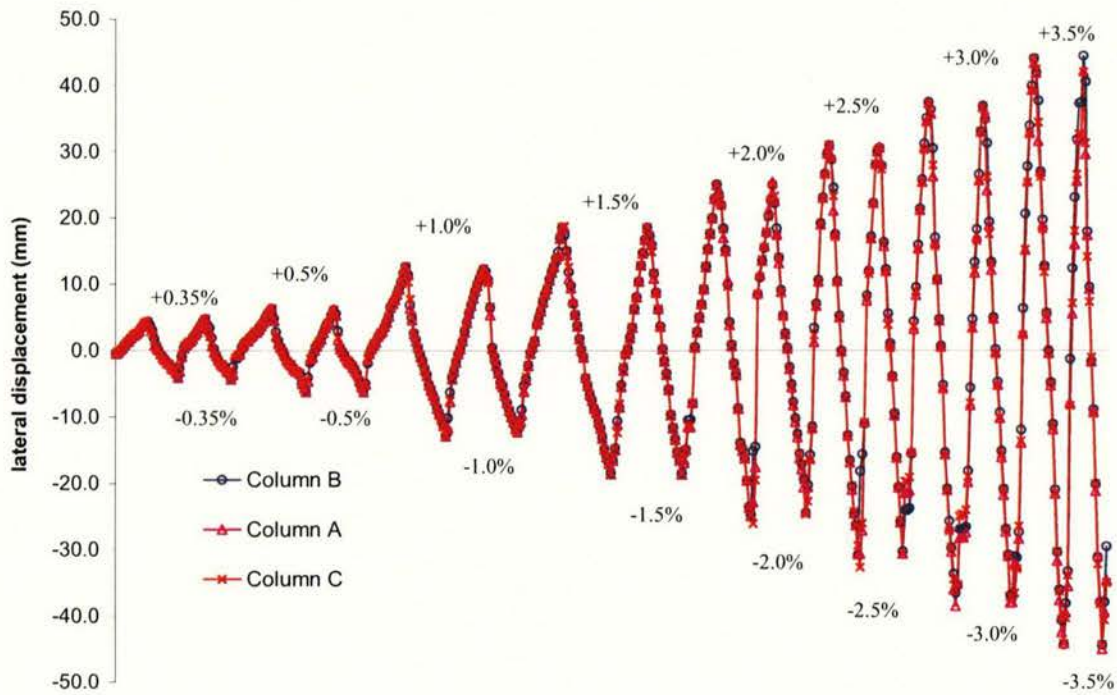

Figure 6.2: Lateral displacement history of columns from 65% of F_y to 3.5% interstorey drift.

6.3 General Behaviour and Observations During Test

Shrinkage cracks in the frame were located and marked before the test. The shrinkage cracks were difficult to see with the unaided eye as they were less than 0.1mm in width. It took two weeks to complete the test. The initial elastic cycles were performed in four days.

Displacement cycles from 0.1% interstorey drift to displacement at 65% of frame theoretical strength

The unit was displaced to ± 0.1% interstorey drift for three cycles. This corresponded to a displacement of ± 1.2mm at the top of the columns relative to the bottom (hence referred to as relative displacement in this document). Over these cycles, the maximum lateral load was 24.6kN. The unit was then displaced up to ± 0.2% interstorey drift. In these load cycles fine flexural cracks had formed in the beams. However, cracks were not present in the beam-column joint zones.

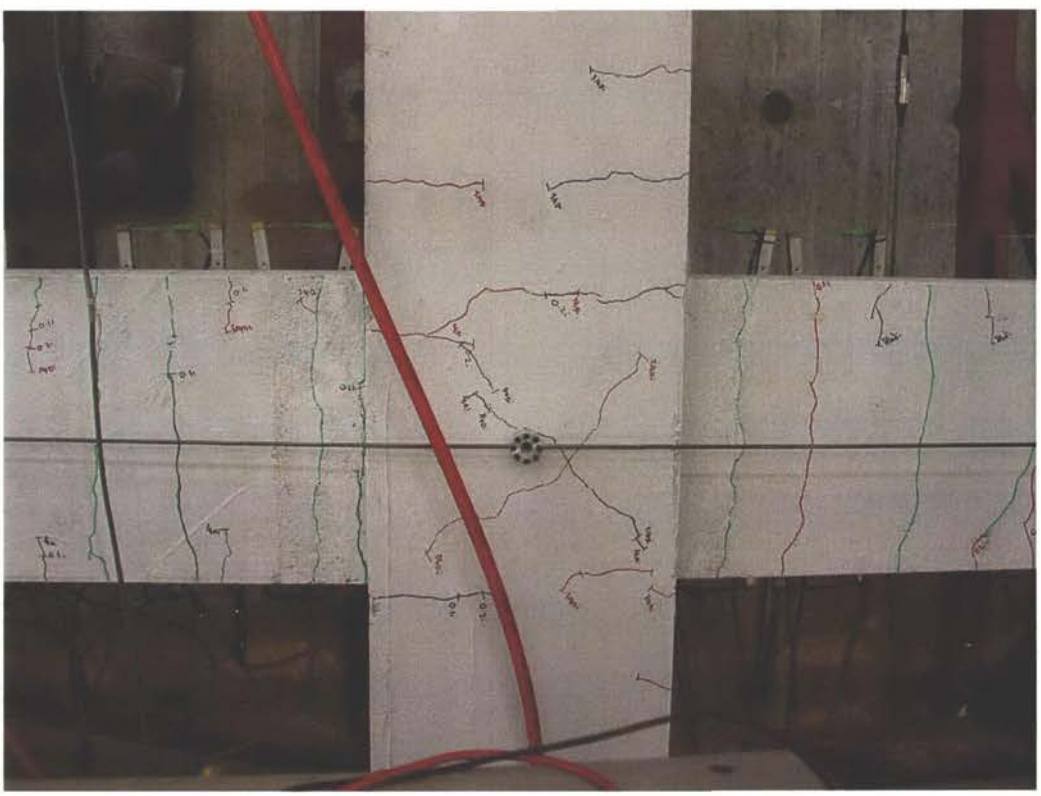

Figure 6.3: Joint cracks in joint 'B' at 65% of frame theoretical lateral strength.

The unit was then loaded up to around of 67kN in both directions for two cycles. This corresponded to 65% of the theoretical lateral strength of the test unit. The average displacement was 0.35% interstorey drift. During these load cycles diagonal cracks had formed in beam-column joint 'B' (central joint, also refer to Figure 3.11 in *Chapter 3*) as shown in Figure 6.3. The red lines represent cracks formed at displacement in the positive direction (southward), while the black lines indicate cracks formed at negative displacement direction.

Data collected from the experiment was downloaded for checks on readings from the instrumentation. Tape measurements and theodolite readings taken between a reference point and the top of the columns were used to check against the electronic readings of the column displacements. Tape measurements were also taken between the centres of the joints to check against elongation readings from the displacement transducers.

Displacement cycles up to 1.5% interstorey drift

The next step in testing was to displace the unit to $\pm 0.5\%$ interstorey drift. Two displacement cycles to this level was applied. More flexural cracking was apparent in the beams and columns, but these cracks did not exceed 0.15mm in width.

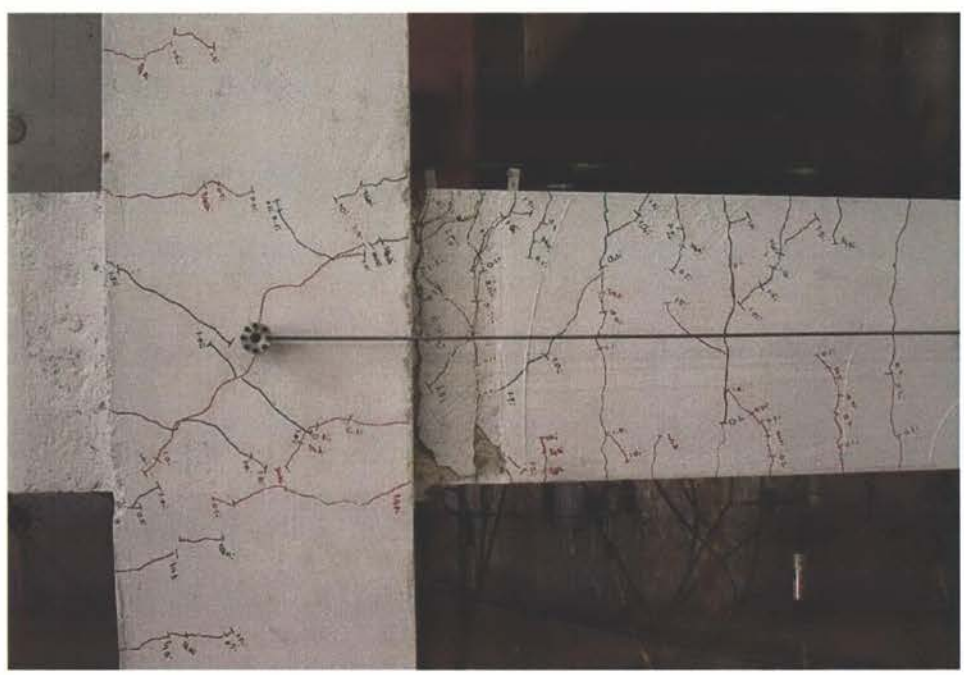

Figure 6.4: Beam-column joint 'A', at 1.5% interstorey drift.

The unit was then subjected to displacements up to ± 1.0% interstorey drift for two cycles. Cracking was mainly confined to the plastic hinge zones and beam-column joints. Most of the cracking was concentrated in the beam at the column face. In the beam plastic hinge zones next to joints 'A' and 'C' diagonal cracks formed at approximately 60° to the horizontal. Diagonal cracks also formed in the joint zones of all the columns. As expected, at displacements up to ± 1.5% interstorey drift, the cracks formed in the previous cycles had extended and widened. A picture of the beam-column joint of joint 'A' is shown by Figure 6.4.

Displacement cycles up to 3.5% interstorey drift

The unit was then displaced to ± 2.0% interstorey drift for two cycles. Diagonal cracks formed in the beam plastic hinge zones next to joint 'B'. During this stage, some abnormal movement was detected at the base of column 'B'. This was thought to be caused by the slack in the pin connections at the base. The test unit was then displaced up to ± 2.5% interstorey drift. On closer inspection during the first cycle of this displacement step, the loading frame at the base of column 'B' was actually sliding by around 8mm both ways. This was thought to be caused by the shrinkage of the mortar bed at the base of the loading frame as the frame was put in place some months before testing began. The test was stopped and loads released after the first cycle to 2.5% interstorey drift. The mortar was replaced and the frame was restressed down to the strong floor. Testing recommenced on the following day.

On displacement up to ± 3.0% interstorey drift, diagonal cracks in the beams had increased in width and damage had also spread along the plastic hinge zone by about one beam depth. Significant spalling of cover concrete had occurred resulting in the exposing of beam reinforcement in the beams adjacent to the outside columns. At the central columns, spalling of concrete on the column faces next to beams indicate some pulling out of the beam reinforcement in the joint zone. The unit was then displaced to ± 3.5% interstorey drift for two cycles before testing was concluded. The plastic hinges in the beams at the end of the test is shown by Figure 6.5.

(a) Beam-column joint 'B'

(b) Beam adjacent to column 'C'

Figure 6.5: Test unit at end of test.

In these latter stages, it became increasingly difficult to control the test by adjusting the hydraulic pumps such that the columns would remain parallel. It was discovered during displacement step to $\pm 3.5\%$ interstorey drift that column 'A' had rotated out of the plane of the frame. This rotation was caused by the rotation of the swivelling pin which connected the load cell to the base of the column. This meant that the elongation measurement along the beam of bay 'A'-'B' had been less than the actual elongation (see Figure 6.6). This measurement was critical for accurate control of the test as shown by *Equations 3.18 – 3.20* in *Chapter 3*.

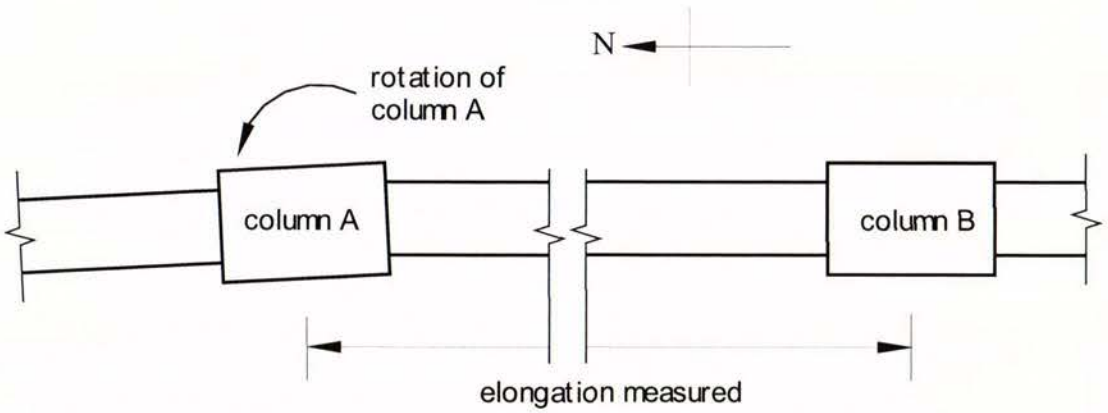

Figure 6.6: Rotation of column 'A'.

This problem was highlighted during the negative displacement cycles (in northwards direction). Due to the under-measured elongation of the beam between column 'A' and column 'B', the base of column 'A' was displaced by a lesser amount than what should have been had the column remained plane (see *Equation 3.19*), and in order to maintain parallel columns (see *Equation 3.1*), the top of column 'A' had been subjected to lesser displacements that what would have been likely. Therefore very little load was recorded at the top of column 'A' while higher loads were measured at the base of the column. Due to the distribution of forces in the frames, a higher force was applied at the top of column 'B' and lower force at base of column 'B'. This meant that the beam in bay 'A'-'B' sustained an appreciable level of axial force. This problem with the rotating pin was not detected in columns 'B' and 'C'.

6.4 Force versus Displacement Response

The force versus displacement response in the elastic stages is shown in Figure 6.7. The maximum lateral force applied at this stage was 67.8kN at a lateral displacement of 4.7mm, and 68.8kN in the reverse direction at a lateral displacement of 4.3mm. By interpolation, the average yield displacement is 6.7mm, which corresponds to an interstorey drift of 0.55%.

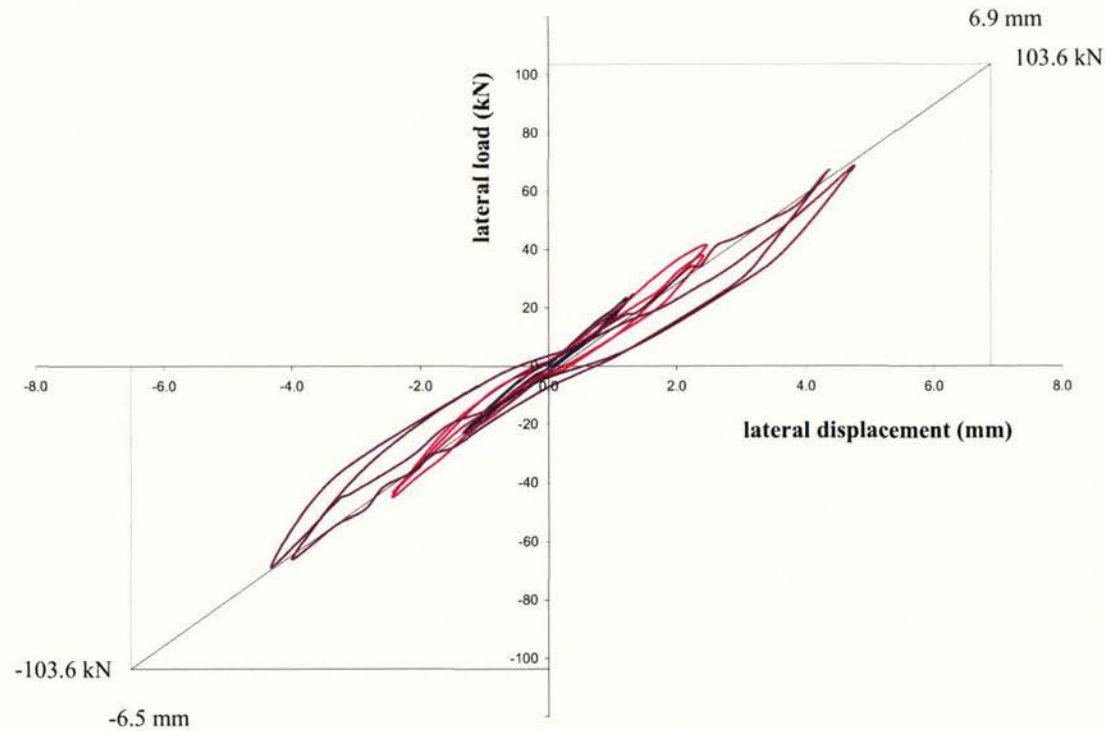

Figure 6.7: Force versus displacement response in the elastic range, up to 65% of nominal lateral strength of frame.

The lateral force versus displacement response for the whole test is shown in Figure 6.8. Solid lines indicate the first cycle for each interstorey drift level and subsequent cycles are marked with dashed lines. The maximum lateral force in the positive direction was reached at the peak of displacement to 1.0% interstorey drift. The maximum value in the positive direction was 114.2kN. In the other direction, the maximum lateral strength of 125.6kN was reached at 2.5% interstorey drift. The figure also shows the theoretical lateral strength of 103.6kN, calculated based on material tests and assuming a rectangular compression stress block as defined in the New Zealand Concrete Standard

[S1]. The maximum value in the positive direction was 10.2% greater than the theoretical value, while it was 21.2% more in the negative direction.

The test unit failed to reach 80% of the maximum lateral strength in the negative direction following the second cycle to 3.0% interstorey drift. As expected, due to strength degradation and opening of cracks, the lateral strength recorded in the second displacement cycles at each displacement step was less than the value recorded in the first cycles. Pinching of the curves was more evident following the displacement cycles to ± 2.0% interstorey drift as shear deformations increased as displacements got larger.

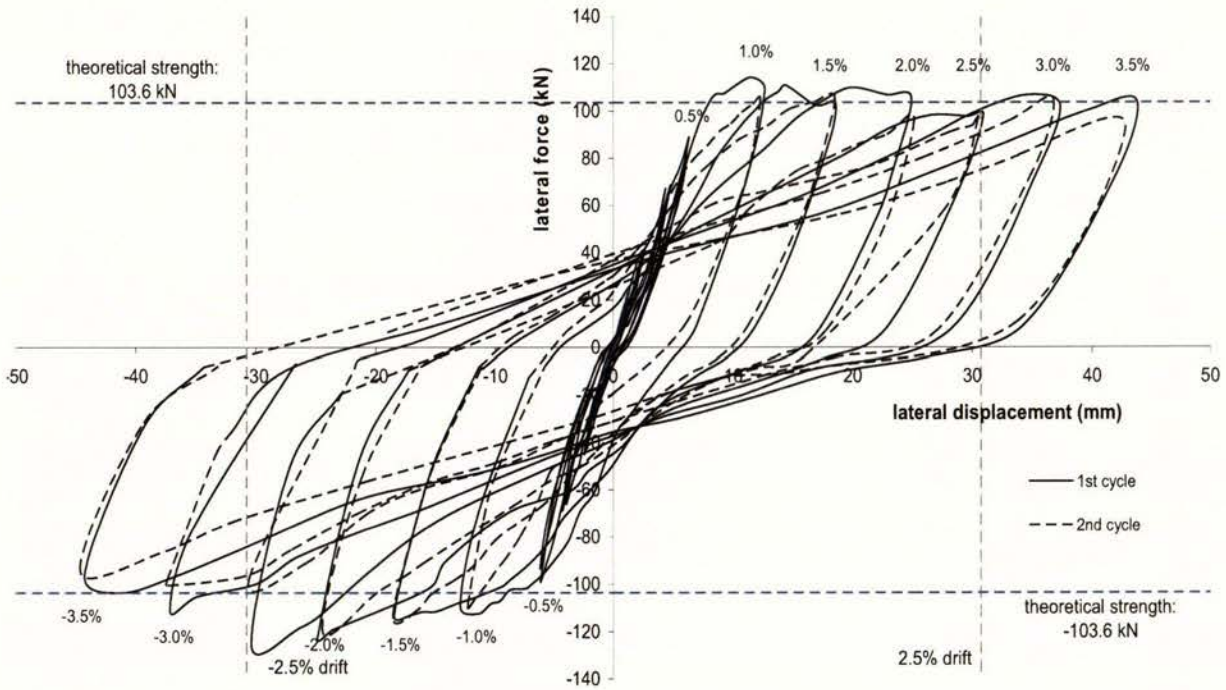

Figure 6.8: Lateral force versus displacement response of test unit.

The differences in the sum of the lateral force applied at the top of the columns and the sum of the lateral forces resisted at the column bases at different stages of the experiment were small. This is shown by Table 6.1. The difference between the sum of the top and bottom lateral forces were typically no more than 5 percent at the peak of the displacement cycles.

Table 6.1: Difference in sum of force applied to top and bottom of columns at peaks of displacement cycles.

drift displacement	load at top (kN)	load at bottom (kN)	difference (kN)	difference (%)
0.5%	88.0	89.0	1.0	1.1
	-98.3	-96.9	-1.4	1.4
1.0%	108.7	112.6	3.9	3.6
	-109.3	-108.9	-0.4	0.4
1.5%	103.7	107.2	3.5	3.4
	-113.3	-113.6	-0.3	0.3
2.0%	105.3	108.9	3.6	3.4
	-122.8	-123.0	-0.2	0.2
2.5%	98.0	102.2	4.2	4.3
	-125.6	-123.0	-2.6	2.1
3.0%	102.5	105.9	3.4	3.3
	-113.3	-112.3	-1.0	0.9
3.5%	104.3	108.5	4.2	4.0
	-95.2	-95.4	-0.2	0.2
Note: Values are for 1st cycle of displacement step.				

6.5 Moment Input to Beam-Column Joints

The moment applied to each beam-column joint was calculated from the sum of the lateral forces applied at the top and bottom of each column multiplied by the corresponding distance to the centre of the joint. Figure 6.9 shows a plot of the moment input for each of the beam-column joint at peaks of each cycle. Clearly for all stages, the moment applied to the central joint, joint 'B', was higher than the moment applied at either joints 'A' and 'C'. The moment input to joints 'A' and 'C' were in reasonable agreement. Further from the displacement steps to 2.5% interstorey drift, it can be seen that most of the lost or decrease in the strength of the unit was associated with the decrease in the strength of joint 'B'.

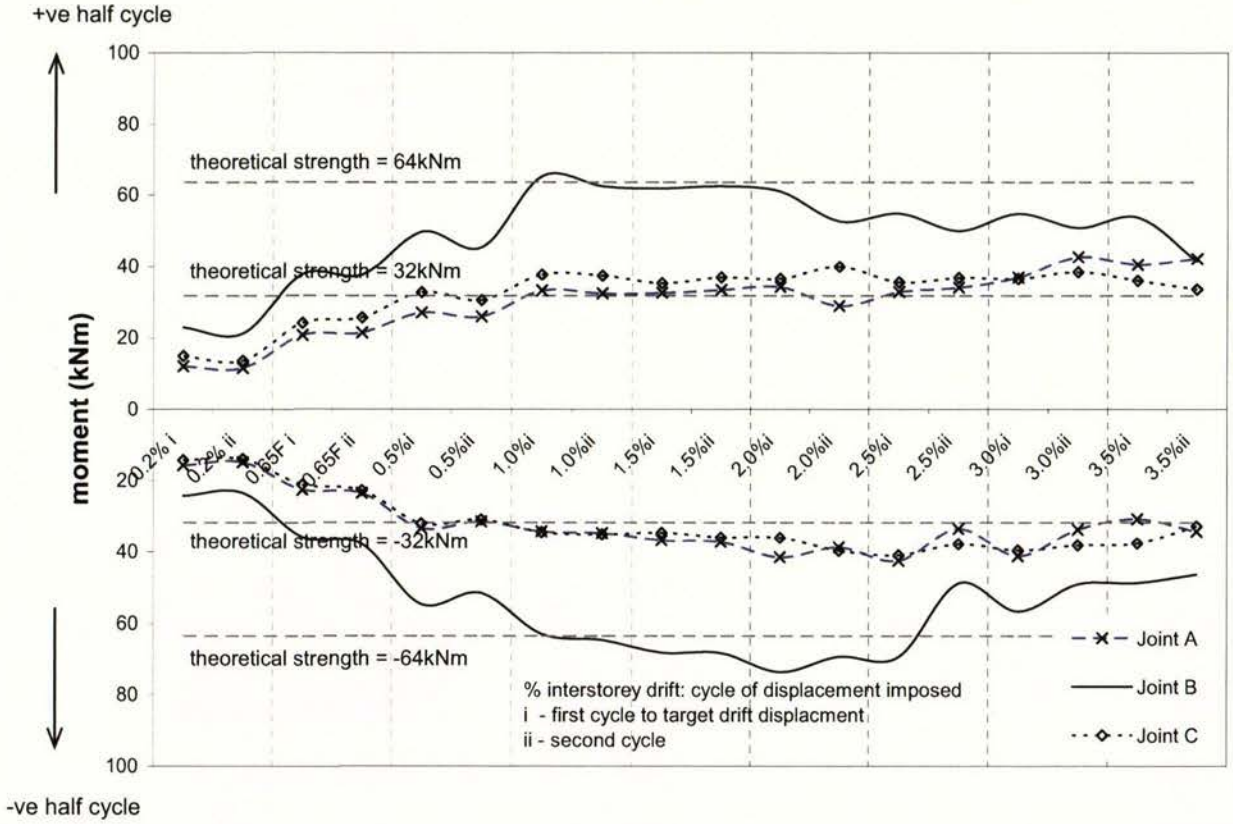

Figure 6.9: Moment input to each beam-column joint at cycle peaks.

The theoretical joint strength calculated from the flexural strength of the beam sections are shown on Figure 6.9. For the outer joints, the theoretical strength was 32kNm, and was 64kNm for Joint 'B'. The experimental peak value for Joint 'B' in the positive direction was 2% greater, and was 15% greater in the negative direction. For the outer joints, the experimental peak values were 33% greater than the theoretical value in both directions.

The comparisons also show that while the outer hinge strengths were maintained in the larger drift cycles, but the central joint strength decreased markedly in these cycles (from 2.5% drift onwards).

6.6 Components of Deformation

The method and equations set out in *Section 3.7.4* were used to calculate the average lateral displacement at the top of the columns from the flexural and shear deformations measured on the beams and columns and joint zones. Figure 6.10 compares the average

lateral displacement measured directly at the top and bottom of the columns with the calculated displacements derived from the measurements taken. The results shown in the figure are the average values from the two beams bays and the three columns. The figure shows that the calculated displacements are in reasonable agreement with the displacement derived from direct measurements, up to displacement cycles to $\pm 2.0\%$ interstorey drift. However further from 2.0% interstorey drift, the difference became increasingly large. This may be due to errors in the transducers and also combined with the twisting of column 'A' (see Figure 6.6) where the deformation recorded at the column face, on the east face of the frame (location of the transducers) would have been greater than the centre-line displacements.

The displacements from direct measurements and the displacements derived from beam and column deformations are also compared by Figure 6.11 with the exception that only columns 'B' and 'C', and the beam between columns 'B' and 'C' were considered. Similar to Figure 6.10, the derived measurements tended to overestimate the lateral displacements of the frame obtained from direct measurements. However, in this case the curves are in reasonable agreement up to $\pm 2.5\%$ interstorey drift, and the errors in both directions are more uniformly spread compared to Figure 6.10.

As expected, the contribution from shear deformation increased as the lateral displacements got larger. Figure 6.12 shows the lateral displacement due to flexural deformation versus the sum of lateral load and the graph of lateral displacement due to shear deformation shown in Figure 6.13. From Figure 6.12, it can be seen that the lateral displacement from flexural deformation was greater in the positive direction than the negative from displacements to $\pm 2.5\%$ drift and onwards. Conversely, the shear deformations were greater in the negative direction than the positive direction. Lateral displacements in the second cycles due to flexural deformation were smaller than that in the first cycle of the same displacement step for the later cycles. This observation can be linked to the increased lateral displacement due to shear deformation in the second cycle of each displacement step. This also explained the pinching in the lateral force versus displacement plot for the second cycles, shown earlier in Figure 6.8.

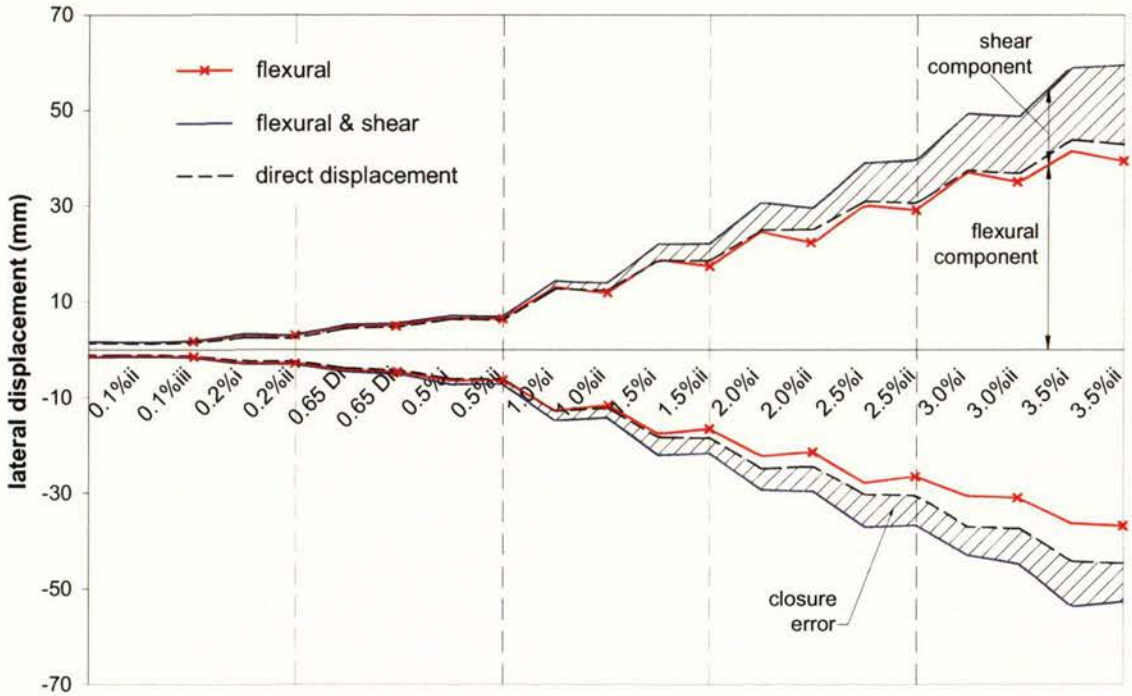

Figure 6.10: Flexural and shear components of deformation in Unit 3.

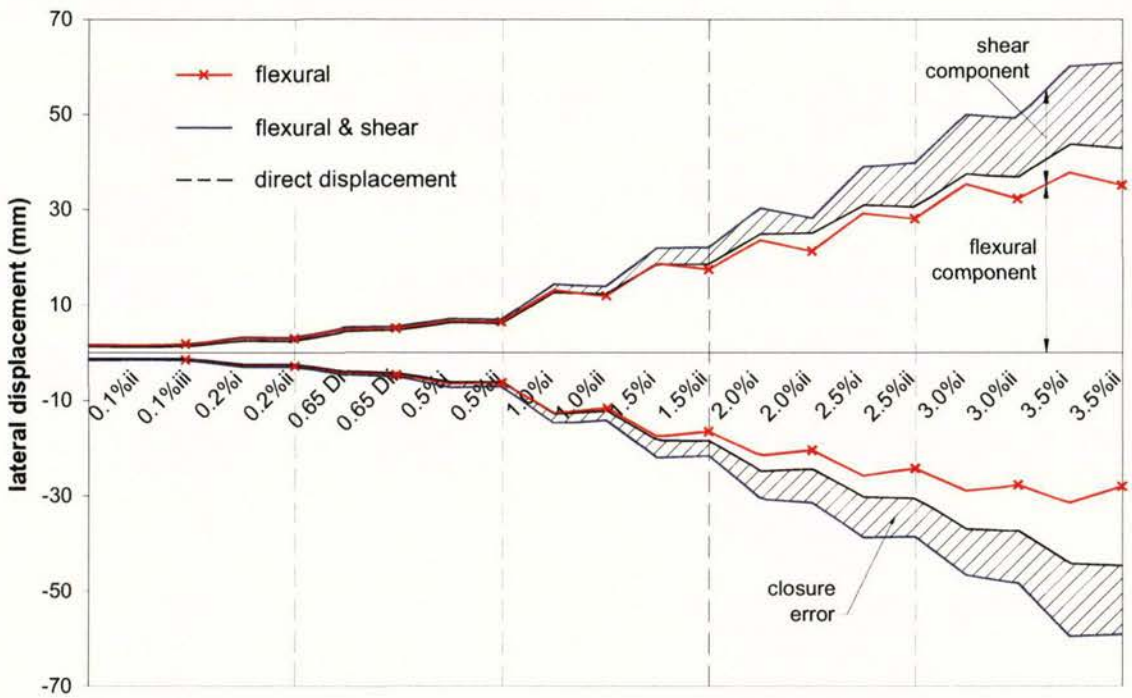

Figure 6.11: Flexural and shear components of deformation of only bay 'B'-'C' of Unit 3.

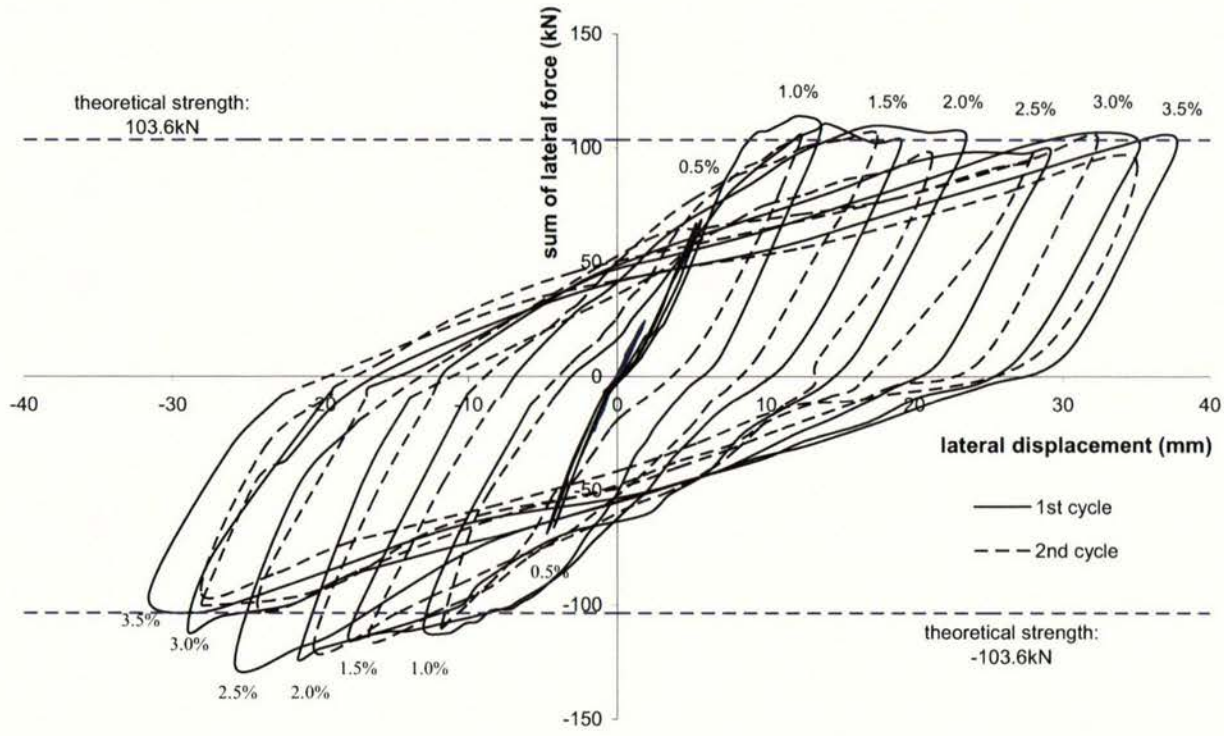

Figure 6.12: Lateral displacements from flexural deformations against the sum of lateral load.

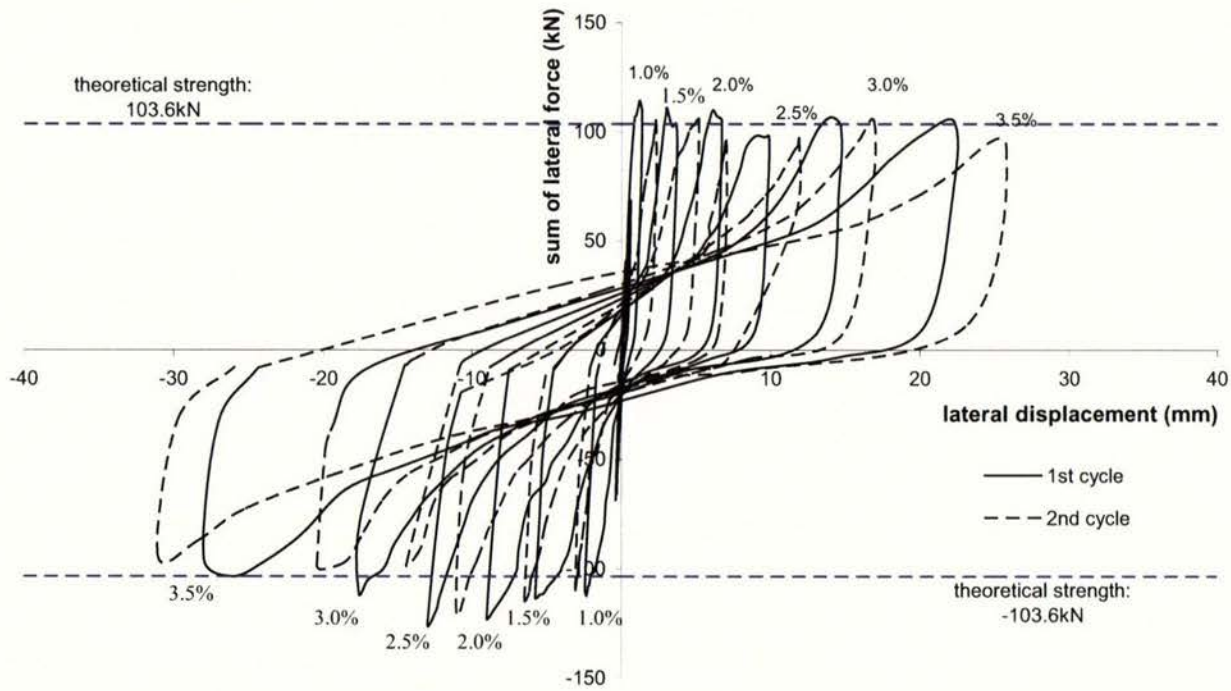

Figure 6.13: Lateral displacements from shear deformations against the sum of lateral load.

Figure 6.14 shows the shear deformation within the central beam-column joints at peak drift levels in the positive direction of lateral displacement. As expected, the shear deformation in joint 'B' was greater than the outer joints. This figure shows that shear deformation in joint 'B' increased at a greater rate up to 1.0% drift then slows from 1.0 to 2.0% drift. It then held an approximately constant level from 2.0% onwards.

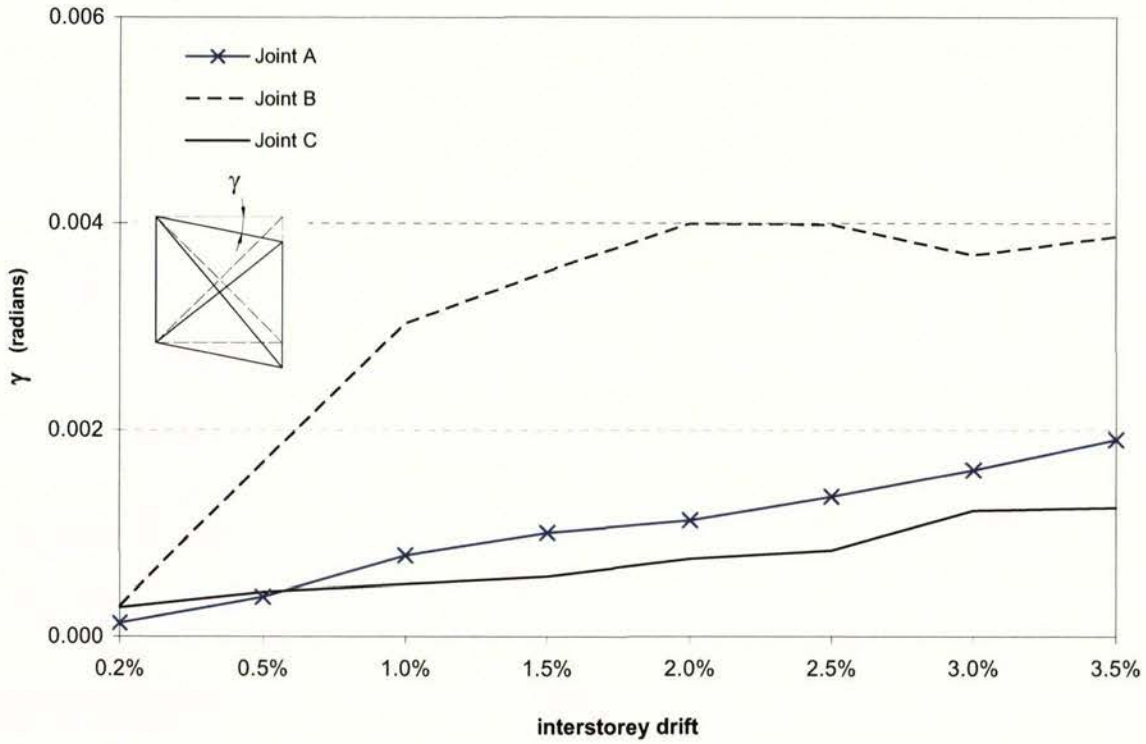

Figure 6.14: Shear deformation in beam-column joints.

6.7 Elongation of Beams

The total elongation of the unit is shown in Figure 6.15 in terms of elongation at the peak of interstorey drift. The elongation of the beam bay 'B'-'C' is shown in Figure 6.16. Two lines were plotted for each of the figures. The solid line was the measurement taken directly between the column centres for both cases, as described in *Section 3.7.3* The dashed line represents the calculated elongation from the measurements taken from the portal transducers mounted on the beams, which was used to measure the flexural deformation. The elongation was calculated from the sum of the elongation measured in each segment, as indicated by *Equation 3.3*.

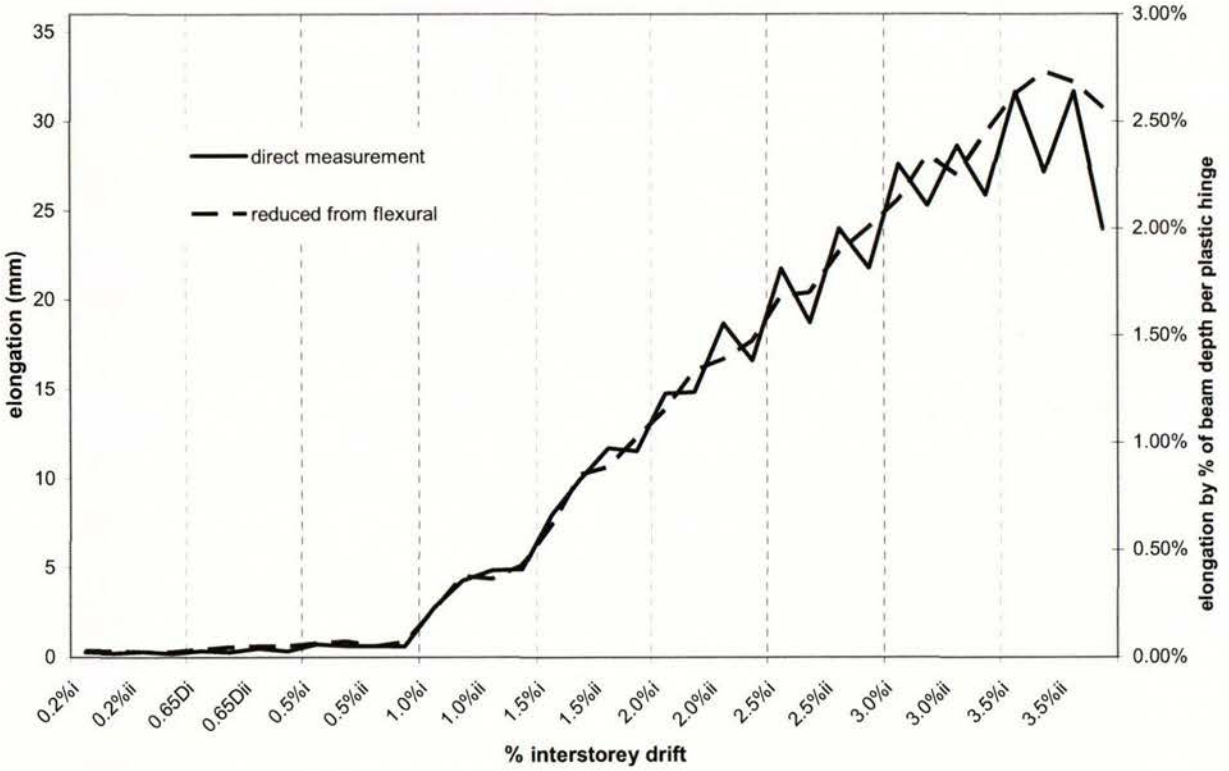

Figure 6.15: Elongation of beams at peak of displacement steps.

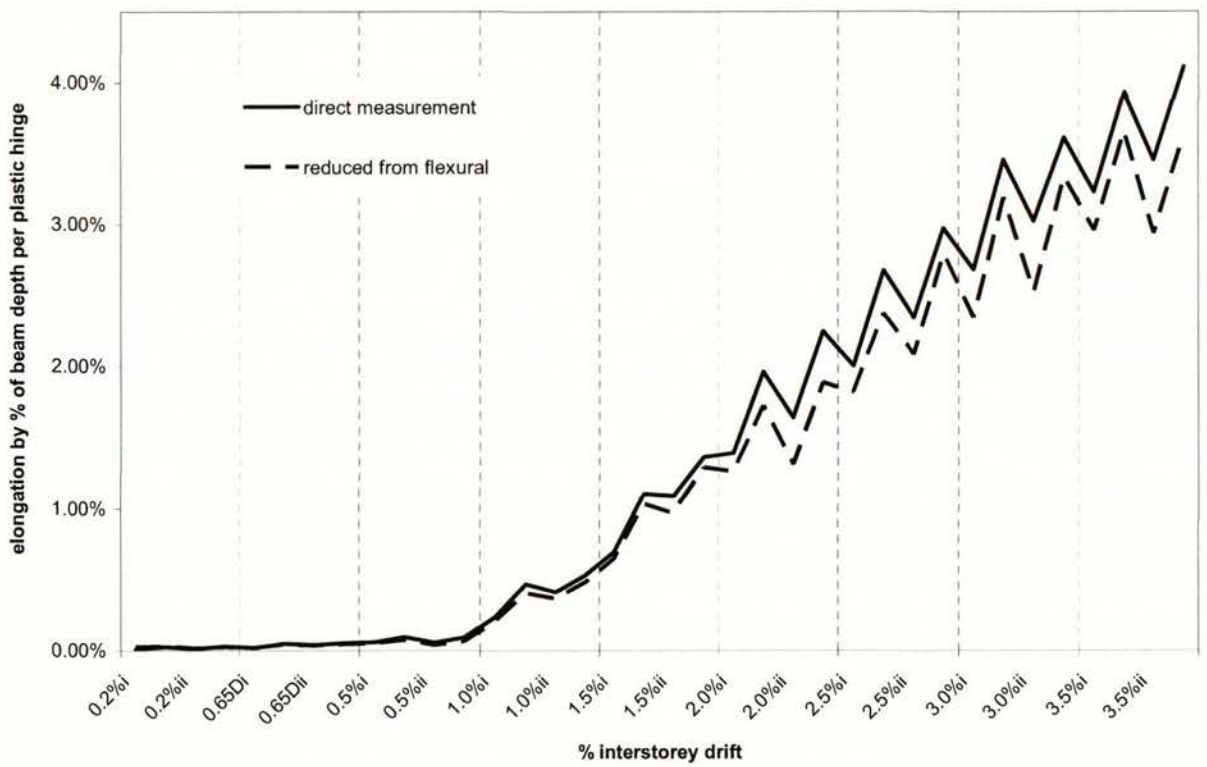

Figure 6.16: Elongation of beam bay 'B' – 'C' at peak of displacement steps.

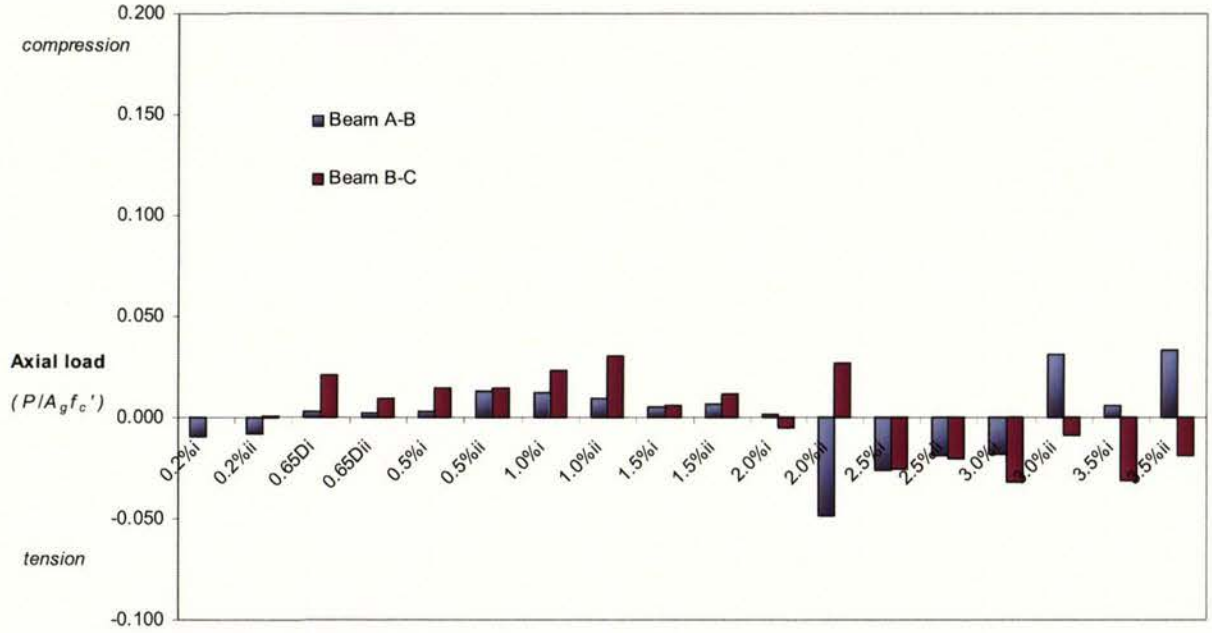

(a) In positive direction

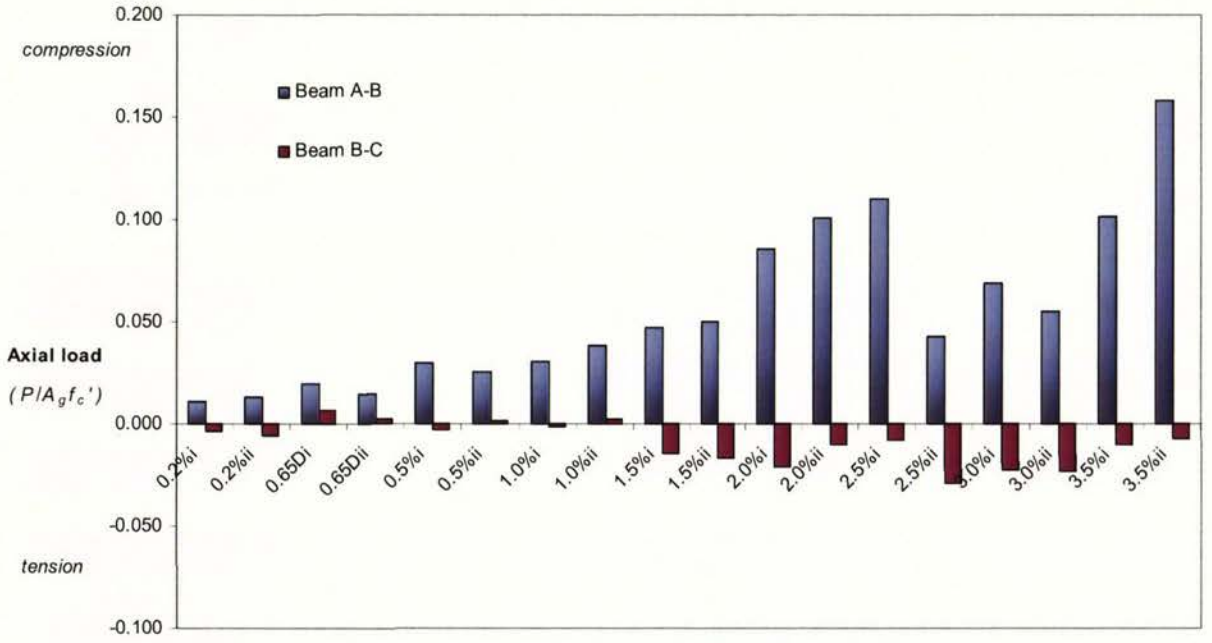

(b) In negative direction

Figure 6.17: Axial load levels in beams.

From Figures 6.15 and 6.16, it can be seen that the elongation of the beams started to increase in a linear fashion from the onset of displacement to ± 1.0% interstorey drift. At 3.0% interstorey drift, which corresponds to about a displacement ductility of 5.5, the average elongation per plastic hinge was 2.4% of beam depth, while for the plastic

hinges between columns 'B' and 'C' the corresponding value was 3.6% of beam depth. The maximum total elongation measured for the unit was 31.7mm or 2.6% of beam depth per plastic hinge (see Figure 6.15). This was recorded at 3.5% interstorey drift. In comparison, the maximum elongation recorded in beam bay 'B'-'C' was 24.7mm or 4.1% of beam depth (see Figure 6.16). The elongation of the beam between columns 'A' and 'B' was restricted by the axial compression force applied due to the errors in testing caused by the rotation of column 'A'. This is shown by Figure 6.17 which plots levels of axial loads sustained by each beam. These values were calculated from the out of balance forces applied at the top and bottom of each column.

The beam between columns 'B' and 'C' was subjected to axial tension forces, which would explain the higher elongation measurements. However, the tension forces were low compared to the axial compression forces sustained by the beam between columns 'A' and 'B', particularly further from ± 2.0% interstorey drift.

Chapter 7

Analytical Model of Test Unit

7.1 Introduction

An inelastic model was developed for the hinge region of a beam to enable the interaction of elongation, axial load and strength to be modelled and assist in the study of the interaction between floor slabs and frames. The results of numerical models of beams and frames with the elongating hinge model were compared against experimental results. A numerical model of the frame with floor slab test unit, Unit 2, was constructed. This model incorporated elongating hinge models in the beams and flexible slab models to model horizontal and vertical shear transfer between the floor slab and the perimeter frame. The results from the computer analyses were compared against the experimental results.

The properties of the connections between the frame and the floor slab were modified to investigate the effects on performance. A two-bay perimeter frame with floor slab model featuring the elongating hinge and the flexible floor slab models was constructed to study the effects of beam elongation and interaction of the floor slab with the frame for this common structural configuration.

7.2 Elongating Hinge Model

The main intention was to develop an inelastic hinge model that includes the influence of axial load on both strength and elongation, so that it may be used to study the interaction between floor slabs and frames. It is essentially a simple empirical plastic hinge model, which reproduces some of the features of the mechanism of elongation described in Chapter 2. However, it does not model shear deformations and contact stress effects in the plastic hinge. The hinge model was developed using a nonlinear building analysis program, SAP 2000 Nonlinear v. 8.1 [C4]. This model is shown in

Figure 7.1. All the members within the hinge, except the rigid vertical end elements, are axial (truss) members. Therefore their member stiffness is defined by:

$$\text{member stiffness} = EA/L \qquad \textit{Equation 7.1}$$

where E is the modulus of elasticity; A the area of member; and L its length.

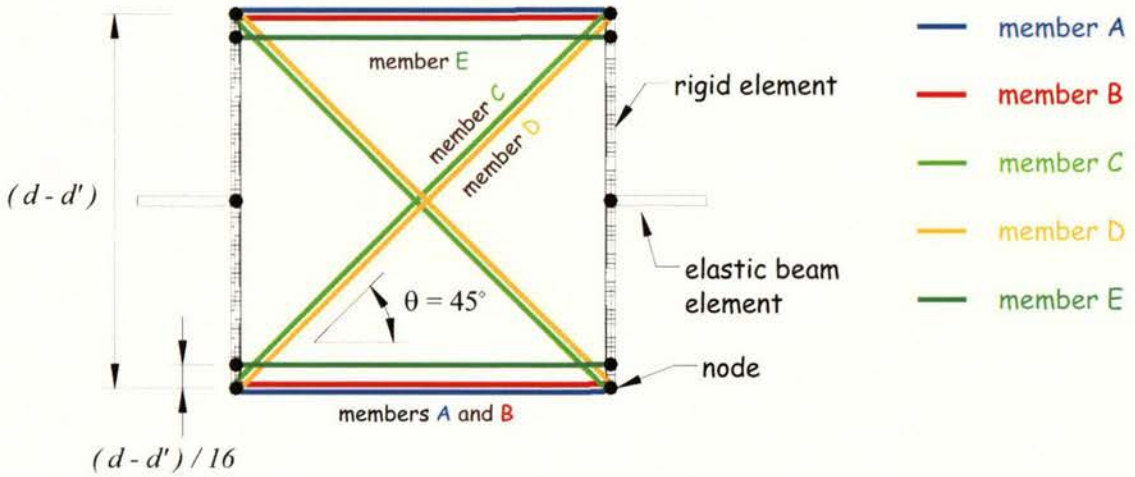

Figure 7.1: Model of elongating hinge.

The plastic hinge model is shown in Figure 7.1. The following is a brief description and parameters of each member in the plastic hinge model, with the force displacement relationships shown in Figures 7.2:

Member A – represents longitudinal steel reinforcement, where E_s and A_s are the appropriate elastic modulus and area for the reinforcement in the beam. A bilinear relationship is used and it is given tension yield strength, $A_s f_y$, such that the product of $A_s f_y$ $(d - d')$ is equal to the flexural strength of the rectangular beam (based on an assumed rectangular compression stress block in concrete and with no allowance for reinforcement in the slab). The strength of the member in compression is discussed in a later section. Strain hardening of the element is matched to the stress-strain plot of the reinforcement from tests.

Member B – is the longitudinal concrete element representing the concrete in the compression zone, where E_c is based on the elastic modulus for concrete and the area of the element, $A_B = b_w\, d/2$. This is an elastic compression member and does not carry tension as it forms a gap in tension.

Member C – this member is a very simplified model of the diagonal compression strut found in cracked reinforced concrete beams. This is an elastic compression member, and it forms a gap when subjected to tension. This member is not limited in compressive strength, but its stiffness is defined by the elastic modulus of the concrete and its area, A_C, is such that the vertical component of $A_C f_c'$ is 0.8 of the shear resistance provided by the transverse reinforcement (stirrup reinforcement) in the potential plastic hinge zone, ie. $A_C f_c' \sin\theta = 0.80 A_v f_v d / s$, where s is the actual spacing between stirrup sets, d is the effective depth, and θ as shown in Figure 7.1. This number (and member 'D') was chosen together with calibration of members 'A' and 'E' such that the level of elongation reached (see later) would yield the best match to the elongation measured from beam tests (see pgs 171-174).

Member D – is a diagonal element, which resists tension and compression. The pair of 'D' members together with the two 'C' members resist the shear in the plastic hinge model. The 'D' members are important for shear resistance particularly at low load levels during unloading and reloading cycles, as they provide some shear resistance when both the diagonal compression members (members 'C') are not loaded due to gapping of these members. The 'D' members are necessary to allow the shear resisted in the transverse reinforcement of a beam and by contact stress effects in the concrete during these unloading and reloading stages. The yield strength and stiffness of this member is such that the vertical component of $A_D f_c'$ is 0.10 of the shear resistance provided by the transverse reinforcement in the potential plastic hinge zone, ie. $A_D f_c' \sin\theta = 0.10 A_v f_v d / s$. Therefore, member 'D' is one eighth the stiffness of member 'C'. Members 'C' and 'D' are only crude elements and are not sophisticated enough to model shear component of deformation in plastic hinge zones.

Member E – this member, together with the adjusted yield strength in compression of member 'A', is used to calibrate the elongation characteristics of the hinge, particularly to account for axial load effects. The stiffness and yield strength vary with the reinforcing steel to concrete ratios in beams. Therefore a trial and error approach is required to calibrate this member and the yield strength in compression of member 'A', as described in the following.

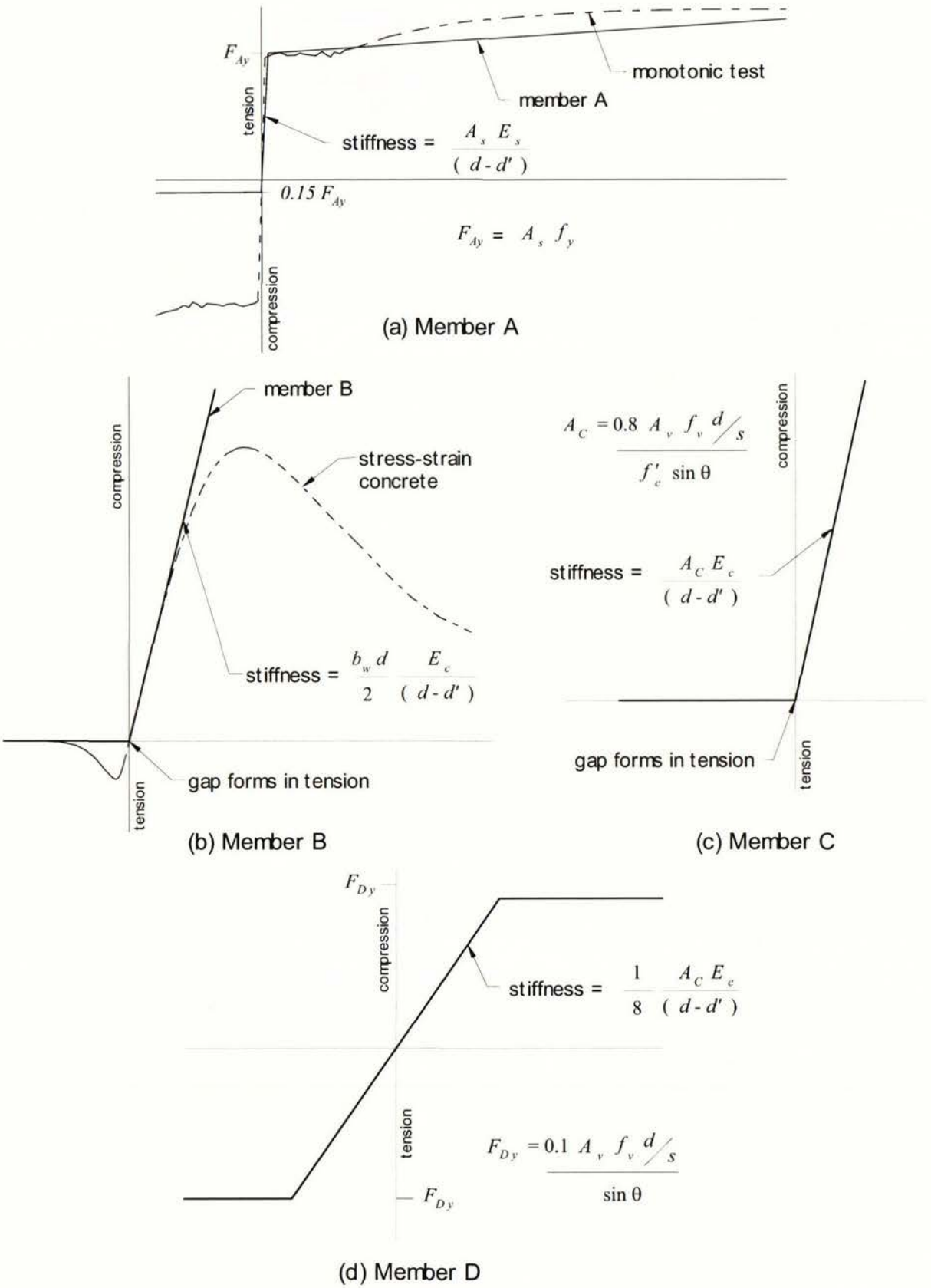

Figures 7.2: Members in elongating hinge model. (continued)

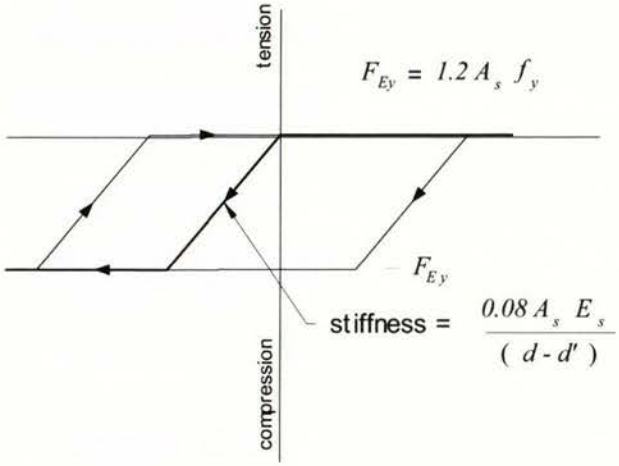

(e) Member E

Figures 7.2: Members in elongating hinge model. (concluded)

Calibration of members 'A' and 'E'

The results from experiments on cantilever beams [F7, T2] were used to calibrate the hinge model of an equivalent computer modelled beam, so that effects of axial compression on elongation can be approximately represented. The beams were subjected to two cycles at displacement ductility two, followed by two cycles to ductility four and another two cycles to ductility six. The axial force was varied in each experiment and were zero, 0.039 $A_g f_c'$, 0.068 $A_g f_c'$ and 0.145 $A_g f_c'$, where A_g is the cross-sectional area of the beam and f_c' is the crushing strength of the concrete, taken at the time of the commencement of testing.

The test beams were 500mm deep and 200mm wide. These were reinforced longitudinally with five 20mm diameter bars in both the top and bottom of the beams and transverse reinforcement consisted of two legged 10mm stirrup and a single 6mm tie. The cantilevers were loaded at 1.5m from the fixed end of the beams.

The parameters described earlier were applied to the plastic hinge members of the model (see Figure 7.1). A trial and error method was used where the compression strength of member 'A', the stiffness of member 'E' and both the tension and compressive strength of member 'E' were adjusted so that the numerical results best fitted those recorded from the experiments (see pg. 173). This method is described in the following text.

The stiffness of members 'E' were set to 8% of the stiffness of member 'A'. Increasing the stiffness of member 'E' has an overall effect of increasing elongation and also increasing the sensitivity of the hinge towards any changes made to the yield strength of this member. The reverse is true when reducing the stiffness. This value may vary for different beams and would require some adjustments by trial and error, typically ranging from 6 to 10%. The next step was to reduce the yield strength in compression of members 'A', and setting the yield strength in compression (almost zero in tension) of members 'E' to the same reduction applied to members 'A', as given by *Equation 7.2*.

$$C_y^{\,E} = T_y^{\,A} - C_y^{\,A} \qquad \textit{Equation 7.2}$$

where C_y denotes yield compression (positive number), T_y is yield in tension, superscript imply member nomination.

This step was repeated until a desired level of elongation is reached. In the case of the test beam (500mm deep, 200mm wide, five 20mm diameter bars in both top and bottom of beam), the following was obtained: $T_y^{\,A}$ = 559.9kN and $C_y^{\,A}$ = 84.0kN (15% of $T_y^{\,A}$). The resulting elongation was 2.8% of the beam depth at displacement ductily six. At this stage, any increase in the compression strength of members 'E' beyond that given by *Equation 7.2* had very little bearing on the elongation of the hinge.

The next step was to apply an axial force to the beam. An axial force of 0.034 $A_g f_c'$ was applied and the elongation of the beam was 1.1% of the beam depth at ductility six. The compression strength of members 'E' had to be increased to assist in resisting the applied axial force. Elongation of the beam was 1.8% of the beam depth at ductility six, when the compression strength of members 'E' was set to 559.9kN (ie. $C_y^{\,E}$ = 1.0 $T_y^{\,A}$). Any increase in the compression strength beyond this did not have an effect on the total elongation of the beam.

In the following step an axial force of 0.068 $A_g f_c'$ was applied, and this resulted in total elongation of 1.0% of the beam depth at displacement ductility six. The compression

strength of members 'E' was increased to 657.9kN (ie. $C_y^E = 1.2\ T_y^A$), resulting in elongation of 1.2% of the beam depth at displacement ductility six.

At applied axial force of 0.145 $A_g f_c'$, increase in the compression strength of members 'E' was not required, as the elongation recorded at ductility six was at 1.0% of beam depth. In summary, the parameters for members 'A' and 'E' obtained from this exercise were:

(i) the stiffness of member 'E' is 0.08 $E_s A_s$ / (d-d')

(ii) the tensile strength of member 'E' is 0.0

(iii) the compressive strength of member 'E' is 1.2 $A_s f_y$

(iv) the compression strength of member 'A' is 0.15 $A_s f_y$

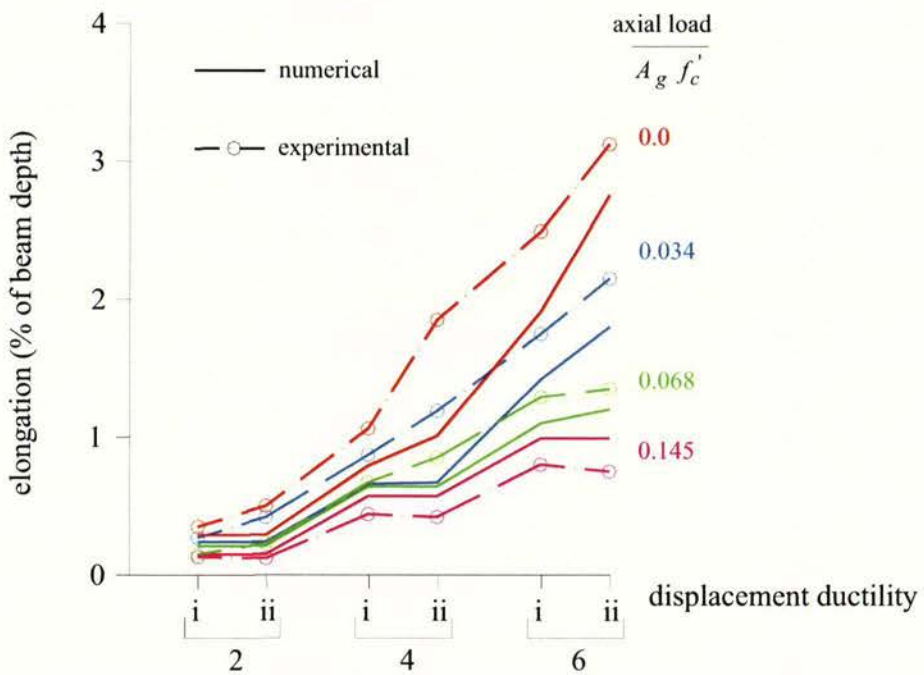

Figure 7.3: Elongation of cantilever beam at varying axial load.

The elongation versus displacement ductility response of the cantilever beams for both the experimental and numerical tests are shown in Figure 7.3. With the exception at axial load of 0.145 $A_g f_c'$, the elongation of the numerical beams was less than that recorded in the physical experiments, especially at displacement ductility 4 and lower. The rate of increase in elongation in the numerical beams is greater between ductility 4

and 6 compared to the physical experiments. However, the model does exhibit similar levels of decrease in elongation with increasing axial load applied.

Figure 7.4 shows the force versus deflection curve of the cantilever beam tested with no axial compression force applied [T2]. The force versus deflection response of the equivalent numerical model is shown in Figure 7.5.

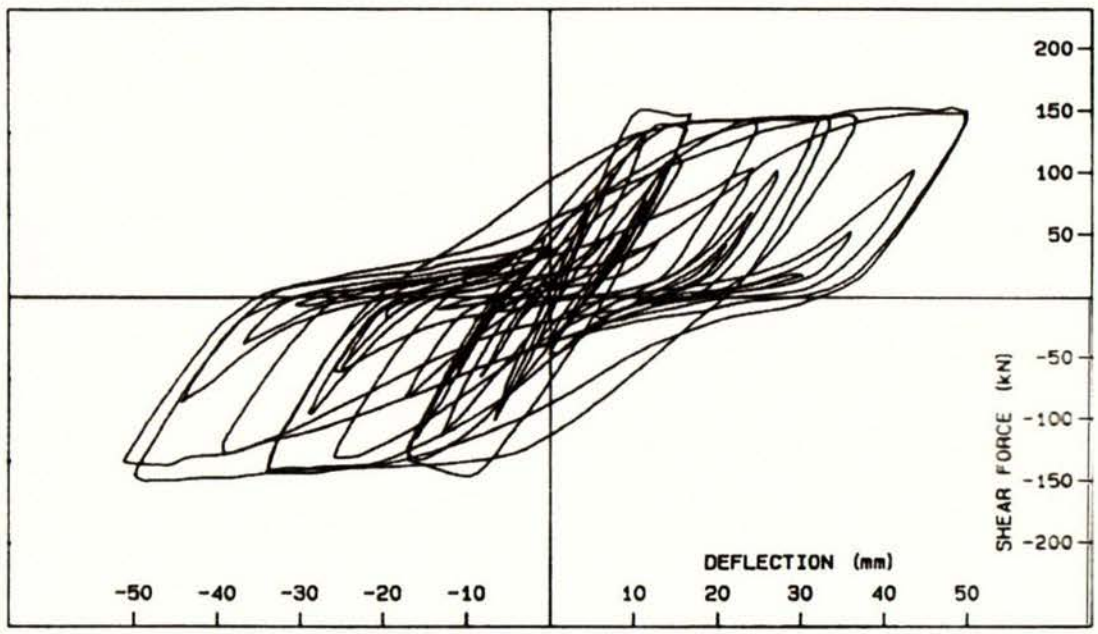

Figure 7.4: Force versus displacement response of cantilever beam [T2].

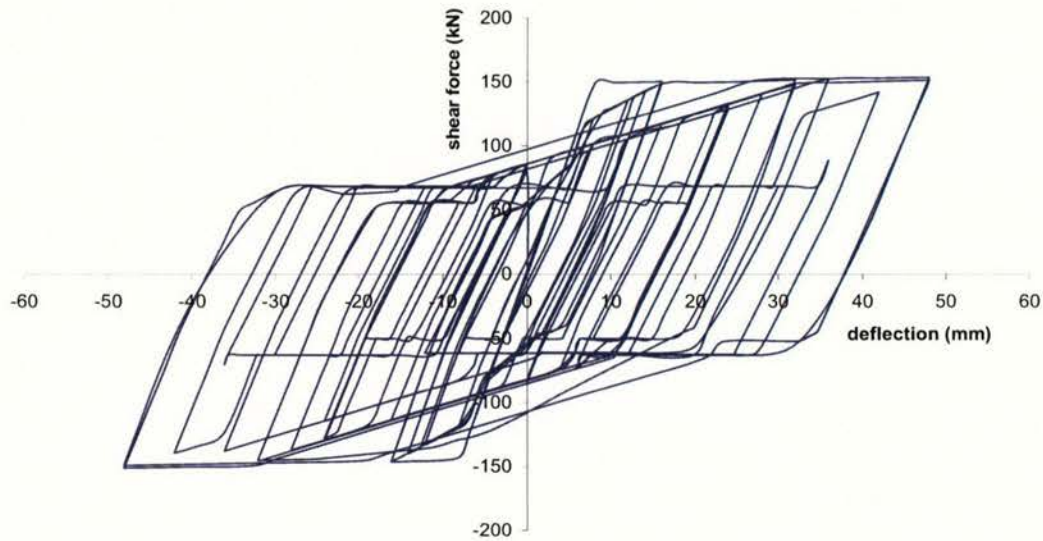

Figure 7.5: Load versus displacement response of modeled cantilever beam.

It can be seen that the model fails to follow the actual response of the test beam at low load levels during the reloading phase. This is because the model does not predict the shear component of deformation, the loss of stiffness of members subjected to cyclic yielding and probable bar slip in the joint. This was not included as standard degrading stiffness elements were not available to the program. However, the strength and displacements levels at peak displacements are in satisfactory agreement with the experimental values.

As a further check of the performance of the hinge model, equivalent numerical models were analysed for three cantilever beams in which no axial loading was applied [F7]. The properties of these beams are summarised in Table 7.1.

Table 7.1: Details of cantilever beams.

Beam	beam size $D \times B$ (mm)	longitudinal reinforcement	$\frac{A_s}{d \times B}$	f_y (MPa)	f_c' (MPa)	span length, M/V (m)	M_y (kNm)	V_s (kN)
B1	500 x 200	5-D20 top 5-D20 bottom	0.0178	290	30	1.329	184	254
B2	500 x 200	5-D20 top 5-D20 bottom	0.0178	280	31	1.735	178	188
B3	500 x 200	2-D28 top 2-D28 bottom	0.0135	317	43	1.300	167	195

* A_s is the area of longitudinal reinforcement, f_y is the yield stress of the longitudinal reinforcement from tension tests, f_c' is the compression strength of the concrete at the commencement of test, M_y is the flexural strength based on rectangular stress block and V_s is the shear strength provided by the transverse reinforcement.

The parameters for the hinge elements described earlier were used for the models. The parameters for members A and E were not calibrated for these beams, but were kept at the same proportions. The numerical and experimentally measured elongation at ductilities 2, 4, 6 and 8 are compared in Table 7.2.

While the elongation for all three beams at ductility 6 are well matched, the elongation for ductilities 2 and 4 are underestimated by the numerical models, especially for beams B2 and B3. The elongation at ductility 8 was significantly overestimated by the numerical models. This may be due to the inability of the hinge to model buckling of the reinforcement, therefore reducing (or the rate of) elongation. This occurs in beam when wide cracks form in the plastic hinges and concrete around the longitudinal reinforcement are dislodged from the beams. The parameters of the members in the hinge were calibrated such that the elongation values gave a best match at ductility 6, such that it could be used to assess the behaviour of the model (see sections 7.3 and 7.4) at higher drift displacements.

Table 7.2: Elongation of cantilever beams and equivalent numerical model.

Beam		elongation (% of beam depth)			
		ductility 2	ductility 4	ductility 6	ductility 8
B1	experiment	0.6	1.5	2.8	4.0
	numerical model	0.3	1.2	3.2	5.8
B2	experiment	0.8	1.8	2.9	3.6
	numerical model	0.3	0.9	2.9	5.7
B3	experiment	0.8	1.9	2.2	3.0
	numerical model	0.3	0.6	1.9	3.6

Two cantilever beam tests were performed by Liddell [L1]. The cantilever beams used in his experiment were 600mm deep, 270mm wide, with four 16mm diameter bars in top and bottom of the beam. The yield stress of the longitudinal reinforcement was 467MPa and the concrete compression strength was 38MPa. The beams were not subjected to axial compression, but were subjected to differing cyclic displacements. The first was subjected the typical New Zealand test regime [P11], the second a procedure often used at the University of California at Berkeley [M5]. The New Zealand loading history requires two displacement cycles for each ductility level for ductilities 2, 4, 6 and 8. For the University of California Berkeley procedure, three

displacement cycles are taken at each ductility level, from ductility 2 through to ductility 8 at single ductility increments.

The same parameters described in the sections above were used in the numerical model. Following the same process of trial and error described earlier, the parameters obtained for members 'A' and 'E' were:

(i) the stiffness of member 'E' is 0.11 $E_s A_s$ / (d-d')

(ii) the tensile strength of member 'E' is 0.0

(iii) the compressive strength of member 'E' is 1.2 $A_s f_y$

(iv) the compression strength of member 'A' is 0.15 $A_s f_y$

A summary of the results is given in Table 7.3. For the New Zealand load history, the elongation at ductilities 2, 4 and 6 are in close agreement while for ductility 8 it is overestimated by the model. For the University of California at Berkeley load history, the elongations predicted by the numerical model are in close agreement with the experimental values. These analyses show that the model is not particularly sensitive to the change in loading history. From these initial tests, it was considered that for the purposes of this project the proposed plastic hinge model provided an adequate tool to represent the elongation phenomenon in beams.

Table 7.3: Elongation in Liddell experiments and equivalent numerical model.

Beam		elongation (% of beam depth)			
		ductility 2	ductility 4	ductility 6	ductility 8
New Zealand load history	experiment	0.2	0.8	1.7	2.7
	numerical model	0.3	0.7	1.8	3.9
University of California at Berkeley load history	experiment	0.3	1.1	2.8	4.3
	numerical model	0.3	0.7	2.3	4.3

7.3 Numerical Model of Frame without Floor Slab.

A numerical model of the two-bay frame experimental unit was developed incorporating the elongating plastic hinge model described in the previous section. The stiffness and strength values as described in the previous section for members 'B' through 'D' (as shown in Figure 7.1) were taken for the members in the plastic hinge of the model. The parameters for the longitudinal reinforcement and the axial member (members 'A' and 'E' respectively) were not altered. In brief, the stiffness of member 'E' was 0.08 $E_s A_s / (d - d')$, the compression strength of member 'E' was 1.2 $A_s f_y$ and does not resist tension, and the compression strength of member 'A' was 0.15 $A_s f_y$.

The following were the values to the member variables: A_s = 339.3mm^2, E_s = 200GPa, f_y = 309MPa. The stress-strain curve used for yielding members within the hinges (ie. members 'A', 'D' and 'E') are shown in Figure 7.6 below. This stress-strain relationship was derived from tension tests of samples taken from the reinforcement used in the experimental frame unit (see *Appendix 2*). The member extended beyond 75ε_y , as the numerical model tended to become unstable during analyses when members failed (by extending beyond provided strain range). The effect of this was mainly negated by removing failing members as the analyses progressed (see section 7.4.3, pg 196).

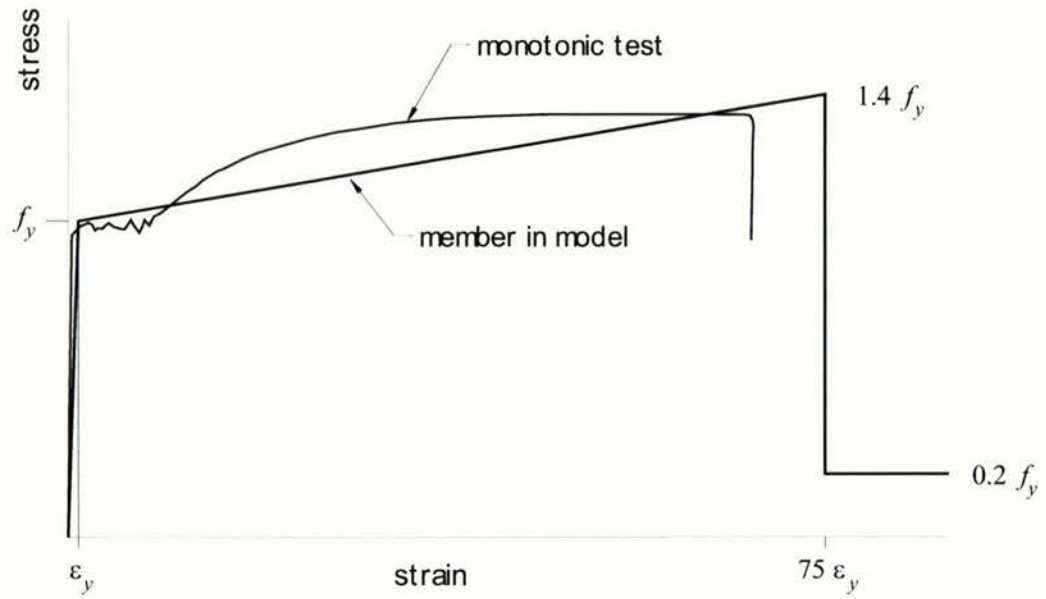

Figure 7.6: Stress-strain relationship used for yielding members in elongating plastic hinge.

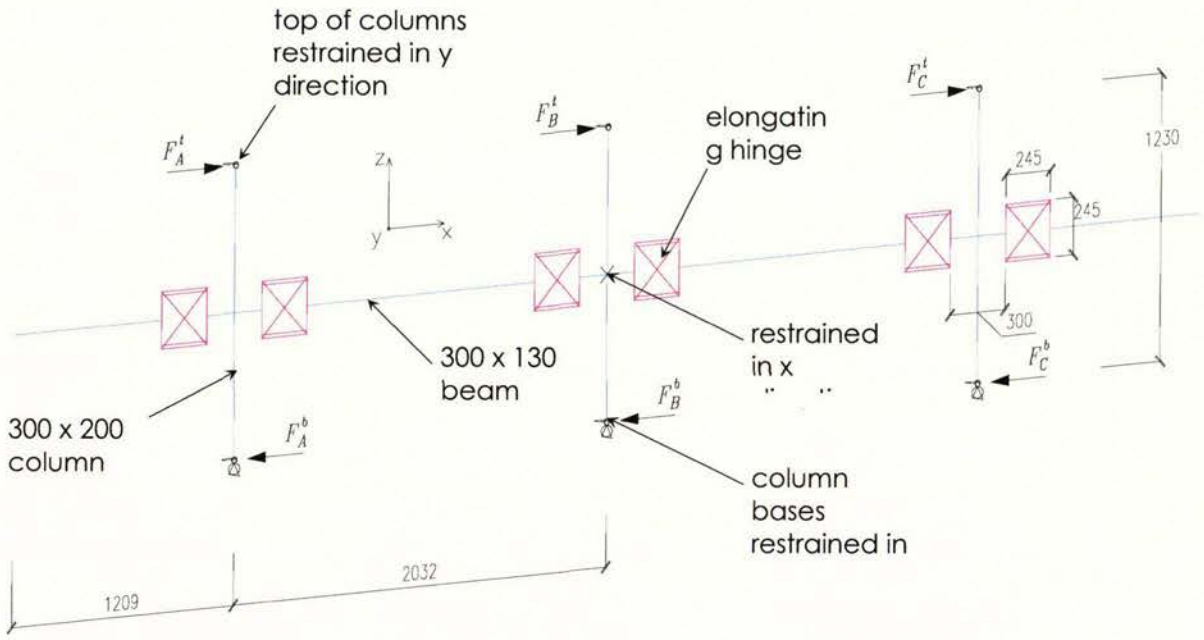

Figure 7.7: Schematic of frame model.

The lateral force versus displacement response of experimental Unit 3 (see *Chapter 6*) is shown in Figure 7.8, and the lateral force versus displacement response of the equivalent numerical model is shown in Figure 7.9. The most obvious difference between the experimental and numerical model response is the inaccuracy of the model in modelling shear component of deformation and the lack of stiffness degrading properties in members.

The lateral force versus displacement at 2.5% drift displacement cycle of the experimental unit and numerical model is compared in Figure 7.10. The numerical loop is significantly fatter than the experimental. At 2.5% drift, the peak force in the numerical model is 110kN compared to 98kN for the experimental unit in the positive direction of displacement. In the reverse direction, the larger force is recorded for the experimental unit at 125kN while for the numerical model the peak force was 111kN.

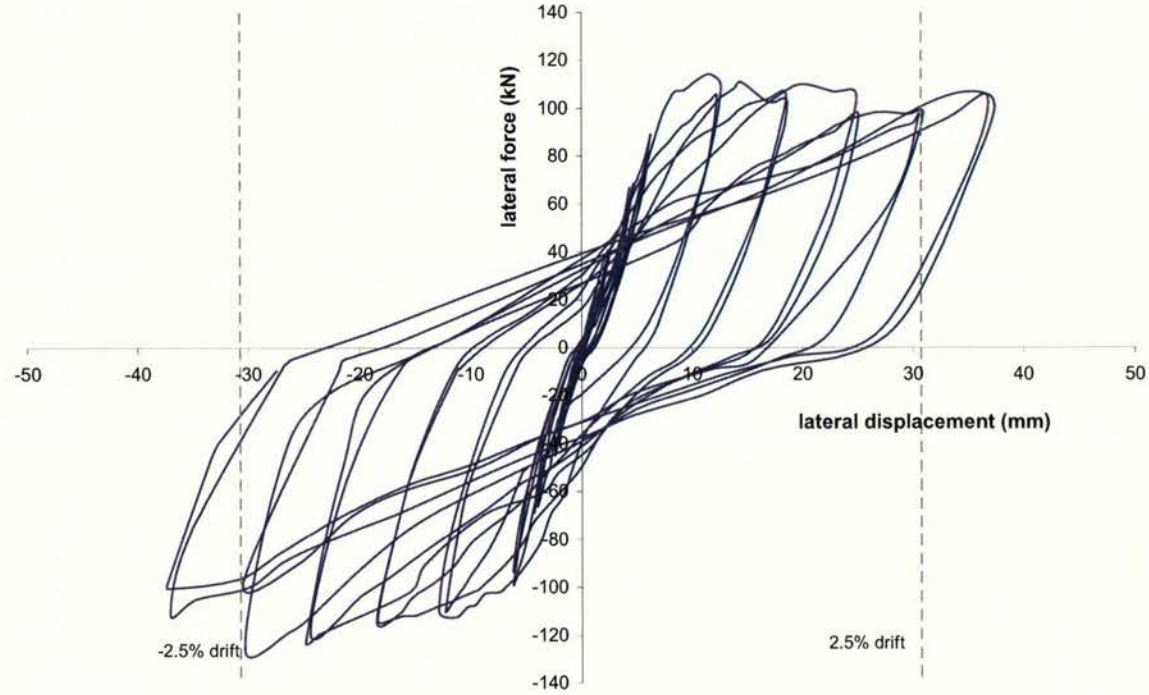

Figure 7.8: Lateral force versus displacement of experimental Unit 3.

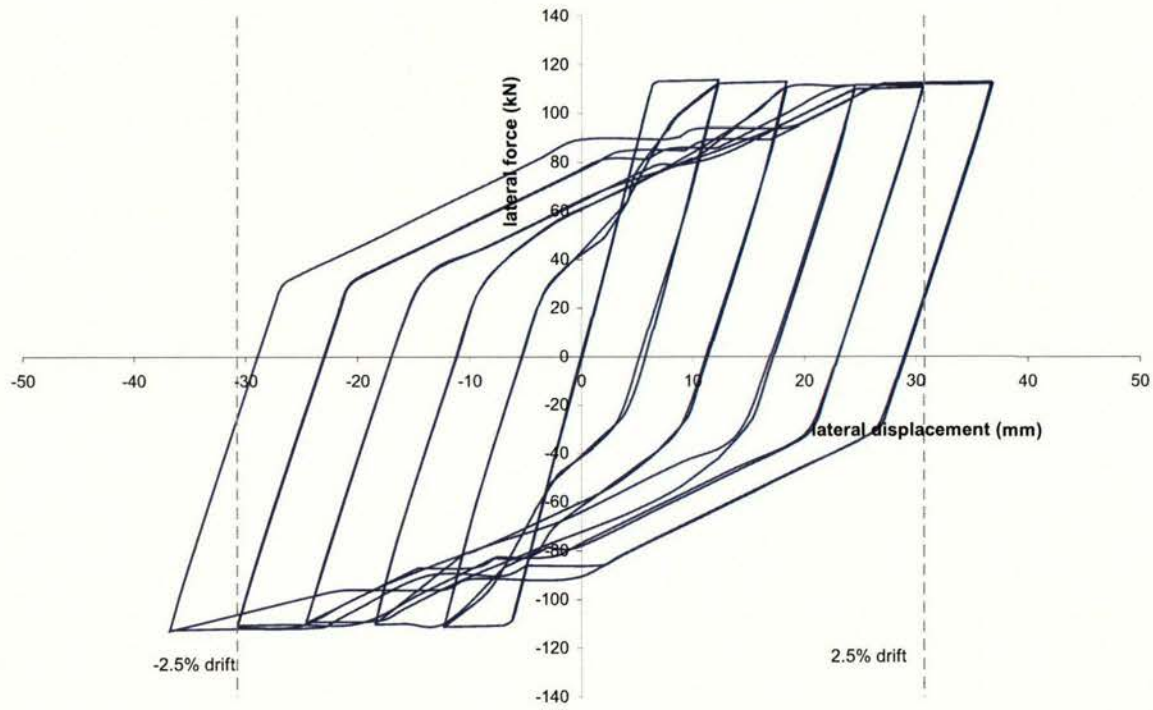

Figure 7.9: Lateral force versus displacement of numerical model of Unit 3.

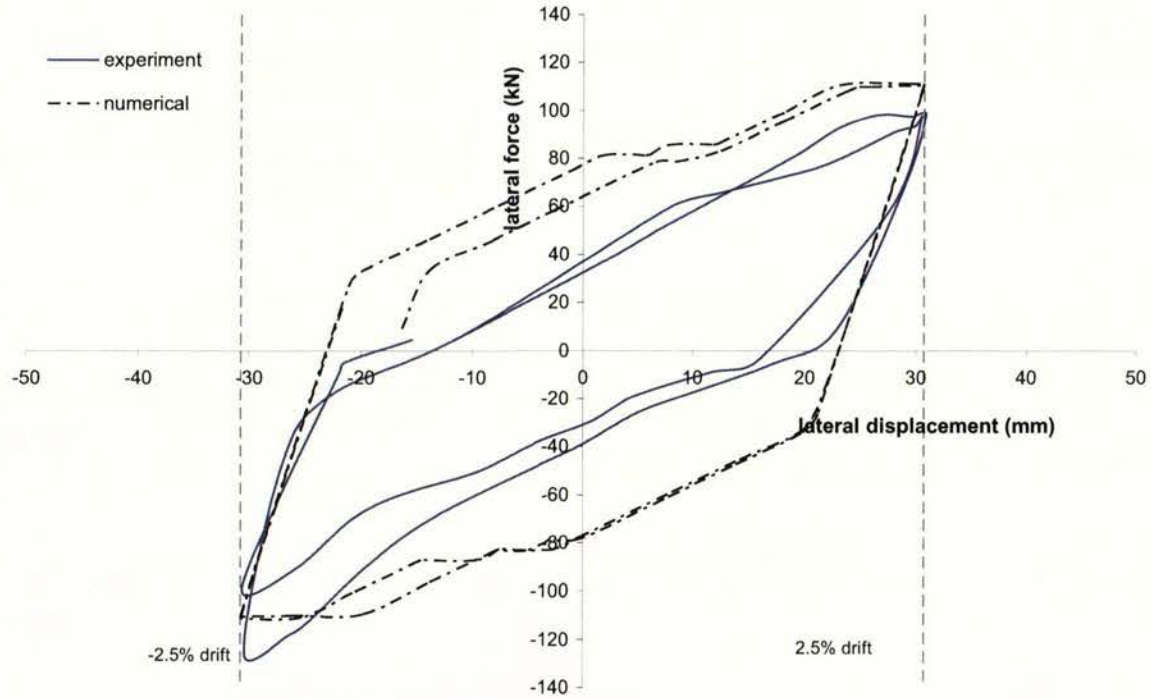

Figure 7.10: Comparison of lateral force versus displacement cycle at 2.5% drift displacement of experimental and numerical model of Unit 3.

Figure 7.11 compares the average elongation of the beams of experimental units, Unit 1 and Unit 3, and the numerical model. The numerical model underestimates the elongation of the beams between 1.0% to just less than 2.5% interstorey drift displacement. After 2.0% drift displacement, elongation in the numerical model increases at a greater rate compared to the two experimental units. The average elongation at 3.0% drift displacement was 3.2% of beam depth for the numerical model, 2.8% of beam depth of Unit 3, and 2.5% of beam depth for Unit 1.

Figure 7.12 shows the average elongation of the beams in the numerical model subjected to varying axial load levels. These were constant axial loads applied over the entire duration of the analysis. The figure shows that the difference in elongation between the beams was small up to 2.0% drift displacement. As discussed for Figure 7.11, elongation was underestimated by the model at the lower drift levels. There was better match at 3.0% drift displacement. At 3.0% drift, the average elongation of the beams was 1.7% of beam depth for axial load level at 0.034 $A_g f_c'$, 1.2% of beam depth at 0.068 $A_g f_c'$, and 1.0% of beam depth at 0.145 $A_g f_c'$. For the experimental frame unit at 3.0% drift displacement corresponded to approximately displacement ductility of 5.5 (see section 6.4 of *Chapter 6*). For comparison, the average elongation of the test

cantilever beams subjected to axial loads (see section 7.2 and Figure 7.3) at displacement ductility six was 2.1% of beam depth at applied axial force of 0.034 $A_g f_c'$, 1.4% of beam depth at 0.068 $A_g f_c'$, and 0.8% of beam depth at 0.145 $A_g f_c'$.

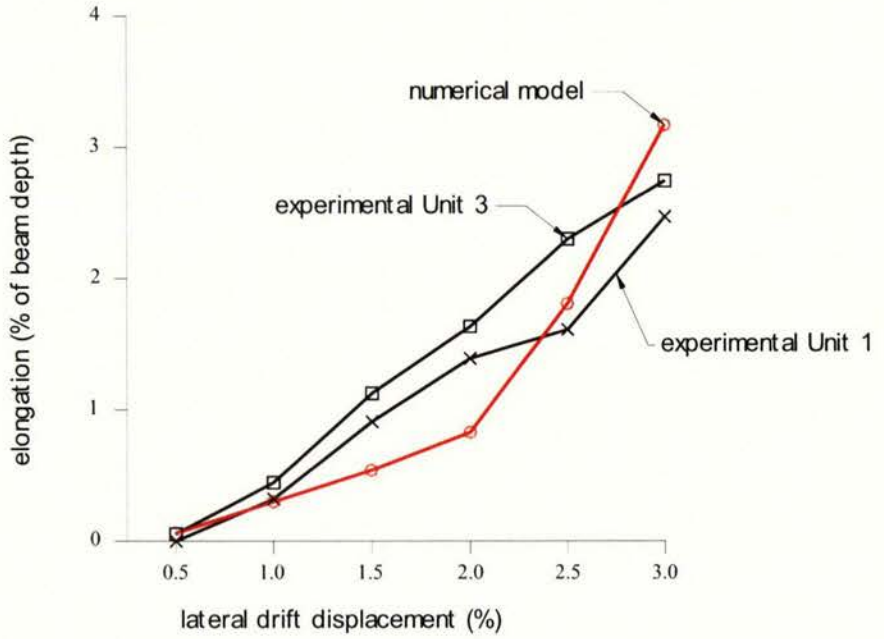

Figure 7.11: Comparison of average elongation of beams in experimental units and numerical model.

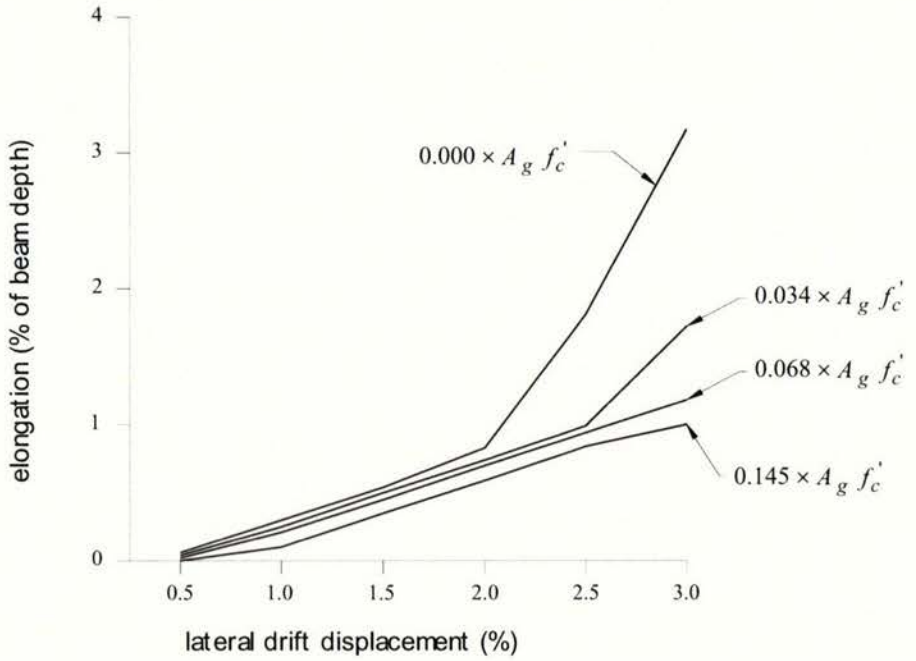

Figure 7.12: Average elongation of numerical frame model subjected to varying axial load levels.

7.4 Numerical Model of Frame with Floor Slab

7.4.1 Description of model

A numerical model of the frame with floor slab unit is shown in Figure 7.13. The numerical model was set-up following the dimensions of the experimental frame with floor slab, Unit 2, as described in Section 3.3.1 and Figures 3.2 and 3.3 of *Chapter 3*. This incorporated the same frame model described in section 7.3 and shown in Figure 7.7. The parameters for the elongating hinge are identical. The difference lies in the addition of the floor slab, supporting transverse beams and connecting elements between the floor and beams.

As can be seen in Figure 7.13, the lines represent the centrelines of the elements and members in the model. These were placed in accordance to their corresponding physical locations within the experimental unit. The insitu floor slab was formed by an elastic mesh shown in red, the blue lines represent the perimeter beams, floor supporting transverse beams and columns. The prestressed floor ribs are in green and floor slab to beam connections are in cyan. The member properties are briefly described in Table 7.4 (also refer to Appendix 4 for additional details).

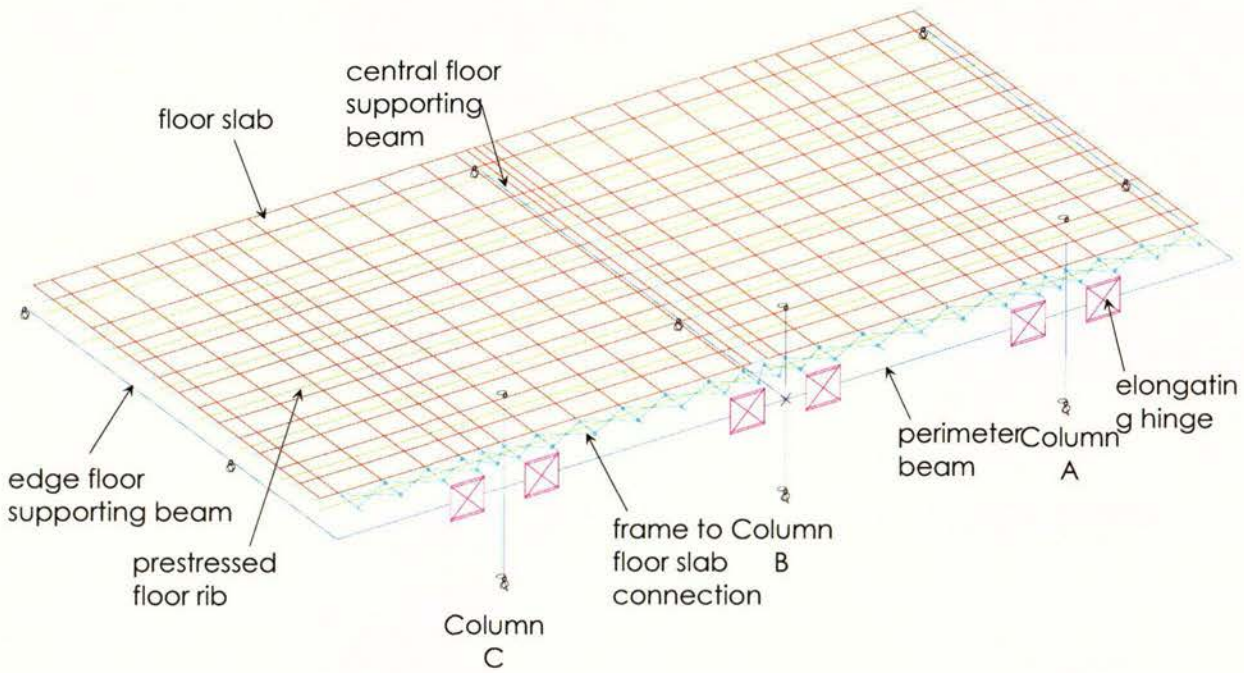

Figure 7.13: Schematic of numerical model of Unit 2.

Table 7.4: Member properties in numerical model of Unit 2.

Member	Dimensions ($D \times b$)	effective moment of inertia, I_e
perimeter beam & edge supporting beam	300mm × 130mm	$0.3 \times \frac{b\ D^3}{12}$
column	300mm × 200mm	$0.55 \times \frac{b\ D^3}{12}$
central supporting beam	285mm × 120mm	$0.3 \times \frac{b\ D^3}{12}$
prestressed rib	165mm × 150mm	$1.0 \times \frac{b\ D^3}{12}$

The beam flexural stiffness was taken from analysis of an analytical model of Units 1 & 3 (frames without floor slab). The analytical model was subjected to the same lateral load as the test units. In order to achieve the same displacement the beams were multiplied by 0.28 for Unit 1 and 0.31 for Unit 3 (see *Chapter 8*, section 8.2.3, pgs. 230-233). The effective stiffness for the column section was calculated from equation 3-4 given by the Concrete Structures Standard [S2]:

$$I_e = \left(\frac{M_{cr}}{M_a}\right)^3 I_g + \left[1 - \left(\frac{M_{cr}}{M_a}\right)^3\right] I_{cr} \qquad \textit{Equation 8.1}$$

where M_{cr} is the cracking moment (= 13.6kNm),

M_a is the moment applied (=54kNm),

I_g is the moment of inertia of gross concrete section (=450x10^6 mm^4),

I_{cr} is the moment of inertia of cracked section (=244x10^6 mm^4).

Figure 7.14 shows a section through the supporting edge beam and the floor slab. The centre of the floor slab was at a different elevation to the centre-line of the prestressed rib, therefore 'weld' constraints were used to connect the floor slab to the prestressed rib at member nodes. These constraints are effectively rigid members which act to tie the nodes together such that the forces and deformations are compatible. Welded nodes translate equally plus relative translation due to rotation between the two nodes. Similarly, where the floor members meet the edge supporting beam, 'weld' constraints were used between the member nodes.

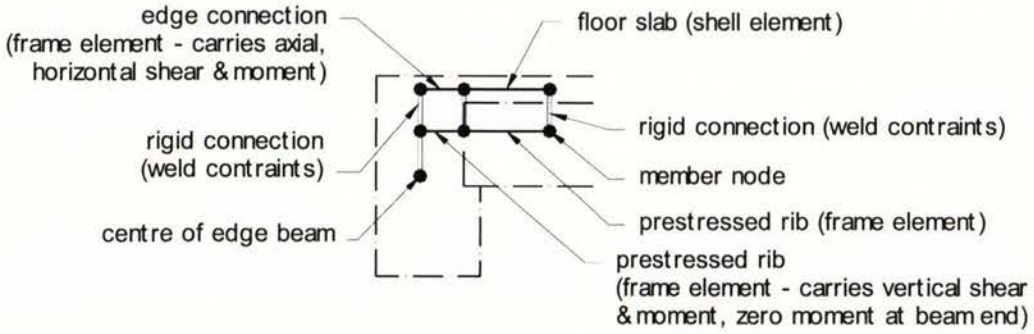

Figure 7.14: Section of numerical model at supported edge of floor slab.

The connections between the prestressed rib and the edge beam carries vertical and horizontal shear between the floor rib and the edge beam. The direct connection between the floor rib and the beam carries only vertical shear, and is pin ended at the beam end such that no bending moment is transferred. The edge connection, which carries axial, horizontal shear and bending forces represents starter reinforcement between the floor slab and the edge beam. In the experimental Unit 2 (see Figure 3.3(c)), these were 10mm diameter reinforcement spaced at 225mm. The following values were used for the edge connection member: A_s = 78.5mm^2, E_s = 200GPa, f_y = 313MPa. The stress-strain relationship used for this member is shown in Figure 7.6.

In the direction perpendicular to the slab the axial stiffness was reduced. This was clear as cracks formed parallel to the frame (see Figure 5.26 in *Chapter 5*). In the direction parallel to the frame (parallel prestressed ribs), the axial stiffness was based on the gross section stiffness of a 40mm thick slab. In this direction the floor slab was assumed to be axially stiff due to the prestressed ribs, though some cracks formed (perpendicular to the perimeter frame) in the floor closer to the frame. Initial results indicated that reducing the stiffness of the floor in the direction perpendicular to the slab made little difference to overall performance, and this would probably have been the case for the stiffness in the parallel direction.

The actual axial horizontal stiffness of the floor should lie in between the two limits; the stiffness of the gross section and the stiffness of the reinforcement in the slab (3.125mm wires at 75mm spacings) assuming that wide cracks (crack width greater than 0.15mm) had formed such that the reinforcement was yielding. From test observations, it was clear that these cracks were not so wide. The tensile resistance of concrete should be

considered here. Figure 7.15 shows the assumed concrete tensile stress-strain behaviour developed by Fenwick & Dickson [F14, D4]. For an assumed crack width of 0.1mm (for unit length of crack and gauge length of 75mm), the sum of concrete tension force and the reinforcement crossing the crack was 34kN (7kN in concrete, 27kN in reinforcement), giving an equivalent stiffness of 0.13 times the gross stiffness of the slab. For an assumed crack width of 0.05mm, the sum of forces was 43kN (30kN in concrete, 13kN in reinforcement), with an equivalent stiffness of 0.29 times the gross stiffness of the slab. This value was chosen for the axial stiffness of the slab in the direction perpendicular to the frame. In the experiment, the cracks were actually wider nearer to the central beam, and the crack widths decreased with distance away from the central beam. For simplicity, this was not incorporated in the numerical model.

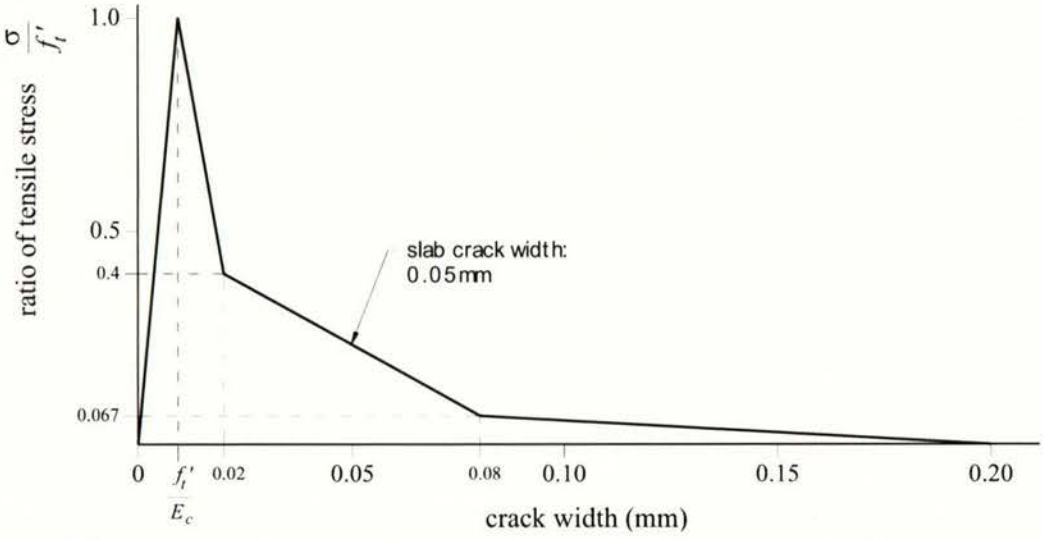

Figure 7.15: Assumed concrete tensile stress-strain behaviour [D4].

Figure 7.16 shows a section through the central floor supporting beam and the floor slab. Similarly, 'weld constraints were used as rigid connections between the member nodes between the floor slab and prestressed ribs, and between the floor member nodes and the central supporting beam. The central connection, between the floor slab and the supporting beam carries axial, horizontal shear and bending forces which represent the reinforcement crossing between the floor slab and the supporting central beam. This consisted of 3.125mm diameter wires spaced at 75mm and two 4.0mm wires above each rib at 450mm spacings between rib centrelines (see Figure 3.3(d)). The following values were used for the member representing the 3.125mm wire mesh: $A_s = 23.0\text{mm}^2$, $E_s = 200\text{GPa}$, $f_y = 408\text{MPa}$. For the 4.0mm wire the parameters were: $A_s = 25.1\text{mm}^2$, E_s

= 200GPa, f_y = 430MPa. The stress-strain relationships used for the 3.125mm wire is shown in Figure 7.17(a) and the 4.0mm wire in Figure 7.17(b).

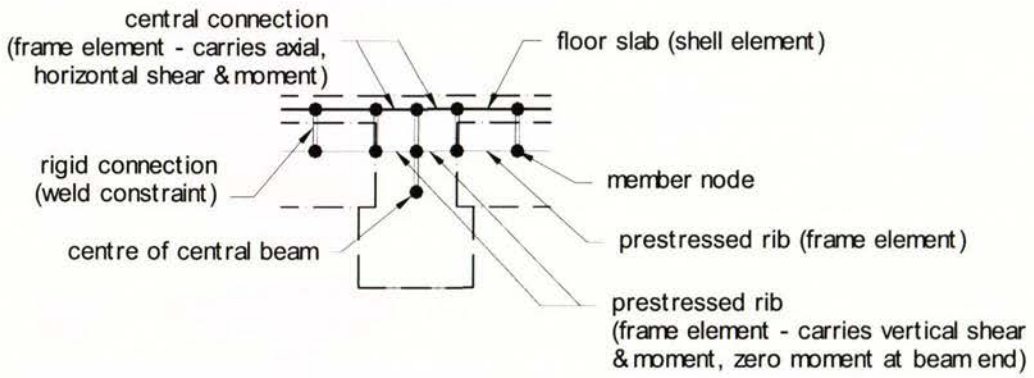

Figure 7.16: Section of numerical model at central floor supporting beam.

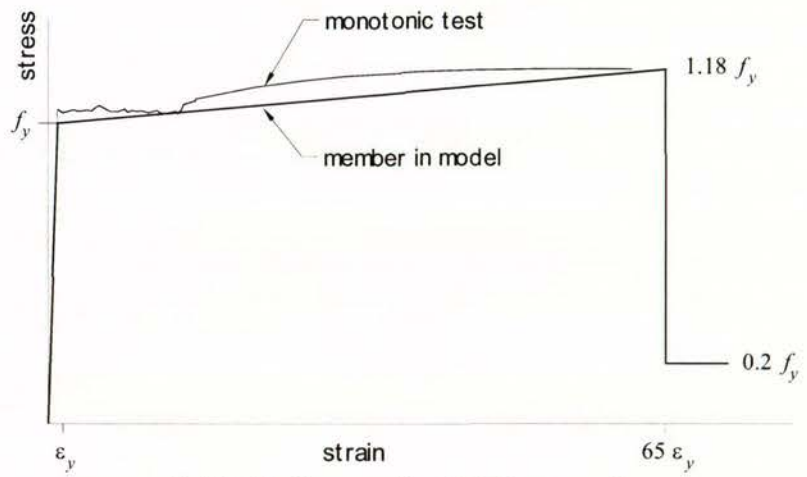

(a) 3.125mm wire @ 75mm c/c

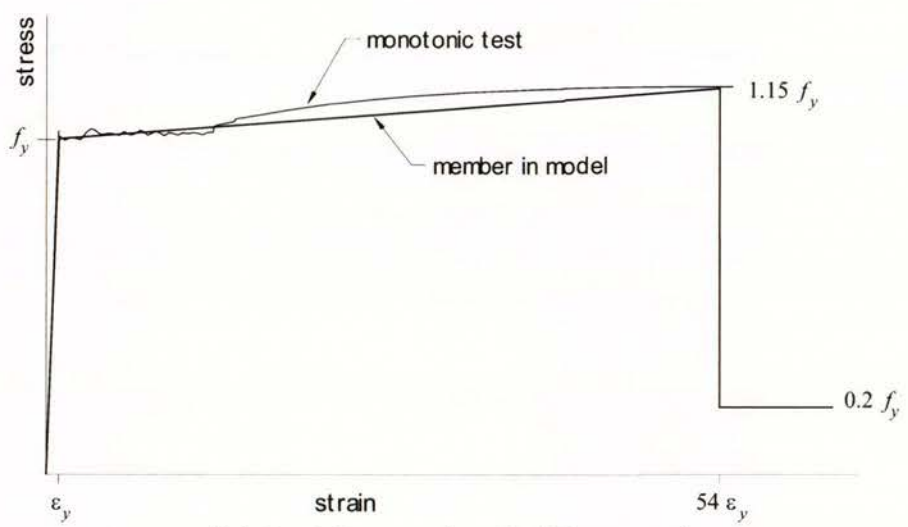

(b) 2 - 4.0mm wire @ 450mm c/c

Figure 7.17: Stress-strain relationship of reinforcement across central transverse beam and floor slab.

7.4.2 Development of flexible slab model

A flexible slab model was developed to model the horizontal shear transfer in the plane of the floor and vertical differential movement between the floor slab and frame (see *Chapter 5*, Figures 5.7 and 5.8). The model connects the floor slab at the first prestressed rib and the perimeter frame, as shown in Figures 7.18. The model consisted of a number of frame elements, with stiffness and strengths chosen to represent the actions of the starter bars of the floor and the concrete in that region (refer to following text for development of member properties and summarised in Appendix 4). The geometry of the elements used in the flexible slab were restricted by the inclusion of the model for the elongating hinge, as shown by Figure 7.18(c). In this figure the flexible slab model is narrower in between the column centre-line and the edge of the elongating plastic hinge. This was followed by a group of elements placed within a width of the plastic hinge. Then, four groups of flexible slab elements were spaced evenly between the two elongating plastic hinges within the length of the beam bay.

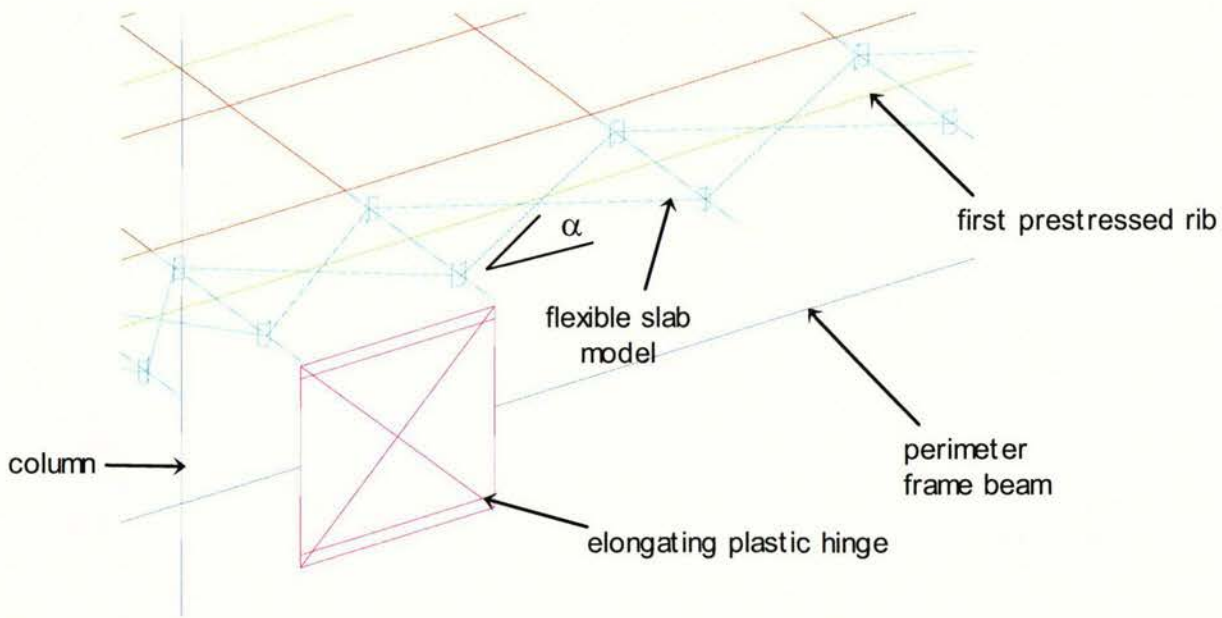

(a) Enlarged view of numerical model

Figures 7.18: Flexible slab model forming connection between floor slab and perimeter frame beam. (continued)

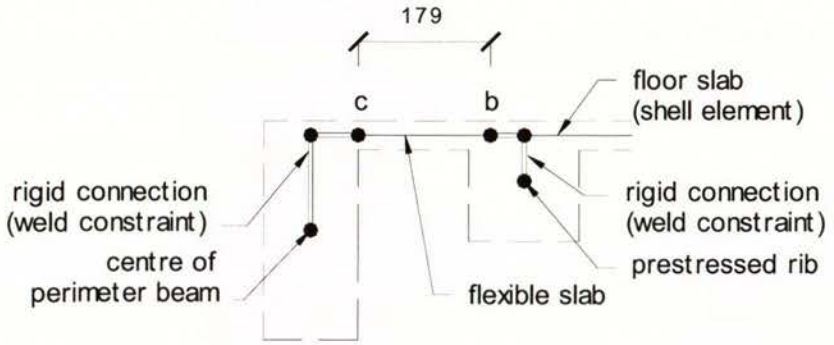

(b) Sectional view through beam and first prestressed rib

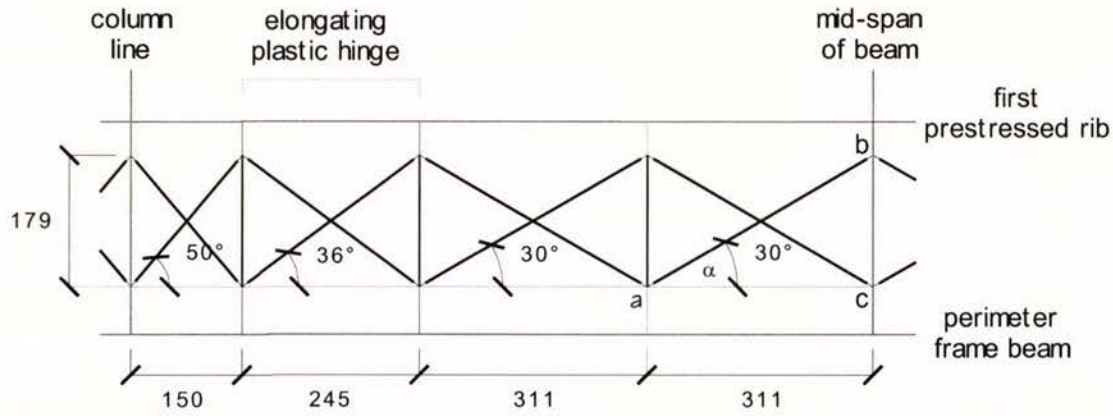

(c) Plan view of flexible slab model

Figures 7.18: Flexible slab model forming connection between floor slab and perimeter frame beam. (concluded)

Figure 7.19 shows the forces acting in the flexible slab. The magnitude of shear transferred across the interface between the floor slab and the perimeter frame beam is determined by the magnitude of the force in the tension tie and the angle of the diagonal compression strut. The tension tie represents the tie reinforcement between the beam and the floor slab, which in the case of the experimental unit, Unit 2, consisted of 10mm reinforcement spaced at 225mm. The diagonal compression strut angle, α, determines the magnitude of shear transferred across the interface between the floor slab and the main beam. The New Zealand Concrete Structures Standard limits this to 35° for shear friction across interfaces where concrete is placed monolithically or roughed to a full amplitude of not less than 5mm [S1]. However a compression strut angle of 30° was selected for the model as the angle adopted by the standard was considered to be conservative. The angle of compression struts determined for the groups of flexible slab model adjacent to the columns and elongating plastic hinges were limited by dimensions of the model (see Figure 7.18(c)).

The model developed for the flexible slab region was also required to represent the relative vertical movement between the perimeter frame and the first prestressed floor rib (see *Chapter 5*, Figures 5.7 and 5.8). This was achieved by the numerical model shown in Figures 7.19. The numerical values for the elements of this model are developed below and are summarised in Appendix 4.

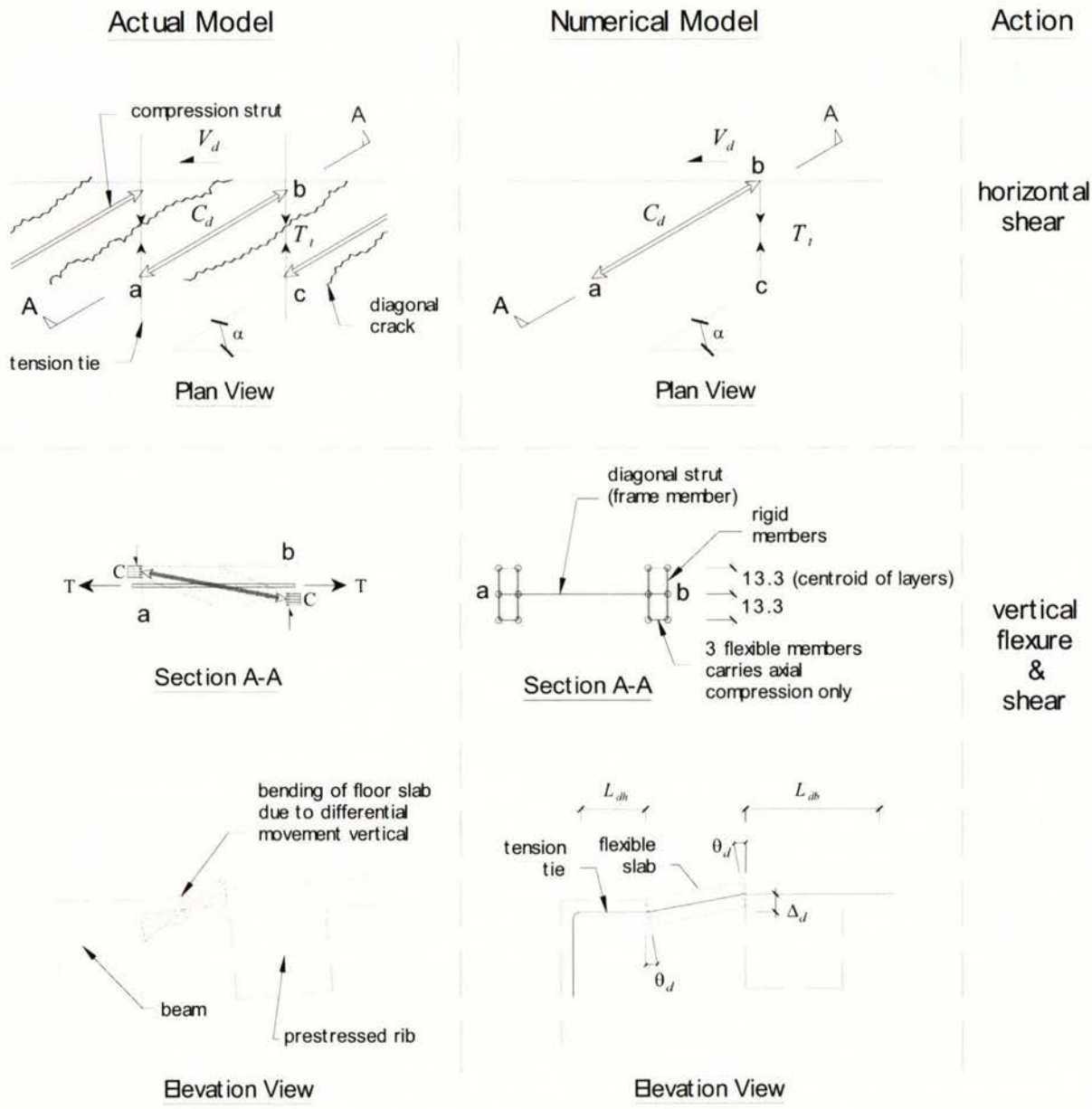

Figure 7.19: Forces acting in flexible slab between first prestressed rib and main beam in perimeter frame.

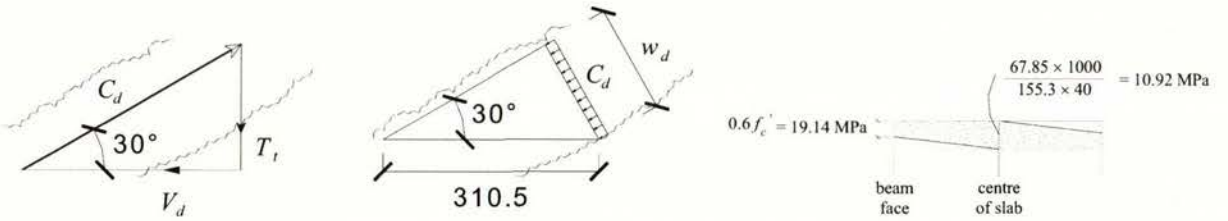

Free body diagram (refer to Figure 7.19) | Width of compression strut | Compression stresses along flexible slab

Figure 7.20: Free body diagram of forces in flexible slab and the width of compression strut.

Figure 7.20 shows a free body diagram of forces in single group of flexible slab model where the angle of the compression strut, α, was set at 30°. The strength of the flexible slab was determined by first calculating the force in the tension ties, T_t, within a length of 310.5mm where the reinforcement was 10mm at 225mm spacings with yield stress of 313 MPa:

$$T_t = \frac{\pi 10^2}{4} \times \frac{310.5}{225} \times \frac{313}{1000} = 33.9\,\text{kN}$$

Therefore the shear along the interface between slab and beam, V_d, for an angle of 30° are given by:

$$V_d = \frac{33.9}{\tan 30^\circ} = 58.8\,\text{kN}$$

And the diagonal compression force, C_d, for an angle of 30° is given by:

$$C_d = \frac{33.9}{\sin 30^\circ} = 67.8\,\text{kN}$$

And the width of concrete, w_d, which can resist C_d is given by:

$$w_d = 310.5 \times \sin 30^\circ = 155.3\,\text{mm}$$

The decrease in compressive strength and stiffness of cracked reinforced concrete has to be allowed in modelling of the flexible slab. This is related to the degree of cracking and straining (diagonal compression cracks as shown in Figure 7.19) in the concrete. Collected experimental data by Vecchio and Collins indicate that the degree of softening lies between 0.2 to 0.8 f_c' [V1]. Experimental data collected by Fenwick on

diagonal compression of webs in beams indicate that at failure, only 2 of 26 beams tested failed at stresses below $0.4 f_c'$ [F13]. The experimental data indicated that most web crushing occurred at stressed between 0.5 and $0.6 f_c'$. A value of $0.6 f_c'$ was selected for this exercise. Therefore, the depth of the compression stress block of the flexible slab at the beam face is given by (where $0.6 f_c' = 19.14$ MPa):

$$d_d = \frac{67.8 \times 1000}{155.3 \times 19.14} = 22.8 \text{ mm}$$

Therefore the moment that can be resisted by the slab is given by:

$$M_d = 33.9 \times \left(20 - \frac{22.8}{2} \right) \Big/ 0.3105 = 0.93 \text{ kNm per m width of slab}$$

In order to estimate the stiffness of the slab, it was assumed that the rotation of the slab is concentrated at the beam and prestressed rib faces, as shown by the elevation view of the analytical model in Figure 7.19. The rotation of the slab is made up of two components; the extension of the tension tie and the compression shortening of the diagonal compression strut. The extension of the tension tie was estimated by calculating the development lengths of the reinforcement (tension tie) based on equations given by the New Zealand Standard [S1], with the exception of decreasing the development length by 25% due to the conservative nature of standard given equations. Therefore the estimated length of tension tie under yield extension is given as the sum of half of the development lengths and the slab width (150mm), calculated below:

$$L_t = \frac{L_{dh} \times 0.75}{2} + \frac{L_{db} \times 0.75}{2} + 150$$

$$= \frac{99.75}{2} + \frac{207.8}{2} + 150 = 303.8 \text{ mm}$$

The extension of the tension tie is given by (where $f_y = 313$ MPa, $E = 200$ GPa):

$$\text{extension of tension tie} = 303.8 \times \frac{313}{200000} = 0.475 \text{ mm}$$

The compression shortening of the diagonal compression strut can be estimated by taking the average compression stress on the top fibre of concrete. At the slab end the stress is taken as $0.6 f_c'$ (19.14MPa) and at mid-span the stress (15.03MPa) is calculated by dividing the compression force, C_d, by the area of the diagonal strut (see Figure 7.20). Therefore the average stress is given by:

$$\text{average stress on diagonal strut} = \frac{19.14 + 10.92}{2} = 15.03 \text{ MPa}$$

The compression shortening of the diagonal strut is given by:

$$\frac{15.03}{0.6 \times E_c} \times \frac{150}{\sin 30^\circ} = 0.293 \text{ mm}$$

where $0.6 \times E_c = 0.6 \times 25.65$ GPa due to softening of cracked concrete as described above (pg.191).

Therefore the compression shortening normal to beam is given by:

$$0.293 \text{ mm} \times \sin 30^\circ = 0.147 \text{ mm}$$

Therefore, at the onset of yield of the reinforcement, from the shortening of the slab and extension of the tension tie, the rotation of the slab, θ_d, is given by:

$$\theta_d = \frac{\left(\frac{0.475 + 0.147}{2}\right)}{20} = 0.0156 \text{ rads}$$

And the vertical deflection, Δ_d, at first yield are given by multiplying the rotation with the width of the flexible slab:

$$\Delta_d = 0.0156 \times 150 = 2.34 \text{ mm}$$

The numerical model of the flexible slab is shown in Figure 7.19. This was developed by having a group of members in three layers at both ends of the diagonal member. These members carry axial compression forces only and were connected by a rigid member. Therefore rotation was concentrated to the ends of the diagonal member as the

flexible slab displaces vertically. These layered members were also limited to $0.6 f_c'$ in compression stress. The stiffness of the layered members was obtained by trial and error where the group of members (diagonal member and tension tie) were subjected to a shear force, V_d, while a vertical displacement of Δ_d (=2.34mm) was applied. The stiffnesses were adjusted such that the bending moment at first yield matched the bending moment calculated.

Table 7.5 presents a summary of the properties of the layered members in the diagonal slab member. Comparison of the moment due to the eccentric compression force in the diagonal slab shows that the numerical (computer) model predicts a lesser value than the analytical (calculated) model. Figure 7.21 shows plots of the moment due to the eccentric force against the horizontal shear force in the slab, V_d, of the analytical model and the numerical model for diagonal struts at 30° to the horizontal. It can be seen that even though the values predicted are lesser for the numerical model, it still provides a close match with the analytical model.

Table 7.5: Member properties in diagonal slab model.

angle of diagonal strut *	moment from an eccentric force (kNm)		layered member		
	analytical (calculated) model	numerical (computer) model	size (mm)	yield force (kN)	γ **
30°	0.58	0.51	13.3 × 155.3	39.6	0.045
36°	0.54	0.52	13.3 × 144.7	36.9	0.053
50°	0.32	0.31	13.3 × 115.0	29.4	0.069

* angle of diagonal strut, see Figure 7.18(c)

** multiplier, layered member stiffness = $\gamma \times \frac{E_c A}{l}$, where E_c = 25.65 GPa, l = 10 mm.

The stress-strain relationship defined for each of the layered members representing the concrete in the diagonal slab is shown in Figure 7.22. The numerical model assumes that all rotation occurs at the ends of the slab, whereas in reality, the deformation spreads along the width of the flexible slab. Therefore, the point of failure defined in

Figure 7.22 was assessed by trial and error (of the numerical model with floor slab) to approximately correspond with the observed point of failure of the slab at similar drift displacement during the experiment on Unit 2.

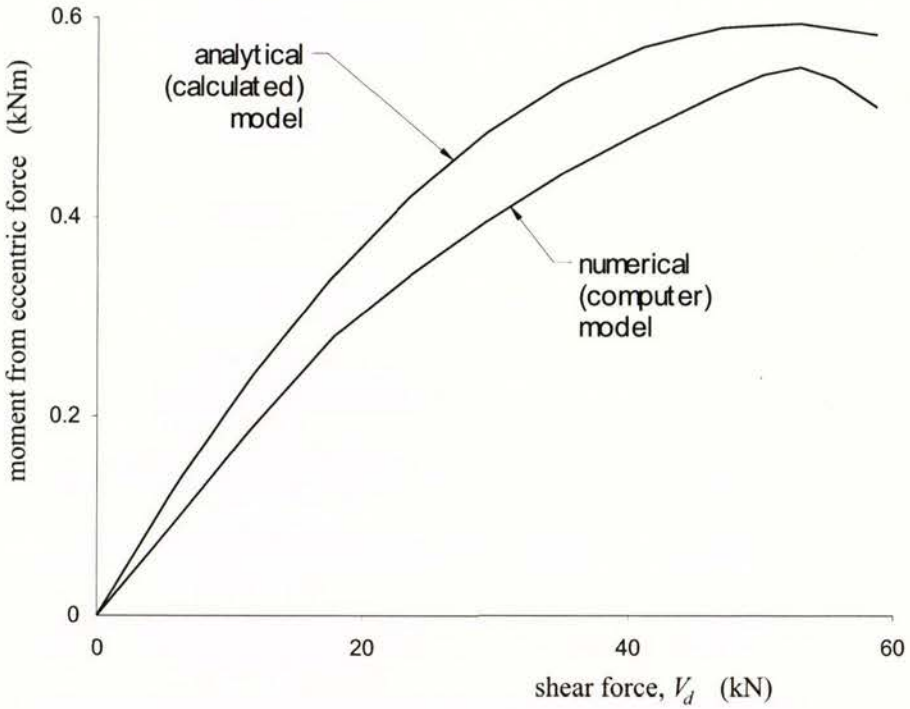

Figure 7.21: Interaction diagram of horizontal shear and moment from eccentric compression force in flexible slab.

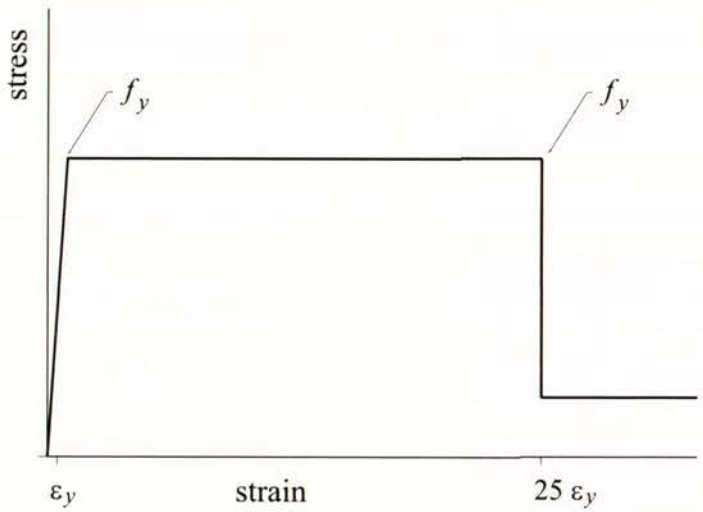

Figure 7.22: Stress-strain relationship of layered members in diagonal slab model.

7.4.3 Results of analysis

With the exception of starting the analysis by displacing the numerical model to 0.5% interstorey drift, it was subjected to a displacement history identical to that of the experimental Unit 2, as shown in Figure 5.1 of *Chapter 5*. During certain stages of the analysis it was found that the analysis became unstable and stopped running as multiple elements were failing. In order to allow the analysis to proceed to latter stages, the analysis was stopped at these stages and the failed or failing members were removed. The first of these was during the second displacement cycle to 2.0% interstorey drift in the positive direction. At this point, the diagonal flexible slab groups labelled 'C_{1a}' and 'C_{1b}' were failing and consequently removed (see Figure 7.23). Eventually a number of diagonal flexible slab groups had failed and removed before the analysis failed to continue on the second half cycle to 4.0% interstorey drift in the negative direction. This is summarised in Table 7.6.

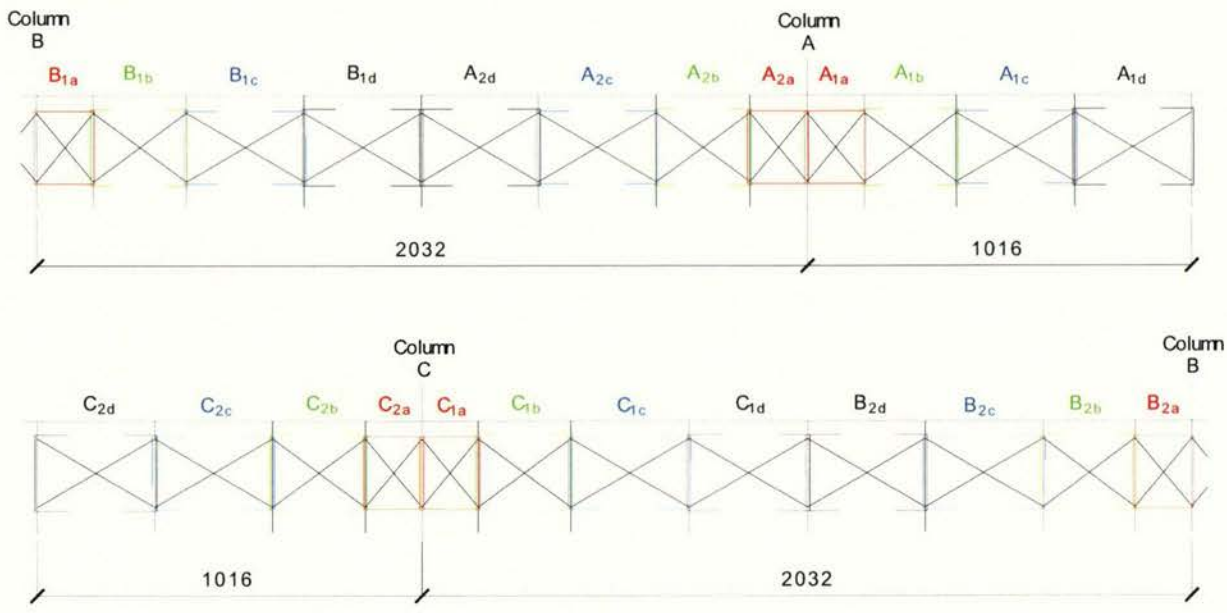

Figure 7.23: Named diagonal flexible slab groups.

As expected, the flexible slab members around the outer columns, columns 'A' and 'C', failed. By the end of the numerical experiment, all the members in the cantilevered extension past the outer columns had failed. The extent of damage around the outer columns corresponded with experimental observations of Unit 2. The numerical experiment also indicated that the flexible slab groups around the central column, column 'B', had failed. This was not so apparent in the experimental unit.

Table 7.6: Flexible slab group that failed during analysis.

displacement stage			Flexible slab group failed (removed)
drift	cycle	direction	
2.0%	2nd	positive	C_{1a} , C_{1b}
2.0%	2nd	negative	A_{2a} , A_{2b}
2.5%	1st	positive	C_{2a}
2.5%	1st	negative	C_{2b} , A_{1a} , B_{2a}
2.5%	2nd	positive	A_{1b}
3.0%	2nd	positive	B_{1a} , B_{1b} , B_{2b}
3.0%	2nd	negative	A_{1c}
3.5%	1st	negative	C_{2c}
4.0%	1st	positive	C_{2d}
4.0%	1st	negative	A_{1d}

The lateral force versus deflection response of the model is shown by Figure 7.24. The lateral force versus deflection chart of the experimental unit is reproduced in Figure 7.25. Because of the inability of the elongating hinge to accurately model degradation of stiffness, the numerical model does not show a response that is typical of an actual frame during the unloading and reloading phases as shown by the response curve of the experimental unit. The lateral force peaked at 3.0% interstorey drift for the numerical model, while in the experimental unit peak lateral strength was at 2.5% interstorey drift. The maximum numerical lateral strength recorded was 276kN in the positive direction and in the reverse direction, the maximum value was 266kN. In comparison, the maximum values in the experiment were 313kN in the positive direction and 284kN in the negative direction. These correspond to a difference of about 12% and 6% in the respective directions. Near the end of the analysis, at the second cycle to 4.0% interstorey drift in the positive direction the lateral strength of the numerical model was 208kN while for the experimental the value was 204kN. While the lateral strength prediction is reasonable, it the peak strength could be improved by having an angle of slightly less than 30° for the diagonal members in the flexible slab model.

The average elongation of the beams at peaks of displacement cycles are shown in Figure 7.26. The results show that the numerical model predicts elongation of beams rather well up to the second cycle to 3.5% interstorey drift. At this point the average elongation of the beams in the numerical model was 1.3% of beam depth compared with 1.5% in the experimental unit. Beyond this point, the elongation in the experimental unit increased at a greater rate, but this was not replicated in the numerical model. This was most likely due to the inability of the model to account for contact stress effects in the test unit where concrete becomes dislodged and acts to prop the cracks open in the hinges. Figure 7.27 shows the average elongation in the plastic hinges within the beam bay (internal beam between columns) and the average elongation in the cantilever extensions. It can be clearly seen that the predicted elongation in the plastic hinges located in the cantilever extension by the numerical model was significantly greater than that measured in the experiment. The elongation in the internal hinges predicted by the numerical model matched the values from the experiment up to 3.0% interstorey drift, but under-predicts at higher drifts.

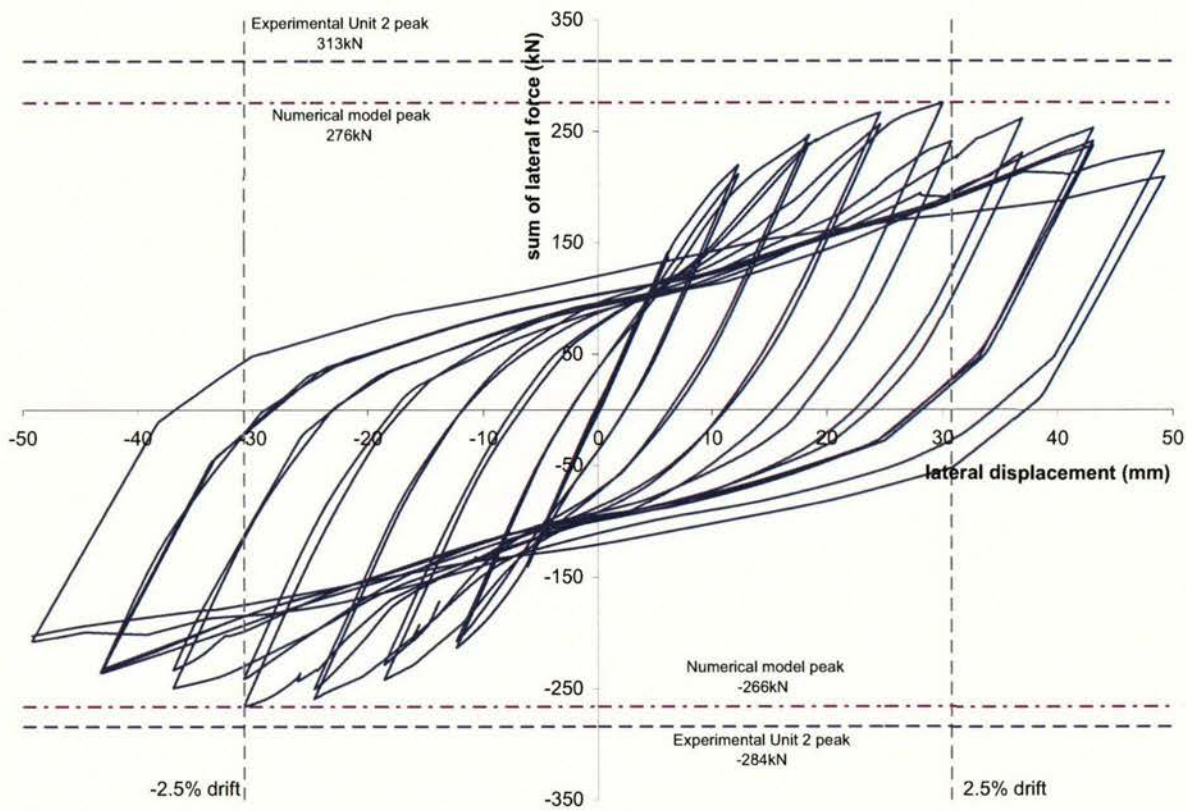

Figure 7.24: Lateral force versus displacement response of numerical model.

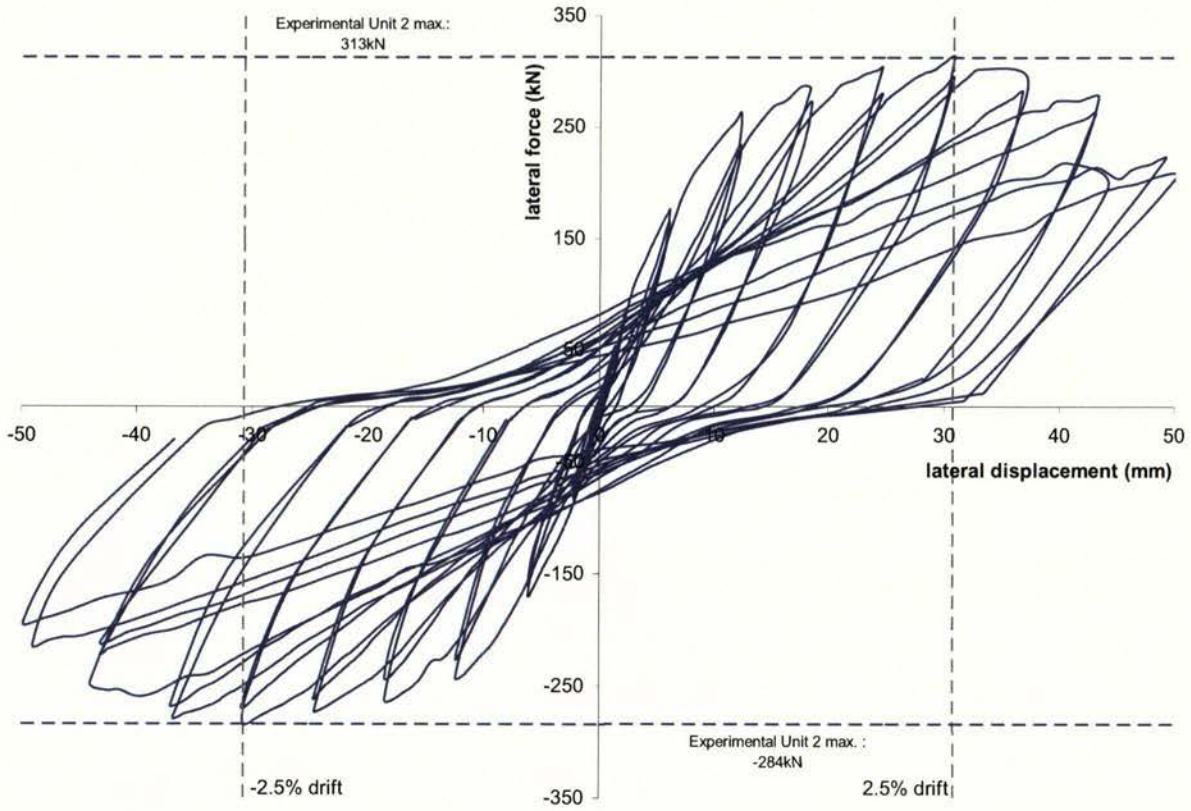

Figure 7.25: Lateral force versus displacement response of experimental Unit 2.

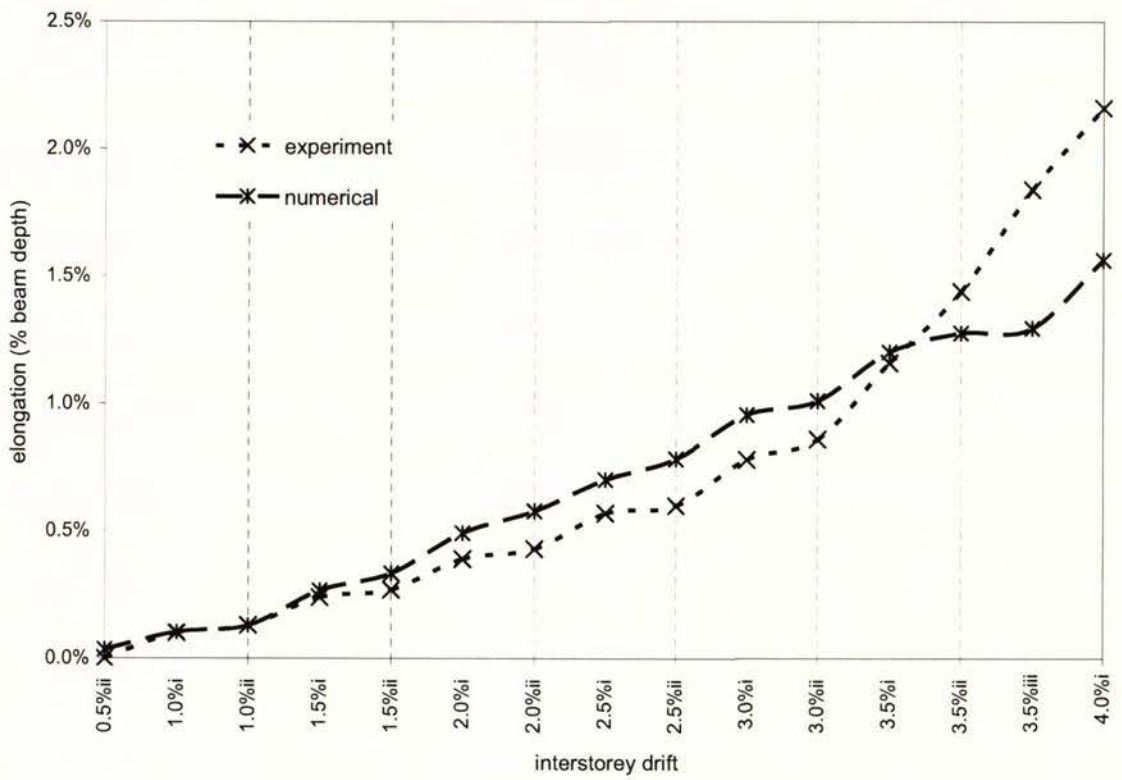

Figure 7.26: Comparison of average elongation of beams in experimental unit and numerical model.

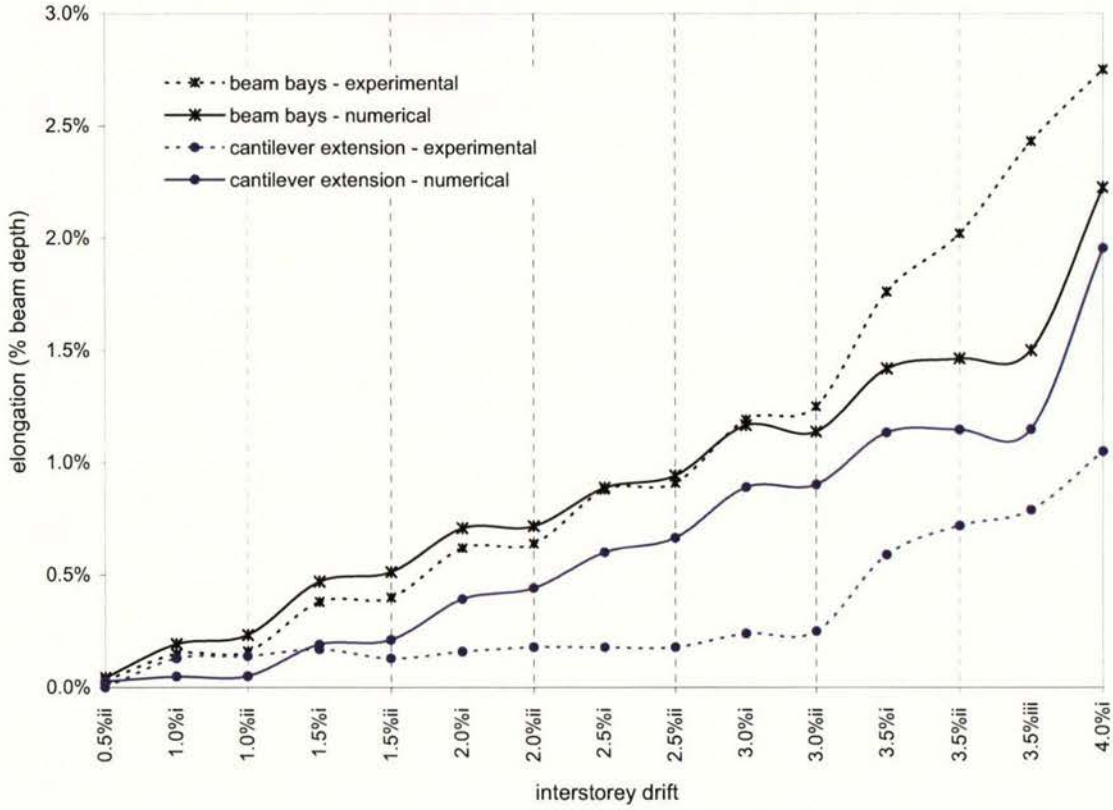

Figure 7.27: Comparison of average elongation of beams within beam bays and cantilever extensions.

Figures 7.28 show the differential vertical movement calculated at peaks of displacement cycles. Figure 7.29 shows the points between which the vertical displacement was reported. Line 'a' indicates the end of the floor slab at the beam face, while line 'b' is near the first prestressed rib in the floor. The largest movements occurred at the inside of the outer joints, where it was a maximum of 8.4mm for 'A2' (next to joint 'A') when displaced in the positive direction. In the reverse direction, the maximum vertical movement was 7.4mm for 'C1' (next to joint 'C'). These correspond to 4.7% and 4.1% of the flexible slab length (179mm) respectively. The figures also indicate that there was a large margin in the vertical movement between the floor slabs on either side of the outer columns. No experimental measurements were made of the magnitude of vertical movement, however this corresponds with observations where the damage around the outer columns was substantial due to rotation concentrated around the beam-column regions. The relative vertical movement at yield from numerical analysis of the flexible slab was 2.3mm. This equates to a displacement ductility of 3.7 for the maximum vertical movement recorded (ie. 8.4mm at 'A2').

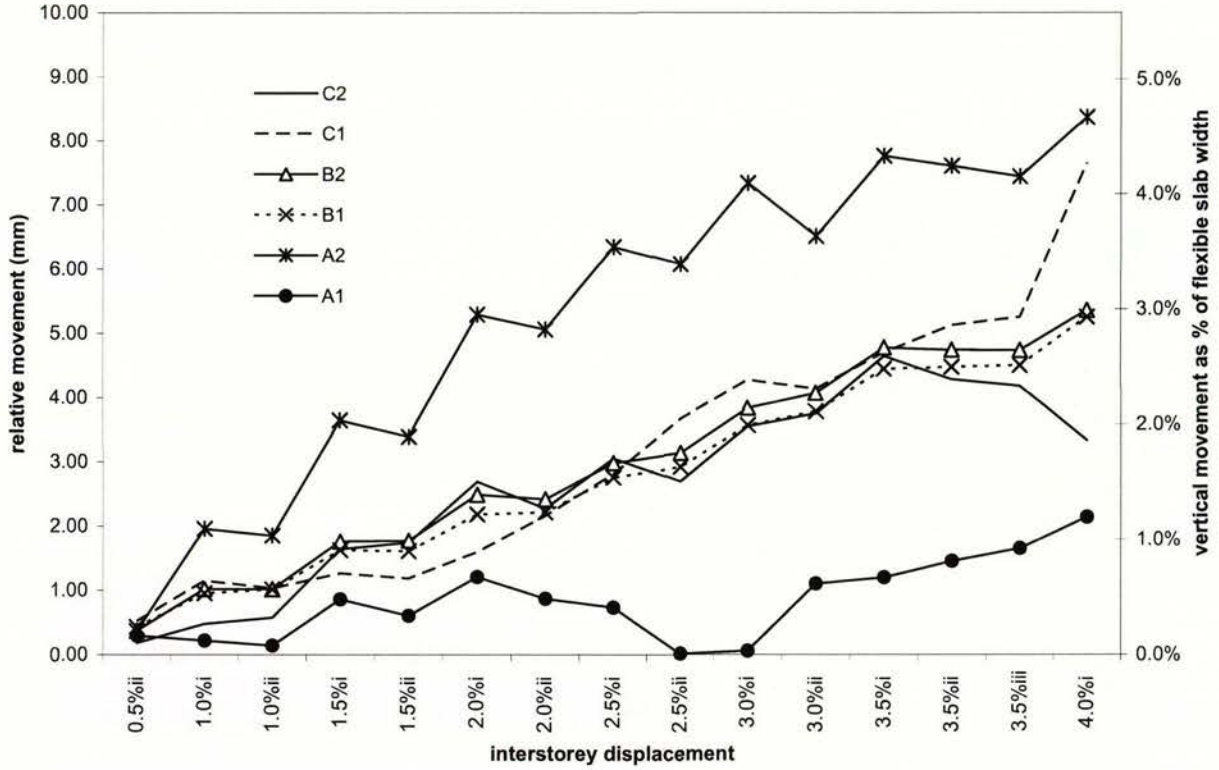

(a) Positive direction of displacement

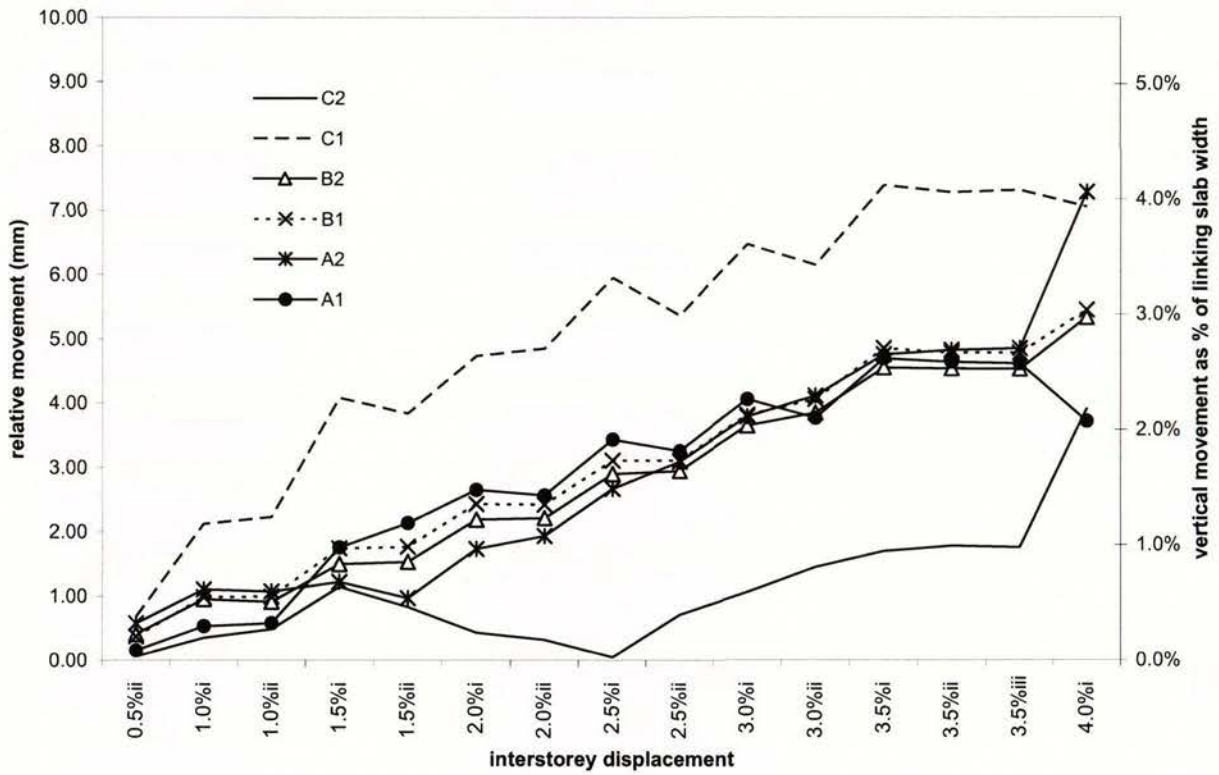

(b) Negative direction of displacement

Figures 7.28: Differential vertical movement of flexible floor slab.

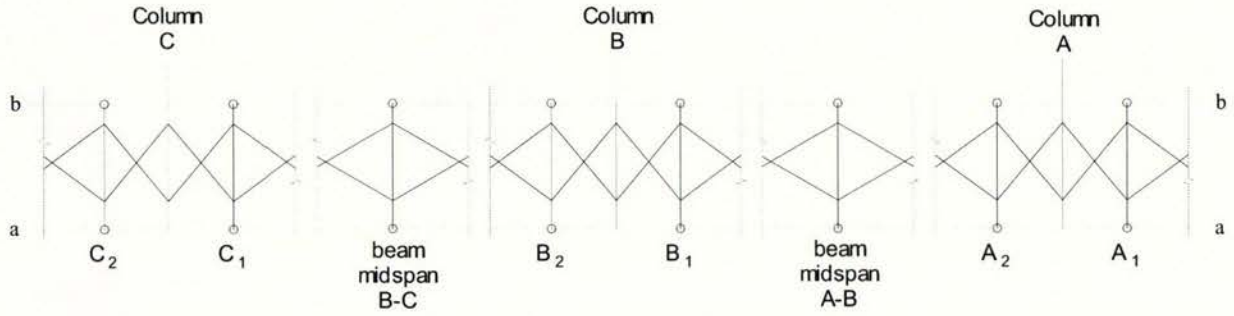

Figure 7.29: Points of differential vertical movement of floor slab between perimeter frame beam and first prestressed floor rib.

7.4.4 Comparison of initial stiffness

The initial stiffness of the experimental model and the numerical model are compared in Figure 7.30. The initial stiffness was obtained from the cycles to 0.5% interstorey drift in the experimental model. The initial stiffness of the experimental unit was 27kN/mm, while the stiffness of the numerical model was 22kN/mm. This equates to a 22% greater stiffness of the experimental unit over the numerical model. There are a number of possible reasons for this lack of agreement. For example, in the numerical model the connections between the floor slab elements and the beam members were based only on equivalent steel reinforcement stiffness. Added to this, the floor stiffness in the direction perpendicular to the perimeter frame was reduced. In comparison, during the initial stages, large areas of the experimental unit remained uncracked.

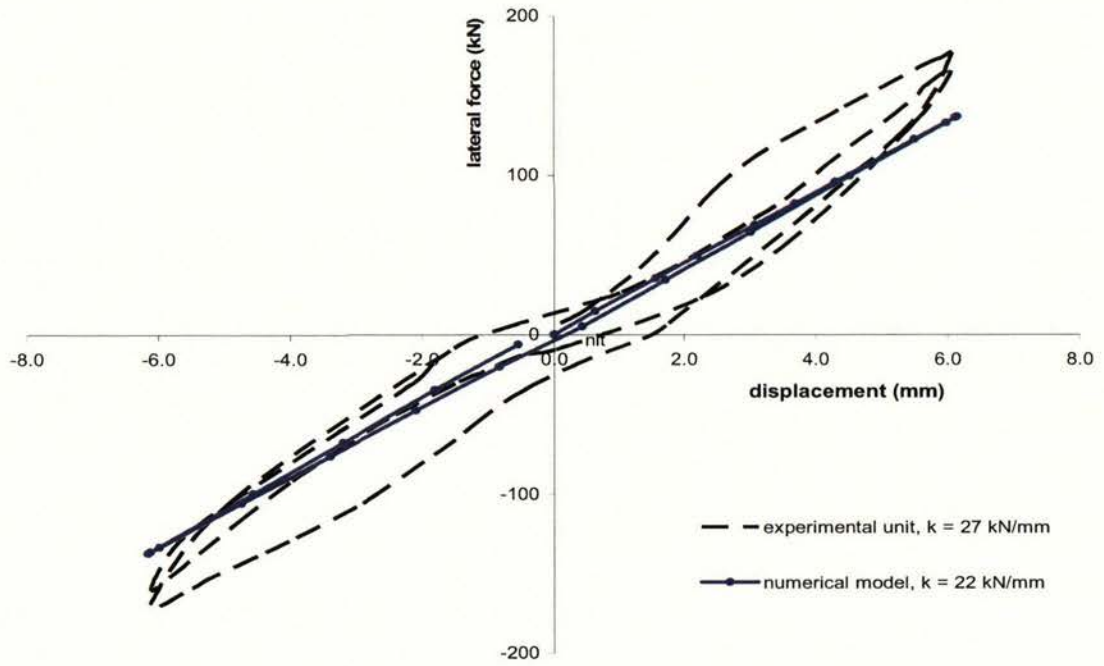

Figure 7.30: Comparison of initial stiffness of experimental and numerical model.

7.5 Variations to Numerical Model of Unit 2

In this section, the numerical model of Unit 2 was modified by changing the support conditions and the properties of the connections between the frame and the floor. The purpose was to investigate the effects that these changes would have on performance in comparison with the unmodified numerical model of Unit 2.

7.5.1 Fixing ends of cantilevers against vertical movement

The numerical model of Unit 2 (described in section 7.4) was modified by fixing the ends of the cantilevers against vertical deflection. This is illustrated in Figure 7.31.

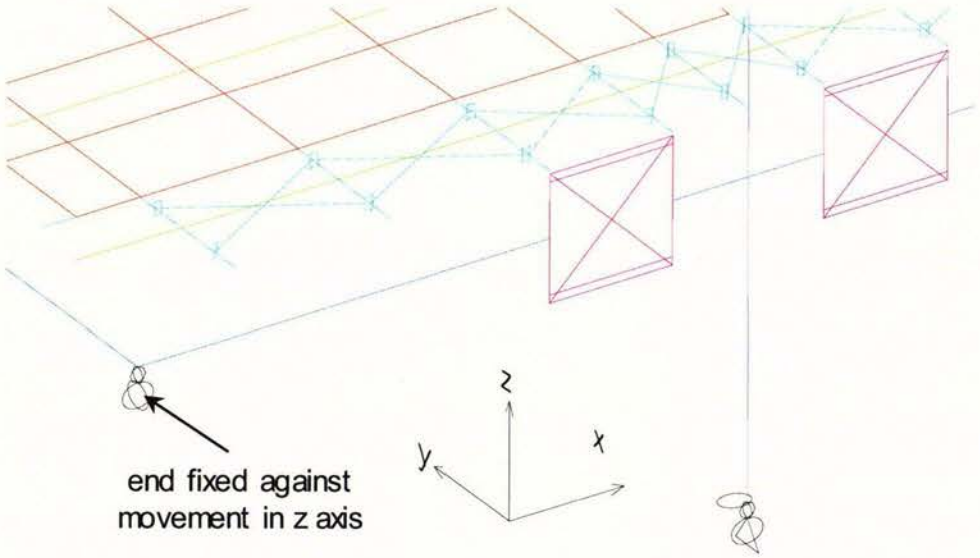

Figure 7.31: End of cantilever fixed against vertical movement.

Figure 7.32 compares the lateral force versus displacement envelope of the numerical model of Unit 2 and the modified model. The modification did not result in much change to the lateral force response. The peak force in the positive direction was 260kN (276kN for model of Unit 2) and 252kN (266kN for model of Unit 2) in the negative direction.

Figures 7.33 shows the differential vertical movement between the first prestressed floor rib and the main beam in the perimeter frame. In comparison with the differential movement for the numerical model of Unit 2 shown in Figures 7.28, the vertical movement around the outer beam-column joints 'A' and 'C' had reduced significantly.

In the positive direction of displacement, the difference in vertical movements between each side of joint 'A' had closed to a maximum of 0.7mm, which had been 7.3mm for the model of Unit 2.

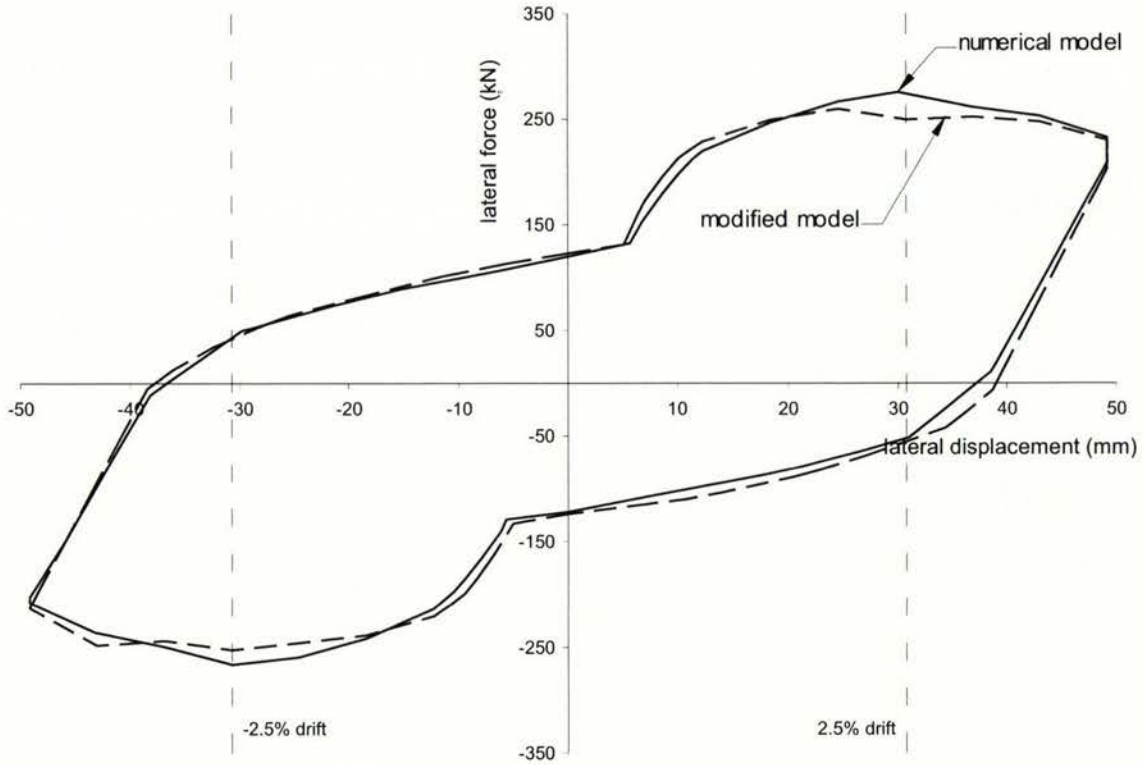

Figure 7.32: Lateral force versus displacement envelope of numerical model of Unit 2 and modified model.

In the negative direction for joint 'C', the difference in movements was 1.1mm, which had been 5.7mm for the model of Unit 2. These values indicate that in fixing the ends of the cantilevers (such as buildings with corner columns) less damage in the floor slab due to vertical movement can be expected around the columns (where floor units span past the columns) than that observed in Unit 2. This is illustrated in Figure 7.33(c).

Figure 7.34 compares the total elongation for the modified model against the numerical model of Unit 2. The elongation recorded for the modified model was slightly greater than that for the numerical model.

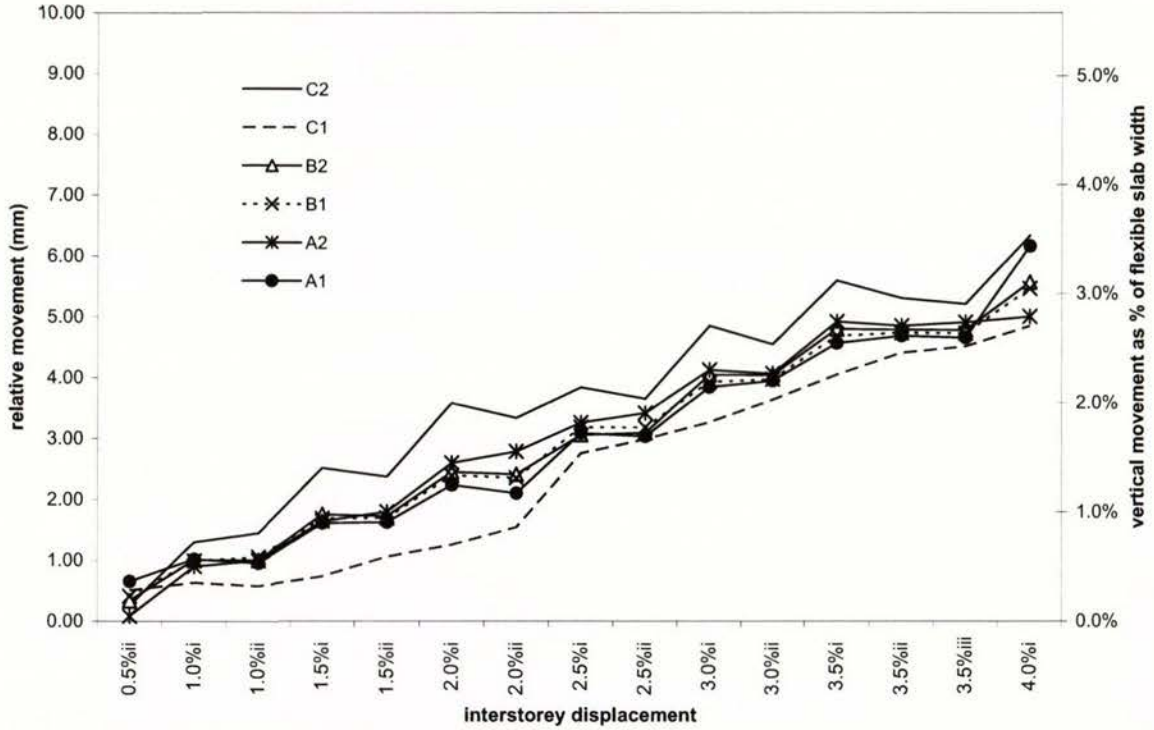

(a) Positive direction of displacement

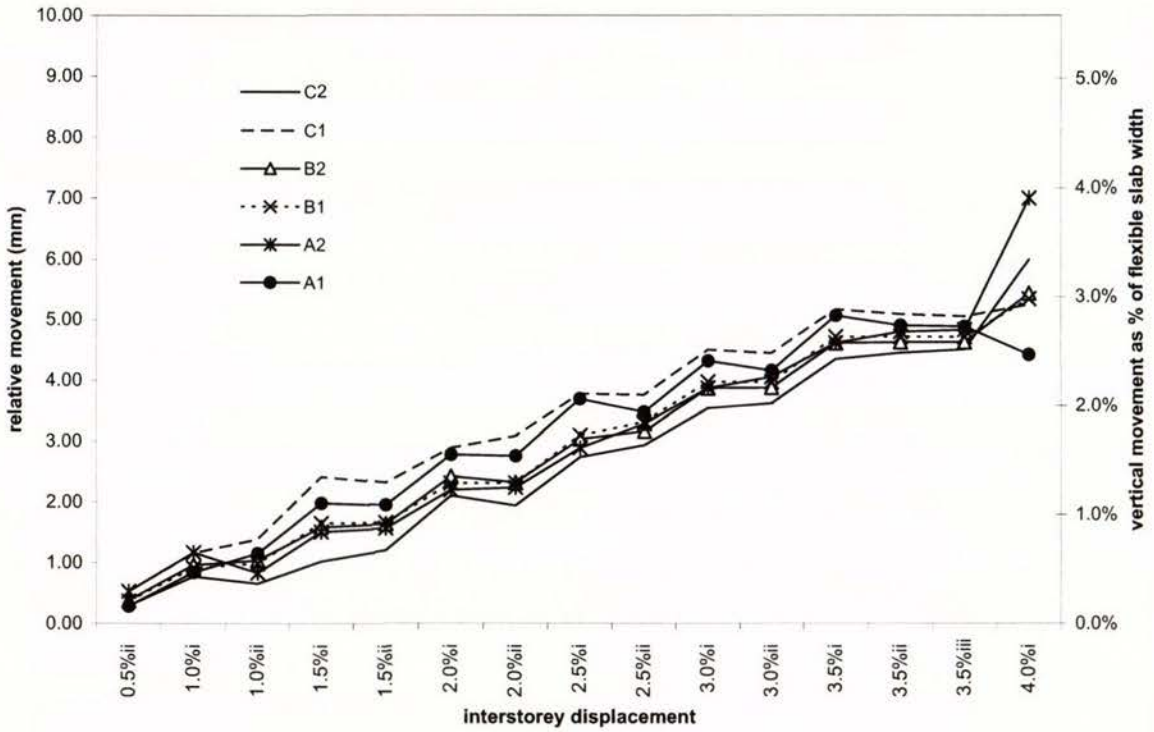

(b) Negative direction of displacement

Figure 7.33: Differential vertical movement of flexible floor slab for modified model. (continued)

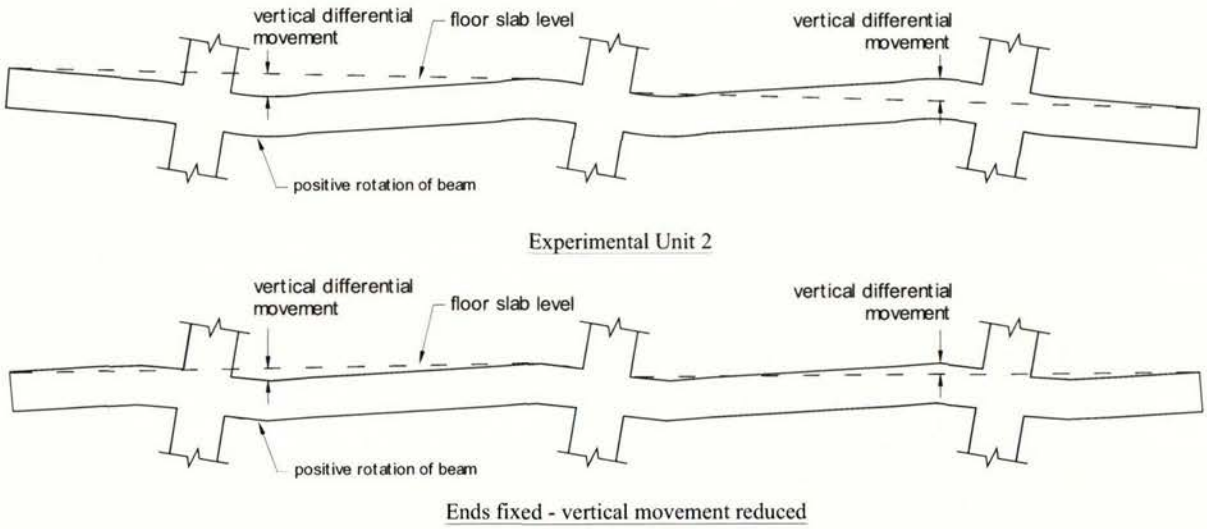

(c) Illustration of vertical movement in Unit 2 and modified model

Figure 7.33: Differential vertical movement of flexible floor slab for modified model. (concluded)

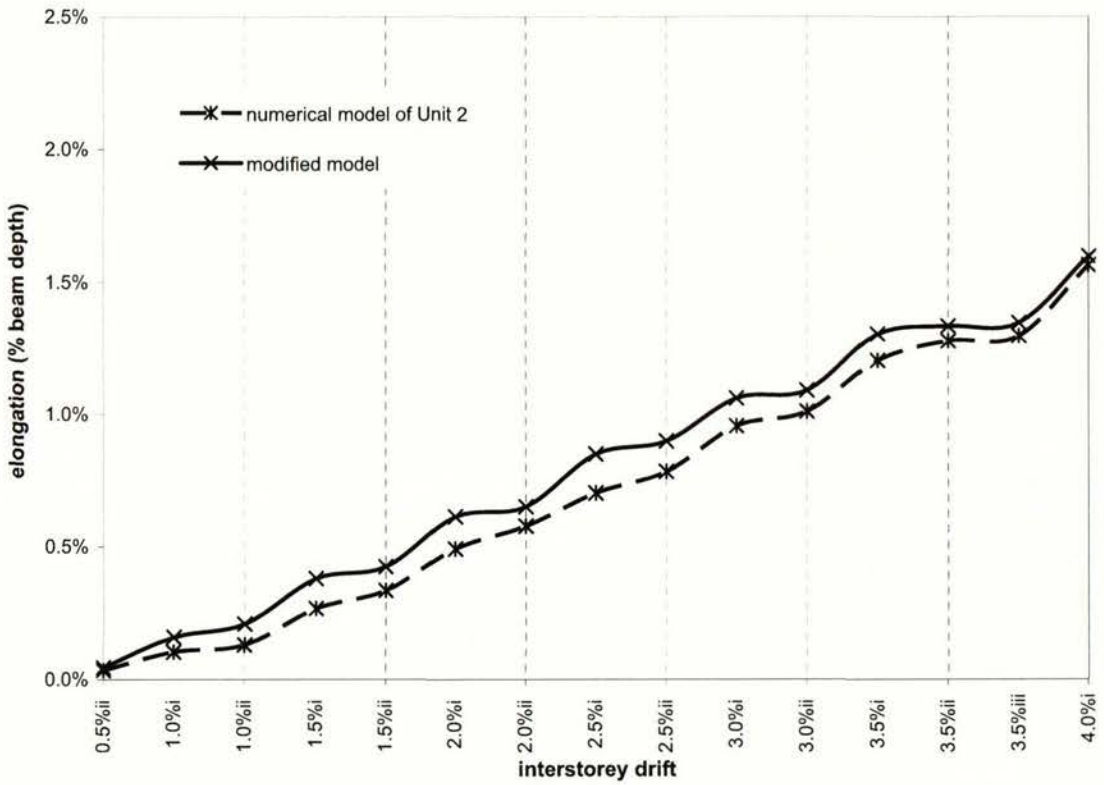

Figure 7.34: Comparison of average elongation in beams between numerical model of Unit 2 and modified model.

7.5.2 Removing flexible slab members and tension ties

Selected flexible slab members were removed from the original numerical model of the floor slab to assess the effect on performance. These changes are described below in reference to Figure 7.35.

Model A - Four diagonal slab members and tension tie members around the centre column, column 'B', were removed.

Model B - Four groups of diagonal slab members and tension tie members around each of the outer columns, columns 'A' and 'C', were removed.

Model C - Two groups of diagonal slab members either side of the mid-span of the beam in each beam bay were removed.

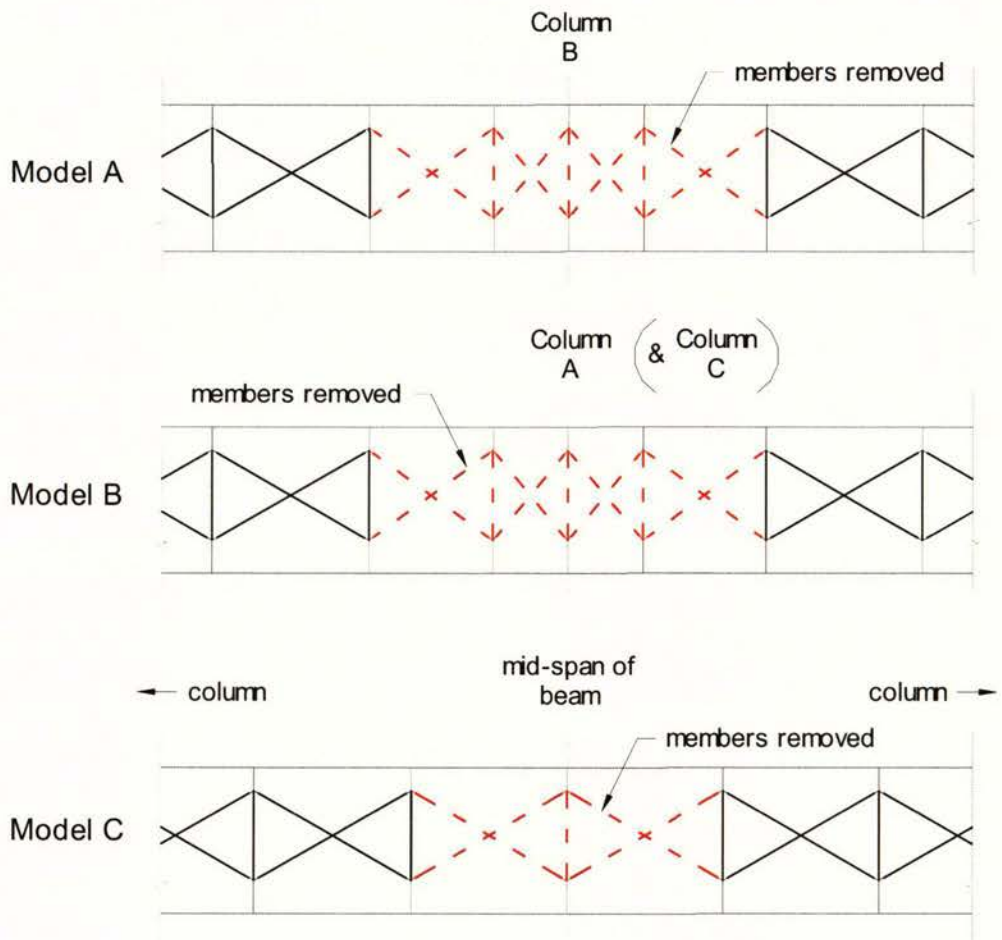

Figure 7.35: Variations to numerical model by removing flexible slab members.

The envelope of lateral force versus displacement responses of the modified models are shown in Figure 7.36. The results are summarised in Table 7.7. The changes in Model A did not make much difference to the lateral force versus displacement response of the model.

Table 7.7: Lateral strength of floor slab models.

	Peak lateral strength		Peak at 3.5% drift	
	lateral strength (kN)	% of numerical model of Unit 2	lateral strength (kN)	% of numerical model of Unit 2
Model A	278 at +2.5% drift	100.7	256 at +3.5% drift	101.2
	-261 at -2.5% drift	98.1	-243 at -3.5% drift	103.4
Model B	248 at +2.5% drift	89.9	228 at +3.5% drift	90.1
	-237 at -3.0% drift	89.1	-221 at -3.5% drift	93.6
Model C	268 at +2.5% drift	97.1	268 at +3.5% drift	105.9
	-261 at -3.0% drift	98.1	-240 at -3.5% drift	101.7

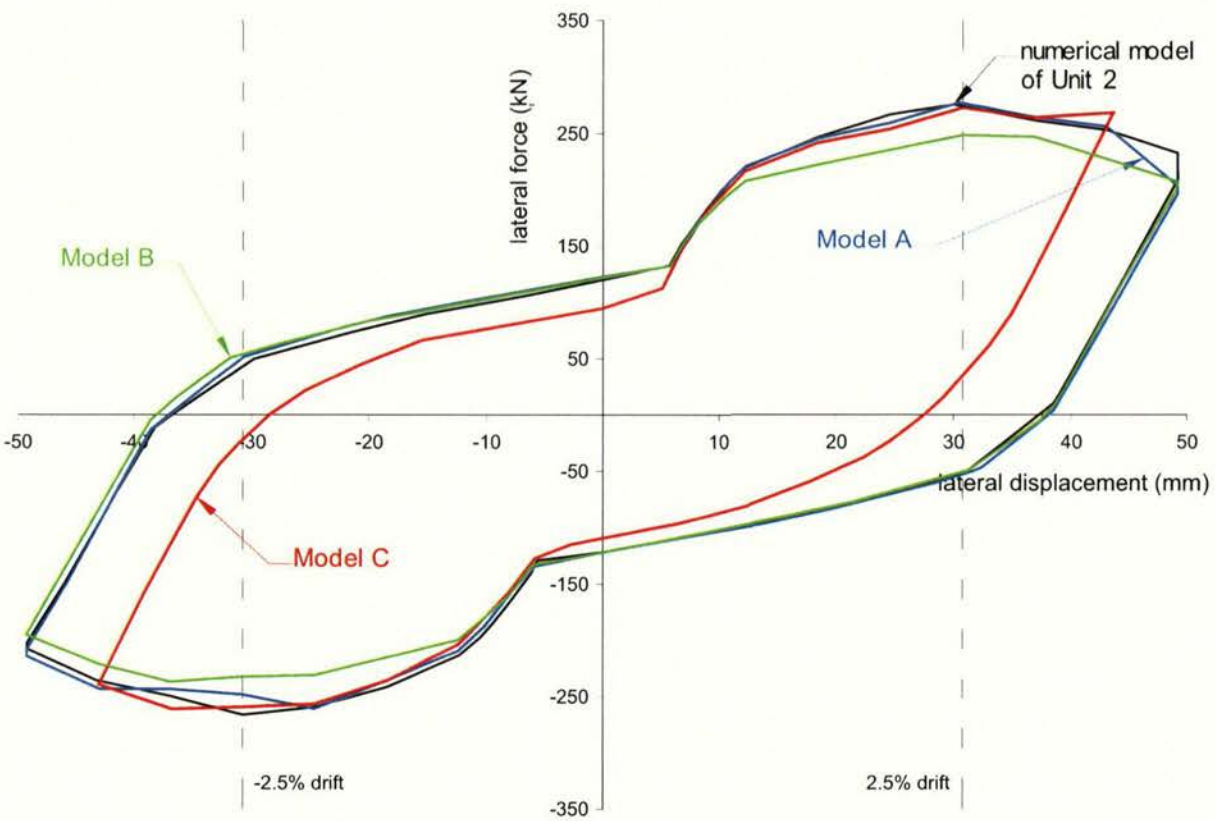

Figure 7.36: Lateral force versus displacement response of modified models.

The changes in Model B resulted in the decrease in peak lateral strengths by 10.1% in the positive direction of displacement and by 10.9% in the negative direction. This may seem to be a favourable result but removing connections to the floor slab around the outer columns may result in the columns not being laterally supported over a number of floors. Therefore the columns may be susceptible of buckling. There may be scope here for design of connections to tie the columns to the floor diaphragm while allowing the beam plastic hinges in the region to rotate more freely. The changes in Model C did not make significant difference to the peak lateral strength. However, the model did not achieve displacement to 4.0% drift as all the floor slab to frame connections along the entire bay from the centre column, column 'B', to the end of the cantilever past column 'C' had failed on the second cycle to 3.5% drift displacement.

Figures 7.37 show the differential vertical movement of the floor slab for the modified models. Only the differential movements resulting from displacing the frame in the positive direction are shown. These can be compared against the vertical movement recorded for the numerical model of Unit 2 shown in Figure 7.28(a).

As shown by Figure 7.37(a), the patterns of differential vertical movement in Model A are rather similar to that shown by the original model. As shown by Figure 7.37(b), the removal of the members around the outer columns in Model B did not result in overall reduction of vertical differential movement. However the difference in vertical movement between the points either side of the columns ('A1' & 'A2') had reduced. The failure of the diagonal groups along the cantilever extension past joint 'C' from the second cycle to 3.0% drift displacement resulted in the increased vertical movement around this region. Figure 7.37(c) shows the differential movement of Model C. The vertical differential movement around the outer columns (columns 'A' and 'C'), had increased significantly in comparison to the numerical model of Unit 2. The model failed on the second cycle to 3.5% interstorey drift.

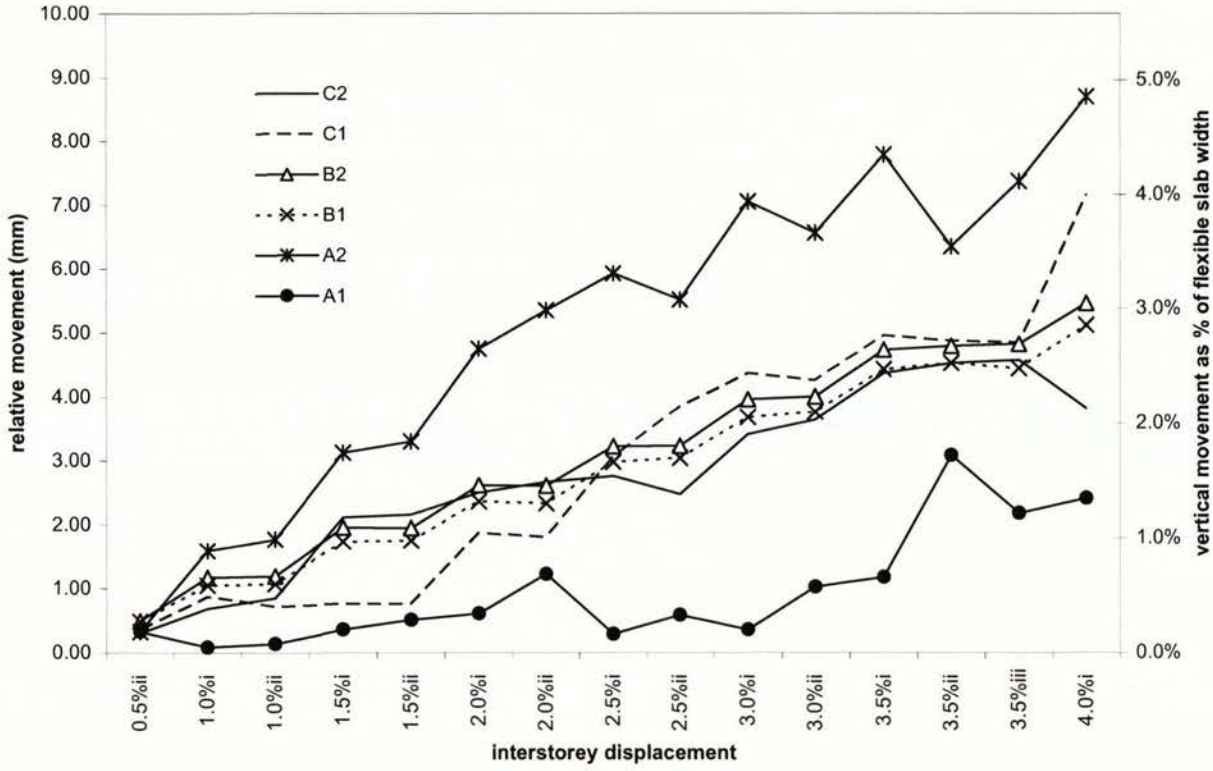

(a) Model A

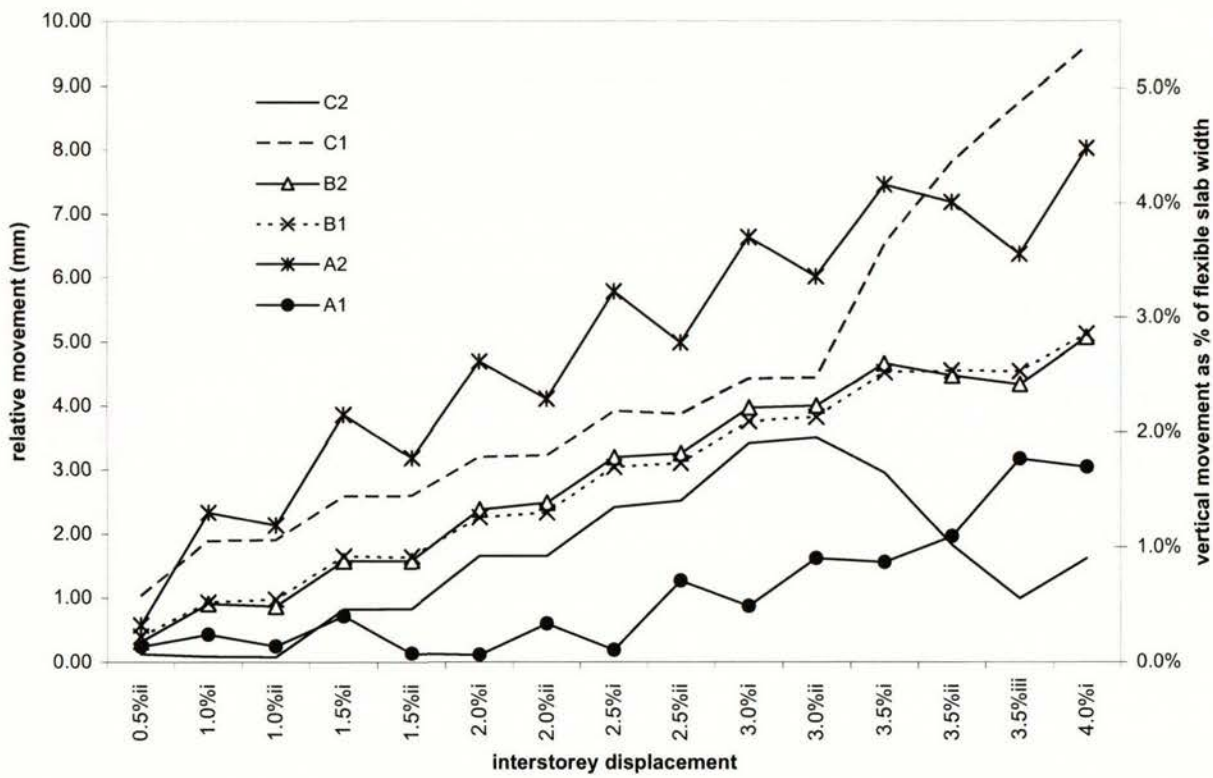

(c) Model B

Figures 7.37: Differential vertical movement of flexible floor slab in modified models in the positive direction of displacement. (continued)

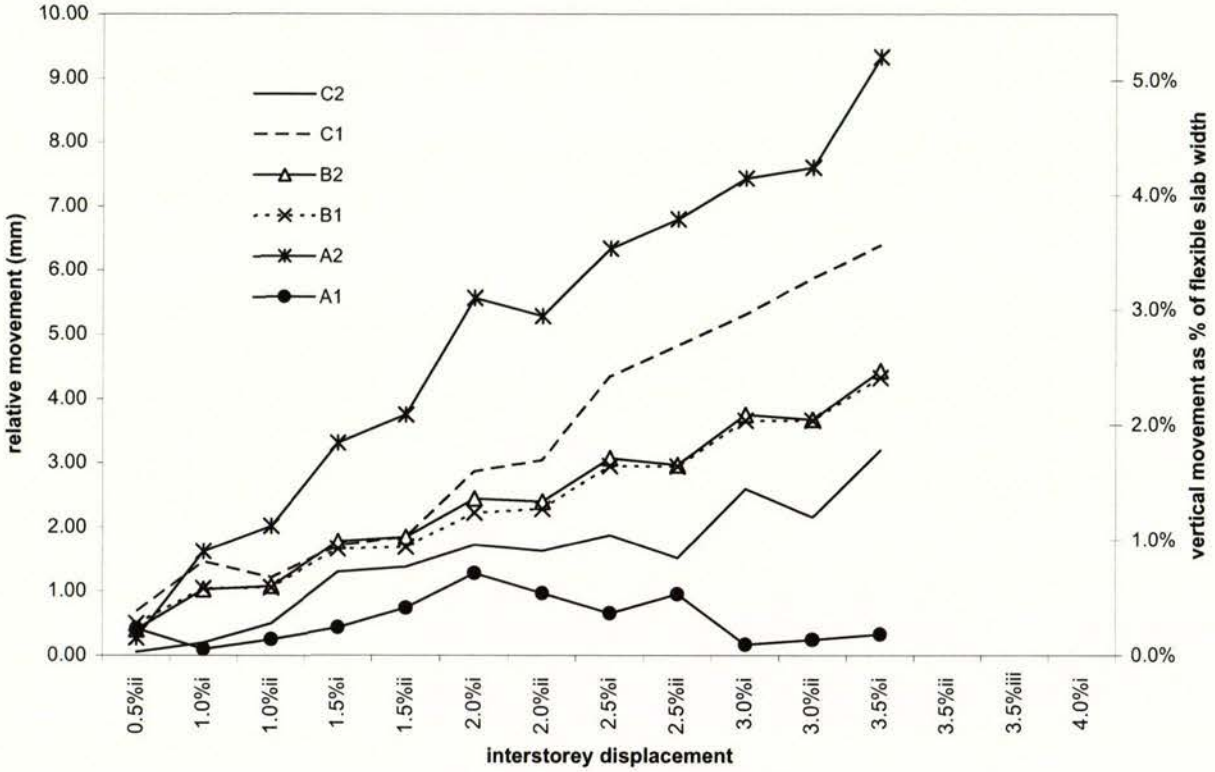

(c) Model C

Figures 7.37: Differential vertical movement of flexible floor slab in modified models in the positive direction of displacement. (concluded)

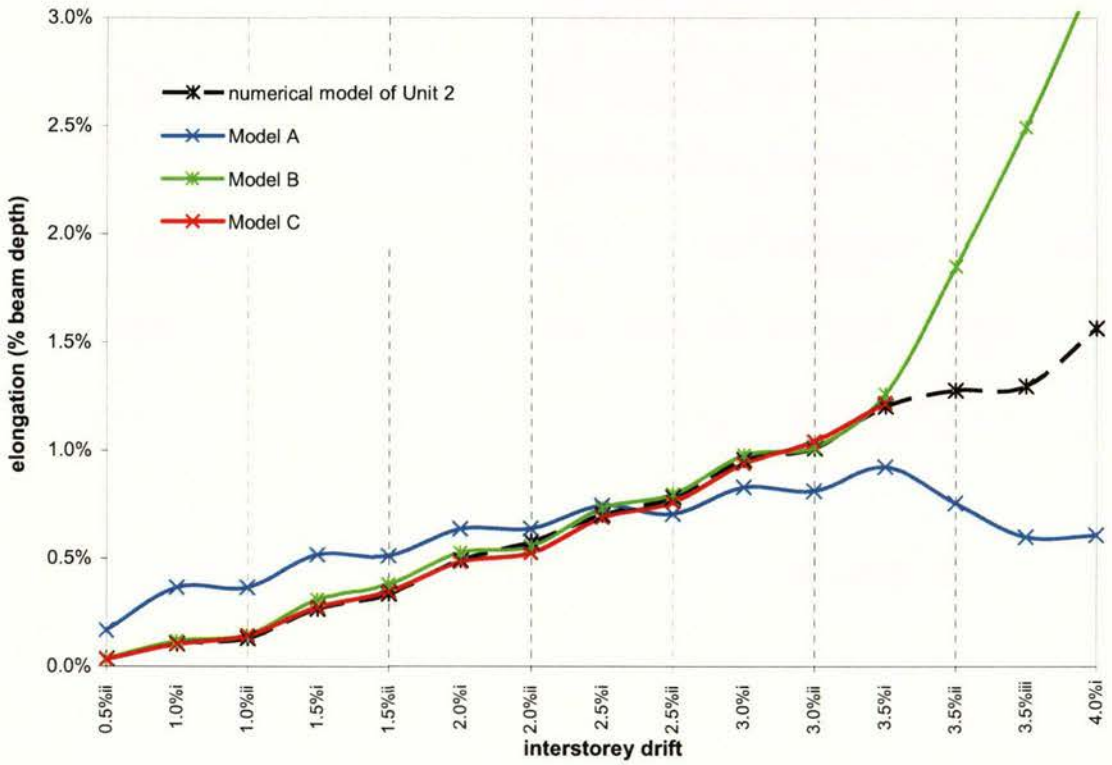

Figure 7.38: Elongation in modified models and numerical model of Unit 2.

Figure 7.38 compares the elongation of the modified models with the numerical model of Unit 2. In Model A, the elongation was higher than the model of Unit 2 up to 2.5% drift displacement, but was lesser thereafter. The rate of increase in elongation was lesser compared to the other models. The elongation in Model B matched well with the elongation of the numerical model of Unit 2. However, the elongation in Model B increased significantly from 3.5% interstorey drift after the flexible slab models in the cantilever extensions failed, releasing the restraint to beam elongation. This indicates that the majority of the restraint to elongation of the model was due to the forces transferred from the slab to the frame around the exterior joints (columns 'A' and 'C'). Model C failed during the second cycle to 3.5% drift displacement. Prior to this, the elongation recorded matched well with the numerical model.

7.5.3 Halving the strength of reinforcement between main beam in perimeter frame and floor slab

The numerical model of Unit 2 was modified by reducing the strength of the tension ties (reinforcement) connecting the perimeter frame to the floor slab by half. The strength and stiffness of the flexible slab model described in section 7.4.2 were recalculated. This modification represents halving the number of reinforcement crossing between the interface between the beam face and the floor slab.

The lateral force versus displacement response of the modified model is shown in Figure 7.39. As observed for the numerical model of unit 2, the modified model does not show a typical response of a reinforced concrete frame mainly due to the inability of the elongating hinge to accurately model degradation of stiffness.

The lateral force envelopes of the numerical model of Unit 2 and the modified model are shown by Figure 7.40. The peak lateral force was achieved at 2.0% drift displacement. The peak force was 229kN in the positive direction and 216kN in the negative direction. These equate to a decrease in peak lateral strength of 17% in the positive direction, and 19% in the negative direction. The modified model failed on the second cycle to 3.0% drift displacement. This was poor compared to the numerical model, where 4.0% drift displacement was achieved.

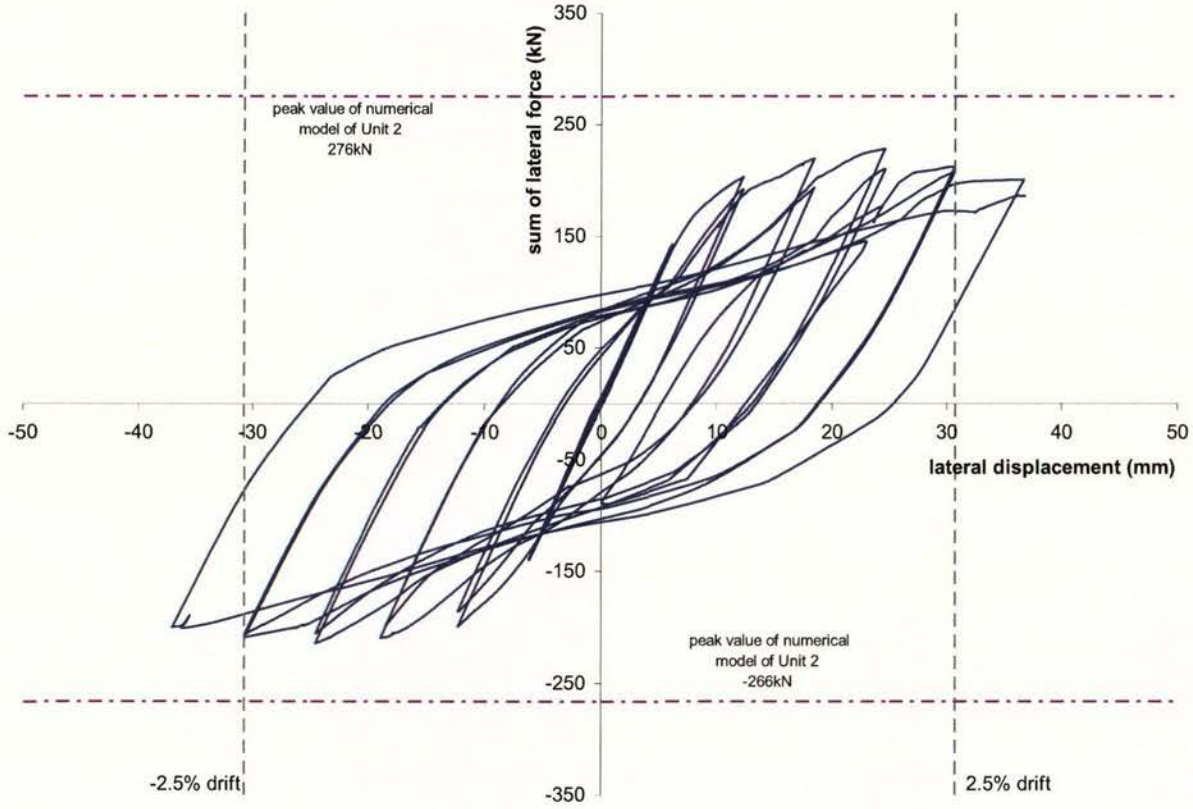

Figure 7.39: Lateral force versus displacement response of modified model.

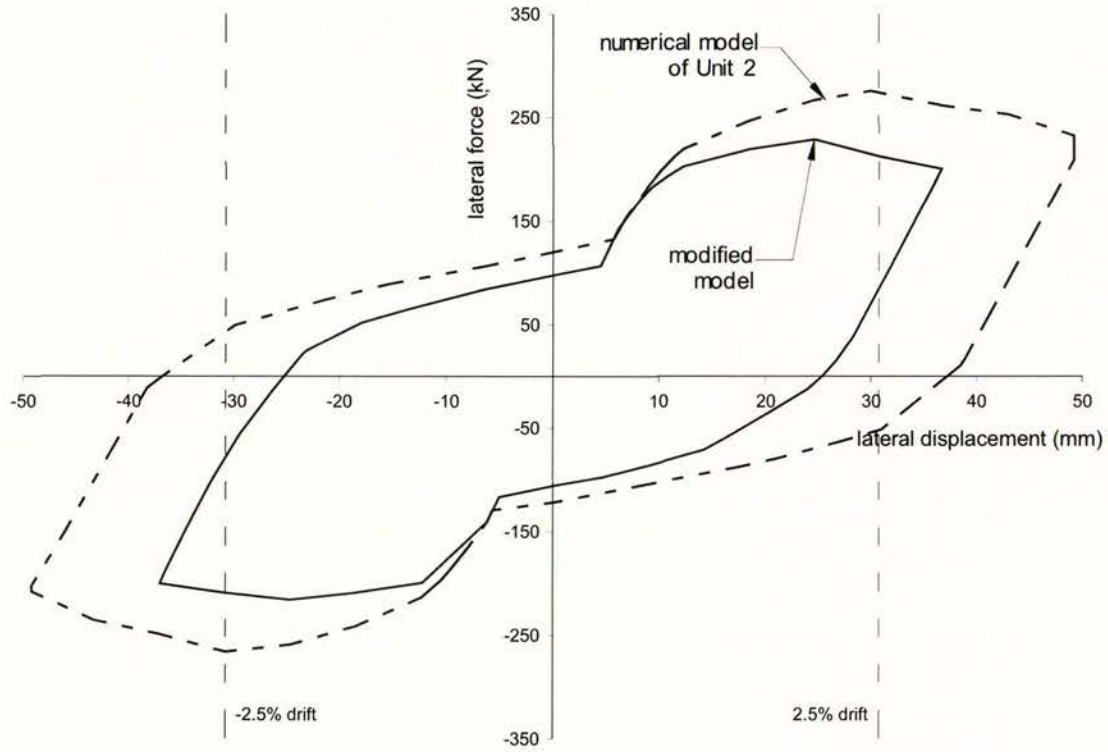

Figure 7.40: Lateral force versus displacement envelope of numerical model of Unit 2 and modified model.

The differential vertical movement of the floor slab relative to the beam is shown by Figures 7.41. The maximum vertical movement reached was 3.6% of the slab width. Compared to the numerical model of Unit 2, the vertical movement was 4.1% at the same displacement. In the negative direction, the maximum vertical movement was 3.6% of the flexible slab width, which was the same as the numerical model of Unit 2 at the same displacement. The noticeable difference to the numerical model of Unit 2 is how the vertical displacements at the inside of both the outer joints, 'C1' and 'A2' were similar (see Figure 7.28 for vertical movement of numerical model of Unit 2). In the numerical model of Unit 2, the magnitude of vertical movement of the slab to the inside of the outer joints changed with lateral direction of movement. In the positive drift direction, the movement at 'C1' was lesser to 'A2'. On reversal of drift direction, the vertical movement of 'C1' increased while 'A1' decreased. In the modified model, the vertical movement at 'C1' and 'A2' stayed at approximately the same level, regardless of the drift direction. The earlier failure of the model compared to the numerical model of Unit 2 was most likely due to this increase in vertical movement of the flexible slab.

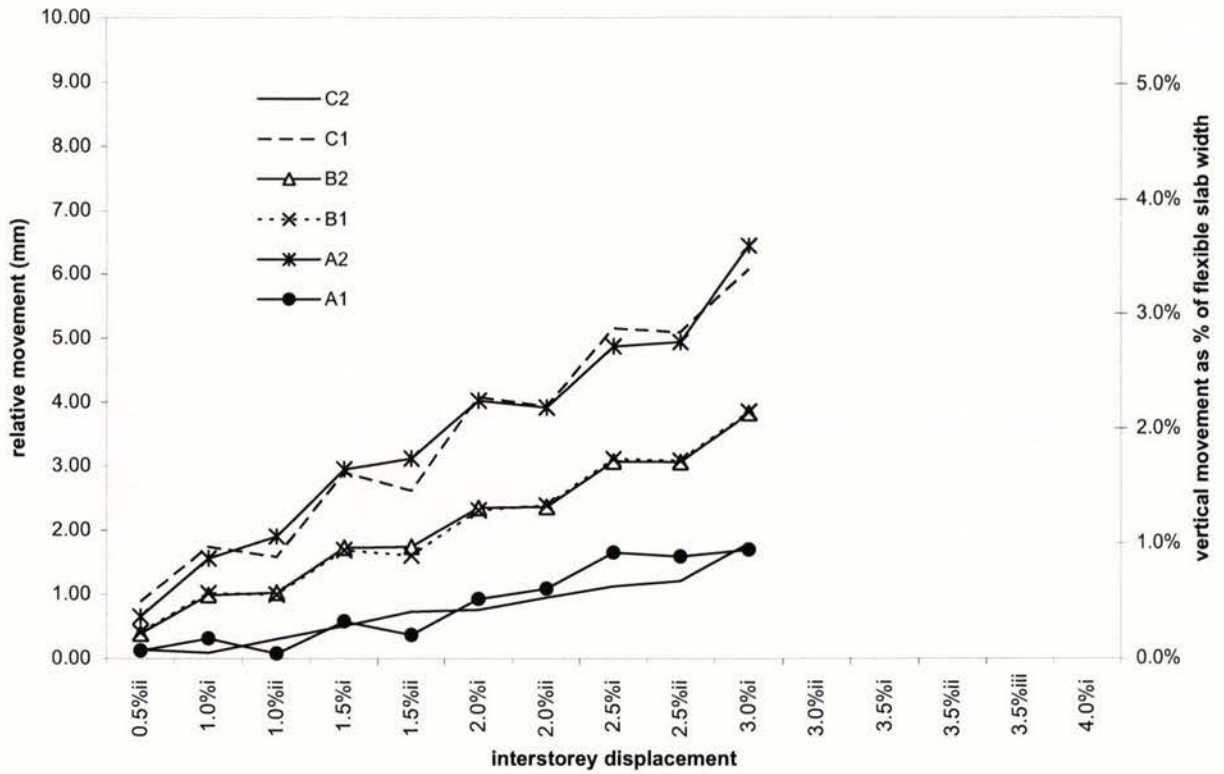

(a) Positive direction of displacement

Figure 7.41: Differential vertical movement of flexible floor slab in modified model. (continued)

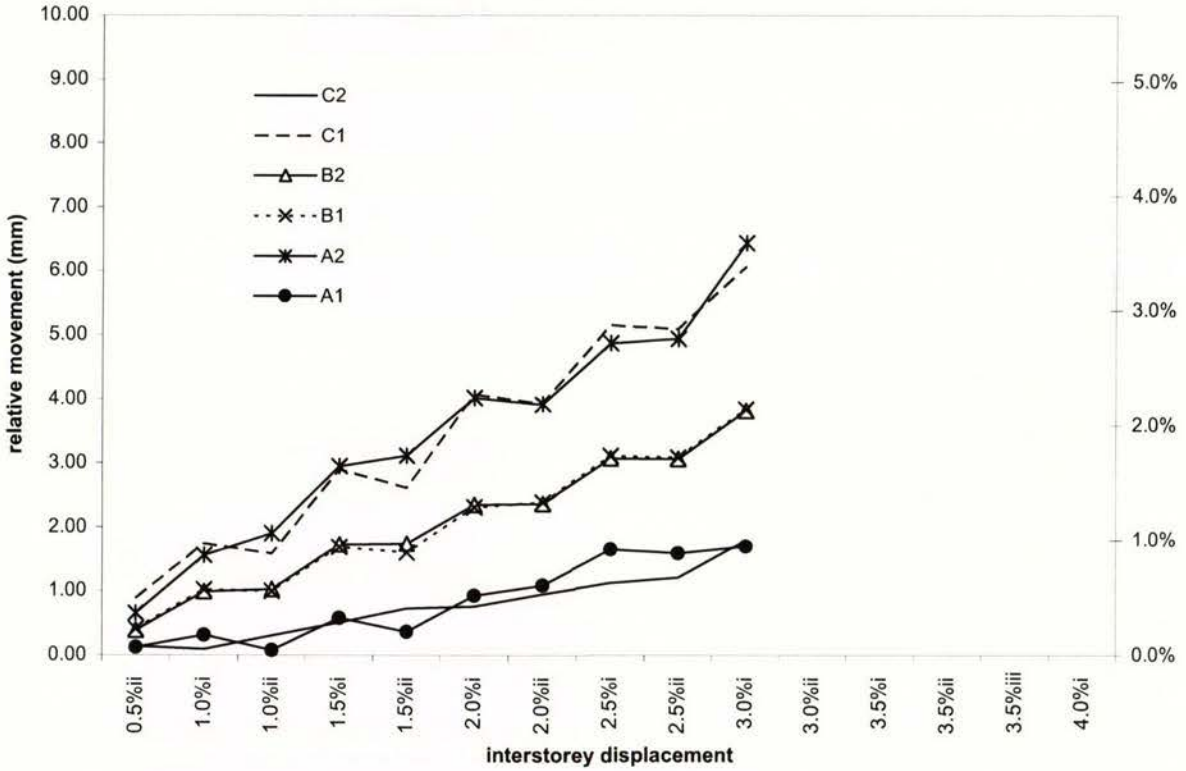

(b) Negative direction of displacement

Figure 7.41: Differential vertical movement of flexible floor slab in modified model. (concluded)

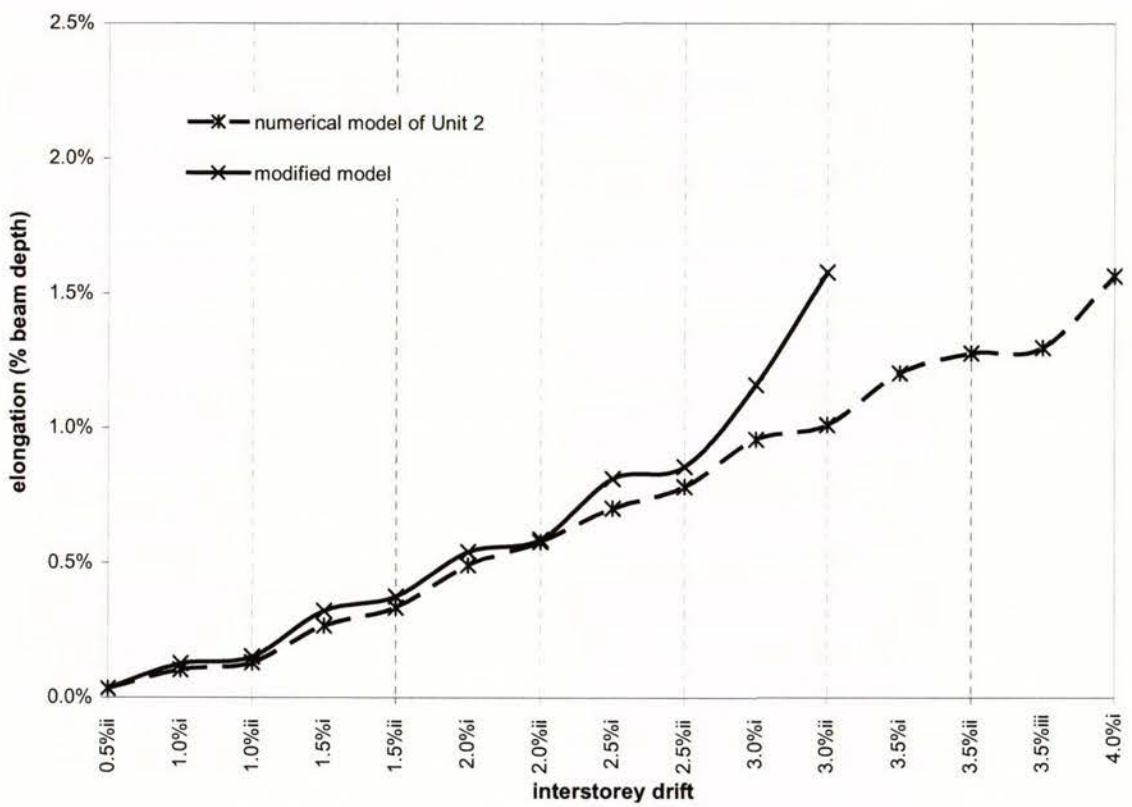

Figure 7.42: Average elongation in modified and numerical model of Unit 2.

Figure 7.42 compares the elongation of the numerical model and the modified model. The level of elongation of the modified model was similar to that of the numerical model up to 2.0% drift displacement. As the flexible slab members in the modified model started to fail (earlier than those in numerical model of Unit 2), the decrease in axial restraint to the beams resulted in the increase in elongation. Elongation was at 1.6% of the beam depth at 3.0% drift displacement before the model failed.

7.6 Two-bay Frame with Floor Slab Model

In this section, a two-bay frame was created using the same members and flexible slab model developed for the numerical model of Unit 2 (see Section 7.4). The purpose was to investigate the possible behaviour of this structural configuration.

7.6.1 Description of model

A two-bay frame, with floor spanning along the frame bays was modelled. The member sizes and properties, plastic hinge and diagonal slab models were the same as the numerical model of Unit 2 described in section. However, the floor slab now spans the entire distance, between the transverse beams connected to the outer columns. The columns were spaced at 2.032m apart. The model is shown in Figure 7.43.

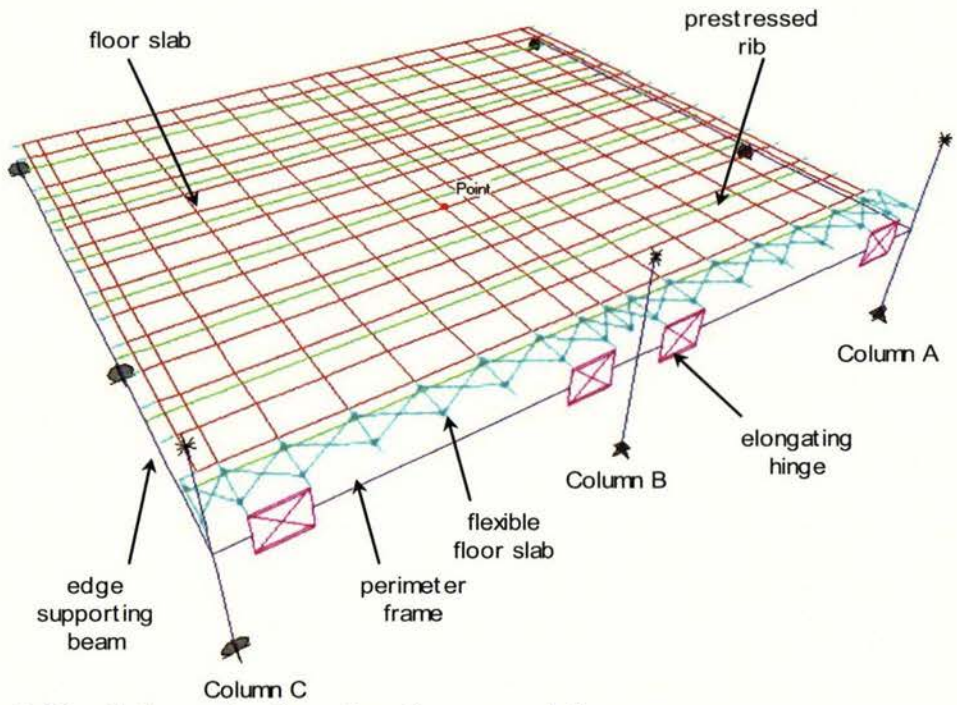

Figure 7.43: Schematic of two bay frame model.

7.6.2 Results of analysis of two-bay frame model

The model was subjected to two cycles at each lateral drift step of 0.5%, up to 3.0% interstorey drift. The analysis ended on the second cycle in the negative direction of displacement to 4.0% drift when the analysis failed to continue.

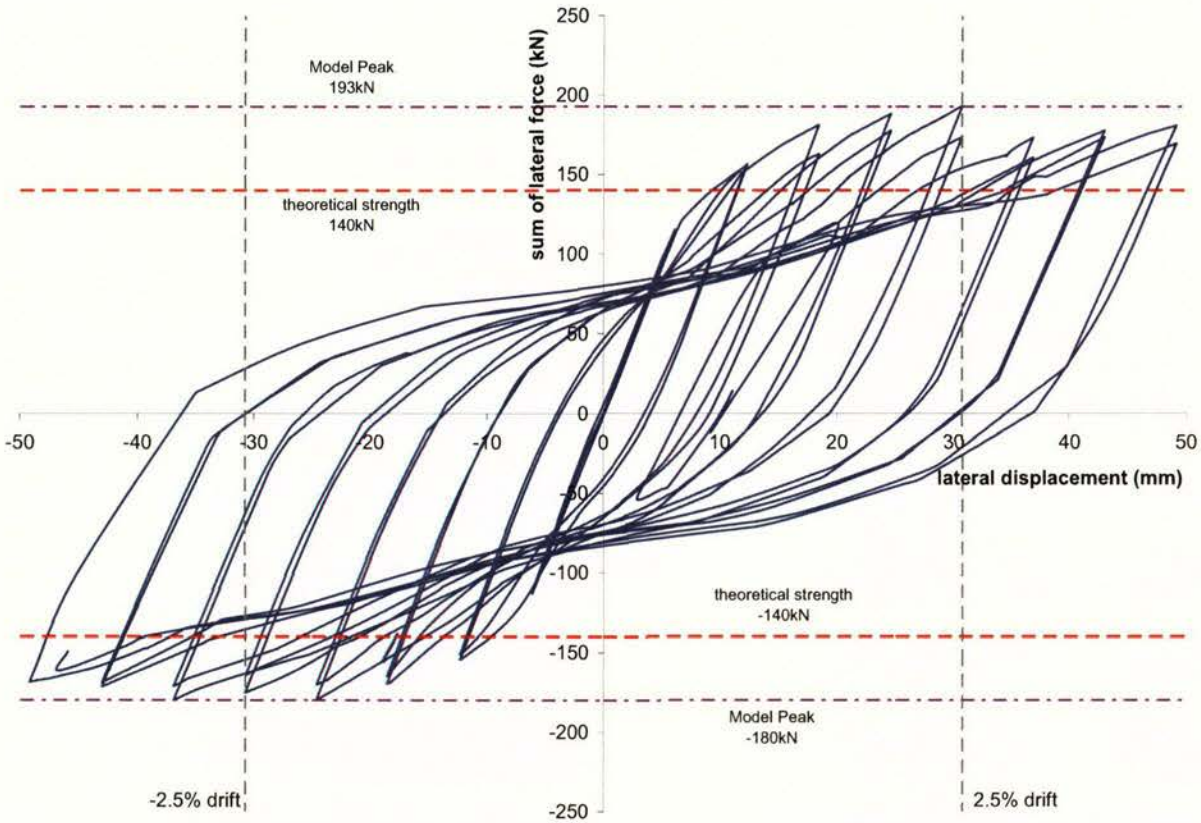

Figure 7.44: Lateral force versus displacement response of two-bay frame model.

The lateral force versus lateral displacement plot is shown by Figure 7.44. The theoretical strength shown in the figure was calculated by including the longitudinal reinforcement effectively anchored within effective slab width for beam strength in negative bending, as recommended in the New Zealand Concrete Structures Standard [S2]. In addition to this, the strands within the first prestressed rib within the effective slab width were included for calculation of the beam strength. The tension force acting at mid-height of the slab is eccentric to the prestressed section. In calculating the strength of the prestressed rib, allowance must also be made for the bending moments due to gravity loads (using same approach described in *Chapter 5*, section 5.4, with corresponding worked example in *Appendix 1*, A1.6). Assuming that the compression strength of the rib concrete is 50MPa, and the prestressing strands (56mm^2 each) were

initially stressed to 980MPa, an ultimate strength analysis indicates that a rib can resist an eccentric force of 81kN at the beam section adjacent to the centre column. Adding to this the 68kN sustained by the passive reinforcement within the effective slab width gives a tension force capacity of 149kN. Using this approach, the beam strength at the column faces could be calculated, and the interpolated joint strength at Columns A, B and C was 34.7kNm, 101.1kNm and 36.8kNm respectively. From these values, the lateral strength of the structure was 140kN.

The peak lateral strength of the numerical model was 193kN in the positive and 180kN in the negative direction. The strength estimated by the model was 38% greater than the calculated strength in the positive direction and 28% greater in the negative direction. This is a significant difference in peak strength assuming that the predicted strength by the model is close to the strength that may be in an actual structure.

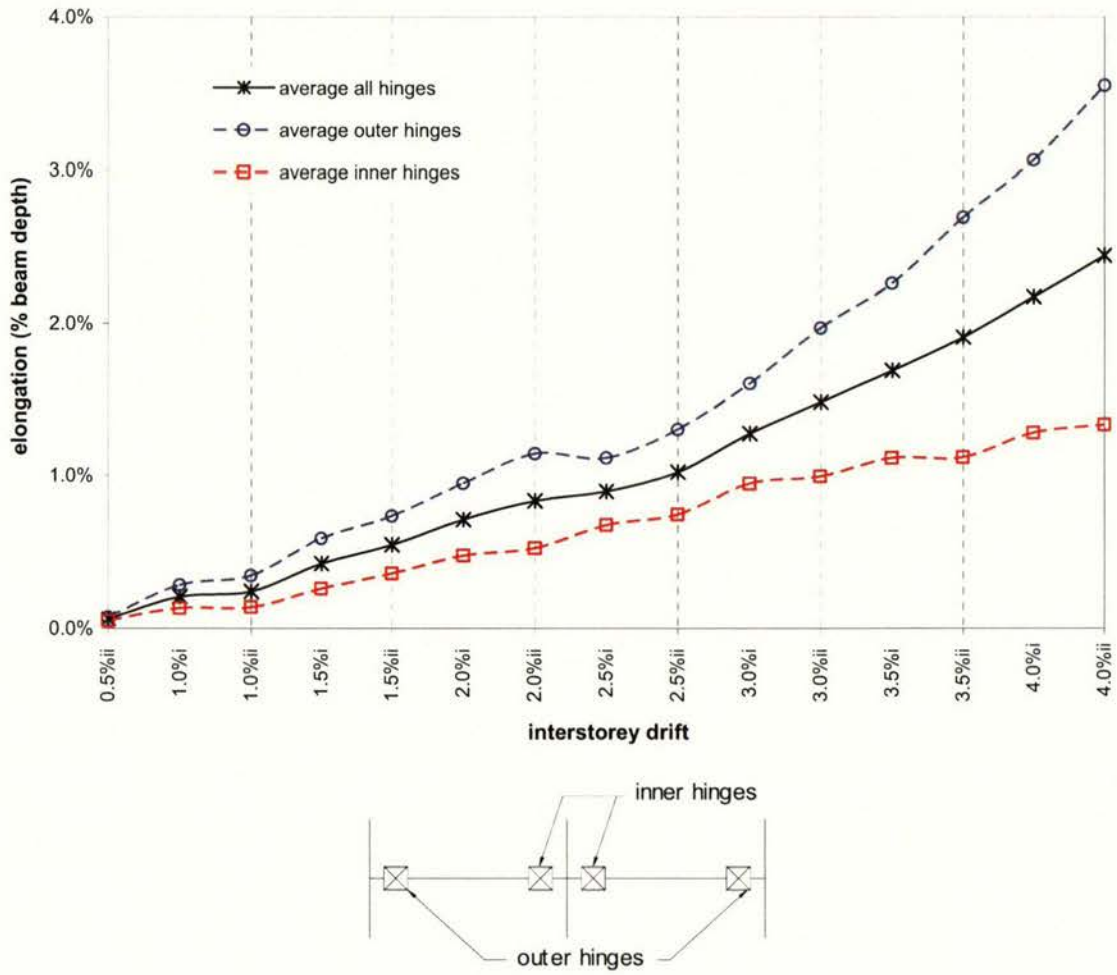

Figure 7.45: Elongation of beams in two-bay frame model.

The elongation in the beams is shown in Figure 7.45. The average elongation rose steadily to 1.0% of beam depth at 2.5% drift displacement, up to 2.4% of beam depth at 4.0% drift displacement. The average elongation was greater than the numerical model of Unit 2, where at 4.0% drift displacement, the average elongation was 1.6% of beam depth. This was due to the lower axial loads sustained by the beam at the outer columns of the two-bay frame, compared to the outer columns of the model of Unit 2 where the floor spanned past the outer columns. This is shown by Figure 7.45 where the average elongation in the hinges adjacent to the outer columns was significantly higher than those recorded for those adjacent to the central joint. At 4.0% interstorey drift, the average elongation was 3.6% of beam depth for the outer hinges while for the inner hinges the average elongation was 1.3% of beam depth.

The vertical differential movement of the floor slab relative to the perimeter frame is shown in Figures 7.46. The locations of the points where the movement measurements were taken are shown by Figure 7.47. As expected, the relative vertical movement the next to the central joint was greater than those recorded for the outer joints. The magnitude and pattern of vertical movement of the central joint was similar to the outer joints of the numerical model of Unit 2 (see Figure 7.28). Significant damage was sustained in the region around the outer joints in the experimental unit. Therefore, it can be expected that the region around the central joint of two-bay frame where the floor span past the joint is most susceptible to damage.

The ratio of bending moment input to the centre-line of the individual columns and the total bending moment input of the two-bay frame and the numerical model of Unit 2 are compared in Figures 7.48. This figure highlights the difference in the source of lateral resistance of perimeter frames with different configurations. In the model of Unit 2, the average moment input of the outer joints were similar to the moment input to the central joint up to 2.5% interstorey drift. Following from this, as the floor slab started to fail around the outer columns (see earlier in section 7.4.3), the moment input to the outer joints decreased relative to the central joint. For the 2-bay frame, it can be seen that the resistance of the central joint was approximately 3 times the resistance of the outer joints. It is clear that the restraint to elongation of the beams by the floor slab causes at

significant increase in the lateral resistance provided by the central joint, while the restraint to the outer joints was significantly lesser.

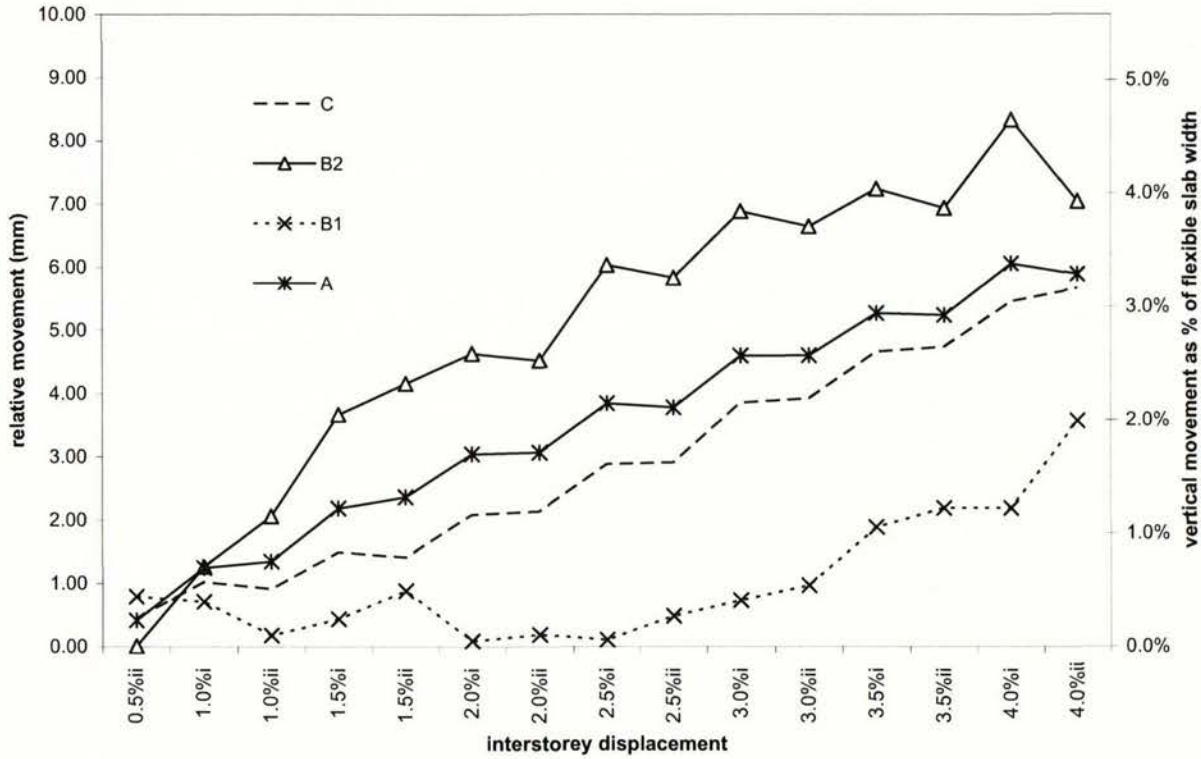

(a) In positive direction

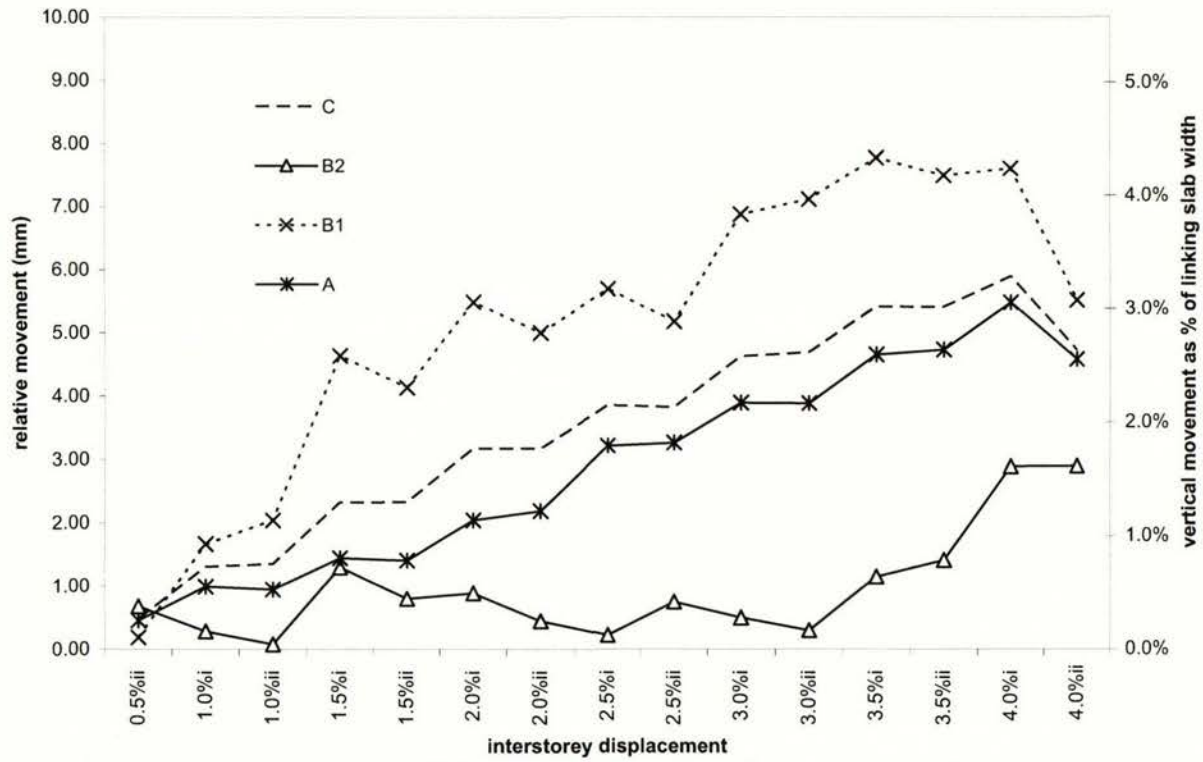

(b) In negative direction

Figures 7.46: Relative vertical displacement of flexible floor slab at cycle peaks.

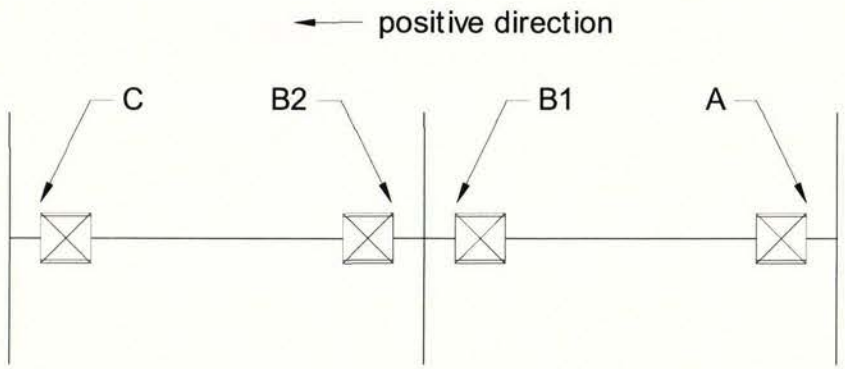

Figure 7.47: Location of points of vertical differential movement.

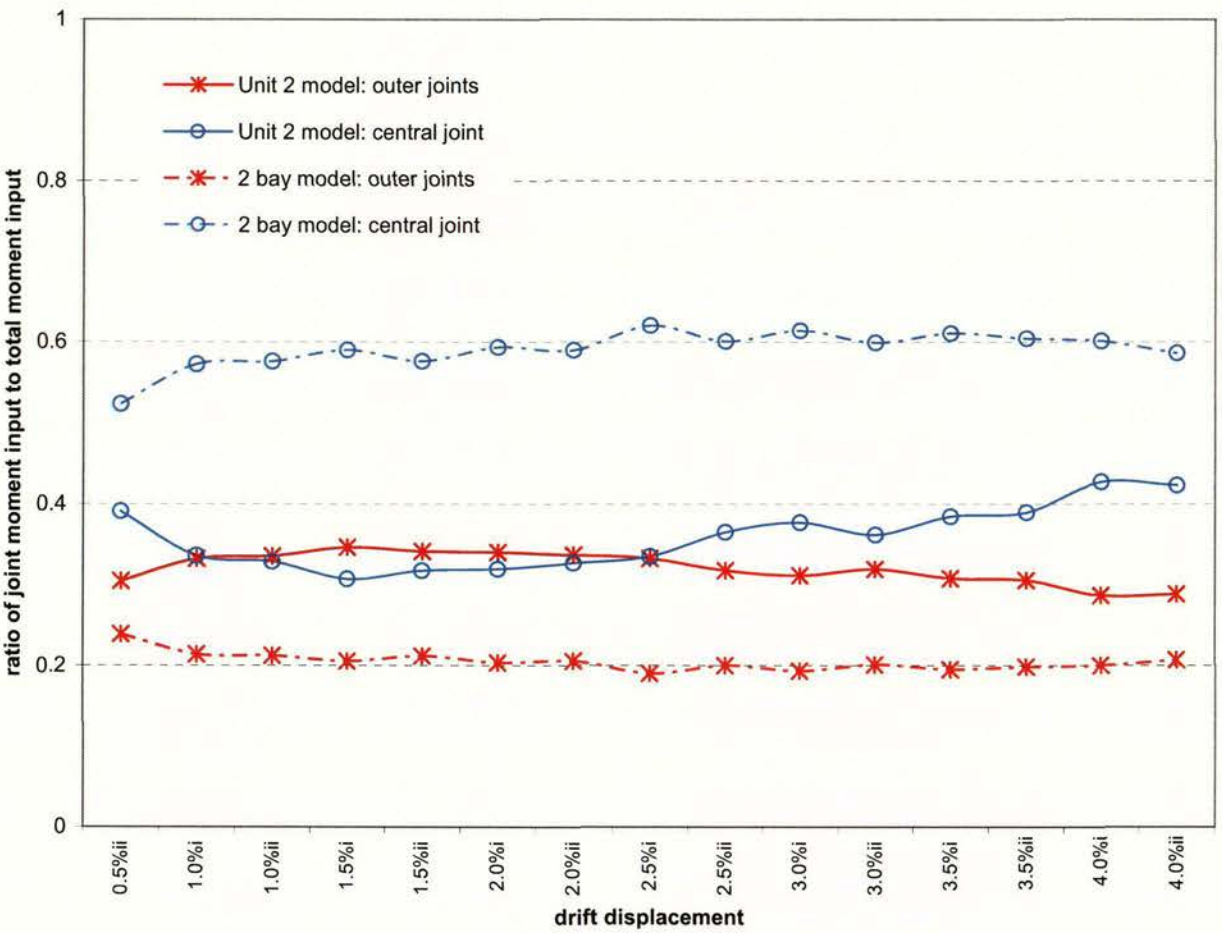

Figure 7.48: Comparison of moment input to beam-column joints of numerical model of Unit 2 and 2-bay model.

7.6.3 Halving the strength of reinforcement between the frame and the floor slab of the two-bay frame model

The two-bay frame model was modified by reducing the strength of the reinforcement connecting the perimeter frame to the floor slab by half. This modification represents

halving the number of reinforcement crossing between the interface between the beam face and the floor slab. The lateral force versus displacement envelope of the two-bay frame model and the modified model is shown in Figure 7.49.

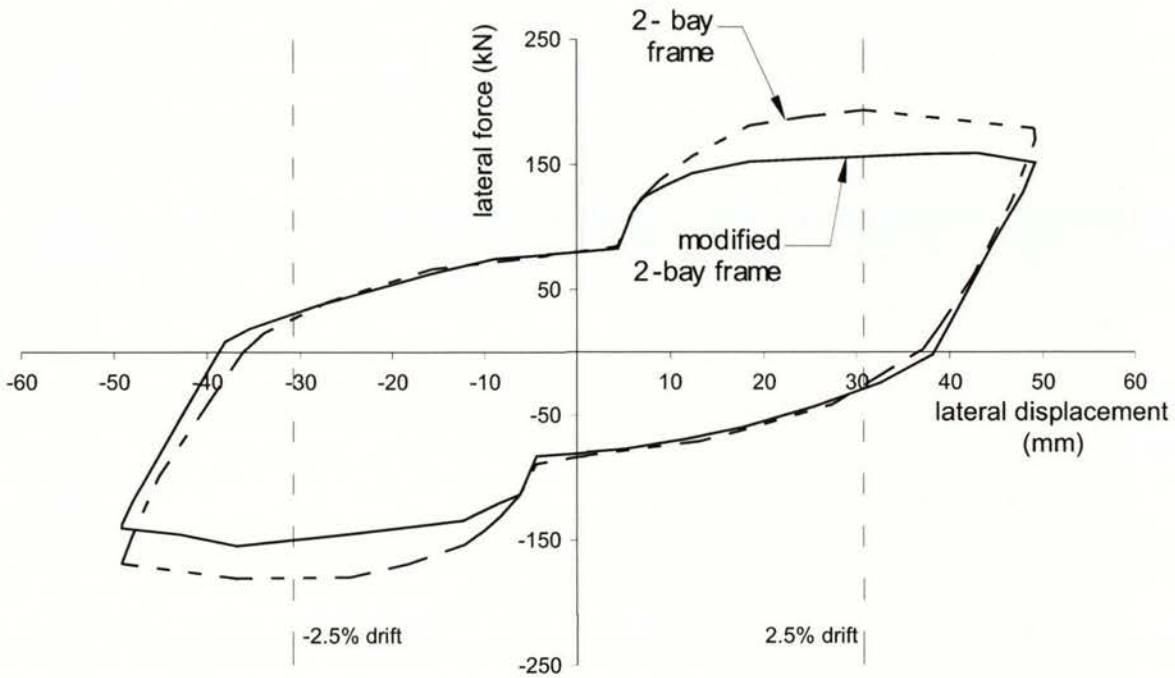

Figure 7.49: Lateral force versus displacement response of modified model.

The peak lateral force was 159kN in the positive direction at 3.5% drift displacement and peaked at 155kN in the negative direction at 3.0% drift displacement. These equate to a decrease in peak lateral strength of 18% in the positive direction, and 14% in the negative direction.

The differential vertical movement of the floor slab relative to the beam is shown by Figures 7.50. The maximum vertical movement reached was 3.9% of the slab width which occurred adjacent to the central joint, B2. Compared to the two-bay frame model, the vertical movement was 4.6% at the same displacement (see Figure 7.46(a)). The vertical movement on the other side of the central joint, B1, increased in comparison to the two-bay frame model. Therefore the change in the vertical movement between one side of the joint to the other was lesser in the modified model than the two-bay frame model. The movement at the outer joints, A and C, remained at about the same levels in comparison with the two-bay frame model.

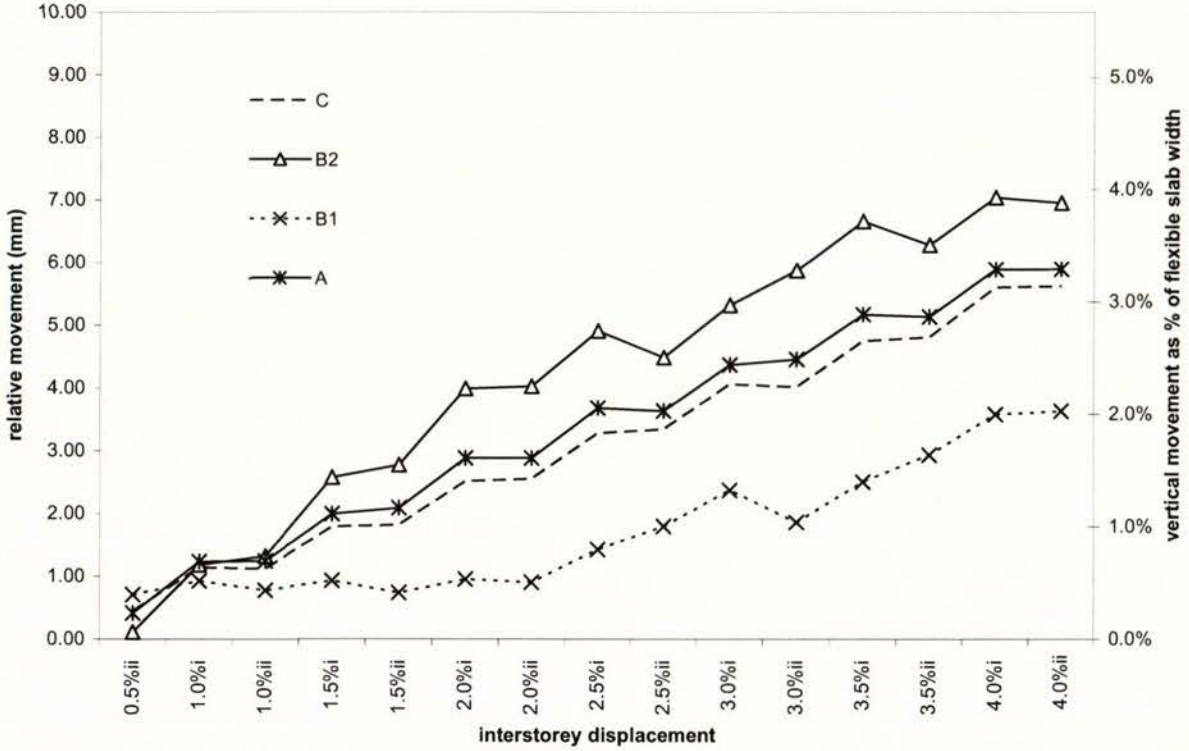

Figure 7.50: Differential vertical movement of flexible floor slab in modified model of two-bay frame in the positive direction.

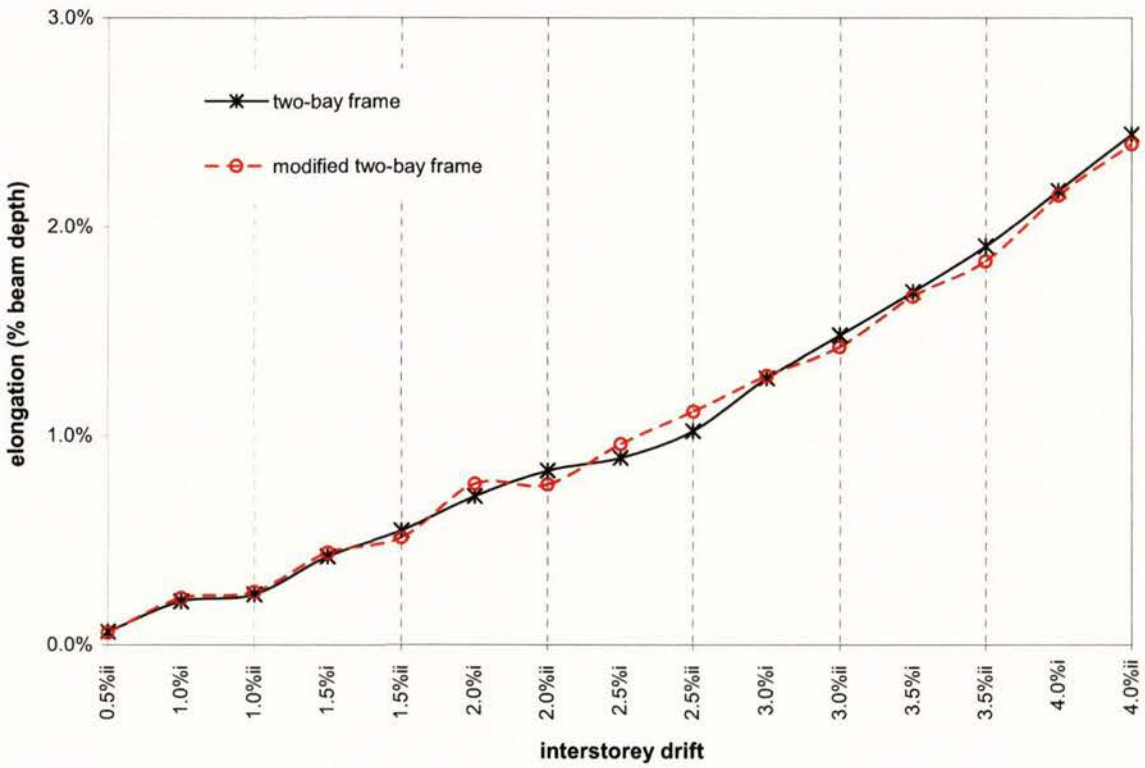

Figure 7.51: Average elongation of two-bay frame model and modified model.

Figure 7.51 compares the elongation of the two-bay frame model and the modified model. Halving the strength of the slab to frame connections did not have effect on the magnitude of the average elongation of the model.

Chapter 8

Summary and Discussion

8.1 Introduction

The increase in lateral strength of the frame and floor slab unit, Unit 2, is compared with Units 1 and 3. The mechanisms of strength increase are investigated. The initial stiffness and elongation characteristics of the three units are compared. The axial forces resisted by the joints of the numerical model of Unit 2 are compared with the corresponding values from the test unit, Unit 2.

8.2 Comparison of Results from Experimental Work

8.2.1 Lateral force resistance

The lateral force resistance of the three experimental units, in terms of the sum of the lateral force applied at the top of the columns at nominal interstorey drift levels are compared in Figures 8.1. The first frame unit, Unit 1, was subjected to load-displacement sequences dissimilar to the latter two units (see *Chapter 3*). Therefore, for Unit 1, the lateral forces indicated in Figures 8.1 were taken from the point at which the nominated interstorey drift level was first reached, while for Units 2 and 3 the values indicated are at peak of the drift displacement cycles. The information plotted on Figure 8.1(b) for Unit 1 is only up to 2.5% drift, as this unit was not displaced any further than 2.9% drift in the negative direction (see *Chapter 4, Section 4.2*). The first and second column of the charts show the sum of the lateral forces applied to the columns in Units 1 and 3 respectively, while the corresponding value for Unit 2 is shown by the fourth column. In Units 1 and 3 only four plastic hinges could develop under cyclic loading. However in Unit 2, which had the floor slab acting compositely with the beams in the perimeter frame, the flexural stiffness of the transverse beams combined with floor slab enabled two additional plastic hinges to form, giving a 50% increase in the number of plastic hinges (see test unit details in *Chapter 3*, section 3.3). For this reason, the third column in Figures 8.1 shows the average lateral strength of

Units 1 and 3 increased by 50% to enable comparison to be made with Unit 2. In practise this would vary with the level of drift displacement, but an increase of 50% was chosen for comparative purposes.

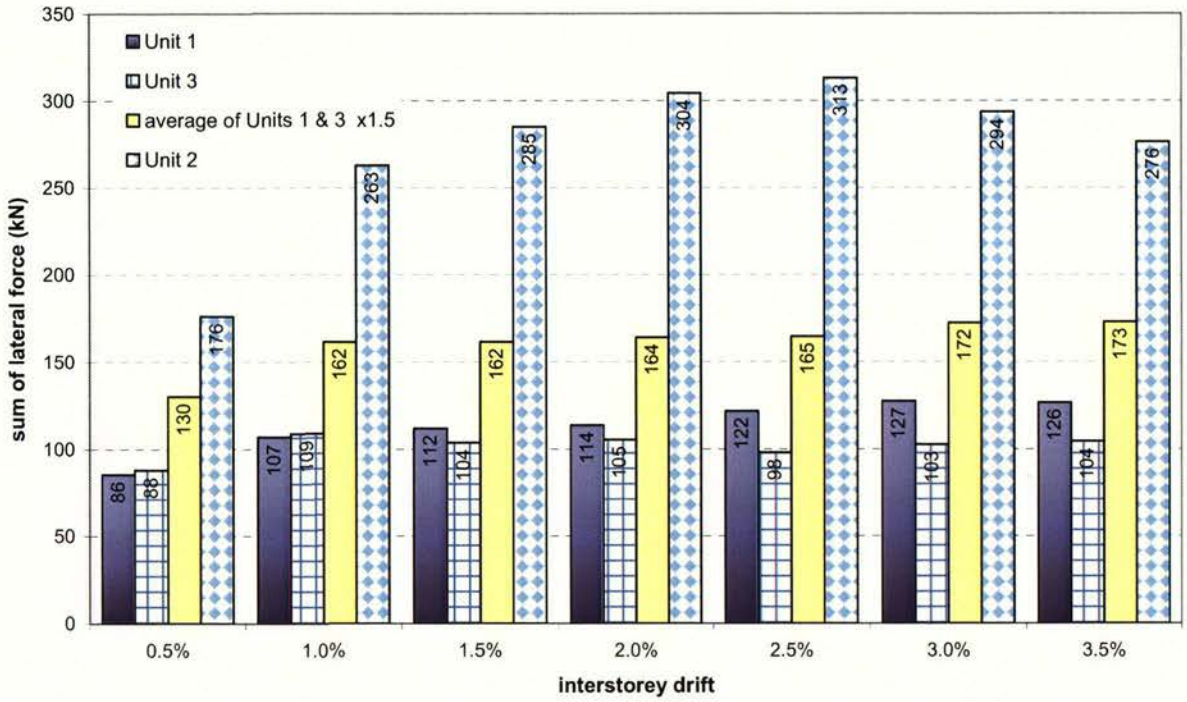

(a) Lateral displacement in positive direction

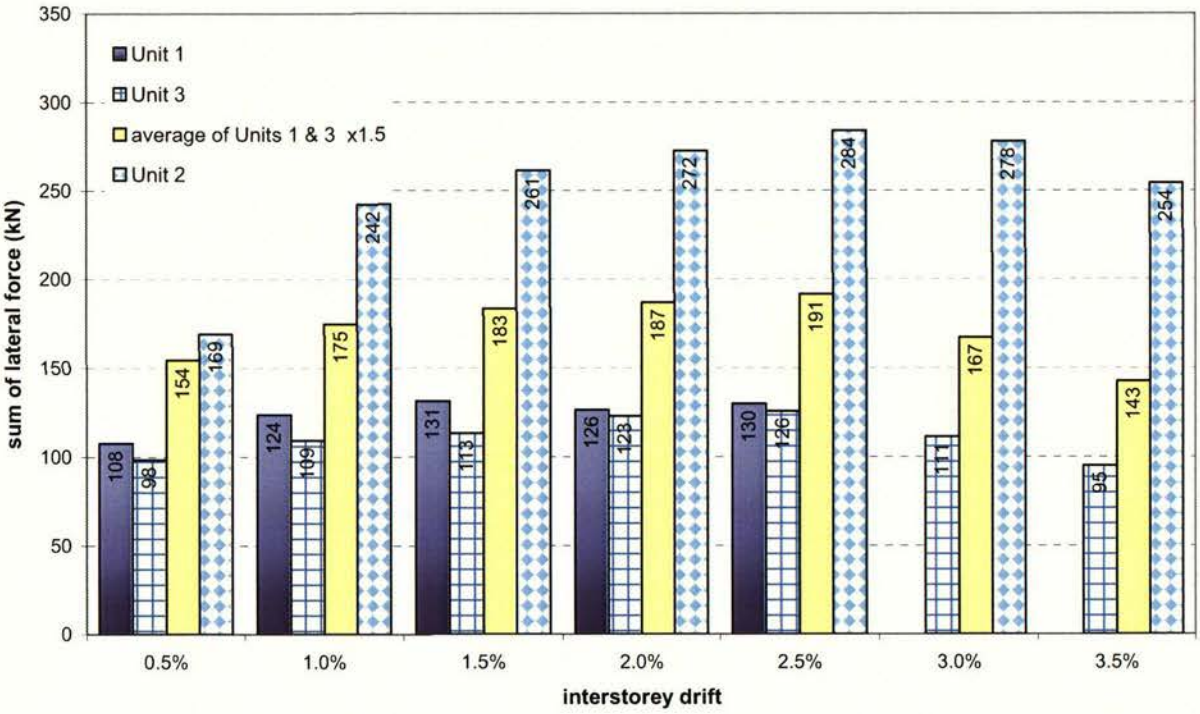

(b) Lateral displacement in negative direction

Figures 8.1: Lateral force resisted by experimental units at peak displacements.

It can be seen from Figure 8.1 that the addition of the slab had a significant influence on the lateral force sustained particularly above 1.0% lateral drift displacement. In the positive direction of displacement, the peak lateral forces of Unit 2 varied from 2.3 to 2.7 times the value of Unit 1 and 2.4 to 3.2 times the corresponding values of Unit 3. In the negative direction of displacement, between interstorey drift levels of 1.0% to 3.0%, the lateral forces in Unit 2 was 1.9 to 2.2 times the value of Unit 1. In the same range, the strength in Unit 2 was 2.2 to 2.3 times the value of Unit 3. Even when allowing for 50% increase in the average lateral force resisted by Units 1 and 3, the lateral force resisted by Unit 2 was 1.8 times greater in the positive direction and 1.5 times greater in the negative direction. The difference in lateral strength reduced a little in the cycles to 3.5% interstorey drift, as the influence of the floor slab on the strength of frame decreased due to damage sustained at the interface of the slab and the beams in Unit 2. However, the strength of Unit 2 was still on average 70% higher than that of the frame only units.

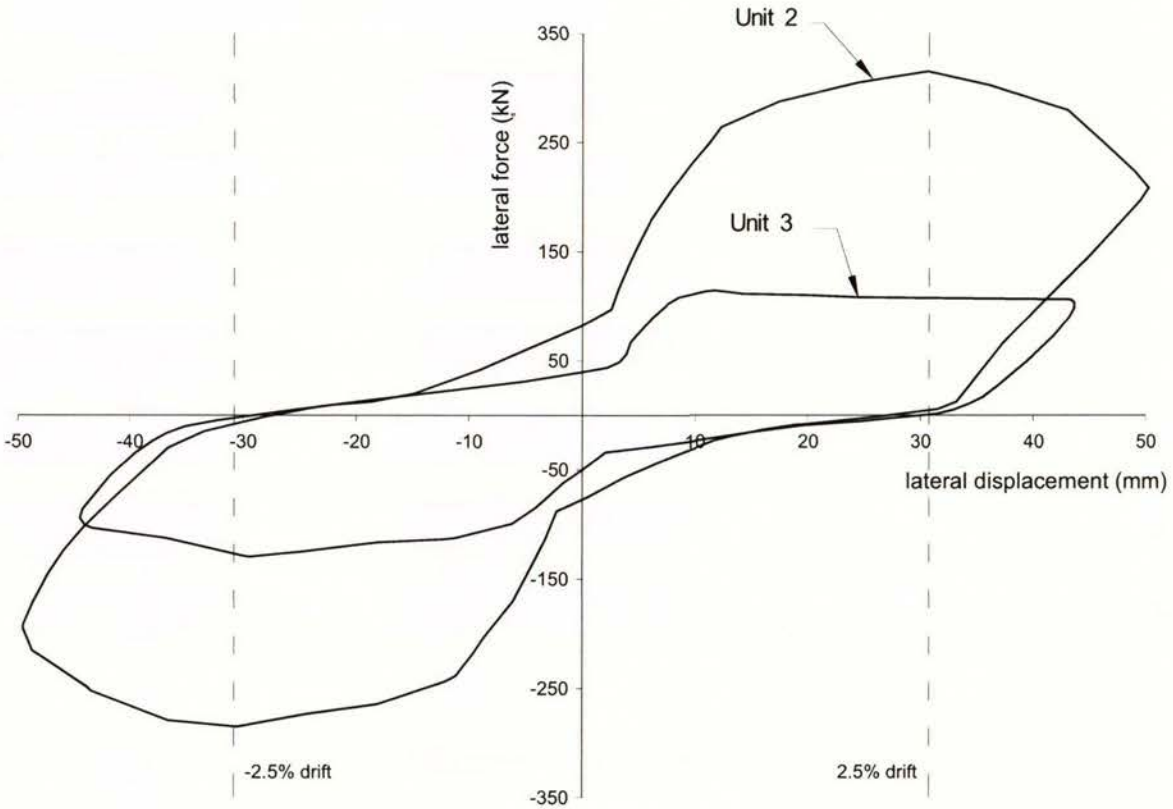

Figure 8.2: Lateral force versus displacement envelope of Units 2 and 3.

The lateral force versus displacement envelopes of Units 2 and 3 are compared in Figure 8.2. This plot shows a significant increase in the lateral force resistance of Unit 2 in

comparison to Unit 3. The peak lateral force values of Unit 3 were steady at approximately 1.0% interstorey drift onwards in the positive direction, while in comparison the lateral force resisted by Unit 2 continued to increase steadily up to a peak value of 313kN at 2.5% drift before decreasing in strength.

A comparison of the bending moment applied to the centre-line of the beam-column joints of Units 2 and 3 is shown by Figure 8.3. The plot shows the obvious increase in the flexural strength of Unit 2 coinciding with the increase in displacement in the inelastic range (0.5% interstorey drift onwards), which activated the influence of the floor slab on the lateral force performance of the frame. The largest difference in the moments applied to the joints of Units 2 and 3 was a factor of 3.3 for joint 'A', 3.1 for joint 'B' and 3.8 for joint 'C'. When the two extra hinges formed in the cantilever extensions of Unit 2 are allowed for, the factors are reduced to 1.7 for joint 'A', 3.1 for joint 'B' and 1.9 for joint 'C'. The increase in bending moment resisted by Unit 2 is discussed in a later section, section 8.3.

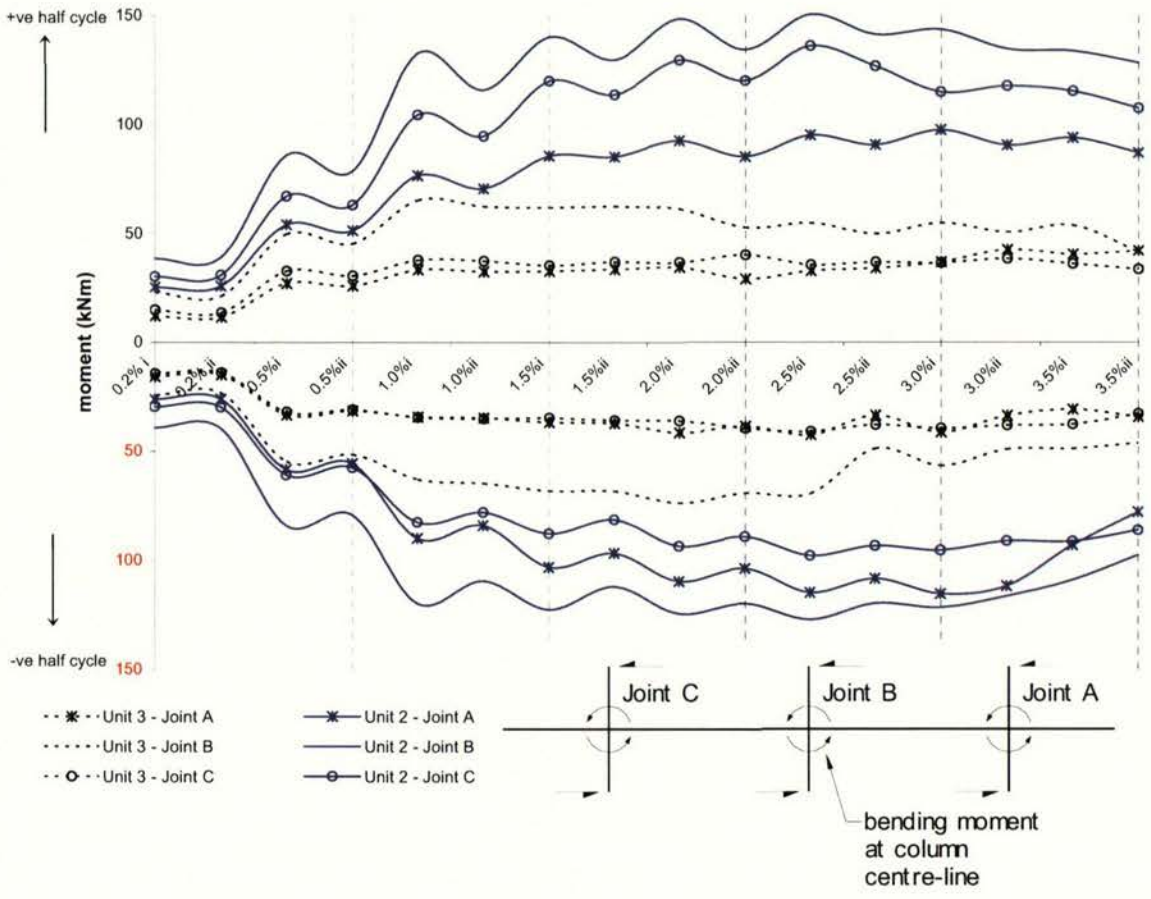

Figure 8.3: Bending moment input to beam-column joints of Units 2 and 3.

8.2.2 Elongation of beams

Beam elongation measured in the experiments is shown in Figure 8.4. The values shown are for average beam elongation due to four plastic hinges formed in the beam bays between the centre and the outer columns of the experimental units. The average elongation of the cantilever extensions of Unit 2 is also shown. The elongation values are expressed as a percentage of the beam depth (300mm). The maximum elongation of 3.3% of beam depth for Unit 1, 3.1% of beam depth for Unit 2, reached at 4.0% interstorey drift. For Unit 3, the maximum value was 2.8% at 3.5% drift. At 3.0% interstorey drift (approximately displacement ductility six), the average elongation for Unit 1 and Unit 3 was 2.5% and 2.4% respectively, while for Unit 2 was significantly lower at 1.3% of beam depth. Clearly the floor slab partially restrained the beam elongation in Unit 2. As indicated by the figure, the elongation in Unit 2 increased from 3.0% interstorey drift onwards, as loss of stiffness and vertical differential movement of the floor slab caused damage at the beam and floor slab interface where the floor had partially restrained the beam from elongating in the previous cycles.

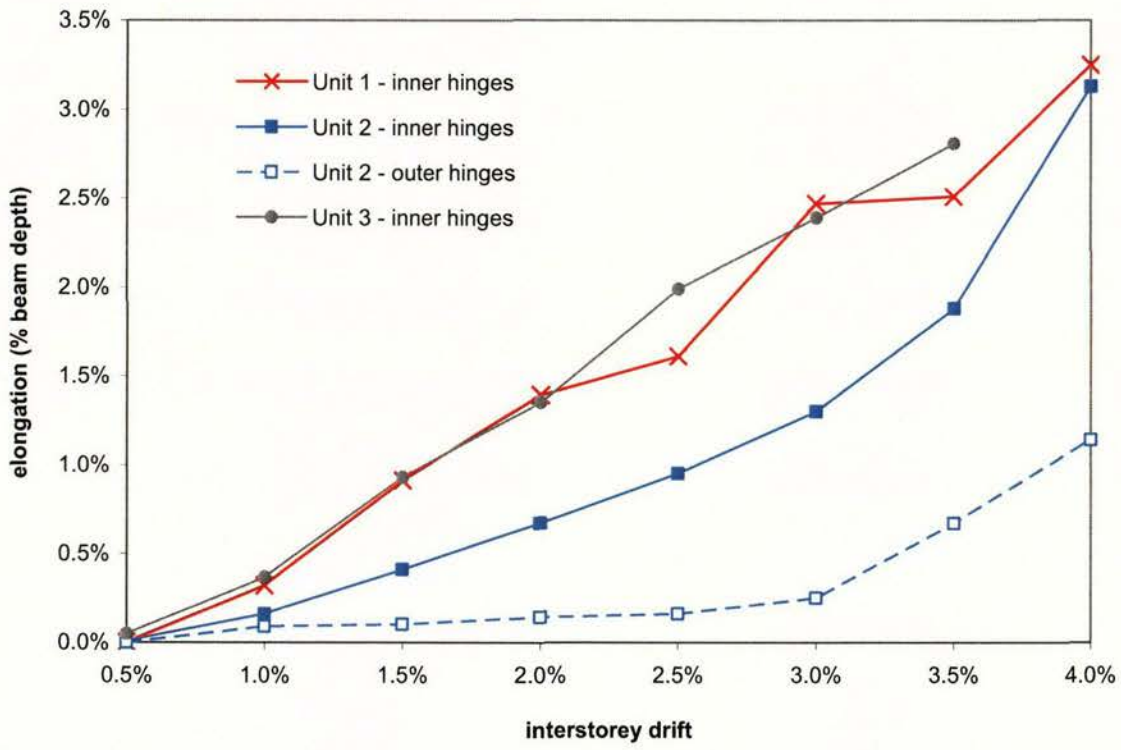

Figure 8.4: Comparison of elongation of beams in experimental units.

Elongation at 1.3% of beam depth per plastic hinge at 3.0% interstorey drift could still be significant when designing for seating widths of floor slabs, particularly when the slabs span past a number of perimeter frame beams. For typical example, a 900mm deep beam and a floor slab unit spanning across three beam bays, up to 70mm of beam elongation could be expected.

8.2.3 Initial lateral stiffness

The force versus displacement response of Unit 1 in the elastic range is shown by Figure 8.5. The theoretical lateral strength of Unit 1 was 105.4kN, calculated based on material tests and an assumed compression stress block as defined in the New Zealand Concrete Structures Standard (see *Chapter 3*). The average extrapolated displacement at 85% of the theoretical value (89.6kN) is 6.4mm, or an equivalent of 0.63% interstorey drift. This gives an initial stiffness of 14.0kN/mm. On closer inspection of the plot, it is apparent that there is 1mm of movement at low lateral force level at the change-over of loading direction. This was attributed to slack in the pins at the base of the columns. Allowing for movement at the supports, the extrapolated displacement was revised to an average value of 5.7mm (0.56% interstorey drift). This corresponds to an initial stiffness of 15.7kN/mm.

The force versus displacement of Unit 3 is shown in Figure 8.6. A best fit line was plotted and extrapolated to 88.1kN which is 85% of the theoretical lateral strength of 103.6kN (see *Chapter 3*). The initial stiffness is 15.7kN/mm, which coincidently is equal to the adjusted stiffness of Unit 1.

The initial stiffnesses of Units 1 and 3 are compared with Unit 2 in Figure 8.7. A best fit line was plotted for displacements up to 0.5% interstorey drift for Unit 2. The initial stiffness of Unit 2 is 27.0kN/mm. This represents a 72% increase in stiffness due to the addition of the floor slab.

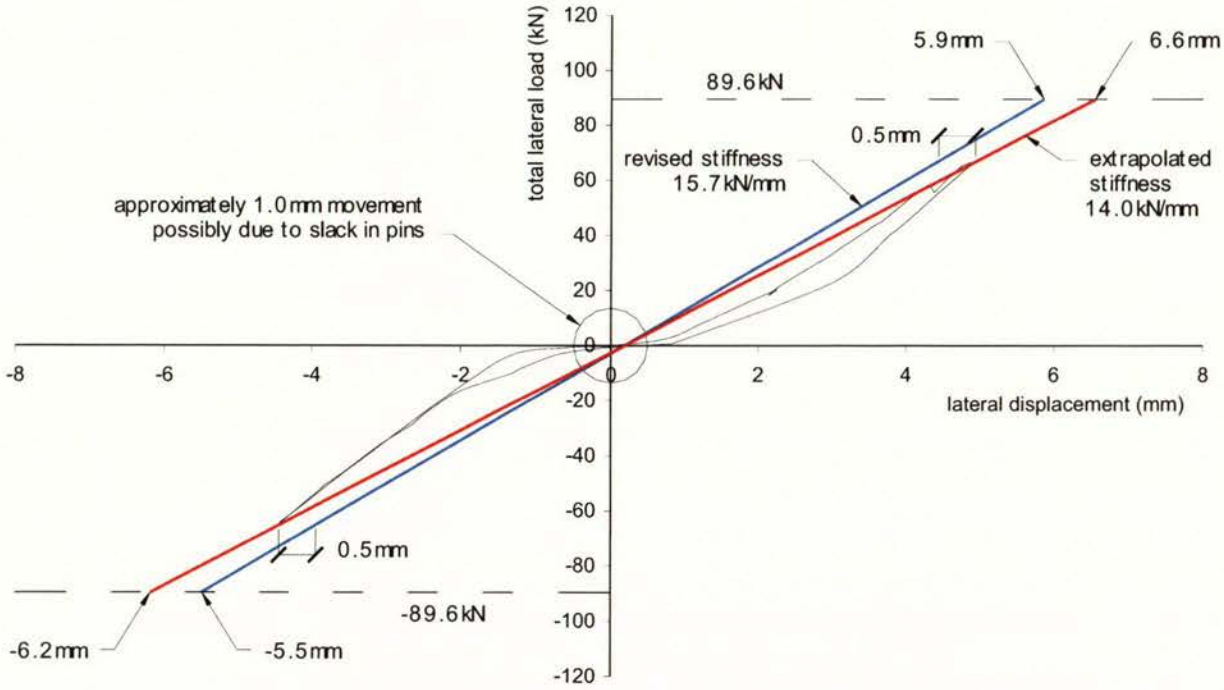

Figure 8.5: Lateral force versus displacement of Unit 1 in the elastic range.

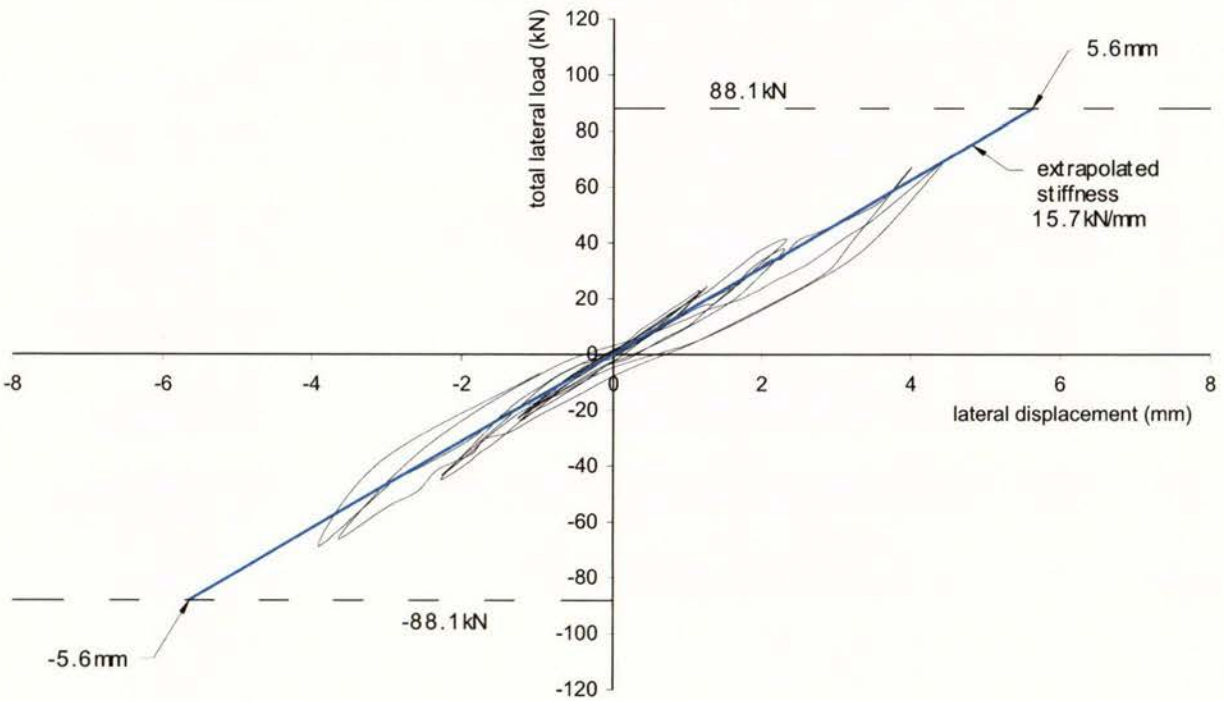

Figure 8.6: Lateral force versus displacement of Unit 3 in the elastic range.

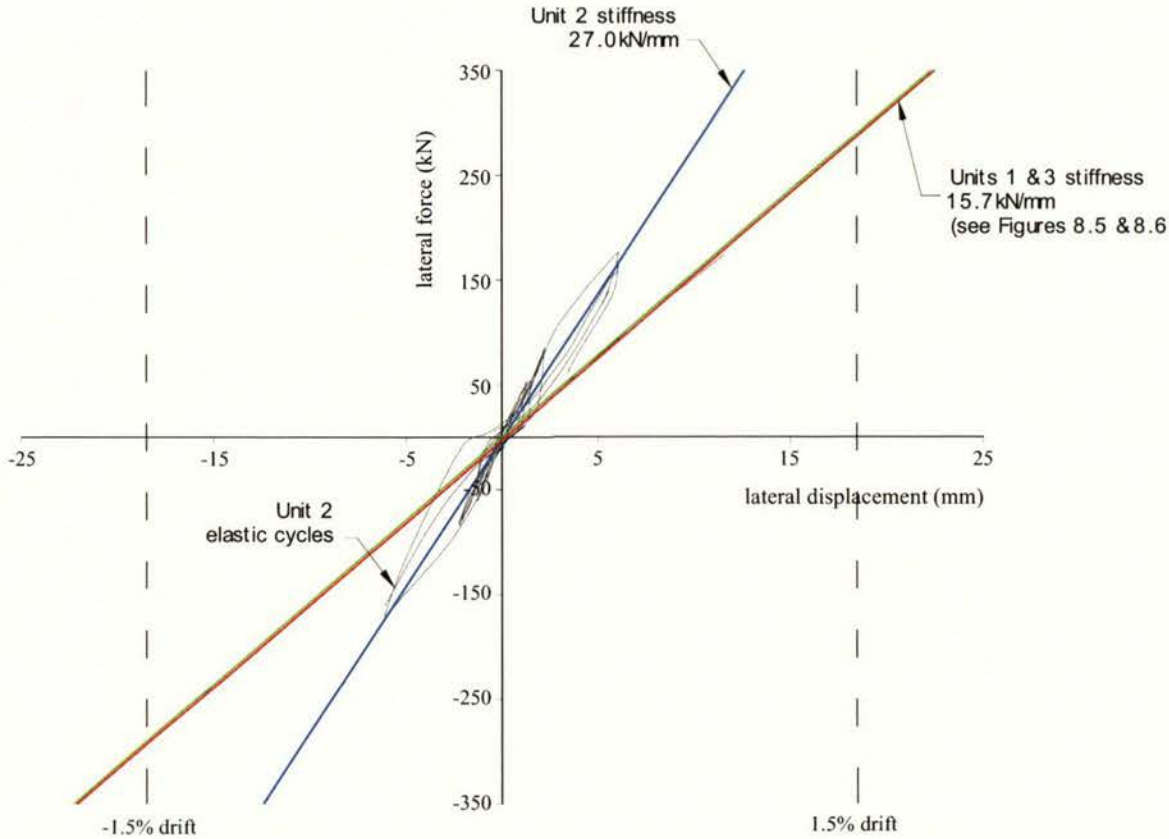

Figure 8.7: Comparison of initial stiffness of experimental units.

The test units were back analysed to find the proportion of the gross section properties that should be used to predict the ductility one displacement. The effective stiffness for the column section was calculated from equation 3-4 given by the Concrete Structures Standard [S2]:

$$I_e = \left(\frac{M_{cr}}{M_a}\right)^3 I_g + \left[1 - \left(\frac{M_{cr}}{M_a}\right)^3\right] I_{cr} \qquad \textit{Equation 8.1}$$

where M_{cr} is the cracking moment,

M_a is the moment applied,

I_g is the moment of inertia of gross concrete section, and

I_{cr} is the moment of inertia of cracked section.

For Unit 1, for an applied lateral force of 89.6kN (therefore M_a=54kNm), the effective moment of inertia of the column section was 0.55 of the gross section moment of inertia, ie. $I_e = 0.55\ I_g$. The effective section stiffness was doubled in the joint zones (as

is common practise derived from previous studies) to represent the local stiffening in these regions. To obtain a displacement of 5.7mm, the beam stiffness was found to be $0.25I_g$. For Unit 3, for an applied lateral force of 88.1kN, the effective moment of inertia of the column section was taken as 0.56 of the gross section moment of inertia. This value was slightly higher than that for Unit 1 due to a greater concrete strength in Unit 1. To obtain a displacement 5.6mm the flexural stiffness of the beam sections in the frame was found to be $0.28I_g$. In comparison, the New Zealand Concrete Structures Standard recommendation is $0.4I_g$ at ultimate limit state [S7].

For Unit 2, the ductility one displacement could not be determined since the yield strength of the unit could not be accurately calculated due to uncertainty concerning the interaction of the frame and the diaphragm. The 0.5% drift displacements and the sum of lateral forces recorded from the experiment to reach this level were used for the analysis. At this level, the average displacement was 6.1mm and the sum of lateral force was 172.8kN. To obtain this value the flexural stiffness of the beam stiffness was taken as $0.29I_g$. For this analysis, 160mm width of slab (four time thickness of slab) was included. The New Zealand Structures Standard recommended value for 'T' and 'L' beams is $0.35I_g$ [S7]. The effective moment of inertia of the column section was taken as 0.53 of the gross section moment of inertia, based on *Equation 8.1* for an applied lateral force of 172.8kN.

8.2.4 Shear deformation in columns

The beam-column joint of all the units performed satisfactorily. There were more diagonal joint shear cracks in the joint areas of Unit 2 than Units 1 and 3 due to the higher shear force sustained. Figure 8.8 compares the shear deformation in beam-column joints of Units 2 & 3. Shear deformation for Unit 1 is not shown here because the peak drift displacements did not match those of the other test units (see *Chapter 3*). The shear deformation in the joints of Unit 2 was significantly greater that that measured in Unit 3. At 3.0% drift displacement, the deformation in joint 'A' was 3.4 times greater than that of Unit 3. At the same displacement, it was 1.9 times for joint 'B', and 3.6 times for joint 'C'. The difference in shear deformation of the joints reflect the significantly larger forces sustained by Unit 2 compared to Unit 3. For the outer

joints, 'A' and 'C', the difference was greater because only one beam hinge formed adjacent to each of the outer joints of Unit 3 while two hinges formed either side of the joints of Unit 2.

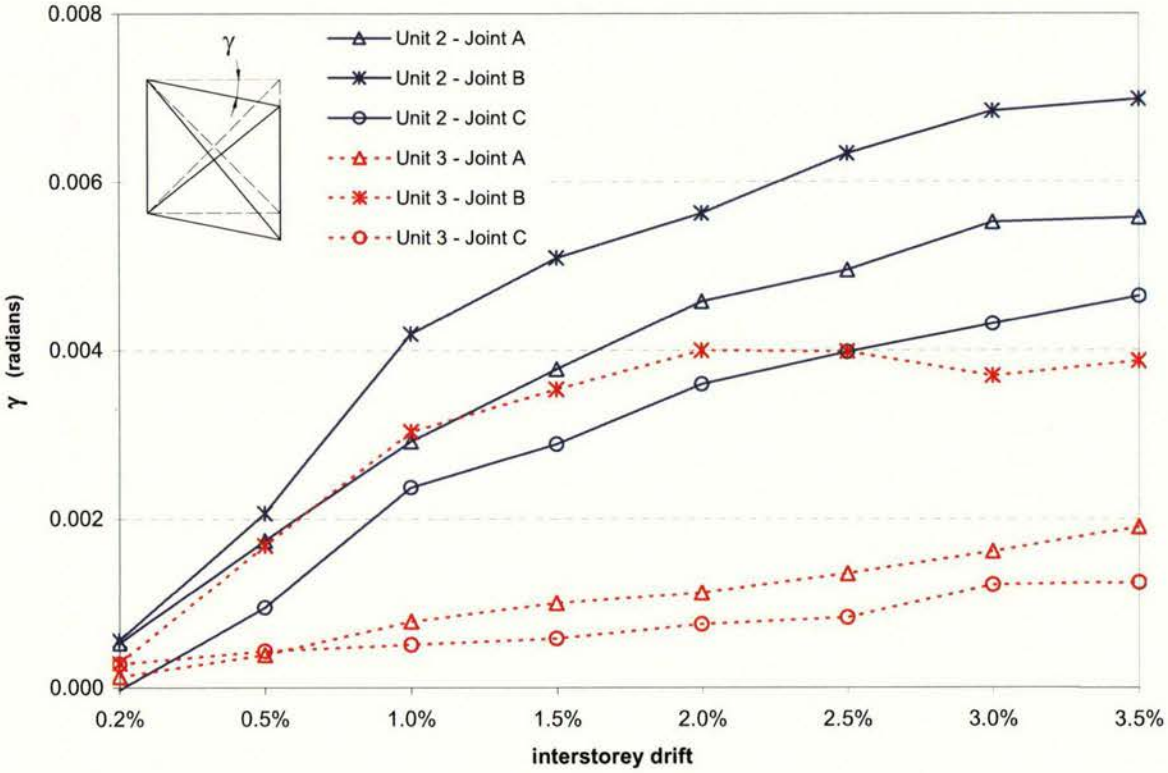

Figure 8.8: Shear deformation of beam-column joints of Units 2 and 3.

8.3 Deformation Incompatibility between Frame and Floor Slab

An important finding from the experiment was the vertical movement of the floor slab relative to the perimeter frame beams of Unit 2 around the exterior columns 'A' and 'C'. As the frame was displaced laterally, the beams rotated about the ends (positive rotation one end and negative rotation on the other). However, due to the relatively stiff prestressed ribs in the floor, the slab had the tendency to remain straight (see Figures 5.8 in *Chapter 5*). This differential movement was taken up by vertical bending of the flexible slab between the frame beam and the first prestressed rib (see Figures 7.19 in *Chapter 7*). It appears that the spalling of concrete was a result of the combined actions of local bending of the flexible slab and the shear transfer induced by the restraining action of the slab to beam elongation. Figures 8.9 show the extent of the damage around the columns at the end of the experiment.

(a) Column A

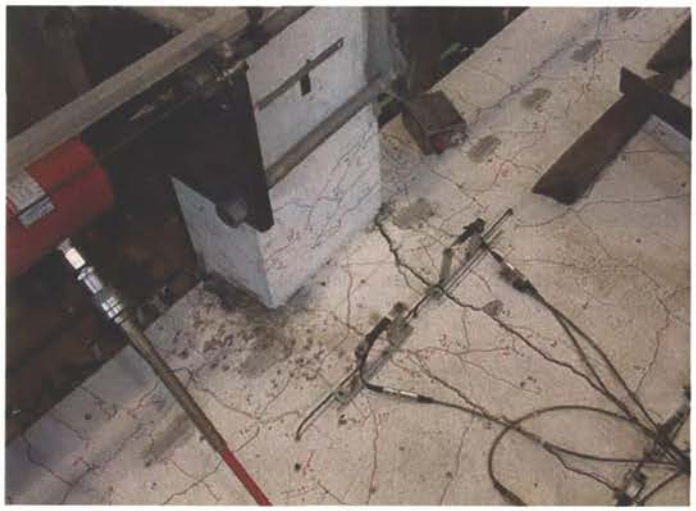

(b) Column B (central)

(c) Column C

Figures 8.9: Extent of damage around columns at the end of experiment.

The separation of the exterior columns from the floor topping could be significant in a multi-storey structure with similar configuration, as the lack of tie-back could result in translation of the column away from the floor. If this occurs over several floors, the columns may be susceptible to failure by buckling.

The relative vertical movement between the beam and the floor slab could well be more significant in cases where stiffer precast units are used and where the first unit is placed close to the perimeter frame. In the test of Unit 2 there was a relatively flexible link, consisting of a 40mm thick slab with a clear span of 150mm between the beam and the first precast unit. If this link had been shorter, failure between the slab and beam would probably have occurred at an earlier stage. This could have more serious implications if other flooring systems were used, in particular the hollowcore system, where it is common for the units to be placed directly alongside the frame beams. This type of floor is significantly stiffer in comparison to the in-situ topping concrete flange with the prestressed ribs used in this experiment.

In an experiment of a full scale, two-bay perimeter frame with hollowcore flooring system by Matthews *et. al.* at University of Canterbury [M4, M7], it was found that the mesh reinforcement failed as a wide crack formed in the topping between the first and second hollowcore floor unit (as shown by Figures 8.10). This was a result of the elongation of the beams against the restraint to elongation provided by the floor which caused the central column to displace outwards. There was also significant longitudinal web splitting in the first hollowcore unit along the floor span as well as transverse splitting to the ends of the unit near the supported edges. On further displacement to -2.0% drift, it was found that the first hollowcore unit rose by 12mm relative to the rest of the floor as shown by Figure 8.10(c). On further testing by loading the structure in the transverse direction and then back to the longitudinal direction up to 2.0% interstorey drift, the entire bottom section of the first hollowcore unit dropped.

In combination with the actions mentioned above, the relative vertical movements between the beams and the floor slab caused by the rotation of the beams and floor slab

could have also contributed to the longitudinal splitting of the hollowcore webs. Had the perimeter frame and floor slab (hollowcore) configuration been the same as the unit tested in this project (ie. two-bay with cantilevered extensions or no corner columns), the differential movements between beams and slab would have been greater. This would increase the possibility of failure by collapse of the bottom section of the hollowcore units. Failure could also occur at smaller drift displacement than that exhibited by the Matthews' experiment.

(a) Plan view of structure

(b) Elevation View

(c) Vertical differential displacement

Figures 8.10: Crack in hollowcore floor in experiment by Matthews [M7].

8.4 Strength Increase of Unit 2 due to Floor Slab

The increase in the strength of the perimeter frame beams due to the restraint to elongation of the beams by the floor slab was documented in *Chapter 5*. In the following sub-sections, the mechanisms involved in the increase of the beam strengths are investigated. The results from the analyses are compared with the results obtained from the numerical model of Unit 2, described in *Chapter 7*.

8.4.1 Strength increase where the precast units span past the columns

At the outer joints of Unit 2, joints 'A' and 'C', where the precast floor units span past the columns, the increase in the strength of the joint can be attributed to the restraint that the floor slab provides to beam elongation. The restraining force is equivalent to the slab providing an additional tension force capacity, T_{slab}, to the beams. This is illustrated in Figures 8.11. The tension force is of similar magnitude on each side of the column, and it acts at a level close to the centre of the insitu floor slab. It can be seen from Figure 8.11(c) that on the positive moment side of the column, the beam sustains the tension force carried by the slab in the compression zone, together with a tension force in the bottom reinforcement in the beam. These two forces are balanced by a compression force in the concrete at the top of the beam. As the insitu concrete in the slab acts with the beam, the resultant compression force can spread into the slab. For the purpose of calculation it has been assumed that the insitu concrete within a distance equal to four times the slab thickness of the beam acts as the compression zone. Hence the tension force in the slab, T_{slab}, is effectively cancelled out by an equal and opposite compression force in the concrete. The net result is that the tension force in the slab makes little difference to the moment capacity on the positive moment side of the column.

The situation is different on the negative moment side of the column. In this case, the effective tension force in the slab, T_{slab}, acts directly with the tension force carried by the reinforcement in the beam. These two forces are balanced by a compression force in the bottom of the beam. The moment capacity of the section is directly increased as is illustrated in Figure 8.11(d). To assess the magnitude of the tension force resisted by the floor slab in Unit 2 at columns 'A' and 'C' at different peak displacements, the following steps were undertaken:

1. The sum of the bending moment resisted by the column at peak drift displacements was calculated from the forces applied by the hydraulic actuators on the columns. In addition the corresponding axial forces acting on the beams from these forces were determined.

2. The sections on each side of the column were analysed when subjected to the axial forces calculated from the step above, with an arbitrary effective tension force sustained by the slab, T_{slab}, acting at the middle of the 40mm thick insitu concrete slab. This arbitrary force was varied until the sum of the moment capacities on each side of the column was equal to the experimentally determined value at the displacement stage being considered. This gave the effective tension force resisted by the slab.

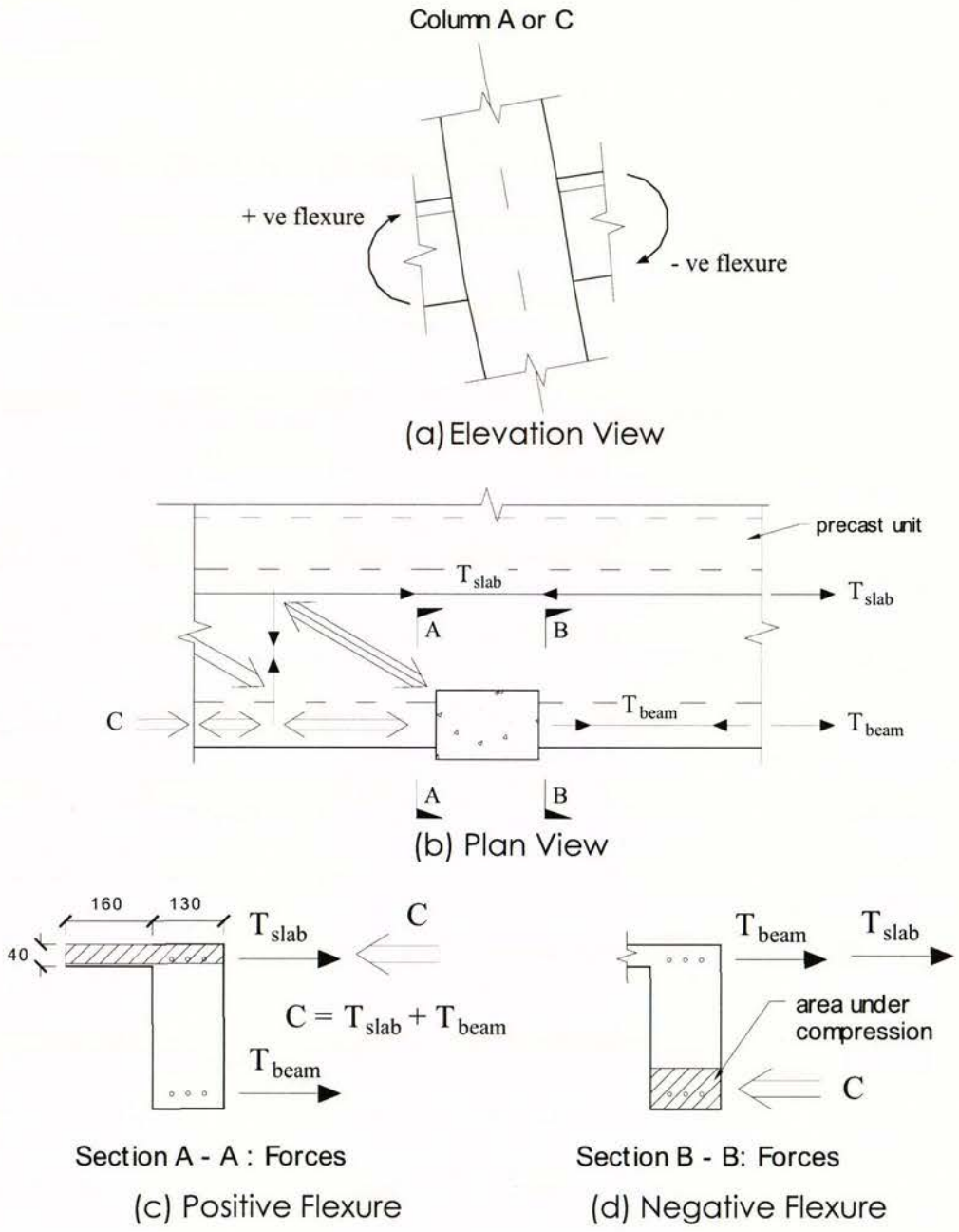

Figures 8.11: Strength increase for beams at columns 'A' and 'C'.

The theoretical strength of each beam calculated in step 2 above was found assuming a rectangular compression stress block as described in the New Zealand Concrete Structures Standard [S2] and a stress-strain relationship for the reinforcement determined from tensile test of the reinforcement. The strain measured at the column to beam junction at the drift displacement being considered was used to estimate the strain at the column face. For this calculation it was assumed that the reinforcement yielded at one beam depth away from the column face (300mm), and the strain increases linearly to peak at the column face, as illustrated in Figure 8.12. The change in strain between the zero load stage and peak displacement was used together with the monotonic stress strain response of the reinforcement to find the force in the reinforcement, as shown in Figure 8.13. As the majority of the measured strains were well above the yield point, the change in strain levels did not have to be known accurately to obtain reasonable estimates of the forces. The approach described above was published by Fenwick *et al* [F16] to estimate the effective tension force in the slab. However the analyses here is more comprehensive as additional strain measurements on the reinforcement were used to estimate the tensile forces.

In order to assess the reliability of the method describe above, the predicted strengths of the plane frame units, Units 1 and 3, were compared with experimentally measured values. This is summarised in Table 8.1. The average predicted strength of the columns is in reasonable agreement with the experimentally measured values. The comparison shows that the approach appeared to be sufficiently reliable to be used for assessing the effective tension forces resisted by the floor slab, T_{slab}, on Unit 2.

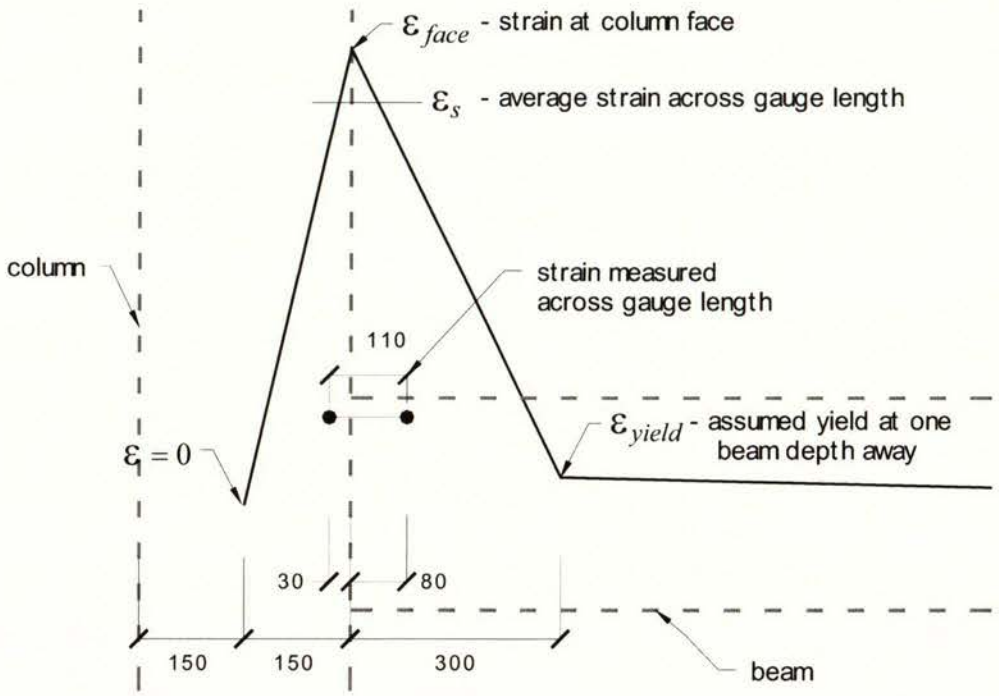

Figure 8.12: Estimating strain level of beam reinforcement at peak displacements.

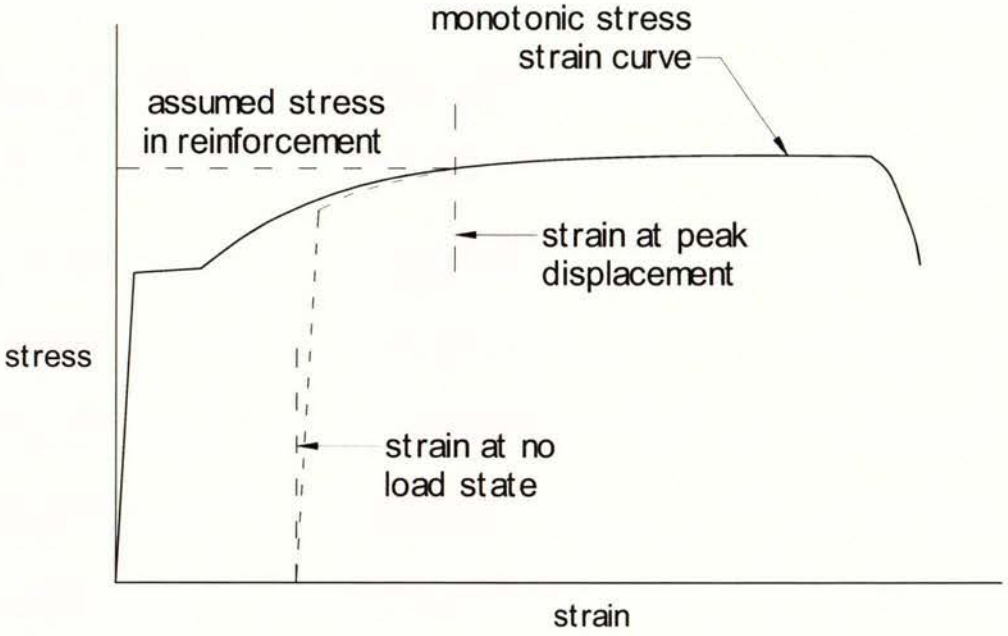

Figure 8.13: Assessing stress levels in reinforcement.

Table 8.1: Comparison of experimentally measured and predicted strengths of beam-column joints in Units 1 and 3.

drift	Unit 1			Unit 3		
	measured moment input (kNm)	predicted moment input (kNm)	ratio of measured to predicted	measured moment input (kNm)	predicted moment input (kNm)	ratio of measured to predicted

±1.0%	127	138	0.92	135	129	1.05
±2.0%	143	150	0.95	147	136	1.08
±2.5%	149	152	0.98	141	139	1.01
±3.0%	148	151	0.98	133	145	0.92

The method described above was applied to the outer columns, columns 'A' and 'C', in Unit 2. In reference to Figure 8.14, the steps taken in determining the moment input on each side of the columns are listed below:

a. The positive bending moments in the beams at the face of columns was determined from strain measurements of the tension reinforcement, assuming that the effective tension force acting at mid-height of the slab did not have significant influence on the strength as the compression force spreads into the slab.

b. The positive bending moment at the centre-line of column 'C' could be extrapolated from the value found in step a.

c. The negative bending moment in the beam at the centre-line of column 'C' is found from the difference of the applied bending moment measured in the test and the value determined in step b.

d. From the values found in steps a and c above, the negative bending moment at the column face of column 'C' and the positive bending moment at the centre-line of column 'B' could be extrapolated.

e. The negative bending moment at the centre-line of column 'B' is found from the difference of the measured values from the test, and the value determined from step d above.

f. From the values from in steps a and e , the negative bending moment at the column face of column 'B' and the positive bending moment at the centre-line of column 'A' could be extrapolated.

g. The negative bending moment in the beam at the centre-line of column 'A' is found from the difference of test measured value and the value from step f. The value at the column face could therefore be extrapolated.

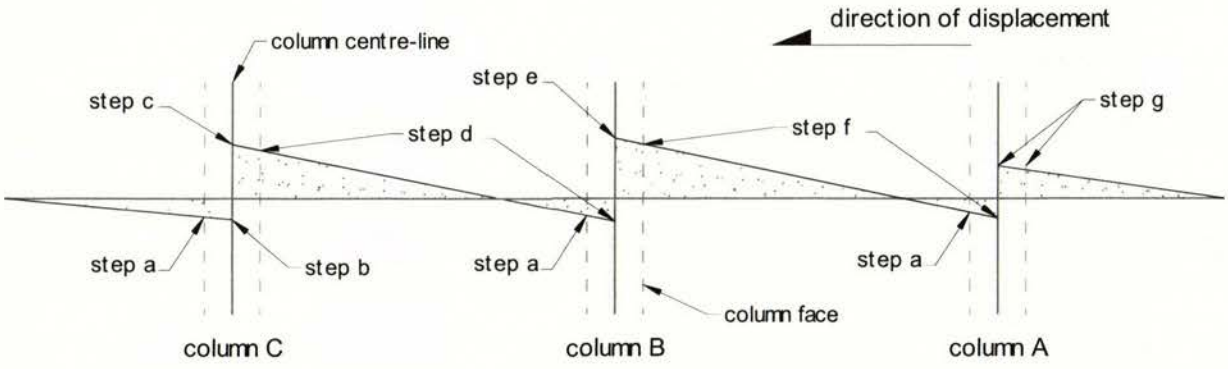

Figure 8.14: Calculating bending moments acting in beams of Unit 2.

From the bending moment resisted by the beams at the column face determined in the steps above, an assumed tension force, T_{slab}, was resisted by the floor at mid-height of the insitu concrete. This force was calculated on a trial and error basis until the bending moments resisted by the beams on both sides of the columns matched those determined from steps 'a' to 'g' above. The average predicted equivalent tension forces sustained by the slab in the positive and negative peak displacements for the two columns are given in Table 8.2. It can be seen that the floor slab made an appreciable contribution to the strength of the beams. The tension force of the passive reinforcement in the beams at yield was 107kN. In the last three drift displacement listed in Table 8.2, the average tension force sustained by the slab was equal to 160kN at column 'A' and 152kN at column 'C', hence approximately increasing the strength of the beam in negative bending by a factor of 2.4.

Table 8.2: Equivalent tension force resisted by floor slab at columns 'A' and 'C'.

drift displacement	average equivalent tension force in slab, T_{slab} (kN)	
	column A	column C
±1.0%	95	123
±2.0%	160	158
±2.5%	165	170
±3.0%	155	128

The current New Zealand Concrete Structures Standard indicates that the strength of the slab within a width of a quarter of the span of the beam from the centre-line of the column contributes to the flexural strength of the beam. This width was equal to 508mm for Unit 2. There are a number of ways that practising engineers might set out to assess the contribution of the floor slab to beam flexural strength, as listed below:

1. The slab reinforcement located in the 40mm topping concrete within this distance of the beam was equal to six 3.125mm wires and two 10mm reinforcement bars. The average yield stress from tension tests was 408MPa for the 3.125mm wires and 312MPa for the 10mm bars. Therefore the tension force at yield is equal to 68kN. At 6% strain, which approximately corresponds to the value at over-strength, the corresponding force for the reinforcement is 80kN.

2. The strength of the precast prestressed rib might be included in this calculation. As the tension force acts at the mid-height of the slab, it is eccentric to the prestressed beam section. In calculating the strength of the precast rib, allowance must also be made for the bending moments resulting from gravity loads which act on it. Within the 508mm from the beam centre-line, there was one precast rib. In terms of the standard, this rib is sufficiently close to the column for it to be effectively anchored (see NZS3101: Part 2:1995, Fig C8.10 [S4]). An ultimate strength analysis indicates that provided the full gravity load acts, each rib can resist an eccentric force of 72kN (also see section 5.4 of *Chapter 5*). Adding this value with the 80kN sustained by the passive reinforcement in the slab (see point 1 above), gives a tension force capacity of 152kN. This value is reasonably close in comparison with the average equivalent tension force shown in Table 8.2. However, for the rib to sustain the 72kN, extensive cracking should have developed across the top surface of the rib, and such cracking was not observed.

3. Another possibility might be assessing the tension force that may be resisted by the prestressed concrete rib and insitu concrete topping without cracking on

the top surface. For a cracking stress of 3.2MPa in the topping concrete, the value of tension in the slab is 57kN. This calculation ignores any existing stresses in the concrete due to creep or shrinkage of the concrete. Under this assumption of uncracked concrete, the tensile capacity of the reinforcement in the concrete cannot be included.

The magnitude of equivalent tension force in the slab shown in Table 8.2 indicates that the width of floor slab contributing to beam strength is most likely greater than the proposed width of 508mm from the beam centre-line. The prestressed rib within this width may have contributed to the beam strength, but may not have reached its ultimate capacity.

In the displacement cycles to ±2.0% drift, appreciable spalling occurred in the flexible slab adjacent to the outer columns, columns 'A' and 'C', due to differential vertical movement between the first precast rib and the beam. In the displacement cycles to ±2.5% drift this spalling extended to approximately 300mm from the column faces (see Figures 5.7 of *Chapter 5*), while in the ±3.0% drift cycles it extended in one case to the middle of one of the beam spans (see Figure 5.9 of *Chapter 5*). This spalling most probably reduced the confinement that the floor diaphragm provided to the beam plastic hinges adjacent to columns 'A' and 'C', hence reducing the effective tension force, T_{slab}, in the slab and flexural strength of the beams.

8.4.2 Strength increase where the precast units are supported on the transverse beam at the column.

In this case, which is represented by the central column, column 'B' in Unit 2, the prestressed rib units were supported on the transverse beam, which framed into column 'B' of the perimeter frame. When plastic hinges form in the perimeter beams at this column, elongation of the beams occurs as shown on Figure 8.15. As a result compression is induced in the beams and a tension force in the slab. This movement causes cracks to develop in the insitu concrete between the transverse beam and the ends of the prestressed units. The compression force in the beams is balanced by an effective tension force in the slab. This tension force, T_{slab}, is made up of the following actions as shown on Figure 8.15:

- Tension forces carried by the reinforcement in the insitu concrete connecting the two halves of the slab at the central transverse beam,
- Shear force resisted by bending action of the floor slab, which acts as a deep beam.

The deep beam action referred to above induces shear, hence diagonal tension and diagonal compression as well as flexural stresses in the floor slab. Figure 8.16 shows the crack pattern sustained in the floor at 3% drift displacement. It can be seen that the slab contains both flexural tension and diagonal tension cracks consistent with the deep beam mechanism, with the extent of these cracks indicating that significant force was resisted by this action.

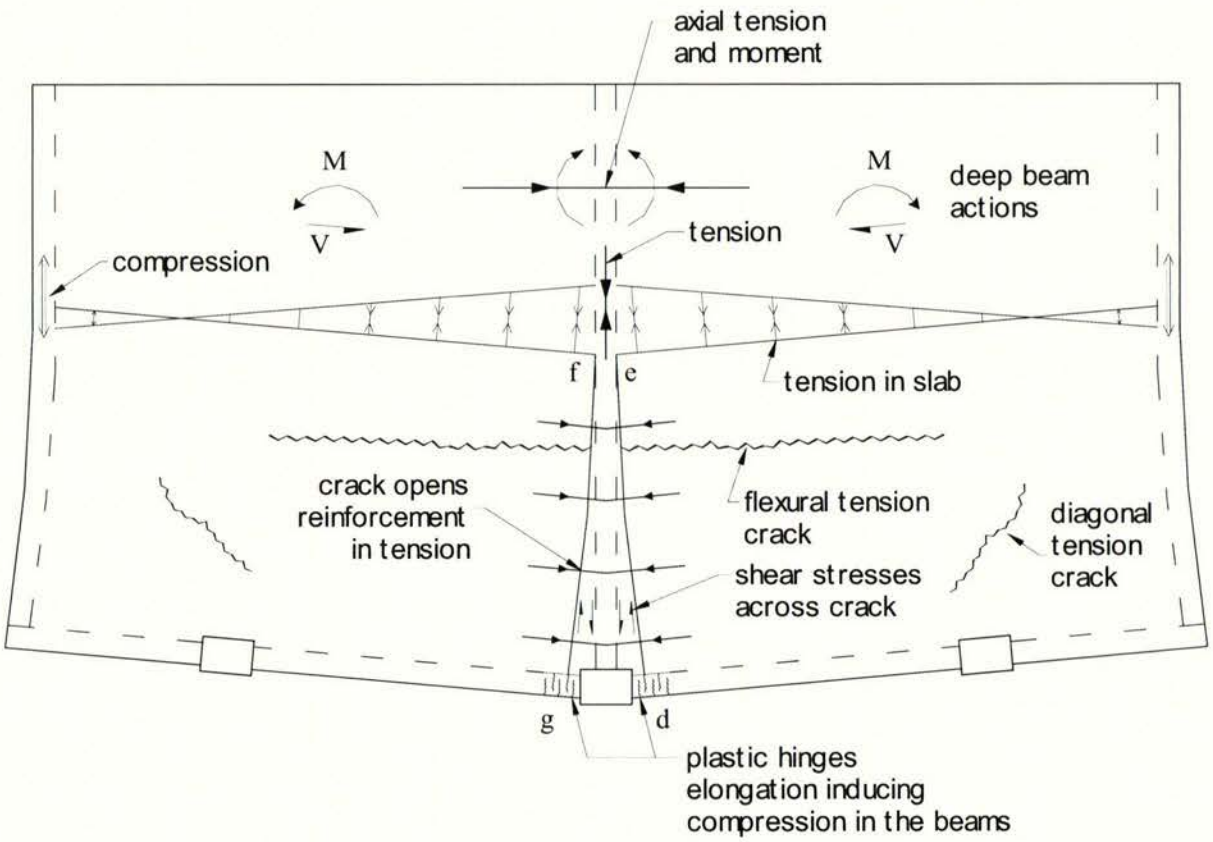

Figure 8.15: Floor slab acting as a deep beam due to elongation in plastic hinges.

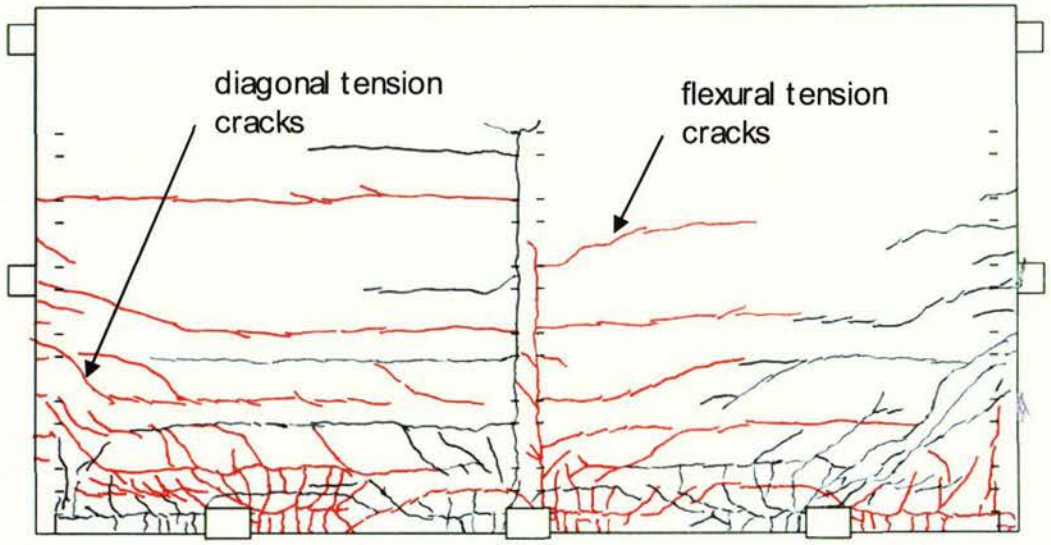

Figure 8.16: Crack pattern in floor slab at 3% drift displacement.

To find the contribution of the slab to the flexural strength of the beam, the same process that was used for columns 'A' and 'C' described in section 8.4.1 was followed. The equivalent tension force resisted by the floor slab, T_{slab}, was calculated based on a trial and error basis to match the bending moments determined from the forces applied by the hydraulic actuators. Having obtained the equivalent tension force in the slab values for different drift levels, the next step was to determine what proportion of this force was carried by the reinforcement crossing the central cracks, d – e and f – g, as shown on Figure 8.15 (see worked example in section A1.7, *Appendix 1*). The remaining force is resisted by the deep beam action of the slab.

The forces sustained by the reinforcement crossing the central cracks, d – e and f – g, were assessed from crack width measurements made during the test and the stress strain response of the reinforcement bars. There were two different types of reinforcement involved. The first consisted of a welded mesh of ductile plaon 3.125mm bars spaced at 75mm centres. This was welded up in the laboratory and it was cast into the 40mm thick insitu topping concrete (also see section 3.3.2 of *Chapter 3*). These 3.125mm bars had an average yield stress of 409MPa and an ultimate stress of 480MPa at a strain of approximately 12.5%. The second type of reinforcement consisted of two 4.0mm diameter deformed bar located directly above each precast rib unit (see Figure 3.3 in *Chapter 3*). These had an average yield strength of 431MPa with an average ultimate stress of 494MPa at an approximate strain of 12%. The strains in the reinforcement at

the cracks were assessed from the crack widths by assuming effective lengths of 75mm for the 3.125mm mesh bars and 120mm for the 4.0mm bars. The change in strain between the zero load stage and peak displacement was used together with the monotonic stress strain response of the reinforcement to find the forces, as illustrated in Figure 8.13. As a majority of the predicted strains were well above the yield point, the strain levels did not have to be known accurately to obtain reasonable estimates of the forces crossing the cracks at the different load stages.

A summary of the results of the analysis is given in Table 8.3 (see worked example in A1.7, *Appendix 1*). The average values are given for the positive and negative peak load displacements to a set drift displacement level. The bending moments resisted by the slabs, acting as deep beams, have been calculated for a section located 1000mm from the centre-line of the perimeter frame at 1.0% drift displacement (in both directions). This was chosen as it was close to the end of the crack, which formed along the central beam at this displacement. For the subsequent drift levels the section was located at 1950mm from the centre-line of the perimeter frame in the negative drift displacement and 1600mm from the centre-line of the frame in the positive drift displacement, as the crack on each side of the transverse beam extended to approximately these locations. To find the effective contribution of the forces carried by the reinforcement across the crack, T_{rein}, moments were taken about this section, as shown by Figure 8.17.

Table 8.3: Contribution of slab to tension force on column 'B' of Unit 2.

drift level	T_{slab} (kN)	T_{rein} * (kN)	T_{beam} ** (kN)	sum of reinforcement forces (kN)	actions resisted by slab as deep beam	
					shear force # (kN)	bending moment (kNm)
±1.0%	225	43	107	36	225 – 189	186
±2.0%	270	66	110	105	270 – 165	368
±2.5%	270	60	116	110	270 – 160	378
±3.0%	235	61	122	113	235 – 122	315

* T_{rein} is the equivalent tension force from the slab reinforcement acting with the perimeter frame beams.

** T_{beam} is the force in the longitudinal reinforcement in the perimeter beam.

The higher value is the shear at the face of the perimeter beam and the lower value is at the end of the crack.

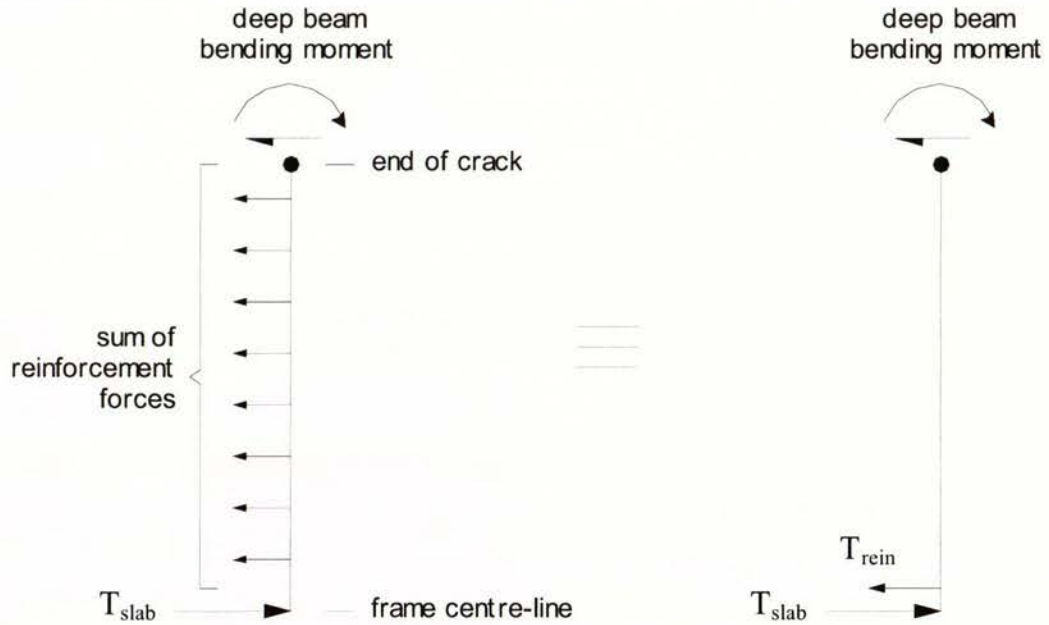

Figure 8.17: Forces acting at central column 'B' of Unit 2.

From Table 8.3 it can be seen that the tension force from the longitudinal reinforcement in the beam, T_{beam}, made up for about 31% of the total tension forces (T_{beam} + T_{slab}) acting on the beam between 2.0 and 3.0% drift displacement. Significantly, the remainder of the source in beam flexural strength comes from deep beam action of the slab.

If the criteria in the New Zealand Standard were used, the tension force capacity of the slab reinforcement would have been taken as 32kN. This value is based on the effective slab width of 508mm from the beam centre-line and the assumption that strain-hardening increases the stress to 1.1 times the yield stress. This value is of the order of 13% of the experimentally determined effective tension forces, T_{slab}, in displacement cycles between 1.0 and 3.0% drift.

The high contribution of the deep beam action in the slab to the strength of the beams adjacent to the central column is supported by the crack pattern as shown in Figure 8.16. The shear force in the slab averages about 258kN in the 2.0, 2.5 and 3.0% drift displacements. This corresponds to an average shear stress of 2.1MPa, which is more than sufficient to account for the diagonal tension cracks that can be observed in Figure

8.16. The average bending moment at the section 1600mm (in the positive direction) and 1950mm (in the negative direction) from the frame centre-line is close to 354kNm. This magnitude of moment can be sustained provided that the longitudinal reinforcement in the central transverse beam can act in tension. This may occur provided that some shear stresses are transmitted across the cracks (along d – e and f – g in Figure 8.15) by aggregate interlock and dowel action of the reinforcement. If this shear transfer is fully effective along this edge (assuming a compression strut angle of 35°), the moment capacity is close to 565kNm, which is well in excess of the calculated moment of 354kNm, which acted on this section.

8.4.3 Comparison of additional tension forces applied to the beams of Unit 2 and the numerical model of Unit 2.

The results from the analysis of the numerical model of Unit 2 were presented in *Chapter 7*. The bending moment input to the centreline of the beam-column joints of the test unit, Unit 2, and the numerical model of Unit 2 are compared in Figure 8.18. It can be seen from the figure that the bending moment input to joint 'A' of the numerical model is in reasonable agreement with the experimentally measured values (similarly joint 'C' in the negative direction). For joint 'C', the numerical results follows the experimental results closely up to 2.5% drift displacement, where on further displacement cycles, the resistance of joint 'C' decreased as flexible slab members around the joint started to fail (and vice versa for joint 'A' in the negative direction). The bending moment resisted by joint 'B' of the numerical model was significantly less than the values measured in the experiment. On average, the bending moment resisted by joint 'B' in the experiment was 32% greater in the positive direction and 14% greater in the negative direction.

The predicted strength of joint 'B' increased from 2.5% drift displacement, as the strengths for joints 'A' and 'C' decreased. This reflected the re-distribution of the resistance provided by the joints as the flexible slab members around columns 'A' and 'C' started to fail. This observation is supported by the appreciable spalling observed in the experiment in the displacement cycles greater than 2.5% drift (see section 5.3 of *Chapter 5*).

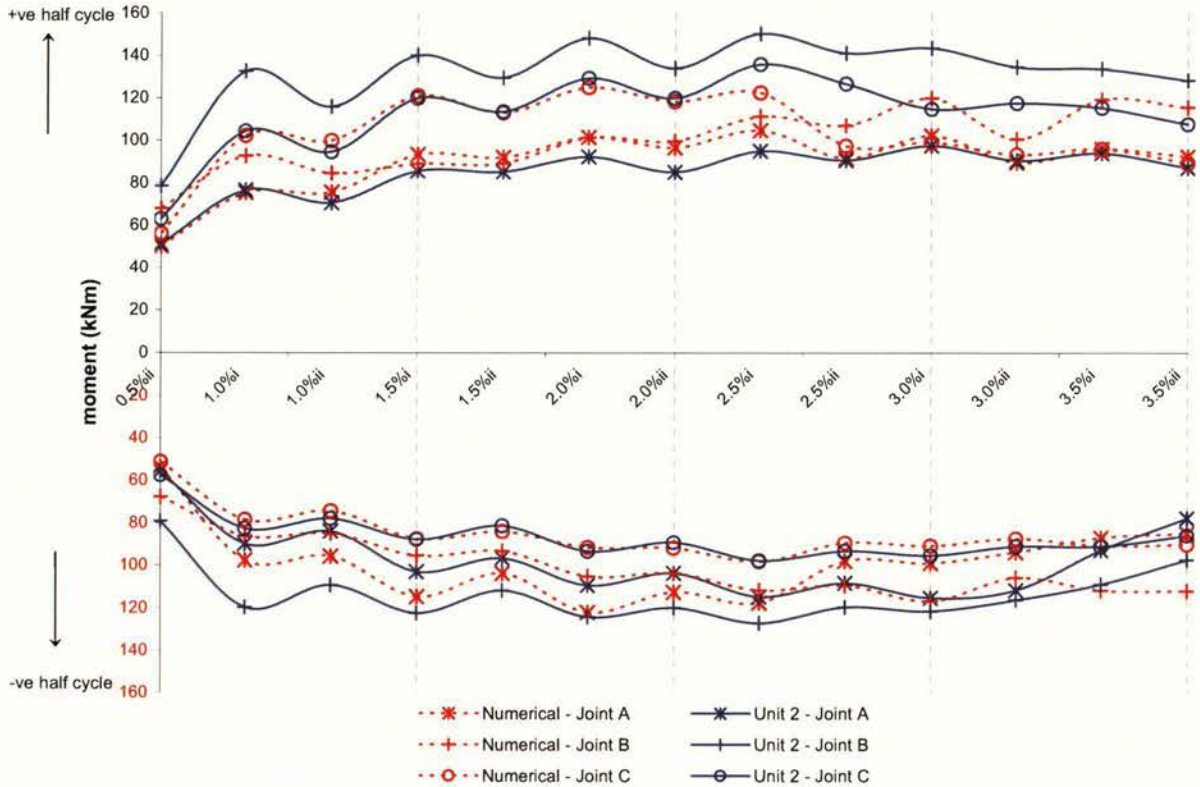

Figure 8.18: Comparison of bending moment input to beam-column center-lines of Unit 2 and numerical model.

To gain a further insight into the accuracy of the model, the effective tension forces resisted by the floor slab calculated from the experimental results and from the model are compared in Table 8.4. The numerical analyses under predicted the strength of the plastic hinge zones adjacent to the outer joints, joints 'A' and 'C'. At 2.0% and 2.5% drift displacement, the difference was within 17%, while at 3.0% the prediction was out by 30%. It is likely that the under-estimation of the strength was due to adopting a lower rotational limit for the flexible slab before failure was assumed to occur (see section 7.4.2 of *Chapter 7*). Another possible reason for the under-estimation of strength could be due to assuming too steep an angle for the compression strut of the flexible slab model, therefore limiting the magnitude of horizontal shear force transferred from the floor slab to the beams.

The strength enhancement of the plastic hinge zones adjacent to the central column, column 'B', was under-estimated by the numerical model. This probably occurred due to the inadequate modelling of the shear transfer from the central transverse beam to the floor slab. In particular this should have included shear across the cracks between the

ends of the floor slab and the central transverse beam by dowel and aggregate interlock actions (cracks marked as d – e and f – g in Figure 8.15). This shear transfer would enable the central beam to contribute the effective strength and stiffness of the deep beam actions in the floor slab.

Table 8.4: Comparison of effective tension force resisted by floor slab of Unit 2 calculated from experimental results and numerical model.

drift level	average force at columns A and C T_{slab} (kN)		average force at column B T_{slab} (kN)	
	experiment	numerical	experiment	numerical
±1.0%	109	89	225	88
±2.0%	159	152	270	143
±2.5%	168	144	270	198
±3.0%	142	100	235	226

8.5 Floor Slab to Frame Connections

The strength enhancement of beams in perimeter frames due to interaction with the prestressed floor places greater demands on the columns and beam-column joints. If the enhancement in beam capacity is not accounted for in the design of columns, a column sway mechanism may develop.

Clause 13.3.7.4 of the Concrete Standard [S2] requires design engineers to ensure that connections by means of reinforcement and shear transfer mechanisms are adequate to resist relevant design forces that are transferred from precast concrete diaphragms to components of the lateral force resisting system. Simply increasing the number of starter reinforcement at the connection between the diaphragm and parallel perimeter frame system may satisfy this clause in the standard, but the results from numerical models indicate that the increased amount of shear reinforcement may actually increase the bending strength of the beams. Therefore, it is important that in the design process, an appropriate amount of starter reinforcement is specified such that the connection

provided is adequate to transfer the likely diaphragm forces due to earthquake inertia forces, but not excessive such that the strength of beam is greatly increased.

In addition, clause 13.4.3.2 of the Concrete Standard [S2] says that 'adequate reinforcement in the cast-in-place topping shall be provided to transfer tension forces across discontinuities caused by the formation of plastic hinges in the supporting beams'. Under seismic actions, beam rotation and elongation, may result in excessively wide cracks between the frame and adjacent floor diaphragm. In the experiment, large cracks were observed in the floor slab around the beam-column joints and plastic hinges. These arose due to the combined action of shear transfer between beam and slab and the relative vertical displacement of the floor to the beams.

However, results from the numerical models in *Chapter 7* indicates that it may be advantageous not to place starter reinforcement between the beam and the floor topping within the potential plastic hinge zones. The results showed that omitting these members helped to reduce the bending strength of the beams. The results also showed that the magnitude of relative vertical movement between the floor and beam was reduced a little, but the movement in between drift cycles reduced significantly. In saying this, adequate reinforcement still has to be provided to satisfy clause 13.3.7.4. Sufficient reinforcement may be provided by starter reinforcement outside of the plastic hinge zones as well as between the floor diaphragm and the beam-column joints. It must be noted that these suggestions are based on results obtained by a simple numerical model, and further research and experiments are required to investigate its viability.

Chapter 9

Conclusions

9.1 Conclusions

The response of structures in major earthquakes is more complex than is usually assumed in both design and research. The effects of elongation are seldom included in structural analyses. The experimental and analytical work described in this thesis indicates the significance of elongation on behaviour and strength of a moment-resisting perimeter frame with prestressed floor components. Listed below are the main conclusions reached from this research:

- Two experimental units representing part of a ductile moment resisting frame were built and tested. These frames consisted of two-bays (ie. three columns) with cantilevered beam extensions on each end. A third identical frame was built with the addition of a floor diaphragm which consisted of precast-prestressed ribs with in-situ concrete topping spanning between outer transverse beams and a central transverse beam. The outer transverse beams branched out from the ends of the cantilevered extensions and the central transverse beam was connected to the central column (see Figures 3.3 of *Chapter 3*). The tests showed that the lateral strength and stiffness of the perimeter beams was significantly enhanced due to the interaction with the floor diaphragm. The initial stiffness of the unit with the floor slab was 72% greater than the initial stiffnesses of the units without the floor slab. The lateral resistance of the unit with the floor slab was typically 2.3 to 3.2 times the lateral force resisted by the units without the slab at equivalent interstorey drift levels. In the units without the floor slab, four plastic hinges could develop under cyclic loading. In the unit with the floor slab acting compositely with the beams in the perimeter frame, the flexural stiffness of the transverse beams combined with floor slab enabled two additional plastic hinges to form, giving a 50% increase in the number of plastic hinges. Allowing for the difference in the number of plastic

hinges formed, the lateral force resisted by the unit with the floor slab was 80% greater than the units without the floor slab.

- This level of observed strength enhancement associated with adding the slab could not be accounted for by including the passive reinforcement in the in-situ concrete in the effective width as defined in the New Zealand Concrete Structures Standard [S2]. The peak lateral strength of the test unit was 66% greater than the calculated lateral strength based on the recommendations in the standard. Even by including the eccentric force (at slab level) which can be resisted by the prestressed rib within the effective width (which is not required by the standard), the lateral strength of the test unit was 44% greater than the calculated value (see section 5.4 in *Chapter 5*). This unaccounted level of increase in strength of the potential plastic hinge zones in the beams becomes a life safety issue, as there is a danger that in a major earthquake a premature non-ductile column failure mechanism may develop instead of the intended ductile beam sway failure mode.

- The floor slab was found to restrain the elongation of the beams in the perimeter frame. At the two outer columns, where the floor slab span past the column, this restraining force acts as an equivalent tension force in the slab, which led to a very significant increase in the bending strength of the beams in negative (hogging) bending. The calculated equivalent tension force in the slab from the test results was found to be 109% greater than the value calculated from passive reinforcement at over-strength values, contained with the effective slab width recommended by the New Zealand Standard. However, with the inclusion of the eccentric force from the prestressed rib section within this width, the calculated equivalent force in the slab from the test was 10% greater.

- At the centre of the unit, elongation of the beams caused cracks to develop between the end of the precast units and the central transverse beam which was connected to the middle of the three columns of the perimeter frame. This generated an effective tension force in the slab which is made up of tension forces in the reinforcement crossing the cracks and the shear force resisted by the floor slab, which acts as a deep beam (see section 8.4 of *Chapter 8* for mechanisms of strength enhancement to

perimeter frame). This effective tension force in the slab is balanced by a compression force in the beams which effectively increased the bending strength of the beams. This deep beam action in the slab is not allowed for in the New Zealand Standard. If the passive reinforcement effectively anchored within the effective width were allowed as per the standard, the contribution of the slab is 22kN. This value is inadequate when compared to the calculated equivalent tension force of 270kN due to deep beam action in the slab.

- It was found that the relatively stiff floor restrained the level of elongation reached in the frame with floor slab experimental unit. At 3.0% interstorey drift the average elongation per plastic hinge zone for the frame-floor slab unit was 1.3% of beam depth, while for the units without floor slab, elongation was recorded at 2.4% of beam depth at the same drift level. Elongation at 1.3% of beam depth per plastic hinge at 3.0% interstorey drift could still be significant when designing for seating widths of floor slabs, particularly when the slabs span across several beam spans. For example, for a 900mm deep beam and a floor slab unit spanning across three beam bays, up to 70mm could be expected.

- The frame-floor slab test unit eventually failed when significant parts of the floor slab separated from the perimeter frame. As the frame was displaced laterally, the beams on each side of the columns rotated (positive rotation on one side and negative rotation on the other), whereas the relatively stiff prestressed ribs in the floor had the tendency to remain straight. This incompatibility in deformation was taken up by vertical bending of the flexible slab between the frame beam and the first prestressed rib, which eventually caused failure in the flexible slab. The damage in floor slab due to the differential movement was mostly limited to the areas surrounding the outer columns, where the differential vertical movement between the beam and slab was greater (see Figures 5.8 in *Chapter 5* and Figures 8.9 in *Chapter 8*). This separation of the exterior columns from the floor topping could be significant in a multi-storey structures with similar configuration, as the lack of tie-back could result in translation of the column away from the floor. If this occurs over several floors, the columns may be susceptible to failure by buckling, particularly in the enhanced moment transfer to the column results in plastic hinges

in the column. The relative vertical movement between the beam and the floor slab could be more significant in cases where stiffer precast units are used and where the first unit is placed close to the perimeter frame in a similar frame-floor slab configuration. In the experiment there was a relatively flexible link, consisting of a 40mm thick slab with a clear span of 150mm between the beam and the first precast unit. If this link was shorter, failure between the slab and beam would probably have occurred at an earlier stage. This could have more serious implications if other types of precast-prestressed flooring systems were used, in particular the hollowcore system, as has been recorded in literature [M7]. This type of floor is significantly stiffer in comparison to the in-situ topping concrete flange with the prestressed ribs used in this experiment.

- A non-linear, semi-empirical model of a plastic hinge zone was developed. The proposed model can predict reasonably the magnitude of both elongation and strength enhancement of plastic hinge zones when axial loads are applied. Analytical results from a numerical model of the frame-floor slab test unit predicted the similar levels of beam elongation. The average peak lateral strength of the test unit in the two directions was 10% greater than the numerical model, while the stiffness was 23% greater. Variations to connection properties were made to the model to assess the influence of these changes to the behaviour of the structure. Refinement to the plastic hinge model is desirable to enable it to model strength degradation in elements as well as better incorporate the effects of shear deformation and the effects of axial loads applied to the beams. Changes to the connections between the floor diaphragm and the supporting beams are also desirable to better model the deep beam action in the slab. However, in its present form the model can reasonably predict the effects that elongations of beams have on the performance of perimeter frame with prestressed floor.

9.2 Recommendations for Future Research Work

The findings from this research have highlighted the need for continuing research, which should be carried out to reach a better understanding of the actions induced from

the interaction of moment-resisting perimeter frames with floor diaphragms containing prestressed elements. The recommendations for future research work are:

- Conduct some direct, push-off experiments of a concrete floor slab connected to a beam, combined with vertical bending of the slab relative to the beam to assess the mechanism of shear transfer between the two interfaces. The magnitude of longitudinal and vertical shear transfer between slab and beam can be assessed with correlation to reinforcement in slab, vertical displacement and the angle of diagonal compression struts in the floor slab.

- Improve the elongating plastic hinge model developed in this study by using strength degrading elements, model shear deformations and a more accurate axial response. Develop a more accurate representation of the mechanism of shear transfer across the floor and frame interface through a better understanding of such action from relevant research. With these two improvements, combined with the use of non-linear shell elements for the floor slab, an analytical model could be effectively used to predict behaviour and performance of such systems without carrying out costly and time consuming physical experiments.

- Conduct analytical studies combined with physical tests to investigate possible retrofitting options to existing structures. It may be that many perimeter frame structures incorporating precast flooring have been designed and built did not allow for the enhanced strength of the beams due to interaction with the floor slab as well as vertical displacement of the floor slab relative to the beams.

The culmination of this research, future research as well as any relevant work, should result in better understanding of the performance of such systems. This knowledge should be reflected in current codes of practice in order that sound design methods can be implemented.

References

A1 Ammerman O.V. and Wolfgram-French C., *R/C Beam-Column-Slab Subassemblages Subjected to Lateral Loads,* Journal of Structural Engineering, ASCE, Vol. 115, No. 6, 1989, pp. 1289 - 1308.

A2 Arnold C., *The Seismic Response of Nonstructural Elements in Buildings*, Proceedings of Pacific Conference on Earthquake Engineering, Auckland, Vol. 1, 1991, pp. 335 - 350.

A3 ACI Committee 318, *Building Code Requirements for Structural Concrete (ACI 318-99) and Commentary (318R-99)*, American Concrete Institute, Michigan, 1999, pp. 391.

B1 Bolong Z., Mingshun W. and Kunlian Z., *A Study of Hysteretic Curve of Reinforced Concrete Member under Cyclic Loading*, Proceedings of the 7th World Conference on Earthquake Engineering, Istanbul, Turkey, 1980.

C1 Cheung P.C., *Seismic Design of Reinforced Concrete Beam-Column Joints with Floor Slab,* Ph.D. Research Report 91-4, Department of Civil Engineering, University of Canterbury, Christchurch, 1991, pp. 328.

C2 Cheung P.C., Paulay T. and Park R., *Mechanisms of slab-contribution in beam-column subassemblages*, ACI Publication, SP-123, American Concrete Institute, Detroit, 1991, pp. 259 - 289.

C3 Cement & Concrete Association of New Zealand, *Examples of Concrete Structural Design to the New Zealand Standard 3101,* 1998.

C4 Computers and Structures, *SAP2000 Nonlinear 8.1 - Structural Analysis Program*, Computers and Structures, Inc., Berkeley, California, 1984 - 2003.

D1 Durrani A.J. and Wight J.K., *Earthquake Resistance of Reinforced Concrete Interior Connections Including a Floor Slab,* American Concrete Institute Structural Journal Vol. 84, No. 5, 1987, pp. 400 - 406.

D2 Douglas K.T., *Development of a Reinforced Concrete Plastic Hinge Model*, Ph.D. Thesis, Department of Civil and Resource Engineering, University of Auckland, 1996, p. 299.

D3 Douglas K.T., Davidson B.J. and Fenwick R.C., *Modelling Reinforced Concrete Plastic Hinges*, Proceedings of 11th World Conference on Earthquake Engineering, Acapulco, Mexico, 1996, Paper No. 468.

D4 Dickson A.R., *The Response of Reinforced Concrete Slabs to Concentrated Loading*, Research Report No. 408, Department of Civil Engineering, The University of Auckland, 1986, pp. 48 - 52.

F1 Farhey D.N., Adin M.A. and Yankelevsky D.Z., 1993, *RC Flat Slab-Column Subassemblages Under Lateral Loading,* Journal of Structural Engineering, ASCE, Vol. 119, No. 6, 1993, pp. 1903 - 1916.

F2 Fenwick R.C., Davidson B.J. and McBride A., *The Influence of Slabs on Elongation in Ductile Seismic Resistant Frames,* Proceedings of New Zealand National Society for Earthquake Engineering Technical Conference, Rotorua, 1995, pp. 36 - 43.

F3 Fenwick R.C. and Davidson B.J., *The Seismic Response of Ductile Reinforced Concrete Frames with Uni-directional Hinges*, Research Report No. 527, Department of Civil Engineering, The University of Auckland, 1993.

F4 Fenwick R.C., Tankut A.T. and Thom C.W., *The Deformation of Reinforced Concrete Beams Subjected to Inelastic Cyclic Loading - Experimental Results*, Report No. 268, Department of Civil Engineering, University of Auckland, 1981, pp. 50 - 72.

F5 Fenwick R.C., Dely, R. and Davidson B., *Ductility Demand for Unidirectional and Reversing Plastic Hinges in Ductile Moment Resisting Frames*, Bulletin of New Zealand Society for Earthquake Engineering, Vol.32, No. 1, pp. 1-12.

F6 Fenwick R.C. and Megget L.M., *Elongations and Load Deflections Characteristics of Reinforced Concrete Members Containing Plastic Hinges*, Bulletin of the New Zealand National Society for Earthquake Engineering, Vol. 26, No. 1, March 1993, pp. 28 - 41.

F7 Fenwick R.C. and Davidson B.J., *Elongation in Ductile Seismic Resistant Reinforced Concrete Frames*, ACI Special Publication, Tom Paulay Symposium, SP-157, American Concrete Institute, 1995, pp. 143 - 170.

F8 Fenwick R.C. and Thom C.W., *Shear Deformation in Reinforced Concrete Beams Subjected to Inelastic Cyclic Loading*, The University of Auckland Research Report No. 279, Department of Civil Engineering, University of Auckland, 1982.

F9 Fenwick R.C. and Fong A., *The Behaviour of Reinforced Concrete Beams Under Cyclic Loading*, Bulletin of New Zealand National Society for Earthquake Engineering, Vol.12, No. 2, 1976, pp. 158 - 167.

F10 Fenwick R.C. and Nguyen H.T., *Reinforced Concrete Beam-Column Joints for Seismic Loading*, Report No. 220, Department of Civil Engineering, University of Auckland, 1981, pp. 56 - 58.

F11 Fenwick R.C., Ingham J.M. and Wuu P.J.Y., *The Performance of Ductile R/C Frames under Seismic Loading*, Proceedings New Zealand National Society for Earthquake Engineering Technical Conference, New Plymouth, 1996, pp. 20 - 26.

F12 Fenwick R.C., Davidson B.J. and Lau D., *Strength Enhancement of Beams in Ductile Seismic Resistant Frames due to Prestressed Components in Floor Slabs,* SESOC Journal, Vol. 12, No. 1, 1999, pp. 35 - 40.

F13 Fenwick R.C., *Shear, Torsion and Section Distortion in Concrete Box Girder Bridges,* Report No. 172, Department of Civil Engineering, University of Auckland, 1978, pp. 39 - 43.

F14 Fenwick R., Deam B. and Bull D., *Failure Modes for Hollowcore Flooring Units*, SESOC Journal, Vol. 17, No. 1, 2004, pp. 52 - 70.

F15 Fenwick R.C., Dickson A.R., *The Flexural Behaviour of Lightly Reinforced Concrete Beams and Slabs*, School of Engineering Report no. 435, University of Auckland, 1987.

F16 Fenwick R.C., Davidson B.J., Lau D.B.N., *Interaction between Ductile RC Perimeter Frames and Floor Slabs containing Precast Units*, Proceedings of New Zealand Society for Earthquake Engineering Technical Conference, Wairakei, 2005.

H1 Hollings J.P., *Reinforced Concrete Seismic Design*, Bulletin of the New Zealand National Society for Earthquake Engineering, Vol. 2, No.3, 1969, pp. 217 - 250.

L1 Liddell D., *Influence of Loading History on Ultimate Displacement of Concrete Structures,* Master of Engineering Thesis, University of Auckland, 2000.

M1 Megget L.M. and Fenwick R.C., *Seismic Behaviour of a Reinforced Concrete Portal Frame Sustaining Gravity Loads*, Bulletin of the New Zealand National Society for Earthquake Engineering, Vol. 22, No. 1, Mar. 1989, pp. 39 - 49.

M2 McBride A., Fenwick R.C. and Davidson B.J., *The Influence of Slabs on the Lateral Cyclic Behaviour of Ductile Concrete Frames*, School of Engineering Report No. 566, University of Auckland, 1996.

M3 Mejia-McMaster J.C. and Park R., *Tests on Special Reinforcement for the End Support of Hollow-Core Slabs*, PCI Journal, Precast/Prestressed Concrete Institute, Vol. 39, 1994, pp. 90 - 105.

M4 Matthews J., Bull D. and Mander J., *Preliminary Results from the Testing of a Precast Hollowcore Floor Slab Building*, Technical Papers TR27 New Zealand Concrete Society Conference 2002, New Zealand Concrete Society, 2002.

M5 Ma S-Y.M., Bertero V.V. and Popov E.P., *Experimental and Analytical Studies on the Hysteretic Behaviour of Reinforced Concrete Rectangular and T-Beams*, Earthquake Engineering Research Centre Report 76-2, 1976.

M6 Matthews J.G., Bull D.K. and Mander J.B., *Preliminary Results from the Testing of a Precast Hollowcore Floor Slab Building*, Conference Proceedings 2003 Pacific Conference on Earthquake Engineering, Christchurch, February 2003.

M7 Matthews J.G., Bull D.K. and Mander J.B., *Hollowcore Floor Slab Performance Following a Severe Earthquake*, Proceedings of fib Symposium: Concrete Structures in Seismic Regions, International Federation for Structural Concrete, Athens, Greece, May 2003.

N1 Norton J.A, King A.B, Bull D.K., Chapman H.E., McVerry G.H., Larkin T.J. and Spring K.C., *Northridge Reconnaissance Report*, Bulletin of the New Zealand National Society for Earthquake Engineering, Vol. 27, No. 4, Dec 1994, pp. 235 - 344.

N2 New Zealand Concrete Society and New Zealand Society for Earthquake Engineering, *Guidelines for the use of structural precast concrete buildings*, Centre for Advance Engineering, University of Canterbury, 1999, Chapter 6.

O1 Oliver S., Bull D.K. and Restrepo J., *Performance of concrete topped precast concrete hollowcore flooring systems with and without dramix steel fibres under*

simulated seismic loading, ASEC Conference Proceedings, Vol. 1, Auckland, 1998, pp. 325 - 332.

P1 Precast/Prestressed Concrete Institute, *Reflections on the Beginnings of Prestressed Concrete in* America, Chicago, 1981.

P2 Pantazopoulou S.J. and Moehle J.P., *The Effect of Slabs on the Flexural Behaviour of Beams,* Report No. UCB/EERC-87/1, Berkeley, 1987.

P3 Park R. and Paulay T., *Reinforced Concrete Structures*, John Wiley & Sons, New York, 1975, pp. 545 - 609.

P4 Paulay T., *Seismic Design of Ductile Moment Resisting Reinforced Concrete Frames, Columns: Evaluation of Actions*, Bulletin of the New Zealand National Society for Earthquake Engineering, Vol. 10, No. 2, June 1977, pp. 85 - 94.

P5 Paulay T., *Capacity Design of Earthquake Resisting Ductile Multistorey Reinforced Concrete Frames*, Proceedings of the 3rd Canadian Conference on Earthquake Engineering, Vol. 2, Montreal, 1979, pp. 917 - 948.

P6 Paulay T., *Deterministic Design Procedure for Ductile Frames in Seismic Areas*, ACI Publication SP-63, American Concrete Institute, Detroit, 1980, pp. 357 - 381.

P7 Park R., *Ductile Design Approach for Reinforced Concrete Frames*, Earthquake Spectra, Vol. 2, no. 3, May 1980, pp. 565 - 620.

P8 Paulay T., *The Coupling of Shear Walls*, Ph.D. Thesis, Department of Civil Engineering, University of Canterbury, Christchurch, 1969.

P9 Pantazopoulou S.J., Moehle J.P. and Shahrooz B.M., *Simple Analytical Model for T-Beams in Flexure*, Journal of Structural Engineering, ASCE, Vol. 114, No. 7, 1988, pp. 1507 - 1523.

P10 Pantazopoulou S.J., French C.W., *Slab Participation in Practical Earthquake Design of Reinforced Concrete Frame*, ACI Structural Journal, American Concrete Institute, Vol. 98, No. 4, July-August 2001, pp. 479 - 489.

P11 Park R., *Evaluation of Ductility of Structures and Structural Assemblages from Laboratory Testing,* Bulletin of the New Zealand National Society for earthquake Engineering, Vol. 22 No. 3, Sept 1989. pp. 155 - 166.

Q1 Qi X. and Pantazopoulou S.J., *Response of RC Frame under Lateral Loads,* Journal of Structural Engineering, ASCE, Vol. 117, No. 4, 1991, pp. 1167 - 1188.

R1 Restrepo J I., *Seismic behaviour of connections between precast concrete elements*, Department of Civil Engineering Report, 93/3, University of Canterbury, 1993, pp. 385.

S1 Standards New Zealand, *Code of Practice for General Structural Design and Design Loadings for Buildings, NZS 4203:1992,* Wellington.

S2 Standards New Zealand, *Concrete Structures Standard NZS 3101:1995 Part 1 - The Design of Concrete Structures*, Wellington.

S3 Suzuki N., Otani S. and Kobayashi Y., *Three-Dimensional Beam-Column Subassemblages Under Bidirectional Earthquake Loadings,* Proceedings of 8th World Conference on Earthquake Engineering, San Francisco, Vol. VI, 1984, pp. 453 - 460.

S4 Standards New Zealand, *Concrete Structures Standard NZS 3101:1995 Part 2 - Commentary on the Design of Concrete Structures*, Wellington, pp. 211 - 212.

S5 Skinner R.I. and McVerry G.H., *Base Isolation for Increased Earthquake Resistance of Buildings*, Bulletin of the New Zealand Society for Earthquake Engineering, Vol. 8, No. 2, 1975, pp. 93 - 101.

S6 Sakata H., and Wada A., *Elasto-plastic Behaviour of One-twentieth Scale of RC frame*, Proceedings of the 10th World Conference on Earthquake Engineering, Madrid, Vol. 6, 1992, pp. 3335 - 3340.

S7 Standards New Zealand, *Concrete Structures Standard NZS 3101:1995 Part 2 - Commentary on the Design of Concrete Structures*, Amendment No.3, Wellington, March 2004, pp. 9 - 11, 25.

T1 Technical Advisory Group of Precast Flooring Systems, *The Seismic Performance of Flooring Systems - Special Research Report - Interim Executive Summary*, SESOC Journal, Vol. 15, No. 2, 2002.

T2 Thom C.W., *The Effects of Inelastic Shear on the Seismic Response of Structures*, Ph.D. Thesis, University of Auckland, March 1983.

V1 Vecchio F.J. and Collins M.P., *Compression Response of Cracked Reinforced Concrete*, Journal of Structural Engineering, ASCE, Vol. 119, No. 12, 1993, pp. 3590 - 3610.

W1 Wight J.K. (ed.), *Earthquake Effects on Reinforced Concrete Structures*, ACI Publication, SP-84, 1984, p. 428.

Z1 Zerbe H.E. and Durrani A.J., *Seismic Response of Connections in Two-Bay R/C Frame Subassemblies,* Journal of Structural Engineering, ASCE, Vol. 115, No. 11, 1989, pp. 2829 - 2844.

Z2 Zerbe H.E. and Durrani A.J., *Seismic Response of Connections in Two-Bay Reinforced Concrete Frame Subassemblies with a Floor Slab,* American Concrete Institute Structural Journal, Vol. 87, No. 4, 1990, pp. 406 - 415.

Appendix 1

Design Calculations

A1.1 Test Unit Beam Design – to NZS 3101:1995 [S2]

A1.1.1 Dimension Check

The beam for the frame is 300 x 130 mm. This must comply with clause *8.5.2.1.*

$$\frac{L_n}{b_w} = \frac{2032-300}{130} = 13.3 < 25 \qquad \text{OK.} \qquad (\text{Eq. 8-17})$$

$$\frac{L_n h}{b_w^{\,2}} = \frac{(2032-300)(300)}{130^2} = 30.7 < 100 \qquad \text{OK.} \qquad (\text{Eq. 8-18})$$

For the cantilevered ends:

$$\frac{L_n}{b_w} = \frac{1220-150}{130} = 8.2 < 15 \qquad \text{OK.} \qquad (\text{Eq. 8-19})$$

$$\frac{L_n h}{b_w^{\,2}} = \frac{(1220-150)(300)}{130^2} = 19.0 < 60 \qquad \text{OK.} \qquad (\text{Eq. 8-20})$$

A1.1.2 Beam Flexural Reinforcement

The minimum reinforcement ratio:

$$p_{\min} = \frac{\sqrt{f_c'}}{4f_y} = \frac{\sqrt{30}}{4(300)} = 0.0046 \qquad (\text{Eq. 8-22})$$

The maximum reinforcement ratio in plastic hinge zone (PHZ):

$$p_{\max} = \frac{f_c^{'} + 10}{6 f_y} = \frac{30 + 10}{6(300)} = 0.0222 \qquad \text{(Eq. 8-21)}$$

The maximum size of longitudinal bar is limited by the bond requirements of bars passing through the beam-column joints, from clause *7.5.2.5*:

$$\frac{d_b}{h_c} \le 3.3 \alpha_f \frac{\sqrt{f_c^{'}}}{\alpha_0 f_y} \qquad \text{(Eq. 7-13)}$$

where $\alpha_f = 1.0$ (one way frame)

$\alpha_0 = 1.25$ (plastic hinge at column faces)

$$\therefore d_b \le 3.3(1.0)\frac{\sqrt{30}}{1.25(300)} = 14.4$$ **maximum bar diameter is 12mm**

Red Book [C3] design: beam sized at 900 x 400mm and longitudinally reinforced with 4-HD24. Reinforcement ratio:

$$p_{RB} = \frac{A_s}{b_w d} = \frac{\pi(4)(24^2/4)}{400(835)} = 0.0054$$

Scale the above for difference in steel grade:

$$0.0054\left(\frac{430}{300}\right) = 0.0077$$

try 3-D12, equal top and bottom, $A_s = 339\text{mm}^2$

$$p = \frac{339}{130(300 - 27.5)} = 0.0096$$

OK. Satisfies $p_{\min}$ & $p_{\max}$, also comparable with Red Book design.

Have 3-D12, equal top and bottom beam longitudinal reinforcement.

Flexural overstrength of beam

Applying capacity design principles used for ductile structures, a reasonable allowance for the increase in the strength of the bars is made. It is generally accepted that the factor used for the overstrength of steel, $\lambda_o = 1.25$.

Flexural overstrength of beam (in both positive and negative bending) at column face:

$$M_{o,f} = \lambda_o A_s f_y \left(d - d'\right) = 1.25(339)(0.3)\frac{(272.5 - 27.5)}{1000} = 31.1\,\text{kNm}$$

Flexural overstrength of beam at column centreline by extrapolation (ignoring beam self-weight):

$$M_{o,cl} = M_o\left(\frac{L}{L_n}\right) = 31.1\left(\frac{2032}{2032 - 300}\right) = 36.5\,\text{kNm}$$

Beam overstrength at column centreline in both positive and negative bending, M_o= 36.5 kNm

A1.1.2 Beam Transverse Reinforcement

Design shear force under overstrength actions:

$$V_o = \frac{2M_o}{L} = \frac{2(36.5)}{(2.032)} = 35.9\,\text{kN}$$ **Design shear force, V_o = 35.9 kN**

The beam potential plastic hinge zone (PPHZ) will be located at the face of the column, and has a length of 2h = 2(300) = 600mm.

Antibuckling and confinement requirements

Within PPHZ: clause *8.5.3.4(a)*: corner bars less than 200mm apart, therefore one set of 2 legged stirrup required.

Clause *8.5.3.4(d)*: The centre-centre spacing of stirrup shall not exceed the lesser of *d*/4 or 6 times the diameter of longitudinal bar, and first stirrup not more than 50mm from column face:

$$s \le \frac{d}{4} = 68\text{mm} \quad \text{or} \quad 6 \times 12 = 72\text{mm}$$

Clause *8.5.3.4(b)*: Diameter not less than 5mm, and area of one leg of a stirrup shall not be less than:

$$A_{te} = \frac{\sum A_b f_y}{96 f_{yt}} \frac{s}{d_b} \qquad \text{(Eq. 8-23)}$$

where: $A_b = 113\text{mm}^2$ (one 12mm bar)

$f_y = f_{yt} = 300\text{MPa}$

$d_b = 12\text{mm}$

try $s = 65\text{mm}$ (within limits of *8.5.3.4(d)*)

$$\therefore A_{te} \ge \frac{113(300)}{96(300)} \frac{65}{12} = 6.4\text{mm}^2$$

with 6mm stirrup bar, $A_{te} = 28.3\text{mm}^2$, OK.

Outside of PPHZ: From clause *9.3.5.4(a)*, spacing limit shall not be less than $0.5d$ = 136mm.

Shear stresses in beam

Nominal shear stress in PPHZ

$$v_n = \frac{V_o}{\phi b_w d} = \frac{35.9(1000)}{1.0(130)(272.5)} = 1.01\text{MPa}$$

This shall not exceed the following from *9.3.1.8*:

$0.2 f_c' = 6\text{MPa}$ OK.

$1.1\sqrt{f_c'} = 6\text{MPa}$ OK.

and 9.0MPa OK.

Therefore beam shear stress, v_n = **1.01MPa**

Check for diagonal reinforcement within PPHZ: From clause *9.4.4.2(a)*, the nominal shear stress v_n = 1.01MPa, shall not exceed:

$0.16f_c^{'} = 4.8\text{MPa}$ OK.

$0.85\sqrt{f_c^{'}} = 4.7\text{MPa}$ OK.

From clause *9.4.4.2(b)*:

$$v_n = 1.01\text{MPa} \le 0.25(2+r)\sqrt{f_c^{'}} = 0.25(2-1)\sqrt{30} = 1.37\text{MPa}$$

Therefore, diagonal reinforcement is not required.

Shear reinforcement

Shear reinforcement required, from clause *9.3.6.3*:

$$A_{v,req} = \frac{(v_n - v_c)b_w s}{f_{yt}} \qquad \text{(Eq. 9-14)}$$

where: $v_c = 0$ (assumed zero, clause *9.4.2.1*)

s = 65mm (from previous)

$$\therefore A_{v,req} = \frac{(1.01)(130)(65)}{300} = 31\text{mm}^2$$

Since there are 3-D12, there is minimum of a 6mm 2-legged stirrup. A_v = 56mm^2.

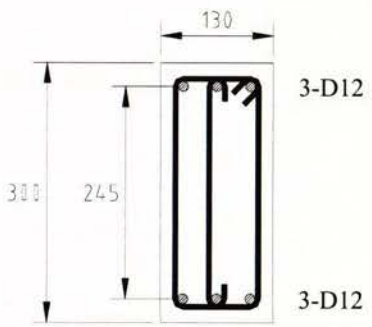

Within PPHZ have 3 legs R6 @ 65 c/c

Outside of PPHZ: Assume s = 100mm

$$\therefore A_{v,req} = \frac{(1.01)(130)(100)}{300} = 48\text{mm}^2 \qquad \text{OK.}$$

Have transverse reinforcement outside of PPHZ: 3 legs R6@100 c/c

A1.2 Test Unit Column Design

A1.2.1 Dimension Check

The columns are members of the primary lateral force resisting system, therefore the dimension requirements of *8.5.2.1* must be satisfied.

$$\frac{L_n}{b_w} = \frac{1230-300}{200} = 4.7 < 25 \qquad \text{OK.} \qquad (\text{Eq. 8-17})$$

$$\frac{L_n h}{b_w^{\,2}} = \frac{(1230-300)(300)}{200^2} = 7.0 < 100 \qquad \text{OK.} \qquad (\text{Eq. 8-18})$$

A1.2.2 Column Flexural Reinforcement

The longitudinal reinforcement ratio limitations are:

$$0.008 \le p_t \le 0.08 \qquad \text{clause 8.4.6.1}$$

From clauses 8.5.4.2 (a) and (b):

$$0.008 \le p_t \le \frac{18}{f_y} = 0.042 \qquad f_y = 430\text{MPa}$$

The aim in deciding on the column proportions and reinforcement was to ensure that the columns are substantially stronger than the beams. Consider case where there are 6 plastic hinges forming simultaneously in the beam (Note that this does not apply for Unit 1 and does not consider the strength contribution from the flooring system). From section A1.1.2, $M_{o,cl}$ = 36.5 kNm. Therefore, the sum of lateral load applied is:

$$\frac{36.5\times 6}{1.23} = 178\text{ kN}$$

Therefore, the axial load acting on columns 'A' and 'C' is given by:

$$178\times 1.23 = N\times 4.064$$

where the distance between 'A' and 'C' is 4.064m

$$\therefore N = \pm 53.9\text{ kN}$$

Try 12-HD12 for column longitudinal reinforcement.

$$p_t = \frac{A_s}{A_g} = 12\frac{\pi(6^2)}{300(200)} = 0.0226$$ OK, within limits.

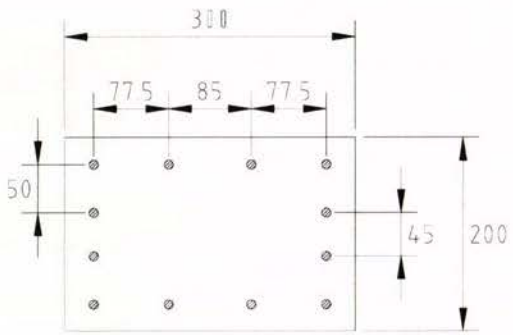

This arrangement satisfies clause *8.5.4.2(c)*, where the distance between each cross-linked bar shall not exceed larger of 1/4 of the adjacent lateral dimension of the section or 200mm.

From analysis of column strength:

N (kN)	$M_{n,col}$	$\frac{M_{n,col}}{M_{o,cl}}$
+53.9	84.6 kNm	2.32
0	72.0 kNm	1.97
-53.9	63.0 kNm	1.73

It can be seen from the table above that the nominal flexural strength of the columns is at least 1.73 times the flexural overstrength of the beams.

Have column flexural reinforcement of 12-HD12

A1.2.3 Column Transverse Reinforcement

Antibuckling and confinement requirements

Within PPHZ (taken as 2h = 600mm from beam face): From clause *8.5.4.3(b)ii*, maximum spacing of stirrup sets is to be the lesser of:

$6\,d_b = 6 \times 12 = 72\text{mm}$

or

$\frac{b}{4} = \frac{200}{4} = 50\text{mm}$ therefore spacing shall not be more than 50mm.

From clause *8.5.4.3(b)i*, the minimum effective area of stirrup bars in the principal direction is given by Eq. 8-26, and no individual leg shall be less than that given by Eq.8-23:

$$A_{sh} \geq \frac{(1.3 - p_t m)s_h h''}{3.3}\frac{A_g}{A_c}\frac{f_c'}{f_{yt}}\frac{N^*}{\phi f_c' A_g} - 0.006 s_h h'' \qquad \text{(Eq. 8-26)}$$

where $p_t m = p_t \frac{f_y}{0.85 f_c'} = 0.0226\frac{430}{0.85(30)} = 0.38$ OK. as < 0.4.

$f_{yt} = 300\text{MPa}$

$\frac{A_g}{A_c} = \frac{300(200)}{(300-60)(200-55)} = 1.72$ OK. as > 1.2.

$\phi = 1.0$

$h'' = 151\text{mm}$

$$\therefore \frac{A_{sh}}{s_h} \geq \left[\frac{(1.3-0.38)(151)}{3.3}(1.72)\frac{30}{300}\frac{(53.9\times10^3)}{1.0(30)(300\times200)}\right] - 0.006(151) = -0.689$$

negative value, therefore not critical.

$$A_{te} \geq \frac{\sum A_b f_y}{96 f_{yt}}\frac{s_h}{d_b} \qquad \text{(Eq. 8-23)}$$

where $\sum A_b = 4\times\frac{\pi(12^2)}{4} = 452.4$ ie. 4 bars reliant on tie

$$\therefore \frac{A_{te}}{s_h} \geq \frac{452.4\times300}{96(300)(12)} = 0.393$$

$\therefore$ if s_h = 50mm (max allowable), $A_{te} \geq 20\text{mm}^2$

If use 6mm stirrup, bar area = 28mm^2, therefore OK.

Outside of PPHZ: From clause *8.4.7.2(b)*, maximum spacing of stirrup sets is to be the lesser of:

$10\ d_b = 10 \times 12 = 120\text{mm}$

or

$$\frac{b}{3} = \frac{200}{3} = 67\text{mm}$$

Therefore spacing shall not be more than 67mm.

From clause *8.4.7.2(a)*, the minimum effective area of stirrup bars in the principal direction is given by Eq. 8-8, and no individual leg shall be less than that given by Eq. 8-9:

$$A_{sh} \geq \frac{(1.0-p_t m)s_h h''}{3.3}\frac{A_g}{A_c}\frac{f_c'}{f_{yt}}\frac{N^*}{\phi f_c' A_g} - 0.0065 s_h h'' \qquad \text{(Eq. 8-8)}$$

from previous result (Eq. 8-26), this will not be critical.

$$A_{te} \geq \frac{\sum A_b f_y}{135 f_{yt}} \frac{s_h}{d_b} \qquad \text{(Eq. 8-9)}$$

$0.393\left(\frac{96}{135}\right) = 0.279$ scaling from previous calculation of Eq. 8-23.

$\therefore$ if $s_h = 65\text{mm}$, $A_{te} \geq 18\text{mm}^2$ OK. as 6mm bar area is 28mm^2.

Shear stresses in column

Estimate design shear force from:

$$V_{col}^* = \frac{1.25 M_{n,col}}{\left(\frac{1.23}{2}\right)}$$

Shear stress is given by:

$$v_n = \frac{V_{col}^*}{\phi\, b_w d}$$

This shall not exceed the following from *9.3.1.8*:

$0.2 f_c' = 6\text{MPa}$, $1.1\sqrt{f_c'} = 6\text{MPa}$ or 9.0MPa

Therefore most critical case is $M_{n,col} = 84.6$ kNm.

$\therefore V_{col}^* = 172\text{ kN}$

$v_n = \frac{172 \times 10^3}{1.0(200)(270)} = 3.2\text{ MPa}$ OK. within limits.

Concrete shear stress, v_c, is given by:

$v_c = \left(1 + \frac{3N^*}{A_g f_c'}\right) v_b$ for members subjected to axial compression. (Eq. 9-6)

$$v_c = \left(1 + \frac{12N^*}{A_g f_c'}\right) v_b \qquad \text{for members subjected to axial tension.} \qquad (\text{Eq. 9-7})$$

where N^* is negative for tension

$$v_b = (0.07 + 10p_w)\sqrt{f_c'} \qquad (\text{Eq. 9-3})$$

$$\text{where } p_w = \frac{(A_s + A_{ps})}{b_w d} = \frac{(12(\pi \times 6^2) + 0)}{200(270)} = 0.025$$

$\therefore v_b = 1.75\text{MPa}$

$M_{n,col}$	V_{col}^*	v_n	v_c	$v_n - v_c$
84.6	172	3.2	1.9	1.3
72.0	146	2.7	1.7	1.0
63.0	128	2.4	1.1	1.3

Critical case is where ($v_n - v_c$) = 1.3 MPa.

Shear reinforcement

The required shear reinforcement is given by *9.3.6.3*:

$$A_v = \frac{(v_n - v_c) b_w s}{f_{yt}} \qquad (\text{Eq. 9-14})$$

$$\therefore \frac{A_v}{s} \geq \frac{(1.3)200}{300} = 0.87$$

Outside of PPHZ, s = 65mm, $A_v \geq 57\text{mm}^2$

There are 4 legs of 6mm bar, giving a combined area, $A_v = 113\text{mm}^2$ OK.

Transverse reinforcement within PPHZ: R6 stirrup sets @ 50 c/c

Transverse reinforcement outside PPHZ: R6 stirrup sets @ 65 c/c

This stirrup arrangement is shown below:

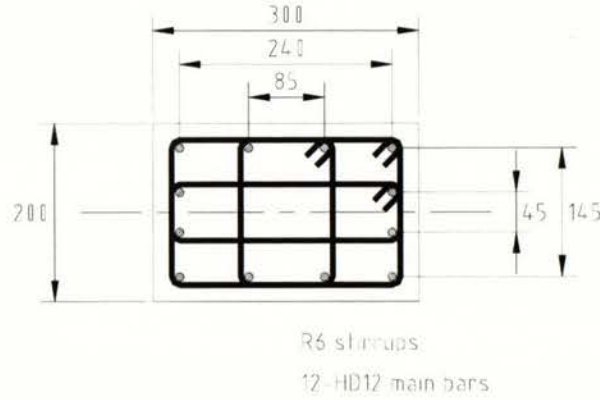

A1.3 Test Unit Beam-Column Joint Design

The column shear based on the beam overstrength moments at the column centreline is:

$$V_{col}^{*} = \frac{2\left(2\,M_{o,cl}\right)}{\left(L_c + L_c^{'}\right)}$$

where $M_{o,cl} = 36.5$ (Section A1.1.2)

$L_c = L_c^{'} = 1.23$

$$\therefore V_{col}^{*} = \frac{2\left(2\left(36.5\right)\right)}{\left(1.23+1.23\right)} = 59.3\text{kN}$$

The horizontal joint shear force is calculated from:

$$V_{jh} = 1.25 f_y \left(A_{s1} + A_{s2}\right) - V_{col}^{*} \qquad \text{(Eq. C11-2)}$$

where A_{s1} and A_{s2} are the top and bottom beam longitudinal steel respectively

$$\therefore V_{jh} = 1.25\left(0.3\right)\left(2 \times 3\left(\frac{\pi\left(12^{2}\right)}{4}\right)\right) - 59.3 = 195.2\text{kN}$$

V_{jh} = 195.2kN

The nominal horizontal joint shear stress is calculated from:

$$v_{jh} = \frac{V_{jh}}{b_j h_c} \qquad \text{(Eq. 11-3)}$$

where $h_c = 300\text{mm}$

b_j is smaller of $b_c = 200\text{mm}$ or $b_w + 0.5h_c = 130 + 150 = 280\text{mm}$

$$\therefore v_{jh} = \frac{195.2 \times 1000}{200(300)} = 3.25\text{MPa}$$

And shall not exceed $0.20f_c' = 0.2(30) = 6\text{MPa}$ OK.

v_{jh} = 3.25MPa

Horizontal joint reinforcement

The area of reinforcement required to resist the applied horizontal joint shear force is calculated from (interior joints):

$$A_{jh} = \frac{6v_{jh}}{f_c'} \alpha_i \frac{f_y}{f_{yh}} A_s^* \qquad \text{(Eq.11-4)}$$

where $\alpha_I = 1.4$ or $1.4 - 1.6\dfrac{C_j N^*}{f_c' A_g}$

$C_j = 1.0$, $N^* = -54.9\text{kN}$

A^*_s is the greater of top and bottom beam reinforcement (= 339mm^2)

$$0.85 \le \frac{6v_{jh}}{f_c'} = 0.65 \le 1.20$$ therefore equal 0.85 (*11.4.4.1(c)*)

$$A_{jh} = 0.85\left(1.4 - 1.6\frac{1.0(-54900)}{30(300 \times 200)}\right)\frac{300}{300}(339) = 418\text{mm}^2$$

Check that not less than:

$$0.4\frac{V_{jh}}{f_{yh}} = 260\text{mm}^2 \qquad \text{OK.}$$

Therefore the required area of joint horizontal steel is: $A_{jh,req}$ = **418mm²**

Try same configuration as column transverse reinforcement, ie. 4-legged R6 per set, giving an area of 113mm².

Number of sets required: $\frac{A_{jh,req}}{113} = \frac{418}{113} = 3.7 \text{ sets} \Rightarrow$ Have 5 sets.

Try spacing at 40mm c/c.

Leaving distance between beam bar and tie set: $\frac{245 - 4(40)}{2} = 22.5\text{mm}$

$$\frac{22.5}{40} = 0.56 > 0.5 \qquad \text{OK.}$$

Beam-column horizontal shear reinforcement 5-R6 stirrup sets @ 40 c/c

Vertical joint reinforcement

The area of reinforcement required to resist the vertical joint shear force is calculated from:

$$A_{jv} = \alpha_v \frac{h_b}{h_c} A_{jh} \frac{f_{yh}}{f_{yv}} \qquad \text{(Eq.11-7)}$$

where $\alpha_v = \dfrac{0.7}{1 + \dfrac{N^*}{f_c^{'} A_g}} = \dfrac{0.7}{1 + \dfrac{-54900}{30(300 \times 200)}} = 0.722$

$$A_{jv,req} = 0.722\frac{300}{300}(418)\frac{300}{430} = 211\text{mm}^2$$

There are 4-HD12 crossing the potential failure plane, therefore the area of the vertical joint shear reinforcement provided is:

$$A_{jv} = 4\left(\frac{\pi\left(12^2\right)}{4}\right) = 452\,\text{mm}^2 \qquad \text{OK.} > 211\,\text{mm}^2$$

No additional vertical joint shear reinforcement is required.

A1.4 Test Unit Corner Half-Hinge Joint Design – Unit 2

The method used for the design of the corner half-hinge joint was obtained from a design example contained in the 'Red Book' [C3]. The normal forces on the joint were derived from the flexural strength of the connecting beam. The longitudinal force is taken as 0.2 times the compressive vertical force. The values and dimensions are shown below:

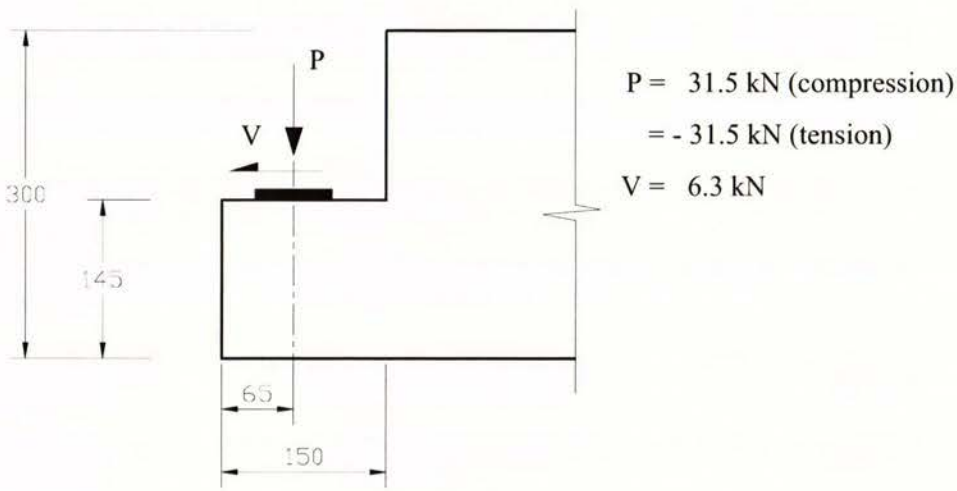

The tension force of 31.5kN may be carried by a RB12H (12mm Reid bar with 500MPa), which has a capacity of 56.5kN. Footplates are screwed on for anchorage.

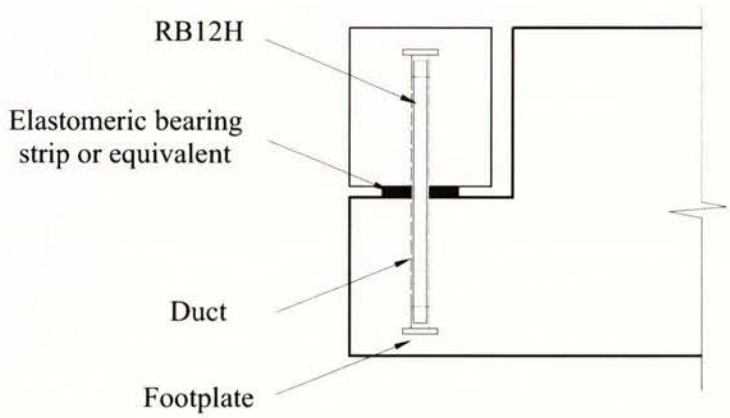

A1.4.1 Upward force on half hinge

The sketch below shows the strut and tie model and free body diagram for upward loading on the half hinge.

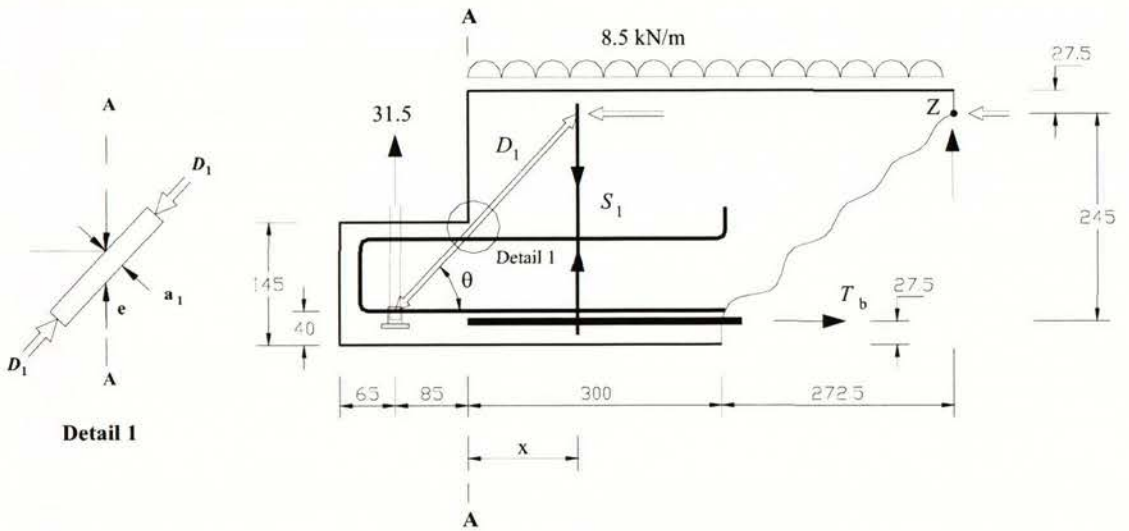

Assume centre of D_1 is 15mm below top surface of the nib at Section A-A (meaning e/2=15).

$$\therefore\ \theta = \tan^{-1}\left(\frac{105-15}{85}\right) = 46.6°$$

$$\text{hence } D_1 = \frac{31.5}{\sin 46.6°} = 43.4\text{ kN}$$

With a compression stress of $0.65 f_c^{'}$ and using the full width of the beam:

$$a_1 = \frac{43.4\times10^3}{0.65\times30\times130} = 17.1\text{ mm}$$

which gives a distance on the vertical plane A-A of:

$$e = \frac{17.1}{\cos 46.6°} = 24.9\text{ mm}$$

Hence the centre of D_1 is 24.9/2 = 12.45mm down on section A-A, which is close to the assumed value of 15mm.

Assuming that the centre of D_1 is 12.5mm below the top surface of the nib at Section A-A gives:

$$\theta = \tan^{-1}\left(\frac{105-12.5}{85}\right) = 47.4°$$

Then

$$D_1 = \frac{31.5}{\sin 47.4°} = 42.8\,\text{kN}$$

$$a_1 = \frac{42.8\times10^3}{0.65\times30\times130} = 16.9\,\text{mm}$$

and:

$$e = \frac{16.9}{\cos 47.4°} = 25.0\,\text{mm}$$

Hence the centre of D_1 is 12.5mm down on section A-A, which is equal to the assumed value.

$$\therefore\ T_a = \frac{31.5}{\tan 47.4°} = 29.0\,\text{kN}$$

T_b is the force in the bottom 3-D12 bars, and is calculated from the free body shown in the sketch by taking moments about point Z. The longitudinal projection of the diagonal crack starting from the end of the lap is equal to an effective depth, *d*.

$$T_b = \frac{\left(31.5(0.085+0.3+0.2725) - 8.5(0.2725+0.3)^2\right)}{(0.2725-0.0275)} = 73.1\,\text{kN}$$

<u>Lap length for 12mm bars:</u>

$$L_{db} = 0.5\times\frac{1.0}{\sqrt{30}}\times300\times12 = 329\,\text{mm}$$

$$\alpha_b = \frac{73.1/0.3}{3\times\pi 12^2/4} = 0.718$$

Assume there are 3 legged 6mm stirrups @ 100 c/c:

$$\alpha_d = 1+\sqrt{\frac{85}{100}\times\frac{300}{80\times3\times12}} = 1.3$$

Therefore:

$$L_d = \frac{0.718}{1.0\times1.3}\times329 = 182\text{ mm} < 300\text{ mm provided. OK.}$$

Bars for $T_a = 29.0$ kN

$$A_{s,req.} \geq \frac{29}{0.3} = 97\text{ mm}^2$$

Check minimum reinforcement:

$$p_{\min} = \frac{\sqrt{30}}{4\times300} = 0.004564$$

$$A_{s,\min} = 0.004654\times130\times105 = 62\text{ mm}^2$$

Hence have 2-D10 bars, $A_s = 157$ mm^2.

Stirrup reinforcement

The force $S_1 = 31.5$ kN is carried by a band of stirrups over a distance of 2x, which equals 260mm. For 3 legged 6mm stirrups @ 100 c/c, the tension capacity is:

$$3\times\frac{\pi 6^2}{4}\times0.3\times\frac{272.5}{100} = 69.3\text{ kN} > 31.5\text{ kN, OK.}$$

A1.4.2 Downward force on half hinge

Downward force on the joint can be resisted in two ways shown by the following diagrams. For a robust connection, the total load should be split between the two strut

and tie models. The maximum actions consist of a downward force of 31.5 kN and lateral force of 6.3 kN. These are divided between the two models.

Strut and Tie Model 1

$T_1 = 27.2$ kN
$C_1 = 20.0$ kN
$C_2 = 18.4$ kN
$C_3 = 28.3$ kN

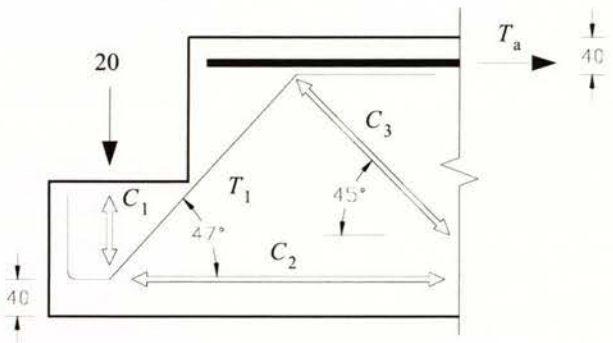

Assume T_1 consists of 2-D10. Therefore $A_s f_y = 47.1$ kN.

Vertical load balance giving, 47.1 × sin 47.4 = 34.7 kN, but round this down to 20 kN, given the arbitary division of actions between models 1 and 2. Hence:

$$C_1 = 20\,\text{kN},\ C_2 = 18.4\,\text{kN} \text{ and } C_3 = 24.3\,\text{kN}.$$

Design C_1

Using maximum concrete stress of $0.55 f'_c$, the area of concrete required is 1212mm^2. For a width of 130mm, the thickness of the compression strut is 9.3mm. This is small enough to affect the geometry of the chosen mechanism.

Design T_1

Force = 20 / sin 47.4 = 27.2 kN, therefore $A_{s,req} = 90.7\text{mm}^2$

Anchorage force for the 2-D10 bars is $C_2 = 18.4$ kN.

$$\frac{A_{s,req}}{A_{s,prvd}} = \frac{18.4}{47.1} = 0.39$$

$$\therefore\ L_{dh} = 0.24 \times 0.39 \times 1.0 \times 0.8 \times \frac{300 \times 10}{\sqrt{30}} = 41\,\text{mm}$$ OK as 45mm provided.

Anchorage for T_1 bars at top of half hinge:

$$L_{db} = \frac{0.5 \times 0.77 \times 300 \times 10}{\sqrt{30}} = 159 \text{ mm}$$

Design C_3

Force = 28.3 kN. Compression area at $0.55 f'_c$ is 1715mm^2. For beam width of 130mm, the width of compression strut is 13mm. OK.

Strut and Tie Model 2

Compression load to be carried on model 2 is: 31.5 – 20.0 = 11.5 kN. Assume D_1, T_3, C_4 meet at the centroid of bottom longitudinal bars, 40mm, and centroid of the top bars is 23mm below the top surface. The resultant of the applied forces is inclined so that the centroid meets the top steel centroid at 85 + 13mm from the face of the half hinge. Resultant forces are shown on the sketch of the model below.

T_2 = 11.5 kN
T_3 = 22.7 kN
C_4 = 16.4 kN
D_1 = 20.0 kN
D_2 = 16.3 kN
D_3 = 16.3 kN
S_2 = 11.5 kN

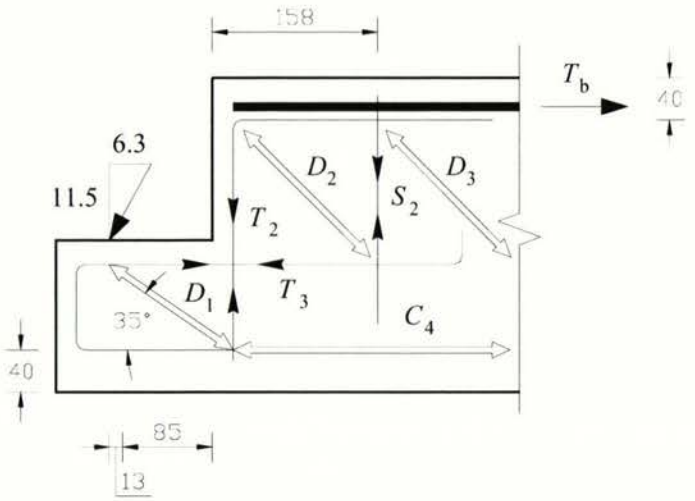

Design for T_3

Force = 22.7 kN. $A_{s,req}$ = 22.7 / 0.3 = 76 mm^2.From previous design, 2-D10 provided. Therefore, $A_{s,prvd}$ = 157 mm^2. OK.

Anchorage for T_3 reinforcement:

$$L_{dh} = 0.24 \times \frac{76}{157} \times 1.0 \times \frac{300 \times 10}{\sqrt{30}} = 64 \text{ mm} < 8 d_b = 80 \text{ mm}$$

Design for D_1

Force = 20.0 kN. At $0.55 f'_c$ the compression strut thickness is 9.3mm. OK.

Design for T_2

Force = 11.5 kN. Provide 2-D10 with 47.1 kN at yield. These bars are bent round the top corner and run parallel to the 3-D12 longitudinal bars. The tension force is carried round the corner and the development length for the bars is:

$$L_{db} = \frac{0.5 \times 1.3 \times 300}{\sqrt{30}} \times 10 = 356 \text{ mm}$$

However this may be reduced as the required force is substantially less than yield strength of bars provided.

Design for D_2

Force = 16.3 kN. At $0.45 f'_c$ the compression strut thickness is 9.3mm. OK.

Anchorage for T_3 bars must extend beyond the intersection with the compression strut of D_2. Provide anchorage length of 140mm.

Design for S_2

Force = 11.5 kN. Previously designed for S_1 with 3 leg R6 stirrups @ 100 c/c providing 69.3 kN. OK.

The final reinforcing layout is shown by Figure 3.4 in *Chapter 3*.

A1.5 Calculation of design lateral strength of Unit 1

Overall depth of beam, D = 300mm, width of beam, b_w = 130mm,
depth from extreme compression fibre to centroid of tension steel, d = 272.5mm
distance between top and bottom steel reinforcement, d-d' = 245mm
average reinforcing yield stress, f_y = 309.3MPa,
average concrete compression strength, f_c' = 30.8MPa

tension in steel reinforcing, $T_s = 3 \times \frac{\pi 12^2}{4} \times 309.3 \times 10^{-3} = 104.95 \text{ kN}$

depth of compression stress block, $a = \dfrac{104.9 \times 10^3}{0.85 \times 30.8 \times 130} = 30.8\,\text{mm}$

beam sectional flexural strength, $M_n = 104.9 \times \left(272.5 - \dfrac{30.8}{2} \right) / 10^{-3} = 26.95\,\text{kNm}$

beam flexural overstrength, $M_o = 1.15 \times 104.9 \times 0.245 = 29.6\,\text{kNm}$

The theoretical lateral strength of the frame is calculated by extrapolating the beam sectional flexural strength at column face (26.95kNm) to the column centreline, which equals 31.62kNm. Therefore the sum of joint bending moment is 31.62×4=126.48kNm. The total lateral strength is given dividing the sum of joint bending moment by the distance between the load applied at the top and the bottom of the columns:

$$\frac{126.48}{1.2} = 105.4\,\text{kN}$$

A1.6 Calculation of theoretical lateral strength of Unit 2

For calculation of beam flexural strength in negative bending, the code recommended flange width of 443mm from the beam centreline. Within this width there were 6/3.125mm wires, 2/D10 (not anchored at joint B) over a prestressed rib (see *Chapter 5,* Figure 5.14).

from beam reinforcement, $T_{beam} = 3 \times \dfrac{\pi \times 12^2}{4} \times \dfrac{309.3}{10^3} = 104.95\,\text{kN}$

from mesh wire, $T_{wire} = 6 \times \dfrac{\pi \times 3.125^2}{4} \times \dfrac{408}{10^3} = 18.8\,\text{kN}$

from 2/D10 along top of rib, $T_{D10} = 2 \times \dfrac{\pi \times 10^2}{4} \times \dfrac{313.3}{10^3} = 49.2\,\text{kN}$

Eccentric force due to prestressed rib

Assume rib compression strength, $f_c{}'_{rib}$ = 50MPa,

pretension strands A_{sp} = 225.2mm2, stressed initially to f_{sp} = 980MPa,

by trial and error approach, say eccentric tension force due to rib T_{slab} = 68kN,

say depth of in compression, c = 61mm

effective stress in strands, $f_{sp}{}' = 980 - 200000 \times \left(\dfrac{61 - 52}{61} \right) \times 0.003 = 891.48\,\text{MPa}$

therefore tension force in strands, $T_{sp} = 225.2 \times 891.48 \times 10^{-3} = 200.76\text{kN}$

compression force, $C = T_{slab} + T_{sp} = 268.76\text{kN}$,

therefore, $a = \dfrac{268.76 \times 10^3}{0.85 \times 50 \times 150} = 42.16\,\text{mm}$,

therefore, $c = \dfrac{42.16}{0.69} = 61.1\,\text{mm}$, compared to 61mm guess above, OK.

Floor self weight and imposed dead load is 2.25kN/m, span of floor 3.125m.

Bending moment due to gravity is given by:

$$\text{Adjacent to joint 'A'} = 2.25 \times \left(\frac{3.125 \times 1.817}{2} - \frac{1.817^2}{2} \right) = 2.67\,\text{kNm}$$

$$\text{Adjacent to joint 'C'} = 2.25 \times \left(\frac{3.125 \times 2.117}{2} - \frac{2.117^2}{2} \right) = 2.40\,\text{kNm}$$

Taking moments about centre of rectangular compression stress block ($a/2$) adjacent to joint 'A':

$$T_{slab} \times \left(165 - \frac{42.16}{2} - 20 \right) / 10^3 - 2.67 - 200.76 \times \left(52 - \frac{42.16}{2} \right) / 10^3 = 0$$

Therefore, $T_{slab} = 71.6\text{kN}$, compared to 68kN trial value, OK.

Say $T_{slab}{}^{A} = 72\text{kN}$

Taking moments about centre of rectangular compression stress block ($a/2$) adjacent to joint 'C':

$$T_{slab} \times \left(165 - \frac{42.16}{2} - 20 \right) / 10^3 - 2.4 - 200.76 \times \left(52 - \frac{42.16}{2} \right) / 10^3 = 0$$

Therefore, $T_{slab} = 69.4\text{kN}$, compared to 68kN trial value, OK.

Say $T_{slab}{}^{C} = 69\text{kN}$

<u>Beam flexural strength at Joint 'A'</u>

In positive bending:

Given by steel reinforcement in beam only, M_n = 27.0kNm (neglecting flange as negligible, therefore same as that for Unit 1, see section A1.5 above)

In negative bending neglecting rib strands:

$C = T_{beam} + T_{wire} + T_{D10} = 172.95\text{kN}$, $a = (172.95 \times 10^3)/0.85 \times 32.5 \times 130 = 48.2\text{mm}$

$M_n = 104.95 \times (272.5 - 48.2/2)/10^3 + (18.8 + 49.2) \times (280 - 48.2/2)/10^3 = 43.5\text{kNm}$

In negative bending including rib strands:

$C = T_{beam} + T_{wire} + T_{D10} + T_{slab} = 244.95\text{kN}$,

$a = (244.95 \times 10^3)/0.85 \times 32.5 \times 130 = 68.2\text{mm}$

$M_n = 104.95 \times (272.5-68.2/2)/10^3 + (18.8+49.2+72) \times (280-68.2/2)/10^3 = 59.4\text{kNm}$

Beam flexural strength at Joint 'C'

In positive bending: as per joint 'A' above

In negative bending neglecting rib strands: as per joint 'A' above

In negative bending including rib strands:

$C = T_{beam} + T_{wire} + T_{D10} + T_{slab} = 241.95\text{kN}$,

$a = (241.95 \times 10^3)/0.85 \times 32.5 \times 130 = 67.4\text{mm}$

$M_n = 104.95 \times (272.5-67.4/2)/10^3 + (18.8+49.2+69) \times (280-67.4/2)/10^3 = 58.8\text{kNm}$

Beam flexural strength at Joint 'B'

In positive bending: as per joint 'A' above

In negative bending, rib and 2/D10 not effectively anchored, therefore to be ignored:

$C = T_{beam} + T_{wire} = 123.75\text{kN}$,

$a = (123.75 \times 10^3)/0.85 \times 32.5 \times 130 = 34.5\text{mm}$

$M_n = 104.95 \times (272.5-34.5/2)/10^3 + 18.8 \times (280-34.5/2)/10^3 = 31.7\text{kNm}$

The bending moment at the centreline of the beams and columns can be extrapolated from the values calculated above. These are summarised below:

	beam flexural strength at column centreline (kNm)					
	Joint 'A'		Joint 'B'		Joint 'C'	
	-ve bending	+ve bending	-ve bending	+ve bending	-ve bending	+ve bending
excluding strands	-50	31	-36	32	-50	32
including strands	-67	31	-36	34	-67	32

The total lateral strength is given dividing the sum of joint bending moment by the distance between the load applied at the top and the bottom of the columns:

Neglecting prestressed strands: 231/1.23 = 188kN

Including prestressed strands: 267/1.23 = 217kN

A1.7 Example of calculating forces acting in deep beam mechanism

An example of calculating the forces acting at ±2.5% drift displacement to increase the flexural strength of the beam in negative bending at the central joint, joint 'B', is set out below. This action (deep beam action) is described in section 8.4.2 of *Chapter 8*.

The bending moment acting at joint 'B' was determined from the forces applied at the top and the bottom of the columns. From the strains measured at the column faces, the tension force in the beam reinforcement, T_{beam}, can be estimated with reasonable accuracy (see section 8.4.1). Knowing the negative bending moment in the beam (see section 8.4.1), the axial load, N, from the out of balance jack forces, and the force in the beam reinforcement, T_{beam}, the equivalent tension force in the slab, T_{slab}, can be calculated.

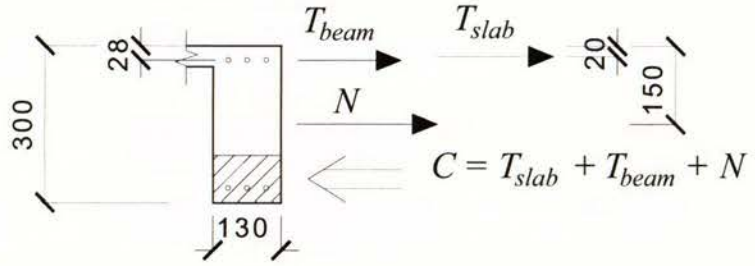

Forces in Beam

At +2.5% drift displacement:

M_{beam} = 93kNm, N = 10kN, T_{beam} = 121kN, f_c' = 32.5MPa, T_{slab} = 300kN

At –2.5% drift displacement:

M_{beam} = 81kNm, N = 15kN, T_{beam} = 111kN, f_c' = 32.5MPa, T_{slab} = 240kN

The forces sustained by the reinforcement crossing the central cracks, d – e and f – g (see Figure 8.15), were assessed from crack width measurements made during the test and the stress strain response of the reinforcement bars. There were two different types of reinforcement involved. The first consisted of a welded mesh of ductile plain 3.125mm bars spaced at 75mm centres. The second type of reinforcement consisted of two 4.0mm diameter deformed bar located directly above each precast rib unit. The

strains in the reinforcement at the cracks were assessed from the crack widths by assuming effective lengths of 75mm for the 3.125mm mesh bars and 120mm for the 4.0mm bars. The change in strain between the zero load stage and peak displacement was used together with the monotonic stress strain response of the reinforcement to find the forces, as illustrated in Figure 8.13. As a majority of the predicted strains were well above the yield point, the strain levels did not have to be known accurately to obtain reasonable estimates of the forces crossing the cracks at the different load stages. The figures below shows the forces obtained along the length of the crack between the floor and the central transverse beam:

At +2.5% drift displacement:

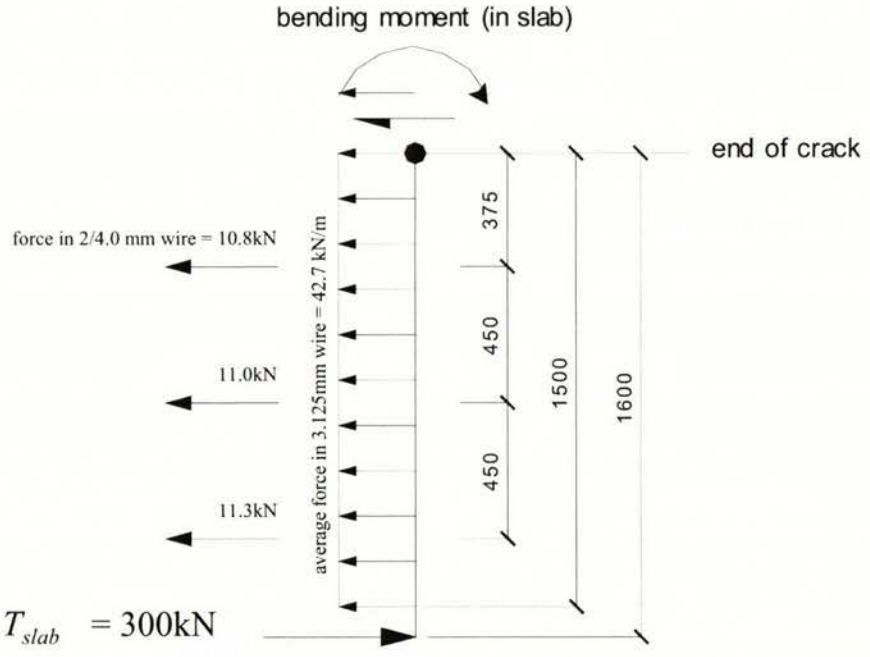

Therefore, the bending moment in the slab is given by:

$$(300\times1.6)-(11.3\times1.275)-(11\times0.825)-(10.8\times0.375)-\left(\frac{42.7\times1.5^2}{2}\right)=404.4\,\text{kNm}$$

The sum of reinforcement forces crossing the crack is:

$(42.7\times1.5) + 10.8 + 11.0 + 11.3 = 97.2\text{kN}$

At –2.5% drift displacement:

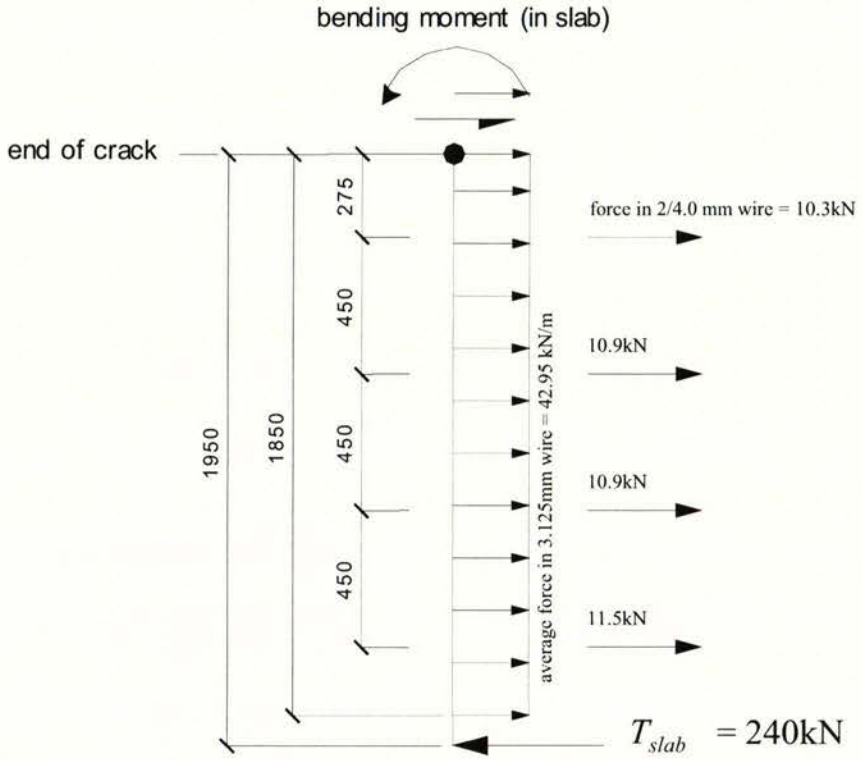

Therefore, the bending moment in the slab is given by:

$$(240\times1.95)-(11.5\times1.625)-(10.9\times1.175)-(10.9\times0.725)-(10.3\times0.275)-\left(\frac{42.95\times1.85^2}{2}\right)$$

= 352 kNm

The sum of reinforcement forces crossing the crack is:

(42.95×1.85) + 11.5 + 10.9 + 10.9 + 10.3 = 123kN

In summary:

drift level	T_{slab} (kN)	T_{beam} ** (kN)	sum of reinforcement forces (kN)	Slab bending moment (kNm)
+2.5%	300	121	97	404
–2.5%	240	111	123	352
(average) ±2.5%	270	116	110	378

The above average values are tabulated in Table 8.3 (*Chapter 8*). From the average forces above, the equivalent tension force, T_{rein}, from the slab reinforcement acting with

the perimeter frame beams (see Figure 8.17), using an average crack length of 1.775m (ie. 1.95m in negative drift displacement and 1.6m in positive drift displacement)is given by:

$$T_{rein} = \frac{(270 \times 1.775) - 378}{1.675} = 60.4\,\text{kN}$$

Appendix 2

Steel Reinforcement Stress-Strain Response

A2.1 Batch A

D12 - 1 to 3 12mm diameter deformed bar used for *longitudinal reinforcement in frame beams.*

HD12 - 1 to 3 12mm diameter deformed bar used for *longitudinal reinforcement in columns.*

R6 - 1 to 3 6mm diameter plain bar used for *transverse reinforcement in beams.*

A2.2 Batch B

WireA - 1 to 3 3.125mm diameter wire used for *mesh reinforcing in topping slab.*

WireB - 1 to 3 4.0mm diameter wire used for *continuity bar between precast rib ends and central transverse beam.*

D10 - 1 to 3 10mm diameter deformed bar used for *starter bars from main beam into floor slab, half-hinge joint and transverse beam.*

A2.3 Batch C

D12 - 1 to 3 12mm diameter deformed bar used for *longitudinal reinforcement in frame beams.*

HD12 - 1 to 3 12mm diameter deformed bar used for *longitudinal reinforcement in columns.*

R6 - 1 to 3 6mm diameter plain bar used for transverse *reinforcement in beams.*

A2.1 Batch A

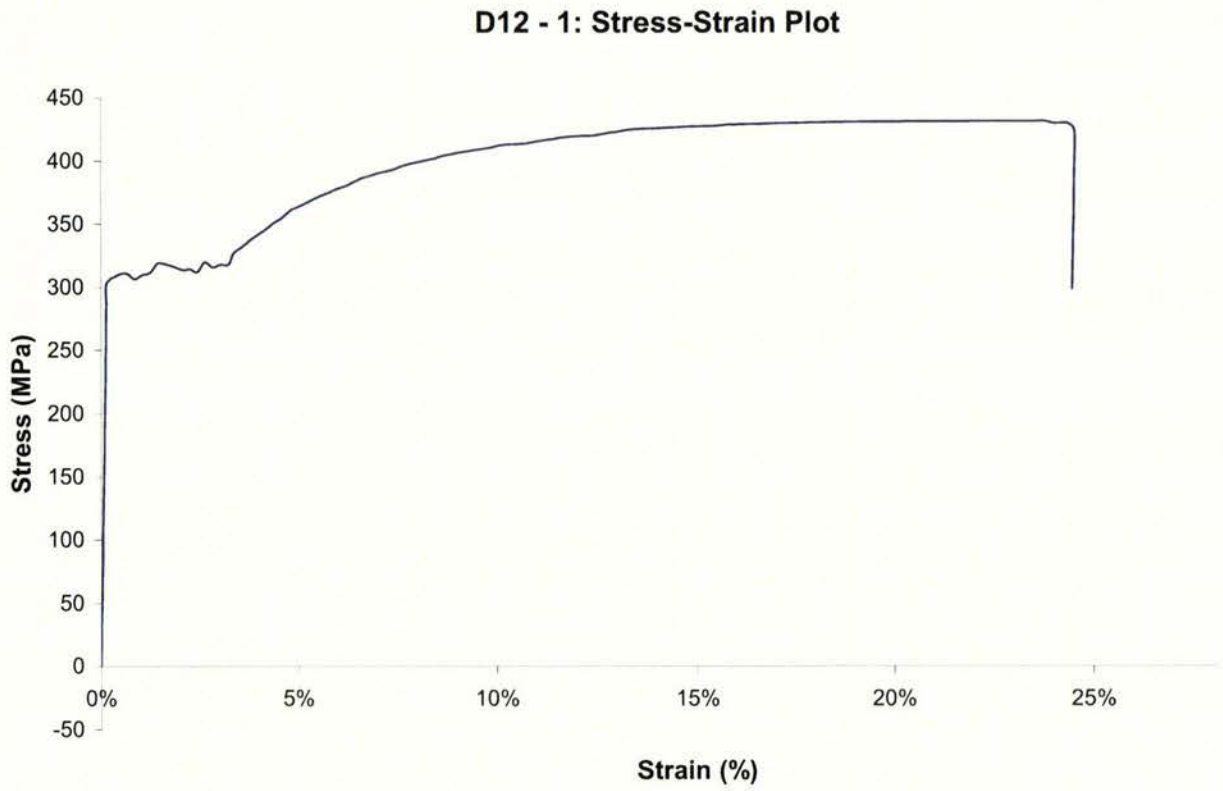
D12 - 1: Stress-Strain Plot
Stress (MPa)
450
400
350
300
250
200
150
100
50
0
-50
0%
5%
10%
15%
20%
25%
Strain (%)

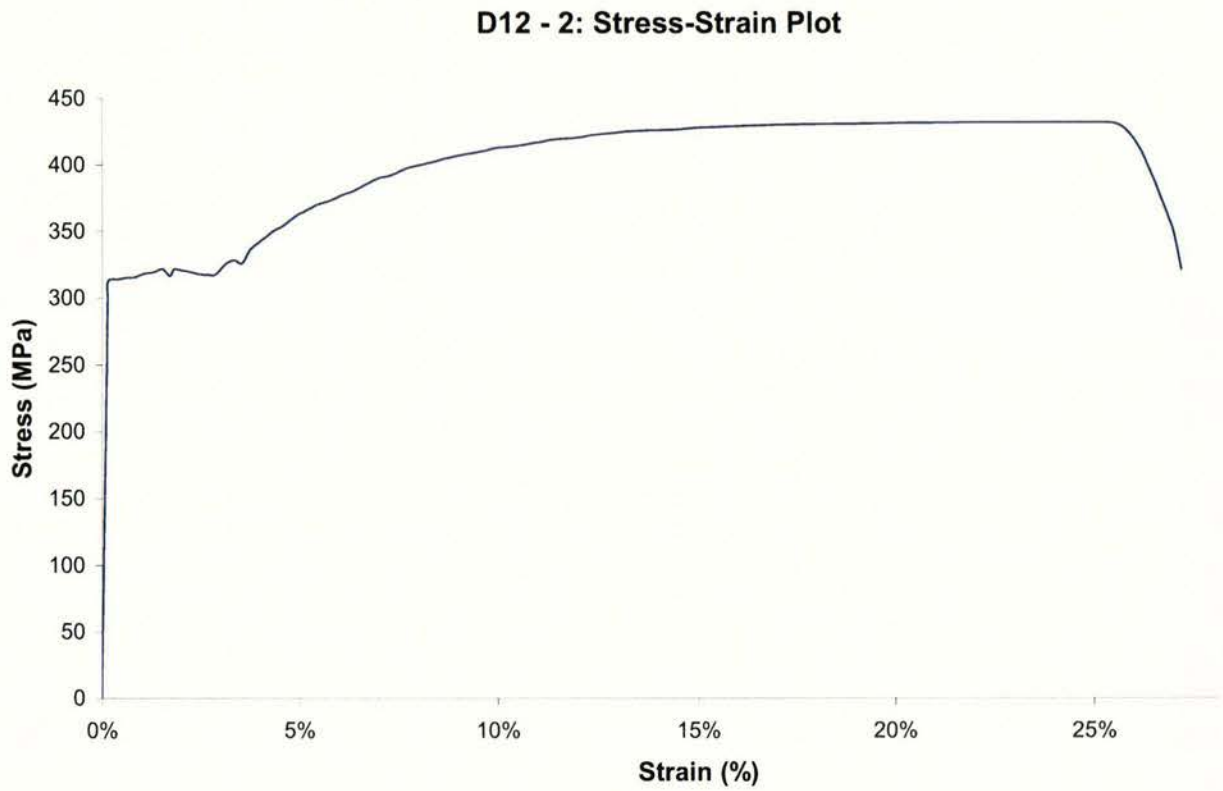
D12 - 2: Stress-Strain Plot
Stress (MPa)
450
400
350
300
250
200
150
100
50
0
0%
5%
10%
15%
20%
25%
Strain (%)

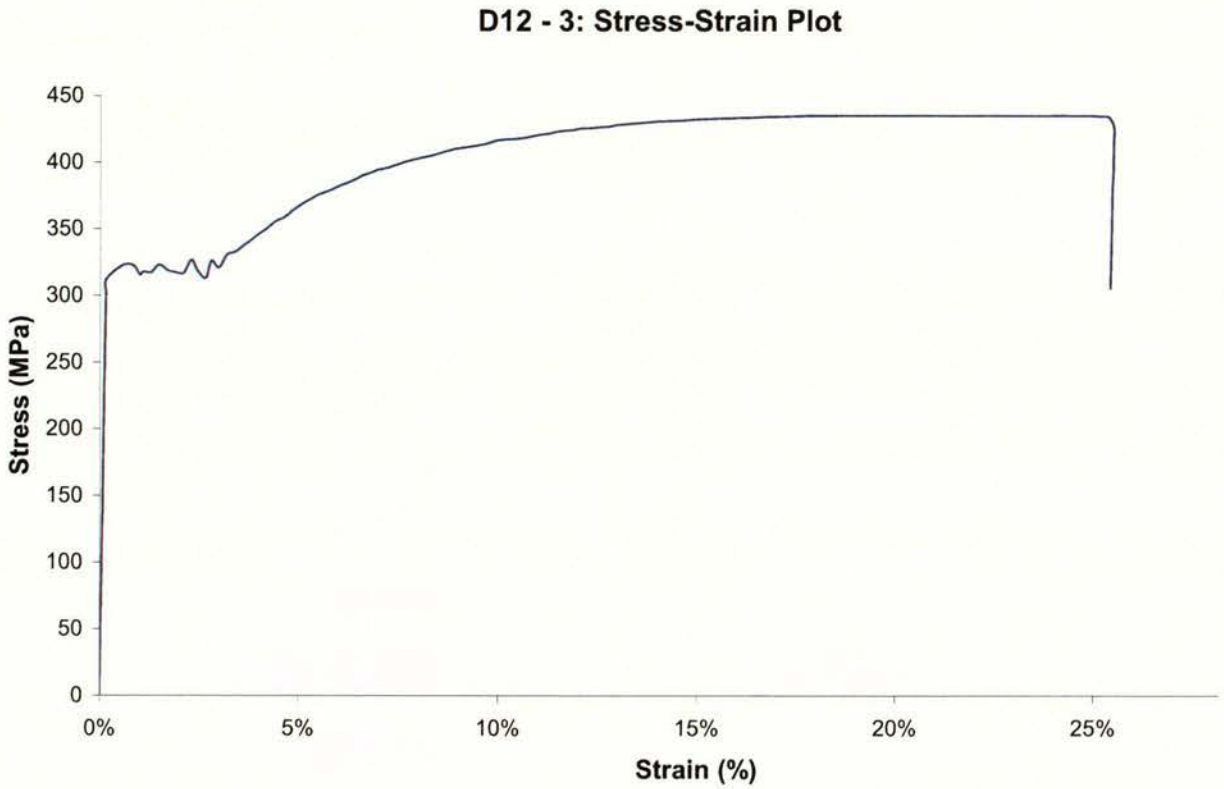
D12 - 3: Stress-Strain Plot
Stress (MPa)
450
400
350
300
250
200
150
100
50
0
0%
5%
10%
15%
20%
25%
Strain (%)

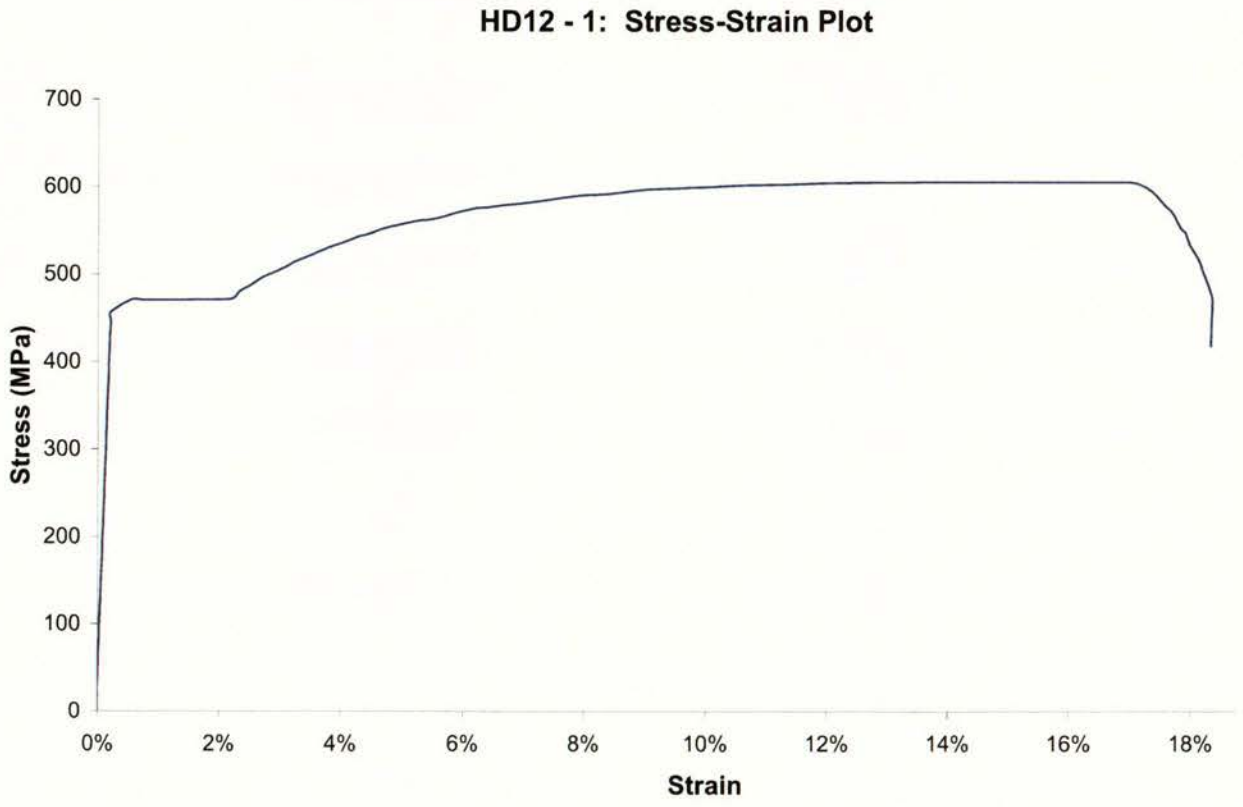
HD12 - 1: Stress-Strain Plot
Stress (MPa)
700
600
500
400
300
200
100
0
0%
2%
4%
6%
8%
10%
12%
14%
16%
18%
Strain

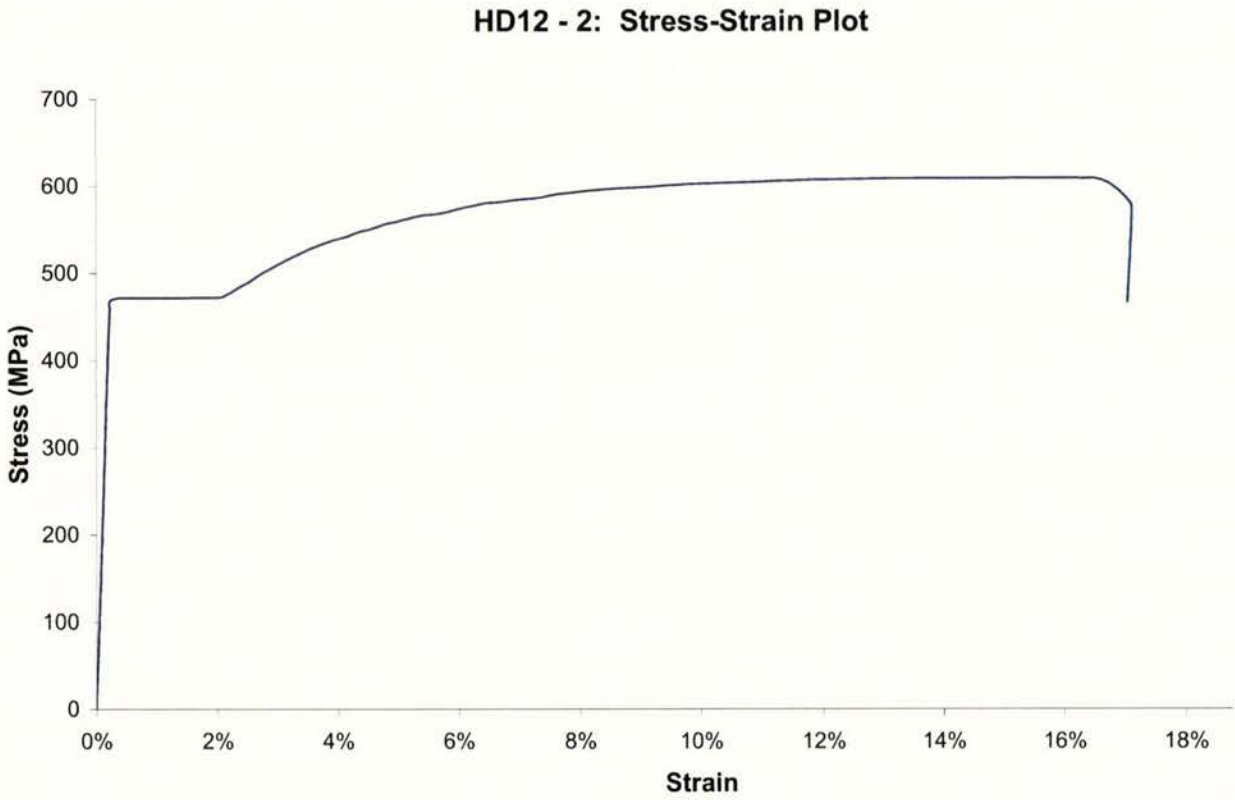
HD12 - 2: Stress-Strain Plot
Stress (MPa)
700
600
500
400
300
200
100
0
0%
2%
4%
6%
8%
10%
12%
14%
16%
18%
Strain

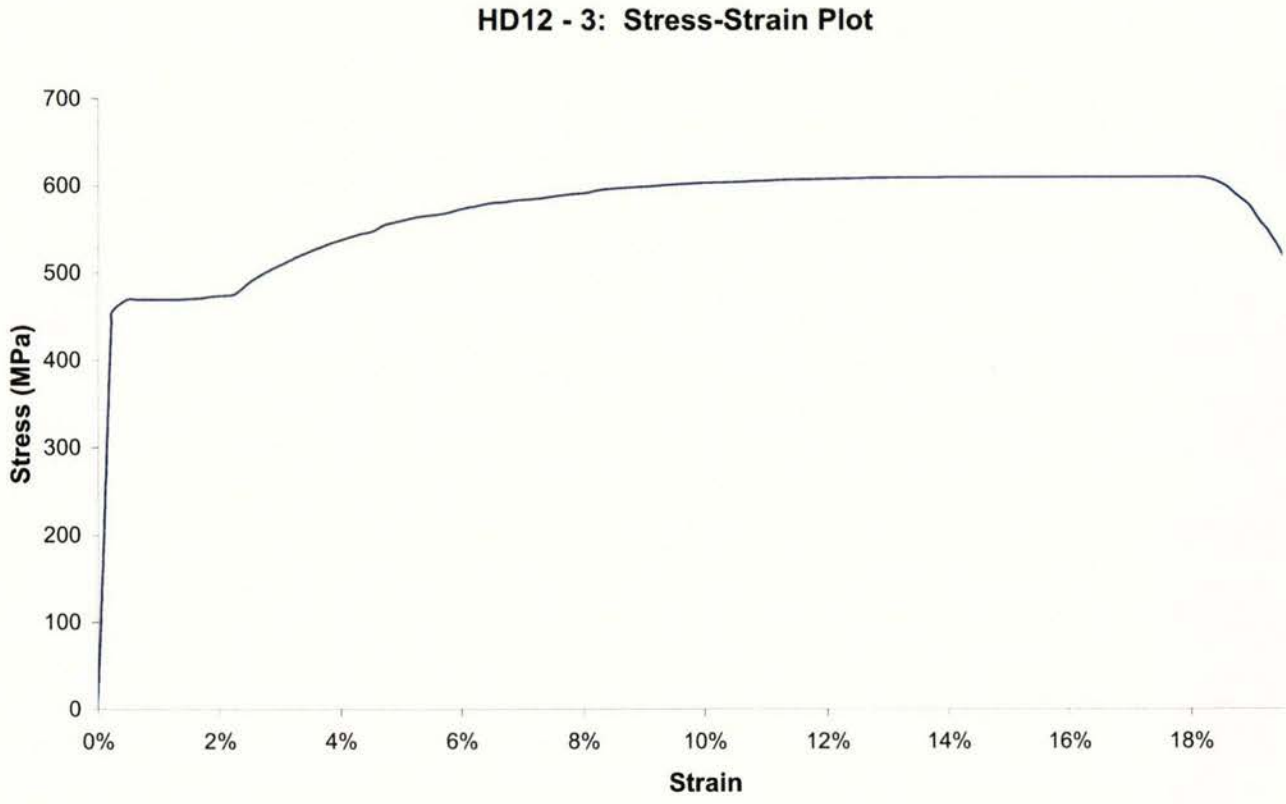
HD12 - 3: Stress-Strain Plot
Stress (MPa)
700
600
500
400
300
200
100
0
0%
2%
4%
6%
8%
10%
12%
14%
16%
18%
Strain

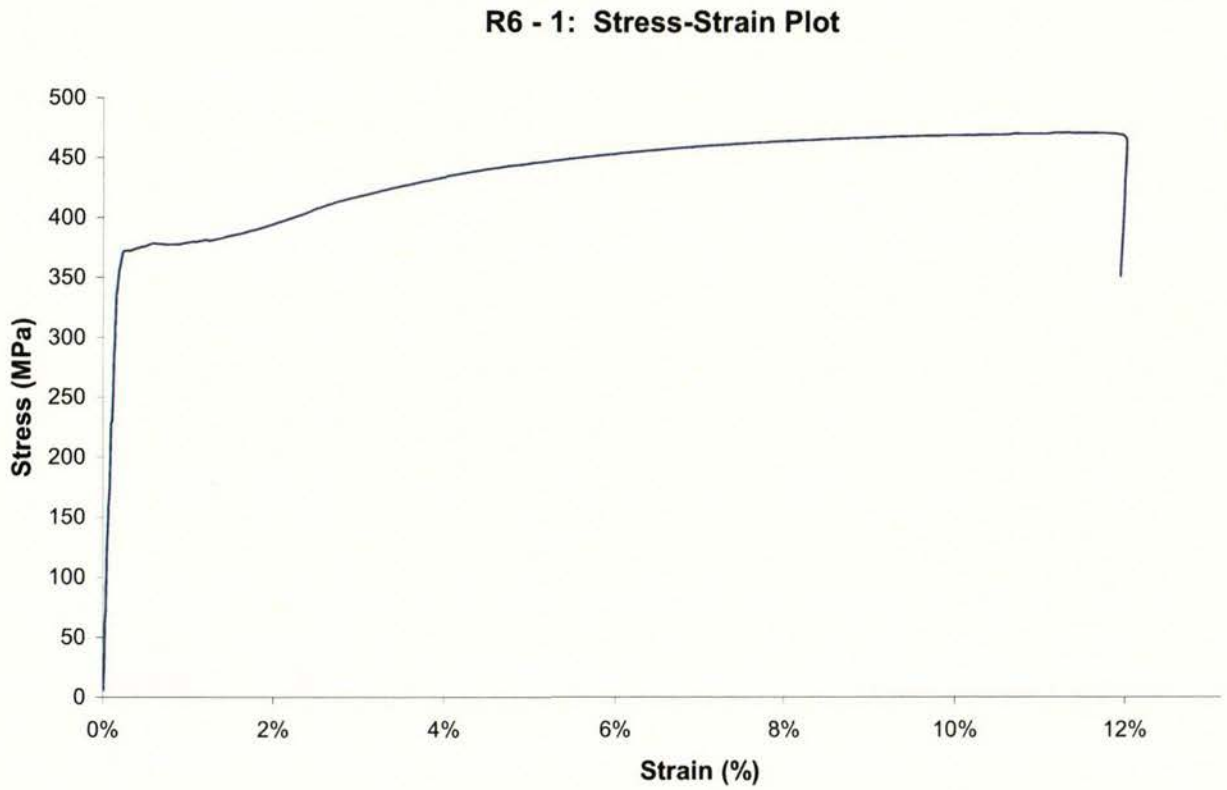
R6 - 1: Stress-Strain Plot
Stress (MPa)
500
450
400
350
300
250
200
150
100
50
0
0%
2%
4%
6%
8%
10%
12%
Strain (%)

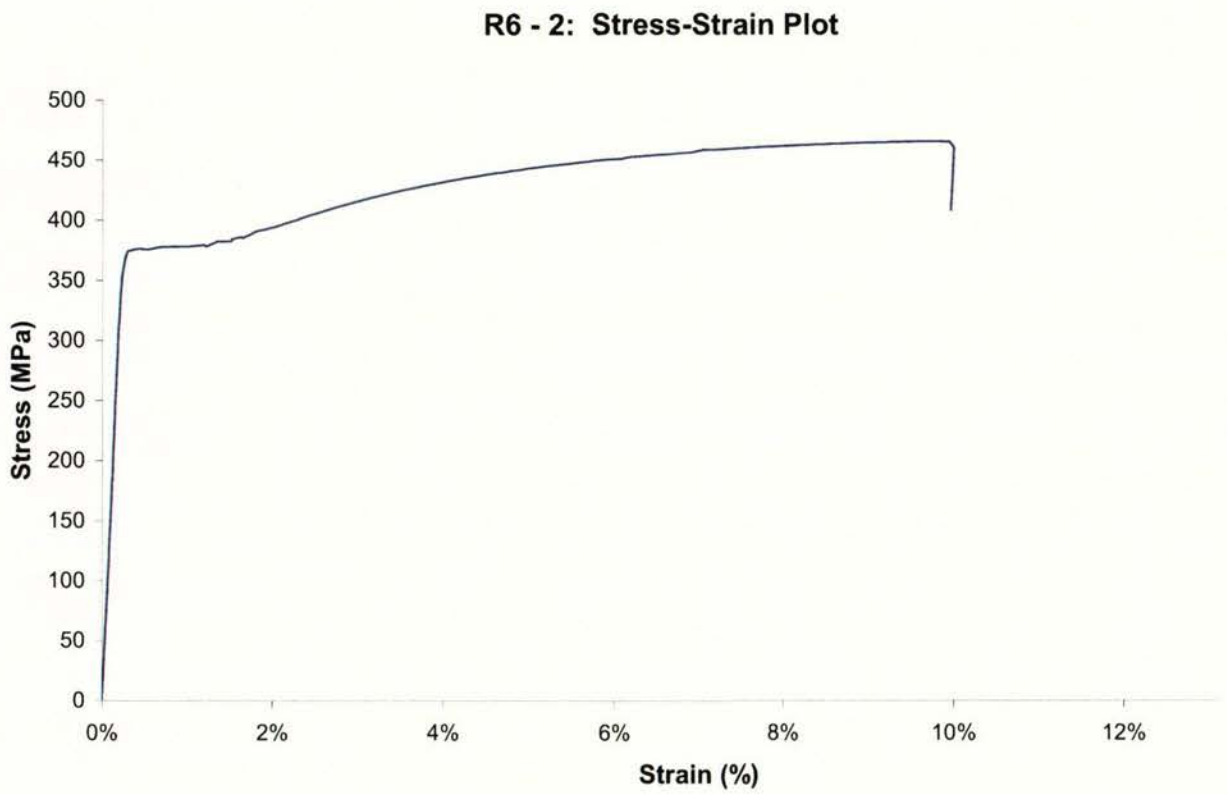
R6 - 2: Stress-Strain Plot
Stress (MPa)
500
450
400
350
300
250
200
150
100
50
0
0%
2%
4%
6%
8%
10%
12%
Strain (%)

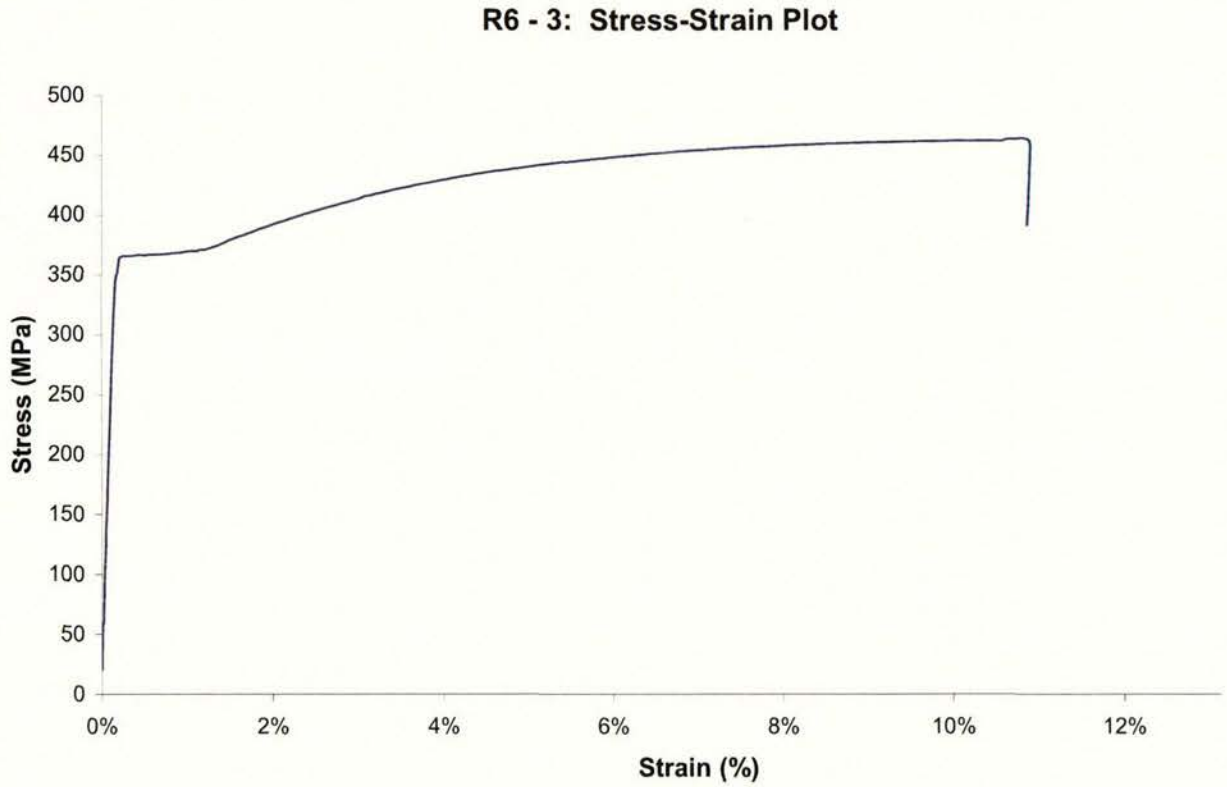
R6 - 3: Stress-Strain Plot
Stress (MPa)
500
450
400
350
300
250
200
150
100
50
0
0%
2%
4%
6%
8%
10%
12%
Strain (%)

A2.2 Batch B

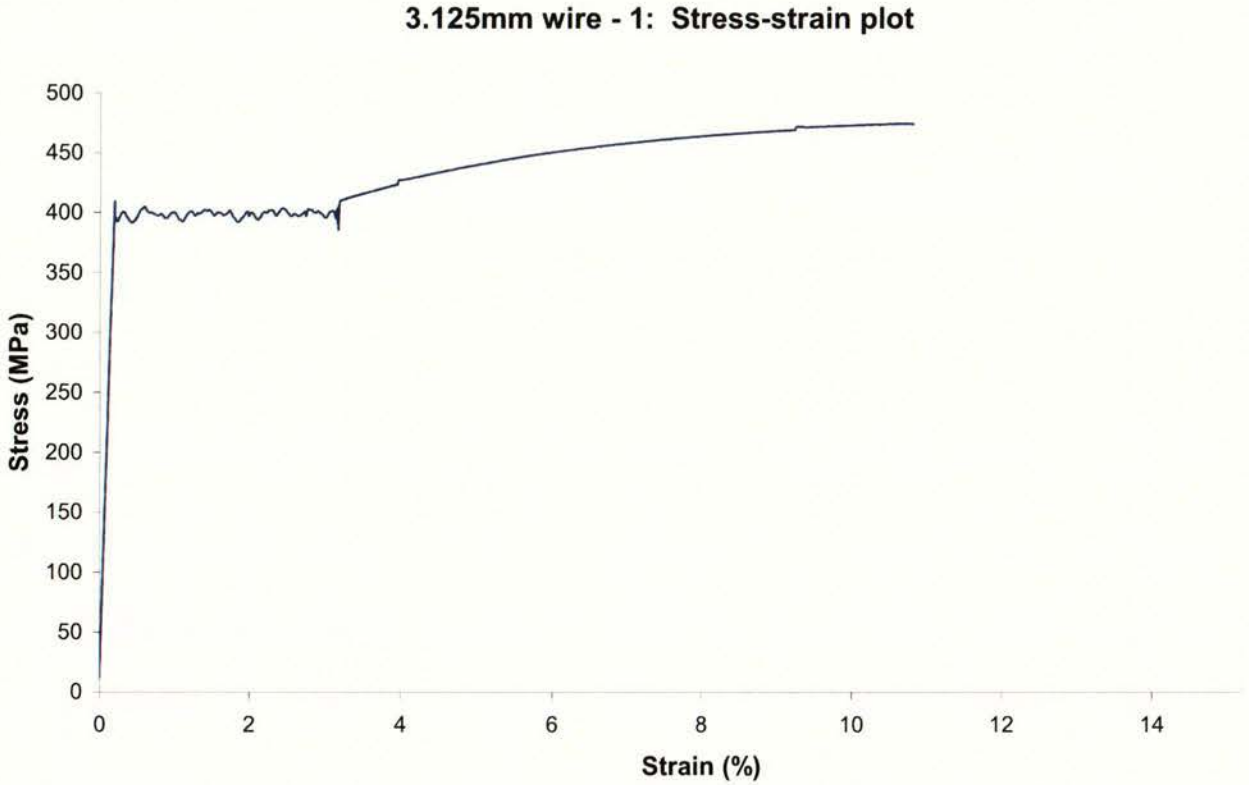
3.125mm wire - 1: Stress-strain plot
Stress (MPa)
500
450
400
350
300
250
200
150
100
50
0
0
2
4
6
8
10
12
14
Strain (%)

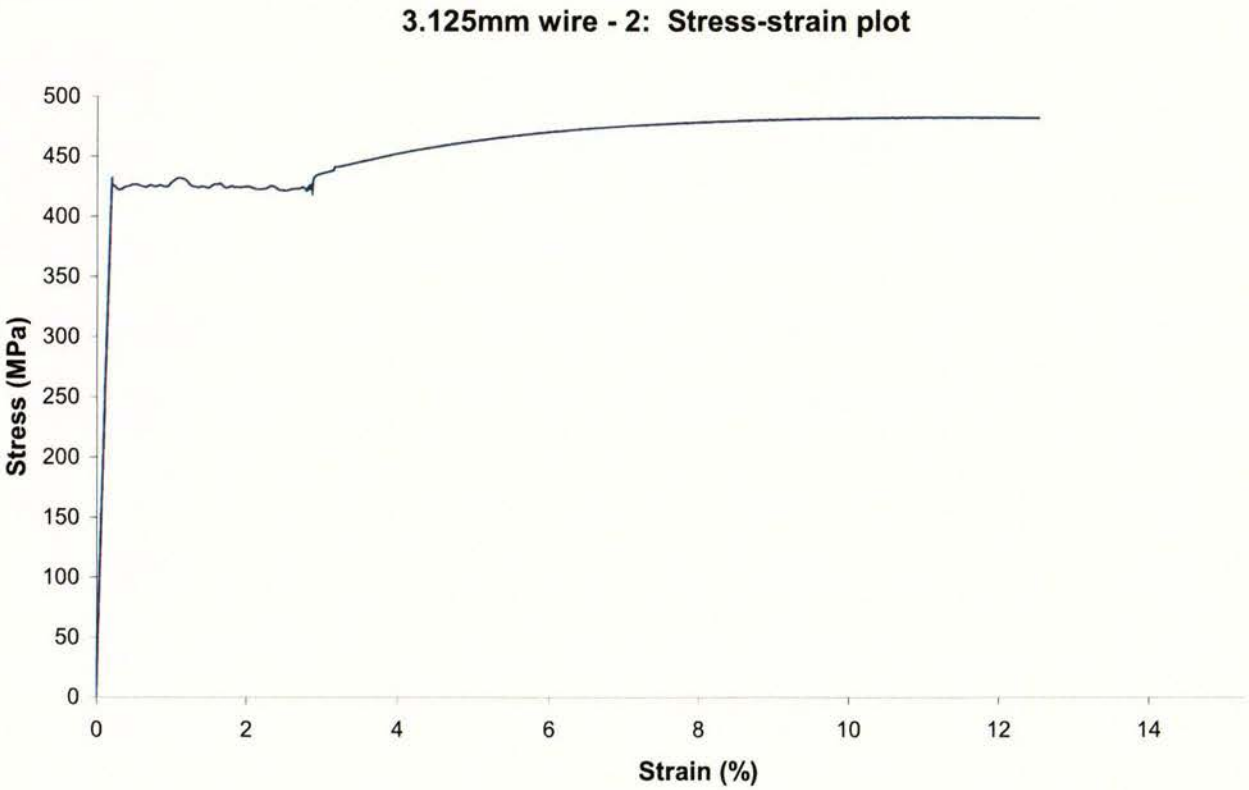
3.125mm wire - 2: Stress-strain plot
Stress (MPa)
500
450
400
350
300
250
200
150
100
50
0
0
2
4
6
8
10
12
14
Strain (%)

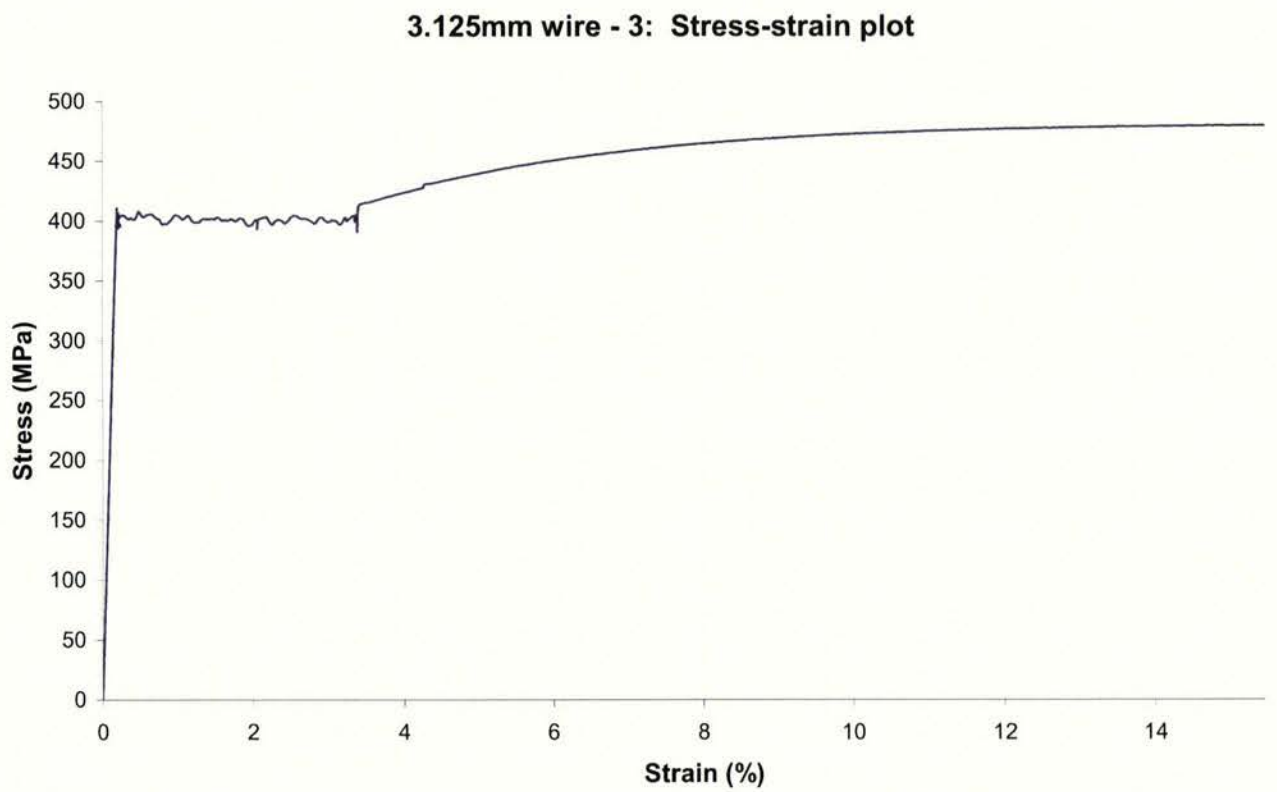
3.125mm wire - 3: Stress-strain plot
Stress (MPa)
500
450
400
350
300
250
200
150
100
50
0
0
2
4
6
8
10
12
14
Strain (%)

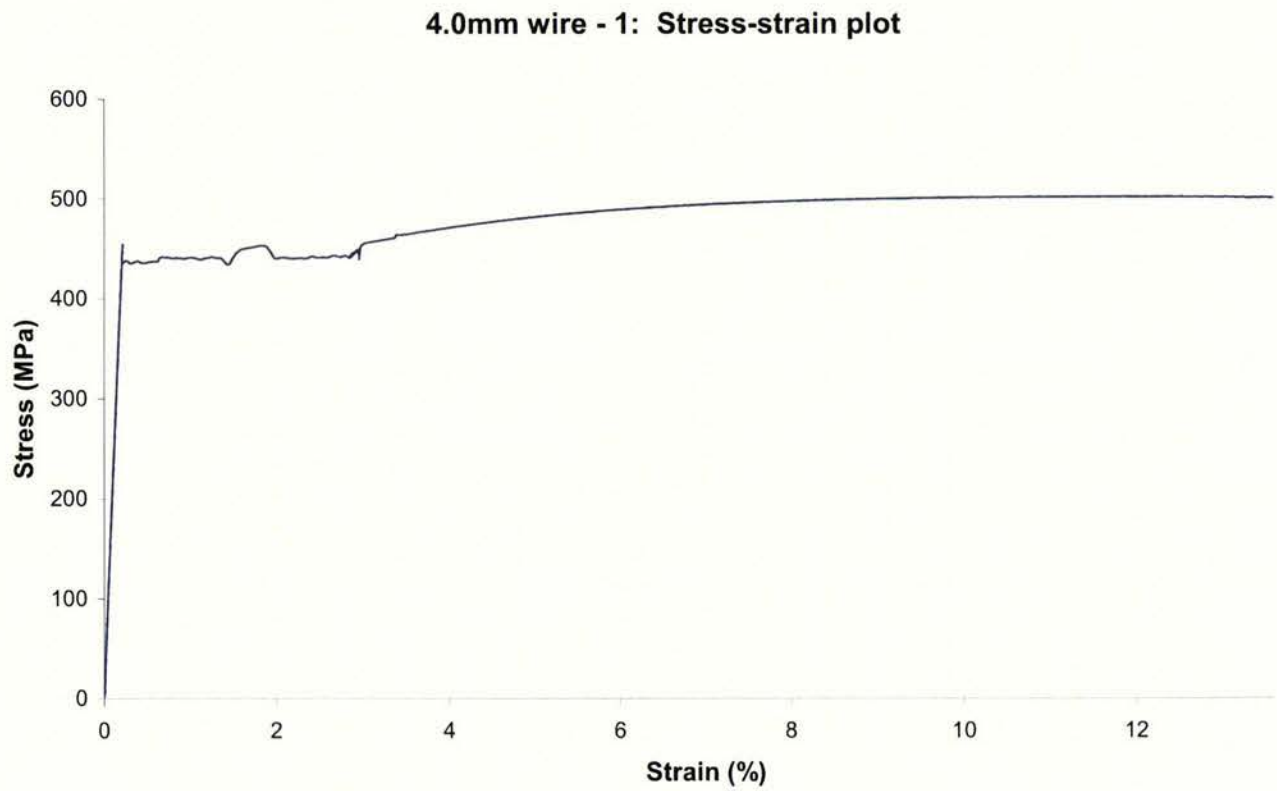
4.0mm wire - 1: Stress-strain plot
Stress (MPa)
600
500
400
300
200
100
0
0
2
4
6
8
10
12
Strain (%)

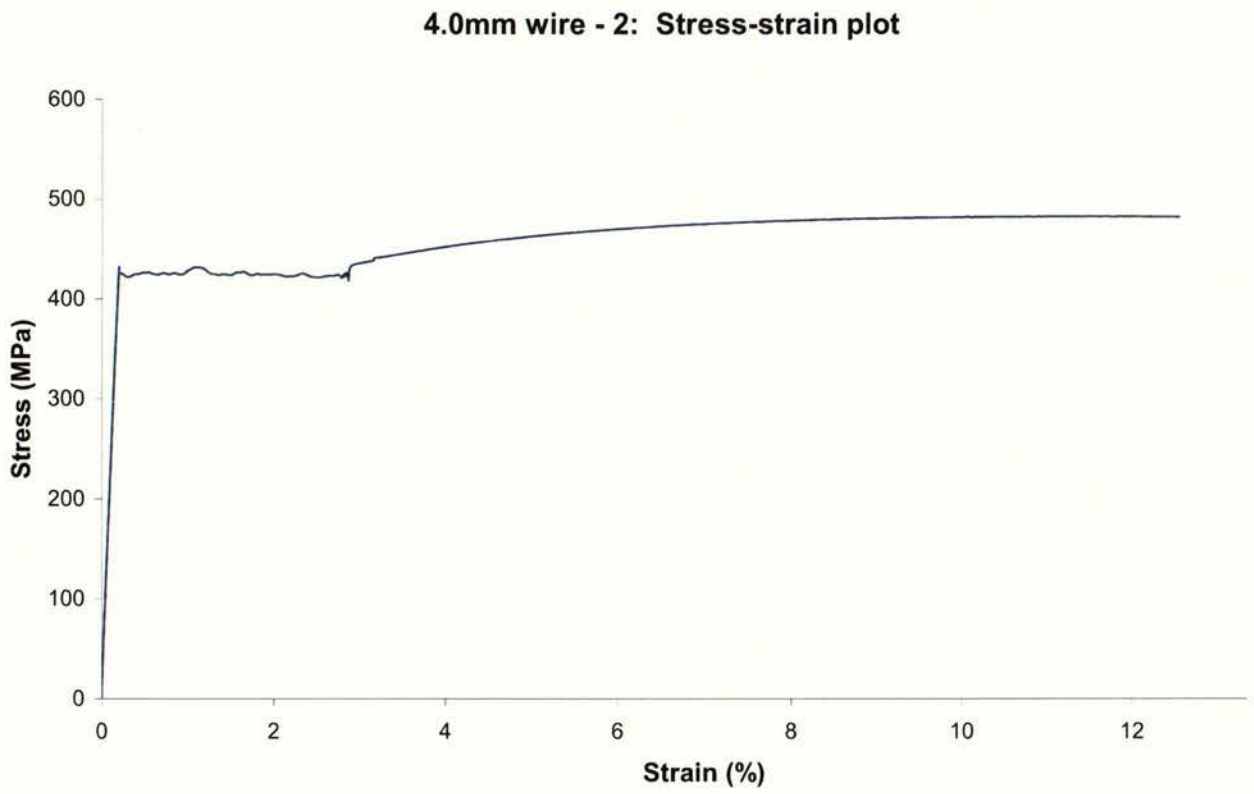
4.0mm wire - 2: Stress-strain plot
Stress (MPa)
600
500
400
300
200
100
0
0
2
4
6
8
10
12
Strain (%)

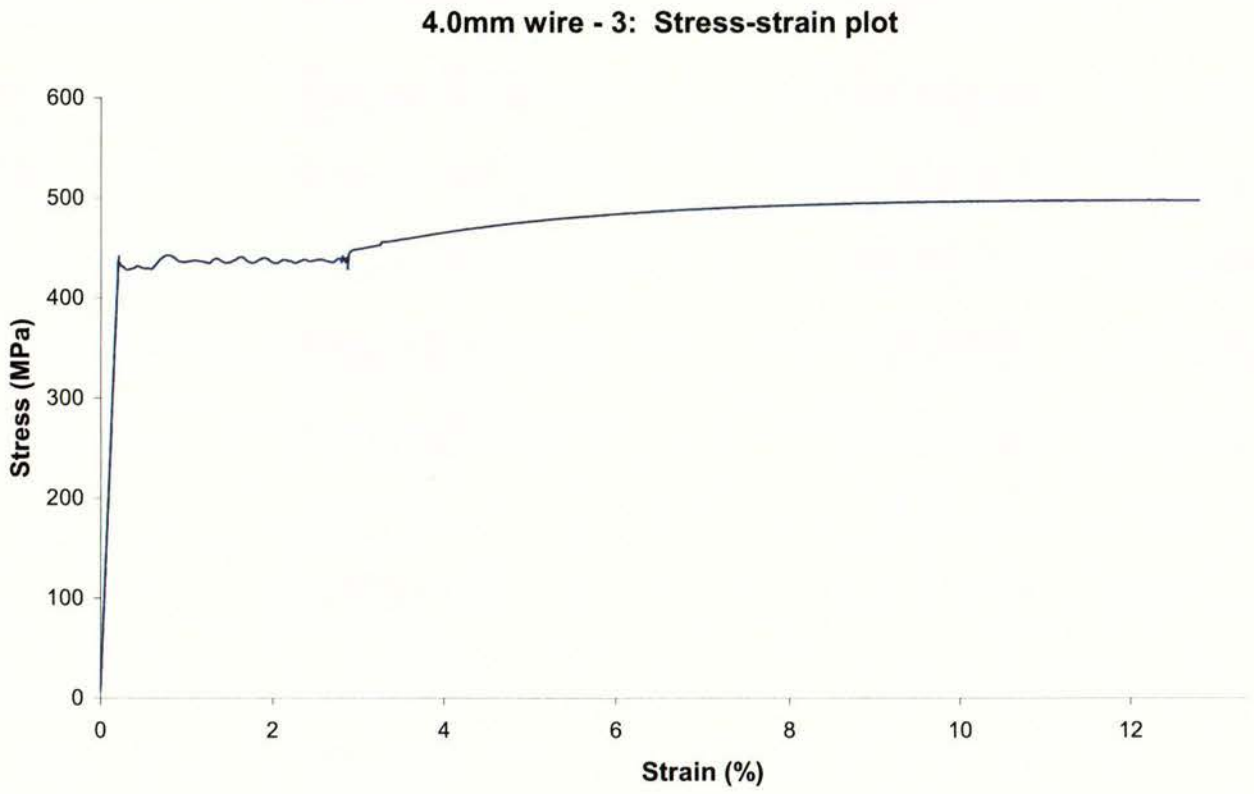
4.0mm wire - 3: Stress-strain plot
Stress (MPa)
600
500
400
300
200
100
0
0
2
4
6
8
10
12
Strain (%)

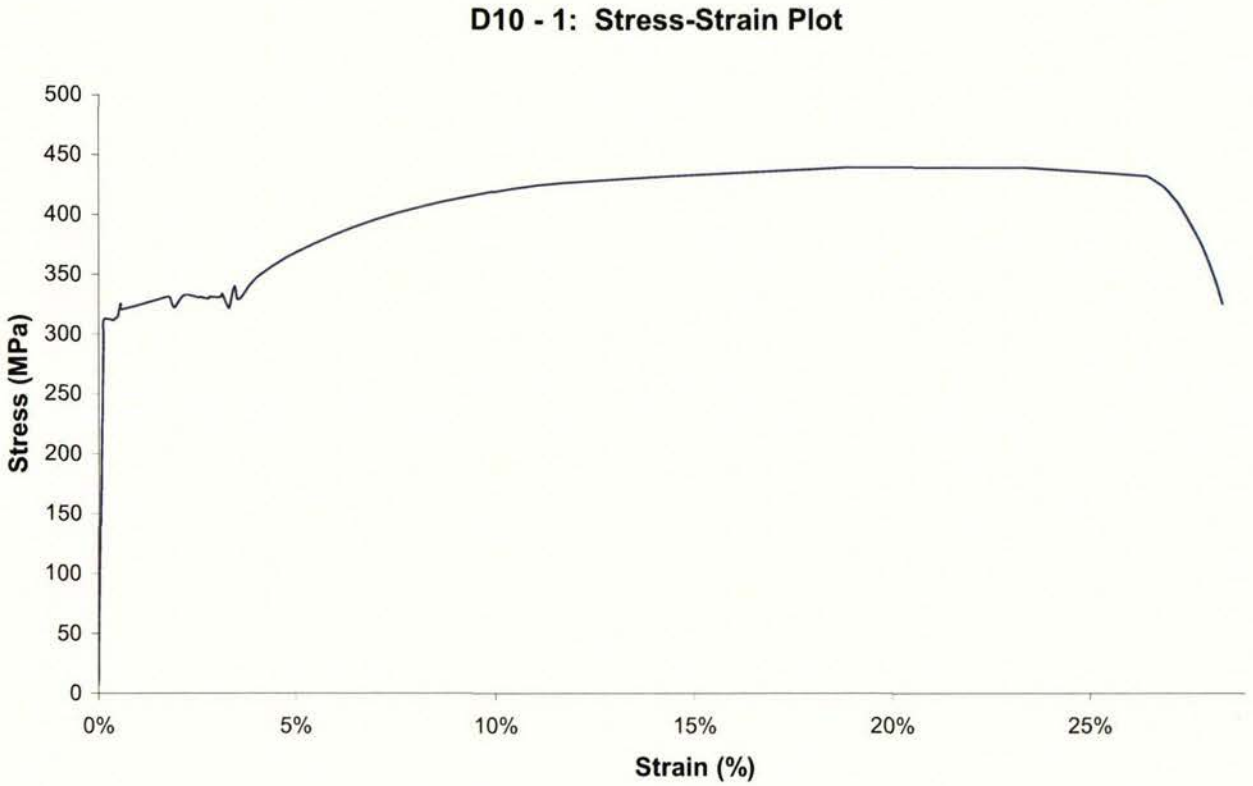
D10 - 1: Stress-Strain Plot
Stress (MPa)
500
450
400
350
300
250
200
150
100
50
0
0%
5%
10%
15%
20%
25%
Strain (%)

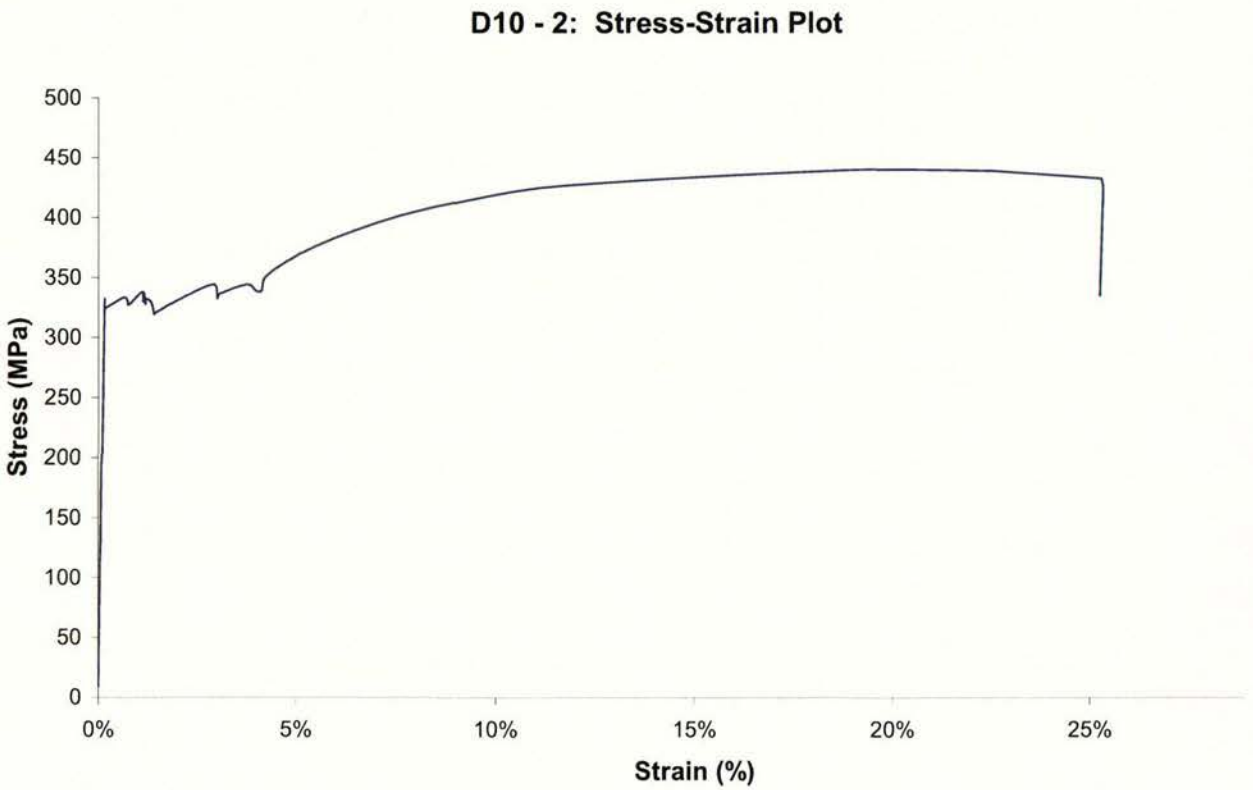
D10 - 2: Stress-Strain Plot
Stress (MPa)
500
450
400
350
300
250
200
150
100
50
0
0%
5%
10%
15%
20%
25%
Strain (%)

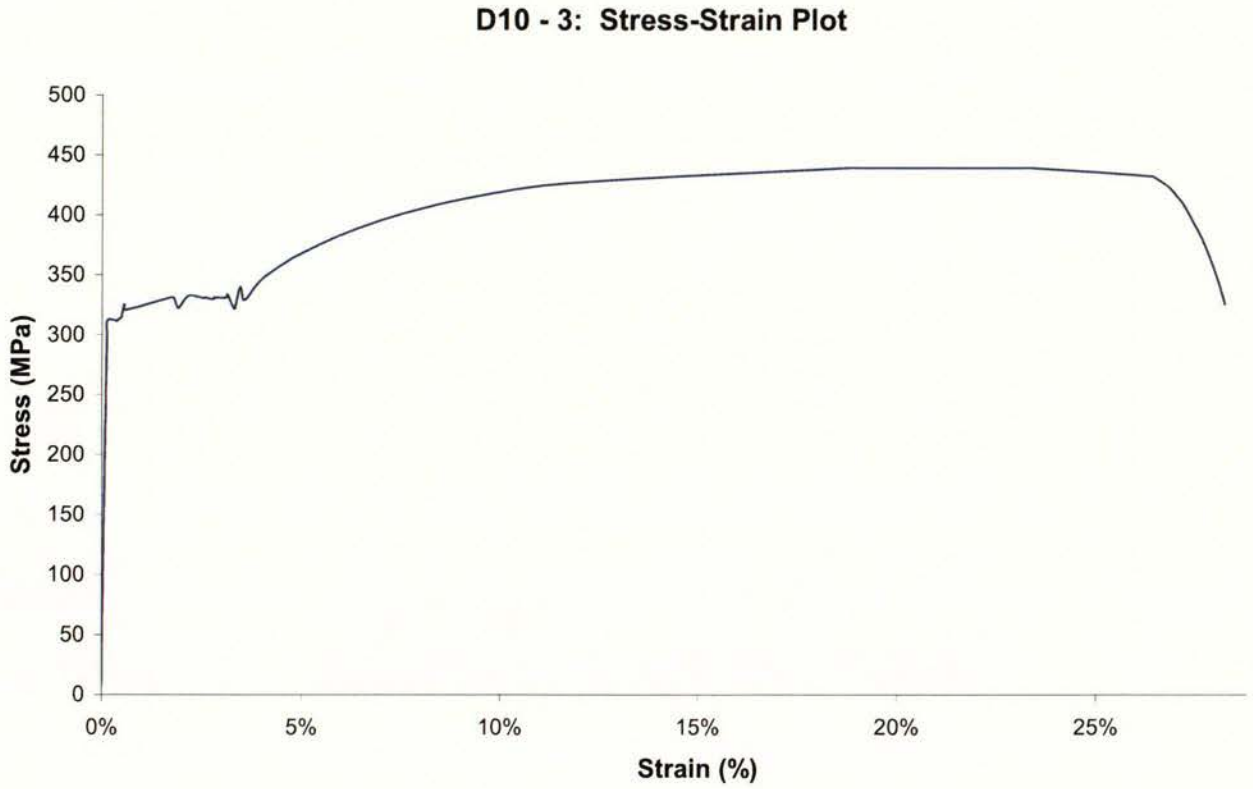
D10 - 3: Stress-Strain Plot
Stress (MPa)
500
450
400
350
300
250
200
150
100
50
0
0%
5%
10%
15%
20%
25%
Strain (%)

A2.3 Batch C

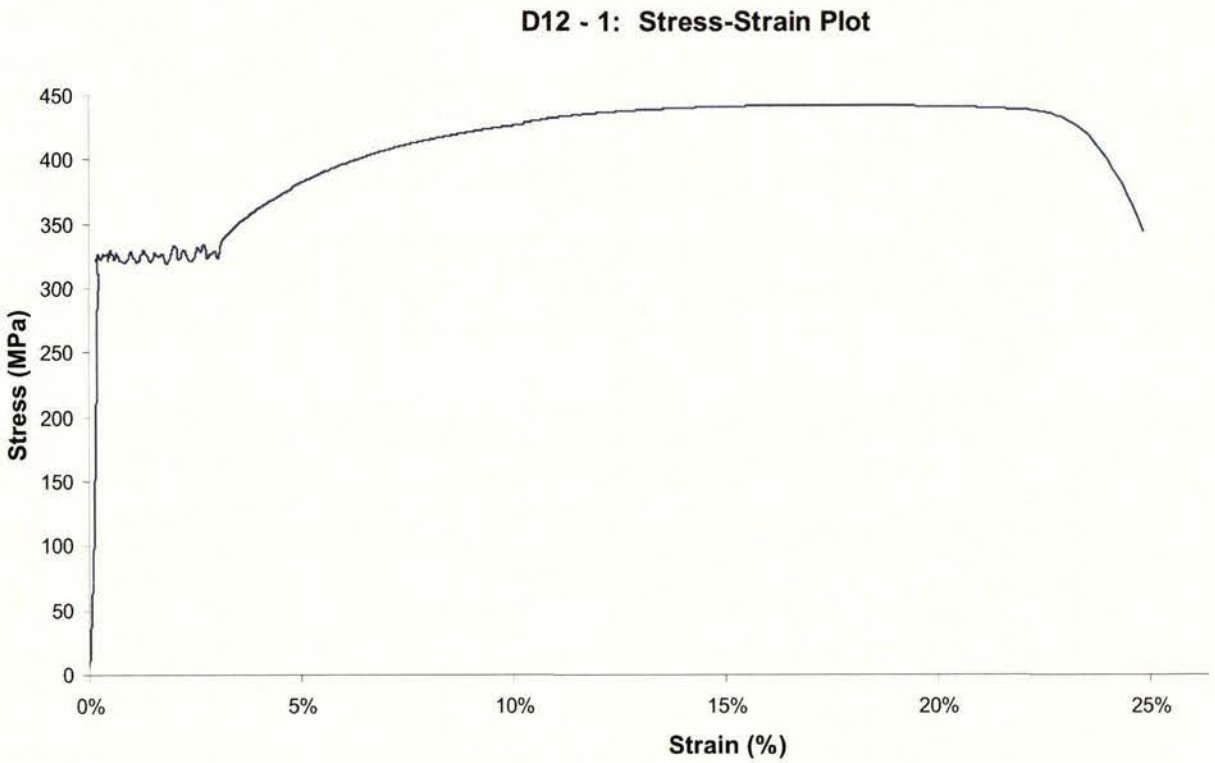
D12 - 1: Stress-Strain Plot
Stress (MPa)
450
400
350
300
250
200
150
100
50
0
0%
5%
10%
15%
20%
25%
Strain (%)

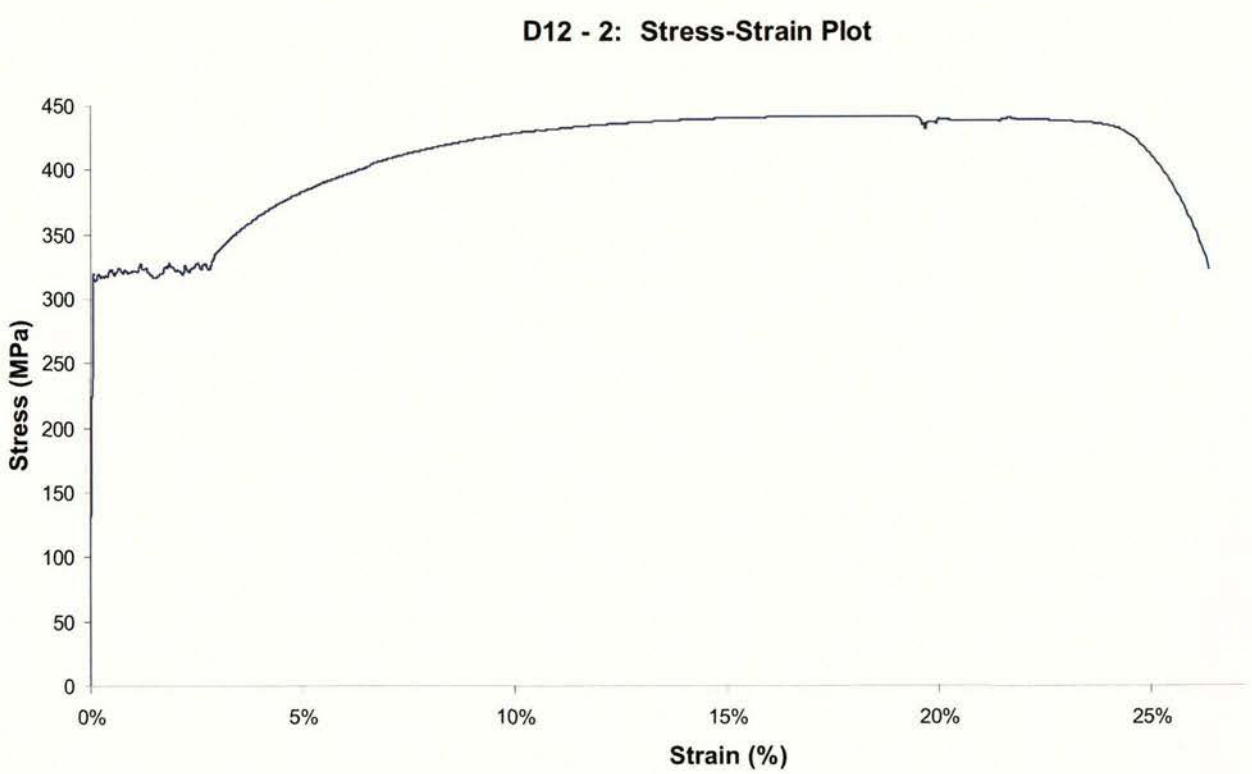
D12 - 2: Stress-Strain Plot
Stress (MPa)
450
400
350
300
250
200
150
100
50
0
0%
5%
10%
15%
20%
25%
Strain (%)

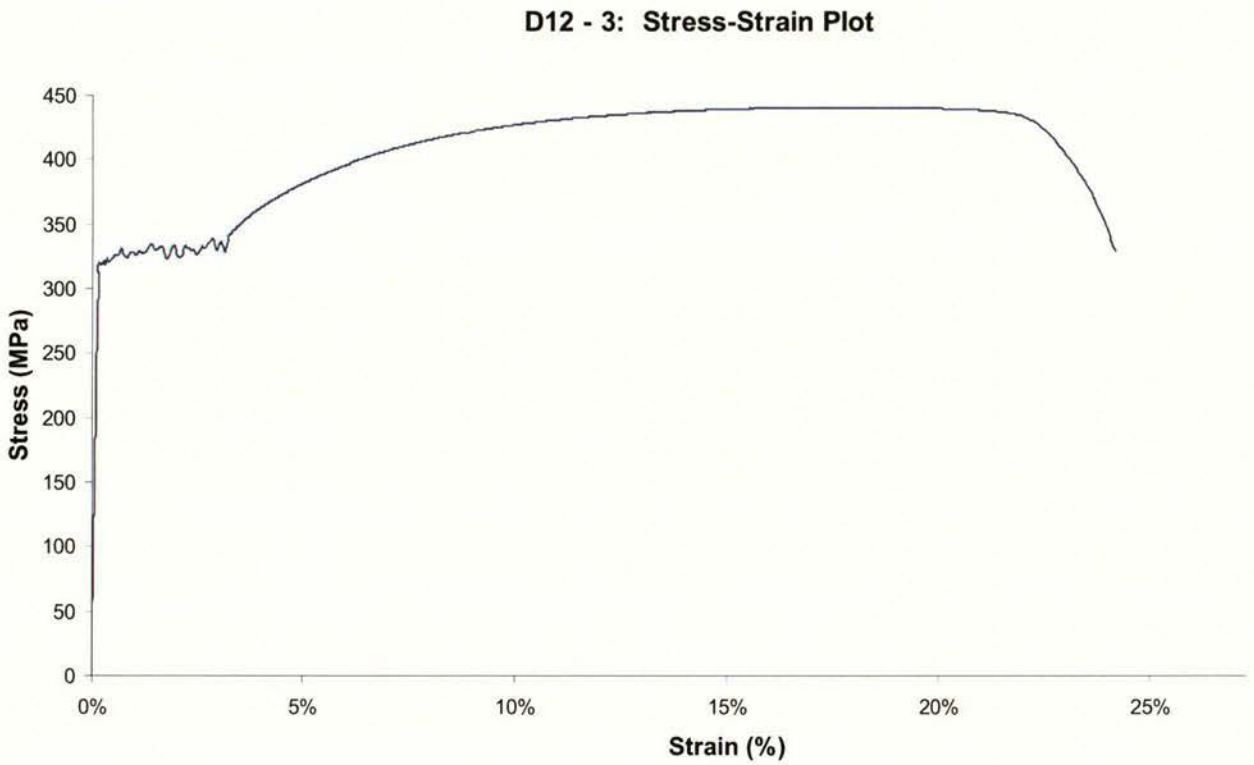
D12 - 3: Stress-Strain Plot
Stress (MPa)
450
400
350
300
250
200
150
100
50
0
0%
5%
10%
15%
20%
25%
Strain (%)

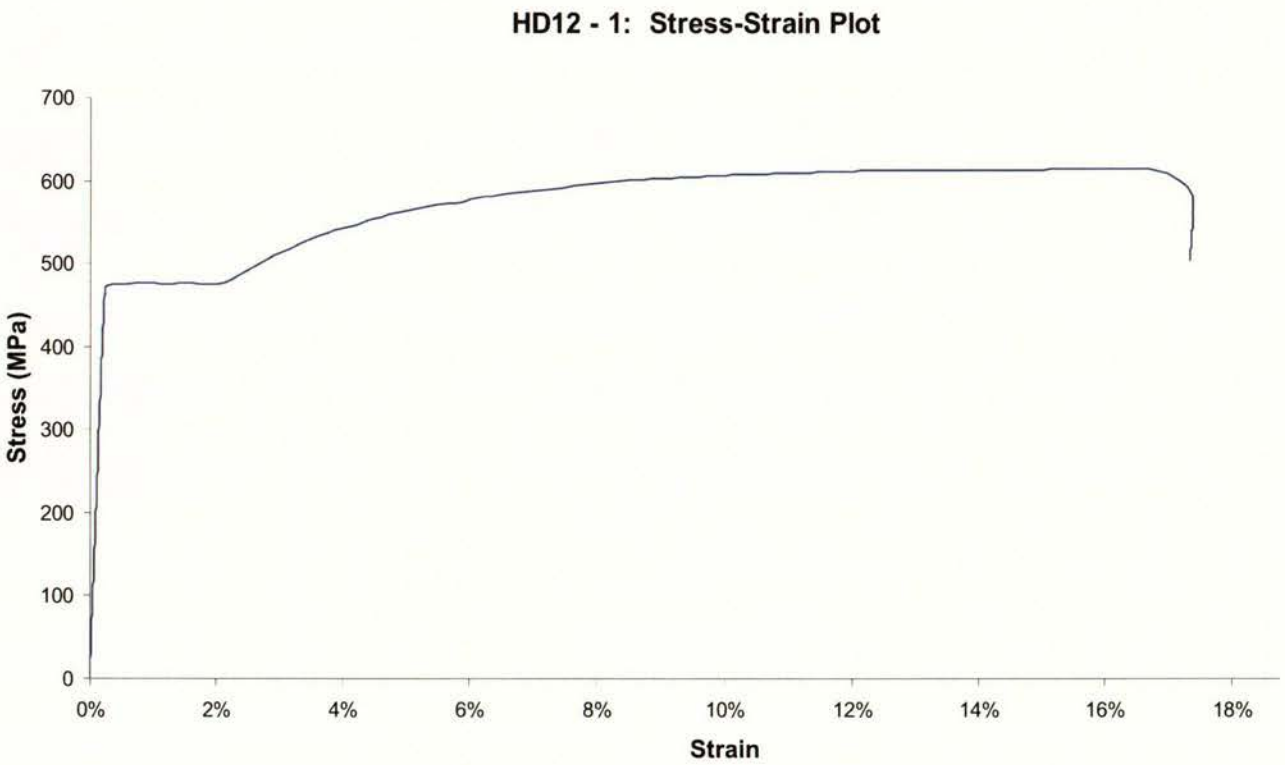
HD12 - 1: Stress-Strain Plot
Stress (MPa)
700
600
500
400
300
200
100
0
0%
2%
4%
6%
8%
10%
12%
14%
16%
18%
Strain

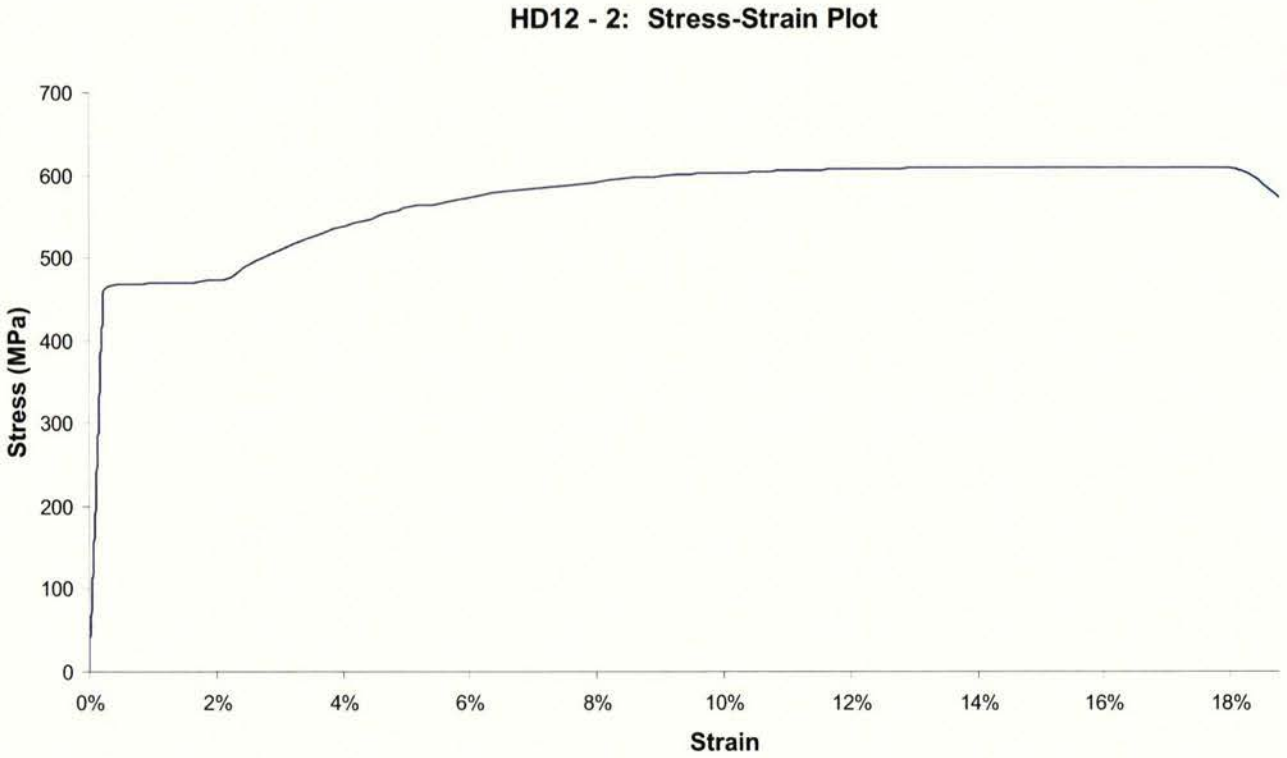
HD12 - 2: Stress-Strain Plot
Stress (MPa)
700
600
500
400
300
200
100
0
0%
2%
4%
6%
8%
10%
12%
14%
16%
18%
Strain

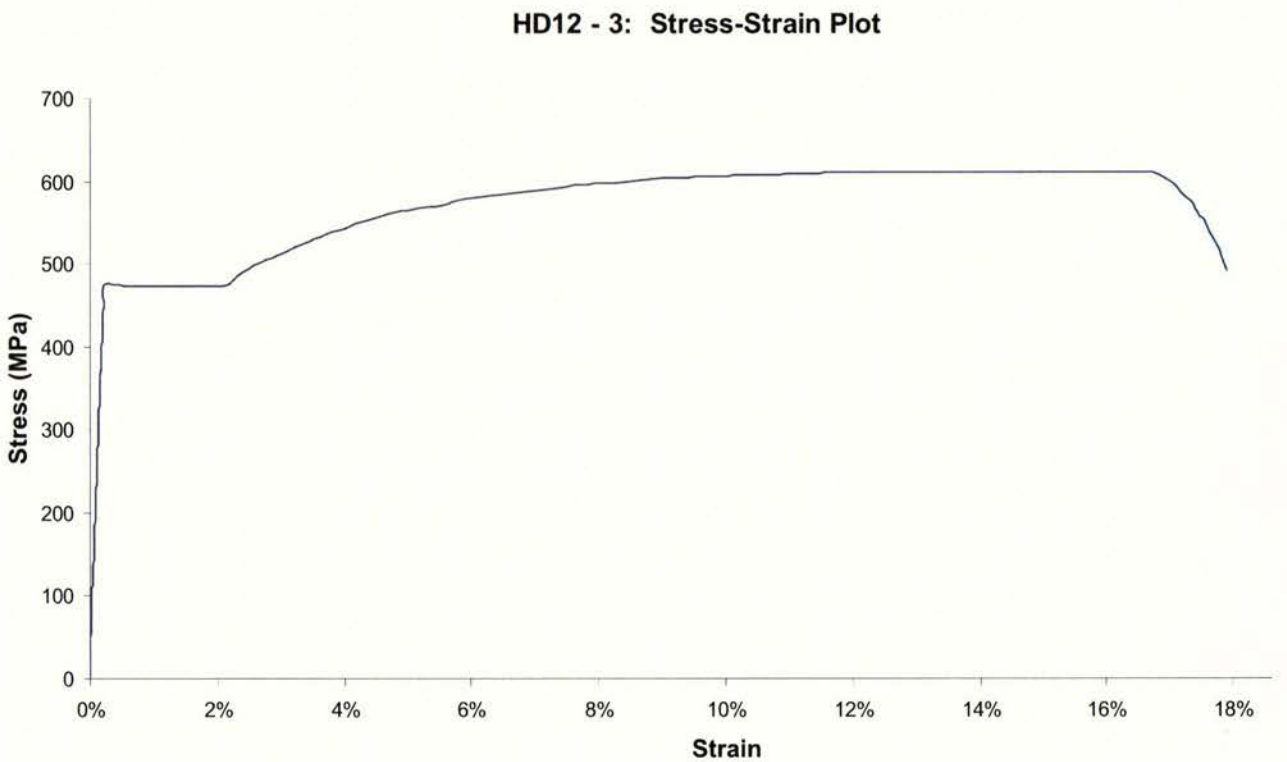
HD12 - 3: Stress-Strain Plot
Stress (MPa)
700
600
500
400
300
200
100
0
0%
2%
4%
6%
8%
10%
12%
14%
16%
18%
Strain

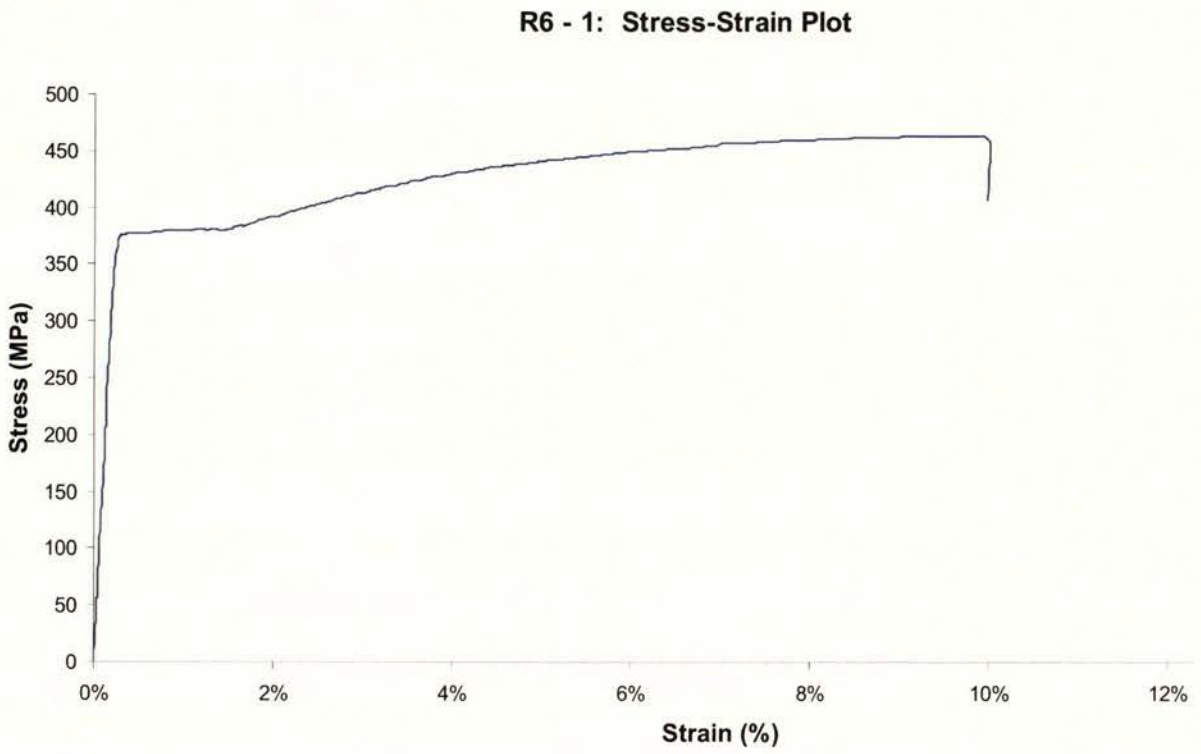
R6 - 1: Stress-Strain Plot
Stress (MPa)
500
450
400
350
300
250
200
150
100
50
0
0%
2%
4%
6%
8%
10%
12%
Strain (%)

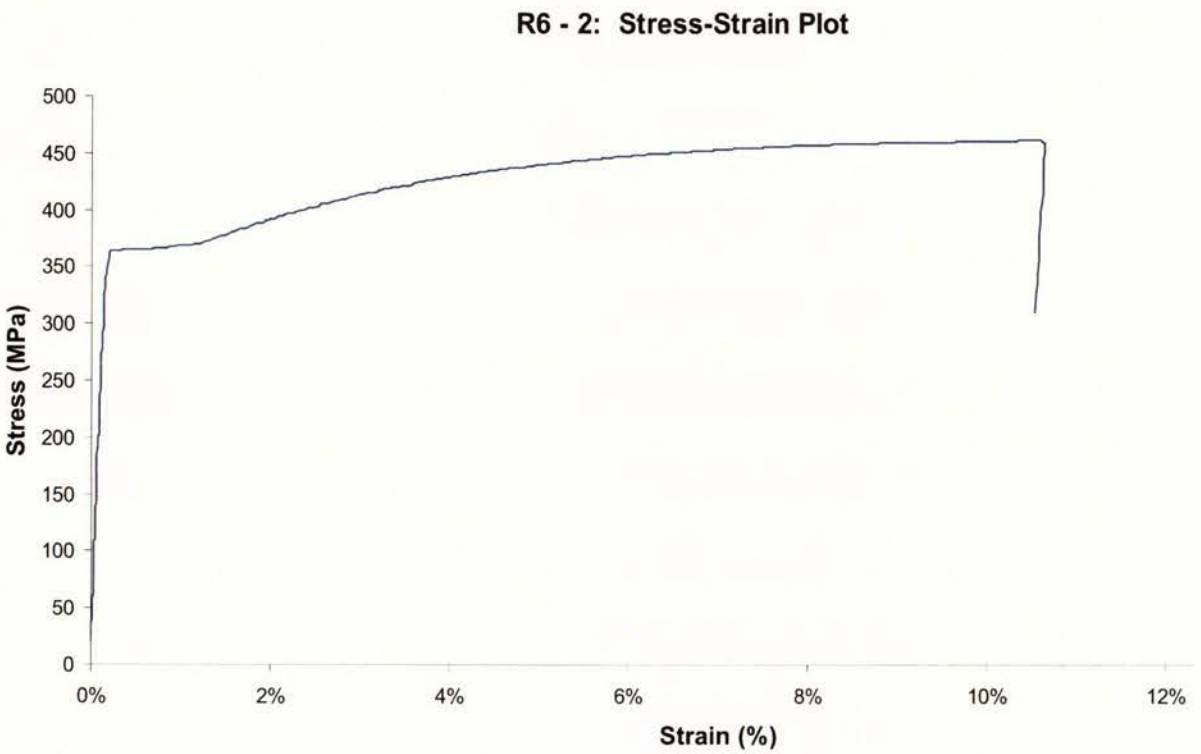
R6 - 2: Stress-Strain Plot
Stress (MPa)
500
450
400
350
300
250
200
150
100
50
0
0%
2%
4%
6%
8%
10%
12%
Strain (%)

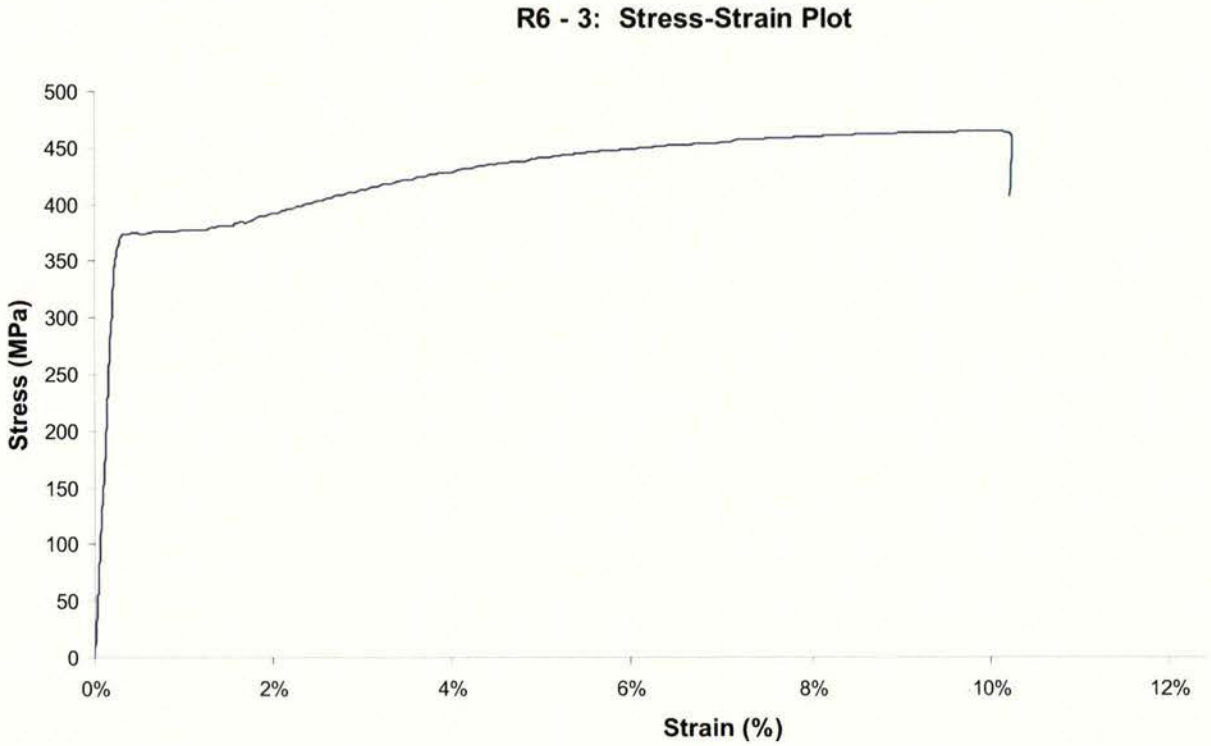
R6 - 3: Stress-Strain Plot
Stress (MPa)
500
450
400
350
300
250
200
150
100
50
0
0%
2%
4%
6%
8%
10%
12%
Strain (%)

Appendix 3

Test Data

A3.1 Experimental Data of Unit 1 (see *Chapter 4*)

Table A3.1: Forces and displacements at top and bottom of columns of Unit 1.

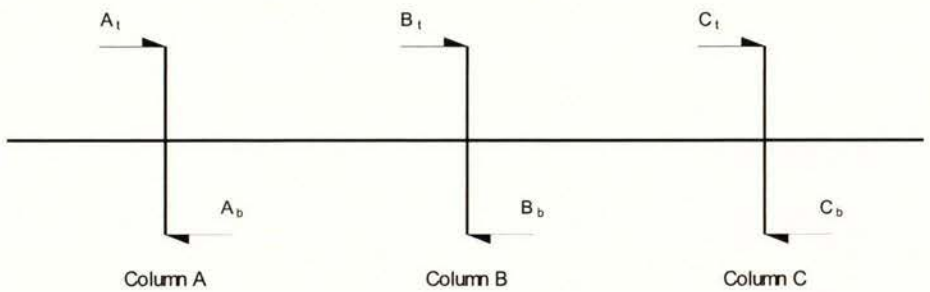

Where: F - sum of lateral force applied.
D - absolute displacement at top of column A.
A_t - lateral force applied at top of column A.
A_b - lateral force applied at bottom of column A.
B_t - lateral force applied at top of column B.
B_b - lateral force applied at bottom of column B.
C_t - lateral force applied at top of column C.
C_b - lateral force applied at bottom of column C.
d_A - relative lateral displacement between top and bottom of column A.
d_B - relative lateral displacement between top and bottom of column B.
d_C - relative lateral displacement between top and bottom of column C.

step	F (kN)	D (mm)	A_t (kN)	B_t (kN)	C_t (kN)	A_b (kN)	B_b (kN)	C_b (kN)	d_A (mm)	d_B (mm)	d_C (mm)
$+0.6F_y$	0.00	0.00	0.00	0.00	0.00	0.00	0.00	0.00	0.00	0.00	0.00
	7.78	1.94	7.26	7.38	0.40	0.62	4.50	0.60	1.56	1.44	0.79
	20.26	2.63	8.09	17.74	2.52	6.85	3.92	6.98	2.60	2.09	2.30
	21.71	2.97	7.31	13.97	7.74	6.66	10.91	1.83	2.31	2.49	2.35
	30.34	4.00	14.03	21.44	8.90	7.60	18.00	1.96	3.16	3.16	2.51
	44.96	4.28	13.69	33.19	11.77	10.05	17.93	14.47	3.36	3.75	4.34
	55.59	5.16	14.63	38.93	16.66	15.36	25.24	11.57	4.20	4.65	4.84
	67.12	5.71	14.74	52.98	14.14	24.23	22.19	18.60	5.16	5.27	5.06
	39.86	5.45	35.84	39.67	0.19	3.60	22.37	11.21	5.84	2.57	3.33
$-0.6F_y$	0.74	0.57	0.33	1.51	-0.77	0.38	-0.05	0.19	1.14	0.43	1.04
	-8.17	-2.60	-7.90	-6.94	-1.24	-0.17	-5.77	-0.36	-1.57	-1.58	-0.50
	-24.46	-3.46	-10.13	-20.78	-3.68	-6.44	-6.44	-8.32	-2.66	-2.55	-2.46
	-35.80	-4.33	-14.55	-28.74	-7.06	-8.61	-14.09	-9.06	-3.29	-3.27	-3.00
	-49.75	-4.75	-13.11	-37.69	-12.06	-17.40	-15.22	-12.97	-3.82	-3.87	-4.10

step	F (kN)	D (mm)	A_t (kN)	B_t (kN)	C_t (kN)	A_b (kN)	B_b (kN)	C_b (kN)	d_A (mm)	d_B (mm)	d_C (mm)
	-65.16	-5.69	-16.96	-50.52	-14.64	-24.68	-21.76	-14.21	-4.63	-4.72	-4.51
+2Di	-0.18	0.05	-0.23	2.52	-2.71	-0.08	0.15	-0.16	-0.14	0.30	-0.20
	7.66	2.21	7.20	10.02	-2.36	0.12	5.59	0.36	1.70	1.70	0.59
	19.17	3.10	7.27	14.94	4.23	8.67	9.79	-0.73	2.88	2.34	1.80
	51.92	5.19	13.76	41.60	10.33	17.16	20.30	13.20	4.66	4.45	4.16
	107.23	8.57	36.71	86.88	20.35	24.47	49.44	28.70	7.74	7.70	7.51
	80.09	10.96	11.18	48.07	32.02	38.45	44.95	-4.38	11.57	11.56	11.90
	80.66	13.84	17.98	49.02	31.64	31.03	47.52	-0.68	15.81	14.46	18.31
	95.24	15.79	15.34	78.51	16.73	37.25	33.43	23.77	18.03	18.18	18.52
	17.66	12.04	11.73	19.72	-2.06	7.22	10.05	-0.97	15.22	12.14	13.41
-2Di	1.09	9.36	-0.86	3.76	-2.67	0.03	1.74	-0.31	11.77	10.71	12.97
	-7.52	5.04	-9.04	-4.44	-3.08	-0.65	-5.26	-0.29	8.66	8.05	11.81
	-30.23	4.25	-7.87	-27.73	-2.51	-12.61	-0.32	-17.66	6.88	5.86	8.13
	-47.83	2.61	-15.21	-38.07	-9.76	-14.49	-5.20	-24.28	5.50	5.39	5.08
	-65.30	0.55	-22.46	-51.45	-13.85	-17.00	-17.34	-25.66	3.84	3.40	3.75
	-79.17	-1.54	-19.33	-61.39	-17.78	-29.91	-18.52	-27.23	1.30	0.93	0.75
	-94.24	-4.51	-26.74	-71.99	-22.25	-31.80	-32.16	-26.32	-1.54	-1.65	-1.87
	-103.36	-7.93	-26.06	-75.43	-27.93	-36.59	-40.60	-22.29	-4.61	-4.76	-4.62
	-106.02	-10.47	-25.65	-80.99	-25.03	-38.79	-35.89	-27.33	-6.96	-7.13	-7.61
	-115.38	-13.34	-23.56	-82.40	-32.98	-45.76	-43.57	-23.11	-9.49	-9.58	-10.01
	-116.42	-16.39	-27.42	-87.08	-29.34	-43.23	-42.30	-26.08	-12.50	-11.41	-10.86
	-53.85	-13.23	-7.04	-50.48	-3.37	-21.64	-5.32	-12.78	-10.05	-9.85	-8.29
+2Dii	-0.78	-8.99	-1.30	2.12	-2.90	-0.55	-0.52	0.20	-5.98	-4.13	-3.61
	8.32	-5.60	3.78	7.20	1.12	6.57	0.47	0.01	-2.30	-2.27	-2.11
	18.82	-3.46	6.03	14.73	4.09	12.25	1.31	5.80	-0.35	0.26	0.21
	41.99	-0.34	10.63	32.56	9.43	20.93	6.47	13.97	2.81	3.08	3.16
	63.66	2.59	18.55	49.17	14.49	24.68	17.76	18.69	5.58	5.67	5.78
	80.39	5.82	19.64	61.27	19.12	31.01	26.33	21.61	8.85	8.91	8.99
	108.46	12.98	30.42	86.01	22.44	31.57	48.40	27.63	16.61	16.28	16.46
	112.35	15.46	34.91	88.88	23.47	29.80	55.06	27.05	19.21	19.23	19.99
	90.92	16.40	19.82	69.70	21.23	36.30	38.31	16.88	21.29	21.05	21.37
	38.47	14.22	16.55	39.54	-1.08	2.00	34.95	-0.67	15.46	20.49	13.88
-2Dii	1.54	8.64	-0.08	4.61	-3.08	-0.13	3.58	-0.71	12.25	14.05	13.89
	-32.47	1.63	-10.44	-24.91	-7.56	-12.96	0.93	-18.34	5.94	6.11	6.09
	-60.36	-4.07	-16.37	-45.82	-14.55	-21.25	-10.65	-23.70	1.19	1.49	1.59
	-88.30	-8.40	-27.48	-69.44	-18.86	-26.44	-27.42	-29.63	-2.79	-2.69	-2.48
	-95.00	-10.70	-24.43	-72.29	-22.71	-37.45	-33.70	-19.72	-5.37	-5.34	-5.23
	-109.70	-13.25	-28.98	-81.39	-28.32	-38.39	-42.29	-24.89	-7.86	-7.52	-7.03
	-115.34	-15.93	-27.53	-83.71	-31.63	-41.46	-46.26	-24.11	-10.37	-9.86	-9.31
	-25.91	-12.91	-19.95	-21.59	-4.32	-1.33	-21.60	-0.94	-8.45	-4.73	-1.94
+4Di	-1.37	-8.86	-0.81	1.65	-3.02	0.13	-2.18	0.25	-4.64	-2.00	-1.17
	13.74	-3.07	5.90	10.65	3.10	10.90	1.29	0.11	1.85	1.10	2.39
	32.53	0.94	11.14	25.79	6.73	19.16	5.98	6.78	5.52	5.64	5.60
	43.38	3.04	11.16	33.39	9.99	23.07	8.89	11.01	7.62	7.84	8.07
	80.60	10.30	17.41	60.46	20.14	33.72	28.02	18.12	14.97	15.10	15.20
	107.66	15.26	31.66	80.88	26.78	32.73	53.49	20.23	20.10	19.89	20.10
	116.05	20.31	32.69	90.02	26.04	34.87	57.50	24.54	25.95	26.01	26.27
	97.48	22.30	19.20	73.05	24.43	40.04	47.20	11.55	28.87	29.16	28.67
	125.70	26.61	45.33	102.40	23.30	28.26	68.06	30.48	33.84	33.19	31.79
	128.86	32.17	47.85	111.58	17.27	25.99	65.53	38.42	40.91	40.13	40.17
	53.54	30.03	0.70	52.84	0.70	35.98	18.69	0.24	39.10	40.97	36.81
-4Di	-0.59	19.91	-2.37	4.05	-4.64	-0.17	-0.80	-0.63	29.45	31.33	34.36
	-9.40	16.53	-11.49	-3.84	-5.56	-0.43	-8.04	-0.97	27.02	28.27	33.57
	-46.74	10.56	-15.30	-37.66	-9.08	-18.70	1.78	-26.76	18.87	19.26	20.86
	-64.15	5.65	-16.97	-50.36	-13.79	-27.03	-4.62	-27.62	14.48	15.76	16.82
	-79.80	0.25	-21.02	-61.40	-18.40	-24.98	-22.74	-28.90	9.98	10.06	10.29
	-92.56	-3.58	-21.66	-70.52	-22.04	-34.83	-26.46	-28.45	6.22	5.80	5.79
	-110.89	-10.85	-27.52	-81.83	-29.06	-41.38	-40.79	-27.21	-0.99	-1.12	-1.00

step	F (kN)	D (mm)	A_t (kN)	B_t (kN)	C_t (kN)	A_b (kN)	B_b (kN)	C_b (kN)	d_A (mm)	d_B (mm)	d_C (mm)
	-110.83	-14.03	-26.43	-79.66	-31.17	-41.44	-42.53	-25.23	-4.00	-4.15	-3.95
	-123.82	-20.28	-28.87	-93.22	-30.60	-49.18	-41.78	-30.90	-9.77	-10.04	-9.97
	-128.10	-25.33	-26.23	-91.66	-36.44	-53.98	-44.57	-27.61	-14.52	-14.77	-13.99
	-131.89	-30.08	-30.38	-97.13	-34.76	-51.46	-46.23	-31.23	-19.32	-18.49	-18.18
	-124.41	-31.77	-25.61	-94.77	-29.64	-52.99	-36.36	-32.23	-20.83	-20.24	-20.22
+4Dii	0.90	-20.29	0.55	2.80	-1.90	0.34	0.06	-0.11	-10.36	-9.14	-9.51
	19.21	-13.88	7.68	16.17	3.04	9.34	3.60	5.63	-3.59	-4.19	-3.83
	29.37	-9.89	8.44	23.44	5.93	16.82	4.41	9.45	0.41	0.70	0.35
	52.44	-3.11	15.93	42.71	9.73	25.56	13.92	14.28	7.27	7.42	7.43
	58.48	0.01	10.96	42.71	15.77	30.16	17.01	12.12	10.34	11.13	11.88
	86.68	6.22	24.68	67.18	19.50	33.92	34.58	19.78	16.63	17.04	17.60
	101.47	11.09	25.92	77.94	23.53	38.07	41.88	23.93	21.82	22.14	22.61
	100.24	15.48	22.86	74.60	25.64	40.70	45.32	16.62	26.46	26.97	26.67
	119.17	20.80	30.96	92.20	26.97	39.97	52.76	29.68	32.37	32.65	32.17
	124.64	26.48	41.83	99.99	24.65	32.35	62.29	33.30	38.50	38.39	37.85
	129.55	31.07	41.87	106.98	22.57	35.47	62.27	35.72	44.32	44.10	44.68
	101.33	32.19	18.95	74.27	27.06	46.07	49.09	10.03	46.15	46.50	45.98
	88.98	31.56	16.38	77.69	11.29	40.36	34.89	15.64	45.58	46.19	43.86
-4Dii	0.61	19.09	-2.46	3.36	-2.75	-0.43	1.91	-0.71	31.89	33.85	34.76
	-15.57	9.66	-3.48	-10.69	-4.87	-14.05	11.03	-12.25	22.55	22.36	22.53
	-32.04	4.81	-6.62	-23.84	-8.19	-22.50	4.97	-15.28	17.42	17.56	17.85
	-45.12	-2.01	-11.22	-34.30	-10.82	-26.01	-0.18	-17.31	10.87	11.50	11.17
	-56.61	-6.13	-16.62	-43.02	-13.59	-26.99	-8.33	-19.67	7.23	7.95	7.65
	-80.95	-12.13	-25.07	-62.69	-18.26	-33.34	-22.08	-24.31	1.91	1.49	1.85
	-99.24	-17.81	-27.35	-76.98	-22.26	-40.56	-29.26	-28.67	-4.15	-4.65	-4.42
	-102.43	-21.52	-22.05	-76.25	-26.18	-45.96	-29.68	-26.12	-8.40	-8.67	-8.34
	-114.68	-26.25	-27.98	-86.69	-27.99	-45.54	-38.76	-29.79	-13.10	-13.29	-13.20
	-126.01	-31.21	-30.10	-94.03	-31.98	-50.24	-46.53	-29.89	-17.79	-17.84	-17.57
	-123.37	-32.06	-28.76	-91.86	-31.51	-49.25	-44.99	-29.35	-18.64	-18.69	-18.41
	-25.67	-26.58	-18.68	-21.93	-3.73	-6.82	-14.80	-0.93	-14.24	-11.68	-8.59
+6Di	0.51	-20.57	-1.00	4.30	-3.78	-0.23	-0.35	0.37	-7.97	-7.13	-6.44
	10.84	-14.08	4.08	7.46	3.37	0.64	8.07	1.07	-3.41	-1.45	1.07
	25.32	-4.89	9.10	19.35	5.96	8.41	15.26	0.97	6.78	6.93	6.23
	34.14	-0.04	8.03	27.72	6.43	17.47	8.42	8.95	12.28	13.01	13.34
	42.52	4.00	8.42	29.10	13.42	24.68	16.90	2.25	16.46	16.95	17.23
	64.17	12.85	15.59	48.41	15.76	29.85	28.67	6.95	25.81	26.08	25.31
	81.93	18.57	21.43	62.83	19.10	30.35	38.19	15.25	31.54	31.95	31.81
	94.06	23.38	17.86	70.04	24.02	39.82	40.77	16.25	36.90	37.42	37.43
	116.24	30.15	28.54	88.48	27.76	41.00	56.61	22.44	44.33	44.69	44.92
	100.77	34.00	21.14	76.25	24.52	41.76	46.72	14.97	49.72	49.33	49.05
	129.65	41.28	43.44	103.71	25.94	34.57	70.79	29.57	57.49	57.03	56.85
	127.44	48.24	45.66	104.12	23.32	30.49	70.60	31.58	64.89	65.28	66.25
	49.51	43.91	0.58	45.00	4.50	31.22	15.85	1.75	61.89	62.78	60.60
-6Di	-0.41	33.68	-2.39	0.51	-0.92	0.18	0.72	-0.85	51.53	51.41	53.42
	-5.04	27.56	-0.47	-2.61	-2.43	-0.75	-5.26	-1.13	50.58	42.55	50.82
	-14.73	22.95	-4.64	-11.80	-2.93	-12.03	4.23	-7.74	41.08	39.29	44.83
	-23.33	18.30	-6.26	-18.00	-5.33	-15.66	4.47	-13.55	35.56	34.95	35.18
	-32.67	14.04	-7.65	-24.17	-8.50	-21.87	0.95	-13.25	31.06	30.72	30.87
	-38.12	9.40	-9.22	-29.54	-8.58	-22.45	0.00	-14.68	26.66	26.41	26.47
	-51.78	3.92	-13.39	-40.11	-11.67	-29.27	-6.49	-16.30	21.59	21.22	21.31
	-76.18	-6.24	-23.76	-69.76	-6.42	-34.95	-10.98	-27.17	10.74	10.24	11.98
	-89.35	-11.58	-25.38	-70.69	-18.66	-38.17	-24.65	-26.40	5.15	4.79	4.48
	-100.67	-16.38	-25.37	-77.04	-23.64	-43.46	-30.80	-26.91	-0.11	-0.37	-0.41
	-109.79	-22.22	-31.73	-85.58	-24.21	-42.11	-36.09	-30.50	-5.97	-6.30	-6.66
	-118.33	-27.53	-29.44	-88.13	-30.20	-48.07	-42.83	-28.76	-11.97	-11.79	-12.05
	-122.36	-32.56	-32.54	-88.14	-34.23	-47.05	-51.27	-25.24	-16.96	-16.59	-16.41
	-125.07	-37.33	-34.54	-93.49	-31.57	-46.86	-49.75	-30.61	-21.67	-21.38	-20.75
	-129.76	-45.53	-35.29	-95.39	-34.36	-48.64	-52.27	-31.17	-29.68	-30.27	-30.26

step	F (kN)	D (mm)	A_t (kN)	B_t (kN)	C_t (kN)	A_b (kN)	B_b (kN)	C_b (kN)	d_A (mm)	d_B (mm)	d_C (mm)
	-126.56	-47.92	-33.69	-89.88	-36.68	-47.13	-53.96	-28.01	-32.08	-32.64	-32.64
+6Dii	-0.14	-36.84	-0.21	1.76	-1.90	-0.39	2.35	-0.56	-22.18	-24.42	-23.21
	16.18	-23.38	3.88	9.64	6.54	5.14	11.60	0.47	-10.05	-9.36	-8.33
	28.00	-13.72	9.33	22.67	5.33	10.33	8.17	9.21	0.70	1.03	0.72
	32.83	-8.90	6.36	24.09	8.74	16.98	8.83	8.40	6.07	6.62	6.15
	40.76	-2.36	11.77	32.08	8.68	16.41	13.37	12.11	12.41	13.77	13.27
	45.68	4.60	6.42	33.07	12.61	30.47	7.42	9.82	21.44	21.76	21.41
	63.48	12.51	19.99	47.69	15.78	28.42	21.03	16.34	29.54	30.18	29.37
	61.84	18.77	13.70	47.76	14.08	36.24	7.20	20.84	37.44	38.26	36.44
	77.47	27.23	24.22	58.59	18.88	34.32	21.90	22.88	45.69	47.92	44.64
	78.63	33.07	17.51	59.24	19.40	40.42	14.58	25.61	52.83	54.95	54.60
	100.84	42.36	34.02	76.21	24.63	37.51	39.05	28.08	62.40	64.55	64.24
	99.26	47.70	36.55	73.46	25.80	33.72	44.67	24.92	67.99	69.77	69.61
	34.02	42.44	-2.74	29.10	4.93	33.21	0.32	0.70	65.68	67.46	61.11
-6Dii	1.84	35.49	-0.47	2.52	-0.68	0.68	-0.16	-0.43	56.51	60.68	56.42
	-5.90	27.41	-7.59	-3.25	-2.65	0.14	-6.54	-1.21	48.98	53.01	52.53
	-4.20	20.37	1.47	-0.39	-3.81	-0.96	-4.03	-1.30	50.92	33.94	48.94
	-19.83	7.65	-6.73	-13.93	-5.90	-16.08	10.13	-14.33	26.44	26.53	25.29
	-33.63	-5.55	-8.91	-25.62	-8.01	-25.43	11.82	-20.13	11.36	11.14	12.39
	-45.49	-14.53	-13.20	-33.38	-12.11	-30.79	11.22	-25.88	1.23	-0.04	1.28
	-46.97	-19.62	-6.91	-35.38	-11.59	-35.75	18.57	-29.63	-5.48	-6.82	-5.38
	-56.70	-27.10	-9.24	-44.04	-12.65	-38.00	15.48	-33.23	-14.34	-15.30	-13.06
	-71.20	-34.06	-19.58	-55.91	-15.29	-35.19	1.41	-36.85	-21.35	-22.22	-21.86
	-83.61	-41.34	-23.97	-65.55	-18.07	-37.94	-6.63	-35.99	-28.34	-28.13	-28.33
	-97.66	-47.54	-27.95	-72.03	-25.63	-40.06	-23.72	-32.89	-34.33	-34.33	-34.76
end	-0.64	-37.33	-1.34	3.31	-3.94	-0.30	2.15	-0.66	-23.62	-26.78	-22.97

Table A3.2: Elongation of beams at peak of displacement step of Unit 1.

displacement step	E_{A-B}	E_{B-C}
+0.64Fy	0.0375	-0.004
-0.64Fy	0.187	-0.0245
+2Di	2.6895	2.397
-2Di	3.5255	3.1015
+2Dii	4.2495	4.9265
-2Dii	4.536	4.958
+4Di	7.941	10.0665
-4Di	9.299	12.14
+4Dii	9.425	14.354
-4Dii	10.94	14.5975
+6Di	12.115	18.0215
-6Di	12.761	18.9195
+6Dii	14.7975	18.119
-6Dii	9.976	20.7955

Where: E_{A-B} - beam elongation measured between columns A and B.
E_{B-C} - beam elongation measured between columns B and C.

A3.2 Experimental Data of Unit 2 (see *Chapter 5*)

Table A3.3: Forces and displacements at top and bottom of columns of Unit 2.

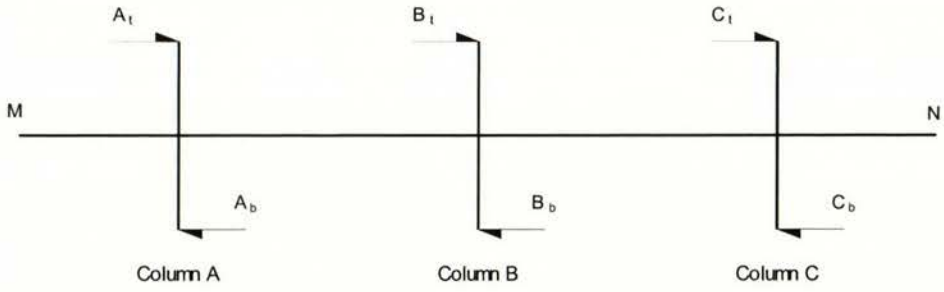

Where: F - sum of lateral force applied.
d - average displacement columns.
A_t - lateral force applied at top of column A.
A_b - lateral force applied at bottom of column A.
B_t - lateral force applied at top of column B.
B_b - lateral force applied at bottom of column B.
C_t - lateral force applied at top of column C.
C_b - lateral force applied at bottom of column C.
d_A - relative lateral displacement between top and bottom of column A.
d_B - relative lateral displacement between top and bottom of column B.
d_C - relative lateral displacement between top and bottom of column C.

step	F (kN)	d (mm)	A_t (kN)	B_t (kN)	C_t (kN)	A_b (kN)	B_b (kN)	C_b (kN)	d_A (mm)	d_B (mm)	d_C (mm)
+0.2%i	1.83	-0.19	0.44	2.14	-0.75	-0.41	-4.42	3.72	-0.18	-0.18	-0.21
	18.05	0.49	7.38	8.91	1.75	1.98	0.24	10.45	0.51	0.48	0.48
	33.96	0.98	11.39	18.05	4.52	5.50	4.78	16.66	0.99	0.98	0.96
	60.07	1.67	22.18	27.05	10.84	9.70	16.26	24.97	1.70	1.64	1.66
	83.41	2.19	26.97	37.21	19.23	15.67	25.85	30.05	2.20	2.17	2.19
	40.32	1.46	20.35	9.18	10.80	9.85	26.36	1.88	1.79	1.97	0.61
-0.2%i	-3.91	0.14	0.74	-6.52	1.87	-1.96	3.27	0.35	0.13	0.15	0.14
	-18.40	-0.49	-1.99	-10.61	-5.81	-6.53	-2.77	-2.29	-0.49	-0.49	-0.50
	-29.78	-0.87	-4.98	-14.03	-10.78	-10.59	-7.75	-4.34	-0.87	-0.88	-0.87
	-52.14	-1.53	-10.96	-19.34	-21.84	-17.16	-20.24	-8.70	-1.55	-1.52	-1.54
	-63.79	-1.83	-12.81	-25.75	-25.22	-21.20	-24.12	-12.65	-1.82	-1.83	-1.83
	-81.22	-2.22	-17.55	-32.59	-31.09	-25.28	-31.45	-17.18	-2.21	-2.22	-2.23
	-58.27	-1.93	-22.14	-5.09	-31.03	-12.66	-32.15	-12.87	-1.97	-1.55	-2.27
+0.2%ii	-13.66	-0.70	-9.37	-0.78	-3.50	-0.86	-15.15	0.26	-0.66	-0.96	-0.47
	14.83	0.47	6.30	4.09	4.44	1.70	2.78	7.18	0.48	0.45	0.48
	34.92	1.05	13.95	15.86	5.11	4.61	7.35	16.66	1.06	1.06	1.04
	51.49	1.49	17.64	24.03	9.82	8.74	12.91	21.42	1.49	1.50	1.50
	64.28	1.80	23.00	28.57	12.71	10.51	18.71	25.52	1.79	1.80	1.79
	83.31	2.21	26.88	38.08	18.36	15.03	25.31	31.65	2.19	2.21	2.23
	30.41	1.30	9.26	5.67	15.48	1.23	14.49	17.15	0.88	1.20	1.83
-0.2%ii	6.45	0.58	4.15	-2.26	4.56	0.13	9.72	1.28	0.49	0.87	0.37

step	F (kN)	d (mm)	A_t (kN)	B_t (kN)	C_t (kN)	A_b (kN)	B_b (kN)	C_b (kN)	d_A (mm)	d_B (mm)	d_C (mm)
	-6.55	0.01	1.65	-5.70	-2.51	-2.78	1.75	0.45	0.07	0.06	-0.10
	-19.28	-0.55	-0.45	-9.07	-9.76	-8.32	-4.25	0.30	-0.55	-0.56	-0.54
	-37.96	-1.15	-5.41	-16.39	-16.16	-13.78	-11.34	-4.91	-1.14	-1.16	-1.13
	-58.28	-1.70	-11.32	-23.67	-23.29	-19.12	-20.93	-11.05	-1.70	-1.70	-1.70
	-81.51	-2.23	-16.71	-33.26	-31.54	-25.89	-31.05	-16.98	-2.22	-2.23	-2.23
	-60.05	-2.00	-20.82	-4.33	-34.90	-14.09	-33.15	-12.09	-2.03	-1.58	-2.39
	-8.33	-0.57	-4.62	-0.49	-3.22	0.17	-11.67	0.39	-0.40	-0.81	-0.49
+0.5%i	7.11	0.10	3.03	1.05	3.04	0.95	0.46	3.30	0.11	0.10	0.09
	26.93	0.87	10.69	9.49	6.74	3.54	7.35	12.41	0.87	0.86	0.89
	62.12	1.82	20.82	25.33	15.97	11.25	19.95	22.71	1.82	1.82	1.81
	89.61	2.43	29.75	35.91	23.94	16.29	31.57	31.43	2.44	2.41	2.44
	121.94	3.52	39.35	51.23	31.36	21.61	43.28	44.15	3.50	3.51	3.54
	142.91	4.45	44.57	61.15	37.18	26.08	51.24	51.15	4.42	4.42	4.51
	169.50	5.68	57.14	70.06	42.30	28.11	62.94	62.80	5.67	5.68	5.68
	176.30	6.06	58.92	74.13	43.26	29.00	65.61	65.89	6.05	6.07	6.07
	127.42	5.33	55.53	38.44	33.46	10.53	58.60	56.54	4.90	5.25	5.83
-0.5%i	-5.11	1.17	1.89	-6.68	-0.33	-2.57	3.35	1.46	1.17	1.17	1.17
	-33.70	-0.42	-7.48	-16.30	-9.92	-9.78	-8.03	-7.98	-0.41	-0.43	-0.43
	-65.77	-1.50	-12.47	-27.60	-25.69	-21.33	-23.42	-12.12	-1.49	-1.52	-1.49
	-96.56	-2.57	-19.59	-40.13	-36.84	-30.89	-36.95	-20.45	-2.54	-2.58	-2.60
	-119.53	-3.56	-25.74	-50.68	-43.11	-37.50	-46.48	-27.51	-3.53	-3.57	-3.58
	-138.52	-4.50	-31.84	-57.67	-49.02	-43.48	-54.99	-32.71	-4.49	-4.50	-4.50
	-161.78	-5.63	-38.91	-66.91	-55.95	-52.28	-63.84	-38.32	-5.63	-5.63	-5.63
	-169.10	-6.12	-40.41	-69.24	-59.45	-54.61	-67.59	-39.55	-6.10	-6.12	-6.16
	-104.57	-4.91	-24.76	-25.15	-54.67	-25.07	-56.82	-25.24	-4.29	-4.76	-5.69
+0.5%ii	3.69	-0.79	-1.87	2.99	2.57	0.56	-2.63	1.17	-0.84	-0.76	-0.78
	21.17	0.64	7.68	8.08	5.40	2.18	3.98	9.01	0.64	0.63	0.64
	36.30	1.55	13.46	12.57	10.27	4.56	10.28	14.60	1.55	1.54	1.56
	60.39	2.59	21.54	21.84	17.01	9.98	19.48	21.78	2.64	2.57	2.57
	84.74	3.54	26.21	32.59	25.94	16.34	28.92	28.66	3.52	3.54	3.55
	118.39	4.55	37.19	49.51	31.68	22.76	39.80	41.55	4.56	4.56	4.52
	150.61	5.56	48.76	62.22	39.63	27.32	53.53	53.50	5.55	5.58	5.54
	165.42	6.05	54.53	67.45	43.44	29.03	60.38	59.24	6.04	6.06	6.05
	60.83	3.67	15.69	8.96	36.19	0.70	29.26	34.39	2.19	3.39	5.42
-0.5%ii	-9.25	0.01	-0.98	-4.11	-4.16	-2.96	-0.10	0.14	-0.12	0.21	-0.06
	-30.38	-1.50	-2.73	-15.63	-12.02	-12.58	-6.43	-4.54	-1.46	-1.49	-1.54
	-52.34	-2.51	-8.44	-23.34	-20.56	-19.32	-15.83	-9.91	-2.50	-2.50	-2.53
	-82.11	-3.64	-16.69	-35.96	-29.46	-27.94	-28.31	-19.02	-3.63	-3.65	-3.64
	-111.41	-4.62	-23.07	-47.30	-41.04	-38.18	-41.26	-25.46	-4.62	-4.62	-4.63
	-141.85	-5.54	-30.78	-61.42	-49.65	-47.97	-52.86	-34.09	-5.53	-5.54	-5.56
	-159.79	-6.12	-36.13	-68.77	-54.89	-54.30	-59.91	-38.64	-6.12	-6.12	-6.11
	-29.70	-2.11	-5.30	-16.91	-7.50	-0.15	-26.09	-0.36	-1.30	-3.21	-1.82
+1.0%i	5.87	-0.36	0.66	2.21	3.00	1.17	3.18	7.31	-0.36	-0.39	-0.32
	26.93	1.50	7.72	7.55	11.65	4.76	12.15	14.96	1.50	1.49	1.50
	62.26	3.06	18.21	23.05	21.01	12.01	24.16	26.60	3.05	3.06	3.07
	114.17	4.80	34.18	45.45	34.54	22.82	43.68	43.94	4.79	4.80	4.79
	169.16	6.50	52.75	67.87	48.53	31.81	66.72	63.23	6.50	6.50	6.49
	214.39	8.53	69.03	85.07	60.29	35.51	87.08	85.75	8.51	8.49	8.59
	244.96	10.91	73.97	102.33	68.66	40.56	98.00	91.45	10.91	10.90	10.91
	262.86	12.34	82.86	109.21	70.78	41.68	106.67	98.95	12.31	12.34	12.39
	98.26	8.05	46.64	32.67	18.95	2.26	47.90	51.08	7.45	8.18	8.53
-1.0%i	-5.37	3.01	-1.46	-6.77	2.85	-1.69	8.06	-1.35	3.03	3.14	2.85
	-17.91	1.11	-5.75	-9.45	-2.71	-7.21	2.79	-2.03	1.17	1.13	1.04
	-50.73	-0.99	-16.14	-18.67	-15.91	-19.33	-11.20	-8.31	-0.99	-0.98	-1.01

step	F (kN)	d (mm)	A_t (kN)	B_t (kN)	C_t (kN)	A_b (kN)	B_b (kN)	C_b (kN)	d_A (mm)	d_B (mm)	d_C (mm)
	-84.02	-2.91	-26.21	-32.34	-25.47	-27.40	-24.85	-20.29	-2.92	-2.91	-2.90
	-106.44	-3.99	-32.14	-41.72	-32.58	-33.49	-34.25	-27.91	-4.00	-3.98	-3.97
	-143.87	-5.58	-43.36	-57.87	-42.64	-44.17	-49.37	-40.19	-5.62	-5.59	-5.53
	-181.53	-7.40	-53.13	-74.13	-54.28	-58.51	-65.61	-47.32	-7.43	-7.38	-7.39
	-209.74	-9.08	-60.43	-87.55	-61.76	-68.92	-78.55	-52.27	-9.07	-9.08	-9.10
	-226.69	-10.48	-62.27	-92.84	-71.58	-76.99	-87.45	-52.13	-10.45	-10.40	-10.60
	-242.34	-12.39	-65.64	-101.60	-75.10	-80.63	-93.04	-59.19	-12.38	-12.31	-12.47
	-165.60	-10.58	-44.95	-53.74	-66.91	-53.98	-75.50	-32.83	-10.66	-10.28	-10.81
+1.0%ii	6.69	-2.44	-0.23	1.47	5.44	0.98	4.14	4.09	-2.51	-2.59	-2.22
	23.67	0.06	6.53	0.80	16.34	2.54	13.95	9.91	0.03	0.00	0.14
	50.17	2.37	16.03	11.30	22.84	8.02	21.99	20.96	2.35	2.34	2.40
	83.89	4.71	25.91	26.58	31.40	17.88	33.39	29.83	4.70	4.72	4.73
	113.13	6.45	36.85	37.63	38.65	24.70	45.66	37.95	6.46	6.44	6.46
	161.22	8.89	50.63	57.04	53.55	34.79	65.44	54.74	8.83	8.80	9.03
	198.15	10.50	59.13	74.37	64.65	40.66	81.58	64.93	10.50	10.49	10.51
	234.80	12.26	72.28	91.88	70.64	42.55	96.59	83.32	12.25	12.26	12.26
	135.51	9.71	52.16	27.81	55.54	32.40	82.84	14.89	10.70	10.16	8.26
	21.85	4.52	4.50	-0.13	17.48	0.52	31.84	-0.32	3.57	6.31	3.69
-1.0%ii	5.86	3.21	2.99	-0.29	3.16	-0.06	19.15	-1.42	2.92	4.99	1.72
	-9.51	0.05	-3.16	-5.76	-0.59	-1.11	5.56	-1.17	-0.01	0.11	0.05
	-30.28	-1.82	-10.05	-12.98	-7.25	-11.81	0.97	-6.56	-1.84	-1.81	-1.82
	-76.34	-5.06	-22.52	-31.16	-22.66	-25.66	-15.33	-22.48	-5.09	-5.04	-5.05
	-113.03	-7.05	-34.56	-44.62	-33.84	-33.12	-33.07	-34.89	-7.07	-7.07	-7.02
	-156.70	-9.01	-42.00	-63.96	-50.73	-49.26	-51.66	-43.33	-9.00	-9.01	-9.01
	-191.01	-10.60	-56.29	-81.34	-53.38	-58.45	-65.58	-55.62	-10.63	-10.61	-10.57
	-226.48	-12.36	-63.31	-95.54	-67.62	-73.34	-82.30	-59.08	-12.37	-12.34	-12.37
	-142.36	-10.25	-47.36	-46.83	-48.17	-35.88	-66.81	-36.59	-9.91	-10.36	-10.50
	-86.03	-8.15	-36.53	-22.87	-26.63	-23.94	-46.31	-11.61	-8.50	-8.55	-7.38
+1.5%i	-10.20	-3.82	-6.49	-0.92	-2.79	-0.35	-7.61	3.14	-3.03	-4.92	-3.50
	17.43	0.08	6.64	1.99	8.80	0.90	10.72	11.33	0.02	0.07	0.16
	35.45	2.04	13.53	6.70	15.22	3.20	17.06	20.11	2.04	2.04	2.05
	76.33	4.98	23.90	22.51	29.91	16.15	31.43	30.21	4.97	4.95	5.02
	111.16	7.00	35.45	37.41	38.31	25.38	45.36	39.00	6.98	7.02	6.98
	157.88	9.22	50.63	55.95	51.30	35.12	65.25	52.03	9.22	9.22	9.22
	205.50	11.25	62.80	78.01	64.69	40.38	85.84	71.76	11.24	11.25	11.27
	248.03	13.40	76.64	98.49	72.90	44.73	102.19	91.86	13.33	13.41	13.45
	269.75	15.17	87.25	104.32	78.18	46.22	111.48	102.73	15.14	15.18	15.19
	285.10	18.35	98.00	107.65	79.44	41.17	120.33	115.71	17.96	18.56	18.55
	103.58	12.39	33.82	50.52	19.23	6.16	43.26	59.84	10.66	13.84	12.68
-1.5%i	-4.99	5.25	0.59	-8.49	2.91	-1.17	11.05	-0.73	5.52	5.79	4.45
	-45.62	-0.56	-11.66	-21.80	-12.16	-17.18	-6.27	-8.32	-0.57	-0.54	-0.57
	-75.50	-3.06	-16.41	-33.28	-25.82	-27.86	-17.96	-15.90	-3.12	-3.00	-3.05
	-101.90	-5.19	-21.07	-46.30	-34.54	-35.73	-26.70	-24.92	-5.25	-5.19	-5.14
	-148.18	-8.39	-38.25	-61.80	-48.13	-45.73	-46.54	-41.32	-8.39	-8.39	-8.39
	-194.32	-11.14	-53.34	-81.68	-59.31	-63.73	-64.34	-52.04	-11.17	-11.13	-11.12
	-228.13	-14.50	-69.16	-93.71	-65.26	-76.46	-76.62	-62.47	-14.54	-14.50	-14.46
	-255.24	-16.76	-74.50	-103.12	-77.63	-83.48	-90.05	-67.85	-16.75	-16.75	-16.80
	-261.44	-18.50	-78.77	-106.40	-76.26	-88.84	-92.70	-66.53	-18.52	-18.48	-18.49
+1.5%ii	-13.63	-7.88	-7.85	-0.98	-4.79	0.26	-8.62	1.23	-6.03	-9.78	-7.85
	5.11	-5.74	-2.46	5.99	1.59	0.92	5.50	4.20	-5.42	-5.79	-6.02
	39.90	0.05	15.96	8.89	15.06	2.14	21.26	20.72	0.09	0.03	0.03
	72.68	3.20	25.78	21.84	25.06	11.17	33.97	28.67	3.23	3.17	3.20
	94.61	5.20	31.36	31.85	31.40	18.17	42.06	33.09	5.20	5.20	5.20
	132.14	8.56	43.38	44.89	43.87	28.29	57.82	42.46	8.53	8.56	8.58

step	F (kN)	d (mm)	A_t (kN)	B_t (kN)	C_t (kN)	A_b (kN)	B_b (kN)	C_b (kN)	d_A (mm)	d_B (mm)	d_C (mm)
	156.74	10.39	50.55	55.23	50.96	33.87	66.57	51.97	10.37	10.37	10.43
	186.79	12.57	62.72	66.18	57.89	35.68	80.11	65.03	12.57	12.59	12.56
	217.46	14.58	72.02	77.66	67.79	39.53	92.96	77.78	14.56	14.59	14.59
	234.11	15.79	77.35	83.46	73.29	41.68	99.76	85.08	15.75	15.79	15.82
	271.61	18.47	93.63	96.19	81.79	44.86	114.74	103.06	18.46	18.47	18.48
	198.07	16.54	98.61	50.70	48.76	15.43	98.46	85.75	16.69	16.45	16.49
-1.5%ii	0.64	6.32	4.75	-9.65	5.54	-1.04	18.48	-1.31	6.33	7.86	4.77
	-18.41	1.14	-10.05	-6.54	-1.81	-4.68	3.71	-2.33	1.12	1.40	0.89
	-44.62	-1.78	-10.79	-18.45	-15.38	-18.57	-4.48	-6.40	-1.83	-1.76	-1.75
	-68.72	-4.13	-15.26	-30.17	-23.29	-25.81	-12.85	-14.92	-4.16	-4.10	-4.13
	-91.70	-6.30	-23.94	-37.07	-30.68	-28.83	-24.73	-23.15	-6.30	-6.29	-6.31
	-110.66	-8.13	-31.95	-45.27	-33.44	-32.01	-32.38	-32.59	-8.15	-8.11	-8.14
	-146.82	-11.08	-41.34	-61.06	-44.42	-44.48	-46.46	-42.34	-11.10	-11.08	-11.05
	-189.63	-14.13	-56.67	-79.67	-53.30	-60.26	-63.25	-52.59	-14.13	-14.14	-14.11
	-220.34	-16.26	-67.59	-90.56	-62.18	-71.12	-76.32	-58.55	-16.27	-16.24	-16.27
	-241.59	-18.52	-78.64	-96.01	-66.93	-78.66	-85.86	-65.38	-18.55	-18.47	-18.54
	-168.87	-16.35	-48.95	-52.42	-67.50	-55.86	-68.70	-35.53	-15.96	-16.16	-16.91
+2.0%i	-10.85	-7.63	-7.21	-0.87	-2.77	0.83	-6.35	0.90	-5.85	-9.48	-7.56
	4.11	-5.88	-2.61	6.30	0.43	1.55	5.69	3.66	-5.16	-6.18	-6.30
	21.02	-1.90	7.55	2.12	11.35	1.11	14.75	11.41	-1.84	-1.91	-1.95
	57.95	2.71	22.56	14.56	20.82	7.44	28.41	26.45	2.66	2.69	2.77
	95.29	6.27	35.09	30.11	30.09	17.92	42.62	35.06	6.28	6.25	6.27
	135.78	9.89	46.81	43.37	45.60	29.66	61.02	41.85	9.88	9.90	9.89
	171.20	12.60	54.15	59.70	57.36	37.08	73.86	55.92	12.56	12.61	12.64
	235.28	16.69	79.93	84.02	71.33	40.63	100.14	87.77	16.70	16.70	16.67
	278.56	20.16	93.67	99.79	85.11	48.48	118.39	103.75	20.13	20.14	20.22
	292.44	22.06	99.39	105.19	87.86	45.94	125.01	113.69	22.03	22.07	22.06
	304.45	24.61	103.63	113.41	87.41	46.58	127.70	122.97	24.62	24.62	24.60
	143.73	19.80	52.35	43.15	48.23	27.63	82.50	36.98	20.57	21.49	17.34
-2.0%i	-5.26	8.85	-1.27	-6.21	2.22	0.28	12.59	-4.19	9.65	10.64	6.26
	-34.22	1.89	-20.55	-6.48	-7.19	-9.65	-10.97	-5.41	1.79	2.23	1.64
	-68.38	-1.62	-23.32	-27.07	-17.99	-20.24	-18.97	-16.90	-1.66	-1.59	-1.61
	-88.49	-4.27	-18.47	-40.31	-29.71	-31.84	-22.88	-20.32	-4.33	-4.25	-4.22
	-111.40	-6.85	-26.12	-47.79	-37.49	-36.63	-32.64	-28.49	-6.92	-6.83	-6.81
	-135.31	-9.55	-35.36	-55.68	-44.27	-42.17	-42.69	-37.20	-9.55	-9.55	-9.54
	-175.86	-13.58	-50.59	-71.31	-53.95	-57.19	-58.51	-47.47	-13.60	-13.58	-13.56
	-208.07	-16.28	-59.81	-84.65	-63.61	-71.73	-69.16	-53.66	-16.30	-16.24	-16.31
	-239.49	-19.15	-72.06	-92.57	-74.86	-82.00	-83.80	-59.55	-19.14	-19.13	-19.19
	-260.77	-22.35	-82.75	-101.75	-76.26	-87.62	-90.90	-70.36	-22.37	-22.32	-22.37
	-272.38	-24.61	-84.89	-106.87	-80.62	-93.24	-95.32	-71.34	-24.64	-24.59	-24.61
	-133.93	-20.11	-42.28	-34.89	-56.76	-48.69	-49.99	-25.47	-19.93	-19.49	-20.91
+2.0%ii	2.93	-10.03	-3.07	5.45	0.55	1.61	5.32	2.16	-8.53	-10.55	-11.02
	27.07	-3.51	7.65	5.63	13.79	1.33	16.50	15.29	-3.77	-3.72	-3.05
	51.69	-0.05	19.23	14.47	17.99	4.34	28.79	23.99	-0.02	-0.08	-0.05
	67.53	2.26	20.71	23.47	23.35	10.10	33.79	29.02	2.26	2.26	2.25
	93.43	4.91	32.21	32.41	28.81	15.79	44.22	34.20	4.88	4.92	4.91
	125.85	9.00	43.23	42.50	40.12	23.61	59.14	41.96	8.99	9.01	9.00
	149.37	11.97	49.21	50.39	49.78	30.26	69.57	47.27	11.99	11.95	11.96
	176.23	14.75	56.63	61.57	58.03	34.96	78.73	58.99	14.74	14.75	14.77
	203.01	17.64	65.73	69.32	67.95	36.78	90.97	71.36	17.62	17.62	17.69
	235.51	20.52	76.20	80.34	78.97	40.95	104.48	84.11	20.48	20.52	20.55
	260.19	22.72	84.32	89.36	86.51	44.52	113.83	94.78	22.72	22.72	22.71
	279.75	24.58	92.53	95.54	91.67	45.88	122.74	103.46	24.57	24.58	24.59
	88.71	17.36	24.32	0.25	64.14	-0.23	84.88	15.42	13.92	20.45	17.70

step	F (kN)	d (mm)	A_t (kN)	B_t (kN)	C_t (kN)	A_b (kN)	B_b (kN)	C_b (kN)	d_A (mm)	d_B (mm)	d_C (mm)
-2.0%ii	-4.13	8.02	-1.08	-6.88	3.83	-1.01	10.85	-2.38	8.70	8.92	6.43
	-44.99	0.10	-15.86	-18.54	-10.60	-16.03	-6.01	-10.41	0.05	0.10	0.14
	-72.41	-3.69	-13.95	-32.99	-25.47	-28.94	-15.77	-15.38	-3.71	-3.65	-3.70
	-91.41	-6.01	-20.99	-39.06	-31.36	-30.65	-26.14	-22.00	-6.06	-6.01	-5.96
	-113.44	-9.02	-27.41	-47.26	-38.77	-36.11	-36.54	-29.22	-9.03	-9.03	-8.99
	-136.38	-11.92	-33.92	-54.09	-48.37	-43.31	-46.66	-34.59	-11.90	-11.92	-11.94
	-162.46	-15.01	-44.31	-64.84	-53.32	-52.64	-56.59	-41.90	-15.04	-15.00	-14.99
	-193.63	-18.05	-54.21	-76.16	-63.26	-65.22	-69.19	-47.68	-18.03	-18.06	-18.07
	-220.14	-20.44	-63.94	-86.25	-69.95	-74.36	-78.91	-54.67	-20.41	-20.43	-20.47
	-260.71	-24.65	-80.14	-102.51	-78.06	-88.56	-92.36	-67.07	-24.68	-24.64	-24.62
	-142.55	-20.66	-31.32	-52.19	-59.03	-61.60	-46.89	-23.88	-20.27	-20.60	-21.11
+2.5%i	-10.53	-11.87	-6.83	-1.03	-2.67	0.70	-3.23	1.42	-9.26	-14.31	-12.04
	12.22	-7.04	1.87	0.20	10.15	1.94	13.95	6.02	-7.05	-7.15	-6.93
	39.37	-1.83	13.80	4.91	20.66	3.65	26.65	18.39	-1.83	-1.84	-1.83
	76.93	2.98	29.43	24.39	23.11	10.55	38.17	33.67	3.00	2.97	2.98
	103.40	6.29	37.85	34.82	30.73	17.81	49.75	39.01	6.26	6.25	6.37
	126.32	9.18	43.02	45.32	37.98	24.24	59.07	44.92	9.17	9.16	9.20
	150.32	12.19	49.93	52.51	47.88	29.71	70.80	50.75	12.19	12.21	12.18
	174.32	15.06	55.82	61.57	56.93	34.85	80.04	59.83	15.05	15.08	15.04
	204.28	18.46	64.03	70.66	69.58	38.84	92.84	71.39	18.47	18.47	18.45
	236.64	21.43	73.25	81.85	81.54	43.66	105.49	84.50	21.44	21.43	21.42
	268.98	24.44	83.98	94.47	90.53	47.63	117.71	99.28	24.43	24.43	24.47
	293.79	27.28	93.65	105.86	94.28	51.22	124.73	112.92	27.28	27.26	27.28
	313.19	30.85	101.66	117.52	94.01	52.92	127.23	127.25	30.82	30.87	30.86
	201.77	27.65	64.03	74.44	63.31	39.88	92.04	69.44	27.78	28.79	26.37
	15.90	16.56	8.59	-0.76	8.07	-0.05	29.11	2.36	15.82	21.12	12.73
-2.5%i	-5.11	11.45	-0.04	-8.82	3.75	-2.48	12.64	-1.40	12.24	12.47	9.64
	-44.47	3.09	-9.29	-21.91	-13.26	-17.78	-3.41	-6.72	3.12	3.11	3.03
	-81.44	-2.68	-18.64	-36.29	-26.51	-25.77	-21.75	-18.88	-2.68	-2.67	-2.68
	-102.14	-5.77	-23.15	-44.31	-34.68	-33.12	-30.76	-23.57	-5.77	-5.71	-5.81
	-121.67	-8.75	-29.77	-50.01	-41.89	-37.97	-40.46	-28.95	-8.81	-8.73	-8.71
	-140.97	-11.63	-32.80	-57.33	-50.84	-46.63	-47.32	-32.23	-11.67	-11.63	-11.58
	-171.58	-15.88	-46.16	-67.43	-57.99	-57.01	-59.43	-41.08	-15.88	-15.89	-15.86
	-200.09	-19.29	-56.59	-78.66	-64.83	-69.44	-67.86	-48.29	-19.32	-19.29	-19.24
	-227.53	-22.37	-69.88	-87.73	-69.93	-77.64	-77.45	-57.45	-22.40	-22.38	-22.34
	-262.48	-26.64	-82.81	-98.54	-81.13	-90.13	-91.09	-66.00	-26.68	-26.63	-26.62
	-284.02	-30.77	-88.60	-110.66	-84.76	-98.07	-95.99	-74.35	-30.78	-30.77	-30.75
	-142.49	-25.79	-48.32	-56.59	-37.57	-55.12	-45.03	-30.15	-25.92	-26.71	-24.73
+2.5%ii	-11.26	-15.91	-6.93	-1.07	-3.26	-0.38	-2.52	0.68	-13.06	-19.35	-15.32
	23.18	-6.35	8.67	8.60	5.91	1.39	14.74	15.82	-6.02	-6.46	-6.57
	62.62	0.04	26.90	19.41	16.32	6.02	33.55	29.08	0.06	0.04	0.02
	87.93	3.74	35.19	28.07	24.67	12.47	45.99	34.24	3.77	3.71	3.75
	110.16	7.05	40.01	37.32	32.82	19.04	55.57	38.18	7.06	7.04	7.06
	129.97	10.12	49.74	45.90	34.33	22.14	63.27	46.66	10.15	10.14	10.08
	163.71	15.36	59.39	55.77	48.55	30.79	77.54	56.52	15.32	15.34	15.40
	186.50	18.64	64.54	65.24	56.72	34.43	85.13	66.71	18.61	18.63	18.68
	219.07	22.73	74.29	76.65	68.13	38.79	96.93	81.33	22.74	22.73	22.72
	250.26	26.04	84.62	88.84	76.79	42.17	107.67	96.53	26.01	26.07	26.05
	294.88	30.74	97.61	107.78	89.49	49.82	121.88	116.72	30.75	30.73	30.74
	152.29	26.04	53.53	33.55	65.22	37.11	90.70	23.53	27.27	27.54	23.32
	21.52	17.15	10.33	-0.69	11.88	0.00	34.28	1.86	16.18	21.77	13.49
-2.5%ii	-1.02	12.60	3.52	-9.02	4.48	-0.34	15.28	-1.23	14.78	13.62	9.40
	-16.57	5.58	-4.81	-7.46	-4.30	-10.64	4.94	1.04	5.67	6.15	4.90
	-57.67	-0.33	-10.94	-22.13	-24.59	-22.89	-12.57	-6.61	-0.36	-0.31	-0.33

step	F (kN)	d (mm)	A_t (kN)	B_t (kN)	C_t (kN)	A_b (kN)	B_b (kN)	C_b (kN)	d_A (mm)	d_B (mm)	d_C (mm)
	-77.77	-3.44	-13.61	-33.88	-30.28	-29.29	-19.73	-13.88	-3.51	-3.40	-3.43
	-99.59	-7.00	-18.57	-41.68	-39.34	-34.94	-30.35	-19.59	-7.04	-7.01	-6.96
	-117.84	-10.03	-24.68	-48.58	-44.58	-39.22	-38.34	-26.02	-10.04	-10.04	-10.01
	-138.17	-13.39	-31.80	-55.25	-51.12	-45.25	-46.83	-32.04	-13.35	-13.40	-13.42
	-157.68	-16.53	-42.66	-61.40	-53.63	-49.86	-55.05	-39.50	-16.51	-16.53	-16.54
	-179.11	-19.75	-51.94	-69.15	-58.03	-58.42	-62.63	-44.65	-19.76	-19.74	-19.73
	-207.82	-23.39	-62.33	-78.26	-67.24	-69.73	-73.15	-51.42	-23.39	-23.39	-23.41
	-237.10	-27.10	-77.45	-89.29	-70.35	-77.18	-82.65	-63.76	-27.06	-27.10	-27.15
	-268.25	-30.86	-88.31	-101.13	-78.81	-87.80	-93.38	-72.90	-30.84	-30.89	-30.86
	-197.21	-28.49	-57.35	-73.50	-66.36	-79.83	-76.01	-28.21	-28.97	-29.43	-27.07
+3.0%i	-11.61	-16.30	-8.57	-1.21	-1.83	-0.21	-3.83	2.61	-13.62	-19.84	-15.45
	8.81	-11.37	0.97	4.60	3.24	1.80	9.85	8.16	-10.99	-11.50	-11.62
	24.80	-6.43	8.97	8.58	7.25	1.40	15.71	18.61	-6.36	-6.41	-6.53
	56.22	-0.51	26.50	12.71	17.01	3.09	34.20	28.94	-0.60	-0.56	-0.36
	89.88	4.29	35.70	27.96	26.22	13.58	47.09	36.53	4.28	4.29	4.30
	112.40	7.86	43.00	36.76	32.64	19.51	57.21	41.76	7.86	7.86	7.87
	144.36	13.03	53.71	48.71	41.93	26.65	70.25	51.67	13.04	13.04	13.02
	168.59	16.95	61.21	57.20	50.18	31.55	79.42	61.12	16.93	16.97	16.94
	195.88	20.93	67.95	66.82	61.10	35.84	89.36	72.56	20.92	20.93	20.95
	227.20	24.67	77.71	77.99	71.50	39.99	100.43	86.47	24.68	24.67	24.65
	261.28	28.29	88.20	90.74	82.34	44.64	113.09	101.44	28.31	28.29	28.28
	296.34	32.02	99.04	105.71	91.59	49.99	125.06	117.36	32.03	31.99	32.04
	293.57	37.16	101.88	102.38	89.30	56.74	131.20	97.55	37.16	37.20	37.11
	162.62	32.13	54.66	48.00	59.96	52.10	101.11	5.24	33.97	35.60	26.83
	29.04	23.37	16.88	-0.80	12.96	0.18	41.37	2.41	22.81	28.38	18.91
-3.0%i	-2.16	17.90	0.81	-7.39	4.42	0.03	15.60	-1.95	19.48	20.51	13.70
	-19.35	9.62	-7.46	-10.21	-1.69	-8.60	5.99	-0.61	9.73	9.89	9.24
	-64.76	1.72	-10.39	-29.55	-24.82	-26.23	-13.20	-11.11	1.63	1.78	1.76
	-88.25	-2.34	-15.97	-40.04	-32.23	-31.41	-22.76	-18.54	-2.34	-2.35	-2.33
	-106.78	-6.26	-21.54	-46.61	-38.63	-34.55	-32.73	-24.31	-6.21	-6.28	-6.28
	-126.40	-10.01	-32.82	-52.53	-41.06	-37.98	-41.84	-32.40	-10.01	-10.00	-10.01
	-146.80	-14.28	-40.54	-57.17	-49.08	-45.05	-50.73	-37.88	-14.26	-14.26	-14.32
	-166.88	-18.07	-51.95	-62.87	-52.06	-50.31	-58.10	-44.83	-18.05	-18.07	-18.09
	-201.10	-23.75	-67.89	-74.75	-58.46	-63.39	-68.11	-55.66	-23.77	-23.74	-23.74
	-226.17	-27.39	-77.41	-81.79	-66.97	-73.24	-77.08	-60.88	-27.36	-27.40	-27.42
	-253.10	-31.21	-89.05	-92.53	-71.52	-82.75	-84.80	-70.77	-31.21	-31.22	-31.21
	-272.50	-34.95	-94.45	-103.09	-74.96	-90.30	-90.16	-77.11	-34.96	-34.92	-34.96
	-277.84	-36.78	-94.82	-106.24	-76.77	-92.75	-91.44	-78.34	-36.75	-36.76	-36.82
	-154.92	-31.29	-48.21	-70.02	-36.70	-75.88	-47.75	-11.07	-32.79	-33.69	-27.40
	-18.55	-21.80	-13.65	-1.52	-3.38	2.12	-10.30	0.62	-18.23	-26.16	-21.02
+3.0%ii	1.95	-18.05	-3.31	6.77	-1.51	1.31	7.16	2.99	-15.47	-20.09	-18.58
	12.49	-12.45	0.83	3.31	8.35	2.07	12.39	7.85	-12.14	-12.92	-12.28
	35.52	-5.89	14.80	3.46	17.26	1.91	27.54	15.54	-5.89	-5.90	-5.89
	68.05	-0.11	27.20	12.35	28.50	8.34	43.99	24.18	-0.06	-0.21	-0.07
	92.77	3.79	31.08	25.75	35.94	17.08	51.77	30.04	3.78	3.75	3.85
	120.36	8.84	39.27	37.14	43.95	24.44	63.97	35.68	8.82	8.84	8.87
	139.22	12.31	45.39	46.81	47.03	29.19	69.22	43.33	12.34	12.32	12.28
	159.07	16.37	49.61	53.02	56.44	35.89	77.22	47.26	16.35	16.38	16.37
	177.80	20.44	54.98	58.72	64.10	39.58	84.56	54.08	20.45	20.45	20.41
	198.78	24.51	59.37	65.01	74.39	44.52	92.19	60.99	24.53	24.52	24.49
	224.04	28.42	68.38	72.43	83.23	48.73	102.05	70.64	28.41	28.42	28.44
	249.07	32.03	77.39	81.23	90.44	52.10	111.03	81.37	31.98	32.03	32.07
	272.54	35.10	86.86	92.51	93.17	55.12	118.15	93.31	35.13	35.15	35.02
	282.41	36.73	89.05	99.61	93.75	58.06	119.49	97.72	36.75	36.73	36.72

step	F (kN)	d (mm)	A_t (kN)	B_t (kN)	C_t (kN)	A_b (kN)	B_b (kN)	C_b (kN)	d_A (mm)	d_B (mm)	d_C (mm)
	185.58	33.73	58.14	53.98	73.45	46.72	90.95	47.60	33.99	34.46	32.73
-3.0%ii	-3.34	16.17	-0.51	-6.21	3.38	-0.92	12.78	-1.42	17.80	17.91	12.80
	-25.10	7.62	-8.44	-16.68	0.02	-10.82	10.43	-9.33	7.65	7.87	7.35
	-55.71	0.36	-12.53	-26.06	-17.12	-23.12	-8.01	-13.11	0.33	0.56	0.19
	-84.43	-3.55	-20.37	-38.91	-25.16	-28.03	-19.09	-21.97	-3.61	-3.51	-3.53
	-103.40	-8.00	-22.37	-46.19	-34.84	-35.35	-28.62	-25.28	-7.99	-7.96	-8.06
	-122.94	-11.56	-29.49	-53.98	-39.47	-38.54	-36.83	-32.67	-11.52	-11.55	-11.62
	-141.56	-15.29	-36.23	-60.37	-44.97	-44.80	-44.41	-37.70	-15.26	-15.30	-15.32
	-156.96	-18.58	-43.89	-66.04	-47.03	-49.83	-49.69	-43.36	-18.57	-18.58	-18.58
	-176.28	-22.50	-53.34	-73.61	-49.33	-57.86	-54.83	-49.44	-22.53	-22.50	-22.48
	-208.63	-27.69	-64.86	-83.42	-60.35	-71.22	-65.34	-56.84	-27.64	-27.65	-27.79
	-231.26	-31.05	-75.84	-90.39	-65.04	-78.50	-72.96	-64.15	-31.06	-31.04	-31.06
	-253.45	-34.49	-85.68	-99.19	-68.58	-85.61	-79.29	-72.49	-34.49	-34.48	-34.51
	-267.25	-36.99	-90.77	-105.57	-70.91	-90.80	-83.47	-77.17	-36.95	-36.97	-37.06
	-146.05	-32.08	-75.78	-32.63	-37.63	-32.56	-75.04	-29.33	-31.77	-34.21	-30.27
+3.5%i	-17.96	-21.58	-13.97	-0.94	-3.06	0.78	-9.01	3.63	-17.71	-26.59	-20.45
	9.50	-14.18	0.68	2.10	6.72	1.57	15.51	7.19	-13.84	-14.25	-14.46
	40.11	-5.61	18.17	2.30	19.64	1.79	33.86	19.60	-5.63	-5.64	-5.56
	72.09	-0.13	21.69	15.28	35.13	14.30	47.09	23.58	-0.14	-0.13	-0.12
	101.16	4.90	29.41	27.07	44.68	22.25	60.66	29.95	4.89	4.88	4.93
	129.62	9.74	37.59	38.70	53.32	29.26	72.92	35.94	9.74	9.77	9.73
	152.24	14.52	44.33	47.44	60.47	35.38	81.76	42.50	14.46	14.51	14.60
	173.83	19.27	52.69	54.47	66.67	39.91	89.54	50.65	19.29	19.27	19.24
	199.40	24.75	61.27	60.48	77.65	44.16	100.99	59.31	24.76	24.78	24.70
	230.06	29.87	72.41	71.83	85.82	49.75	111.37	71.28	29.89	29.90	29.84
	244.93	32.84	75.39	76.69	92.85	55.35	117.40	71.85	32.88	32.93	32.70
	265.89	38.71	81.44	74.26	110.19	65.86	132.63	65.97	38.67	38.67	38.79
	276.42	43.33	83.83	83.69	108.90	68.86	133.94	70.69	43.29	43.35	43.35
	176.68	39.51	49.32	49.16	78.20	58.06	99.30	22.35	40.14	41.36	37.04
-3.5%i	25.16	28.09	16.24	-0.76	9.68	-0.20	39.98	5.18	27.34	33.34	23.60
	-8.35	18.56	-5.15	-6.72	3.52	0.09	13.10	-2.18	19.66	19.72	16.29
	-27.53	10.59	-10.49	-8.75	-8.29	-9.95	4.96	-2.12	10.63	10.86	10.29
	-73.14	0.86	-19.32	-35.65	-18.17	-24.74	-6.63	-24.59	0.87	0.94	0.78
	-100.76	-4.75	-29.73	-45.94	-25.08	-28.89	-19.86	-33.89	-4.78	-4.72	-4.74
	-122.16	-9.64	-34.94	-54.79	-32.44	-34.90	-29.19	-39.34	-9.65	-9.64	-9.62
	-141.00	-14.42	-46.07	-60.68	-34.25	-37.68	-37.87	-48.36	-14.43	-14.38	-14.44
	-159.82	-18.69	-54.06	-66.42	-39.34	-44.44	-45.58	-52.22	-18.67	-18.69	-18.70
	-184.95	-23.84	-63.41	-73.08	-48.47	-54.52	-53.27	-57.71	-23.84	-23.86	-23.81
	-214.79	-29.46	-75.44	-81.39	-57.97	-66.70	-62.97	-64.53	-29.41	-29.46	-29.52
	-242.15	-35.69	-91.36	-93.27	-57.52	-77.66	-72.64	-73.68	-35.72	-35.68	-35.68
	-253.50	-41.47	-105.08	-90.61	-57.80	-77.46	-82.47	-80.71	-41.47	-41.52	-41.42
	-246.46	-43.96	-103.10	-83.66	-59.70	-48.05	-93.36	-88.70	-43.95	-43.99	-43.92
	-132.59	-38.52	-46.24	-40.20	-46.15	-28.84	-65.59	-26.36	-37.28	-40.95	-37.34
+3.5%ii	-15.38	-27.97	-7.34	-0.85	-7.19	0.39	-6.59	5.46	-25.25	-32.05	-26.60
	9.79	-20.19	2.01	1.36	6.42	3.93	15.58	6.32	-19.72	-20.34	-20.50
	21.77	-14.17	4.30	-0.58	18.05	9.79	23.42	4.93	-13.79	-14.37	-14.36
	59.58	-5.03	12.81	8.89	37.88	23.26	36.06	13.69	-5.00	-5.06	-5.02
	97.31	2.67	24.95	20.55	51.81	31.62	54.92	21.58	2.67	2.65	2.68
	117.39	7.28	31.66	25.84	59.88	35.98	67.01	24.55	7.28	7.29	7.25
	135.31	11.41	34.66	31.83	68.83	42.30	76.34	26.88	11.40	11.41	11.43
	152.87	16.66	39.67	38.73	74.47	45.92	83.44	32.90	16.68	16.65	16.65
	180.75	24.02	47.17	50.47	83.11	52.38	92.07	43.12	24.08	24.04	23.94
	202.97	29.69	59.03	56.13	87.82	54.70	101.04	52.51	29.75	29.72	29.60
	224.34	34.28	66.43	64.17	93.75	59.18	108.75	59.70	34.28	34.29	34.28

step	F (kN)	d (mm)	A_t (kN)	B_t (kN)	C_t (kN)	A_b (kN)	B_b (kN)	C_b (kN)	d_A (mm)	d_B (mm)	d_C (mm)
	241.10	38.26	69.52	74.19	97.39	62.49	113.28	66.83	38.24	38.31	38.21
	258.95	42.26	75.35	86.23	97.37	65.18	117.58	75.25	42.33	42.36	42.09
	263.14	43.08	76.22	90.63	96.29	65.36	118.11	78.70	43.14	43.21	42.89
	137.71	37.54	50.19	36.99	50.53	26.14	91.51	25.56	37.09	41.00	34.52
	28.09	29.23	16.83	-0.29	11.55	-0.57	42.91	5.57	28.51	34.45	24.74
-3.5%ii	-7.01	15.90	-3.65	-4.09	0.73	-1.42	12.01	0.01	16.72	16.65	14.34
	-33.16	6.62	-19.27	-10.01	-3.89	-6.56	5.07	-11.07	6.66	6.59	6.62
	-60.88	-0.23	-33.05	-16.28	-11.55	-12.68	-6.79	-22.07	-0.23	-0.17	-0.27
	-87.11	-6.13	-44.38	-31.31	-11.41	-15.52	-15.87	-37.89	-6.19	-6.17	-6.03
	-102.26	-9.53	-49.63	-32.16	-20.48	-17.54	-26.58	-40.62	-9.52	-9.49	-9.57
	-118.38	-14.36	-56.06	-41.50	-20.82	-18.94	-33.66	-50.60	-14.24	-14.32	-14.52
	-140.80	-19.99	-67.74	-46.19	-26.87	-22.29	-46.70	-55.76	-19.97	-19.96	-20.03
	-158.73	-25.06	-73.30	-53.85	-31.58	-26.78	-52.93	-63.09	-25.06	-25.05	-25.06
	-177.17	-30.93	-82.75	-58.60	-35.82	-25.07	-62.23	-73.19	-31.02	-30.97	-30.81
	-189.21	-34.20	-86.86	-60.48	-41.87	-26.10	-69.20	-77.02	-34.19	-34.24	-34.16
	-204.82	-39.24	-95.43	-63.88	-45.52	-24.81	-78.83	-85.11	-39.26	-39.25	-39.20
	-221.53	-43.07	-91.89	-74.46	-55.18	-34.71	-84.14	-84.77	-43.05	-43.08	-43.07
	-99.46	-36.19	-19.08	-32.54	-47.84	-18.64	-53.32	-8.02	-33.34	-40.09	-35.15
+3.5%iii	-23.68	-29.40	-19.29	-1.07	-3.32	1.10	-11.21	1.83	-28.71	-32.73	-26.76
	8.45	-19.37	6.53	1.45	0.47	0.51	13.89	10.53	-19.49	-19.65	-18.98
	33.79	-6.78	8.54	-0.09	25.35	15.95	25.12	8.26	-6.70	-6.89	-6.74
	61.94	0.03	21.71	5.20	35.02	22.14	34.77	17.90	0.11	0.03	-0.06
	77.04	4.81	31.38	7.44	38.22	25.65	42.74	22.64	4.81	4.80	4.82
	98.81	9.49	39.10	10.74	48.96	29.14	54.15	27.35	9.43	9.45	9.60
	123.87	15.58	46.64	8.33	68.91	35.98	76.61	24.70	15.60	15.54	15.60
	144.51	20.65	52.39	18.16	73.96	38.71	85.29	31.95	20.66	20.65	20.64
	165.42	25.67	55.04	25.91	84.47	44.43	94.09	36.20	25.64	25.67	25.71
	183.36	30.55	58.41	34.55	90.40	49.24	100.03	42.04	30.56	30.56	30.51
	202.46	35.42	63.35	44.02	95.09	52.92	105.23	49.43	35.48	35.43	35.34
	218.69	40.67	61.80	48.13	108.76	60.73	116.26	44.37	40.63	40.66	40.71
	194.35	44.06	52.28	41.83	100.25	63.35	110.99	21.14	44.05	44.05	44.09
	41.67	33.33	28.28	-0.67	14.06	-0.20	55.27	5.64	31.10	38.15	30.73
-3.5%ii	0.66	23.96	1.36	-0.78	0.08	0.55	13.30	4.30	24.93	25.16	21.79
	-23.02	10.15	-10.81	-9.60	-2.61	-4.33	13.03	-12.15	9.96	10.23	10.25
	-53.87	-0.38	-26.42	-12.08	-15.36	-12.63	3.58	-25.43	-0.41	-0.31	-0.40
	-69.64	-5.41	-46.24	-16.19	-7.21	-4.04	-6.55	-42.82	-5.36	-5.37	-5.49
	-90.48	-10.47	-54.96	-25.82	-9.70	-8.39	-13.08	-53.53	-10.55	-10.45	-10.41
	-110.78	-16.03	-62.10	-33.79	-14.89	-11.91	-24.90	-58.79	-16.05	-16.04	-15.99
	-130.08	-20.59	-64.31	-39.87	-25.90	-18.78	-36.68	-59.44	-20.52	-20.59	-20.68
	-148.69	-25.33	-69.75	-47.73	-31.21	-23.07	-45.12	-65.14	-25.37	-25.34	-25.29
	-170.70	-31.08	-74.04	-56.17	-40.49	-29.46	-55.27	-69.19	-31.04	-31.09	-31.11
	-185.93	-36.10	-78.91	-59.43	-47.60	-31.17	-65.50	-72.43	-36.05	-36.12	-36.12
	-202.81	-40.75	-87.14	-62.74	-52.93	-32.68	-76.25	-76.52	-40.73	-40.72	-40.81
	-209.87	-42.99	-86.95	-67.52	-55.40	-36.92	-78.81	-76.47	-43.00	-42.97	-43.01
+4.0%i	-19.87	-29.22	-16.92	-1.05	-1.89	0.62	-0.62	12.48	-27.92	-33.34	-26.40
	15.37	-13.47	10.60	-1.85	6.62	0.44	32.15	18.20	-12.74	-14.08	-13.59
	24.26	-8.83	11.41	-0.07	12.92	4.81	34.12	20.80	-8.75	-8.86	-8.88
	69.22	4.80	34.86	-0.69	35.05	15.80	52.05	34.15	4.83	4.79	4.77
	85.65	9.66	42.83	-0.13	42.95	20.31	60.37	37.68	9.63	9.70	9.65
	103.33	14.91	52.64	0.04	50.65	23.25	71.17	41.58	14.92	14.92	14.90
	132.09	21.94	60.23	4.44	67.42	30.46	90.00	43.53	21.96	21.96	21.90
	148.69	26.39	73.00	4.36	71.33	26.69	104.97	49.77	26.51	26.33	26.33
	172.36	30.73	74.52	15.19	82.66	35.89	114.14	51.81	30.64	30.68	30.86
	193.96	36.03	78.51	24.75	90.71	41.85	122.87	55.49	36.01	36.04	36.04

step	F (kN)	d (mm)	A_t (kN)	B_t (kN)	C_t (kN)	A_b (kN)	B_b (kN)	C_b (kN)	d_A (mm)	d_B (mm)	d_C (mm)
	203.41	40.75	75.58	35.13	92.71	49.42	126.90	50.85	40.66	40.65	40.94
	204.16	45.03	67.91	22.98	113.26	58.31	144.77	24.17	44.90	44.90	45.29
	222.35	49.16	70.56	40.34	111.45	60.37	149.13	34.35	49.10	49.10	49.28
-4.0%i	11.94	33.04	2.74	-0.60	9.80	-0.25	39.71	10.56	28.56	36.91	33.65
	-11.55	17.00	-5.43	-5.58	-0.53	-1.61	24.39	1.04	17.65	17.64	15.73
	-34.77	6.40	-16.37	-10.03	-8.37	-6.56	23.68	-13.21	6.31	6.52	6.37
	-46.65	0.69	-19.93	-11.48	-15.24	-11.10	22.24	-18.72	0.62	0.91	0.55
	-63.73	-5.80	-30.38	-16.95	-16.40	-13.53	18.44	-29.93	-5.83	-5.78	-5.79
	-79.60	-10.09	-38.40	-21.86	-19.34	-15.82	11.41	-37.56	-10.08	-10.02	-10.18
	-95.41	-14.80	-47.41	-28.23	-19.76	-17.66	4.05	-45.14	-14.86	-14.74	-14.78
	-116.52	-20.23	-55.72	-32.99	-27.81	-20.90	-9.62	-49.81	-20.10	-20.13	-20.46
	-141.69	-26.49	-67.80	-40.54	-33.35	-22.35	-26.17	-57.84	-26.45	-26.51	-26.52
	-160.66	-31.57	-73.19	-52.95	-34.52	-27.07	-33.70	-65.23	-31.67	-31.52	-31.53
	-183.35	-37.87	-81.65	-59.59	-42.12	-31.38	-49.48	-67.45	-37.90	-37.89	-37.82
	-203.22	-43.87	-86.69	-69.99	-46.54	-38.36	-58.98	-70.27	-43.92	-43.88	-43.82
	-206.94	-46.43	-94.16	-66.69	-46.09	-29.05	-68.66	-74.61	-46.42	-46.43	-46.43
	-213.34	-49.01	-93.40	-71.40	-48.53	-32.90	-72.31	-74.35	-49.01	-48.97	-49.04
	-145.30	-46.04	-50.19	-51.46	-43.64	-32.54	-44.87	-37.51	-45.62	-46.74	-45.75
+4.0%ii	-11.38	-31.78	-4.54	-1.05	-5.79	0.32	11.04	11.84	-29.12	-34.66	-31.56
	10.39	-21.29	5.30	-0.94	6.03	2.27	27.56	14.97	-21.31	-21.42	-21.15
	35.42	-4.12	16.96	-1.41	19.87	9.96	35.71	23.14	-4.23	-4.03	-4.09
	65.09	8.26	41.73	-1.09	24.45	11.36	50.50	38.34	8.24	8.21	8.34
	83.05	14.27	50.55	-0.98	33.48	14.96	59.64	42.19	14.20	14.29	14.30
	103.46	21.29	59.15	0.87	43.44	19.79	71.24	45.21	21.36	21.29	21.21
	121.44	25.74	62.53	6.32	52.59	26.10	80.09	46.38	25.53	25.82	25.88
	139.79	30.14	65.09	13.33	61.37	32.66	89.46	46.97	29.98	30.29	30.16
	158.78	36.83	76.67	3.24	78.87	32.50	114.14	42.78	36.79	36.86	36.83
	183.84	41.59	78.58	23.03	82.23	39.99	120.50	49.71	41.52	41.65	41.59
	199.62	46.52	89.75	24.46	85.41	33.17	136.92	55.41	46.57	46.53	46.45
	203.92	50.34	77.32	11.10	115.51	50.32	157.03	21.75	50.37	50.63	50.01
-4.0%ii	5.43	31.67	2.80	-0.49	3.12	-0.38	39.15	6.11	29.08	39.26	26.66
	-9.97	17.08	-6.72	-6.37	3.12	-1.14	26.58	2.41	16.89	17.38	16.96
	-32.20	5.62	-8.76	-12.55	-10.88	-12.12	25.26	-4.40	5.42	5.95	5.50
	-37.70	0.39	-9.56	-16.57	-11.57	-14.13	25.08	-11.36	0.29	0.57	0.32
	-46.70	-5.12	-12.91	-24.46	-9.33	-17.73	25.00	-18.81	-5.13	-5.05	-5.19
	-65.40	-9.98	-33.77	-25.89	-5.75	-9.79	18.00	-34.23	-9.94	-10.01	-9.98
	-85.65	-15.49	-42.77	-32.61	-10.27	-14.39	6.88	-40.23	-15.52	-15.50	-15.44
	-104.39	-21.24	-51.20	-39.00	-14.20	-18.83	-3.46	-45.12	-21.31	-21.24	-21.17
	-124.55	-27.03	-58.47	-47.04	-19.05	-23.78	-12.46	-51.36	-26.98	-27.03	-27.09
	-135.62	-30.73	-65.98	-48.78	-20.86	-22.63	-20.18	-56.22	-30.69	-30.71	-30.80
	-154.50	-36.86	-74.21	-60.28	-20.01	-27.00	-27.19	-63.69	-36.91	-36.84	-36.83
	-171.12	-42.65	-82.39	-66.40	-22.33	-26.81	-38.83	-68.74	-42.66	-42.69	-42.60
	-183.11	-45.71	-84.30	-72.59	-26.22	-31.05	-44.40	-72.16	-45.70	-45.69	-45.74
	-192.65	-49.77	-94.07	-74.39	-24.19	-26.26	-53.81	-77.70	-49.74	-49.77	-49.82
	-118.79	-45.73	-52.30	-37.07	-29.42	-24.20	-45.68	-10.51	-45.84	-47.78	-43.56
	-29.70	-36.72	-23.72	-1.05	-4.93	0.90	-10.39	12.43	-34.86	-41.19	-34.10

Table A3.4: Elongation of beams at peak of displacement step of Unit 2.

displacement step	E_{M-A}	E_{A-B}	E_{B-C}	E_{C-N}
+0.2%ii	-0.202	0.096	-0.02	-0.264
-0.2%ii	-0.167	-0.038	0.079	-0.296
+0.5%i	-0.227	0.263	0.029	-0.273
-0.5%i	-0.082	0.05	0.313	-0.291
+0.5%ii	-0.176	0.307	0.115	-0.263
-0.5%ii	-0.045	0.055	0.335	-0.276
+1.0%i	0.369	0.842	0.416	0.135
-1.0%i	0.642	0.576	1.229	0.156
+1.0%ii	0.353	1.084	0.717	0.174
-1.0%ii	0.629	0.659	1.305	0.204
+1.5%i	0.532	2.053	1.473	0.287
-1.5%i	0.747	1.763	2.751	0.271
+1.5%ii	0.293	2.374	1.827	0.31
-1.5%ii	0.492	1.902	2.926	0.312
+2.0%i	0.405	3.482	2.684	0.366
-2.0%i	0.567	3.103	4.339	0.42
+2.0%ii	0.438	3.887	3.094	0.408
-2.0%ii	0.678	3.224	4.476	0.416
+2.5%i	0.59	5.154	3.996	0.481
-2.5%i	0.484	4.456	6.044	0.57
+2.5%ii	0.449	5.582	4.266	0.499
-2.5%ii	0.551	4.663	6.291	0.53
+3.0%i	0.609	6.974	5.713	0.666
-3.0%i	0.644	5.982	8.286	0.774
+3.0%ii	0.625	7.559	6.442	0.883
-3.0%ii	0.62	6.144	8.869	0.86
+3.5%i	0.909	9.147	9.171	1.701
-3.5%i	1.809	8.861	12.216	1.741
+3.5%ii	2.025	11.132	10.751	1.97
-3.5%ii	2.407	12.2	14.292	1.895
+3.5%iii	2.813	14.105	13.704	2.424
-3.5%iii	2.504	15.161	16.957	2.241
+4.0%i	3.405	15.214	17.228	2.945
-4.0%i	3.125	16.979	20.416	3.174
+4.0%ii	4.08	15.139	20.115	2.741
-4.0%ii	3.233	17.456	21.949	4.869

Where: E_{M-A} - beam elongation measured between end of frame at M and column A.

E_{A-B} - beam elongation measured between columns A and B.

E_{B-C} - beam elongation measured between columns B and C.

E_{C-N} - beam elongation measured between column C and end of frame at N.

A3.3 Experimental Data of Unit 3 (see *Chapter 6*)

Table A3.5: Forces and displacements at top and bottom of columns of Unit 3.

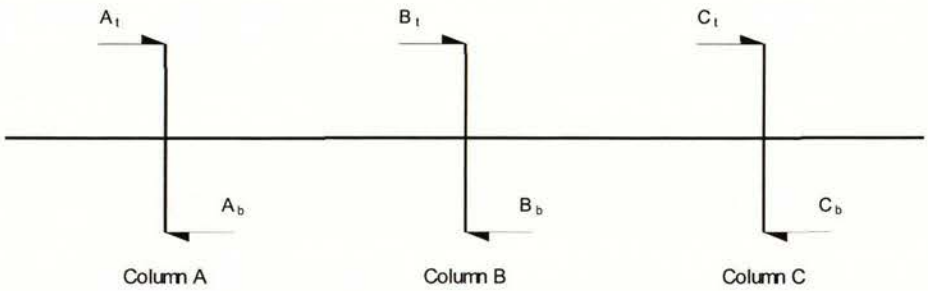

Where: F - sum of lateral force applied.
d - average displacement columns.
A_t - lateral force applied at top of column A.
A_b - lateral force applied at bottom of column A.
B_t - lateral force applied at top of column B.
B_b - lateral force applied at bottom of column B.
C_t - lateral force applied at top of column C.
C_b - lateral force applied at bottom of column C.
d_A - relative lateral displacement between top and bottom of column A.
d_B - relative lateral displacement between top and bottom of column B.
d_C - relative lateral displacement between top and bottom of column C.

step	F (kN)	d (mm)	A_t (kN)	B_t (kN)	C_t (kN)	A_b (kN)	B_b (kN)	C_b (kN)	d_A (mm)	d_B (mm)	d_C (mm)
+0.2%i	0.37	-0.08	0.60	0.04	-0.27	0.20	-0.21	0.09	0.01	-0.17	-0.07
	11.27	0.60	3.29	3.73	4.24	3.63	6.04	1.49	0.61	0.59	0.60
	22.01	1.24	4.60	10.14	7.27	6.69	9.69	5.57	1.25	1.23	1.23
	31.94	1.77	6.19	15.79	9.96	9.73	13.35	9.26	1.77	1.75	1.78
	40.45	2.45	5.15	23.32	11.98	14.41	13.85	12.20	2.47	2.39	2.49
	16.15	1.37	6.17	4.23	5.76	1.80	10.38	4.00	1.22	1.30	1.58
	5.81	0.74	2.06	0.26	3.49	0.46	4.88	0.19	0.55	0.78	0.89
-0.2%i	-1.40	0.22	0.73	-1.11	-1.02	-1.26	0.18	-0.18	0.22	0.26	0.19
	-10.15	-0.45	-2.98	-4.42	-2.74	-2.94	-3.73	-3.00	-0.46	-0.44	-0.46
	-22.14	-1.19	-6.08	-11.07	-4.99	-7.47	-7.95	-6.26	-1.16	-1.16	-1.25
	-30.85	-1.62	-5.90	-17.07	-7.89	-12.42	-9.96	-7.95	-1.61	-1.61	-1.64
	-38.88	-2.10	-7.30	-23.26	-8.33	-15.31	-11.28	-11.59	-2.12	-2.10	-2.08
	-44.68	-2.45	-7.41	-27.46	-9.81	-18.17	-12.12	-13.48	-2.48	-2.40	-2.47
	-26.77	-1.79	-8.08	-12.16	-6.53	-7.46	-12.66	-5.48	-1.89	-1.98	-1.50
	-10.98	-0.99	-3.82	-0.62	-6.54	-2.34	-7.64	-0.26	-1.05	-0.86	-1.07
+0.2%ii	-0.29	-0.22	0.16	0.45	-0.90	0.12	-0.38	0.01	-0.20	-0.24	-0.23
	1.98	0.05	1.00	1.49	-0.52	0.71	-0.14	1.26	0.07	0.02	0.06
	11.54	0.73	4.29	3.12	4.13	2.58	6.84	2.06	0.73	0.70	0.77
	22.82	1.53	5.62	9.97	7.24	5.83	10.47	6.65	1.57	1.49	1.54
	33.56	2.10	5.93	18.84	8.79	10.54	11.63	11.65	2.11	2.07	2.12
	37.63	2.42	5.35	21.79	10.50	13.43	12.67	11.60	2.45	2.39	2.42

step	F (kN)	d (mm)	A_t (kN)	B_t (kN)	C_t (kN)	A_b (kN)	B_b (kN)	C_b (kN)	d_A (mm)	d_B (mm)	d_C (mm)
	18.41	1.63	5.33	6.21	6.87	4.43	9.65	4.33	1.64	1.43	1.83
-0.2%ii	-0.89	0.17	0.51	-0.55	-0.84	-0.10	-0.17	-0.32	0.16	0.17	0.17
	-10.46	-0.62	-2.51	-3.29	-4.66	-3.28	-4.57	-1.99	-0.69	-0.55	-0.63
	-19.15	-1.21	-3.93	-9.54	-5.68	-6.49	-6.92	-5.15	-1.20	-1.19	-1.24
	-30.16	-1.81	-5.24	-18.20	-6.72	-11.73	-8.19	-9.44	-1.81	-1.79	-1.83
	-43.05	-2.43	-5.49	-29.19	-8.37	-18.66	-9.00	-14.37	-2.40	-2.40	-2.48
	-10.23	-0.96	-3.11	-0.60	-6.53	-2.53	-6.97	-0.21	-1.05	-0.76	-1.08
	-2.83	-0.38	-1.18	-0.68	-0.96	-0.39	-1.38	-0.45	-0.42	-0.50	-0.23
+0.35%i	0.48	-0.07	1.22	-0.13	-0.61	0.19	-0.19	0.30	0.09	-0.22	-0.09
	12.51	0.83	5.84	3.14	3.53	1.69	7.61	3.50	0.84	0.82	0.84
	18.54	1.41	6.84	6.93	4.76	2.63	9.36	6.66	1.39	1.34	1.49
	34.01	2.23	7.91	19.03	7.06	8.45	11.55	14.23	2.19	2.16	2.33
	41.15	2.62	10.35	23.58	7.22	10.21	14.04	17.44	2.59	2.58	2.69
	50.25	3.48	11.03	26.82	12.40	15.42	18.41	16.73	3.55	3.44	3.45
	66.80	4.35	18.14	39.92	8.73	15.46	21.49	30.42	4.36	4.34	4.36
	28.03	2.90	8.73	9.86	9.44	8.46	16.30	3.40	3.20	3.04	2.45
	5.76	1.27	1.89	0.13	3.74	0.48	6.19	-0.45	0.72	1.69	1.41
-0.35%i	-2.56	0.47	-0.13	-1.13	-1.31	-0.39	-0.13	-1.31	0.28	0.64	0.50
	-15.42	-0.63	-4.49	-5.04	-5.89	-2.85	-6.96	-4.69	-0.60	-0.58	-0.70
	-27.84	-1.46	-2.75	-16.69	-8.41	-11.20	-7.25	-8.36	-1.45	-1.43	-1.51
	-35.81	-2.07	-6.53	-22.04	-7.24	-13.47	-9.72	-11.46	-2.10	-2.06	-2.05
	-49.28	-2.88	-4.06	-31.71	-13.51	-22.97	-12.11	-13.04	-2.85	-2.78	-3.00
	-65.47	-3.99	-8.35	-36.42	-20.69	-28.41	-21.73	-13.73	-4.06	-3.95	-3.95
	-32.66	-2.76	-9.37	-15.56	-7.73	-10.84	-13.47	-7.20	-3.11	-2.75	-2.42
+0.35%ii	-4.72	-0.91	-2.31	-0.68	-1.73	-0.55	-2.91	-0.75	-0.95	-1.00	-0.79
	10.72	0.81	5.71	2.50	2.51	0.92	6.14	3.84	0.82	0.81	0.81
	16.19	1.34	6.42	6.49	3.28	3.31	6.93	6.09	1.35	1.34	1.33
	26.82	2.31	7.21	12.82	6.79	6.94	10.22	9.81	2.37	2.27	2.31
	42.09	3.34	9.50	20.87	11.73	12.12	16.38	14.17	3.34	3.28	3.40
	59.69	4.30	14.50	32.20	12.99	16.31	22.26	22.12	4.27	4.28	4.35
	67.84	4.74	18.52	33.67	15.64	16.30	27.55	25.09	4.74	4.73	4.74
	39.49	3.68	11.21	19.03	9.25	13.27	18.21	8.31	4.12	3.86	3.04
	5.78	1.27	2.09	0.06	3.63	0.33	6.97	-0.62	0.62	1.91	1.29
-0.35%ii	-4.80	-0.11	-0.44	-1.37	-2.99	-1.08	-0.57	-1.84	-0.34	0.17	-0.15
	-14.24	-0.85	-4.53	-5.33	-4.38	-1.98	-5.52	-5.62	-0.83	-0.84	-0.89
	-29.05	-2.03	-4.88	-16.11	-8.06	-9.89	-8.61	-9.22	-2.01	-1.99	-2.08
	-36.27	-2.53	-4.97	-21.02	-10.29	-14.30	-10.22	-10.25	-2.56	-2.46	-2.55
	-45.43	-3.26	-7.51	-24.18	-13.74	-17.89	-15.91	-10.45	-3.29	-3.23	-3.24
	-68.77	-4.32	-11.64	-37.66	-19.46	-26.63	-23.68	-17.59	-4.35	-4.30	-4.30
	-37.90	-3.32	-16.03	-7.34	-14.53	-6.16	-21.41	-9.82	-3.59	-2.54	-3.84
	-5.40	-0.88	-2.06	-0.96	-2.38	0.13	-4.04	-0.93	-0.53	-1.26	-0.84
+0.5%i	-1.59	-0.58	-1.76	0.62	-0.44	0.62	-1.16	-0.48	-0.57	-0.58	-0.57
	9.15	0.87	3.86	1.69	3.61	1.74	5.22	2.47	0.84	0.78	1.00
	21.03	1.94	6.11	11.29	3.63	4.58	7.12	10.21	1.92	1.93	1.97
	30.10	2.78	8.28	13.17	8.66	7.43	13.58	9.72	2.71	2.73	2.89
	54.30	4.18	11.75	29.51	13.03	15.73	20.22	19.37	4.18	4.21	4.16
	74.18	5.40	15.43	39.11	19.63	22.30	28.27	24.92	5.40	5.39	5.42
	88.00	6.29	23.49	45.30	19.21	20.43	35.59	33.94	6.27	6.29	6.31
	12.32	2.33	7.31	-0.26	5.26	0.51	12.65	0.21	2.06	2.70	2.23
-0.5%i	1.15	1.27	1.95	-1.81	1.02	0.18	3.07	-0.70	1.07	1.45	1.28
	-3.91	0.38	-0.13	-1.90	-1.88	-0.44	-0.05	-1.81	0.34	0.43	0.36
	-14.49	-0.74	-5.57	-5.29	-3.63	-1.13	-5.14	-6.80	-0.74	-0.71	-0.78
	-27.90	-1.93	-1.98	-15.88	-10.04	-12.28	-7.18	-6.51	-1.95	-1.90	-1.94
	-44.39	-3.07	-7.24	-27.74	-9.40	-16.72	-10.84	-15.09	-3.11	-3.03	-3.08
	-48.14	-3.51	-5.59	-35.19	-7.37	-22.07	-7.40	-17.01	-3.59	-3.48	-3.47
	-91.11	-5.66	-11.26	-57.29	-22.55	-39.13	-24.60	-25.84	-5.70	-5.64	-5.64
	-98.35	-6.17	-12.03	-61.56	-24.76	-42.18	-27.34	-27.39	-6.21	-6.16	-6.13

step	F (kN)	d (mm)	A_t (kN)	B_t (kN)	C_t (kN)	A_b (kN)	B_b (kN)	C_b (kN)	d_A (mm)	d_B (mm)	d_C (mm)
	-49.12	-4.43	-12.57	-22.73	-13.82	-15.01	-19.60	-12.71	-4.68	-4.12	-4.49
+0.5%ii	2.03	0.06	1.00	0.11	0.92	1.20	-0.38	1.38	0.00	-0.10	0.28
	7.11	0.68	2.75	1.34	3.01	2.39	3.07	1.73	0.64	0.61	0.78
	15.05	1.72	4.55	6.12	4.38	5.20	6.00	4.46	1.72	1.71	1.73
	35.29	3.39	7.57	20.27	7.45	11.21	10.56	14.55	3.40	3.37	3.40
	44.15	3.95	8.70	26.42	9.04	13.96	12.74	18.60	3.88	3.95	4.01
	65.57	5.26	16.12	36.92	12.53	17.10	22.08	28.06	5.25	5.25	5.28
	81.44	6.12	27.87	36.06	17.50	14.27	37.66	32.00	6.18	6.08	6.10
	59.70	5.34	18.14	25.41	16.14	13.69	30.52	16.46	5.34	5.55	5.13
-0.5%ii	-3.87	0.25	0.09	-2.35	-1.61	-0.52	0.05	-1.65	0.20	0.29	0.27
	-10.95	-0.85	-4.37	-3.58	-2.99	-1.17	-4.16	-3.83	-0.91	-0.87	-0.78
	-22.37	-2.07	-2.15	-11.37	-8.85	-9.03	-6.78	-4.79	-2.07	-2.04	-2.09
	-34.32	-2.97	-7.08	-18.56	-8.68	-11.49	-10.84	-10.12	-3.10	-2.96	-2.86
	-59.38	-4.59	-10.88	-35.10	-13.40	-22.31	-18.16	-17.59	-4.59	-4.62	-4.56
	-77.48	-5.45	-13.12	-44.53	-19.83	-29.09	-25.36	-21.70	-5.43	-5.49	-5.42
	-93.20	-6.21	-12.79	-54.33	-26.08	-38.39	-29.49	-24.27	-6.21	-6.21	-6.21
	-62.08	-5.13	-15.17	-28.47	-18.44	-18.27	-26.63	-15.29	-5.09	-5.02	-5.27
+1.0%i	0.02	-0.52	-0.36	0.00	0.38	0.61	-0.55	0.13	-0.44	-0.63	-0.50
	8.51	0.93	3.66	2.67	2.19	1.24	2.89	4.73	0.85	0.88	1.06
	19.52	2.04	5.35	10.90	3.26	5.23	5.13	9.91	2.05	1.96	2.09
	32.83	3.52	8.13	14.87	9.83	9.13	14.00	10.20	3.56	3.50	3.50
	84.04	6.45	25.62	34.38	24.05	16.80	41.81	28.05	6.40	6.42	6.52
	111.07	10.28	36.57	59.26	15.24	18.14	49.17	47.22	10.22	10.26	10.35
	108.72	12.66	33.13	56.78	18.81	20.89	49.34	42.39	12.61	12.66	12.69
	69.60	11.04	22.73	35.96	10.92	15.55	35.99	19.34	11.42	11.38	10.33
-1.0%i	-5.41	4.81	-0.05	-0.81	-4.55	-1.44	0.04	-2.44	4.57	4.86	5.01
	-28.05	1.48	-3.18	-10.58	-14.28	-11.55	-6.19	-8.33	1.41	1.59	1.45
	-69.35	-2.83	-11.23	-38.30	-19.83	-27.58	-18.93	-22.17	-2.90	-2.81	-2.78
	-91.42	-5.24	-10.81	-53.82	-26.79	-39.34	-26.45	-24.93	-5.22	-5.21	-5.27
	-102.40	-8.73	-13.79	-66.60	-22.01	-36.70	-33.93	-30.44	-8.78	-8.73	-8.69
	-108.19	-10.33	-8.46	-72.40	-27.33	-45.26	-34.13	-27.88	-10.35	-10.25	-10.39
	-109.34	-12.92	-12.30	-69.90	-27.14	-43.43	-36.49	-28.96	-12.90	-12.84	-13.01
	-69.18	-11.37	-18.87	-19.40	-30.92	-14.84	-42.75	-10.08	-11.68	-10.20	-12.22
+1.0%ii	5.57	-4.16	4.24	-1.43	2.76	1.24	2.17	2.96	-4.28	-4.12	-4.09
	15.37	-1.78	10.92	-0.75	5.20	3.98	4.67	7.11	-1.79	-1.79	-1.75
	42.89	2.81	16.41	12.18	14.30	12.92	15.71	15.67	2.71	2.77	2.94
	58.17	4.17	20.82	21.21	16.14	16.89	21.28	21.18	4.14	4.17	4.20
	79.91	6.78	23.89	37.15	18.87	22.14	28.69	31.73	6.77	6.77	6.79
	99.36	10.70	28.66	53.26	17.45	22.59	39.77	40.69	10.65	10.70	10.76
	105.36	12.26	31.28	59.32	14.76	21.42	42.20	45.92	12.23	12.27	12.29
	82.39	11.60	21.76	38.92	21.71	22.44	42.30	19.19	11.79	11.87	11.14
-1.0%ii	-18.07	0.27	-9.43	-0.68	-7.96	-1.60	-5.99	-8.96	0.21	0.36	0.24
	-33.13	-2.15	-6.79	-15.58	-10.77	-14.12	-3.46	-14.29	-2.24	-2.10	-2.10
	-50.04	-4.95	-7.06	-29.81	-13.17	-20.32	-6.15	-21.41	-4.99	-4.85	-5.00
	-88.43	-9.03	-12.12	-52.36	-23.95	-35.73	-23.83	-28.05	-9.08	-8.98	-9.02
	-109.74	-12.30	-8.55	-71.46	-29.73	-47.93	-33.70	-27.36	-12.30	-12.26	-12.33
	-72.91	-10.98	-13.52	-41.87	-17.52	-22.92	-26.92	-21.76	-10.93	-10.58	-11.43
	-7.93	-5.83	-4.00	-0.90	-3.03	0.23	-6.57	-0.93	-6.19	-5.32	-6.00
	8.22	-2.26	4.48	-1.34	5.09	3.04	3.29	1.79	-2.32	-2.29	-2.18
+1.5%i	14.80	-0.40	10.23	-1.49	6.06	3.58	5.58	5.50	-0.43	-0.36	-0.40
	45.78	4.78	21.18	15.45	9.15	11.13	12.88	22.39	4.67	4.73	4.94
	67.29	7.30	24.58	21.19	21.52	16.72	29.11	23.34	7.25	7.28	7.37
	85.00	9.28	27.17	36.77	21.07	20.88	34.54	32.17	9.27	9.29	9.27
	108.21	13.81	34.28	58.04	15.89	19.70	46.13	46.17	13.78	13.83	13.80
	103.70	18.57	29.11	48.95	25.64	23.90	51.70	31.63	18.54	18.53	18.64
	39.46	14.82	13.57	14.04	11.84	6.84	27.17	6.55	14.42	15.01	15.05
	-17.54	5.39	-4.80	-4.16	-8.58	-6.29	-1.50	-8.67	5.39	5.38	5.39

step	F (kN)	d (mm)	A_t (kN)	B_t (kN)	C_t (kN)	A_b (kN)	B_b (kN)	C_b (kN)	d_A (mm)	d_B (mm)	d_C (mm)
-1.5%i	-49.32	0.02	-8.41	-27.27	-13.65	-21.28	-4.27	-22.98	-0.06	0.04	0.07
	-71.37	-4.13	-8.75	-39.22	-23.40	-31.63	-17.10	-22.14	-4.12	-4.12	-4.16
	-89.08	-6.67	-13.66	-53.54	-21.88	-34.52	-23.52	-31.08	-6.70	-6.66	-6.64
	-98.29	-8.76	-13.97	-60.94	-23.38	-38.10	-29.10	-31.16	-8.80	-8.74	-8.74
	-108.11	-13.14	-9.61	-76.26	-22.24	-47.06	-29.19	-32.07	-13.22	-13.11	-13.08
	-111.69	-16.04	-7.55	-83.37	-20.77	-50.89	-26.49	-34.80	-16.07	-16.06	-16.00
	-113.35	-18.47	-6.04	-86.63	-20.67	-53.71	-24.25	-35.68	-18.56	-18.43	-18.41
	-73.11	-16.59	-12.17	-39.54	-21.40	-24.94	-33.99	-12.30	-16.58	-16.67	-16.51
	-44.63	-14.80	-13.45	-21.51	-9.67	-9.93	-23.97	-9.86	-14.92	-14.74	-14.73
+1.5%ii	28.45	-0.55	14.34	1.34	12.76	11.41	9.62	7.99	-0.40	-0.54	-0.70
	50.29	3.47	21.87	9.92	18.50	13.75	21.09	17.09	3.47	3.45	3.49
	68.69	6.29	23.82	22.15	22.72	18.95	28.88	23.68	6.23	6.28	6.35
	87.51	10.40	26.93	36.13	24.45	22.09	39.03	29.54	10.42	10.40	10.39
	100.71	14.69	30.91	43.64	26.16	22.59	51.35	30.66	14.69	14.71	14.67
	105.75	18.53	30.60	51.23	23.91	23.76	50.31	36.00	18.51	18.55	18.54
	77.96	17.24	21.54	40.80	15.62	18.63	34.95	26.81	17.07	17.30	17.35
	10.23	11.35	5.11	-0.28	5.39	0.47	12.13	-0.88	10.83	11.56	11.66
-1.5%ii	-34.91	0.24	-7.73	-18.71	-8.46	-16.80	1.30	-19.01	0.22	0.28	0.20
	-44.45	-1.59	-6.64	-25.76	-12.05	-22.89	0.61	-21.87	-1.62	-1.59	-1.55
	-66.06	-5.88	-8.39	-41.16	-16.51	-30.75	-5.64	-29.25	-5.88	-5.87	-5.87
	-80.01	-9.70	-10.06	-48.61	-21.34	-35.73	-15.90	-29.14	-9.72	-9.69	-9.68
	-110.95	-16.51	-3.82	-83.58	-23.55	-54.91	-22.12	-35.04	-16.55	-16.44	-16.53
	-114.42	-18.56	-4.68	-89.09	-20.65	-55.87	-21.95	-37.83	-18.66	-18.51	-18.50
	-76.53	-16.78	-15.65	-47.03	-13.86	-25.14	-29.45	-21.51	-16.86	-17.10	-16.38
	-47.08	-14.91	-13.30	-25.78	-8.00	-11.66	-20.90	-14.29	-14.94	-14.86	-14.93
	3.63	-7.87	2.80	-1.86	2.69	1.11	2.10	0.23	-7.85	-7.89	-7.87
+2.0%i	27.84	0.42	13.81	-1.92	15.95	9.25	15.07	3.79	0.37	0.48	0.40
	35.87	2.69	20.56	-0.04	15.35	8.86	16.66	10.99	2.63	2.71	2.71
	58.27	6.90	28.95	9.50	19.83	11.85	27.25	20.85	6.94	6.88	6.89
	69.42	9.18	30.70	16.54	22.19	14.40	32.94	24.21	9.17	9.16	9.20
	96.42	15.22	35.46	36.89	24.07	18.69	47.24	33.89	15.24	15.24	15.18
	106.92	22.80	30.66	46.65	29.61	25.20	55.00	30.44	22.79	22.84	22.77
	105.26	24.92	28.68	44.38	32.21	26.96	54.82	27.12	24.88	25.01	24.87
	75.28	23.40	25.33	32.35	17.60	17.60	38.80	20.84	23.65	23.43	23.11
	54.48	21.97	19.36	21.40	13.72	13.20	29.47	13.43	22.25	21.89	21.77
	-11.02	9.96	-5.48	-1.90	-3.65	-0.55	-1.17	-8.84	10.51	9.85	9.52
-2.0%i	-41.84	0.72	-8.30	-21.85	-11.69	-21.76	-0.02	-19.67	0.59	0.78	0.79
	-51.72	-2.05	-5.70	-32.69	-13.34	-26.01	-0.05	-25.51	-2.15	-1.98	-2.02
	-69.52	-8.85	0.11	-51.70	-17.93	-35.38	-4.80	-28.16	-8.82	-8.79	-8.93
	-89.99	-14.07	21.18	-83.09	-28.08	-63.09	-0.01	-26.18	-14.26	-13.95	-14.01
	-111.07	-19.60	12.14	-104.67	-18.54	-67.89	-5.40	-37.68	-19.59	-19.65	-19.55
	-122.82	-24.88	9.68	-114.05	-18.44	-77.13	-5.66	-40.17	-24.94	-24.81	-24.89
	-47.50	-21.39	-0.49	-2.33	-44.68	-29.12	-17.87	1.04	-22.88	-15.20	-26.11
	-9.46	-17.23	-2.27	-0.85	-6.33	-2.71	-2.98	-2.81	-17.57	-14.56	-19.57
+2.0%ii	43.71	8.43	7.17	18.67	17.87	28.56	7.11	9.58	8.51	8.34	8.45
	68.04	13.55	4.13	43.89	20.02	38.17	1.25	31.66	13.44	13.49	13.70
	79.65	17.80	3.07	54.56	22.01	42.00	6.00	35.09	17.85	17.67	17.88
	89.96	22.87	-0.56	67.83	22.69	46.84	8.51	38.71	23.30	22.60	22.71
	96.42	25.13	-1.02	78.82	18.62	48.04	6.76	46.26	25.41	25.01	24.96
	51.34	22.64	0.18	30.79	20.36	24.74	10.22	16.96	22.53	22.14	23.25
	6.80	17.71	2.20	-0.43	5.03	0.50	5.63	0.88	17.53	18.37	17.23
	-12.86	8.90	-4.64	-3.71	-4.51	-4.68	0.17	-7.97	8.76	9.08	8.86
-2.0%ii	-40.06	0.28	-12.99	-18.37	-8.69	-20.26	1.69	-21.26	0.23	0.36	0.24
	-56.26	-5.36	-8.48	-32.35	-15.43	-32.84	5.00	-28.39	-5.57	-5.14	-5.37
	-73.34	-10.53	-2.69	-49.25	-21.40	-46.23	4.19	-31.46	-10.87	-10.23	-10.49
	-90.52	-15.84	0.42	-70.63	-20.31	-56.57	3.02	-37.37	-16.30	-15.60	-15.61
	-103.43	-19.87	2.37	-86.16	-19.63	-63.80	0.13	-39.66	-20.66	-19.40	-19.56

step	F (kN)	d (mm)	A_t (kN)	B_t (kN)	C_t (kN)	A_b (kN)	B_b (kN)	C_b (kN)	d_A (mm)	d_B (mm)	d_C (mm)
	-119.80	-24.47	19.96	-112.80	-26.97	-82.89	0.15	-37.50	-24.30	-24.39	-24.70
	-55.11	-21.21	0.29	-36.98	-18.42	-27.56	-9.59	-16.48	-20.59	-20.33	-22.70
	-7.99	-16.20	-2.71	-0.81	-4.47	-1.94	-3.17	-1.45	-16.29	-15.77	-16.56
+2.5%i	38.23	2.31	23.14	-2.30	17.39	8.20	24.35	7.36	1.25	3.38	2.30
	50.08	6.81	27.84	-1.71	23.95	11.79	28.56	11.73	6.70	6.98	6.74
	59.14	10.45	29.42	1.02	28.69	15.43	31.40	14.46	10.35	10.61	10.40
	80.76	19.04	28.04	21.96	30.77	24.41	33.60	25.76	18.96	19.15	19.00
	98.11	26.60	22.36	37.56	38.19	33.10	49.28	19.51	26.72	26.62	26.45
	97.47	29.63	17.72	37.47	42.28	36.76	50.99	13.59	29.69	29.66	29.56
	98.01	30.96	13.25	42.87	41.90	40.04	46.32	15.86	30.97	30.92	30.99
	67.38	28.95	27.69	17.69	21.99	12.60	42.79	13.30	29.29	28.77	28.78
	9.03	22.96	4.49	-0.09	4.63	-1.01	10.93	0.16	21.06	24.57	23.23
	-16.81	10.38	-6.15	-3.90	-6.76	-8.15	0.29	-8.42	10.37	10.47	10.30
-2.5%i	-39.28	-0.15	-13.34	-8.11	-17.83	-22.31	-2.45	-14.37	-0.17	-0.05	-0.23
	-54.24	-6.98	-6.86	-26.50	-20.88	-35.51	2.64	-20.85	-7.08	-6.93	-6.94
	-67.89	-12.90	-5.29	-57.53	-5.07	-43.19	18.13	-43.25	-12.86	-12.80	-13.05
	-79.57	-16.74	-4.64	-67.77	-7.16	-48.60	13.60	-44.93	-16.90	-16.56	-16.75
	-112.30	-24.47	15.81	-103.81	-24.30	-80.09	5.23	-37.35	-24.54	-24.55	-24.31
	-125.62	-30.36	21.45	-117.92	-29.15	-90.59	5.04	-37.46	-30.77	-30.87	-29.45
	-50.62	-27.20	0.95	-2.39	-49.17	-42.00	-6.78	0.68	-30.67	-18.21	-32.71
	5.95	-10.96	2.78	-0.81	3.97	5.13	0.07	0.07	-10.87	-11.11	-10.90
+2.5%ii	59.53	7.88	39.39	-2.28	22.42	9.65	25.51	25.57	7.49	8.24	7.89
	65.13	11.89	36.21	3.05	25.87	17.01	23.64	25.65	12.21	11.98	11.49
	77.93	22.17	23.62	12.33	41.97	32.26	37.41	9.59	22.20	22.21	22.09
	90.92	28.07	20.89	27.31	42.72	35.60	43.46	13.79	28.14	27.93	28.13
	97.15	30.54	18.30	38.73	40.11	37.16	42.47	19.68	30.63	30.55	30.44
	58.62	27.71	21.11	24.71	12.80	16.21	21.77	21.89	28.02	27.86	27.25
	-3.54	16.02	-0.53	-0.90	-2.11	-2.93	0.13	-0.83	15.69	16.27	16.09
	-18.86	4.79	-6.68	-1.49	-10.69	-13.99	-0.52	-3.89	5.01	5.53	3.83
-2.5%ii	-29.39	0.77	-15.52	-3.93	-9.94	-14.51	-1.38	-13.87	0.97	1.03	0.30
	-37.61	-3.92	-18.85	-6.79	-11.98	-18.70	-0.46	-18.85	-3.90	-3.88	-4.00
	-50.56	-9.65	-20.63	-15.34	-14.59	-25.48	0.08	-25.94	-9.83	-9.56	-9.57
	-59.78	-16.21	-9.93	-29.64	-20.21	-37.61	6.20	-29.24	-16.15	-16.07	-16.39
	-90.82	-25.77	-9.39	-63.87	-17.56	-49.79	0.24	-41.84	-25.89	-25.75	-25.67
	-97.80	-30.53	-5.68	-75.94	-16.18	-48.87	-3.42	-45.34	-30.63	-30.35	-30.62
	-8.68	-21.78	-3.62	-0.90	-4.16	-1.78	-6.79	-0.79	-21.50	-24.11	-19.73
	4.45	-15.40	4.82	-0.60	0.23	1.80	-0.52	2.43	-15.20	-15.56	-15.46
+3.0%i	42.23	3.71	29.04	-2.26	15.45	11.23	19.65	11.85	3.17	4.34	3.63
	51.73	8.91	38.32	-1.92	15.33	7.81	24.35	20.56	8.29	9.51	8.94
	63.40	15.47	37.30	1.09	25.01	14.92	28.50	21.01	15.31	15.90	15.20
	76.50	21.20	36.43	8.17	31.90	20.68	35.75	21.72	21.18	21.39	21.04
	86.96	25.52	33.48	18.44	35.05	25.53	41.12	22.70	25.40	25.75	25.42
	100.45	30.68	29.09	34.50	36.85	31.25	47.61	24.59	30.64	31.19	30.21
	102.49	37.37	20.74	35.93	45.81	39.21	53.17	13.53	37.34	37.50	37.26
	79.91	35.95	33.73	18.12	28.06	13.65	51.96	15.26	35.72	36.35	35.79
	7.48	28.20	4.20	-0.09	3.36	-1.05	8.43	-0.13	26.22	30.42	27.95
	-20.11	10.68	-11.86	-3.52	-4.72	-8.90	0.09	-12.48	10.67	10.65	10.72
-3.0%i	-36.38	0.53	-17.21	-6.83	-12.34	-20.35	-0.96	-15.85	0.59	0.65	0.35
	-46.64	-5.60	-16.83	-12.40	-17.41	-27.13	-0.15	-20.42	-5.56	-5.27	-5.96
	-67.27	-15.60	-16.61	-35.81	-14.86	-36.37	3.07	-35.44	-15.65	-15.36	-15.79
	-76.98	-20.97	-8.86	-47.03	-21.09	-46.19	1.72	-33.87	-21.07	-20.82	-21.03
	-88.40	-26.54	-6.26	-59.68	-22.46	-52.44	0.03	-37.36	-26.70	-25.72	-27.20
	-104.99	-34.77	-0.11	-81.43	-23.45	-65.44	-0.15	-40.82	-36.14	-33.72	-34.46
	-111.27	-37.11	1.38	-92.05	-20.59	-68.42	-0.15	-43.75	-38.55	-36.66	-36.12
	-76.68	-35.23	-0.16	-56.08	-20.44	-40.06	-7.33	-29.35	-34.97	-35.36	-35.36
	-7.20	-26.76	-3.17	-0.79	-3.24	-2.82	-2.35	-1.85	-28.30	-26.95	-25.02
	6.34	-19.04	7.77	-2.54	1.11	0.63	4.53	1.84	-19.90	-18.19	-19.03

step	F (kN)	d (mm)	A_t (kN)	B_t (kN)	C_t (kN)	A_b (kN)	B_b (kN)	C_b (kN)	d_A (mm)	d_B (mm)	d_C (mm)
+3.0%ii	45.54	3.78	35.66	-2.18	12.05	9.52	19.65	17.61	3.39	4.66	3.30
	57.97	12.31	41.19	-2.28	19.06	10.76	26.00	22.87	11.64	13.32	11.97
	64.98	17.29	45.43	-1.86	21.40	11.07	31.19	24.76	17.11	18.26	16.50
	80.29	25.91	46.96	-0.30	33.63	14.70	46.23	21.69	25.56	26.57	25.62
	95.52	33.01	51.27	6.91	37.33	15.55	61.42	21.60	32.94	33.07	33.00
	105.17	36.76	50.58	19.16	35.43	18.67	63.38	26.95	36.70	36.86	36.71
	74.45	35.05	40.85	6.87	26.74	11.86	46.97	16.79	35.10	34.88	35.17
	7.57	27.13	3.20	-0.04	4.41	-0.09	8.02	-0.55	24.06	31.21	26.13
	-11.28	12.83	-4.84	-3.95	-2.50	-8.21	2.85	-6.27	12.06	13.30	13.13
-3.0%ii	-31.55	-0.28	-11.97	-5.14	-14.43	-22.55	0.08	-9.55	-0.27	0.12	-0.68
	-39.49	-5.14	-12.68	-8.75	-18.06	-28.38	0.08	-11.72	-5.18	-4.83	-5.40
	-48.70	-9.97	-11.81	-16.60	-20.29	-33.96	0.16	-15.53	-10.25	-9.44	-10.23
	-57.13	-15.66	-10.24	-35.25	-11.63	-38.81	13.20	-32.36	-16.16	-15.18	-15.65
	-69.22	-21.25	-3.55	-48.99	-16.68	-50.05	13.51	-33.36	-21.84	-20.93	-20.96
	-96.53	-30.95	1.97	-75.20	-23.30	-64.43	4.78	-37.54	-31.05	-30.83	-30.97
	-100.44	-37.38	0.91	-81.79	-19.56	-56.27	0.05	-44.15	-38.04	-36.95	-37.14
	-45.39	-33.34	-2.15	-23.49	-19.75	-18.17	-1.40	-26.30	-32.29	-31.09	-36.64
	-37.00	-32.25	-0.35	-20.23	-16.43	-21.74	-3.21	-11.52	-32.46	-31.32	-32.97
	-9.37	-27.45	-3.40	-0.96	-5.01	-2.86	-3.70	-2.26	-28.45	-27.40	-26.52
+3.5%i	38.54	3.69	31.22	-2.48	9.79	10.21	16.80	12.89	2.57	6.31	2.19
	55.96	16.98	38.66	-2.11	19.40	13.09	25.67	18.92	15.15	20.59	15.19
	73.25	26.18	43.72	-1.26	30.79	15.53	40.63	19.39	25.47	27.72	25.35
	99.96	39.55	39.19	15.73	45.05	26.37	64.77	12.09	39.32	39.97	39.35
	104.35	43.80	35.88	23.15	45.31	29.97	65.32	13.26	43.29	44.04	44.06
	73.29	42.08	32.51	7.77	33.01	19.07	49.85	5.86	41.91	41.92	42.40
	10.55	34.54	5.13	-0.11	5.53	0.05	11.33	-0.87	31.57	37.64	34.39
	-10.17	18.90	-4.44	-0.87	-4.86	-5.75	-0.38	-4.33	18.81	19.65	18.25
-3.5%i	-35.87	-0.25	-17.41	-3.97	-14.49	-23.32	-1.64	-11.38	-0.46	-0.04	-0.24
	-43.93	-5.04	-20.14	-10.05	-13.74	-25.25	0.13	-19.61	-5.32	-4.87	-4.93
	-53.15	-11.52	-16.32	-19.80	-17.02	-33.26	2.07	-22.58	-11.96	-11.16	-11.43
	-64.01	-21.39	1.80	-48.25	-17.56	-53.31	20.82	-31.85	-21.62	-21.05	-21.50
	-84.32	-30.87	2.17	-66.45	-20.04	-63.46	14.53	-35.95	-31.78	-30.46	-30.36
	-96.68	-36.72	1.80	-77.69	-20.79	-65.49	7.79	-39.61	-37.73	-36.10	-36.35
	-103.59	-41.30	2.18	-86.66	-19.12	-67.81	6.23	-42.96	-42.55	-40.77	-40.59
	-95.19	-44.28	26.62	-96.32	-25.49	-76.76	17.07	-35.66	-44.21	-44.40	-44.24
	-33.56	-39.36	-0.04	-19.23	-14.30	-20.75	0.15	-12.52	-39.54	-38.16	-40.37
	-8.15	-34.30	-2.27	-0.77	-5.11	-3.11	-2.11	-1.96	-35.55	-33.40	-33.96
+3.5%ii	29.69	-5.92	29.48	-2.30	2.51	4.15	14.06	12.86	-7.99	-1.37	-8.40
	45.23	8.30	38.41	-1.81	8.64	7.44	20.41	18.75	5.48	12.35	7.07
	56.31	19.01	44.61	-1.26	12.96	8.55	26.33	23.18	15.98	23.07	17.97
	69.97	27.95	46.12	-0.70	24.55	14.07	39.57	18.38	25.54	31.83	26.48
	81.43	33.93	42.43	5.48	33.51	19.58	48.57	15.92	31.77	37.46	32.56
	93.60	42.85	51.35	5.27	36.98	17.11	62.04	17.56	42.07	44.45	42.02
	11.02	33.79	5.53	-0.17	5.66	-0.32	11.70	-0.15	29.57	40.54	31.25
	-9.06	16.44	-0.36	-2.09	-6.60	-8.92	0.20	-0.25	17.34	17.89	14.10
-3.5%ii	-29.21	-1.51	15.98	-36.51	-8.68	-46.65	31.87	-13.55	-1.76	-1.68	-1.10
	-40.41	-9.28	9.19	-41.44	-8.16	-46.93	27.61	-20.40	-9.24	-8.99	-9.62
	-56.08	-20.53	18.34	-59.26	-15.16	-65.80	32.81	-21.39	-21.24	-20.22	-20.13
	-72.82	-31.49	19.87	-80.79	-11.90	-77.34	40.39	-34.09	-30.99	-31.19	-32.30
	-86.79	-37.97	37.88	-106.07	-18.60	-98.01	45.29	-32.03	-37.63	-37.96	-38.34
	-94.14	-44.65	52.44	-123.51	-23.07	-108.13	48.15	-30.39	-45.04	-44.51	-44.40
	-31.67	-39.33	-0.27	-24.26	-7.14	-19.34	6.40	-17.15	-39.34	-37.97	-40.69
	-7.76	-33.12	-2.00	-0.96	-4.80	-2.23	-0.99	-2.98	-34.65	-29.62	-35.08

Table A3.6: Elongation of beams at peak of displacement step of Unit 3.

displacement step	E_{A-B}	E_{B-C}
+0.2%i	0.210	0.065
-0.2%i	0.081	0.158
+0.2%ii	0.226	0.079
-0.2%ii	0.034	0.178
+0.35%i	0.260	0.114
-0.35%i	-0.015	0.302
+0.35%ii	0.256	0.229
-0.35%ii	0.033	0.313
+0.5%i	0.376	0.351
-0.5%i	0.054	0.569
+0.5%ii	0.287	0.342
-0.5%ii	0.069	0.544
+1.0%i	1.297	1.438
-1.0%i	1.457	2.808
+1.0%ii	2.378	2.481
-1.0%ii	1.713	3.193
+1.5%i	3.809	4.165
-1.5%i	3.345	6.614
+1.5%ii	5.179	6.527
-1.5%ii	3.368	8.163
+2.0%i	6.433	8.329
-2.0%i	3.087	11.753
+2.0%ii	8.831	9.836
-2.0%ii	3.107	13.479
+2.5%i	9.733	12.016
-2.5%i	2.673	16.055
+2.5%ii	9.940	14.059
-2.5%ii	3.929	17.834
+3.0%i	11.499	16.088
-3.0%i	4.534	20.729
+3.0%ii	10.458	18.136
-3.0%ii	4.204	21.679
+3.5%i	12.277	19.375
-3.5%i	3.593	23.573
+3.5%ii	10.946	20.724
-3.5%ii	-0.700	24.661

Where: E_{A-B} - beam elongation measured between columns A and B.
E_{B-C} - beam elongation measured between columns B and C.

Appendix 4

Properties of Members in Analytical Models

A4.1 Numerical Model of Frame without Floor Slab (see Figure 7.7).

Members of Elongating Hinge Model (see section 7.2 and Figures 7.1 and 7.2).

Member A: E_s=200GPa, A_s=339.3mm^2, d=272.5mm, d'=27.5mm, F_{Ay}=104.8kN

Member B: b_w=130mm, d=272.5mm, E_c=25GPa

Member C: A_v=28.3mm, f_v=358MPa, d=272.5mm, s=65mm, f_c'=32MPa

Member D: as for Member C

Member E: as for Member A

Members of Frame Model

Member	Type of Element	Section size (mm)	Moduls of Elasticity	Stiffness
beam	Frame	300x130	25GPa	$I_e = 0.3\ I_{gross}$
column	Frame	300x200	25GPa	$I_e = 0.55\ I_{gross}$

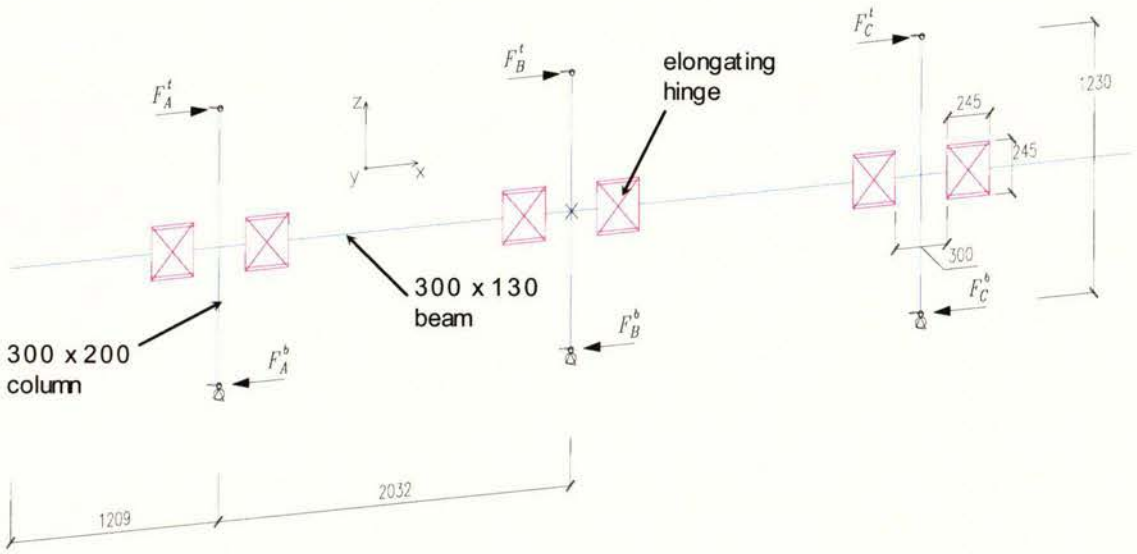

A4.2 Numerical Model of Frame with Floor Slab (see Figure 7.13)

Members of Elongating Hinge Model

As detailed in A4.1 above.

Members of Frame and Floor Slab Model

Member	Type of Element	Section size (mm)	Moduls of Elasticity	Stiffness
perimeter beam	Frame	300x130	25GPa	$I_e = 0.3\ I_{gross}$
column	Frame	300x200	25GPa	$I_e = 0.55\ I_{gross}$
edge supporting beam	Frame	300x130	25GPa	$I_e = 0.3\ I_{gross}$
centre supporting beam	Frame	285x120	25GPa	$I_e = 0.3\ I_{gross}$
prestressed rib	Frame	165x150	28.5GPa	$I_e = 1.0\ I_{gross}$
Floor slab	shell	40mm thick	25GPa	axial stiffness reduced on in direction perpendicular to frame 0.29 EA/L

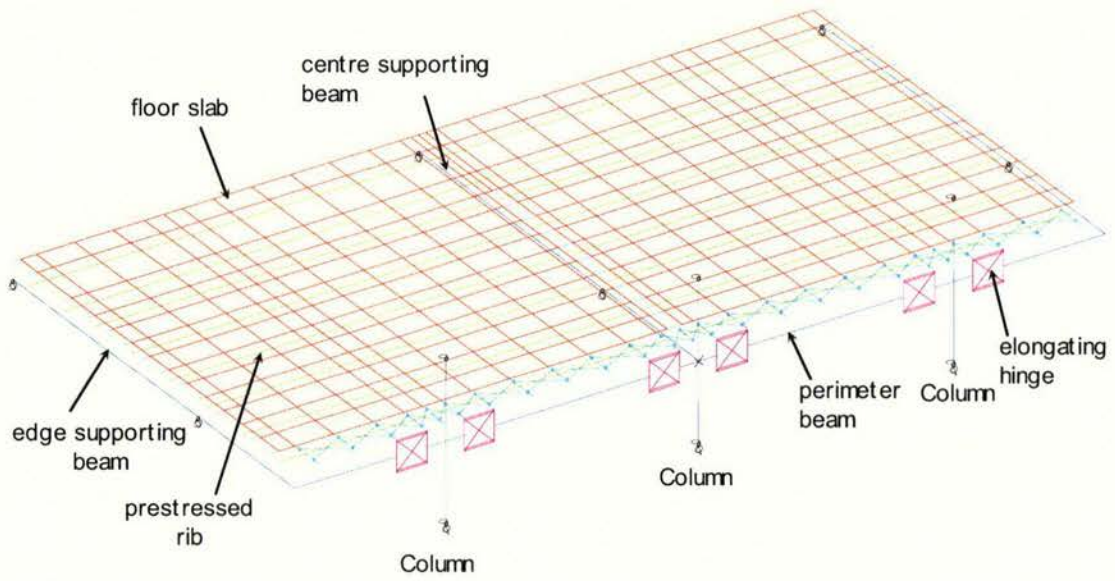

Flexible Floor Slab Model (see Figures 7.18 – 7.20)

Member name	Member α	Type of Element	Section size (mm)	Moduls of Elasticity	Stiffness
tension tie	30°	Frame	10mm diameter	200GPa	0.807 *EA/L*
diagonal strut	30°	Frame	40x155.3	25GPa	1.0 *EA/L*
flexible member	30°	Frame	13.3x155.3	25GPa	0.045 *EA/L*
tension tie	36°	Frame	10mm diameter	200GPa	0.870 *EA/L*
diagonal strut	36°	Frame	40x144.7	25GPa	1.0 *EA/L*
flexible member	36°	Frame	13.3x144.7	25GPa	0.053 *EA/L*
tension tie	50°	Frame	10mm diameter	200GPa	0.637 *EA/L*
diagonal strut	50°	Frame	40x115.0	25GPa	1.0 *EA/L*
flexible member	50°	Frame	13.3x115.0	25GPa	0.069 *EA/L*

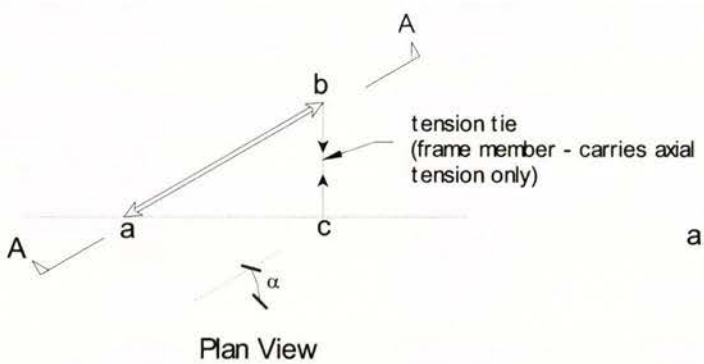

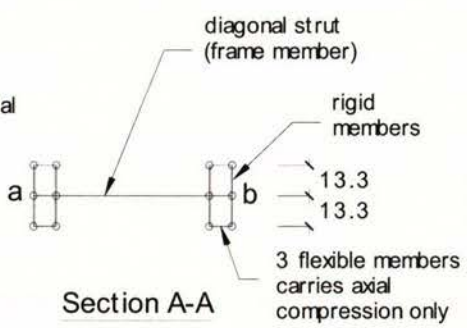

Appendix 5

Input File of Numerical Model of Unit 2

A4.1 Input File (see *Chapter 7*)

```
TABLE:  "ACTIVE DEGREES OF FREEDOM"
   UX=Yes   UY=Yes   UZ=Yes   RX=Yes   RY=Yes   RZ=Yes

TABLE:  "CONSTRAINT DEFINITIONS - LOCAL"
   Name=LOCAL1   U1=No   U2=No   U3=No   R1=No   R2=Yes   R3=No

TABLE:  "CONSTRAINT DEFINITIONS - WELD"
   Name=WELD1   CoordSys=GLOBAL   UX=Yes   UY=Yes   UZ=Yes   RX=Yes   RY=Yes   RZ=Yes
Tolerance=0.131
   Name=WELD2   CoordSys=GLOBAL   UX=Yes   UY=Yes   UZ=Yes   RX=Yes   RY=Yes   RZ=Yes
Tolerance=0.008
   Name=WELD3   CoordSys=GLOBAL   UX=Yes   UY=Yes   UZ=Yes   RX=Yes   RY=Yes   RZ=Yes
Tolerance=0.066
   Name=WELD4   CoordSys=GLOBAL   UX=Yes   UY=Yes   UZ=Yes   RX=Yes   RY=Yes   RZ=Yes
Tolerance=0.0826
   Name=WELD5   CoordSys=GLOBAL   UX=Yes   UY=Yes   UZ=Yes   RX=Yes   RY=Yes   RZ=Yes   Tolerance=0.1
   Name=WELD6   CoordSys=GLOBAL   UX=Yes   UY=Yes   UZ=Yes   RX=Yes   RY=Yes   RZ=Yes
Tolerance=0.019
   Name=WELD7   CoordSys=GLOBAL   UX=Yes   UY=Yes   UZ=Yes   RX=Yes   RY=Yes   RZ=Yes
Tolerance=0.15
   Name=WELD8   CoordSys=GLOBAL   UX=Yes   UY=Yes   UZ=Yes   RX=Yes   RY=Yes   RZ=Yes
Tolerance=0.048

TABLE:  "MATERIAL LIST 1 - BY OBJECT TYPE"
   ObjectType=Frame   Material=STEEL   TotalWeight=0   NumPieces=409
   ObjectType=Frame   Material=CONC   TotalWeight=39.4463921347968   NumPieces=615
   ObjectType=Frame   Material=OTHER   TotalWeight=22.6798542432   NumPieces=168
   ObjectType=Area   Material=CONC   TotalWeight=19.101696

TABLE:  "MATERIAL LIST 2 - BY SECTION PROPERTY"
   Section=COLUMN   ObjectType=Frame   NumPieces=16   TotalLength=3.708   TotalWeight=5.33952
   Section=BEAM   ObjectType=Frame   NumPieces=103   TotalLength=14.864   TotalWeight=12.611664
   Section=MAINLOGITUDINALSTEEL   ObjectType=Frame   NumPieces=24   TotalLength=5.88   TotalWeight=0
   Section=MAINCONCLONGITUDINAL   ObjectType=Frame   NumPieces=12   TotalLength=2.94
TotalWeight=1.37592
   Section=MAINCONCDIAGONAL   ObjectType=Frame   NumPieces=24   TotalLength=8.3155757467538
TotalWeight=0
   Section=CENTRETRANSVERSE   ObjectType=Frame   NumPieces=16   TotalLength=3.465
TotalWeight=2.79072
   Section=ENDSLAB   ObjectType=Frame   NumPieces=60   TotalLength=12.964   TotalWeight=16.5291
   Section=RIB   ObjectType=Frame   NumPieces=168   TotalLength=38.892   TotalWeight=22.6798542432
   Section=CENTRECONNECTION   ObjectType=Frame   NumPieces=28   TotalLength=1.68   TotalWeight=0
   Section=2-4.0MMWIRE   ObjectType=Frame   NumPieces=12   TotalLength=0.72   TotalWeight=0
   Section=DIAGSLAB   ObjectType=Frame   NumPieces=24   TotalLength=8.12487186931585   TotalWeight=0
   Section=SLABLINK   ObjectType=Frame   NumPieces=48   TotalLength=2.65719
TotalWeight=0.7994681347968
   Section=EDGESTARTER   ObjectType=Frame   NumPieces=28   TotalLength=1.82   TotalWeight=0
   Section=TENSIONTIE   ObjectType=Frame   NumPieces=25   TotalLength=4.48208   TotalWeight=0
   Section=DIAGSLABLAYER   ObjectType=Frame   NumPieces=144   TotalLength=1.44014872800732
TotalWeight=0
   Section=STIFFMEMBER   ObjectType=Frame   NumPieces=292   TotalLength=3.89074067524408
TotalWeight=0
   Section=DIAGSLAB.245   ObjectType=Frame   NumPieces=12   TotalLength=3.4029697391724
TotalWeight=0
   Section=DIAGSLABLAYER.245   ObjectType=Frame   NumPieces=72   TotalLength=0.720244038329184
TotalWeight=0
   Section=DIAGSLAB.15   ObjectType=Frame   NumPieces=12   TotalLength=2.56498054942047
TotalWeight=0
   Section=DIAGSLABLAYER.15   ObjectType=Frame   NumPieces=72   TotalLength=0.720186084817609
TotalWeight=0
   Section=slab   ObjectType=Area   TotalWeight=19.101696

TABLE:  "JOINT COORDINATES"
Too big to list, eg:
   Joint=1   CoordSys=GLOBAL   CoordType=Cartesian   XorR=-2.032   Y=0   Z=-0.615   SpecialJt=Yes
GlobalX=-2.032   GlobalY=0   GlobalZ=-0.615
   to
```

```
   Joint=1272   CoordSys=GLOBAL   CoordType=Cartesian   XorR=0   Y=2.54   Z=0.0475   SpecialJt=No
GlobalX=0   GlobalY=2.54   GlobalZ=0.0475

TABLE:  "CONNECTIVITY - FRAME/CABLE"
Too big to list, eg:
   Frame=1   JointI=1   JointJ=2   Length=0.465
   to
   Frame=1192   JointI=1272   JointJ=709   Length=0.06

TABLE:  "MATERIAL PROPERTIES 1 - GENERAL"
   Material=ALUM   Type=Isotropic   DesignType=Aluminum   UnitMass=7.82709980453528
UnitWeight=76.81954656429   E=75152860.995722   U=0.3   A=0.0000117   MDampRatio=0   VDampMass=0
VDampStiff=0   HDampMass=0   HDampStiff=0 _
       NumAdvance=0   Color=Red
   Material=CONC   Type=Isotropic   DesignType=Concrete   UnitMass=2.4465   UnitWeight=24
E=25739350   U=0.2   A=0.0000099   MDampRatio=0   VDampMass=0   VDampStiff=0   HDampMass=0
HDampStiff=0   NumAdvance=0   Color=Cyan
   Material=OTHER   Type=Isotropic   DesignType=None   UnitMass=2.4007   UnitWeight=23.5616
E=28416059   U=0.2   A=0.0000099   MDampRatio=0   VDampMass=0   VDampStiff=0   HDampMass=0
HDampStiff=0   NumAdvance=0   Color=Magenta
   Material=STEEL   Type=Isotropic   DesignType=Steel   UnitMass=7.849   UnitWeight=76.9729
E=200000000   U=0.3   A=0.0000117   MDampRatio=0   VDampMass=0   VDampStiff=0   HDampMass=0
HDampStiff=0   NumAdvance=0   Color=Green

TABLE:  "MATERIAL PROPERTIES 3 - DESIGN STEEL"
   Material=STEEL   Fy=248211.28   Fu=399896

TABLE:  "MATERIAL PROPERTIES 4 - DESIGN CONCRETE"
   Material=CONC   Fc=27579.032   RebarFy=413685.5   RebarFys=275790.32   LtWtConc=No   LtWtFact=1

TABLE:  "FRAME SECTION PROPERTIES 1 - GENERAL"
   SectionName=2-4.0MMWIRE   Material=STEEL   Shape=Rectangular   t3=0.004   t2=0.006283
Area=0.000025132   TorsConst=8.10132874395738E-11   I33=3.35093333333333E-11   I22=8.26760890623333E-
11   AS2=2.09433333333333E-05 _
       AS3=2.09433333333333E-05   S33=1.67546666666667E-08   S22=2.63173926666667E-08
Z33=0.000000025132   Z22=0.000000039476089   R33=1.15470053837925E-03   R22=1.81374587065921E-03
ConcCol=No   ConcBeam=No   Color=White   TotalWt=0 _
       TotalMass=0   FromFile=No   AMod=1   A2Mod=0   A3Mod=1000   JMod=1000   I2Mod=1000   I3Mod=0
MMod=0   WMod=0
   SectionName=BEAM   Material=CONC   Shape=Rectangular   t3=0.3   t2=0.13   Area=0.039
TorsConst=1.5989813999209E-04   I33=0.0002925   I22=0.000054925   AS2=0.0325   AS3=0.0325
S33=0.00195   S22=0.000845   Z33=0.002925   Z22=0.0012675 _
       R33=8.66025403784439E-02   R22=3.75277674973257E-02   ConcCol=No   ConcBeam=Yes
Color=Magenta   TotalWt=12.611664   TotalMass=1.285601499   FromFile=No   AMod=1   A2Mod=1   A3Mod=1
JMod=1   I2Mod=1   I3Mod=1   MMod=1   WMod=1
   SectionName=CENTRECONNECTION   Material=STEEL   Shape=Rectangular   t3=0.003125   t2=0.007363
Area=0.000023009375   TorsConst=5.49273017892601E-11   I33=1.87250773111979E-11
I22=1.039520784236 98E-10   AS2=1.91744791666667E-05 _
       AS3=1.91744791666667E-05   S33=1.19840494791667E-08   S22=2.82363380208333E-08
Z33=1.797607421875E-08   Z22=4.235450703125E-08   R33=9.0210979560879E-04   R22=2.12551501602161E-03
ConcCol=No   ConcBeam=Yes   Color=Yellow _
       TotalWt=0   TotalMass=0   FromFile=No   AMod=0.8   A2Mod=0   A3Mod=3.71   JMod=1000
I2Mod=1000   I3Mod=0   MMod=0   WMod=0
   SectionName=CENTRETRANSVERSE   Material=CONC   Shape=Rectangular   t3=0.285   t2=0.12
Area=0.0342   TorsConst=1.20728454849504E-04   I33=0.00023149125   I22=0.00004104   AS2=0.0285
AS3=0.0285   S33=0.0016245   S22=0.000684 _
       Z33=0.00243675   Z22=0.001026   R33=8.22724133595217E-02   R22=3.46410161513775E-02
ConcCol=No   ConcBeam=Yes   Color=White   TotalWt=2.79072   TotalMass=0.28447902   FromFile=No
AMod=1   A2Mod=1   A3Mod=1   JMod=1   I2Mod=1 _
       I3Mod=1   MMod=1   WMod=1
   SectionName=COLUMN   Material=CONC   Shape=Rectangular   t3=0.3   t2=0.2   Area=0.06
TorsConst=4.69530874711496E-04   I33=0.00045   I22=0.0002   AS2=0.05   AS3=0.05   S33=0.003
S22=0.002   Z33=0.0045   Z22=0.003 _
       R33=8.66025403784439E-02   R22=5.77350269189626E-02   ConcCol=Yes   ConcBeam=No   Color=Cyan
TotalWt=5.33952   TotalMass=0.54429732   FromFile=No   AMod=1   A2Mod=1   A3Mod=1   JMod=1   I2Mod=1
I3Mod=1   MMod=1   WMod=1
   SectionName=DIAGSLAB   Material=CONC   Shape=Rectangular   t3=0.04   t2=0.1553   Area=0.006212
TorsConst=2.77566384951147E-06   I33=8.28266666666667E-07   I22=1.24851312566667E-05
AS2=5.17666666666667E-03   AS3=5.17666666666667E-03 _
       S33=4.14133333333333E-05   S22=1.60787266666667E-04   Z33=0.00006212   Z22=0.0002411809
R33=1.15470053837925E-02   R22=4.48312484025744E-02   ConcCol=No   ConcBeam=Yes   Color=Blue
TotalWt=0   TotalMass=0   FromFile=No   AMod=1 _
       A2Mod=10   A3Mod=10   JMod=10   I2Mod=10   I3Mod=10   MMod=0   WMod=0
   SectionName=DIAGSLAB.15   Material=CONC   Shape=Rectangular   t3=0.04   t2=0.115   Area=0.0046
TorsConst=1.9163890824831E-06   I33=6.13333333333333E-07   I22=5.06958333333333E-06
AS2=3.83333333333333E-03   AS3=3.83333333333333E-03 _
       S33=3.06666666666667E-05   S22=8.81666666666667E-05   Z33=0.000046   Z22=0.00013225
R33=1.15470053837925E-02   R22=3.31976404784035E-02   ConcCol=No   ConcBeam=Yes   Color=White
TotalWt=0   TotalMass=0   FromFile=No   AMod=1 _
       A2Mod=10   A3Mod=10   JMod=10   I2Mod=10   I3Mod=10   MMod=0   WMod=0
   SectionName=DIAGSLAB.245   Material=CONC   Shape=Rectangular   t3=0.04   t2=0.1447   Area=0.005788
TorsConst=2.54959495380266E-06   I33=7.71733333333333E-07   I22=1.00991387433333E-05
AS2=4.82333333333333E-03 _
```

```
        AS3=4.82333333333333E-03   S33=3.85866666666667E-05   S22=1.39587266666667E-04
Z33=0.00005788   Z22=0.0002093809   R33=1.15470053837925E-02   R22=4.17712919758694E-02   ConcCol=No
ConcBeam=Yes   Color=White   TotalWt=0 _
        TotalMass=0   FromFile=No   AMod=1   A2Mod=10   A3Mod=10   JMod=10   I2Mod=10   I3Mod=10
MMod=0   WMod=0
   SectionName=DIAGSLABLAYER   Material=CONC   Shape=Rectangular   t3=0.0133   t2=0.1553
Area=0.00206549   TorsConst=1.1521728988625E-07   I33=3.04470438416667E-08   I22=4.15130614284167E-06
AS2=1.72124166666667E-03
        AS3=1.72124166666667E-03   S33=4.57850283333333E-06   S22=5.34617661666667E-05
Z33=0.00000686775425   Z22=0.00008019264925   R33=3.83937929011101E-03   R22=4.48312484025744E-02
ConcCol=No   ConcBeam=Yes   Color=Gray8Dark _
        TotalWt=0   TotalMass=0   FromFile=No   AMod=0.01   A2Mod=1   A3Mod=10   JMod=1   I2Mod=10
I3Mod=1   MMod=0   WMod=0
   SectionName=DIAGSLABLAYER.15   Material=CONC   Shape=Rectangular   t3=0.0133   t2=0.115
Area=0.0015295   TorsConst=8.36136013599773E-08   I33=2.25461045833333E-08   I22=1.68563645833333E-06
AS2=1.27458333333333E-03
        AS3=1.27458333333333E-03   S33=3.39039166666667E-06   S22=2.93154166666667E-05
Z33=0.0000050855875   Z22=0.000043973125   R33=3.83937929011101E-03   R22=3.31976404784035E-02
ConcCol=No   ConcBeam=Yes   Color=Blue   TotalWt=0 _
        TotalMass=0   FromFile=No   AMod=0.01534   A2Mod=1   A3Mod=10   JMod=1   I2Mod=10   I3Mod=1
MMod=0   WMod=0
   SectionName=DIAGSLABLAYER.245   Material=CONC   Shape=Rectangular   t3=0.0133   t2=0.1447
Area=0.00192451   TorsConst=1.06904648779512E-07   I33=2.83688811583333E-08   I22=3.35796363215833E-
06   AS2=1.60375833333333E-03
        AS3=1.60375833333333E-03   S33=4.26599716666667E-06   S22=4.64127661666667E-05
Z33=0.00000639899575   Z22=0.00006961914925   R33=3.83937929011101E-03   R22=4.17712919758694E-02
ConcCol=No   ConcBeam=Yes   Color=Blue   TotalWt=0 _
        TotalMass=0   FromFile=No   AMod=0.01181   A2Mod=1   A3Mod=10   JMod=1   I2Mod=10   I3Mod=1
MMod=0   WMod=0
   SectionName=EDGECONNECTION   Material=CONC   Shape=Rectangular   t3=0.02   t2=0.225   Area=0.0045
TorsConst=5.66400175851664E-07   I33=0.00000015   I22=0.000018984375   AS2=0.00375   AS3=0.00375
S33=0.000015   S22=0.00016875 _
        Z33=0.0000225   Z22=0.000253125   R33=5.77350269189626E-03   R22=6.49519052838329E-02
ConcCol=No   ConcBeam=Yes   Color=White   TotalWt=0   TotalMass=0   FromFile=No   AMod=1   A2Mod=1
A3Mod=1   JMod=1   I2Mod=1   I3Mod=1 _
        MMod=0   WMod=0
   SectionName=EDGESTARTER   Material=STEEL   Shape=Circle   t3=0.01   Area=7.85398163397448E-05
TorsConst=9.8174770424681E-10   I33=4.90873852123405E-10   I22=4.90873852123405E-10
AS2=7.06858328332352E-05   AS3=7.06858328332352E-05 _
        S33=9.8174770424681E-08   S22=9.8174770424681E-08   Z33=1.66666666666667E-07
Z22=1.66666666666667E-07   R33=0.0025   R22=0.0025   ConcCol=No   ConcBeam=No   Color=White
TotalWt=0   TotalMass=0   FromFile=No   AMod=0.259 _
        A2Mod=0   A3Mod=1.16   JMod=1000   I2Mod=1000   I3Mod=0   MMod=0   WMod=0
   SectionName=ENDSLAB   Material=CONC   Shape=Rectangular   t3=0.125   t2=0.425   Area=0.053125
TorsConst=2.254551501414 89E-04   I33=6.917317708333333E-05   I22=7.99641927083333E-04
AS2=4.42708333333333E-02   AS3=4.42708333333333E-02 _
        S33=1.106770833333333E-03   S22=3.763020833333333E-03   Z33=0.00166015625   Z22=0.00564453125
R33=3.60843918243516E-02   R22=0.122686932202795   ConcCol=No   ConcBeam=Yes   Color=Blue
TotalWt=16.5291   TotalMass=1.68493513125 _
        FromFile=No   AMod=1   A2Mod=1   A3Mod=1   JMod=1   I2Mod=1   I3Mod=1   MMod=1   WMod=1
   SectionName=MAINCONCDIAGONAL   Material=CONC   Shape=Rectangular   t3=0.031   t2=0.13
Area=0.00403   TorsConst=1.09705618803908E-06   I33=3.227358333333333E-07   I22=5.67558333333333E-06
AS2=3.35833333333333E-03
        AS3=3.358333333333333E-03   S33=2.08216666666667E-05   S22=8.73166666666667E-05
Z33=0.0000312325   Z22=0.000130975   R33=8.9489291724392E-03   R22=3.75277674973257E-02   ConcCol=No
ConcBeam=Yes   Color=Blue   TotalWt=0 _
        TotalMass=0   FromFile=No   AMod=1   A2Mod=0   A3Mod=0   JMod=0   I2Mod=0   I3Mod=0   MMod=0
WMod=0
   SectionName=MAINCONCLONGITUDINAL   Material=CONC   Shape=Rectangular   t3=0.15   t2=0.13
Area=0.0195   TorsConst=5.26917117843634E-05   I33=0.0000365625   I22=0.0000274625   AS2=0.01625
AS3=0.01625   S33=0.0004875   S22=0.0004225 _
        Z33=0.00073125   Z22=0.00063375   R33=4.33012701892219E-02   R22=3.75277674973257E-02
ConcCol=No   ConcBeam=Yes   Color=Magenta   TotalWt=1.37592   TotalMass=0.140257845   FromFile=No
AMod=1   A2Mod=0   A3Mod=0   JMod=0 _
        I2Mod=0   I3Mod=0   MMod=1   WMod=1
   SectionName=MAINLOGITUDINALSTEEL   Material=STEEL   Shape=Rectangular   t3=0.012   t2=0.0283
Area=0.0003396   TorsConst=1.19579713315764E-08   I33=0.0000000040752   I22=0.000000022665187
AS2=0.000283   AS3=0.000283   S33=0.0000006792 _
        S22=0.00000160178   Z33=0.0000010188   Z22=0.00000240267   R33=3.46410161513775E-03
R22=8.1695063090332E-03   ConcCol=No   ConcBeam=No   Color=Cyan   TotalWt=0   TotalMass=0
FromFile=No   AMod=1   A2Mod=0   A3Mod=0   JMod=0 _
        I2Mod=0   I3Mod=0   MMod=0   WMod=0
   SectionName=RIB   Material=OTHER   Shape=Rectangular   t3=0.165   t2=0.15   Area=0.02475
TorsConst=8.53635756761209E-05   I33=0.0000561515625   I22=0.00004640625   AS2=0.020625
AS3=0.020625   S33=0.000680625   S22=0.00061875 _
        Z33=0.0010209375   Z22=0.000928125   R33=4.76313972081441E-02   R22=4.33012701892219E-02
ConcCol=No   ConcBeam=No   Color=White   TotalWt=22.6798542432   TotalMass=2.31085860390001
FromFile=No   AMod=1.1   A2Mod=1   A3Mod=1 _
        JMod=1   I2Mod=1   I3Mod=1   MMod=1   WMod=1
   SectionName=SLABLINK   Material=CONC   Shape=Rectangular   t3=0.04   t2=0.3105   Area=0.01242
TorsConst=6.08641235554598E-06   I33=0.000001656   I22=0.00009978460875   AS2=0.01035   AS3=0.01035
S33=0.0000828   S22=0.000642735 _
        Z33=0.0001242   Z22=0.0009641025   R33=1.15470053837925E-02   R22=8.96336292916894E-02
ConcCol=No   ConcBeam=Yes   Color=Blue   TotalWt=0.7994681347968   TotalMass=8.14957829908487E-02
FromFile=No   AMod=10   A2Mod=10   A3Mod=10 _
```

```
        JMod=10    I2Mod=10    I3Mod=10    MMod=1    WMod=1
   SectionName=STIFFMEMBER    Material=STEEL    Shape=Rectangular    t3=0.5    t2=0.5    Area=0.25
TorsConst=8.80208374777188E-03    I33=5.20833333333333E-03    I22=5.20833333333333E-03
AS2=0.208333333333333    AS3=0.208333333333333 _
        S33=2.08333333333333E-02    S22=2.08333333333333E-02    Z33=0.03125    Z22=0.03125
R33=0.144337567297406    R22=0.144337567297406    ConcCol=No    ConcBeam=No    Color=Green    TotalWt=0
TotalMass=0    FromFile=No    AMod=1    A2Mod=1 _
        A3Mod=1    JMod=1    I2Mod=1    I3Mod=1    MMod=0    WMod=0
   SectionName=TENSIONTIE    Material=STEEL    Shape=Circle    t3=0.01    Area=7.85398163397448E-05
TorsConst=9.8174770424681E-10    I33=4.90873852123405E-10    I22=4.90873852123405E-10
AS2=7.06858328332352E-05    AS3=7.06858328332352E-05 _
        S33=9.8174770424681E-08    S22=9.8174770424681E-08    Z33=1.66666666666667E-07
Z22=1.66666666666667E-07    R33=0.0025    R22=0.0025    ConcCol=No    ConcBeam=No    Color=Cyan
TotalWt=0    TotalMass=0    FromFile=No    AMod=0.8066 _
        A2Mod=0    A3Mod=0    JMod=0    I2Mod=0    I3Mod=0    MMod=0    WMod=0

TABLE:  "FRAME SECTION PROPERTIES 2 - CONCRETE COLUMN"
   SectionName=COLUMN    ReinfConfig=Rectangular    LatReinf=Ties    Cover=0.03    NumBars3Dir=0
NumBars2Dir=0    BarSize=12Ø    ReinfType=Design

TABLE:  "FRAME SECTION PROPERTIES 3 - CONCRETE BEAM"
   SectionName=BEAM    TopCover=0    BotCover=0    TopLeftArea=0    TopRghtArea=0    BotLeftArea=0
BotRghtArea=0
   SectionName=CENTRECONNECTION    TopCover=0    BotCover=0    TopLeftArea=0    TopRghtArea=0
BotLeftArea=0    BotRghtArea=0
   SectionName=CENTRETRANSVERSE    TopCover=0    BotCover=0    TopLeftArea=0    TopRghtArea=0
BotLeftArea=0    BotRghtArea=0
   SectionName=DIAGSLAB    TopCover=0    BotCover=0    TopLeftArea=0    TopRghtArea=0    BotLeftArea=0
BotRghtArea=0
   SectionName=DIAGSLAB.15    TopCover=0    BotCover=0    TopLeftArea=0    TopRghtArea=0    BotLeftArea=0
BotRghtArea=0
   SectionName=DIAGSLAB.245    TopCover=0    BotCover=0    TopLeftArea=0    TopRghtArea=0    BotLeftArea=0
BotRghtArea=0
   SectionName=DIAGSLABLAYER    TopCover=0    BotCover=0    TopLeftArea=0    TopRghtArea=0
BotLeftArea=0    BotRghtArea=0
   SectionName=DIAGSLABLAYER.15    TopCover=0    BotCover=0    TopLeftArea=0    TopRghtArea=0
BotLeftArea=0    BotRghtArea=0
   SectionName=DIAGSLABLAYER.245    TopCover=0    BotCover=0    TopLeftArea=0    TopRghtArea=0
BotLeftArea=0    BotRghtArea=0
   SectionName=EDGECONNECTION    TopCover=0    BotCover=0    TopLeftArea=0    TopRghtArea=0
BotLeftArea=0    BotRghtArea=0
   SectionName=ENDSLAB    TopCover=0    BotCover=0    TopLeftArea=0    TopRghtArea=0    BotLeftArea=0
BotRghtArea=0
   SectionName=MAINCONCDIAGONAL    TopCover=0    BotCover=0    TopLeftArea=0    TopRghtArea=0
BotLeftArea=0    BotRghtArea=0
   SectionName=MAINCONCLONGITUDINAL    TopCover=0    BotCover=0    TopLeftArea=0    TopRghtArea=0
BotLeftArea=0    BotRghtArea=0
   SectionName=SLABLINK    TopCover=0    BotCover=0    TopLeftArea=0    TopRghtArea=0    BotLeftArea=0
BotRghtArea=0

TABLE:  "HINGE PROPS 1 - OVERVIEW"
   HingeName=2-4.0mm    Type=User    NumDOFs=1    P=Yes    V2=No    V3=No    T=No    M2=No    M3=No    PMM=No
   HingeName=axialmember    Type=User    NumDOFs=1    P=Yes    V2=No    V3=No    T=No    M2=No    M3=No
PMM=No
   HingeName=diaglayer    Type=User    NumDOFs=1    P=Yes    V2=No    V3=No    T=No    M2=No    M3=No
PMM=No
   HingeName=diaglayer.15    Type=User    NumDOFs=1    P=Yes    V2=No    V3=No    T=No    M2=No    M3=No
PMM=No
   HingeName=diaglayer.245    Type=User    NumDOFs=1    P=Yes    V2=No    V3=No    T=No    M2=No    M3=No
PMM=No
   HingeName=diagshear    Type=User    NumDOFs=1    P=Yes    V2=No    V3=No    T=No    M2=No    M3=No
PMM=No
   HingeName=edgestarter    Type=User    NumDOFs=1    P=Yes    V2=No    V3=No    T=No    M2=No    M3=No
PMM=No
   HingeName=edgestarter0.5    Type=User    NumDOFs=1    P=Yes    V2=No    V3=No    T=No    M2=No    M3=No
PMM=No
   HingeName=edgestarter1.389    Type=User    NumDOFs=1    P=Yes    V2=No    V3=No    T=No    M2=No    M3=No
PMM=No
   HingeName=edgestarter1.5    Type=User    NumDOFs=1    P=Yes    V2=No    V3=No    T=No    M2=No    M3=No
PMM=No
   HingeName=edgestarter1.722    Type=User    NumDOFs=1    P=Yes    V2=No    V3=No    T=No    M2=No    M3=No
PMM=No
   HingeName=halfhinge    Type=User    NumDOFs=1    P=Yes    V2=No    V3=No    T=No    M2=No    M3=No
PMM=No
   HingeName=mainlongsteel    Type=User    NumDOFs=1    P=Yes    V2=No    V3=No    T=No    M2=No    M3=No
PMM=No
   HingeName=mesh    Type=User    NumDOFs=1    P=Yes    V2=No    V3=No    T=No    M2=No    M3=No    PMM=No
   HingeName=mesh0.5    Type=User    NumDOFs=1    P=Yes    V2=No    V3=No    T=No    M2=No    M3=No    PMM=No
   HingeName=mesh1.389    Type=User    NumDOFs=1    P=Yes    V2=No    V3=No    T=No    M2=No    M3=No
PMM=No
   HingeName=mesh1.5    Type=User    NumDOFs=1    P=Yes    V2=No    V3=No    T=No    M2=No    M3=No    PMM=No
   HingeName=mesh1.722    Type=User    NumDOFs=1    P=Yes    V2=No    V3=No    T=No    M2=No    M3=No
PMM=No
   HingeName=tensiontie    Type=User    NumDOFs=1    P=Yes    V2=No    V3=No    T=No    M2=No    M3=No
PMM=No
```

```
   HingeName=tensiontie.15   Type=User   NumDOFs=1   P=Yes   V2=No   V3=No   T=No   M2=No   M3=No
PMM=No
   HingeName=tensiontie.245   Type=User   NumDOFs=1   P=Yes   V2=No   V3=No   T=No   M2=No   M3=No
PMM=No
   HingeName=tensiontie.335   Type=User   NumDOFs=1   P=Yes   V2=No   V3=No   T=No   M2=No   M3=No
PMM=No

TABLE:  "HINGE PROPS 2 - GENERAL"
   HingeName=2-4.0mm   Type="User defined"   DOF=P   RigidPlast=Yes   Symmetric=Yes   FDType=Force-
Displ   UseYldForce=No   UseYldDispl=No   FDPosForSF=10.82   FDPosDisSF=0.0002386   FDNegForSF=10.82
FDNegDisSF=0.0002386
   HingeName=axialmember   Type="User defined"   DOF=P   RigidPlast=Yes   Symmetric=No
FDType=Force-Displ   UseYldForce=No   UseYldDispl=No   FDPosForSF=1   FDPosDisSF=0.005
FDNegForSF=132.48   FDNegDisSF=0.005
   HingeName=diaglayer   Type="User defined"   DOF=P   RigidPlast=Yes   Symmetric=No   FDType=Force-
Displ   UseYldForce=No   UseYldDispl=No   FDPosForSF=0.1   FDPosDisSF=0.0001465   FDNegForSF=39.62
FDNegDisSF=0.0001465
   HingeName=diaglayer.15   Type="User defined"   DOF=P   RigidPlast=Yes   Symmetric=No
FDType=Force-Displ   UseYldForce=No   UseYldDispl=No   FDPosForSF=0.1   FDPosDisSF=0.0000755
FDNegForSF=29.348   FDNegDisSF=0.0000755
   HingeName=diaglayer.245   Type="User defined"   DOF=P   RigidPlast=Yes   Symmetric=No
FDType=Force-Displ   UseYldForce=No   UseYldDispl=No   FDPosForSF=0.1   FDPosDisSF=0.0001113
FDNegForSF=36.92   FDNegDisSF=0.0001113
   HingeName=diagshear   Type="User defined"   DOF=P   RigidPlast=Yes   Symmetric=Yes   FDType=Force-
Displ   UseYldForce=No   UseYldDispl=No   FDPosForSF=16.22   FDPosDisSF=0.00054   FDNegForSF=16.22
FDNegDisSF=0.00054
   HingeName=edgestarter   Type="User defined"   DOF=P   RigidPlast=Yes   Symmetric=Yes
FDType=Force-Displ   UseYldForce=No   UseYldDispl=No   FDPosForSF=24.6   FDPosDisSF=0.000214
FDNegForSF=24.6   FDNegDisSF=0.000214
   HingeName=edgestarter0.5   Type="User defined"   DOF=P   RigidPlast=Yes   Symmetric=Yes
FDType=Force-Displ   UseYldForce=No   UseYldDispl=No   FDPosForSF=12.3   FDPosDisSF=0.000214
FDNegForSF=12.3   FDNegDisSF=0.000214
   HingeName=edgestarter1.389   Type="User defined"   DOF=P   RigidPlast=Yes   Symmetric=Yes
FDType=Force-Displ   UseYldForce=No   UseYldDispl=No   FDPosForSF=34.1694   FDPosDisSF=0.000214
FDNegForSF=34.1694   FDNegDisSF=0.000214
   HingeName=edgestarter1.5   Type="User defined"   DOF=P   RigidPlast=Yes   Symmetric=Yes
FDType=Force-Displ   UseYldForce=No   UseYldDispl=No   FDPosForSF=36.9   FDPosDisSF=0.000214
FDNegForSF=36.9   FDNegDisSF=0.000214
   HingeName=edgestarter1.722   Type="User defined"   DOF=P   RigidPlast=Yes   Symmetric=Yes
FDType=Force-Displ   UseYldForce=No   UseYldDispl=No   FDPosForSF=42.3612   FDPosDisSF=0.000214
FDNegForSF=42.3612   FDNegDisSF=0.000214
   HingeName=halfhinge   Type="User defined"   DOF=P   RigidPlast=Yes   Symmetric=Yes   FDType=Force-
Displ   UseYldForce=No   UseYldDispl=No   FDPosForSF=34.4   FDPosDisSF=0.0002   FDNegForSF=34.4
FDNegDisSF=0.0002
   HingeName=mainlongsteel   Type="User defined"   DOF=P   RigidPlast=Yes   Symmetric=No
FDType=Force-Displ   UseYldForce=No   UseYldDispl=No   FDPosForSF=110.4   FDPosDisSF=0.001
FDNegForSF=11.04   FDNegDisSF=0.001
   HingeName=mesh   Type="User defined"   DOF=P   RigidPlast=Yes   Symmetric=Yes   FDType=Force-Displ
UseYldForce=No   UseYldDispl=No   FDPosForSF=9.388   FDPosDisSF=0.000153   FDNegForSF=9.388
FDNegDisSF=0.000153
   HingeName=mesh0.5   Type="User defined"   DOF=P   RigidPlast=Yes   Symmetric=Yes   FDType=Force-
Displ   UseYldForce=No   UseYldDispl=No   FDPosForSF=4.694   FDPosDisSF=0.000153   FDNegForSF=4.694
FDNegDisSF=0.000153
   HingeName=mesh1.389   Type="User defined"   DOF=P   RigidPlast=Yes   Symmetric=Yes   FDType=Force-
Displ   UseYldForce=No   UseYldDispl=No   FDPosForSF=13.0399   FDPosDisSF=0.000153
FDNegForSF=13.0399   FDNegDisSF=0.000153
   HingeName=mesh1.5   Type="User defined"   DOF=P   RigidPlast=Yes   Symmetric=Yes   FDType=Force-
Displ   UseYldForce=No   UseYldDispl=No   FDPosForSF=14.082   FDPosDisSF=0.000153   FDNegForSF=14.082
FDNegDisSF=0.000153
   HingeName=mesh1.722   Type="User defined"   DOF=P   RigidPlast=Yes   Symmetric=Yes   FDType=Force-
Displ   UseYldForce=No   UseYldDispl=No   FDPosForSF=16.1661   FDPosDisSF=0.000153
FDNegForSF=16.1661   FDNegDisSF=0.000153
   HingeName=tensiontie   Type="User defined"   DOF=P   RigidPlast=Yes   Symmetric=No   FDType=Force-
Displ   UseYldForce=No   UseYldDispl=No   FDPosForSF=33.924   FDPosDisSF=0.00048   FDNegForSF=0.1
FDNegDisSF=0.00048
   HingeName=tensiontie.15   Type="User defined"   DOF=P   RigidPlast=Yes   Symmetric=No
FDType=Force-Displ   UseYldForce=No   UseYldDispl=No   FDPosForSF=16.39   FDPosDisSF=0.00048
FDNegForSF=0.1   FDNegDisSF=0.00048
   HingeName=tensiontie.245   Type="User defined"   DOF=P   RigidPlast=Yes   Symmetric=No
FDType=Force-Displ   UseYldForce=No   UseYldDispl=No   FDPosForSF=26.77   FDPosDisSF=0.00048
FDNegForSF=0.1   FDNegDisSF=0.00048
   HingeName=tensiontie.335   Type="User defined"   DOF=P   RigidPlast=Yes   Symmetric=No
FDType=Force-Displ   UseYldForce=No   UseYldDispl=No   FDPosForSF=36.61   FDPosDisSF=0.00048
FDNegForSF=0.1   FDNegDisSF=0.00048

TABLE:  "HINGE PROPS 3 - FORCE-DEFORMATION DATA"
   HingeName=2-4.0mm   Type=User   DOF=P   FDPoint=-E   Force=-0.2   Displ=-59
   HingeName=2-4.0mm   Type=User   DOF=P   FDPoint=-D   Force=-0.2   Displ=-53
   HingeName=2-4.0mm   Type=User   DOF=P   FDPoint=-C   Force=-1.15   Displ=-53
   HingeName=2-4.0mm   Type=User   DOF=P   FDPoint=-B   Force=-1   Displ=0
   HingeName=2-4.0mm   Type=User   DOF=P   FDPoint=A   Force=0   Displ=0
   HingeName=2-4.0mm   Type=User   DOF=P   FDPoint=B   Force=1   Displ=0
   HingeName=2-4.0mm   Type=User   DOF=P   FDPoint=C   Force=1.15   Displ=53
   HingeName=2-4.0mm   Type=User   DOF=P   FDPoint=D   Force=0.2   Displ=53
   HingeName=2-4.0mm   Type=User   DOF=P   FDPoint=E   Force=0.2   Displ=59
```

```
HingeName=axialmember   Type=User   DOF=P   FDPoint=-E   Force=-1.4   Displ=-75
HingeName=axialmember   Type=User   DOF=P   FDPoint=-D   Force=-1.4   Displ=-35
HingeName=axialmember   Type=User   DOF=P   FDPoint=-C   Force=-1.1   Displ=-10
HingeName=axialmember   Type=User   DOF=P   FDPoint=-B   Force=-1   Displ=-1
HingeName=axialmember   Type=User   DOF=P   FDPoint=A   Force=0   Displ=0
HingeName=axialmember   Type=User   DOF=P   FDPoint=B   Force=1   Displ=1
HingeName=axialmember   Type=User   DOF=P   FDPoint=C   Force=1.1   Displ=10
HingeName=axialmember   Type=User   DOF=P   FDPoint=D   Force=1.4   Displ=35
HingeName=axialmember   Type=User   DOF=P   FDPoint=E   Force=1.4   Displ=75
HingeName=diaglayer   Type=User   DOF=P   FDPoint=-E   Force=-0.2   Displ=-49
HingeName=diaglayer   Type=User   DOF=P   FDPoint=-D   Force=-0.2   Displ=-25
HingeName=diaglayer   Type=User   DOF=P   FDPoint=-C   Force=-1.01   Displ=-25
HingeName=diaglayer   Type=User   DOF=P   FDPoint=-B   Force=-1   Displ=0
HingeName=diaglayer   Type=User   DOF=P   FDPoint=A   Force=0   Displ=0
HingeName=diaglayer   Type=User   DOF=P   FDPoint=B   Force=1   Displ=0
HingeName=diaglayer   Type=User   DOF=P   FDPoint=C   Force=1.01   Displ=25
HingeName=diaglayer   Type=User   DOF=P   FDPoint=D   Force=0.2   Displ=25
HingeName=diaglayer   Type=User   DOF=P   FDPoint=E   Force=0.2   Displ=49
HingeName=diaglayer.15   Type=User   DOF=P   FDPoint=-E   Force=-0.2   Displ=-49
HingeName=diaglayer.15   Type=User   DOF=P   FDPoint=-D   Force=-0.2   Displ=-25
HingeName=diaglayer.15   Type=User   DOF=P   FDPoint=-C   Force=-1.01   Displ=-25
HingeName=diaglayer.15   Type=User   DOF=P   FDPoint=-B   Force=-1   Displ=0
HingeName=diaglayer.15   Type=User   DOF=P   FDPoint=A   Force=0   Displ=0
HingeName=diaglayer.15   Type=User   DOF=P   FDPoint=B   Force=1   Displ=0
HingeName=diaglayer.15   Type=User   DOF=P   FDPoint=C   Force=1.01   Displ=25
HingeName=diaglayer.15   Type=User   DOF=P   FDPoint=D   Force=0.2   Displ=25
HingeName=diaglayer.15   Type=User   DOF=P   FDPoint=E   Force=0.2   Displ=49
HingeName=diaglayer.245   Type=User   DOF=P   FDPoint=-E   Force=-0.2   Displ=-49
HingeName=diaglayer.245   Type=User   DOF=P   FDPoint=-D   Force=-0.2   Displ=-25
HingeName=diaglayer.245   Type=User   DOF=P   FDPoint=-C   Force=-1.01   Displ=-25
HingeName=diaglayer.245   Type=User   DOF=P   FDPoint=-B   Force=-1   Displ=0
HingeName=diaglayer.245   Type=User   DOF=P   FDPoint=A   Force=0   Displ=0
HingeName=diaglayer.245   Type=User   DOF=P   FDPoint=B   Force=1   Displ=0
HingeName=diaglayer.245   Type=User   DOF=P   FDPoint=C   Force=1.01   Displ=25
HingeName=diaglayer.245   Type=User   DOF=P   FDPoint=D   Force=0.2   Displ=25
HingeName=diaglayer.245   Type=User   DOF=P   FDPoint=E   Force=0.2   Displ=49
HingeName=diagshear   Type=User   DOF=P   FDPoint=-E   Force=-0.2   Displ=-150
HingeName=diagshear   Type=User   DOF=P   FDPoint=-D   Force=-0.2   Displ=-75
HingeName=diagshear   Type=User   DOF=P   FDPoint=-C   Force=-1.4   Displ=-75
HingeName=diagshear   Type=User   DOF=P   FDPoint=-B   Force=-1   Displ=0
HingeName=diagshear   Type=User   DOF=P   FDPoint=A   Force=0   Displ=0
HingeName=diagshear   Type=User   DOF=P   FDPoint=B   Force=1   Displ=0
HingeName=diagshear   Type=User   DOF=P   FDPoint=C   Force=1.4   Displ=75
HingeName=diagshear   Type=User   DOF=P   FDPoint=D   Force=0.2   Displ=75
HingeName=diagshear   Type=User   DOF=P   FDPoint=E   Force=0.2   Displ=150
HingeName=edgestarter   Type=User   DOF=P   FDPoint=-E   Force=-0.2   Displ=-75
HingeName=edgestarter   Type=User   DOF=P   FDPoint=-D   Force=-0.2   Displ=-34
HingeName=edgestarter   Type=User   DOF=P   FDPoint=-C   Force=-1.4   Displ=-34
HingeName=edgestarter   Type=User   DOF=P   FDPoint=-B   Force=-1   Displ=0
HingeName=edgestarter   Type=User   DOF=P   FDPoint=A   Force=0   Displ=0
HingeName=edgestarter   Type=User   DOF=P   FDPoint=B   Force=1   Displ=0
HingeName=edgestarter   Type=User   DOF=P   FDPoint=C   Force=1.4   Displ=34
HingeName=edgestarter   Type=User   DOF=P   FDPoint=D   Force=0.2   Displ=34
HingeName=edgestarter   Type=User   DOF=P   FDPoint=E   Force=0.2   Displ=75
HingeName=edgestarter0.5   Type=User   DOF=P   FDPoint=-E   Force=-0.2   Displ=-75
HingeName=edgestarter0.5   Type=User   DOF=P   FDPoint=-D   Force=-0.2   Displ=-34
HingeName=edgestarter0.5   Type=User   DOF=P   FDPoint=-C   Force=-1.4   Displ=-34
HingeName=edgestarter0.5   Type=User   DOF=P   FDPoint=-B   Force=-1   Displ=0
HingeName=edgestarter0.5   Type=User   DOF=P   FDPoint=A   Force=0   Displ=0
HingeName=edgestarter0.5   Type=User   DOF=P   FDPoint=B   Force=1   Displ=0
HingeName=edgestarter0.5   Type=User   DOF=P   FDPoint=C   Force=1.4   Displ=34
HingeName=edgestarter0.5   Type=User   DOF=P   FDPoint=D   Force=0.2   Displ=34
HingeName=edgestarter0.5   Type=User   DOF=P   FDPoint=E   Force=0.2   Displ=75
HingeName=edgestarter1.389   Type=User   DOF=P   FDPoint=-E   Force=-0.2   Displ=-75
HingeName=edgestarter1.389   Type=User   DOF=P   FDPoint=-D   Force=-0.2   Displ=-34
HingeName=edgestarter1.389   Type=User   DOF=P   FDPoint=-C   Force=-1.4   Displ=-34
HingeName=edgestarter1.389   Type=User   DOF=P   FDPoint=-B   Force=-1   Displ=0
HingeName=edgestarter1.389   Type=User   DOF=P   FDPoint=A   Force=0   Displ=0
HingeName=edgestarter1.389   Type=User   DOF=P   FDPoint=B   Force=1   Displ=0
HingeName=edgestarter1.389   Type=User   DOF=P   FDPoint=C   Force=1.4   Displ=34
HingeName=edgestarter1.389   Type=User   DOF=P   FDPoint=D   Force=0.2   Displ=34
HingeName=edgestarter1.389   Type=User   DOF=P   FDPoint=E   Force=0.2   Displ=75
HingeName=edgestarter1.5   Type=User   DOF=P   FDPoint=-E   Force=-0.2   Displ=-75
HingeName=edgestarter1.5   Type=User   DOF=P   FDPoint=-D   Force=-0.2   Displ=-34
HingeName=edgestarter1.5   Type=User   DOF=P   FDPoint=-C   Force=-1.4   Displ=-34
HingeName=edgestarter1.5   Type=User   DOF=P   FDPoint=-B   Force=-1   Displ=0
HingeName=edgestarter1.5   Type=User   DOF=P   FDPoint=A   Force=0   Displ=0
HingeName=edgestarter1.5   Type=User   DOF=P   FDPoint=B   Force=1   Displ=0
HingeName=edgestarter1.5   Type=User   DOF=P   FDPoint=C   Force=1.4   Displ=34
HingeName=edgestarter1.5   Type=User   DOF=P   FDPoint=D   Force=0.2   Displ=34
HingeName=edgestarter1.5   Type=User   DOF=P   FDPoint=E   Force=0.2   Displ=75
HingeName=edgestarter1.722   Type=User   DOF=P   FDPoint=-E   Force=-0.2   Displ=-75
HingeName=edgestarter1.722   Type=User   DOF=P   FDPoint=-D   Force=-0.2   Displ=-34
HingeName=edgestarter1.722   Type=User   DOF=P   FDPoint=-C   Force=-1.4   Displ=-34
HingeName=edgestarter1.722   Type=User   DOF=P   FDPoint=-B   Force=-1   Displ=0
```

```
HingeName=edgestarter1.722   Type=User   DOF=P   FDPoint=A   Force=0   Displ=0
HingeName=edgestarter1.722   Type=User   DOF=P   FDPoint=B   Force=1   Displ=0
HingeName=edgestarter1.722   Type=User   DOF=P   FDPoint=C   Force=1.4   Displ=34
HingeName=edgestarter1.722   Type=User   DOF=P   FDPoint=D   Force=0.2   Displ=34
HingeName=edgestarter1.722   Type=User   DOF=P   FDPoint=E   Force=0.2   Displ=75
HingeName=halfhinge   Type=User   DOF=P   FDPoint=-E   Force=-0.2   Displ=-100
HingeName=halfhinge   Type=User   DOF=P   FDPoint=-D   Force=-0.2   Displ=-50
HingeName=halfhinge   Type=User   DOF=P   FDPoint=-C   Force=-1.05   Displ=-50
HingeName=halfhinge   Type=User   DOF=P   FDPoint=-B   Force=-1   Displ=0
HingeName=halfhinge   Type=User   DOF=P   FDPoint=A   Force=0   Displ=0
HingeName=halfhinge   Type=User   DOF=P   FDPoint=B   Force=1   Displ=0
HingeName=halfhinge   Type=User   DOF=P   FDPoint=C   Force=1.05   Displ=50
HingeName=halfhinge   Type=User   DOF=P   FDPoint=D   Force=0.2   Displ=50
HingeName=halfhinge   Type=User   DOF=P   FDPoint=E   Force=0.2   Displ=100
HingeName=mainlongsteel   Type=User   DOF=P   FDPoint=-E   Force=-0.2   Displ=-100
HingeName=mainlongsteel   Type=User   DOF=P   FDPoint=-D   Force=-0.2   Displ=-75
HingeName=mainlongsteel   Type=User   DOF=P   FDPoint=-C   Force=-1.4   Displ=-75
HingeName=mainlongsteel   Type=User   DOF=P   FDPoint=-B   Force=-1   Displ=0
HingeName=mainlongsteel   Type=User   DOF=P   FDPoint=A   Force=0   Displ=0
HingeName=mainlongsteel   Type=User   DOF=P   FDPoint=B   Force=1   Displ=0
HingeName=mainlongsteel   Type=User   DOF=P   FDPoint=C   Force=1.4   Displ=75
HingeName=mainlongsteel   Type=User   DOF=P   FDPoint=D   Force=0.2   Displ=75
HingeName=mainlongsteel   Type=User   DOF=P   FDPoint=E   Force=0.2   Displ=100
HingeName=mesh   Type=User   DOF=P   FDPoint=-E   Force=-0.2   Displ=-70
HingeName=mesh   Type=User   DOF=P   FDPoint=-D   Force=-0.2   Displ=-65
HingeName=mesh   Type=User   DOF=P   FDPoint=-C   Force=-1.18   Displ=-65
HingeName=mesh   Type=User   DOF=P   FDPoint=-B   Force=-1   Displ=-1
HingeName=mesh   Type=User   DOF=P   FDPoint=A   Force=0   Displ=0
HingeName=mesh   Type=User   DOF=P   FDPoint=B   Force=1   Displ=1
HingeName=mesh   Type=User   DOF=P   FDPoint=C   Force=1.18   Displ=65
HingeName=mesh   Type=User   DOF=P   FDPoint=D   Force=0.2   Displ=65
HingeName=mesh   Type=User   DOF=P   FDPoint=E   Force=0.2   Displ=70
HingeName=mesh0.5   Type=User   DOF=P   FDPoint=-E   Force=-0.2   Displ=-70
HingeName=mesh0.5   Type=User   DOF=P   FDPoint=-D   Force=-0.2   Displ=-65
HingeName=mesh0.5   Type=User   DOF=P   FDPoint=-C   Force=-1.18   Displ=-65
HingeName=mesh0.5   Type=User   DOF=P   FDPoint=-B   Force=-1   Displ=-1
HingeName=mesh0.5   Type=User   DOF=P   FDPoint=A   Force=0   Displ=0
HingeName=mesh0.5   Type=User   DOF=P   FDPoint=B   Force=1   Displ=1
HingeName=mesh0.5   Type=User   DOF=P   FDPoint=C   Force=1.18   Displ=65
HingeName=mesh0.5   Type=User   DOF=P   FDPoint=D   Force=0.2   Displ=65
HingeName=mesh0.5   Type=User   DOF=P   FDPoint=E   Force=0.2   Displ=70
HingeName=mesh1.389   Type=User   DOF=P   FDPoint=-E   Force=-0.2   Displ=-70
HingeName=mesh1.389   Type=User   DOF=P   FDPoint=-D   Force=-0.2   Displ=-65
HingeName=mesh1.389   Type=User   DOF=P   FDPoint=-C   Force=-1.18   Displ=-65
HingeName=mesh1.389   Type=User   DOF=P   FDPoint=-B   Force=-1   Displ=-1
HingeName=mesh1.389   Type=User   DOF=P   FDPoint=A   Force=0   Displ=0
HingeName=mesh1.389   Type=User   DOF=P   FDPoint=B   Force=1   Displ=1
HingeName=mesh1.389   Type=User   DOF=P   FDPoint=C   Force=1.18   Displ=65
HingeName=mesh1.389   Type=User   DOF=P   FDPoint=D   Force=0.2   Displ=65
HingeName=mesh1.389   Type=User   DOF=P   FDPoint=E   Force=0.2   Displ=70
HingeName=mesh1.5   Type=User   DOF=P   FDPoint=-E   Force=-0.2   Displ=-70
HingeName=mesh1.5   Type=User   DOF=P   FDPoint=-D   Force=-0.2   Displ=-65
HingeName=mesh1.5   Type=User   DOF=P   FDPoint=-C   Force=-1.18   Displ=-65
HingeName=mesh1.5   Type=User   DOF=P   FDPoint=-B   Force=-1   Displ=-1
HingeName=mesh1.5   Type=User   DOF=P   FDPoint=A   Force=0   Displ=0
HingeName=mesh1.5   Type=User   DOF=P   FDPoint=B   Force=1   Displ=1
HingeName=mesh1.5   Type=User   DOF=P   FDPoint=C   Force=1.18   Displ=65
HingeName=mesh1.5   Type=User   DOF=P   FDPoint=D   Force=0.2   Displ=65
HingeName=mesh1.5   Type=User   DOF=P   FDPoint=E   Force=0.2   Displ=70
HingeName=mesh1.722   Type=User   DOF=P   FDPoint=-E   Force=-0.2   Displ=-70
HingeName=mesh1.722   Type=User   DOF=P   FDPoint=-D   Force=-0.2   Displ=-65
HingeName=mesh1.722   Type=User   DOF=P   FDPoint=-C   Force=-1.18   Displ=-65
HingeName=mesh1.722   Type=User   DOF=P   FDPoint=-B   Force=-1   Displ=-1
HingeName=mesh1.722   Type=User   DOF=P   FDPoint=A   Force=0   Displ=0
HingeName=mesh1.722   Type=User   DOF=P   FDPoint=B   Force=1   Displ=1
HingeName=mesh1.722   Type=User   DOF=P   FDPoint=C   Force=1.18   Displ=65
HingeName=mesh1.722   Type=User   DOF=P   FDPoint=D   Force=0.2   Displ=65
HingeName=mesh1.722   Type=User   DOF=P   FDPoint=E   Force=0.2   Displ=70
HingeName=tensiontie   Type=User   DOF=P   FDPoint=-E   Force=-0.2   Displ=-100
HingeName=tensiontie   Type=User   DOF=P   FDPoint=-D   Force=-0.2   Displ=-75
HingeName=tensiontie   Type=User   DOF=P   FDPoint=-C   Force=-1.2   Displ=-75
HingeName=tensiontie   Type=User   DOF=P   FDPoint=-B   Force=-1   Displ=0
HingeName=tensiontie   Type=User   DOF=P   FDPoint=A   Force=0   Displ=0
HingeName=tensiontie   Type=User   DOF=P   FDPoint=B   Force=1   Displ=0
HingeName=tensiontie   Type=User   DOF=P   FDPoint=C   Force=1.2   Displ=75
HingeName=tensiontie   Type=User   DOF=P   FDPoint=D   Force=0.2   Displ=75
HingeName=tensiontie   Type=User   DOF=P   FDPoint=E   Force=0.2   Displ=100
HingeName=tensiontie.15   Type=User   DOF=P   FDPoint=-E   Force=-0.2   Displ=-100
HingeName=tensiontie.15   Type=User   DOF=P   FDPoint=-D   Force=-0.2   Displ=-75
HingeName=tensiontie.15   Type=User   DOF=P   FDPoint=-C   Force=-1.2   Displ=-75
HingeName=tensiontie.15   Type=User   DOF=P   FDPoint=-B   Force=-1   Displ=0
HingeName=tensiontie.15   Type=User   DOF=P   FDPoint=A   Force=0   Displ=0
HingeName=tensiontie.15   Type=User   DOF=P   FDPoint=B   Force=1   Displ=0
HingeName=tensiontie.15   Type=User   DOF=P   FDPoint=C   Force=1.2   Displ=75
HingeName=tensiontie.15   Type=User   DOF=P   FDPoint=D   Force=0.2   Displ=75
```

```
   HingeName=tensiontie.15   Type=User   DOF=P   FDPoint=E   Force=0.2   Displ=100
   HingeName=tensiontie.245   Type=User   DOF=P   FDPoint=-E   Force=-0.2   Displ=-100
   HingeName=tensiontie.245   Type=User   DOF=P   FDPoint=-D   Force=-0.2   Displ=-75
   HingeName=tensiontie.245   Type=User   DOF=P   FDPoint=-C   Force=-1.2   Displ=-75
   HingeName=tensiontie.245   Type=User   DOF=P   FDPoint=-B   Force=-1   Displ=0
   HingeName=tensiontie.245   Type=User   DOF=P   FDPoint=A   Force=0   Displ=0
   HingeName=tensiontie.245   Type=User   DOF=P   FDPoint=B   Force=1   Displ=0
   HingeName=tensiontie.245   Type=User   DOF=P   FDPoint=C   Force=1.2   Displ=75
   HingeName=tensiontie.245   Type=User   DOF=P   FDPoint=D   Force=0.2   Displ=75
   HingeName=tensiontie.245   Type=User   DOF=P   FDPoint=E   Force=0.2   Displ=100
   HingeName=tensiontie.335   Type=User   DOF=P   FDPoint=-E   Force=-0.2   Displ=-100
   HingeName=tensiontie.335   Type=User   DOF=P   FDPoint=-D   Force=-0.2   Displ=-75
   HingeName=tensiontie.335   Type=User   DOF=P   FDPoint=-C   Force=-1.2   Displ=-75
   HingeName=tensiontie.335   Type=User   DOF=P   FDPoint=-B   Force=-1   Displ=0
   HingeName=tensiontie.335   Type=User   DOF=P   FDPoint=A   Force=0   Displ=0
   HingeName=tensiontie.335   Type=User   DOF=P   FDPoint=B   Force=1   Displ=0
   HingeName=tensiontie.335   Type=User   DOF=P   FDPoint=C   Force=1.2   Displ=75
   HingeName=tensiontie.335   Type=User   DOF=P   FDPoint=D   Force=0.2   Displ=75
   HingeName=tensiontie.335   Type=User   DOF=P   FDPoint=E   Force=0.2   Displ=100

TABLE:  "HINGE PROPS 4 - ACCEPTANCE CRITERIA"
   HingeName=2-4.0mm   Type=User   DOF=P   ACPoint=IO   ACPos=13   ACNeg=-13
   HingeName=2-4.0mm   Type=User   DOF=P   ACPoint=LS   ACPos=26   ACNeg=-26
   HingeName=2-4.0mm   Type=User   DOF=P   ACPoint=CP   ACPos=53   ACNeg=-53
   HingeName=axialmember   Type=User   DOF=P   ACPoint=IO   ACPos=9   ACNeg=-9
   HingeName=axialmember   Type=User   DOF=P   ACPoint=LS   ACPos=18   ACNeg=-18
   HingeName=axialmember   Type=User   DOF=P   ACPoint=CP   ACPos=35   ACNeg=-35
   HingeName=diaglayer   Type=User   DOF=P   ACPoint=IO   ACPos=6   ACNeg=-6
   HingeName=diaglayer   Type=User   DOF=P   ACPoint=LS   ACPos=13   ACNeg=-13
   HingeName=diaglayer   Type=User   DOF=P   ACPoint=CP   ACPos=25   ACNeg=-25
   HingeName=diaglayer.15   Type=User   DOF=P   ACPoint=IO   ACPos=6   ACNeg=-6
   HingeName=diaglayer.15   Type=User   DOF=P   ACPoint=LS   ACPos=13   ACNeg=-13
   HingeName=diaglayer.15   Type=User   DOF=P   ACPoint=CP   ACPos=25   ACNeg=-25
   HingeName=diaglayer.245   Type=User   DOF=P   ACPoint=IO   ACPos=6   ACNeg=-6
   HingeName=diaglayer.245   Type=User   DOF=P   ACPoint=LS   ACPos=13   ACNeg=-13
   HingeName=diaglayer.245   Type=User   DOF=P   ACPoint=CP   ACPos=23   ACNeg=-25
   HingeName=diagshear   Type=User   DOF=P   ACPoint=IO   ACPos=9   ACNeg=-9
   HingeName=diagshear   Type=User   DOF=P   ACPoint=LS   ACPos=18   ACNeg=-18
   HingeName=diagshear   Type=User   DOF=P   ACPoint=CP   ACPos=35   ACNeg=-35
   HingeName=edgestarter   Type=User   DOF=P   ACPoint=IO   ACPos=8   ACNeg=-8
   HingeName=edgestarter   Type=User   DOF=P   ACPoint=LS   ACPos=17   ACNeg=-17
   HingeName=edgestarter   Type=User   DOF=P   ACPoint=CP   ACPos=34   ACNeg=-34
   HingeName=edgestarter0.5   Type=User   DOF=P   ACPoint=IO   ACPos=8   ACNeg=-8
   HingeName=edgestarter0.5   Type=User   DOF=P   ACPoint=LS   ACPos=17   ACNeg=-17
   HingeName=edgestarter0.5   Type=User   DOF=P   ACPoint=CP   ACPos=34   ACNeg=-34
   HingeName=edgestarter1.389   Type=User   DOF=P   ACPoint=IO   ACPos=8   ACNeg=-8
   HingeName=edgestarter1.389   Type=User   DOF=P   ACPoint=LS   ACPos=17   ACNeg=-17
   HingeName=edgestarter1.389   Type=User   DOF=P   ACPoint=CP   ACPos=34   ACNeg=-34
   HingeName=edgestarter1.5   Type=User   DOF=P   ACPoint=IO   ACPos=8   ACNeg=-8
   HingeName=edgestarter1.5   Type=User   DOF=P   ACPoint=LS   ACPos=17   ACNeg=-17
   HingeName=edgestarter1.5   Type=User   DOF=P   ACPoint=CP   ACPos=34   ACNeg=-34
   HingeName=edgestarter1.722   Type=User   DOF=P   ACPoint=IO   ACPos=8   ACNeg=-8
   HingeName=edgestarter1.722   Type=User   DOF=P   ACPoint=LS   ACPos=17   ACNeg=-17
   HingeName=edgestarter1.722   Type=User   DOF=P   ACPoint=CP   ACPos=34   ACNeg=-34
   HingeName=halfhinge   Type=User   DOF=P   ACPoint=IO   ACPos=12   ACNeg=-12
   HingeName=halfhinge   Type=User   DOF=P   ACPoint=LS   ACPos=25   ACNeg=-25
   HingeName=halfhinge   Type=User   DOF=P   ACPoint=CP   ACPos=50   ACNeg=-50
   HingeName=mainlongsteel   Type=User   DOF=P   ACPoint=IO   ACPos=9   ACNeg=-9
   HingeName=mainlongsteel   Type=User   DOF=P   ACPoint=LS   ACPos=18   ACNeg=-18
   HingeName=mainlongsteel   Type=User   DOF=P   ACPoint=CP   ACPos=35   ACNeg=-35
   HingeName=mesh   Type=User   DOF=P   ACPoint=IO   ACPos=16   ACNeg=-16
   HingeName=mesh   Type=User   DOF=P   ACPoint=LS   ACPos=32   ACNeg=-32
   HingeName=mesh   Type=User   DOF=P   ACPoint=CP   ACPos=65   ACNeg=-65
   HingeName=mesh0.5   Type=User   DOF=P   ACPoint=IO   ACPos=16   ACNeg=-16
   HingeName=mesh0.5   Type=User   DOF=P   ACPoint=LS   ACPos=32   ACNeg=-32
   HingeName=mesh0.5   Type=User   DOF=P   ACPoint=CP   ACPos=65   ACNeg=-65
   HingeName=mesh1.389   Type=User   DOF=P   ACPoint=IO   ACPos=16   ACNeg=-16
   HingeName=mesh1.389   Type=User   DOF=P   ACPoint=LS   ACPos=32   ACNeg=-32
   HingeName=mesh1.389   Type=User   DOF=P   ACPoint=CP   ACPos=65   ACNeg=-65
   HingeName=mesh1.5   Type=User   DOF=P   ACPoint=IO   ACPos=16   ACNeg=-16
   HingeName=mesh1.5   Type=User   DOF=P   ACPoint=LS   ACPos=32   ACNeg=-32
   HingeName=mesh1.5   Type=User   DOF=P   ACPoint=CP   ACPos=65   ACNeg=-65
   HingeName=mesh1.722   Type=User   DOF=P   ACPoint=IO   ACPos=16   ACNeg=-16
   HingeName=mesh1.722   Type=User   DOF=P   ACPoint=LS   ACPos=32   ACNeg=-32
   HingeName=mesh1.722   Type=User   DOF=P   ACPoint=CP   ACPos=65   ACNeg=-65
   HingeName=tensiontie   Type=User   DOF=P   ACPoint=IO   ACPos=8   ACNeg=-8
   HingeName=tensiontie   Type=User   DOF=P   ACPoint=LS   ACPos=17   ACNeg=-17
   HingeName=tensiontie   Type=User   DOF=P   ACPoint=CP   ACPos=34   ACNeg=-34
   HingeName=tensiontie.15   Type=User   DOF=P   ACPoint=IO   ACPos=8   ACNeg=-8
   HingeName=tensiontie.15   Type=User   DOF=P   ACPoint=LS   ACPos=17   ACNeg=-17
   HingeName=tensiontie.15   Type=User   DOF=P   ACPoint=CP   ACPos=34   ACNeg=-34
   HingeName=tensiontie.245   Type=User   DOF=P   ACPoint=IO   ACPos=8   ACNeg=-8
   HingeName=tensiontie.245   Type=User   DOF=P   ACPoint=LS   ACPos=17   ACNeg=-17
   HingeName=tensiontie.245   Type=User   DOF=P   ACPoint=CP   ACPos=34   ACNeg=-34
   HingeName=tensiontie.335   Type=User   DOF=P   ACPoint=IO   ACPos=8   ACNeg=-8
```

```
   HingeName=tensiontie.335   Type=User   DOF=P   ACPoint=LS   ACPos=17   ACNeg=-17
   HingeName=tensiontie.335   Type=User   DOF=P   ACPoint=CP   ACPos=34   ACNeg=-34

TABLE:  "AREA SECTION PROPERTIES"
   Section=slab   Material=CONC   MatAngle=0   AreaType=Shell   Type=Shell-Thick   Thickness=0.04
BendThick=0.04   Color=Magenta   TotalWt=19.101696   TotalMass=1.947179136   F11Mod=1   F22Mod=1
F12Mod=1   M11Mod=1   M22Mod=1   M12Mod=1
        V13Mod=1   V23Mod=1   MMod=1   WMod=1

TABLE:  "LINK PROPERTY DEFINITIONS 01 - GENERAL"
   Link=LIN1   LinkType=Linear   Mass=0   Weight=0   RotInert1=0   RotInert2=0   RotInert3=0
PDM2I=0   PDM2J=0   PDM3I=0   PDM3J=0   Color=Red

TABLE:  "LOAD CASE DEFINITIONS"
   LoadCase=DEAD   DesignType=DEAD   SelfWtMult=1
   LoadCase=Lateral   DesignType=OTHER   SelfWtMult=0
   LoadCase=A   DesignType=OTHER   SelfWtMult=0
   LoadCase=B   DesignType=OTHER   SelfWtMult=0
   LoadCase=C   DesignType=OTHER   SelfWtMult=0

TABLE:  "ANALYSIS CASE DEFINITIONS"
   Case=DEAD   Type=NonStatic   InitialCond=Zero
   Case=+0.5i   Type=NonStatic   InitialCond=DEAD
   Case=-0.5i   Type=NonStatic   InitialCond=+0.5i
   Case=+0.5ii   Type=NonStatic   InitialCond=-0.5i
   Case=-0.5ii   Type=NonStatic   InitialCond=+0.5ii
   Case=+1.0i   Type=NonStatic   InitialCond=-0.5ii
   Case=-1.0i   Type=NonStatic   InitialCond=+1.0i
   Case=+1.0ii   Type=NonStatic   InitialCond=-1.0i
   Case=-1.0ii   Type=NonStatic   InitialCond=+1.0ii
   Case=+1.5i   Type=NonStatic   InitialCond=-1.0ii
   Case=-1.5i   Type=NonStatic   InitialCond=+1.5i
   Case=+1.5ii   Type=NonStatic   InitialCond=-1.5i
   Case=-1.5ii   Type=NonStatic   InitialCond=+1.5ii
   Case=+2.0ia   Type=NonStatic   InitialCond=-1.5ii
   Case=-2.0ia   Type=NonStatic   InitialCond=+2.0ia
   Case=+2.0iia   Type=NonStatic   InitialCond=-2.0ia
   Case="remove C1 C1a"   Type=NonStatic   InitialCond=+2.0iia
   Case=+2.0iib   Type=NonStatic   InitialCond="remove C1 C1a"
   Case=-2.0iia   Type=NonStatic   InitialCond=+2.0iib
   Case="remove A2 A2a"   Type=NonStatic   InitialCond=-2.0iia
   Case=-2.0iib   Type=NonStatic   InitialCond="remove A2 A2a"
   Case=+2.5ia   Type=NonStatic   InitialCond=-2.0iib
   Case="remove C2"   Type=NonStatic   InitialCond=+2.5ia
   Case=+2.5ib   Type=NonStatic   InitialCond="remove C2"
   Case=-2.5ia   Type=NonStatic   InitialCond=+2.5ib
   Case="removes C2a"   Type=NonStatic   InitialCond=-2.5ia
   Case=-2.5ib   Type=NonStatic   InitialCond="removes C2a"
   Case="remove A1 B2"   Type=NonStatic   InitialCond=-2.5ib
   Case=-2.5ic   Type=NonStatic   InitialCond="remove A1 B2"
   Case=+2.5iia   Type=NonStatic   InitialCond=-2.5ic
   Case="removes A1a"   Type=NonStatic   InitialCond=+2.5iia
   Case=+2.5iib   Type=NonStatic   InitialCond="removes A1a"
   Case=-2.5ii   Type=NonStatic   InitialCond=+2.5iib
   Case=+3.0ia   Type=NonStatic   InitialCond=-2.5ii
   Case=-3.0ia   Type=NonStatic   InitialCond=+3.0ia
   Case=+3.0iia   Type=NonStatic   InitialCond=-3.0ia
   Case="remove B1a"   Type=NonStatic   InitialCond=+3.0iia
   Case="removes B1 B2a"   Type=NonStatic   InitialCond="remove B1a"
   Case=+3.0iib   Type=NonStatic   InitialCond="removes B1 B2a"
   Case=-3.0iia   Type=NonStatic   InitialCond=+3.0iib
   Case="removes A1b"   Type=NonStatic   InitialCond=-3.0iia
   Case=-3.0iib   Type=NonStatic   InitialCond="removes A1b"
   Case=+3.5ia   Type=NonStatic   InitialCond=-3.0iib
   Case=-3.5ia   Type=NonStatic   InitialCond=+3.5ia
   Case="remove C2b"   Type=NonStatic   InitialCond=-3.5ia
   Case=+3.5ii   Type=NonStatic   InitialCond="remove C2b"
   Case=-3.5ii   Type=NonStatic   InitialCond=+3.5ii
   Case=+3.5iii   Type=NonStatic   InitialCond=-3.5ii
   Case=-3.5iii   Type=NonStatic   InitialCond=+3.5iii
   Case=+4.0ia   Type=NonStatic   InitialCond=-3.5iii
   Case="remove C2c"   Type=NonStatic   InitialCond=+4.0ia
   Case=+4.0ib   Type=NonStatic   InitialCond="remove C2c"
   Case=-4.0ia   Type=NonStatic   InitialCond=+4.0ib
   Case="remove A1c"   Type=NonStatic   InitialCond=-4.0ia
   Case=-4.0ib   Type=NonStatic   InitialCond="remove A1c"
   Case=+4.0ii   Type=NonStatic   InitialCond=-4.0ib
   Case=-4.0ii   Type=NonStatic   InitialCond=+4.0ii

TABLE:  "CASE - STATIC 1 - LOAD ASSIGNMENTS"
   Case=DEAD   LoadType="Load case"   LoadName=DEAD   LoadSF=1
   Case=+0.5i   LoadType="Load case"   LoadName=Lateral   LoadSF=1
   Case=-0.5i   LoadType="Load case"   LoadName=Lateral   LoadSF=-1
   Case=+0.5ii   LoadType="Load case"   LoadName=Lateral   LoadSF=1
   Case=-0.5ii   LoadType="Load case"   LoadName=Lateral   LoadSF=-1
```

```
   Case=+1.0i   LoadType="Load case"   LoadName=Lateral   LoadSF=1
   Case=-1.0i   LoadType="Load case"   LoadName=Lateral   LoadSF=-1
   Case=+1.0ii   LoadType="Load case"   LoadName=Lateral   LoadSF=1
   Case=-1.0ii   LoadType="Load case"   LoadName=Lateral   LoadSF=-1
   Case=+1.5i   LoadType="Load case"   LoadName=Lateral   LoadSF=1
   Case=-1.5i   LoadType="Load case"   LoadName=Lateral   LoadSF=-1
   Case=+1.5ii   LoadType="Load case"   LoadName=Lateral   LoadSF=1
   Case=-1.5ii   LoadType="Load case"   LoadName=Lateral   LoadSF=-1
   Case=+2.0ia   LoadType="Load case"   LoadName=Lateral   LoadSF=1
   Case=-2.0ia   LoadType="Load case"   LoadName=Lateral   LoadSF=-1
   Case=+2.0iia   LoadType="Load case"   LoadName=Lateral   LoadSF=1
   Case="remove C1 C1a"   LoadType="Load case"   LoadName=Lateral   LoadSF=0
   Case=+2.0iib   LoadType="Load case"   LoadName=Lateral   LoadSF=1
   Case=-2.0iia   LoadType="Load case"   LoadName=Lateral   LoadSF=-1
   Case="remove A2 A2a"   LoadType="Load case"   LoadName=Lateral   LoadSF=0
   Case=-2.0iib   LoadType="Load case"   LoadName=Lateral   LoadSF=-1
   Case=+2.5ia   LoadType="Load case"   LoadName=Lateral   LoadSF=1
   Case="remove C2"   LoadType="Load case"   LoadName=Lateral   LoadSF=0
   Case=+2.5ib   LoadType="Load case"   LoadName=Lateral   LoadSF=1
   Case=-2.5ia   LoadType="Load case"   LoadName=Lateral   LoadSF=-1
   Case="removes C2a"   LoadType="Load case"   LoadName=Lateral   LoadSF=0
   Case=-2.5ib   LoadType="Load case"   LoadName=Lateral   LoadSF=-1
   Case="remove A1 B2"   LoadType="Load case"   LoadName=Lateral   LoadSF=0
   Case=-2.5ic   LoadType="Load case"   LoadName=Lateral   LoadSF=-1
   Case=+2.5iia   LoadType="Load case"   LoadName=Lateral   LoadSF=1
   Case="removes A1a"   LoadType="Load case"   LoadName=Lateral   LoadSF=0
   Case=+2.5iib   LoadType="Load case"   LoadName=Lateral   LoadSF=1
   Case=-2.5ii   LoadType="Load case"   LoadName=Lateral   LoadSF=-1
   Case=+3.0ia   LoadType="Load case"   LoadName=Lateral   LoadSF=1
   Case=-3.0ia   LoadType="Load case"   LoadName=Lateral   LoadSF=-1
   Case=+3.0iia   LoadType="Load case"   LoadName=Lateral   LoadSF=1
   Case="remove B1a"   LoadType="Load case"   LoadName=Lateral   LoadSF=0
   Case="removes B1 B2a"   LoadType="Load case"   LoadName=Lateral   LoadSF=0
   Case=+3.0iib   LoadType="Load case"   LoadName=Lateral   LoadSF=1
   Case=-3.0iia   LoadType="Load case"   LoadName=Lateral   LoadSF=-1
   Case="removes A1b"   LoadType="Load case"   LoadName=Lateral   LoadSF=0
   Case=-3.0iib   LoadType="Load case"   LoadName=Lateral   LoadSF=-1
   Case=+3.5ia   LoadType="Load case"   LoadName=Lateral   LoadSF=1
   Case=-3.5ia   LoadType="Load case"   LoadName=Lateral   LoadSF=-1
   Case="remove C2b"   LoadType="Load case"   LoadName=Lateral   LoadSF=0
   Case=+3.5ii   LoadType="Load case"   LoadName=Lateral   LoadSF=1
   Case=-3.5ii   LoadType="Load case"   LoadName=Lateral   LoadSF=-1
   Case=+3.5iii   LoadType="Load case"   LoadName=Lateral   LoadSF=1
   Case=-3.5iii   LoadType="Load case"   LoadName=Lateral   LoadSF=-1
   Case=+4.0ia   LoadType="Load case"   LoadName=Lateral   LoadSF=1
   Case="remove C2c"   LoadType="Load case"   LoadName=Lateral   LoadSF=0
   Case=+4.0ib   LoadType="Load case"   LoadName=Lateral   LoadSF=1
   Case=-4.0ia   LoadType="Load case"   LoadName=Lateral   LoadSF=-1
   Case="remove A1c"   LoadType="Load case"   LoadName=Lateral   LoadSF=0
   Case=-4.0ib   LoadType="Load case"   LoadName=Lateral   LoadSF=-1
   Case=+4.0ii   LoadType="Load case"   LoadName=Lateral   LoadSF=1
   Case=-4.0ii   LoadType="Load case"   LoadName=Lateral   LoadSF=-1

TABLE:  "CASE - STATIC 2 - NONLINEAR LOAD APPLICATION"
   Case=DEAD   LoadApp="Full Load"   MonitorDOF=U1   MonitorJt=5
   Case=+0.5i   LoadApp="Displ Ctrl"   DisplType=Monitored   TargetDispl=0.00615   MonitorDOF=U1
MonitorJt=10
   Case=-0.5i   LoadApp="Displ Ctrl"   DisplType=Monitored   TargetDispl=0.0123   MonitorDOF=U1
MonitorJt=10
   Case=+0.5ii   LoadApp="Displ Ctrl"   DisplType=Monitored   TargetDispl=0.0123   MonitorDOF=U1
MonitorJt=10
   Case=-0.5ii   LoadApp="Displ Ctrl"   DisplType=Monitored   TargetDispl=0.0123   MonitorDOF=U1
MonitorJt=10
   Case=+1.0i   LoadApp="Displ Ctrl"   DisplType=Monitored   TargetDispl=0.01845   MonitorDOF=U1
MonitorJt=10
   Case=-1.0i   LoadApp="Displ Ctrl"   DisplType=Monitored   TargetDispl=0.0246   MonitorDOF=U1
MonitorJt=10
   Case=+1.0ii   LoadApp="Displ Ctrl"   DisplType=Monitored   TargetDispl=0.0246   MonitorDOF=U1
MonitorJt=10
   Case=-1.0ii   LoadApp="Displ Ctrl"   DisplType=Monitored   TargetDispl=0.0246   MonitorDOF=U1
MonitorJt=10
   Case=+1.5i   LoadApp="Displ Ctrl"   DisplType=Monitored   TargetDispl=0.03075   MonitorDOF=U1
MonitorJt=10
   Case=-1.5i   LoadApp="Displ Ctrl"   DisplType=Monitored   TargetDispl=0.037   MonitorDOF=U1
MonitorJt=10
   Case=+1.5ii   LoadApp="Displ Ctrl"   DisplType=Monitored   TargetDispl=0.037   MonitorDOF=U1
MonitorJt=10
   Case=-1.5ii   LoadApp="Displ Ctrl"   DisplType=Monitored   TargetDispl=0.037   MonitorDOF=U1
MonitorJt=10
   Case=+2.0ia   LoadApp="Displ Ctrl"   DisplType=Monitored   TargetDispl=0.04315   MonitorDOF=U1
MonitorJt=10
   Case=-2.0ia   LoadApp="Displ Ctrl"   DisplType=Monitored   TargetDispl=0.0492   MonitorDOF=U1
MonitorJt=10
   Case=+2.0iia   LoadApp="Displ Ctrl"   DisplType=Monitored   TargetDispl=0.0321   MonitorDOF=U1
MonitorJt=10
```

```
   Case="remove C1 C1a"   LoadApp="Full Load"   MonitorDOF=U1   MonitorJt=10
   Case=+2.0iib   LoadApp="Displ Ctrl"   DisplType=Monitored   TargetDispl=0.01708   MonitorDOF=U1
MonitorJt=10
   Case=-2.0iia   LoadApp="Displ Ctrl"   DisplType=Monitored   TargetDispl=0.0326   MonitorDOF=U1
MonitorJt=10
   Case="remove A2 A2a"   LoadApp="Full Load"   MonitorDOF=U1   MonitorJt=10
   Case=-2.0iib   LoadApp="Displ Ctrl"   DisplType=Monitored   TargetDispl=0.01661   MonitorDOF=U1
MonitorJt=10
   Case=+2.5ia   LoadApp="Displ Ctrl"   DisplType=Monitored   TargetDispl=0.0301   MonitorDOF=U1
MonitorJt=10
   Case="remove C2"   LoadApp="Full Load"   MonitorDOF=U1   MonitorJt=10
   Case=+2.5ib   LoadApp="Displ Ctrl"   DisplType=Monitored   TargetDispl=0.02413   MonitorDOF=U1
MonitorJt=10
   Case=-2.5ia   LoadApp="Displ Ctrl"   DisplType=Monitored   TargetDispl=0.024   MonitorDOF=U1
MonitorJt=10
   Case="removes C2a"   LoadApp="Full Load"   MonitorDOF=U1   MonitorJt=10
   Case=-2.5ib   LoadApp="Displ Ctrl"   DisplType=Monitored   TargetDispl=0.02995   MonitorDOF=U1
MonitorJt=10
   Case="remove A1 B2"   LoadApp="Full Load"   MonitorDOF=U1   MonitorJt=10
   Case=-2.5ic   LoadApp="Displ Ctrl"   DisplType=Monitored   TargetDispl=0.00637   MonitorDOF=U1
MonitorJt=10
   Case=+2.5iia   LoadApp="Displ Ctrl"   DisplType=Monitored   TargetDispl=0.05475   MonitorDOF=U1
MonitorJt=10
   Case="removes A1a"   LoadApp="Full Load"   MonitorDOF=U1   MonitorJt=10
   Case=+2.5iib   LoadApp="Displ Ctrl"   DisplType=Monitored   TargetDispl=0.00659   MonitorDOF=U1
MonitorJt=10
   Case=-2.5ii   LoadApp="Displ Ctrl"   DisplType=Monitored   TargetDispl=0.0615   MonitorDOF=U1
MonitorJt=10
   Case=+3.0ia   LoadApp="Displ Ctrl"   DisplType=Monitored   TargetDispl=0.06765   MonitorDOF=U1
MonitorJt=10
   Case=-3.0ia   LoadApp="Displ Ctrl"   DisplType=Monitored   TargetDispl=0.0738   MonitorDOF=U1
MonitorJt=10
   Case=+3.0iia   LoadApp="Displ Ctrl"   DisplType=Monitored   TargetDispl=0.0649   MonitorDOF=U1
MonitorJt=10
   Case="remove B1a"   LoadApp="Full Load"   MonitorDOF=U1   MonitorJt=10
   Case="removes B1 B2a"   LoadApp="Full Load"   MonitorDOF=U1   MonitorJt=10
   Case=+3.0iib   LoadApp="Displ Ctrl"   DisplType=Monitored   TargetDispl=0.00667   MonitorDOF=U1
MonitorJt=10
   Case=-3.0iia   LoadApp="Displ Ctrl"   DisplType=Monitored   TargetDispl=0.0689   MonitorDOF=U1
MonitorJt=10
   Case="removes A1b"   LoadApp="Full Load"   MonitorDOF=U1   MonitorJt=10
   Case=-3.0iib   LoadApp="Displ Ctrl"   DisplType=Monitored   TargetDispl=0.00454   MonitorDOF=U1
MonitorJt=10
   Case=+3.5ia   LoadApp="Displ Ctrl"   DisplType=Monitored   TargetDispl=0.07995   MonitorDOF=U1
MonitorJt=10
   Case=-3.5ia   LoadApp="Displ Ctrl"   DisplType=Monitored   TargetDispl=0.0861   MonitorDOF=U1
MonitorJt=10
   Case="remove C2b"   LoadApp="Full Load"   MonitorDOF=U1   MonitorJt=10
   Case=+3.5ii   LoadApp="Displ Ctrl"   DisplType=Monitored   TargetDispl=0.0863   MonitorDOF=U1
MonitorJt=10
   Case=-3.5ii   LoadApp="Displ Ctrl"   DisplType=Monitored   TargetDispl=0.0861   MonitorDOF=U1
MonitorJt=10
   Case=+3.5iii   LoadApp="Displ Ctrl"   DisplType=Monitored   TargetDispl=0.0861   MonitorDOF=U1
MonitorJt=10
   Case=-3.5iii   LoadApp="Displ Ctrl"   DisplType=Monitored   TargetDispl=0.0861   MonitorDOF=U1
MonitorJt=10
   Case=+4.0ia   LoadApp="Displ Ctrl"   DisplType=Monitored   TargetDispl=0.08005   MonitorDOF=U1
MonitorJt=10
   Case="remove C2c"   LoadApp="Full Load"   MonitorDOF=U1   MonitorJt=10
   Case=+4.0ib   LoadApp="Displ Ctrl"   DisplType=Monitored   TargetDispl=0.00828   MonitorDOF=U1
MonitorJt=10
   Case=-4.0ia   LoadApp="Displ Ctrl"   DisplType=Monitored   TargetDispl=0.0884   MonitorDOF=U1
MonitorJt=10
   Case="remove A1c"   LoadApp="Full Load"   MonitorDOF=U1   MonitorJt=10
   Case=-4.0ib   LoadApp="Displ Ctrl"   DisplType=Monitored   TargetDispl=0.00454   MonitorDOF=U1
MonitorJt=10
   Case=+4.0ii   LoadApp="Displ Ctrl"   DisplType=Monitored   TargetDispl=0.0984   MonitorDOF=U1
MonitorJt=10
   Case=-4.0ii   LoadApp="Displ Ctrl"   DisplType=Monitored   TargetDispl=0.0984   MonitorDOF=U1
MonitorJt=10

TABLE:  "CASE - STATIC 3 - NONLINEAR STAGE INFORMATION"
   Case="remove C1 C1a"   Stage=1   Operation=Remove   GroupName=C1
   Case="remove C1 C1a"   Stage=2   Operation=Remove   GroupName=C1a
   Case="remove A2 A2a"   Stage=1   Operation=Remove   GroupName=A2
   Case="remove A2 A2a"   Stage=2   Operation=Remove   GroupName=A2a
   Case="remove C2"   Stage=1   Operation=Remove   GroupName=C2
   Case="removes C2a"   Stage=1   Operation=Remove   GroupName=C2a
   Case="remove A1 B2"   Stage=1   Operation=Remove   GroupName=A1
   Case="remove A1 B2"   Stage=2   Operation=Remove   GroupName=B2
   Case="removes A1a"   Stage=1   Operation=Remove   GroupName=A1a
   Case="remove B1a"   Stage=1   Operation=Remove   GroupName=B1a
   Case="removes B1 B2a"   Stage=1   Operation=Remove   GroupName=B1
   Case="removes B1 B2a"   Stage=2   Operation=Remove   GroupName=B2a
   Case="removes A1b"   Stage=1   Operation=Remove   GroupName=A1b
```

```
   Case="remove C2b"   Stage=1   Operation=Remove   GroupName=C2b
   Case="remove C2c"   Stage=1   Operation=Remove   GroupName=C2c
   Case="remove A1c"   Stage=1   Operation=Remove   GroupName=A1c

TABLE:  "CASE - STATIC 4 - NONLINEAR PARAMETERS"
   Case=DEAD   Unloading="Unload Entire"   GeoNonLin=None   ResultsSave="Multiple States"
MinNumState=10   MaxNumState=100   PosIncOnly=Yes   MaxTotal=200   MaxNull=50   MaxIter=10
ItConvTol=0.0001   EvLumpTol=0.01   FrameTC=No
       FrameHinge=No   CableTC=No   LinkTC=No   LinkOther=No
   Case=+0.5i   Unloading="Unload Entire"   GeoNonLin=None   ResultsSave="Multiple States"
MinNumState=10   MaxNumState=100   PosIncOnly=No   MaxTotal=300   MaxNull=150   MaxIter=10
ItConvTol=0.0001   EvLumpTol=0.01   FrameTC=Yes
       FrameHinge=Yes   CableTC=Yes   LinkTC=Yes   LinkOther=Yes
   Case=-0.5i   Unloading="Unload Entire"   GeoNonLin=None   ResultsSave="Multiple States"
MinNumState=10   MaxNumState=100   PosIncOnly=No   MaxTotal=300   MaxNull=150   MaxIter=10
ItConvTol=0.0001   EvLumpTol=0.01   FrameTC=Yes
       FrameHinge=Yes   CableTC=Yes   LinkTC=Yes   LinkOther=Yes
   Case=+0.5ii   Unloading="Unload Entire"   GeoNonLin=None   ResultsSave="Multiple States"
MinNumState=10   MaxNumState=100   PosIncOnly=No   MaxTotal=300   MaxNull=150   MaxIter=10
ItConvTol=0.0001   EvLumpTol=0.01   FrameTC=Yes
       FrameHinge=Yes   CableTC=Yes   LinkTC=Yes   LinkOther=Yes
   Case=-0.5ii   Unloading="Unload Entire"   GeoNonLin=None   ResultsSave="Multiple States"
MinNumState=10   MaxNumState=100   PosIncOnly=No   MaxTotal=300   MaxNull=150   MaxIter=10
ItConvTol=0.0001   EvLumpTol=0.01   FrameTC=Yes
       FrameHinge=Yes   CableTC=Yes   LinkTC=Yes   LinkOther=Yes
   Case=+1.0i   Unloading="Unload Entire"   GeoNonLin=None   ResultsSave="Multiple States"
MinNumState=10   MaxNumState=100   PosIncOnly=No   MaxTotal=300   MaxNull=150   MaxIter=10
ItConvTol=0.0001   EvLumpTol=0.01   FrameTC=Yes
       FrameHinge=Yes   CableTC=Yes   LinkTC=Yes   LinkOther=Yes
   Case=-1.0i   Unloading="Unload Entire"   GeoNonLin=None   ResultsSave="Multiple States"
MinNumState=10   MaxNumState=100   PosIncOnly=No   MaxTotal=300   MaxNull=150   MaxIter=10
ItConvTol=0.0001   EvLumpTol=0.01   FrameTC=Yes
       FrameHinge=Yes   CableTC=Yes   LinkTC=Yes   LinkOther=Yes
   Case=+1.0ii   Unloading="Unload Entire"   GeoNonLin=None   ResultsSave="Multiple States"
MinNumState=10   MaxNumState=100   PosIncOnly=No   MaxTotal=300   MaxNull=150   MaxIter=10
ItConvTol=0.0001   EvLumpTol=0.01   FrameTC=Yes
       FrameHinge=Yes   CableTC=Yes   LinkTC=Yes   LinkOther=Yes
   Case=-1.0ii   Unloading="Unload Entire"   GeoNonLin=None   ResultsSave="Multiple States"
MinNumState=10   MaxNumState=100   PosIncOnly=No   MaxTotal=300   MaxNull=150   MaxIter=10
ItConvTol=0.0001   EvLumpTol=0.01   FrameTC=Yes
       FrameHinge=Yes   CableTC=Yes   LinkTC=Yes   LinkOther=Yes
   Case=+1.5i   Unloading="Unload Entire"   GeoNonLin=None   ResultsSave="Multiple States"
MinNumState=10   MaxNumState=100   PosIncOnly=No   MaxTotal=300   MaxNull=150   MaxIter=10
ItConvTol=0.0001   EvLumpTol=0.01   FrameTC=Yes
       FrameHinge=Yes   CableTC=Yes   LinkTC=Yes   LinkOther=Yes
   Case=-1.5i   Unloading="Unload Entire"   GeoNonLin=None   ResultsSave="Multiple States"
MinNumState=10   MaxNumState=100   PosIncOnly=No   MaxTotal=500   MaxNull=250   MaxIter=10
ItConvTol=0.0001   EvLumpTol=0.02   FrameTC=Yes
       FrameHinge=Yes   CableTC=Yes   LinkTC=Yes   LinkOther=Yes
   Case=+1.5ii   Unloading="Unload Entire"   GeoNonLin=None   ResultsSave="Multiple States"
MinNumState=10   MaxNumState=100   PosIncOnly=No   MaxTotal=300   MaxNull=150   MaxIter=10
ItConvTol=0.0001   EvLumpTol=0.01   FrameTC=Yes
       FrameHinge=Yes   CableTC=Yes   LinkTC=Yes   LinkOther=Yes
   Case=-1.5ii   Unloading="Unload Entire"   GeoNonLin=None   ResultsSave="Multiple States"
MinNumState=10   MaxNumState=100   PosIncOnly=No   MaxTotal=300   MaxNull=150   MaxIter=10
ItConvTol=0.0001   EvLumpTol=0.01   FrameTC=Yes
       FrameHinge=Yes   CableTC=Yes   LinkTC=Yes   LinkOther=Yes
   Case=+2.0ia   Unloading="Unload Entire"   GeoNonLin=None   ResultsSave="Multiple States"
MinNumState=10   MaxNumState=100   PosIncOnly=No   MaxTotal=300   MaxNull=150   MaxIter=10
ItConvTol=0.0001   EvLumpTol=0.01   FrameTC=Yes
       FrameHinge=Yes   CableTC=Yes   LinkTC=Yes   LinkOther=Yes
   Case=-2.0ia   Unloading="Unload Entire"   GeoNonLin=None   ResultsSave="Multiple States"
MinNumState=10   MaxNumState=100   PosIncOnly=No   MaxTotal=500   MaxNull=300   MaxIter=10
ItConvTol=0.0001   EvLumpTol=0.01   FrameTC=Yes
       FrameHinge=Yes   CableTC=Yes   LinkTC=Yes   LinkOther=Yes
   Case=+2.0iia   Unloading="Unload Entire"   GeoNonLin=None   ResultsSave="Multiple States"
MinNumState=10   MaxNumState=100   PosIncOnly=No   MaxTotal=500   MaxNull=250   MaxIter=10
ItConvTol=0.0001   EvLumpTol=0.01   FrameTC=Yes
       FrameHinge=Yes   CableTC=Yes   LinkTC=Yes   LinkOther=Yes
   Case="remove C1 C1a"   Unloading="Unload Entire"   GeoNonLin=None   ResultsSave="Multiple States"
MinNumState=10   MaxNumState=100   PosIncOnly=No   MaxTotal=300   MaxNull=150   MaxIter=10
ItConvTol=0.001   EvLumpTol=0.01
       FrameTC=Yes   FrameHinge=Yes   CableTC=Yes   LinkTC=Yes   LinkOther=Yes
   Case=+2.0iib   Unloading="Unload Entire"   GeoNonLin=None   ResultsSave="Multiple States"
MinNumState=10   MaxNumState=100   PosIncOnly=No   MaxTotal=500   MaxNull=250   MaxIter=10
ItConvTol=0.0001   EvLumpTol=0.01   FrameTC=Yes
       FrameHinge=Yes   CableTC=Yes   LinkTC=Yes   LinkOther=Yes
   Case=-2.0iia   Unloading="Unload Entire"   GeoNonLin=None   ResultsSave="Multiple States"
MinNumState=10   MaxNumState=100   PosIncOnly=No   MaxTotal=500   MaxNull=250   MaxIter=10
ItConvTol=0.0001   EvLumpTol=0.01   FrameTC=Yes
       FrameHinge=Yes   CableTC=Yes   LinkTC=Yes   LinkOther=Yes
   Case="remove A2 A2a"   Unloading="Unload Entire"   GeoNonLin=None   ResultsSave="Multiple States"
MinNumState=10   MaxNumState=100   PosIncOnly=No   MaxTotal=300   MaxNull=150   MaxIter=10
ItConvTol=0.001   EvLumpTol=0.01
       FrameTC=Yes   FrameHinge=Yes   CableTC=Yes   LinkTC=Yes   LinkOther=Yes
```

```
   Case=-2.0iib   Unloading="Unload Entire"   GeoNonLin=None   ResultsSave="Multiple States"
MinNumState=10   MaxNumState=100   PosIncOnly=No   MaxTotal=500   MaxNull=250   MaxIter=10
ItConvTol=0.0001   EvLumpTol=0.01   FrameTC=Yes _
       FrameHinge=Yes   CableTC=Yes   LinkTC=Yes   LinkOther=Yes
   Case=+2.5ia   Unloading="Unload Entire"   GeoNonLin=None   ResultsSave="Multiple States"
MinNumState=10   MaxNumState=100   PosIncOnly=No   MaxTotal=400   MaxNull=200   MaxIter=10
ItConvTol=0.0001   EvLumpTol=0.01   FrameTC=Yes _
       FrameHinge=Yes   CableTC=Yes   LinkTC=Yes   LinkOther=Yes
   Case="remove C2"   Unloading="Unload Entire"   GeoNonLin=None   ResultsSave="Multiple States"
MinNumState=10   MaxNumState=100   PosIncOnly=No   MaxTotal=300   MaxNull=150   MaxIter=10
ItConvTol=0.001   EvLumpTol=0.01   FrameTC=Yes _
       FrameHinge=Yes   CableTC=Yes   LinkTC=Yes   LinkOther=Yes
   Case=+2.5ib   Unloading="Unload Entire"   GeoNonLin=None   ResultsSave="Multiple States"
MinNumState=10   MaxNumState=100   PosIncOnly=No   MaxTotal=400   MaxNull=200   MaxIter=10
ItConvTol=0.0001   EvLumpTol=0.01   FrameTC=Yes _
       FrameHinge=Yes   CableTC=Yes   LinkTC=Yes   LinkOther=Yes
   Case=-2.5ia   Unloading="Unload Entire"   GeoNonLin=None   ResultsSave="Multiple States"
MinNumState=10   MaxNumState=100   PosIncOnly=No   MaxTotal=400   MaxNull=200   MaxIter=10
ItConvTol=0.0001   EvLumpTol=0.01   FrameTC=Yes _
       FrameHinge=Yes   CableTC=Yes   LinkTC=Yes   LinkOther=Yes
   Case="removes C2a"   Unloading="Unload Entire"   GeoNonLin=None   ResultsSave="Multiple States"
MinNumState=10   MaxNumState=100   PosIncOnly=No   MaxTotal=300   MaxNull=150   MaxIter=10
ItConvTol=0.001   EvLumpTol=0.01   FrameTC=Yes _
       FrameHinge=Yes   CableTC=Yes   LinkTC=Yes   LinkOther=Yes
   Case=-2.5ib   Unloading="Unload Entire"   GeoNonLin=None   ResultsSave="Multiple States"
MinNumState=10   MaxNumState=100   PosIncOnly=No   MaxTotal=400   MaxNull=200   MaxIter=10
ItConvTol=0.0001   EvLumpTol=0.01   FrameTC=Yes _
       FrameHinge=Yes   CableTC=Yes   LinkTC=Yes   LinkOther=Yes
   Case="remove A1 B2"   Unloading="Unload Entire"   GeoNonLin=None   ResultsSave="Multiple States"
MinNumState=10   MaxNumState=100   PosIncOnly=No   MaxTotal=300   MaxNull=150   MaxIter=10
ItConvTol=0.001   EvLumpTol=0.01 _
       FrameTC=Yes   FrameHinge=Yes   CableTC=Yes   LinkTC=Yes   LinkOther=Yes
   Case=-2.5ic   Unloading="Unload Entire"   GeoNonLin=None   ResultsSave="Multiple States"
MinNumState=10   MaxNumState=100   PosIncOnly=No   MaxTotal=400   MaxNull=200   MaxIter=10
ItConvTol=0.0001   EvLumpTol=0.01   FrameTC=Yes _
       FrameHinge=Yes   CableTC=Yes   LinkTC=Yes   LinkOther=Yes
   Case=+2.5iia   Unloading="Unload Entire"   GeoNonLin=None   ResultsSave="Multiple States"
MinNumState=10   MaxNumState=100   PosIncOnly=No   MaxTotal=400   MaxNull=200   MaxIter=10
ItConvTol=0.0001   EvLumpTol=0.01   FrameTC=Yes _
       FrameHinge=Yes   CableTC=Yes   LinkTC=Yes   LinkOther=Yes
   Case="removes A1a"   Unloading="Unload Entire"   GeoNonLin=None   ResultsSave="Multiple States"
MinNumState=10   MaxNumState=100   PosIncOnly=No   MaxTotal=300   MaxNull=150   MaxIter=10
ItConvTol=0.001   EvLumpTol=0.01   FrameTC=Yes _
       FrameHinge=Yes   CableTC=Yes   LinkTC=Yes   LinkOther=Yes
   Case=+2.5iib   Unloading="Unload Entire"   GeoNonLin=None   ResultsSave="Multiple States"
MinNumState=10   MaxNumState=100   PosIncOnly=No   MaxTotal=400   MaxNull=200   MaxIter=10
ItConvTol=0.0001   EvLumpTol=0.01   FrameTC=Yes _
       FrameHinge=Yes   CableTC=Yes   LinkTC=Yes   LinkOther=Yes
   Case=-2.5ii   Unloading="Unload Entire"   GeoNonLin=None   ResultsSave="Multiple States"
MinNumState=10   MaxNumState=100   PosIncOnly=No   MaxTotal=600   MaxNull=300   MaxIter=10
ItConvTol=0.0001   EvLumpTol=0.01   FrameTC=Yes _
       FrameHinge=Yes   CableTC=Yes   LinkTC=Yes   LinkOther=Yes
   Case=+3.0ia   Unloading="Unload Entire"   GeoNonLin=None   ResultsSave="Multiple States"
MinNumState=10   MaxNumState=100   PosIncOnly=No   MaxTotal=500   MaxNull=300   MaxIter=10
ItConvTol=0.0001   EvLumpTol=0.01   FrameTC=Yes _
       FrameHinge=Yes   CableTC=Yes   LinkTC=Yes   LinkOther=Yes
   Case=-3.0ia   Unloading="Unload Entire"   GeoNonLin=None   ResultsSave="Multiple States"
MinNumState=10   MaxNumState=100   PosIncOnly=No   MaxTotal=700   MaxNull=400   MaxIter=10
ItConvTol=0.0001   EvLumpTol=0.01   FrameTC=Yes _
       FrameHinge=Yes   CableTC=Yes   LinkTC=Yes   LinkOther=Yes
   Case=+3.0iia   Unloading="Unload Entire"   GeoNonLin=None   ResultsSave="Multiple States"
MinNumState=10   MaxNumState=100   PosIncOnly=No   MaxTotal=500   MaxNull=300   MaxIter=10
ItConvTol=0.0001   EvLumpTol=0.01   FrameTC=Yes _
       FrameHinge=Yes   CableTC=Yes   LinkTC=Yes   LinkOther=Yes
   Case="remove B1a"   Unloading="Unload Entire"   GeoNonLin=None   ResultsSave="Multiple States"
MinNumState=10   MaxNumState=100   PosIncOnly=No   MaxTotal=300   MaxNull=150   MaxIter=10
ItConvTol=0.001   EvLumpTol=0.01   FrameTC=Yes _
       FrameHinge=Yes   CableTC=Yes   LinkTC=Yes   LinkOther=Yes
   Case="removes B1 B2a"   Unloading="Unload Entire"   GeoNonLin=None   ResultsSave="Multiple States"
MinNumState=10   MaxNumState=100   PosIncOnly=No   MaxTotal=300   MaxNull=150   MaxIter=10
ItConvTol=0.001   EvLumpTol=0.01 _
       FrameTC=Yes   FrameHinge=Yes   CableTC=Yes   LinkTC=Yes   LinkOther=Yes
   Case=+3.0iib   Unloading="Unload Entire"   GeoNonLin=None   ResultsSave="Multiple States"
MinNumState=10   MaxNumState=100   PosIncOnly=No   MaxTotal=500   MaxNull=300   MaxIter=10
ItConvTol=0.0001   EvLumpTol=0.01   FrameTC=Yes _
       FrameHinge=Yes   CableTC=Yes   LinkTC=Yes   LinkOther=Yes
   Case=-3.0iia   Unloading="Unload Entire"   GeoNonLin=None   ResultsSave="Multiple States"
MinNumState=10   MaxNumState=100   PosIncOnly=No   MaxTotal=600   MaxNull=300   MaxIter=10
ItConvTol=0.0001   EvLumpTol=0.01   FrameTC=Yes _
       FrameHinge=Yes   CableTC=Yes   LinkTC=Yes   LinkOther=Yes
   Case="removes A1b"   Unloading="Unload Entire"   GeoNonLin=None   ResultsSave="Multiple States"
MinNumState=10   MaxNumState=100   PosIncOnly=No   MaxTotal=300   MaxNull=150   MaxIter=10
ItConvTol=0.001   EvLumpTol=0.01   FrameTC=Yes _
       FrameHinge=Yes   CableTC=Yes   LinkTC=Yes   LinkOther=Yes
```

```
   Case=-3.0iib   Unloading="Unload Entire"   GeoNonLin=None   ResultsSave="Multiple States"
MinNumState=10   MaxNumState=100   PosIncOnly=No   MaxTotal=600   MaxNull=300   MaxIter=10
ItConvTol=0.0001   EvLumpTol=0.01   FrameTC=Yes _
       FrameHinge=Yes   CableTC=Yes   LinkTC=Yes   LinkOther=Yes
   Case=+3.5ia   Unloading="Unload Entire"   GeoNonLin=None   ResultsSave="Multiple States"
MinNumState=10   MaxNumState=100   PosIncOnly=No   MaxTotal=600   MaxNull=300   MaxIter=10
ItConvTol=0.0001   EvLumpTol=0.01   FrameTC=Yes _
       FrameHinge=Yes   CableTC=Yes   LinkTC=Yes   LinkOther=Yes
   Case=-3.5ia   Unloading="Unload Entire"   GeoNonLin=None   ResultsSave="Multiple States"
MinNumState=10   MaxNumState=100   PosIncOnly=No   MaxTotal=500   MaxNull=300   MaxIter=10
ItConvTol=0.0001   EvLumpTol=0.01   FrameTC=Yes _
       FrameHinge=Yes   CableTC=Yes   LinkTC=Yes   LinkOther=Yes
   Case="remove C2b"   Unloading="Unload Entire"   GeoNonLin=None   ResultsSave="Multiple States"
MinNumState=10   MaxNumState=100   PosIncOnly=No   MaxTotal=300   MaxNull=150   MaxIter=10
ItConvTol=0.001   EvLumpTol=0.01   FrameTC=Yes _
       FrameHinge=Yes   CableTC=Yes   LinkTC=Yes   LinkOther=Yes
   Case=+3.5ii   Unloading="Unload Entire"   GeoNonLin=None   ResultsSave="Multiple States"
MinNumState=10   MaxNumState=100   PosIncOnly=No   MaxTotal=500   MaxNull=300   MaxIter=10
ItConvTol=0.0001   EvLumpTol=0.01   FrameTC=Yes _
       FrameHinge=Yes   CableTC=Yes   LinkTC=Yes   LinkOther=Yes
   Case=-3.5ii   Unloading="Unload Entire"   GeoNonLin=None   ResultsSave="Multiple States"
MinNumState=10   MaxNumState=100   PosIncOnly=No   MaxTotal=600   MaxNull=300   MaxIter=10
ItConvTol=0.0001   EvLumpTol=0.01   FrameTC=Yes _
       FrameHinge=Yes   CableTC=Yes   LinkTC=Yes   LinkOther=Yes
   Case=+3.5iii   Unloading="Unload Entire"   GeoNonLin=None   ResultsSave="Multiple States"
MinNumState=10   MaxNumState=100   PosIncOnly=No   MaxTotal=500   MaxNull=300   MaxIter=10
ItConvTol=0.0001   EvLumpTol=0.01   FrameTC=Yes _
       FrameHinge=Yes   CableTC=Yes   LinkTC=Yes   LinkOther=Yes
   Case=-3.5iii   Unloading="Unload Entire"   GeoNonLin=None   ResultsSave="Multiple States"
MinNumState=10   MaxNumState=100   PosIncOnly=No   MaxTotal=600   MaxNull=300   MaxIter=10
ItConvTol=0.0001   EvLumpTol=0.01   FrameTC=Yes _
       FrameHinge=Yes   CableTC=Yes   LinkTC=Yes   LinkOther=Yes
   Case=+4.0ia   Unloading="Unload Entire"   GeoNonLin=None   ResultsSave="Multiple States"
MinNumState=10   MaxNumState=100   PosIncOnly=No   MaxTotal=500   MaxNull=300   MaxIter=10
ItConvTol=0.0001   EvLumpTol=0.01   FrameTC=Yes _
       FrameHinge=Yes   CableTC=Yes   LinkTC=Yes   LinkOther=Yes
   Case="remove C2c"   Unloading="Unload Entire"   GeoNonLin=None   ResultsSave="Multiple States"
MinNumState=10   MaxNumState=100   PosIncOnly=No   MaxTotal=300   MaxNull=150   MaxIter=10
ItConvTol=0.001   EvLumpTol=0.01   FrameTC=Yes _
       FrameHinge=Yes   CableTC=Yes   LinkTC=Yes   LinkOther=Yes
   Case=+4.0ib   Unloading="Unload Entire"   GeoNonLin=None   ResultsSave="Multiple States"
MinNumState=10   MaxNumState=100   PosIncOnly=No   MaxTotal=500   MaxNull=300   MaxIter=10
ItConvTol=0.0001   EvLumpTol=0.01   FrameTC=Yes _
       FrameHinge=Yes   CableTC=Yes   LinkTC=Yes   LinkOther=Yes
   Case=-4.0ia   Unloading="Unload Entire"   GeoNonLin=None   ResultsSave="Multiple States"
MinNumState=10   MaxNumState=100   PosIncOnly=No   MaxTotal=500   MaxNull=300   MaxIter=10
ItConvTol=0.0001   EvLumpTol=0.01   FrameTC=Yes _
       FrameHinge=Yes   CableTC=Yes   LinkTC=Yes   LinkOther=Yes
   Case="remove A1c"   Unloading="Unload Entire"   GeoNonLin=None   ResultsSave="Multiple States"
MinNumState=10   MaxNumState=100   PosIncOnly=No   MaxTotal=300   MaxNull=150   MaxIter=10
ItConvTol=0.001   EvLumpTol=0.01   FrameTC=Yes _
       FrameHinge=Yes   CableTC=Yes   LinkTC=Yes   LinkOther=Yes
   Case=-4.0ib   Unloading="Unload Entire"   GeoNonLin=None   ResultsSave="Multiple States"
MinNumState=10   MaxNumState=100   PosIncOnly=No   MaxTotal=500   MaxNull=300   MaxIter=10
ItConvTol=0.0001   EvLumpTol=0.01   FrameTC=Yes _
       FrameHinge=Yes   CableTC=Yes   LinkTC=Yes   LinkOther=Yes
   Case=+4.0ii   Unloading="Unload Entire"   GeoNonLin=None   ResultsSave="Multiple States"
MinNumState=10   MaxNumState=100   PosIncOnly=No   MaxTotal=500   MaxNull=300   MaxIter=10
ItConvTol=0.0001   EvLumpTol=0.01   FrameTC=Yes _
       FrameHinge=Yes   CableTC=Yes   LinkTC=Yes   LinkOther=Yes
   Case=-4.0ii   Unloading="Unload Entire"   GeoNonLin=None   ResultsSave="Multiple States"
MinNumState=10   MaxNumState=100   PosIncOnly=No   MaxTotal=500   MaxNull=300   MaxIter=10
ItConvTol=0.0001   EvLumpTol=0.01   FrameTC=Yes _
       FrameHinge=Yes   CableTC=Yes   LinkTC=Yes   LinkOther=Yes

TABLE:  "JOINT CONSTRAINT ASSIGNMENTS"
Too many to list, some for eg.
   Joint=3   Constraint=LOCAL1   Type=Local
   Joint=8   Constraint=LOCAL1   Type=Local
   Joint=13   Constraint=LOCAL1   Type=Local
   Joint=18   Constraint=WELD1   Type=Weld
   Joint=19   Constraint=WELD1   Type=Weld
   Joint=24   Constraint=WELD1   Type=Weld
   Joint=25   Constraint=WELD1   Type=Weld
   Joint=26   Constraint=WELD1   Type=Weld
   Joint=33   Constraint=WELD1   Type=Weld
   Joint=34   Constraint=WELD1   Type=Weld
   Joint=35   Constraint=WELD1   Type=Weld
   Joint=40   Constraint=WELD1   Type=Weld
   Joint=41   Constraint=WELD1   Type=Weld
   Joint=50   Constraint=WELD2   Type=Weld
   Joint=51   Constraint=WELD2   Type=Weld
   Joint=58   Constraint=WELD2   Type=Weld
   Joint=59   Constraint=WELD2   Type=Weld
   Joint=66   Constraint=WELD2   Type=Weld
```

```
   Joint=67   Constraint=WELD2   Type=Weld
   Joint=74   Constraint=WELD2   Type=Weld
   Joint=75   Constraint=WELD2   Type=Weld
   Joint=82   Constraint=WELD2   Type=Weld
   Joint=83   Constraint=WELD2   Type=Weld
   Joint=90   Constraint=WELD2   Type=Weld
   Joint=91   Constraint=WELD2   Type=Weld
   Joint=95   Constraint=WELD1   Type=Weld
   to
   Joint=1272   Constraint=WELD8   Type=Weld

TABLE:  "JOINT RESTRAINT ASSIGNMENTS"
   Joint=1   U1=No   U2=Yes   U3=Yes   R1=No   R2=No   R3=No
   Joint=5   U1=No   U2=Yes   U3=No   R1=No   R2=No   R3=No
   Joint=6   U1=Yes   U2=Yes   U3=Yes   R1=No   R2=No   R3=No
   Joint=10   U1=No   U2=Yes   U3=No   R1=No   R2=No   R3=No
   Joint=11   U1=No   U2=Yes   U3=Yes   R1=No   R2=No   R3=No
   Joint=15   U1=No   U2=Yes   U3=No   R1=No   R2=No   R3=No
   Joint=119   U1=No   U2=No   U3=Yes   R1=No   R2=No   R3=No
   Joint=128   U1=No   U2=No   U3=Yes   R1=No   R2=No   R3=No
   Joint=135   U1=No   U2=No   U3=Yes   R1=No   R2=No   R3=No
   Joint=144   U1=No   U2=No   U3=Yes   R1=No   R2=No   R3=No
   Joint=167   U1=No   U2=No   U3=Yes   R1=No   R2=No   R3=No
   Joint=176   U1=No   U2=No   U3=Yes   R1=No   R2=No   R3=No

TABLE:  "FRAME SECTION ASSIGNMENTS"
Too many to list, some for eg.
   Frame=1   SectionType=Rectangular   AutoSelect=N.A.   AnalSect=COLUMN   DesignSect=COLUMN
MatProp=Default
to
   Frame=15   SectionType=Rectangular   AutoSelect=N.A.   AnalSect=COLUMN   DesignSect=COLUMN
MatProp=Default
   Frame=16   SectionType=Rectangular   AutoSelect=N.A.   AnalSect=BEAM   DesignSect=BEAM
MatProp=Default
to
   Frame=41   SectionType=Rectangular   AutoSelect=N.A.   AnalSect=DIAGSLABLAYER   DesignSect=COLUMN
MatProp=Default
   Frame=42   SectionType=Rectangular   AutoSelect=N.A.   AnalSect=MAINLOGITUDINALSTEEL
DesignSect=MAINLOGITUDINALSTEEL   MatProp=Default
   Frame=43   SectionType=Rectangular   AutoSelect=N.A.   AnalSect=MAINLOGITUDINALSTEEL
DesignSect=MAINLOGITUDINALSTEEL   MatProp=Default
   Frame=44   SectionType=Rectangular   AutoSelect=N.A.   AnalSect=DIAGSLABLAYER   DesignSect=COLUMN
MatProp=Default
   Frame=45   SectionType=Rectangular   AutoSelect=N.A.   AnalSect=DIAGSLABLAYER   DesignSect=COLUMN
MatProp=Default
   Frame=98   SectionType=Rectangular   AutoSelect=N.A.   AnalSect=DIAGSLAB   DesignSect=COLUMN
MatProp=Default
   Frame=99   SectionType=Rectangular   AutoSelect=N.A.   AnalSect=DIAGSLABLAYER   DesignSect=COLUMN
MatProp=Default
   Frame=211   SectionType=Rectangular   AutoSelect=N.A.   AnalSect=ENDSLAB   DesignSect=COLUMN
MatProp=Default
   Frame=212   SectionType=Rectangular   AutoSelect=N.A.   AnalSect=ENDSLAB   DesignSect=COLUMN
MatProp=Default
   Frame=213   SectionType=Rectangular   AutoSelect=N.A.   AnalSect=SLABLINK   DesignSect=SLABLINK
MatProp=Default
   Frame=214   SectionType=Rectangular   AutoSelect=N.A.   AnalSect=SLABLINK   DesignSect=SLABLINK
MatProp=Default
   Frame=253   SectionType=Rectangular   AutoSelect=N.A.   AnalSect=RIB   DesignSect=N.A.
MatProp=Default
   Frame=254   SectionType=Rectangular   AutoSelect=N.A.   AnalSect=RIB   DesignSect=N.A.
MatProp=Default
   Frame=353   SectionType=Circle   AutoSelect=N.A.   AnalSect=TENSIONTIE   DesignSect=TENSIONTIE
MatProp=Default
   Frame=354   SectionType=Circle   AutoSelect=N.A.   AnalSect=TENSIONTIE   DesignSect=TENSIONTIE
MatProp=Default
   Frame=368   SectionType=Circle   AutoSelect=N.A.   AnalSect=EDGESTARTER   DesignSect=EDGESTARTER
MatProp=Default
   Frame=369   SectionType=Circle   AutoSelect=N.A.   AnalSect=EDGESTARTER   DesignSect=EDGESTARTER
MatProp=Default
   Frame=397   SectionType=Rectangular   AutoSelect=N.A.   AnalSect=CENTRECONNECTION
DesignSect=COLUMN   MatProp=Default
   Frame=398   SectionType=Rectangular   AutoSelect=N.A.   AnalSect=STIFFMEMBER   DesignSect=COLUMN
MatProp=Default
   Frame=433   SectionType=Circle   AutoSelect=N.A.   AnalSect=TENSIONTIE   DesignSect=TENSIONTIE
MatProp=Default
   Frame=434   SectionType=Rectangular   AutoSelect=N.A.   AnalSect=DIAGSLAB.245   DesignSect=COLUMN
MatProp=Default
   Frame=444   SectionType=Rectangular   AutoSelect=N.A.   AnalSect=2-4.0MMWIRE   DesignSect=2-
4.0MMWIRE   MatProp=Default
   Frame=445   SectionType=Rectangular   AutoSelect=N.A.   AnalSect=2-4.0MMWIRE   DesignSect=2-
4.0MMWIRE   MatProp=Default
   Frame=503   SectionType=Rectangular   AutoSelect=N.A.   AnalSect=SLABLINK   DesignSect=SLABLINK
MatProp=Default
   Frame=504   SectionType=Rectangular   AutoSelect=N.A.   AnalSect=SLABLINK   DesignSect=SLABLINK
MatProp=Default
```

```
   Frame=585   SectionType=Rectangular   AutoSelect=N.A.   AnalSect=DIAGSLABLAYER   DesignSect=COLUMN
MatProp=Default
   Frame=886   SectionType=Rectangular   AutoSelect=N.A.   AnalSect=DIAGSLABLAYER.245
DesignSect=DIAGSLABLAYER.245   MatProp=Default
   Frame=887   SectionType=Rectangular   AutoSelect=N.A.   AnalSect=DIAGSLABLAYER.245
DesignSect=COLUMN   MatProp=Default
   Frame=990   SectionType=Rectangular   AutoSelect=N.A.   AnalSect=DIAGSLAB.15   DesignSect=COLUMN
MatProp=Default
   Frame=991   SectionType=Rectangular   AutoSelect=N.A.   AnalSect=DIAGSLAB.15   DesignSect=COLUMN
MatProp=Default
   Frame=1143   SectionType=Rectangular   AutoSelect=N.A.   AnalSect=MAINLOGITUDINALSTEEL
DesignSect=MAINLOGITUDINALSTEEL   MatProp=Default
   Frame=1144   SectionType=Rectangular   AutoSelect=N.A.   AnalSect=MAINLOGITUDINALSTEEL
DesignSect=MAINLOGITUDINALSTEEL   MatProp=Default
   Frame=1145   SectionType=Rectangular   AutoSelect=N.A.   AnalSect=MAINCONCDIAGONAL
DesignSect=MAINCONCDIAGONAL   MatProp=Default
   Frame=1146   SectionType=Rectangular   AutoSelect=N.A.   AnalSect=MAINCONCDIAGONAL
DesignSect=MAINCONCDIAGONAL   MatProp=Default

TABLE:  "FRAME PROPERTY MODIFIERS"
Too many to list, some eg.
   Frame=1   AMod=1   AS2Mod=1   AS3Mod=1   JMod=1   I22Mod=1   I33Mod=0.4   MassMod=1   WeightMod=1
to
   Frame=1192   PI=Yes   V2I=No   V3I=No   TI=Yes   M2I=Yes   M3I=Yes   PJ=No   V2J=No   V3J=No
TJ=No   M2J=No   M3J=No   PartialFix=No

TABLE:  "FRAME TENSION AND COMPRESSION LIMITS"
   Frame=40   TensLimit=Yes   CompLimit=Yes   Tension=0   Compression=-40.0162
   Frame=41   TensLimit=Yes   CompLimit=Yes   Tension=0   Compression=-40.0162
   Frame=44   TensLimit=Yes   CompLimit=Yes   Tension=0   Compression=-40.0162
   Frame=45   TensLimit=Yes   CompLimit=Yes   Tension=0   Compression=-40.0162
   Frame=54   TensLimit=Yes   CompLimit=No   Tension=0
   Frame=55   TensLimit=Yes   CompLimit=No   Tension=0
   Frame=58   TensLimit=Yes   CompLimit=Yes   Tension=0   Compression=-40.0162
   Frame=59   TensLimit=Yes   CompLimit=Yes   Tension=0   Compression=-40.0162
   Frame=72   TensLimit=Yes   CompLimit=No   Tension=0
   Frame=73   TensLimit=Yes   CompLimit=No   Tension=0
   Frame=90   TensLimit=Yes   CompLimit=No   Tension=0
   Frame=91   TensLimit=Yes   CompLimit=No   Tension=0
   Frame=98   TensLimit=Yes   CompLimit=No   Tension=0
   Frame=99   TensLimit=Yes   CompLimit=Yes   Tension=0   Compression=-40.0162
   Frame=108   TensLimit=Yes   CompLimit=No   Tension=0
   Frame=109   TensLimit=Yes   CompLimit=No   Tension=0
   Frame=112   TensLimit=Yes   CompLimit=Yes   Tension=0   Compression=-40.0162
   Frame=113   TensLimit=Yes   CompLimit=Yes   Tension=0   Compression=-40.0162
   Frame=116   TensLimit=Yes   CompLimit=Yes   Tension=0   Compression=-40.0162
   Frame=117   TensLimit=Yes   CompLimit=Yes   Tension=0   Compression=-40.0162
   Frame=126   TensLimit=Yes   CompLimit=No   Tension=0
   Frame=127   TensLimit=Yes   CompLimit=No   Tension=0
   Frame=130   TensLimit=Yes   CompLimit=Yes   Tension=0   Compression=-40.0162
   Frame=144   TensLimit=Yes   CompLimit=No   Tension=0
   Frame=145   TensLimit=Yes   CompLimit=No   Tension=0
   Frame=406   TensLimit=Yes   CompLimit=No   Tension=0
   Frame=410   TensLimit=Yes   CompLimit=Yes   Tension=0   Compression=-40.0162
   Frame=412   TensLimit=Yes   CompLimit=Yes   Tension=0   Compression=-40.0162
   Frame=414   TensLimit=Yes   CompLimit=Yes   Tension=0   Compression=-40.0162
   Frame=416   TensLimit=Yes   CompLimit=Yes   Tension=0   Compression=-40.0162
   Frame=418   TensLimit=Yes   CompLimit=Yes   Tension=0   Compression=-40.0162
   Frame=420   TensLimit=Yes   CompLimit=Yes   Tension=0   Compression=-40.0162
   Frame=434   TensLimit=Yes   CompLimit=No   Tension=0
   Frame=456   TensLimit=Yes   CompLimit=No   Tension=0
   Frame=457   TensLimit=Yes   CompLimit=No   Tension=0
   Frame=458   TensLimit=Yes   CompLimit=Yes   Tension=0   Compression=-40.0162
   Frame=465   TensLimit=Yes   CompLimit=No   Tension=0
   Frame=466   TensLimit=Yes   CompLimit=Yes   Tension=0   Compression=-40.0162
   Frame=467   TensLimit=Yes   CompLimit=Yes   Tension=0   Compression=-40.0162
   Frame=468   TensLimit=Yes   CompLimit=Yes   Tension=0   Compression=-40.0162
   Frame=469   TensLimit=Yes   CompLimit=Yes   Tension=0   Compression=-40.0162
   Frame=470   TensLimit=Yes   CompLimit=Yes   Tension=0   Compression=-40.0162
   Frame=471   TensLimit=Yes   CompLimit=Yes   Tension=0   Compression=-40.0162
   Frame=472   TensLimit=Yes   CompLimit=Yes   Tension=0   Compression=-40.0162
   Frame=473   TensLimit=Yes   CompLimit=Yes   Tension=0   Compression=-40.0162
   Frame=481   TensLimit=Yes   CompLimit=No   Tension=0
   Frame=482   TensLimit=Yes   CompLimit=Yes   Tension=0   Compression=-40.0162
   Frame=483   TensLimit=Yes   CompLimit=Yes   Tension=0   Compression=-40.0162
   Frame=484   TensLimit=Yes   CompLimit=Yes   Tension=0   Compression=-40.0162
   Frame=485   TensLimit=Yes   CompLimit=Yes   Tension=0   Compression=-40.0162
   Frame=486   TensLimit=Yes   CompLimit=Yes   Tension=0   Compression=-40.0162
   Frame=487   TensLimit=Yes   CompLimit=Yes   Tension=0   Compression=-40.0162
   Frame=501   TensLimit=Yes   CompLimit=No   Tension=0
   Frame=502   TensLimit=Yes   CompLimit=Yes   Tension=0   Compression=-37.2892
   Frame=579   TensLimit=Yes   CompLimit=No   Tension=0
   Frame=580   TensLimit=Yes   CompLimit=Yes   Tension=0   Compression=-40.0162
   Frame=581   TensLimit=Yes   CompLimit=Yes   Tension=0   Compression=-40.0162
   Frame=582   TensLimit=Yes   CompLimit=Yes   Tension=0   Compression=-40.0162
```

```
Frame=583   TensLimit=Yes   CompLimit=Yes   Tension=0   Compression=-40.0162
Frame=584   TensLimit=Yes   CompLimit=Yes   Tension=0   Compression=-40.0162
Frame=585   TensLimit=Yes   CompLimit=Yes   Tension=0   Compression=-40.0162
Frame=594   TensLimit=Yes   CompLimit=No    Tension=0
Frame=595   TensLimit=Yes   CompLimit=Yes   Tension=0   Compression=-40.0162
Frame=596   TensLimit=Yes   CompLimit=Yes   Tension=0   Compression=-40.0162
Frame=597   TensLimit=Yes   CompLimit=Yes   Tension=0   Compression=-40.0162
Frame=598   TensLimit=Yes   CompLimit=Yes   Tension=0   Compression=-40.0162
Frame=599   TensLimit=Yes   CompLimit=Yes   Tension=0   Compression=-40.0162
Frame=600   TensLimit=Yes   CompLimit=Yes   Tension=0   Compression=-40.0162
Frame=601   TensLimit=Yes   CompLimit=Yes   Tension=0   Compression=-40.0162
Frame=602   TensLimit=Yes   CompLimit=Yes   Tension=0   Compression=-40.0162
Frame=609   TensLimit=Yes   CompLimit=No    Tension=0
Frame=610   TensLimit=Yes   CompLimit=Yes   Tension=0   Compression=-40.0162
Frame=611   TensLimit=Yes   CompLimit=Yes   Tension=0   Compression=-40.0162
Frame=612   TensLimit=Yes   CompLimit=Yes   Tension=0   Compression=-40.0162
Frame=613   TensLimit=Yes   CompLimit=Yes   Tension=0   Compression=-40.0162
Frame=614   TensLimit=Yes   CompLimit=Yes   Tension=0   Compression=-40.0162
Frame=615   TensLimit=Yes   CompLimit=Yes   Tension=0   Compression=-40.0162
Frame=616   TensLimit=Yes   CompLimit=Yes   Tension=0   Compression=-40.0162
Frame=624   TensLimit=Yes   CompLimit=No    Tension=0
Frame=625   TensLimit=Yes   CompLimit=Yes   Tension=0   Compression=-40.0162
Frame=626   TensLimit=Yes   CompLimit=Yes   Tension=0   Compression=-40.0162
Frame=627   TensLimit=Yes   CompLimit=Yes   Tension=0   Compression=-40.0162
Frame=628   TensLimit=Yes   CompLimit=Yes   Tension=0   Compression=-40.0162
Frame=629   TensLimit=Yes   CompLimit=Yes   Tension=0   Compression=-40.0162
Frame=630   TensLimit=Yes   CompLimit=Yes   Tension=0   Compression=-40.0162
Frame=639   TensLimit=Yes   CompLimit=No    Tension=0
Frame=640   TensLimit=Yes   CompLimit=Yes   Tension=0   Compression=-40.0162
Frame=641   TensLimit=Yes   CompLimit=Yes   Tension=0   Compression=-40.0162
Frame=642   TensLimit=Yes   CompLimit=Yes   Tension=0   Compression=-40.0162
Frame=643   TensLimit=Yes   CompLimit=Yes   Tension=0   Compression=-40.0162
Frame=644   TensLimit=Yes   CompLimit=Yes   Tension=0   Compression=-40.0162
Frame=645   TensLimit=Yes   CompLimit=Yes   Tension=0   Compression=-40.0162
Frame=654   TensLimit=Yes   CompLimit=No    Tension=0
Frame=655   TensLimit=Yes   CompLimit=Yes   Tension=0   Compression=-40.0162
Frame=656   TensLimit=Yes   CompLimit=Yes   Tension=0   Compression=-40.0162
Frame=657   TensLimit=Yes   CompLimit=Yes   Tension=0   Compression=-40.0162
Frame=658   TensLimit=Yes   CompLimit=Yes   Tension=0   Compression=-40.0162
Frame=659   TensLimit=Yes   CompLimit=Yes   Tension=0   Compression=-40.0162
Frame=660   TensLimit=Yes   CompLimit=Yes   Tension=0   Compression=-40.0162
Frame=669   TensLimit=Yes   CompLimit=No    Tension=0
Frame=670   TensLimit=Yes   CompLimit=Yes   Tension=0   Compression=-40.0162
Frame=671   TensLimit=Yes   CompLimit=Yes   Tension=0   Compression=-40.0162
Frame=672   TensLimit=Yes   CompLimit=Yes   Tension=0   Compression=-40.0162
Frame=673   TensLimit=Yes   CompLimit=Yes   Tension=0   Compression=-40.0162
Frame=674   TensLimit=Yes   CompLimit=Yes   Tension=0   Compression=-40.0162
Frame=675   TensLimit=Yes   CompLimit=Yes   Tension=0   Compression=-40.0162
Frame=677   TensLimit=Yes   CompLimit=No    Tension=0
Frame=684   TensLimit=Yes   CompLimit=Yes   Tension=0   Compression=-40.0162
Frame=685   TensLimit=Yes   CompLimit=Yes   Tension=0   Compression=-40.0162
Frame=686   TensLimit=Yes   CompLimit=Yes   Tension=0   Compression=-40.0162
Frame=687   TensLimit=Yes   CompLimit=Yes   Tension=0   Compression=-40.0162
Frame=688   TensLimit=Yes   CompLimit=Yes   Tension=0   Compression=-40.0162
Frame=689   TensLimit=Yes   CompLimit=Yes   Tension=0   Compression=-40.0162
Frame=698   TensLimit=Yes   CompLimit=No    Tension=0
Frame=699   TensLimit=Yes   CompLimit=Yes   Tension=0   Compression=-40.0162
Frame=700   TensLimit=Yes   CompLimit=Yes   Tension=0   Compression=-40.0162
Frame=701   TensLimit=Yes   CompLimit=Yes   Tension=0   Compression=-40.0162
Frame=702   TensLimit=Yes   CompLimit=Yes   Tension=0   Compression=-40.0162
Frame=703   TensLimit=Yes   CompLimit=Yes   Tension=0   Compression=-40.0162
Frame=704   TensLimit=Yes   CompLimit=Yes   Tension=0   Compression=-40.0162
Frame=705   TensLimit=Yes   CompLimit=No    Tension=0
Frame=706   TensLimit=Yes   CompLimit=No    Tension=0
Frame=713   TensLimit=Yes   CompLimit=No    Tension=0
Frame=714   TensLimit=Yes   CompLimit=Yes   Tension=0   Compression=-40.0162
Frame=715   TensLimit=Yes   CompLimit=Yes   Tension=0   Compression=-40.0162
Frame=716   TensLimit=Yes   CompLimit=Yes   Tension=0   Compression=-40.0162
Frame=717   TensLimit=Yes   CompLimit=Yes   Tension=0   Compression=-40.0162
Frame=718   TensLimit=Yes   CompLimit=Yes   Tension=0   Compression=-40.0162
Frame=719   TensLimit=Yes   CompLimit=Yes   Tension=0   Compression=-40.0162
Frame=720   TensLimit=Yes   CompLimit=Yes   Tension=0   Compression=-37.2892
Frame=721   TensLimit=Yes   CompLimit=Yes   Tension=0   Compression=-37.2892
Frame=728   TensLimit=Yes   CompLimit=No    Tension=0
Frame=729   TensLimit=Yes   CompLimit=Yes   Tension=0   Compression=-40.0162
Frame=730   TensLimit=Yes   CompLimit=Yes   Tension=0   Compression=-40.0162
Frame=731   TensLimit=Yes   CompLimit=Yes   Tension=0   Compression=-40.0162
Frame=732   TensLimit=Yes   CompLimit=Yes   Tension=0   Compression=-40.0162
Frame=733   TensLimit=Yes   CompLimit=Yes   Tension=0   Compression=-40.0162
Frame=734   TensLimit=Yes   CompLimit=Yes   Tension=0   Compression=-40.0162
Frame=735   TensLimit=Yes   CompLimit=Yes   Tension=0   Compression=-37.2892
Frame=736   TensLimit=Yes   CompLimit=Yes   Tension=0   Compression=-37.2892
Frame=743   TensLimit=Yes   CompLimit=No    Tension=0
Frame=744   TensLimit=Yes   CompLimit=Yes   Tension=0   Compression=-40.0162
Frame=745   TensLimit=Yes   CompLimit=Yes   Tension=0   Compression=-40.0162
```

```
Frame=746   TensLimit=Yes   CompLimit=Yes   Tension=0   Compression=-40.0162
Frame=747   TensLimit=Yes   CompLimit=Yes   Tension=0   Compression=-40.0162
Frame=748   TensLimit=Yes   CompLimit=Yes   Tension=0   Compression=-40.0162
Frame=749   TensLimit=Yes   CompLimit=Yes   Tension=0   Compression=-40.0162
Frame=750   TensLimit=Yes   CompLimit=Yes   Tension=0   Compression=-37.2892
Frame=751   TensLimit=Yes   CompLimit=Yes   Tension=0   Compression=-37.2892
Frame=758   TensLimit=Yes   CompLimit=No    Tension=0
Frame=759   TensLimit=Yes   CompLimit=Yes   Tension=0   Compression=-40.0162
Frame=760   TensLimit=Yes   CompLimit=Yes   Tension=0   Compression=-40.0162
Frame=761   TensLimit=Yes   CompLimit=Yes   Tension=0   Compression=-40.0162
Frame=762   TensLimit=Yes   CompLimit=Yes   Tension=0   Compression=-40.0162
Frame=763   TensLimit=Yes   CompLimit=Yes   Tension=0   Compression=-40.0162
Frame=764   TensLimit=Yes   CompLimit=Yes   Tension=0   Compression=-40.0162
Frame=765   TensLimit=Yes   CompLimit=Yes   Tension=0   Compression=-37.2892
Frame=766   TensLimit=Yes   CompLimit=Yes   Tension=0   Compression=-37.2892
Frame=773   TensLimit=Yes   CompLimit=No    Tension=0
Frame=774   TensLimit=Yes   CompLimit=Yes   Tension=0   Compression=-40.0162
Frame=775   TensLimit=Yes   CompLimit=Yes   Tension=0   Compression=-40.0162
Frame=776   TensLimit=Yes   CompLimit=Yes   Tension=0   Compression=-40.0162
Frame=777   TensLimit=Yes   CompLimit=Yes   Tension=0   Compression=-40.0162
Frame=778   TensLimit=Yes   CompLimit=Yes   Tension=0   Compression=-40.0162
Frame=779   TensLimit=Yes   CompLimit=Yes   Tension=0   Compression=-40.0162
Frame=780   TensLimit=Yes   CompLimit=Yes   Tension=0   Compression=-37.2892
Frame=781   TensLimit=Yes   CompLimit=Yes   Tension=0   Compression=-37.2892
Frame=788   TensLimit=Yes   CompLimit=Yes   Tension=0   Compression=-37.2892
Frame=789   TensLimit=Yes   CompLimit=Yes   Tension=0   Compression=-37.2892
Frame=802   TensLimit=Yes   CompLimit=No    Tension=0
Frame=803   TensLimit=Yes   CompLimit=No    Tension=0
Frame=804   TensLimit=Yes   CompLimit=Yes   Tension=0   Compression=-37.2892
Frame=805   TensLimit=Yes   CompLimit=Yes   Tension=0   Compression=-37.2892
Frame=806   TensLimit=Yes   CompLimit=Yes   Tension=0   Compression=-37.2892
Frame=807   TensLimit=Yes   CompLimit=Yes   Tension=0   Compression=-37.2892
Frame=808   TensLimit=Yes   CompLimit=Yes   Tension=0   Compression=-37.2892
Frame=809   TensLimit=Yes   CompLimit=Yes   Tension=0   Compression=-37.2892
Frame=810   TensLimit=Yes   CompLimit=Yes   Tension=0   Compression=-37.2892
Frame=811   TensLimit=Yes   CompLimit=Yes   Tension=0   Compression=-37.2892
Frame=812   TensLimit=Yes   CompLimit=Yes   Tension=0   Compression=-37.2892
Frame=813   TensLimit=Yes   CompLimit=Yes   Tension=0   Compression=-37.2892
Frame=814   TensLimit=Yes   CompLimit=Yes   Tension=0   Compression=-37.2892
Frame=815   TensLimit=Yes   CompLimit=Yes   Tension=0   Compression=-37.2892
Frame=818   TensLimit=Yes   CompLimit=No    Tension=0
Frame=819   TensLimit=Yes   CompLimit=Yes   Tension=0   Compression=-40.0162
Frame=820   TensLimit=Yes   CompLimit=Yes   Tension=0   Compression=-40.0162
Frame=821   TensLimit=Yes   CompLimit=Yes   Tension=0   Compression=-40.0162
Frame=822   TensLimit=Yes   CompLimit=Yes   Tension=0   Compression=-40.0162
Frame=823   TensLimit=Yes   CompLimit=Yes   Tension=0   Compression=-40.0162
Frame=824   TensLimit=Yes   CompLimit=Yes   Tension=0   Compression=-40.0162
Frame=833   TensLimit=Yes   CompLimit=No    Tension=0
Frame=834   TensLimit=Yes   CompLimit=Yes   Tension=0   Compression=-40.0162
Frame=835   TensLimit=Yes   CompLimit=Yes   Tension=0   Compression=-40.0162
Frame=836   TensLimit=Yes   CompLimit=Yes   Tension=0   Compression=-40.0162
Frame=837   TensLimit=Yes   CompLimit=Yes   Tension=0   Compression=-40.0162
Frame=838   TensLimit=Yes   CompLimit=Yes   Tension=0   Compression=-40.0162
Frame=839   TensLimit=Yes   CompLimit=Yes   Tension=0   Compression=-40.0162
Frame=848   TensLimit=Yes   CompLimit=No    Tension=0
Frame=849   TensLimit=Yes   CompLimit=Yes   Tension=0   Compression=-40.0162
Frame=850   TensLimit=Yes   CompLimit=Yes   Tension=0   Compression=-40.0162
Frame=851   TensLimit=Yes   CompLimit=Yes   Tension=0   Compression=-40.0162
Frame=852   TensLimit=Yes   CompLimit=Yes   Tension=0   Compression=-40.0162
Frame=853   TensLimit=Yes   CompLimit=Yes   Tension=0   Compression=-40.0162
Frame=854   TensLimit=Yes   CompLimit=Yes   Tension=0   Compression=-40.0162
Frame=863   TensLimit=Yes   CompLimit=No    Tension=0
Frame=864   TensLimit=Yes   CompLimit=Yes   Tension=0   Compression=-40.0162
Frame=865   TensLimit=Yes   CompLimit=Yes   Tension=0   Compression=-40.0162
Frame=866   TensLimit=Yes   CompLimit=Yes   Tension=0   Compression=-40.0162
Frame=867   TensLimit=Yes   CompLimit=Yes   Tension=0   Compression=-40.0162
Frame=868   TensLimit=Yes   CompLimit=Yes   Tension=0   Compression=-40.0162
Frame=869   TensLimit=Yes   CompLimit=Yes   Tension=0   Compression=-40.0162
Frame=884   TensLimit=Yes   CompLimit=No    Tension=0
Frame=885   TensLimit=Yes   CompLimit=No    Tension=0
Frame=886   TensLimit=Yes   CompLimit=Yes   Tension=0   Compression=-37.2892
Frame=887   TensLimit=Yes   CompLimit=Yes   Tension=0   Compression=-37.2892
Frame=888   TensLimit=Yes   CompLimit=Yes   Tension=0   Compression=-37.2892
Frame=889   TensLimit=Yes   CompLimit=Yes   Tension=0   Compression=-37.2892
Frame=890   TensLimit=Yes   CompLimit=Yes   Tension=0   Compression=-37.2892
Frame=891   TensLimit=Yes   CompLimit=Yes   Tension=0   Compression=-37.2892
Frame=892   TensLimit=Yes   CompLimit=Yes   Tension=0   Compression=-37.2892
Frame=893   TensLimit=Yes   CompLimit=Yes   Tension=0   Compression=-37.2892
Frame=894   TensLimit=Yes   CompLimit=Yes   Tension=0   Compression=-37.2892
Frame=895   TensLimit=Yes   CompLimit=Yes   Tension=0   Compression=-37.2892
Frame=896   TensLimit=Yes   CompLimit=Yes   Tension=0   Compression=-37.2892
Frame=897   TensLimit=Yes   CompLimit=Yes   Tension=0   Compression=-37.2892
Frame=910   TensLimit=Yes   CompLimit=No    Tension=0
Frame=911   TensLimit=Yes   CompLimit=No    Tension=0
Frame=912   TensLimit=Yes   CompLimit=Yes   Tension=0   Compression=-37.2892
```

```
Frame=913   TensLimit=Yes   CompLimit=Yes   Tension=0   Compression=-37.2892
Frame=914   TensLimit=Yes   CompLimit=Yes   Tension=0   Compression=-37.2892
Frame=915   TensLimit=Yes   CompLimit=Yes   Tension=0   Compression=-37.2892
Frame=916   TensLimit=Yes   CompLimit=Yes   Tension=0   Compression=-37.2892
Frame=917   TensLimit=Yes   CompLimit=Yes   Tension=0   Compression=-37.2892
Frame=922   TensLimit=Yes   CompLimit=Yes   Tension=0   Compression=-37.2892
Frame=923   TensLimit=Yes   CompLimit=Yes   Tension=0   Compression=-37.2892
Frame=924   TensLimit=Yes   CompLimit=Yes   Tension=0   Compression=-37.2892
Frame=925   TensLimit=Yes   CompLimit=Yes   Tension=0   Compression=-37.2892
Frame=926   TensLimit=Yes   CompLimit=Yes   Tension=0   Compression=-37.2892
Frame=927   TensLimit=Yes   CompLimit=Yes   Tension=0   Compression=-37.2892
Frame=936   TensLimit=Yes   CompLimit=Yes   Tension=0   Compression=-37.2892
Frame=937   TensLimit=Yes   CompLimit=Yes   Tension=0   Compression=-37.2892
Frame=938   TensLimit=Yes   CompLimit=Yes   Tension=0   Compression=-37.2892
Frame=939   TensLimit=Yes   CompLimit=Yes   Tension=0   Compression=-37.2892
Frame=940   TensLimit=Yes   CompLimit=Yes   Tension=0   Compression=-37.2892
Frame=941   TensLimit=Yes   CompLimit=Yes   Tension=0   Compression=-37.2892
Frame=942   TensLimit=Yes   CompLimit=Yes   Tension=0   Compression=-37.2892
Frame=943   TensLimit=Yes   CompLimit=Yes   Tension=0   Compression=-37.2892
Frame=944   TensLimit=Yes   CompLimit=Yes   Tension=0   Compression=-37.2892
Frame=945   TensLimit=Yes   CompLimit=Yes   Tension=0   Compression=-37.2892
Frame=946   TensLimit=Yes   CompLimit=Yes   Tension=0   Compression=-37.2892
Frame=949   TensLimit=Yes   CompLimit=No    Tension=0
Frame=960   TensLimit=Yes   CompLimit=No    Tension=0
Frame=961   TensLimit=Yes   CompLimit=No    Tension=0
Frame=962   TensLimit=Yes   CompLimit=Yes   Tension=0   Compression=-37.2892
Frame=963   TensLimit=Yes   CompLimit=Yes   Tension=0   Compression=-37.2892
Frame=964   TensLimit=Yes   CompLimit=Yes   Tension=0   Compression=-37.2892
Frame=965   TensLimit=Yes   CompLimit=Yes   Tension=0   Compression=-37.2892
Frame=966   TensLimit=Yes   CompLimit=Yes   Tension=0   Compression=-37.2892
Frame=967   TensLimit=Yes   CompLimit=Yes   Tension=0   Compression=-37.2892
Frame=968   TensLimit=Yes   CompLimit=Yes   Tension=0   Compression=-37.2892
Frame=969   TensLimit=Yes   CompLimit=Yes   Tension=0   Compression=-37.2892
Frame=970   TensLimit=Yes   CompLimit=Yes   Tension=0   Compression=-37.2892
Frame=977   TensLimit=Yes   CompLimit=Yes   Tension=0   Compression=-37.2892
Frame=978   TensLimit=Yes   CompLimit=Yes   Tension=0   Compression=-37.2892
Frame=979   TensLimit=Yes   CompLimit=Yes   Tension=0   Compression=-37.2892
Frame=990   TensLimit=Yes   CompLimit=No    Tension=0
Frame=991   TensLimit=Yes   CompLimit=No    Tension=0
Frame=992   TensLimit=Yes   CompLimit=No    Tension=0
Frame=993   TensLimit=Yes   CompLimit=No    Tension=0
Frame=994   TensLimit=Yes   CompLimit=No    Tension=0
Frame=995   TensLimit=Yes   CompLimit=No    Tension=0
Frame=996   TensLimit=Yes   CompLimit=No    Tension=0
Frame=1037  TensLimit=Yes   CompLimit=Yes   Tension=0   Compression=-29.641
Frame=1038  TensLimit=Yes   CompLimit=Yes   Tension=0   Compression=-29.641
Frame=1039  TensLimit=Yes   CompLimit=Yes   Tension=0   Compression=-29.641
Frame=1040  TensLimit=Yes   CompLimit=Yes   Tension=0   Compression=-29.641
Frame=1041  TensLimit=Yes   CompLimit=Yes   Tension=0   Compression=-29.641
Frame=1042  TensLimit=Yes   CompLimit=Yes   Tension=0   Compression=-29.641
Frame=1043  TensLimit=Yes   CompLimit=Yes   Tension=0   Compression=-29.641
Frame=1044  TensLimit=Yes   CompLimit=Yes   Tension=0   Compression=-29.641
Frame=1045  TensLimit=Yes   CompLimit=Yes   Tension=0   Compression=-29.641
Frame=1046  TensLimit=Yes   CompLimit=Yes   Tension=0   Compression=-29.641
Frame=1047  TensLimit=Yes   CompLimit=Yes   Tension=0   Compression=-29.641
Frame=1048  TensLimit=Yes   CompLimit=Yes   Tension=0   Compression=-29.641
Frame=1049  TensLimit=Yes   CompLimit=Yes   Tension=0   Compression=-29.641
Frame=1050  TensLimit=Yes   CompLimit=Yes   Tension=0   Compression=-29.641
Frame=1051  TensLimit=Yes   CompLimit=Yes   Tension=0   Compression=-29.641
Frame=1052  TensLimit=Yes   CompLimit=Yes   Tension=0   Compression=-29.641
Frame=1053  TensLimit=Yes   CompLimit=Yes   Tension=0   Compression=-29.641
Frame=1054  TensLimit=Yes   CompLimit=Yes   Tension=0   Compression=-29.641
Frame=1055  TensLimit=Yes   CompLimit=Yes   Tension=0   Compression=-29.641
Frame=1056  TensLimit=Yes   CompLimit=Yes   Tension=0   Compression=-29.641
Frame=1057  TensLimit=Yes   CompLimit=Yes   Tension=0   Compression=-29.641
Frame=1058  TensLimit=Yes   CompLimit=Yes   Tension=0   Compression=-29.641
Frame=1059  TensLimit=Yes   CompLimit=Yes   Tension=0   Compression=-29.641
Frame=1060  TensLimit=Yes   CompLimit=Yes   Tension=0   Compression=-29.641
Frame=1061  TensLimit=Yes   CompLimit=Yes   Tension=0   Compression=-29.641
Frame=1062  TensLimit=Yes   CompLimit=Yes   Tension=0   Compression=-29.641
Frame=1063  TensLimit=Yes   CompLimit=Yes   Tension=0   Compression=-29.641
Frame=1064  TensLimit=Yes   CompLimit=Yes   Tension=0   Compression=-29.641
Frame=1065  TensLimit=Yes   CompLimit=Yes   Tension=0   Compression=-29.641
Frame=1066  TensLimit=Yes   CompLimit=Yes   Tension=0   Compression=-29.641
Frame=1067  TensLimit=Yes   CompLimit=Yes   Tension=0   Compression=-29.641
Frame=1068  TensLimit=Yes   CompLimit=Yes   Tension=0   Compression=-29.641
Frame=1069  TensLimit=Yes   CompLimit=Yes   Tension=0   Compression=-29.641
Frame=1070  TensLimit=Yes   CompLimit=Yes   Tension=0   Compression=-29.641
Frame=1071  TensLimit=Yes   CompLimit=Yes   Tension=0   Compression=-29.641
Frame=1072  TensLimit=Yes   CompLimit=Yes   Tension=0   Compression=-29.641
Frame=1073  TensLimit=Yes   CompLimit=Yes   Tension=0   Compression=-29.641
Frame=1074  TensLimit=Yes   CompLimit=Yes   Tension=0   Compression=-29.641
Frame=1075  TensLimit=Yes   CompLimit=Yes   Tension=0   Compression=-29.641
Frame=1076  TensLimit=Yes   CompLimit=Yes   Tension=0   Compression=-29.641
Frame=1077  TensLimit=Yes   CompLimit=Yes   Tension=0   Compression=-29.641
```

```
   Frame=1078   TensLimit=Yes   CompLimit=Yes   Tension=0   Compression=-29.641
   Frame=1079   TensLimit=Yes   CompLimit=Yes   Tension=0   Compression=-29.641
   Frame=1080   TensLimit=Yes   CompLimit=Yes   Tension=0   Compression=-29.641
   Frame=1081   TensLimit=Yes   CompLimit=Yes   Tension=0   Compression=-29.641
   Frame=1082   TensLimit=Yes   CompLimit=Yes   Tension=0   Compression=-29.641
   Frame=1083   TensLimit=Yes   CompLimit=Yes   Tension=0   Compression=-29.641
   Frame=1084   TensLimit=Yes   CompLimit=Yes   Tension=0   Compression=-29.641
   Frame=1091   TensLimit=Yes   CompLimit=No    Tension=0
   Frame=1092   TensLimit=Yes   CompLimit=No    Tension=0
   Frame=1093   TensLimit=Yes   CompLimit=No    Tension=0
   Frame=1094   TensLimit=Yes   CompLimit=No    Tension=0
   Frame=1115   TensLimit=Yes   CompLimit=Yes   Tension=0   Compression=-29.641
   Frame=1116   TensLimit=Yes   CompLimit=Yes   Tension=0   Compression=-29.641
   Frame=1117   TensLimit=Yes   CompLimit=Yes   Tension=0   Compression=-29.641
   Frame=1118   TensLimit=Yes   CompLimit=Yes   Tension=0   Compression=-29.641
   Frame=1119   TensLimit=Yes   CompLimit=Yes   Tension=0   Compression=-29.641
   Frame=1120   TensLimit=Yes   CompLimit=Yes   Tension=0   Compression=-29.641
   Frame=1121   TensLimit=Yes   CompLimit=Yes   Tension=0   Compression=-29.641
   Frame=1122   TensLimit=Yes   CompLimit=Yes   Tension=0   Compression=-29.641
   Frame=1123   TensLimit=Yes   CompLimit=Yes   Tension=0   Compression=-29.641
   Frame=1124   TensLimit=Yes   CompLimit=Yes   Tension=0   Compression=-29.641
   Frame=1125   TensLimit=Yes   CompLimit=Yes   Tension=0   Compression=-29.641
   Frame=1126   TensLimit=Yes   CompLimit=Yes   Tension=0   Compression=-29.641
   Frame=1127   TensLimit=Yes   CompLimit=Yes   Tension=0   Compression=-29.641
   Frame=1128   TensLimit=Yes   CompLimit=Yes   Tension=0   Compression=-29.641
   Frame=1129   TensLimit=Yes   CompLimit=Yes   Tension=0   Compression=-29.641
   Frame=1130   TensLimit=Yes   CompLimit=Yes   Tension=0   Compression=-29.641
   Frame=1131   TensLimit=Yes   CompLimit=Yes   Tension=0   Compression=-29.641
   Frame=1132   TensLimit=Yes   CompLimit=Yes   Tension=0   Compression=-29.641
   Frame=1133   TensLimit=Yes   CompLimit=Yes   Tension=0   Compression=-29.641
   Frame=1134   TensLimit=Yes   CompLimit=Yes   Tension=0   Compression=-29.641
   Frame=1135   TensLimit=Yes   CompLimit=Yes   Tension=0   Compression=-29.641
   Frame=1136   TensLimit=Yes   CompLimit=Yes   Tension=0   Compression=-29.641
   Frame=1137   TensLimit=Yes   CompLimit=Yes   Tension=0   Compression=-29.641
   Frame=1138   TensLimit=Yes   CompLimit=Yes   Tension=0   Compression=-29.641
   Frame=1145   TensLimit=Yes   CompLimit=No    Tension=0
   Frame=1146   TensLimit=Yes   CompLimit=No    Tension=0
   Frame=1149   TensLimit=Yes   CompLimit=No    Tension=0
   Frame=1150   TensLimit=Yes   CompLimit=No    Tension=0
   Frame=1153   TensLimit=Yes   CompLimit=No    Tension=0
   Frame=1154   TensLimit=Yes   CompLimit=No    Tension=0
   Frame=1157   TensLimit=Yes   CompLimit=No    Tension=0
   Frame=1158   TensLimit=Yes   CompLimit=No    Tension=0
   Frame=1161   TensLimit=Yes   CompLimit=No    Tension=0
   Frame=1162   TensLimit=Yes   CompLimit=No    Tension=0
   Frame=1165   TensLimit=Yes   CompLimit=No    Tension=0
   Frame=1166   TensLimit=Yes   CompLimit=No    Tension=0

TABLE:  "FRAME NL HINGE ASSIGNMENTS"
   Frame=16   AssignHinge=halfhinge   GenHinge=halfhinge   DistType=RelDist   RelDist=0.5
AbsDist=0.0325   ActualDist=0.0325
   Frame=39   AssignHinge=halfhinge   GenHinge=halfhinge   DistType=RelDist   RelDist=0.5
AbsDist=0.0325   ActualDist=0.0325
   Frame=40   AssignHinge=diaglayer   GenHinge=diaglayer   DistType=RelDist   RelDist=0.5
AbsDist=4.99988999878993E-03   ActualDist=4.99988999878993E-03
   Frame=41   AssignHinge=diaglayer   GenHinge=diaglayer   DistType=RelDist   RelDist=0.5
AbsDist=4.99988999878993E-03   ActualDist=4.99988999878993E-03
   Frame=42   AssignHinge=axialmember   GenHinge=axialmember   DistType=RelDist   RelDist=0.5
AbsDist=0.1225   ActualDist=0.1225
   Frame=43   AssignHinge=axialmember   GenHinge=axialmember   DistType=RelDist   RelDist=0.5
AbsDist=0.1225   ActualDist=0.1225
   Frame=44   AssignHinge=diaglayer   GenHinge=diaglayer   DistType=RelDist   RelDist=0.5
AbsDist=4.99988999878993E-03   ActualDist=4.99988999878993E-03
   Frame=45   AssignHinge=diaglayer   GenHinge=diaglayer   DistType=RelDist   RelDist=0.5
AbsDist=4.99988999879011E-03   ActualDist=4.99988999879011E-03
   Frame=56   AssignHinge=diagshear   GenHinge=diagshear   DistType=RelDist   RelDist=0.5
AbsDist=0.173241161390704   ActualDist=0.173241161390704
   Frame=57   AssignHinge=diagshear   GenHinge=diagshear   DistType=RelDist   RelDist=0.5
AbsDist=0.173241161390704   ActualDist=0.173241161390704
   Frame=58   AssignHinge=diaglayer   GenHinge=diaglayer   DistType=RelDist   RelDist=0.5
AbsDist=4.99988999879011E-03   ActualDist=4.99988999879011E-03
   Frame=59   AssignHinge=diaglayer   GenHinge=diaglayer   DistType=RelDist   RelDist=0.5
AbsDist=4.99988999879011E-03   ActualDist=4.99988999879011E-03
   Frame=60   AssignHinge=axialmember   GenHinge=axialmember   DistType=RelDist   RelDist=0.5
AbsDist=0.1225   ActualDist=0.1225
   Frame=61   AssignHinge=axialmember   GenHinge=axialmember   DistType=RelDist   RelDist=0.5
AbsDist=0.1225   ActualDist=0.1225
   Frame=74   AssignHinge=diagshear   GenHinge=diagshear   DistType=RelDist   RelDist=0.5
AbsDist=0.173241161390704   ActualDist=0.173241161390704
   Frame=75   AssignHinge=diagshear   GenHinge=diagshear   DistType=RelDist   RelDist=0.5
AbsDist=0.173241161390704   ActualDist=0.173241161390704
   Frame=78   AssignHinge=axialmember   GenHinge=axialmember   DistType=RelDist   RelDist=0.5
AbsDist=0.1225   ActualDist=0.1225
   Frame=79   AssignHinge=axialmember   GenHinge=axialmember   DistType=RelDist   RelDist=0.5
AbsDist=0.1225   ActualDist=0.1225
```

```
   Frame=92   AssignHinge=diagshear   GenHinge=diagshear   DistType=RelDist   RelDist=0.5
AbsDist=0.173241161390704   ActualDist=0.173241161390704
   Frame=93   AssignHinge=diagshear   GenHinge=diagshear   DistType=RelDist   RelDist=0.5
AbsDist=0.173241161390704   ActualDist=0.173241161390704
   Frame=96   AssignHinge=axialmember   GenHinge=axialmember   DistType=RelDist   RelDist=0.5
AbsDist=0.1225   ActualDist=0.1225
   Frame=97   AssignHinge=axialmember   GenHinge=axialmember   DistType=RelDist   RelDist=0.5
AbsDist=0.1225   ActualDist=0.1225
   Frame=99   AssignHinge=diaglayer   GenHinge=diaglayer   DistType=RelDist   RelDist=0.5
AbsDist=4.99988999878992E-03   ActualDist=4.99988999878992E-03
   Frame=110   AssignHinge=diagshear   GenHinge=diagshear   DistType=RelDist   RelDist=0.5
AbsDist=0.173241161390704   ActualDist=0.173241161390704
   Frame=111   AssignHinge=diagshear   GenHinge=diagshear   DistType=RelDist   RelDist=0.5
AbsDist=0.173241161390704   ActualDist=0.173241161390704
   Frame=112   AssignHinge=diaglayer   GenHinge=diaglayer   DistType=RelDist   RelDist=0.5
AbsDist=4.99988999878992E-03   ActualDist=4.99988999878992E-03
   Frame=113   AssignHinge=diaglayer   GenHinge=diaglayer   DistType=RelDist   RelDist=0.5
AbsDist=4.99988999878992E-03   ActualDist=4.99988999878992E-03
   Frame=114   AssignHinge=axialmember   GenHinge=axialmember   DistType=RelDist   RelDist=0.5
AbsDist=0.1225   ActualDist=0.1225
   Frame=115   AssignHinge=axialmember   GenHinge=axialmember   DistType=RelDist   RelDist=0.5
AbsDist=0.1225   ActualDist=0.1225
   Frame=116   AssignHinge=diaglayer   GenHinge=diaglayer   DistType=RelDist   RelDist=0.5
AbsDist=4.99988999879012E-03   ActualDist=4.99988999879012E-03
   Frame=117   AssignHinge=diaglayer   GenHinge=diaglayer   DistType=RelDist   RelDist=0.5
AbsDist=4.99988999879012E-03   ActualDist=4.99988999879012E-03
   Frame=128   AssignHinge=diagshear   GenHinge=diagshear   DistType=RelDist   RelDist=0.5
AbsDist=0.173241161390704   ActualDist=0.173241161390704
   Frame=129   AssignHinge=diagshear   GenHinge=diagshear   DistType=RelDist   RelDist=0.5
AbsDist=0.173241161390704   ActualDist=0.173241161390704
   Frame=130   AssignHinge=diaglayer   GenHinge=diaglayer   DistType=RelDist   RelDist=0.5
AbsDist=4.99988999879012E-03   ActualDist=4.99988999879012E-03
   Frame=132   AssignHinge=axialmember   GenHinge=axialmember   DistType=RelDist   RelDist=0.5
AbsDist=0.1225   ActualDist=0.1225
   Frame=133   AssignHinge=axialmember   GenHinge=axialmember   DistType=RelDist   RelDist=0.5
AbsDist=0.1225   ActualDist=0.1225
   Frame=146   AssignHinge=diagshear   GenHinge=diagshear   DistType=RelDist   RelDist=0.5
AbsDist=0.173241161390704   ActualDist=0.173241161390704
   Frame=147   AssignHinge=diagshear   GenHinge=diagshear   DistType=RelDist   RelDist=0.5
AbsDist=0.173241161390704   ActualDist=0.173241161390704
   Frame=282   AssignHinge=tensiontie.15   GenHinge=tensiontie.15   DistType=RelDist   RelDist=0.5
AbsDist=0.089635   ActualDist=0.089635
   Frame=291   AssignHinge=tensiontie.245   GenHinge=tensiontie.245   DistType=RelDist   RelDist=0.5
AbsDist=0.089635   ActualDist=0.089635
   Frame=353   AssignHinge=tensiontie.245   GenHinge=tensiontie.245   DistType=RelDist   RelDist=0.5
AbsDist=0.089635   ActualDist=0.089635
   Frame=354   AssignHinge=tensiontie.245   GenHinge=tensiontie.245   DistType=RelDist   RelDist=0.5
AbsDist=0.089635   ActualDist=0.089635
   Frame=363   AssignHinge=tensiontie.245   GenHinge=tensiontie.245   DistType=RelDist   RelDist=0.5
AbsDist=0.08965   ActualDist=0.08965
   Frame=364   AssignHinge=tensiontie.245   GenHinge=tensiontie.245   DistType=RelDist   RelDist=0.5
AbsDist=0.08965   ActualDist=0.08965
   Frame=368   AssignHinge=edgestarter1.5   GenHinge=edgestarter1.5   DistType=RelDist   RelDist=0.5
AbsDist=0.0325   ActualDist=0.0325
   Frame=369   AssignHinge=edgestarter   GenHinge=edgestarter   DistType=RelDist   RelDist=0.5
AbsDist=0.0325   ActualDist=0.0325
   Frame=370   AssignHinge=edgestarter   GenHinge=edgestarter   DistType=RelDist   RelDist=0.5
AbsDist=0.0325   ActualDist=0.0325
   Frame=371   AssignHinge=edgestarter   GenHinge=edgestarter   DistType=RelDist   RelDist=0.5
AbsDist=0.0325   ActualDist=0.0325
   Frame=372   AssignHinge=edgestarter   GenHinge=edgestarter   DistType=RelDist   RelDist=0.5
AbsDist=0.0325   ActualDist=0.0325
   Frame=373   AssignHinge=edgestarter   GenHinge=edgestarter   DistType=RelDist   RelDist=0.5
AbsDist=0.0325   ActualDist=0.0325
   Frame=374   AssignHinge=edgestarter   GenHinge=edgestarter   DistType=RelDist   RelDist=0.5
AbsDist=0.0325   ActualDist=0.0325
   Frame=375   AssignHinge=edgestarter   GenHinge=edgestarter   DistType=RelDist   RelDist=0.5
AbsDist=0.0325   ActualDist=0.0325
   Frame=376   AssignHinge=edgestarter   GenHinge=edgestarter   DistType=RelDist   RelDist=0.5
AbsDist=0.0325   ActualDist=0.0325
   Frame=377   AssignHinge=edgestarter   GenHinge=edgestarter   DistType=RelDist   RelDist=0.5
AbsDist=0.0325   ActualDist=0.0325
   Frame=378   AssignHinge=edgestarter   GenHinge=edgestarter   DistType=RelDist   RelDist=0.5
AbsDist=0.0325   ActualDist=0.0325
   Frame=379   AssignHinge=edgestarter1.722   GenHinge=edgestarter1.722   DistType=RelDist
RelDist=0.5   AbsDist=0.0325   ActualDist=0.0325
   Frame=380   AssignHinge=edgestarter1.389   GenHinge=edgestarter1.389   DistType=RelDist
RelDist=0.5   AbsDist=0.0325   ActualDist=0.0325
   Frame=381   AssignHinge=edgestarter0.5   GenHinge=edgestarter0.5   DistType=RelDist   RelDist=0.5
AbsDist=0.0325   ActualDist=0.0325
   Frame=382   AssignHinge=edgestarter1.5   GenHinge=edgestarter1.5   DistType=RelDist   RelDist=0.5
AbsDist=0.0325   ActualDist=0.0325
   Frame=383   AssignHinge=edgestarter   GenHinge=edgestarter   DistType=RelDist   RelDist=0.5
AbsDist=0.0325   ActualDist=0.0325
```

```
   Frame=384   AssignHinge=edgestarter   GenHinge=edgestarter   DistType=RelDist   RelDist=0.5
AbsDist=0.0325   ActualDist=0.0325
   Frame=385   AssignHinge=edgestarter   GenHinge=edgestarter   DistType=RelDist   RelDist=0.5
AbsDist=0.0325   ActualDist=0.0325
   Frame=386   AssignHinge=edgestarter   GenHinge=edgestarter   DistType=RelDist   RelDist=0.5
AbsDist=0.0325   ActualDist=0.0325
   Frame=387   AssignHinge=edgestarter   GenHinge=edgestarter   DistType=RelDist   RelDist=0.5
AbsDist=0.0325   ActualDist=0.0325
   Frame=388   AssignHinge=edgestarter   GenHinge=edgestarter   DistType=RelDist   RelDist=0.5
AbsDist=0.0325   ActualDist=0.0325
   Frame=389   AssignHinge=edgestarter   GenHinge=edgestarter   DistType=RelDist   RelDist=0.5
AbsDist=0.0325   ActualDist=0.0325
   Frame=390   AssignHinge=edgestarter   GenHinge=edgestarter   DistType=RelDist   RelDist=0.5
AbsDist=0.0325   ActualDist=0.0325
   Frame=391   AssignHinge=edgestarter   GenHinge=edgestarter   DistType=RelDist   RelDist=0.5
AbsDist=0.0325   ActualDist=0.0325
   Frame=392   AssignHinge=edgestarter   GenHinge=edgestarter   DistType=RelDist   RelDist=0.5
AbsDist=0.0325   ActualDist=0.0325
   Frame=393   AssignHinge=edgestarter1.722   GenHinge=edgestarter1.722   DistType=RelDist
RelDist=0.5   AbsDist=0.0325   ActualDist=0.0325
   Frame=394   AssignHinge=edgestarter1.389   GenHinge=edgestarter1.389   DistType=RelDist
RelDist=0.5   AbsDist=0.0325   ActualDist=0.0325
   Frame=395   AssignHinge=edgestarter0.5   GenHinge=edgestarter0.5   DistType=RelDist   RelDist=0.5
AbsDist=0.0325   ActualDist=0.0325
   Frame=397   AssignHinge=mesh   GenHinge=mesh   DistType=RelDist   RelDist=0.5   AbsDist=0.03
ActualDist=0.03
   Frame=399   AssignHinge=mesh   GenHinge=mesh   DistType=RelDist   RelDist=0.5   AbsDist=0.03
ActualDist=0.03
   Frame=401   AssignHinge=mesh   GenHinge=mesh   DistType=RelDist   RelDist=0.5   AbsDist=0.03
ActualDist=0.03
   Frame=403   AssignHinge=mesh   GenHinge=mesh   DistType=RelDist   RelDist=0.5   AbsDist=0.03
ActualDist=0.03
   Frame=405   AssignHinge=mesh   GenHinge=mesh   DistType=RelDist   RelDist=0.5   AbsDist=0.03
ActualDist=0.03
   Frame=407   AssignHinge=mesh1.722   GenHinge=mesh1.722   DistType=RelDist   RelDist=0.5
AbsDist=0.03   ActualDist=0.03
   Frame=408   AssignHinge=mesh1.389   GenHinge=mesh1.389   DistType=RelDist   RelDist=0.5
AbsDist=0.03   ActualDist=0.03
   Frame=409   AssignHinge=mesh0.5   GenHinge=mesh0.5   DistType=RelDist   RelDist=0.5   AbsDist=0.03
ActualDist=0.03
   Frame=410   AssignHinge=diaglayer   GenHinge=diaglayer   DistType=RelDist   RelDist=0.5
AbsDist=4.99988999878993E-03   ActualDist=4.99988999878993E-03
   Frame=411   AssignHinge=mesh   GenHinge=mesh   DistType=RelDist   RelDist=0.5   AbsDist=0.03
ActualDist=0.03
   Frame=412   AssignHinge=diaglayer   GenHinge=diaglayer   DistType=RelDist   RelDist=0.5
AbsDist=4.99988999878993E-03   ActualDist=4.99988999878993E-03
   Frame=413   AssignHinge=mesh   GenHinge=mesh   DistType=RelDist   RelDist=0.5   AbsDist=0.03
ActualDist=0.03
   Frame=414   AssignHinge=diaglayer   GenHinge=diaglayer   DistType=RelDist   RelDist=0.5
AbsDist=4.99988999878993E-03   ActualDist=4.99988999878993E-03
   Frame=415   AssignHinge=mesh   GenHinge=mesh   DistType=RelDist   RelDist=0.5   AbsDist=0.03
ActualDist=0.03
   Frame=416   AssignHinge=diaglayer   GenHinge=diaglayer   DistType=RelDist   RelDist=0.5
AbsDist=4.9998899987903E-03   ActualDist=4.9998899987903E-03
   Frame=417   AssignHinge=mesh   GenHinge=mesh   DistType=RelDist   RelDist=0.5   AbsDist=0.03
ActualDist=0.03
   Frame=418   AssignHinge=diaglayer   GenHinge=diaglayer   DistType=RelDist   RelDist=0.5
AbsDist=4.99988999879012E-03   ActualDist=4.99988999879012E-03
   Frame=419   AssignHinge=mesh   GenHinge=mesh   DistType=RelDist   RelDist=0.5   AbsDist=0.03
ActualDist=0.03
   Frame=420   AssignHinge=diaglayer   GenHinge=diaglayer   DistType=RelDist   RelDist=0.5
AbsDist=4.9998899987903E-03   ActualDist=4.9998899987903E-03
   Frame=421   AssignHinge=mesh1.722   GenHinge=mesh1.722   DistType=RelDist   RelDist=0.5
AbsDist=0.03   ActualDist=0.03
   Frame=422   AssignHinge=mesh1.389   GenHinge=mesh1.389   DistType=RelDist   RelDist=0.5
AbsDist=0.03   ActualDist=0.03
   Frame=423   AssignHinge=mesh0.5   GenHinge=mesh0.5   DistType=RelDist   RelDist=0.5   AbsDist=0.03
ActualDist=0.03
   Frame=424   AssignHinge=tensiontie   GenHinge=tensiontie   DistType=RelDist   RelDist=0.5
AbsDist=0.089635   ActualDist=0.089635
   Frame=425   AssignHinge=tensiontie   GenHinge=tensiontie   DistType=RelDist   RelDist=0.5
AbsDist=0.089635   ActualDist=0.089635
   Frame=426   AssignHinge=tensiontie.245   GenHinge=tensiontie.245   DistType=RelDist   RelDist=0.5
AbsDist=0.089635   ActualDist=0.089635
   Frame=427   AssignHinge=tensiontie.15   GenHinge=tensiontie.15   DistType=RelDist   RelDist=0.5
AbsDist=0.089635   ActualDist=0.089635
   Frame=428   AssignHinge=tensiontie.245   GenHinge=tensiontie.245   DistType=RelDist   RelDist=0.5
AbsDist=0.089635   ActualDist=0.089635
   Frame=429   AssignHinge=tensiontie   GenHinge=tensiontie   DistType=RelDist   RelDist=0.5
AbsDist=0.089635   ActualDist=0.089635
   Frame=430   AssignHinge=tensiontie   GenHinge=tensiontie   DistType=RelDist   RelDist=0.5
AbsDist=0.089635   ActualDist=0.089635
   Frame=431   AssignHinge=tensiontie   GenHinge=tensiontie   DistType=RelDist   RelDist=0.5
AbsDist=0.089635   ActualDist=0.089635
```

```
   Frame=432   AssignHinge=tensiontie.335   GenHinge=tensiontie.335   DistType=RelDist   RelDist=0.5
AbsDist=0.089635   ActualDist=0.089635
   Frame=433   AssignHinge=tensiontie.245   GenHinge=tensiontie.245   DistType=RelDist   RelDist=0.5
AbsDist=0.089635   ActualDist=0.089635
   Frame=435   AssignHinge=tensiontie.335   GenHinge=tensiontie.335   DistType=RelDist   RelDist=0.5
AbsDist=0.08965   ActualDist=0.08965
   Frame=436   AssignHinge=tensiontie   GenHinge=tensiontie   DistType=RelDist   RelDist=0.5
AbsDist=0.08965   ActualDist=0.08965
   Frame=437   AssignHinge=tensiontie   GenHinge=tensiontie   DistType=RelDist   RelDist=0.5
AbsDist=0.08965   ActualDist=0.08965
   Frame=438   AssignHinge=tensiontie   GenHinge=tensiontie   DistType=RelDist   RelDist=0.5
AbsDist=0.08965   ActualDist=0.08965
   Frame=439   AssignHinge=tensiontie.245   GenHinge=tensiontie.245   DistType=RelDist   RelDist=0.5
AbsDist=0.08965   ActualDist=0.08965
   Frame=440   AssignHinge=tensiontie.15   GenHinge=tensiontie.15   DistType=RelDist   RelDist=0.5
AbsDist=0.08965   ActualDist=0.08965
   Frame=441   AssignHinge=tensiontie.245   GenHinge=tensiontie.245   DistType=RelDist   RelDist=0.5
AbsDist=0.08965   ActualDist=0.08965
   Frame=442   AssignHinge=tensiontie   GenHinge=tensiontie   DistType=RelDist   RelDist=0.5
AbsDist=0.08965   ActualDist=0.08965
   Frame=443   AssignHinge=tensiontie   GenHinge=tensiontie   DistType=RelDist   RelDist=0.5
AbsDist=0.08965   ActualDist=0.08965
   Frame=444   AssignHinge=2-4.0mm   GenHinge=2-4.0mm   DistType=RelDist   RelDist=0.5   AbsDist=0.03
ActualDist=0.03
   Frame=445   AssignHinge=2-4.0mm   GenHinge=2-4.0mm   DistType=RelDist   RelDist=0.5   AbsDist=0.03
ActualDist=0.03
   Frame=446   AssignHinge=2-4.0mm   GenHinge=2-4.0mm   DistType=RelDist   RelDist=0.5   AbsDist=0.03
ActualDist=0.03
   Frame=447   AssignHinge=2-4.0mm   GenHinge=2-4.0mm   DistType=RelDist   RelDist=0.5   AbsDist=0.03
ActualDist=0.03
   Frame=448   AssignHinge=2-4.0mm   GenHinge=2-4.0mm   DistType=RelDist   RelDist=0.5   AbsDist=0.03
ActualDist=0.03
   Frame=449   AssignHinge=2-4.0mm   GenHinge=2-4.0mm   DistType=RelDist   RelDist=0.5   AbsDist=0.03
ActualDist=0.03
   Frame=450   AssignHinge=2-4.0mm   GenHinge=2-4.0mm   DistType=RelDist   RelDist=0.5   AbsDist=0.03
ActualDist=0.03
   Frame=451   AssignHinge=2-4.0mm   GenHinge=2-4.0mm   DistType=RelDist   RelDist=0.5   AbsDist=0.03
ActualDist=0.03
   Frame=452   AssignHinge=2-4.0mm   GenHinge=2-4.0mm   DistType=RelDist   RelDist=0.5   AbsDist=0.03
ActualDist=0.03
   Frame=453   AssignHinge=2-4.0mm   GenHinge=2-4.0mm   DistType=RelDist   RelDist=0.5   AbsDist=0.03
ActualDist=0.03
   Frame=454   AssignHinge=2-4.0mm   GenHinge=2-4.0mm   DistType=RelDist   RelDist=0.5   AbsDist=0.03
ActualDist=0.03
   Frame=455   AssignHinge=2-4.0mm   GenHinge=2-4.0mm   DistType=RelDist   RelDist=0.5   AbsDist=0.03
ActualDist=0.03
   Frame=458   AssignHinge=diaglayer   GenHinge=diaglayer   DistType=RelDist   RelDist=0.5
AbsDist=4.99988999878993E-03   ActualDist=4.99988999878993E-03
   Frame=466   AssignHinge=diaglayer   GenHinge=diaglayer   DistType=RelDist   RelDist=0.5
AbsDist=4.99988999878992E-03   ActualDist=4.99988999878992E-03
   Frame=467   AssignHinge=diaglayer   GenHinge=diaglayer   DistType=RelDist   RelDist=0.5
AbsDist=4.99988999878992E-03   ActualDist=4.99988999878992E-03
   Frame=468   AssignHinge=diaglayer   GenHinge=diaglayer   DistType=RelDist   RelDist=0.5
AbsDist=4.99988999878992E-03   ActualDist=4.99988999878992E-03
   Frame=469   AssignHinge=diaglayer   GenHinge=diaglayer   DistType=RelDist   RelDist=0.5
AbsDist=4.99988999879031E-03   ActualDist=4.99988999879031E-03
   Frame=470   AssignHinge=diaglayer   GenHinge=diaglayer   DistType=RelDist   RelDist=0.5
AbsDist=4.99988999879012E-03   ActualDist=4.99988999879012E-03
   Frame=471   AssignHinge=diaglayer   GenHinge=diaglayer   DistType=RelDist   RelDist=0.5
AbsDist=4.99988999879031E-03   ActualDist=4.99988999879031E-03
   Frame=472   AssignHinge=diaglayer   GenHinge=diaglayer   DistType=RelDist   RelDist=0.5
AbsDist=4.99988999878993E-03   ActualDist=4.99988999878993E-03
   Frame=473   AssignHinge=diaglayer   GenHinge=diaglayer   DistType=RelDist   RelDist=0.5
AbsDist=4.99988999878993E-03   ActualDist=4.99988999878993E-03
   Frame=482   AssignHinge=diaglayer   GenHinge=diaglayer   DistType=RelDist   RelDist=0.5
AbsDist=4.99988999878993E-03   ActualDist=4.99988999878993E-03
   Frame=483   AssignHinge=diaglayer   GenHinge=diaglayer   DistType=RelDist   RelDist=0.5
AbsDist=4.99988999878993E-03   ActualDist=4.99988999878993E-03
   Frame=484   AssignHinge=diaglayer   GenHinge=diaglayer   DistType=RelDist   RelDist=0.5
AbsDist=4.99988999878993E-03   ActualDist=4.99988999878993E-03
   Frame=485   AssignHinge=diaglayer   GenHinge=diaglayer   DistType=RelDist   RelDist=0.5
AbsDist=4.99988999879011E-03   ActualDist=4.99988999879011E-03
   Frame=486   AssignHinge=diaglayer   GenHinge=diaglayer   DistType=RelDist   RelDist=0.5
AbsDist=4.99988999879002E-03   ActualDist=4.99988999879002E-03
   Frame=487   AssignHinge=diaglayer   GenHinge=diaglayer   DistType=RelDist   RelDist=0.5
AbsDist=4.99988999879011E-03   ActualDist=4.99988999879011E-03
   Frame=502   AssignHinge=diaglayer.245   GenHinge=diaglayer.245   DistType=RelDist   RelDist=0.5
AbsDist=5.00132482448402E-03   ActualDist=5.00132482448402E-03
   Frame=580   AssignHinge=diaglayer   GenHinge=diaglayer   DistType=RelDist   RelDist=0.5
AbsDist=4.99988999878992E-03   ActualDist=4.99988999878992E-03
   Frame=581   AssignHinge=diaglayer   GenHinge=diaglayer   DistType=RelDist   RelDist=0.5
AbsDist=4.99988999878993E-03   ActualDist=4.99988999878993E-03
   Frame=582   AssignHinge=diaglayer   GenHinge=diaglayer   DistType=RelDist   RelDist=0.5
AbsDist=4.99988999878992E-03   ActualDist=4.99988999878992E-03
```

```
   Frame=583   AssignHinge=diaglayer   GenHinge=diaglayer   DistType=RelDist   RelDist=0.5
AbsDist=4.99988999879012E-03   ActualDist=4.99988999879012E-03
   Frame=584   AssignHinge=diaglayer   GenHinge=diaglayer   DistType=RelDist   RelDist=0.5
AbsDist=4.99988999879002E-03   ActualDist=4.99988999879002E-03
   Frame=585   AssignHinge=diaglayer   GenHinge=diaglayer   DistType=RelDist   RelDist=0.5
AbsDist=4.99988999879012E-03   ActualDist=4.99988999879012E-03
   Frame=595   AssignHinge=diaglayer   GenHinge=diaglayer   DistType=RelDist   RelDist=0.5
AbsDist=4.99988999878983E-03   ActualDist=4.99988999878983E-03
   Frame=596   AssignHinge=diaglayer   GenHinge=diaglayer   DistType=RelDist   RelDist=0.5
AbsDist=4.99988999878993E-03   ActualDist=4.99988999878993E-03
   Frame=597   AssignHinge=diaglayer   GenHinge=diaglayer   DistType=RelDist   RelDist=0.5
AbsDist=4.99988999878983E-03   ActualDist=4.99988999878983E-03
   Frame=598   AssignHinge=diaglayer   GenHinge=diaglayer   DistType=RelDist   RelDist=0.5
AbsDist=4.99988999879011E-03   ActualDist=4.99988999879011E-03
   Frame=599   AssignHinge=diaglayer   GenHinge=diaglayer   DistType=RelDist   RelDist=0.5
AbsDist=4.99988999879002E-03   ActualDist=4.99988999879002E-03
   Frame=600   AssignHinge=diaglayer   GenHinge=diaglayer   DistType=RelDist   RelDist=0.5
AbsDist=4.99988999879011E-03   ActualDist=4.99988999879011E-03
   Frame=601   AssignHinge=diaglayer   GenHinge=diaglayer   DistType=RelDist   RelDist=0.5
AbsDist=4.99988999879011E-03   ActualDist=4.99988999879011E-03
   Frame=602   AssignHinge=diaglayer   GenHinge=diaglayer   DistType=RelDist   RelDist=0.5
AbsDist=5.00740701361498E-03   ActualDist=5.00740701361498E-03
   Frame=610   AssignHinge=diaglayer   GenHinge=diaglayer   DistType=RelDist   RelDist=0.5
AbsDist=4.99988999878982E-03   ActualDist=4.99988999878982E-03
   Frame=611   AssignHinge=diaglayer   GenHinge=diaglayer   DistType=RelDist   RelDist=0.5
AbsDist=4.99988999878993E-03   ActualDist=4.99988999878993E-03
   Frame=612   AssignHinge=diaglayer   GenHinge=diaglayer   DistType=RelDist   RelDist=0.5
AbsDist=4.99988999878982E-03   ActualDist=4.99988999878982E-03
   Frame=613   AssignHinge=diaglayer   GenHinge=diaglayer   DistType=RelDist   RelDist=0.5
AbsDist=4.99988999879012E-03   ActualDist=4.99988999879012E-03
   Frame=614   AssignHinge=diaglayer   GenHinge=diaglayer   DistType=RelDist   RelDist=0.5
AbsDist=4.99988999879002E-03   ActualDist=4.99988999879002E-03
   Frame=615   AssignHinge=diaglayer   GenHinge=diaglayer   DistType=RelDist   RelDist=0.5
AbsDist=4.99988999879012E-03   ActualDist=4.99988999879012E-03
   Frame=616   AssignHinge=diaglayer   GenHinge=diaglayer   DistType=RelDist   RelDist=0.5
AbsDist=4.99988999879011E-03   ActualDist=4.99988999879011E-03
   Frame=625   AssignHinge=diaglayer   GenHinge=diaglayer   DistType=RelDist   RelDist=0.5
AbsDist=4.99988999878983E-03   ActualDist=4.99988999878983E-03
   Frame=626   AssignHinge=diaglayer   GenHinge=diaglayer   DistType=RelDist   RelDist=0.5
AbsDist=4.99988999878993E-03   ActualDist=4.99988999878993E-03
   Frame=627   AssignHinge=diaglayer   GenHinge=diaglayer   DistType=RelDist   RelDist=0.5
AbsDist=4.99988999878983E-03   ActualDist=4.99988999878983E-03
   Frame=628   AssignHinge=diaglayer   GenHinge=diaglayer   DistType=RelDist   RelDist=0.5
AbsDist=4.99988999879011E-03   ActualDist=4.99988999879011E-03
   Frame=629   AssignHinge=diaglayer   GenHinge=diaglayer   DistType=RelDist   RelDist=0.5
AbsDist=4.99988999879002E-03   ActualDist=4.99988999879002E-03
   Frame=630   AssignHinge=diaglayer   GenHinge=diaglayer   DistType=RelDist   RelDist=0.5
AbsDist=4.99988999879011E-03   ActualDist=4.99988999879011E-03
   Frame=640   AssignHinge=diaglayer   GenHinge=diaglayer   DistType=RelDist   RelDist=0.5
AbsDist=4.99988999878982E-03   ActualDist=4.99988999878982E-03
   Frame=641   AssignHinge=diaglayer   GenHinge=diaglayer   DistType=RelDist   RelDist=0.5
AbsDist=4.99988999878993E-03   ActualDist=4.99988999878993E-03
   Frame=642   AssignHinge=diaglayer   GenHinge=diaglayer   DistType=RelDist   RelDist=0.5
AbsDist=4.99988999878982E-03   ActualDist=4.99988999878982E-03
   Frame=643   AssignHinge=diaglayer   GenHinge=diaglayer   DistType=RelDist   RelDist=0.5
AbsDist=4.99988999879012E-03   ActualDist=4.99988999879012E-03
   Frame=644   AssignHinge=diaglayer   GenHinge=diaglayer   DistType=RelDist   RelDist=0.5
AbsDist=4.99988999879002E-03   ActualDist=4.99988999879002E-03
   Frame=645   AssignHinge=diaglayer   GenHinge=diaglayer   DistType=RelDist   RelDist=0.5
AbsDist=4.99988999879012E-03   ActualDist=4.99988999879012E-03
   Frame=655   AssignHinge=diaglayer   GenHinge=diaglayer   DistType=RelDist   RelDist=0.5
AbsDist=4.99988999878973E-03   ActualDist=4.99988999878973E-03
   Frame=656   AssignHinge=diaglayer   GenHinge=diaglayer   DistType=RelDist   RelDist=0.5
AbsDist=4.99988999878983E-03   ActualDist=4.99988999878983E-03
   Frame=657   AssignHinge=diaglayer   GenHinge=diaglayer   DistType=RelDist   RelDist=0.5
AbsDist=4.99988999878973E-03   ActualDist=4.99988999878973E-03
   Frame=658   AssignHinge=diaglayer   GenHinge=diaglayer   DistType=RelDist   RelDist=0.5
AbsDist=4.99988999879011E-03   ActualDist=4.99988999879011E-03
   Frame=659   AssignHinge=diaglayer   GenHinge=diaglayer   DistType=RelDist   RelDist=0.5
AbsDist=4.99988999879012E-03   ActualDist=4.99988999879012E-03
   Frame=660   AssignHinge=diaglayer   GenHinge=diaglayer   DistType=RelDist   RelDist=0.5
AbsDist=4.99988999879011E-03   ActualDist=4.99988999879011E-03
   Frame=670   AssignHinge=diaglayer   GenHinge=diaglayer   DistType=RelDist   RelDist=0.5
AbsDist=4.99988999878973E-03   ActualDist=4.99988999878973E-03
   Frame=671   AssignHinge=diaglayer   GenHinge=diaglayer   DistType=RelDist   RelDist=0.5
AbsDist=4.99988999878983E-03   ActualDist=4.99988999878983E-03
   Frame=672   AssignHinge=diaglayer   GenHinge=diaglayer   DistType=RelDist   RelDist=0.5
AbsDist=4.99988999878973E-03   ActualDist=4.99988999878973E-03
   Frame=673   AssignHinge=diaglayer   GenHinge=diaglayer   DistType=RelDist   RelDist=0.5
AbsDist=4.99988999879012E-03   ActualDist=4.99988999879012E-03
   Frame=674   AssignHinge=diaglayer   GenHinge=diaglayer   DistType=RelDist   RelDist=0.5
AbsDist=4.99988999879012E-03   ActualDist=4.99988999879012E-03
   Frame=675   AssignHinge=diaglayer   GenHinge=diaglayer   DistType=RelDist   RelDist=0.5
AbsDist=4.99988999879012E-03   ActualDist=4.99988999879012E-03
```

```
   Frame=684   AssignHinge=diaglayer   GenHinge=diaglayer   DistType=RelDist   RelDist=0.5
AbsDist=4.99988999878992E-03   ActualDist=4.99988999878992E-03
   Frame=685   AssignHinge=diaglayer   GenHinge=diaglayer   DistType=RelDist   RelDist=0.5
AbsDist=5.00740701361489E-03   ActualDist=5.00740701361489E-03
   Frame=686   AssignHinge=diaglayer   GenHinge=diaglayer   DistType=RelDist   RelDist=0.5
AbsDist=4.99988999878992E-03   ActualDist=4.99988999878992E-03
   Frame=687   AssignHinge=diaglayer   GenHinge=diaglayer   DistType=RelDist   RelDist=0.5
AbsDist=4.99988999879012E-03   ActualDist=4.99988999879012E-03
   Frame=688   AssignHinge=diaglayer   GenHinge=diaglayer   DistType=RelDist   RelDist=0.5
AbsDist=4.99988999879002E-03   ActualDist=4.99988999879002E-03
   Frame=689   AssignHinge=diaglayer   GenHinge=diaglayer   DistType=RelDist   RelDist=0.5
AbsDist=4.99988999879012E-03   ActualDist=4.99988999879012E-03
   Frame=699   AssignHinge=diaglayer   GenHinge=diaglayer   DistType=RelDist   RelDist=0.5
AbsDist=4.99988999878973E-03   ActualDist=4.99988999878973E-03
   Frame=700   AssignHinge=diaglayer   GenHinge=diaglayer   DistType=RelDist   RelDist=0.5
AbsDist=4.99988999878983E-03   ActualDist=4.99988999878983E-03
   Frame=701   AssignHinge=diaglayer   GenHinge=diaglayer   DistType=RelDist   RelDist=0.5
AbsDist=4.99988999878973E-03   ActualDist=4.99988999878973E-03
   Frame=702   AssignHinge=diaglayer   GenHinge=diaglayer   DistType=RelDist   RelDist=0.5
AbsDist=4.99988999879011E-03   ActualDist=4.99988999879011E-03
   Frame=703   AssignHinge=diaglayer   GenHinge=diaglayer   DistType=RelDist   RelDist=0.5
AbsDist=5.00740701361508E-03   ActualDist=5.00740701361508E-03
   Frame=704   AssignHinge=diaglayer   GenHinge=diaglayer   DistType=RelDist   RelDist=0.5
AbsDist=4.99988999879011E-03   ActualDist=4.99988999879011E-03
   Frame=714   AssignHinge=diaglayer   GenHinge=diaglayer   DistType=RelDist   RelDist=0.5
AbsDist=4.99988999878973E-03   ActualDist=4.99988999878973E-03
   Frame=715   AssignHinge=diaglayer   GenHinge=diaglayer   DistType=RelDist   RelDist=0.5
AbsDist=5.00740701361479E-03   ActualDist=5.00740701361479E-03
   Frame=716   AssignHinge=diaglayer   GenHinge=diaglayer   DistType=RelDist   RelDist=0.5
AbsDist=4.99988999878973E-03   ActualDist=4.99988999878973E-03
   Frame=717   AssignHinge=diaglayer   GenHinge=diaglayer   DistType=RelDist   RelDist=0.5
AbsDist=4.99988999879012E-03   ActualDist=4.99988999879012E-03
   Frame=718   AssignHinge=diaglayer   GenHinge=diaglayer   DistType=RelDist   RelDist=0.5
AbsDist=4.99988999879012E-03   ActualDist=4.99988999879012E-03
   Frame=719   AssignHinge=diaglayer   GenHinge=diaglayer   DistType=RelDist   RelDist=0.5
AbsDist=4.99988999879012E-03   ActualDist=4.99988999879012E-03
   Frame=720   AssignHinge=diaglayer.245   GenHinge=diaglayer.245   DistType=RelDist   RelDist=0.5
AbsDist=5.00132482448384E-03   ActualDist=5.00132482448384E-03
   Frame=721   AssignHinge=diaglayer.245   GenHinge=diaglayer.245   DistType=RelDist   RelDist=0.5
AbsDist=5.00132482448402E-03   ActualDist=5.00132482448402E-03
   Frame=729   AssignHinge=diaglayer   GenHinge=diaglayer   DistType=RelDist   RelDist=0.5
AbsDist=4.99988999878993E-03   ActualDist=4.99988999878993E-03
   Frame=730   AssignHinge=diaglayer   GenHinge=diaglayer   DistType=RelDist   RelDist=0.5
AbsDist=4.99988999878993E-03   ActualDist=4.99988999878993E-03
   Frame=731   AssignHinge=diaglayer   GenHinge=diaglayer   DistType=RelDist   RelDist=0.5
AbsDist=4.99988999878993E-03   ActualDist=4.99988999878993E-03
   Frame=732   AssignHinge=diaglayer   GenHinge=diaglayer   DistType=RelDist   RelDist=0.5
AbsDist=4.99988999879011E-03   ActualDist=4.99988999879011E-03
   Frame=733   AssignHinge=diaglayer   GenHinge=diaglayer   DistType=RelDist   RelDist=0.5
AbsDist=5.00740701361498E-03   ActualDist=5.00740701361498E-03
   Frame=734   AssignHinge=diaglayer   GenHinge=diaglayer   DistType=RelDist   RelDist=0.5
AbsDist=4.99988999879011E-03   ActualDist=4.99988999879011E-03
   Frame=735   AssignHinge=diaglayer.245   GenHinge=diaglayer.245   DistType=RelDist   RelDist=0.5
AbsDist=5.00132482448384E-03   ActualDist=5.00132482448384E-03
   Frame=736   AssignHinge=diaglayer.245   GenHinge=diaglayer.245   DistType=RelDist   RelDist=0.5
AbsDist=5.00132482448384E-03   ActualDist=5.00132482448384E-03
   Frame=744   AssignHinge=diaglayer   GenHinge=diaglayer   DistType=RelDist   RelDist=0.5
AbsDist=4.99988999878992E-03   ActualDist=4.99988999878992E-03
   Frame=745   AssignHinge=diaglayer   GenHinge=diaglayer   DistType=RelDist   RelDist=0.5
AbsDist=5.00740701361489E-03   ActualDist=5.00740701361489E-03
   Frame=746   AssignHinge=diaglayer   GenHinge=diaglayer   DistType=RelDist   RelDist=0.5
AbsDist=4.99988999878992E-03   ActualDist=4.99988999878992E-03
   Frame=747   AssignHinge=diaglayer   GenHinge=diaglayer   DistType=RelDist   RelDist=0.5
AbsDist=4.99988999879012E-03   ActualDist=4.99988999879012E-03
   Frame=748   AssignHinge=diaglayer   GenHinge=diaglayer   DistType=RelDist   RelDist=0.5
AbsDist=4.99988999879002E-03   ActualDist=4.99988999879002E-03
   Frame=749   AssignHinge=diaglayer   GenHinge=diaglayer   DistType=RelDist   RelDist=0.5
AbsDist=4.99988999879012E-03   ActualDist=4.99988999879012E-03
   Frame=750   AssignHinge=diaglayer.245   GenHinge=diaglayer.245   DistType=RelDist   RelDist=0.5
AbsDist=5.00132482448403E-03   ActualDist=5.00132482448403E-03
   Frame=751   AssignHinge=diaglayer.245   GenHinge=diaglayer.245   DistType=RelDist   RelDist=0.5
AbsDist=5.00132482448384E-03   ActualDist=5.00132482448384E-03
   Frame=759   AssignHinge=diaglayer   GenHinge=diaglayer   DistType=RelDist   RelDist=0.5
AbsDist=4.99988999878993E-03   ActualDist=4.99988999878993E-03
   Frame=760   AssignHinge=diaglayer   GenHinge=diaglayer   DistType=RelDist   RelDist=0.5
AbsDist=4.99988999879002E-03   ActualDist=4.99988999879002E-03
   Frame=761   AssignHinge=diaglayer   GenHinge=diaglayer   DistType=RelDist   RelDist=0.5
AbsDist=4.99988999878993E-03   ActualDist=4.99988999878993E-03
   Frame=762   AssignHinge=diaglayer   GenHinge=diaglayer   DistType=RelDist   RelDist=0.5
AbsDist=4.99988999879011E-03   ActualDist=4.99988999879011E-03
   Frame=763   AssignHinge=diaglayer   GenHinge=diaglayer   DistType=RelDist   RelDist=0.5
AbsDist=5.00740701361489E-03   ActualDist=5.00740701361489E-03
   Frame=764   AssignHinge=diaglayer   GenHinge=diaglayer   DistType=RelDist   RelDist=0.5
AbsDist=4.99988999879011E-03   ActualDist=4.99988999879011E-03
```

```
   Frame=765   AssignHinge=diaglayer.245   GenHinge=diaglayer.245   DistType=RelDist   RelDist=0.5
AbsDist=5.00132482448402E-03   ActualDist=5.00132482448402E-03
   Frame=766   AssignHinge=diaglayer.245   GenHinge=diaglayer.245   DistType=RelDist   RelDist=0.5
AbsDist=5.00132482448402E-03   ActualDist=5.00132482448402E-03
   Frame=774   AssignHinge=diaglayer   GenHinge=diaglayer   DistType=RelDist   RelDist=0.5
AbsDist=4.99988999878992E-03   ActualDist=4.99988999878992E-03
   Frame=775   AssignHinge=diaglayer   GenHinge=diaglayer   DistType=RelDist   RelDist=0.5
AbsDist=5.00740701361498E-03   ActualDist=5.00740701361498E-03
   Frame=776   AssignHinge=diaglayer   GenHinge=diaglayer   DistType=RelDist   RelDist=0.5
AbsDist=4.99988999878992E-03   ActualDist=4.99988999878992E-03
   Frame=777   AssignHinge=diaglayer   GenHinge=diaglayer   DistType=RelDist   RelDist=0.5
AbsDist=4.99988999879012E-03   ActualDist=4.99988999879012E-03
   Frame=778   AssignHinge=diaglayer   GenHinge=diaglayer   DistType=RelDist   RelDist=0.5
AbsDist=4.99988999878993E-03   ActualDist=4.99988999878993E-03
   Frame=779   AssignHinge=diaglayer   GenHinge=diaglayer   DistType=RelDist   RelDist=0.5
AbsDist=4.99988999879012E-03   ActualDist=4.99988999879012E-03
   Frame=780   AssignHinge=diaglayer.245   GenHinge=diaglayer.245   DistType=RelDist   RelDist=0.5
AbsDist=5.00132482448402E-03   ActualDist=5.00132482448402E-03
   Frame=781   AssignHinge=diaglayer.245   GenHinge=diaglayer.245   DistType=RelDist   RelDist=0.5
AbsDist=5.00132482448402E-03   ActualDist=5.00132482448402E-03
   Frame=788   AssignHinge=diaglayer.245   GenHinge=diaglayer.245   DistType=RelDist   RelDist=0.5
AbsDist=5.00132482448402E-03   ActualDist=5.00132482448402E-03
   Frame=789   AssignHinge=diaglayer.245   GenHinge=diaglayer.245   DistType=RelDist   RelDist=0.5
AbsDist=5.00132482448402E-03   ActualDist=5.00132482448402E-03
   Frame=804   AssignHinge=diaglayer.245   GenHinge=diaglayer.245   DistType=RelDist   RelDist=0.5
AbsDist=5.00132482448384E-03   ActualDist=5.00132482448384E-03
   Frame=805   AssignHinge=diaglayer.245   GenHinge=diaglayer.245   DistType=RelDist   RelDist=0.5
AbsDist=5.00132482448402E-03   ActualDist=5.00132482448402E-03
   Frame=806   AssignHinge=diaglayer.245   GenHinge=diaglayer.245   DistType=RelDist   RelDist=0.5
AbsDist=5.00132482448384E-03   ActualDist=5.00132482448384E-03
   Frame=807   AssignHinge=diaglayer.245   GenHinge=diaglayer.245   DistType=RelDist   RelDist=0.5
AbsDist=5.00132482448384E-03   ActualDist=5.00132482448384E-03
   Frame=808   AssignHinge=diaglayer.245   GenHinge=diaglayer.245   DistType=RelDist   RelDist=0.5
AbsDist=5.01020209173245E-03   ActualDist=5.01020209173245E-03
   Frame=809   AssignHinge=diaglayer.245   GenHinge=diaglayer.245   DistType=RelDist   RelDist=0.5
AbsDist=5.00132482448384E-03   ActualDist=5.00132482448384E-03
   Frame=810   AssignHinge=diaglayer.245   GenHinge=diaglayer.245   DistType=RelDist   RelDist=0.5
AbsDist=5.00132482448402E-03   ActualDist=5.00132482448402E-03
   Frame=811   AssignHinge=diaglayer.245   GenHinge=diaglayer.245   DistType=RelDist   RelDist=0.5
AbsDist=5.00132482448393E-03   ActualDist=5.00132482448393E-03
   Frame=812   AssignHinge=diaglayer.245   GenHinge=diaglayer.245   DistType=RelDist   RelDist=0.5
AbsDist=5.00132482448402E-03   ActualDist=5.00132482448402E-03
   Frame=813   AssignHinge=diaglayer.245   GenHinge=diaglayer.245   DistType=RelDist   RelDist=0.5
AbsDist=5.00132482448402E-03   ActualDist=5.00132482448402E-03
   Frame=814   AssignHinge=diaglayer.245   GenHinge=diaglayer.245   DistType=RelDist   RelDist=0.5
AbsDist=5.01020209173235E-03   ActualDist=5.01020209173235E-03
   Frame=815   AssignHinge=diaglayer.245   GenHinge=diaglayer.245   DistType=RelDist   RelDist=0.5
AbsDist=5.00132482448402E-03   ActualDist=5.00132482448402E-03
   Frame=819   AssignHinge=diaglayer   GenHinge=diaglayer   DistType=RelDist   RelDist=0.5
AbsDist=4.99988999878993E-03   ActualDist=4.99988999878993E-03
   Frame=820   AssignHinge=diaglayer   GenHinge=diaglayer   DistType=RelDist   RelDist=0.5
AbsDist=4.99988999878973E-03   ActualDist=4.99988999878973E-03
   Frame=821   AssignHinge=diaglayer   GenHinge=diaglayer   DistType=RelDist   RelDist=0.5
AbsDist=4.99988999878993E-03   ActualDist=4.99988999878993E-03
   Frame=822   AssignHinge=diaglayer   GenHinge=diaglayer   DistType=RelDist   RelDist=0.5
AbsDist=4.99988999879011E-03   ActualDist=4.99988999879011E-03
   Frame=823   AssignHinge=diaglayer   GenHinge=diaglayer   DistType=RelDist   RelDist=0.5
AbsDist=5.00740701361508E-03   ActualDist=5.00740701361508E-03
   Frame=824   AssignHinge=diaglayer   GenHinge=diaglayer   DistType=RelDist   RelDist=0.5
AbsDist=4.99988999879011E-03   ActualDist=4.99988999879011E-03
   Frame=834   AssignHinge=diaglayer   GenHinge=diaglayer   DistType=RelDist   RelDist=0.5
AbsDist=4.99988999878992E-03   ActualDist=4.99988999878992E-03
   Frame=835   AssignHinge=diaglayer   GenHinge=diaglayer   DistType=RelDist   RelDist=0.5
AbsDist=5.00740701361469E-03   ActualDist=5.00740701361469E-03
   Frame=836   AssignHinge=diaglayer   GenHinge=diaglayer   DistType=RelDist   RelDist=0.5
AbsDist=4.99988999878992E-03   ActualDist=4.99988999878992E-03
   Frame=837   AssignHinge=diaglayer   GenHinge=diaglayer   DistType=RelDist   RelDist=0.5
AbsDist=4.99988999879012E-03   ActualDist=4.99988999879012E-03
   Frame=838   AssignHinge=diaglayer   GenHinge=diaglayer   DistType=RelDist   RelDist=0.5
AbsDist=4.99988999879012E-03   ActualDist=4.99988999879012E-03
   Frame=839   AssignHinge=diaglayer   GenHinge=diaglayer   DistType=RelDist   RelDist=0.5
AbsDist=4.99988999879012E-03   ActualDist=4.99988999879012E-03
   Frame=849   AssignHinge=diaglayer   GenHinge=diaglayer   DistType=RelDist   RelDist=0.5
AbsDist=4.99988999878993E-03   ActualDist=4.99988999878993E-03
   Frame=850   AssignHinge=diaglayer   GenHinge=diaglayer   DistType=RelDist   RelDist=0.5
AbsDist=4.99988999878993E-03   ActualDist=4.99988999878993E-03
   Frame=851   AssignHinge=diaglayer   GenHinge=diaglayer   DistType=RelDist   RelDist=0.5
AbsDist=4.99988999878993E-03   ActualDist=4.99988999878993E-03
   Frame=852   AssignHinge=diaglayer   GenHinge=diaglayer   DistType=RelDist   RelDist=0.5
AbsDist=4.99988999879011E-03   ActualDist=4.99988999879011E-03
   Frame=853   AssignHinge=diaglayer   GenHinge=diaglayer   DistType=RelDist   RelDist=0.5
AbsDist=5.00740701361508E-03   ActualDist=5.00740701361508E-03
   Frame=854   AssignHinge=diaglayer   GenHinge=diaglayer   DistType=RelDist   RelDist=0.5
AbsDist=4.99988999879011E-03   ActualDist=4.99988999879011E-03
```

```
   Frame=864   AssignHinge=diaglayer   GenHinge=diaglayer   DistType=RelDist   RelDist=0.5
AbsDist=4.99988999878992E-03   ActualDist=4.99988999878992E-03
   Frame=865   AssignHinge=diaglayer   GenHinge=diaglayer   DistType=RelDist   RelDist=0.5
AbsDist=5.00740701361489E-03   ActualDist=5.00740701361489E-03
   Frame=866   AssignHinge=diaglayer   GenHinge=diaglayer   DistType=RelDist   RelDist=0.5
AbsDist=4.99988999878992E-03   ActualDist=4.99988999878992E-03
   Frame=867   AssignHinge=diaglayer   GenHinge=diaglayer   DistType=RelDist   RelDist=0.5
AbsDist=4.99988999879012E-03   ActualDist=4.99988999879012E-03
   Frame=868   AssignHinge=diaglayer   GenHinge=diaglayer   DistType=RelDist   RelDist=0.5
AbsDist=4.99988999879012E-03   ActualDist=4.99988999879012E-03
   Frame=869   AssignHinge=diaglayer   GenHinge=diaglayer   DistType=RelDist   RelDist=0.5
AbsDist=4.99988999879012E-03   ActualDist=4.99988999879012E-03
   Frame=886   AssignHinge=diaglayer.245   GenHinge=diaglayer.245   DistType=RelDist   RelDist=0.5
AbsDist=5.00132482448402E-03   ActualDist=5.00132482448402E-03
   Frame=887   AssignHinge=diaglayer.245   GenHinge=diaglayer.245   DistType=RelDist   RelDist=0.5
AbsDist=5.00132482448402E-03   ActualDist=5.00132482448402E-03
   Frame=888   AssignHinge=diaglayer.245   GenHinge=diaglayer.245   DistType=RelDist   RelDist=0.5
AbsDist=5.00132482448402E-03   ActualDist=5.00132482448402E-03
   Frame=889   AssignHinge=diaglayer.245   GenHinge=diaglayer.245   DistType=RelDist   RelDist=0.5
AbsDist=5.00132482448402E-03   ActualDist=5.00132482448402E-03
   Frame=890   AssignHinge=diaglayer.245   GenHinge=diaglayer.245   DistType=RelDist   RelDist=0.5
AbsDist=5.00132482448402E-03   ActualDist=5.00132482448402E-03
   Frame=891   AssignHinge=diaglayer.245   GenHinge=diaglayer.245   DistType=RelDist   RelDist=0.5
AbsDist=5.00132482448402E-03   ActualDist=5.00132482448402E-03
   Frame=892   AssignHinge=diaglayer.245   GenHinge=diaglayer.245   DistType=RelDist   RelDist=0.5
AbsDist=5.00132482448402E-03   ActualDist=5.00132482448402E-03
   Frame=893   AssignHinge=diaglayer.245   GenHinge=diaglayer.245   DistType=RelDist   RelDist=0.5
AbsDist=5.00132482448402E-03   ActualDist=5.00132482448402E-03
   Frame=894   AssignHinge=diaglayer.245   GenHinge=diaglayer.245   DistType=RelDist   RelDist=0.5
AbsDist=5.00132482448402E-03   ActualDist=5.00132482448402E-03
   Frame=895   AssignHinge=diaglayer.245   GenHinge=diaglayer.245   DistType=RelDist   RelDist=0.5
AbsDist=5.00132482448402E-03   ActualDist=5.00132482448402E-03
   Frame=896   AssignHinge=diaglayer.245   GenHinge=diaglayer.245   DistType=RelDist   RelDist=0.5
AbsDist=5.00132482448403E-03   ActualDist=5.00132482448403E-03
   Frame=897   AssignHinge=diaglayer.245   GenHinge=diaglayer.245   DistType=RelDist   RelDist=0.5
AbsDist=5.00132482448402E-03   ActualDist=5.00132482448402E-03
   Frame=912   AssignHinge=diaglayer.245   GenHinge=diaglayer.245   DistType=RelDist   RelDist=0.5
AbsDist=5.00132482448384E-03   ActualDist=5.00132482448384E-03
   Frame=913   AssignHinge=diaglayer.245   GenHinge=diaglayer.245   DistType=RelDist   RelDist=0.5
AbsDist=5.00132482448402E-03   ActualDist=5.00132482448402E-03
   Frame=914   AssignHinge=diaglayer.245   GenHinge=diaglayer.245   DistType=RelDist   RelDist=0.5
AbsDist=5.00132482448384E-03   ActualDist=5.00132482448384E-03
   Frame=915   AssignHinge=diaglayer.245   GenHinge=diaglayer.245   DistType=RelDist   RelDist=0.5
AbsDist=5.00132482448384E-03   ActualDist=5.00132482448384E-03
   Frame=916   AssignHinge=diaglayer.245   GenHinge=diaglayer.245   DistType=RelDist   RelDist=0.5
AbsDist=5.00132482448403E-03   ActualDist=5.00132482448403E-03
   Frame=917   AssignHinge=diaglayer.245   GenHinge=diaglayer.245   DistType=RelDist   RelDist=0.5
AbsDist=5.00132482448384E-03   ActualDist=5.00132482448384E-03
   Frame=922   AssignHinge=diaglayer.245   GenHinge=diaglayer.245   DistType=RelDist   RelDist=0.5
AbsDist=5.00132482448402E-03   ActualDist=5.00132482448402E-03
   Frame=923   AssignHinge=diaglayer.245   GenHinge=diaglayer.245   DistType=RelDist   RelDist=0.5
AbsDist=5.00132482448402E-03   ActualDist=5.00132482448402E-03
   Frame=924   AssignHinge=diaglayer.245   GenHinge=diaglayer.245   DistType=RelDist   RelDist=0.5
AbsDist=5.00132482448402E-03   ActualDist=5.00132482448402E-03
   Frame=925   AssignHinge=diaglayer.245   GenHinge=diaglayer.245   DistType=RelDist   RelDist=0.5
AbsDist=5.00132482448402E-03   ActualDist=5.00132482448402E-03
   Frame=926   AssignHinge=diaglayer.245   GenHinge=diaglayer.245   DistType=RelDist   RelDist=0.5
AbsDist=5.00132482448402E-03   ActualDist=5.00132482448402E-03
   Frame=927   AssignHinge=diaglayer.245   GenHinge=diaglayer.245   DistType=RelDist   RelDist=0.5
AbsDist=5.00132482448402E-03   ActualDist=5.00132482448402E-03
   Frame=936   AssignHinge=diaglayer.245   GenHinge=diaglayer.245   DistType=RelDist   RelDist=0.5
AbsDist=5.00132482448402E-03   ActualDist=5.00132482448402E-03
   Frame=937   AssignHinge=diaglayer.245   GenHinge=diaglayer.245   DistType=RelDist   RelDist=0.5
AbsDist=5.00132482448402E-03   ActualDist=5.00132482448402E-03
   Frame=938   AssignHinge=diaglayer.245   GenHinge=diaglayer.245   DistType=RelDist   RelDist=0.5
AbsDist=5.00132482448402E-03   ActualDist=5.00132482448402E-03
   Frame=939   AssignHinge=diaglayer.245   GenHinge=diaglayer.245   DistType=RelDist   RelDist=0.5
AbsDist=5.00132482448403E-03   ActualDist=5.00132482448403E-03
   Frame=940   AssignHinge=diaglayer.245   GenHinge=diaglayer.245   DistType=RelDist   RelDist=0.5
AbsDist=5.00132482448402E-03   ActualDist=5.00132482448402E-03
   Frame=941   AssignHinge=diaglayer.245   GenHinge=diaglayer.245   DistType=RelDist   RelDist=0.5
AbsDist=5.00132482448402E-03   ActualDist=5.00132482448402E-03
   Frame=942   AssignHinge=diaglayer.245   GenHinge=diaglayer.245   DistType=RelDist   RelDist=0.5
AbsDist=5.00132482448402E-03   ActualDist=5.00132482448402E-03
   Frame=943   AssignHinge=diaglayer.245   GenHinge=diaglayer.245   DistType=RelDist   RelDist=0.5
AbsDist=5.00132482448402E-03   ActualDist=5.00132482448402E-03
   Frame=944   AssignHinge=diaglayer.245   GenHinge=diaglayer.245   DistType=RelDist   RelDist=0.5
AbsDist=5.00132482448402E-03   ActualDist=5.00132482448402E-03
   Frame=945   AssignHinge=diaglayer.245   GenHinge=diaglayer.245   DistType=RelDist   RelDist=0.5
AbsDist=5.00132482448402E-03   ActualDist=5.00132482448402E-03
   Frame=946   AssignHinge=diaglayer.245   GenHinge=diaglayer.245   DistType=RelDist   RelDist=0.5
AbsDist=5.00132482448402E-03   ActualDist=5.00132482448402E-03
   Frame=962   AssignHinge=diaglayer.245   GenHinge=diaglayer.245   DistType=RelDist   RelDist=0.5
AbsDist=5.00132482448402E-03   ActualDist=5.00132482448402E-03
```

```
   Frame=963   AssignHinge=diaglayer.245   GenHinge=diaglayer.245   DistType=RelDist   RelDist=0.5
AbsDist=5.00132482448402E-03   ActualDist=5.00132482448402E-03
   Frame=964   AssignHinge=diaglayer.245   GenHinge=diaglayer.245   DistType=RelDist   RelDist=0.5
AbsDist=5.00132482448402E-03   ActualDist=5.00132482448402E-03
   Frame=965   AssignHinge=diaglayer.245   GenHinge=diaglayer.245   DistType=RelDist   RelDist=0.5
AbsDist=5.00132482448402E-03   ActualDist=5.00132482448402E-03
   Frame=966   AssignHinge=diaglayer.245   GenHinge=diaglayer.245   DistType=RelDist   RelDist=0.5
AbsDist=5.00132482448402E-03   ActualDist=5.00132482448402E-03
   Frame=967   AssignHinge=diaglayer.245   GenHinge=diaglayer.245   DistType=RelDist   RelDist=0.5
AbsDist=5.00132482448402E-03   ActualDist=5.00132482448402E-03
   Frame=968   AssignHinge=diaglayer.245   GenHinge=diaglayer.245   DistType=RelDist   RelDist=0.5
AbsDist=5.00132482448402E-03   ActualDist=5.00132482448402E-03
   Frame=969   AssignHinge=diaglayer.245   GenHinge=diaglayer.245   DistType=RelDist   RelDist=0.5
AbsDist=5.00132482448402E-03   ActualDist=5.00132482448402E-03
   Frame=970   AssignHinge=diaglayer.245   GenHinge=diaglayer.245   DistType=RelDist   RelDist=0.5
AbsDist=5.00132482448402E-03   ActualDist=5.00132482448402E-03
   Frame=977   AssignHinge=diaglayer.245   GenHinge=diaglayer.245   DistType=RelDist   RelDist=0.5
AbsDist=5.00132482448402E-03   ActualDist=5.00132482448402E-03
   Frame=978   AssignHinge=diaglayer.245   GenHinge=diaglayer.245   DistType=RelDist   RelDist=0.5
AbsDist=5.01020209173245E-03   ActualDist=5.01020209173245E-03
   Frame=979   AssignHinge=diaglayer.245   GenHinge=diaglayer.245   DistType=RelDist   RelDist=0.5
AbsDist=5.00132482448402E-03   ActualDist=5.00132482448402E-03
   Frame=1037   AssignHinge=diaglayer.15   GenHinge=diaglayer.15   DistType=RelDist   RelDist=0.15
AbsDist=1.50033971153201E-03   ActualDist=1.50033971153201E-03
   Frame=1038   AssignHinge=diaglayer.15   GenHinge=diaglayer.15   DistType=RelDist   RelDist=0.15
AbsDist=1.50033971153201E-03   ActualDist=1.50033971153201E-03
   Frame=1039   AssignHinge=diaglayer.15   GenHinge=diaglayer.15   DistType=RelDist   RelDist=0.15
AbsDist=1.50033971153201E-03   ActualDist=1.50033971153201E-03
   Frame=1040   AssignHinge=diaglayer.15   GenHinge=diaglayer.15   DistType=RelDist   RelDist=0.15
AbsDist=1.50033971153201E-03   ActualDist=1.50033971153201E-03
   Frame=1041   AssignHinge=diaglayer.15   GenHinge=diaglayer.15   DistType=RelDist   RelDist=0.15
AbsDist=1.50033971153201E-03   ActualDist=1.50033971153201E-03
   Frame=1042   AssignHinge=diaglayer.15   GenHinge=diaglayer.15   DistType=RelDist   RelDist=0.15
AbsDist=1.50033971153201E-03   ActualDist=1.50033971153201E-03
   Frame=1043   AssignHinge=diaglayer.15   GenHinge=diaglayer.15   DistType=RelDist   RelDist=0.15
AbsDist=1.50033971153201E-03   ActualDist=1.50033971153201E-03
   Frame=1044   AssignHinge=diaglayer.15   GenHinge=diaglayer.15   DistType=RelDist   RelDist=0.15
AbsDist=1.50033971153201E-03   ActualDist=1.50033971153201E-03
   Frame=1045   AssignHinge=diaglayer.15   GenHinge=diaglayer.15   DistType=RelDist   RelDist=0.15
AbsDist=1.50033971153201E-03   ActualDist=1.50033971153201E-03
   Frame=1046   AssignHinge=diaglayer.15   GenHinge=diaglayer.15   DistType=RelDist   RelDist=0.15
AbsDist=1.50033971153201E-03   ActualDist=1.50033971153201E-03
   Frame=1047   AssignHinge=diaglayer.15   GenHinge=diaglayer.15   DistType=RelDist   RelDist=0.15
AbsDist=1.50033971153202E-03   ActualDist=1.50033971153202E-03
   Frame=1048   AssignHinge=diaglayer.15   GenHinge=diaglayer.15   DistType=RelDist   RelDist=0.15
AbsDist=1.50033971153201E-03   ActualDist=1.50033971153201E-03
   Frame=1049   AssignHinge=diaglayer.15   GenHinge=diaglayer.15   DistType=RelDist   RelDist=0.15
AbsDist=1.50033971153201E-03   ActualDist=1.50033971153201E-03
   Frame=1050   AssignHinge=diaglayer.15   GenHinge=diaglayer.15   DistType=RelDist   RelDist=0.15
AbsDist=1.50033971153201E-03   ActualDist=1.50033971153201E-03
   Frame=1051   AssignHinge=diaglayer.15   GenHinge=diaglayer.15   DistType=RelDist   RelDist=0.15
AbsDist=1.50033971153201E-03   ActualDist=1.50033971153201E-03
   Frame=1052   AssignHinge=diaglayer.15   GenHinge=diaglayer.15   DistType=RelDist   RelDist=0.15
AbsDist=1.50033971153201E-03   ActualDist=1.50033971153201E-03
   Frame=1053   AssignHinge=diaglayer.15   GenHinge=diaglayer.15   DistType=RelDist   RelDist=0.15
AbsDist=1.50033971153202E-03   ActualDist=1.50033971153202E-03
   Frame=1054   AssignHinge=diaglayer.15   GenHinge=diaglayer.15   DistType=RelDist   RelDist=0.15
AbsDist=1.50033971153201E-03   ActualDist=1.50033971153201E-03
   Frame=1055   AssignHinge=diaglayer.15   GenHinge=diaglayer.15   DistType=RelDist   RelDist=0.15
AbsDist=1.50033971153203E-03   ActualDist=1.50033971153203E-03
   Frame=1056   AssignHinge=diaglayer.15   GenHinge=diaglayer.15   DistType=RelDist   RelDist=0.15
AbsDist=1.50033971153203E-03   ActualDist=1.50033971153203E-03
   Frame=1057   AssignHinge=diaglayer.15   GenHinge=diaglayer.15   DistType=RelDist   RelDist=0.15
AbsDist=1.50033971153203E-03   ActualDist=1.50033971153203E-03
   Frame=1058   AssignHinge=diaglayer.15   GenHinge=diaglayer.15   DistType=RelDist   RelDist=0.15
AbsDist=1.50033971153203E-03   ActualDist=1.50033971153203E-03
   Frame=1059   AssignHinge=diaglayer.15   GenHinge=diaglayer.15   DistType=RelDist   RelDist=0.15
AbsDist=1.50033971153203E-03   ActualDist=1.50033971153203E-03
   Frame=1060   AssignHinge=diaglayer.15   GenHinge=diaglayer.15   DistType=RelDist   RelDist=0.15
AbsDist=1.50033971153203E-03   ActualDist=1.50033971153203E-03
   Frame=1061   AssignHinge=diaglayer.15   GenHinge=diaglayer.15   DistType=RelDist   RelDist=0.15
AbsDist=1.50033971153201E-03   ActualDist=1.50033971153201E-03
   Frame=1062   AssignHinge=diaglayer.15   GenHinge=diaglayer.15   DistType=RelDist   RelDist=0.15
AbsDist=1.50033971153203E-03   ActualDist=1.50033971153203E-03
   Frame=1063   AssignHinge=diaglayer.15   GenHinge=diaglayer.15   DistType=RelDist   RelDist=0.15
AbsDist=1.50033971153201E-03   ActualDist=1.50033971153201E-03
   Frame=1064   AssignHinge=diaglayer.15   GenHinge=diaglayer.15   DistType=RelDist   RelDist=0.15
AbsDist=1.50033971153201E-03   ActualDist=1.50033971153201E-03
   Frame=1065   AssignHinge=diaglayer.15   GenHinge=diaglayer.15   DistType=RelDist   RelDist=0.15
AbsDist=1.50379320386815E-03   ActualDist=1.50379320386815E-03
   Frame=1066   AssignHinge=diaglayer.15   GenHinge=diaglayer.15   DistType=RelDist   RelDist=0.15
AbsDist=1.50033971153201E-03   ActualDist=1.50033971153201E-03
   Frame=1067   AssignHinge=diaglayer.15   GenHinge=diaglayer.15   DistType=RelDist   RelDist=0.15
AbsDist=1.50033971153201E-03   ActualDist=1.50033971153201E-03
```

```
   Frame=1068   AssignHinge=diaglayer.15   GenHinge=diaglayer.15   DistType=RelDist   RelDist=0.15
AbsDist=1.50033971153201E-03   ActualDist=1.50033971153201E-03
   Frame=1069   AssignHinge=diaglayer.15   GenHinge=diaglayer.15   DistType=RelDist   RelDist=0.15
AbsDist=1.50033971153201E-03   ActualDist=1.50033971153201E-03
   Frame=1070   AssignHinge=diaglayer.15   GenHinge=diaglayer.15   DistType=RelDist   RelDist=0.15
AbsDist=1.50033971153201E-03   ActualDist=1.50033971153201E-03
   Frame=1071   AssignHinge=diaglayer.15   GenHinge=diaglayer.15   DistType=RelDist   RelDist=0.15
AbsDist=1.50033971153201E-03   ActualDist=1.50033971153201E-03
   Frame=1072   AssignHinge=diaglayer.15   GenHinge=diaglayer.15   DistType=RelDist   RelDist=0.15
AbsDist=1.50033971153201E-03   ActualDist=1.50033971153201E-03
   Frame=1073   AssignHinge=diaglayer.15   GenHinge=diaglayer.15   DistType=RelDist   RelDist=0.15
AbsDist=1.50033971153201E-03   ActualDist=1.50033971153201E-03
   Frame=1074   AssignHinge=diaglayer.15   GenHinge=diaglayer.15   DistType=RelDist   RelDist=0.15
AbsDist=1.50033971153201E-03   ActualDist=1.50033971153201E-03
   Frame=1075   AssignHinge=diaglayer.15   GenHinge=diaglayer.15   DistType=RelDist   RelDist=0.15
AbsDist=1.50033971153201E-03   ActualDist=1.50033971153201E-03
   Frame=1076   AssignHinge=diaglayer.15   GenHinge=diaglayer.15   DistType=RelDist   RelDist=0.15
AbsDist=1.50033971153201E-03   ActualDist=1.50033971153201E-03
   Frame=1077   AssignHinge=diaglayer.15   GenHinge=diaglayer.15   DistType=RelDist   RelDist=0.15
AbsDist=1.50033971153201E-03   ActualDist=1.50033971153201E-03
   Frame=1078   AssignHinge=diaglayer.15   GenHinge=diaglayer.15   DistType=RelDist   RelDist=0.15
AbsDist=1.50033971153201E-03   ActualDist=1.50033971153201E-03
   Frame=1079   AssignHinge=diaglayer.15   GenHinge=diaglayer.15   DistType=RelDist   RelDist=0.15
AbsDist=1.50033971153201E-03   ActualDist=1.50033971153201E-03
   Frame=1080   AssignHinge=diaglayer.15   GenHinge=diaglayer.15   DistType=RelDist   RelDist=0.15
AbsDist=1.50033971153201E-03   ActualDist=1.50033971153201E-03
   Frame=1081   AssignHinge=diaglayer.15   GenHinge=diaglayer.15   DistType=RelDist   RelDist=0.15
AbsDist=1.50033971153201E-03   ActualDist=1.50033971153201E-03
   Frame=1082   AssignHinge=diaglayer.15   GenHinge=diaglayer.15   DistType=RelDist   RelDist=0.15
AbsDist=1.50033971153201E-03   ActualDist=1.50033971153201E-03
   Frame=1083   AssignHinge=diaglayer.15   GenHinge=diaglayer.15   DistType=RelDist   RelDist=0.15
AbsDist=1.50033971153201E-03   ActualDist=1.50033971153201E-03
   Frame=1084   AssignHinge=diaglayer.15   GenHinge=diaglayer.15   DistType=RelDist   RelDist=0.15
AbsDist=1.50033971153201E-03   ActualDist=1.50033971153201E-03
   Frame=1115   AssignHinge=diaglayer.15   GenHinge=diaglayer.15   DistType=RelDist   RelDist=0.15
AbsDist=1.50033971153201E-03   ActualDist=1.50033971153201E-03
   Frame=1116   AssignHinge=diaglayer.15   GenHinge=diaglayer.15   DistType=RelDist   RelDist=0.15
AbsDist=1.50033971153201E-03   ActualDist=1.50033971153201E-03
   Frame=1117   AssignHinge=diaglayer.15   GenHinge=diaglayer.15   DistType=RelDist   RelDist=0.15
AbsDist=1.50033971153201E-03   ActualDist=1.50033971153201E-03
   Frame=1118   AssignHinge=diaglayer.15   GenHinge=diaglayer.15   DistType=RelDist   RelDist=0.15
AbsDist=1.50033971153201E-03   ActualDist=1.50033971153201E-03
   Frame=1119   AssignHinge=diaglayer.15   GenHinge=diaglayer.15   DistType=RelDist   RelDist=0.15
AbsDist=1.50033971153201E-03   ActualDist=1.50033971153201E-03
   Frame=1120   AssignHinge=diaglayer.15   GenHinge=diaglayer.15   DistType=RelDist   RelDist=0.15
AbsDist=1.50033971153201E-03   ActualDist=1.50033971153201E-03
   Frame=1121   AssignHinge=diaglayer.15   GenHinge=diaglayer.15   DistType=RelDist   RelDist=0.15
AbsDist=1.50033971153201E-03   ActualDist=1.50033971153201E-03
   Frame=1122   AssignHinge=diaglayer.15   GenHinge=diaglayer.15   DistType=RelDist   RelDist=0.15
AbsDist=1.50033971153201E-03   ActualDist=1.50033971153201E-03
   Frame=1123   AssignHinge=diaglayer.15   GenHinge=diaglayer.15   DistType=RelDist   RelDist=0.15
AbsDist=1.50033971153201E-03   ActualDist=1.50033971153201E-03
   Frame=1124   AssignHinge=diaglayer.15   GenHinge=diaglayer.15   DistType=RelDist   RelDist=0.15
AbsDist=1.50033971153201E-03   ActualDist=1.50033971153201E-03
   Frame=1125   AssignHinge=diaglayer.15   GenHinge=diaglayer.15   DistType=RelDist   RelDist=0.15
AbsDist=1.50033971153202E-03   ActualDist=1.50033971153202E-03
   Frame=1126   AssignHinge=diaglayer.15   GenHinge=diaglayer.15   DistType=RelDist   RelDist=0.15
AbsDist=1.50033971153201E-03   ActualDist=1.50033971153201E-03
   Frame=1127   AssignHinge=diaglayer.15   GenHinge=diaglayer.15   DistType=RelDist   RelDist=0.15
AbsDist=1.50033971153201E-03   ActualDist=1.50033971153201E-03
   Frame=1128   AssignHinge=diaglayer.15   GenHinge=diaglayer.15   DistType=RelDist   RelDist=0.15
AbsDist=1.50033971153201E-03   ActualDist=1.50033971153201E-03
   Frame=1129   AssignHinge=diaglayer.15   GenHinge=diaglayer.15   DistType=RelDist   RelDist=0.15
AbsDist=1.50033971153201E-03   ActualDist=1.50033971153201E-03
   Frame=1130   AssignHinge=diaglayer.15   GenHinge=diaglayer.15   DistType=RelDist   RelDist=0.15
AbsDist=1.50033971153201E-03   ActualDist=1.50033971153201E-03
   Frame=1131   AssignHinge=diaglayer.15   GenHinge=diaglayer.15   DistType=RelDist   RelDist=0.15
AbsDist=1.50033971153202E-03   ActualDist=1.50033971153202E-03
   Frame=1132   AssignHinge=diaglayer.15   GenHinge=diaglayer.15   DistType=RelDist   RelDist=0.15
AbsDist=1.50033971153201E-03   ActualDist=1.50033971153201E-03
   Frame=1133   AssignHinge=diaglayer.15   GenHinge=diaglayer.15   DistType=RelDist   RelDist=0.15
AbsDist=1.50033971153203E-03   ActualDist=1.50033971153203E-03
   Frame=1134   AssignHinge=diaglayer.15   GenHinge=diaglayer.15   DistType=RelDist   RelDist=0.15
AbsDist=1.50033971153203E-03   ActualDist=1.50033971153203E-03
   Frame=1135   AssignHinge=diaglayer.15   GenHinge=diaglayer.15   DistType=RelDist   RelDist=0.15
AbsDist=1.50033971153203E-03   ActualDist=1.50033971153203E-03
   Frame=1136   AssignHinge=diaglayer.15   GenHinge=diaglayer.15   DistType=RelDist   RelDist=0.15
AbsDist=1.50033971153203E-03   ActualDist=1.50033971153203E-03
   Frame=1137   AssignHinge=diaglayer.15   GenHinge=diaglayer.15   DistType=RelDist   RelDist=0.15
AbsDist=1.50033971153203E-03   ActualDist=1.50033971153203E-03
   Frame=1138   AssignHinge=diaglayer.15   GenHinge=diaglayer.15   DistType=RelDist   RelDist=0.15
AbsDist=1.50033971153203E-03   ActualDist=1.50033971153203E-03
   Frame=1143   AssignHinge=mainlongsteel   GenHinge=mainlongsteel   DistType=RelDist   RelDist=0.5
AbsDist=0.1225   ActualDist=0.1225
```

```
   Frame=1144   AssignHinge=mainlongsteel   GenHinge=mainlongsteel   DistType=RelDist   RelDist=0.5
AbsDist=0.1225   ActualDist=0.1225
   Frame=1147   AssignHinge=mainlongsteel   GenHinge=mainlongsteel   DistType=RelDist   RelDist=0.5
AbsDist=0.1225   ActualDist=0.1225
   Frame=1148   AssignHinge=mainlongsteel   GenHinge=mainlongsteel   DistType=RelDist   RelDist=0.5
AbsDist=0.1225   ActualDist=0.1225
   Frame=1151   AssignHinge=mainlongsteel   GenHinge=mainlongsteel   DistType=RelDist   RelDist=0.5
AbsDist=0.1225   ActualDist=0.1225
   Frame=1152   AssignHinge=mainlongsteel   GenHinge=mainlongsteel   DistType=RelDist   RelDist=0.5
AbsDist=0.1225   ActualDist=0.1225
   Frame=1155   AssignHinge=mainlongsteel   GenHinge=mainlongsteel   DistType=RelDist   RelDist=0.5
AbsDist=0.1225   ActualDist=0.1225
   Frame=1156   AssignHinge=mainlongsteel   GenHinge=mainlongsteel   DistType=RelDist   RelDist=0.5
AbsDist=0.1225   ActualDist=0.1225
   Frame=1159   AssignHinge=mainlongsteel   GenHinge=mainlongsteel   DistType=RelDist   RelDist=0.5
AbsDist=0.1225   ActualDist=0.1225
   Frame=1160   AssignHinge=mainlongsteel   GenHinge=mainlongsteel   DistType=RelDist   RelDist=0.5
AbsDist=0.1225   ActualDist=0.1225
   Frame=1163   AssignHinge=mainlongsteel   GenHinge=mainlongsteel   DistType=RelDist   RelDist=0.5
AbsDist=0.1225   ActualDist=0.1225
   Frame=1164   AssignHinge=mainlongsteel   GenHinge=mainlongsteel   DistType=RelDist   RelDist=0.5
AbsDist=0.1225   ActualDist=0.1225
   Frame=1167   AssignHinge=mesh1.5   GenHinge=mesh1.5   DistType=RelDist   RelDist=0.5
AbsDist=0.03   ActualDist=0.03
   Frame=1168   AssignHinge=mesh1.5   GenHinge=mesh1.5   DistType=RelDist   RelDist=0.5
AbsDist=0.03   ActualDist=0.03
   Frame=1169   AssignHinge=mesh   GenHinge=mesh   DistType=RelDist   RelDist=0.5   AbsDist=0.03
ActualDist=0.03
   Frame=1170   AssignHinge=mesh   GenHinge=mesh   DistType=RelDist   RelDist=0.5   AbsDist=0.03
ActualDist=0.03
   Frame=1171   AssignHinge=mesh   GenHinge=mesh   DistType=RelDist   RelDist=0.5   AbsDist=0.03
ActualDist=0.03
   Frame=1172   AssignHinge=mesh   GenHinge=mesh   DistType=RelDist   RelDist=0.5   AbsDist=0.03
ActualDist=0.03
   Frame=1173   AssignHinge=mesh   GenHinge=mesh   DistType=RelDist   RelDist=0.5   AbsDist=0.03
ActualDist=0.03
   Frame=1174   AssignHinge=mesh   GenHinge=mesh   DistType=RelDist   RelDist=0.5   AbsDist=0.03
ActualDist=0.03
   Frame=1175   AssignHinge=mesh   GenHinge=mesh   DistType=RelDist   RelDist=0.5   AbsDist=0.03
ActualDist=0.03
   Frame=1176   AssignHinge=mesh   GenHinge=mesh   DistType=RelDist   RelDist=0.5   AbsDist=0.03
ActualDist=0.03
   Frame=1177   AssignHinge=mesh   GenHinge=mesh   DistType=RelDist   RelDist=0.5   AbsDist=0.03
ActualDist=0.03
   Frame=1178   AssignHinge=mesh   GenHinge=mesh   DistType=RelDist   RelDist=0.5   AbsDist=0.03
ActualDist=0.03

TABLE:  "AREA SECTION ASSIGNMENTS"
   Area=1   Section=slab   MatProp=Default
   to
   Area=344   Section=slab   MatProp=Default

TABLE:  "AREA STIFFNESS MODIFIERS"
Selected Areas eg:
   Area=32   f11=0.29   f22=1   f12=1   m11=1   m22=1   m12=1   v13=1   v23=1   MassMod=1
WeightMod=1

END TABLE DATA
```